



# **BACTERIAL MECHANISMS OF ANTIBIOTIC RESISTANCE: A STRUCTURAL PERSPECTIVE**

EDITED BY: Vassiliy Bavro, Graeme L. Conn and Christopher Davies

PUBLISHED IN: Frontiers in Molecular Biosciences and Frontiers in Microbiology



# frontiers

## Frontiers Copyright Statement

© Copyright 2007-2019 Frontiers Media SA. All rights reserved.

All content included on this site, such as text, graphics, logos, button icons, images, video/audio clips, downloads, data compilations and software, is the property of or is licensed to Frontiers Media SA ("Frontiers") or its licensees and/or subcontractors. The copyright in the text of individual articles is the property of their respective authors, subject to a license granted to Frontiers.

The compilation of articles constituting this e-book, wherever published, as well as the compilation of all other content on this site, is the exclusive property of Frontiers. For the conditions for downloading and copying of e-books from Frontiers' website, please see the Terms for Website Use. If purchasing Frontiers e-books from other websites or sources, the conditions of the website concerned apply.

Images and graphics not forming part of user-contributed materials may not be downloaded or copied without permission.

Individual articles may be downloaded and reproduced in accordance with the principles of the CC-BY licence subject to any copyright or other notices. They may not be re-sold as an e-book.

As author or other contributor you grant a CC-BY licence to others to reproduce your articles, including any graphics and third-party materials supplied by you, in accordance with the Conditions for Website Use and subject to any copyright notices which you include in connection with your articles and materials.

All copyright, and all rights therein, are protected by national and international copyright laws.

The above represents a summary only. For the full conditions see the Conditions for Authors and the Conditions for Website Use.

ISSN 1664-8714  
ISBN 978-2-88963-190-2  
DOI 10.3389/978-2-88963-190-2

## About Frontiers

Frontiers is more than just an open-access publisher of scholarly articles: it is a pioneering approach to the world of academia, radically improving the way scholarly research is managed. The grand vision of Frontiers is a world where all people have an equal opportunity to seek, share and generate knowledge. Frontiers provides immediate and permanent online open access to all its publications, but this alone is not enough to realize our grand goals.

## Frontiers Journal Series

The Frontiers Journal Series is a multi-tier and interdisciplinary set of open-access, online journals, promising a paradigm shift from the current review, selection and dissemination processes in academic publishing. All Frontiers journals are driven by researchers for researchers; therefore, they constitute a service to the scholarly community. At the same time, the Frontiers Journal Series operates on a revolutionary invention, the tiered publishing system, initially addressing specific communities of scholars, and gradually climbing up to broader public understanding, thus serving the interests of the lay society, too.

## Dedication to Quality

Each Frontiers article is a landmark of the highest quality, thanks to genuinely collaborative interactions between authors and review editors, who include some of the world's best academicians. Research must be certified by peers before entering a stream of knowledge that may eventually reach the public - and shape society; therefore, Frontiers only applies the most rigorous and unbiased reviews.

Frontiers revolutionizes research publishing by freely delivering the most outstanding research, evaluated with no bias from both the academic and social point of view. By applying the most advanced information technologies, Frontiers is catapulting scholarly publishing into a new generation.

## What are Frontiers Research Topics?

Frontiers Research Topics are very popular trademarks of the Frontiers Journals Series: they are collections of at least ten articles, all centered on a particular subject. With their unique mix of varied contributions from Original Research to Review Articles, Frontiers Research Topics unify the most influential researchers, the latest key findings and historical advances in a hot research area! Find out more on how to host your own Frontiers Research Topic or contribute to one as an author by contacting the Frontiers Editorial Office: [researchtopics@frontiersin.org](mailto:researchtopics@frontiersin.org)



# BACTERIAL MECHANISMS OF ANTIBIOTIC RESISTANCE: A STRUCTURAL PERSPECTIVE

Topic Editors:

**Vassiliy Bavro**, University of Essex, United Kingdom

**Graeme L. Conn**, Emory University School of Medicine, United States

**Christopher Davies**, Medical University of South Carolina, United States

**Citation:** Bavro, V., Conn, G. L., Davies, C., eds. (2019). Bacterial Mechanisms of Antibiotic Resistance: A Structural Perspective. Lausanne: Frontiers Media.  
doi: 10.3389/978-2-88963-190-2

# Table of Contents

- 05 Editorial: Bacterial Mechanisms of Antibiotic Resistance: A Structural Perspective**  
Graeme L. Conn, Vassiliy N. Bavro and Christopher Davies
- 08 Hoisting-Loop in Bacterial Multidrug Exporter AcrB is a Highly Flexible Hinge That Enables the Large Motion of the Subdomains**  
Martijn Zwama, Katsuhiko Hayashi, Keisuke Sakurai, Ryosuke Nakashima, Kimie Kitagawa, Kunihiro Nishino and Akihito Yamaguchi
- 16 Molecular Determinants of the Promiscuity of MexB and MexY Multidrug Transporters of *Pseudomonas aeruginosa***  
Venkata K. Ramaswamy, Attilio V. Vargiu, Giuliano Mallocci, Jürg Dreier and Paolo Ruggerone
- 33 Antibiotic Resistance Mediated by the MacB ABC Transporter Family: A Structural and Functional Perspective**  
Nicholas P. Greene, Elise Kaplan, Allister Crow and Vassilis Koronakis
- 50 Functional Mechanism of the Efflux Pumps Transcription Regulators From *Pseudomonas aeruginosa* Based on 3D Structures**  
Karim Housseini B Issa, Gilles Phan and Isabelle Broutin
- 70 Re-sensitizing Multidrug Resistant Bacteria to Antibiotics by Targeting Bacterial Response Regulators: Characterization and Comparison of Interactions Between 2-Aminoimidazoles and the Response Regulators BfmR From *Acinetobacter baumannii* and QseB From *Francisella* spp.**  
Morgan E. Milton, Bradley M. Minrovic, Danni L. Harris, Brian Kang, David Jung, Caleb P. Lewis, Richele J. Thompson, Roberta J. Melander, Daina Zeng, Christian Melander and John Cavanagh
- 82 Structure-Function Relationships of the Neisserial EptA Enzyme Responsible for Phosphoethanolamine Decoration of Lipid A: Rationale for Drug Targeting**  
Charlene M. Kahler, K. L. Nawrocki, A. Anandan, Alice Vrielink and William M. Shafer
- 93 Bacterial Strategies to Preserve Cell Wall Integrity Against Environmental Threats**  
Akhilesh K. Yadav, Akbar Espaillat and Felipe Cava
- 102 The Mechanisms of Action of Ribosome-Targeting Peptide Antibiotics**  
Yury S. Polikanov, Nikolay A. Aleksashin, Bertrand Beckert and Daniel N. Wilson
- 123 Tetracycline-Inactivating Enzymes**  
Jana L. Markley and Timothy A. Wencewicz
- 145 Look and Outlook on Enzyme-Mediated Macrolide Resistance**  
Tolou Golkar, Michał Zieliński and Albert M. Berghuis
- 160 The Structural and Functional Basis for Recurring Sulfa Drug Resistance Mutations in *Staphylococcus aureus* Dihydropteroate Synthase**  
Elizabeth C. Griffith, Miranda J. Wallace, Yinan Wu, Gyanendra Kumar, Stefan Gajewski, Pamela Jackson, Gregory A. Phelps, Zhong Zheng, Charles O. Rock, Richard E. Lee and Stephen W. White

- 176** *Structural and Mechanistic Basis for Extended-Spectrum Drug-Resistance Mutations in Altering the Specificity of TEM, CTX-M, and KPC  $\beta$ -lactamases*  
Timothy Palzkill
- 195** *Exploring Additional Dimensions of Complexity in Inhibitor Design for Serine  $\beta$ -Lactamases: Mechanistic and Intra- and Inter-molecular Chemistry Approaches*  
Focco van den Akker and Robert A. Bonomo



# Editorial: Bacterial Mechanisms of Antibiotic Resistance: A Structural Perspective

Graeme L. Conn<sup>1\*</sup>, Vassiliy N. Bavro<sup>2\*</sup> and Christopher Davies<sup>3\*</sup>

<sup>1</sup> Department of Biochemistry, Emory University School of Medicine, Atlanta, GA, United States, <sup>2</sup> School of Biological Sciences, University of Essex, Colchester, United Kingdom, <sup>3</sup> Department of Biochemistry and Molecular Biology, Medical University of South Carolina, Charleston, SC, United States

**Keywords:** antibiotic resistance, antibiotic inactivation, multi-drug-resistance, cell wall alteration, efflux pumps, ribosome, bacteria

## Editorial on the Research Topic

### Bacterial Mechanisms of Antibiotic Resistance: A Structural Perspective

Antibiotic-resistant bacteria are responsible for millions of hard-to-treat infections annually. Since antibiotic “miracle drugs” were first introduced into clinical use, resistance has closely followed; more recently, this problem has been greatly exacerbated by their extensive use in medicine and agriculture, combined with the remarkable ability of bacterial populations to rapidly evolve and exchange genetic material. The rise of multidrug resistance (MDR), coupled with declining availability of newly approved or in-development treatments, threatens to fundamentally alter our ability to treat infections. Whether the most pessimistic predictions of a future “post-antibiotic era” become reality over the coming decades will depend on actions taken in the present. This Research Topic collects together articles that highlight the recent contributions of structural biology and related approaches to our understanding of antibiotic resistance and adaptations used by bacteria against drugs that target key cellular structures, complexes or pathways, as well as drug development efforts to counter these resistance mechanisms. New insights from such approaches are likely to be critical in future efforts to develop strategies to overcome existing resistance mechanisms and to identify targets for novel antibiotic development.

## OPEN ACCESS

### Edited by:

Loredano Pollegioni,  
University of Insubria, Italy

### Reviewed by:

Flavia Marinelli,  
University of Insubria, Italy

### \*Correspondence:

Graeme L. Conn  
gconn@emory.edu  
Vassiliy N. Bavro  
v.bavro@essex.ac.uk  
Christopher Davies  
davies@musc.edu

### Specialty section:

This article was submitted to  
Structural Biology,  
a section of the journal  
Frontiers in Molecular Biosciences

**Received:** 05 June 2019

**Accepted:** 31 July 2019

**Published:** 14 August 2019

### Citation:

Conn GL, Bavro VN and Davies C  
(2019) Editorial: Bacterial Mechanisms  
of Antibiotic Resistance: A Structural  
Perspective. *Front. Mol. Biosci.* 6:71.  
doi: 10.3389/fmolb.2019.00071

## EFFLUX PUMPS AND TRANSPORTERS

The tripartite assemblies built around the Resistance-Nodulation-Division (RND) family of proton-powered secondary transporters play a prominent MDR role in Gram-negative bacteria. While RND assemblies have been a focus of a recent dedicated Frontiers Research Topic (Vargiu et al., 2016), their structural biology is one of the most rapidly advancing directions within the MDR field and two important experimental studies are reported within this collection.

First, Zwama et al. use X-ray crystallography to dissect the role of the so-called hoisting loop, located at the border of transmembrane helix 8 and the PC2 subdomain, in the prototypical RND family member AcrB. This study demonstrates how the random coil-to- $\alpha$ -helix transition of this loop leads to opening and closing of the drug-channel entrance. Crucially, this work elucidates one of the last remaining problematic areas regarding the functional RND-pump cycle, namely the energy transduction and conformational coupling between remote regions of the RND-transporters.

Another persistent question within the RND field is the structural basis for the apparent broad-substrate specificity provided by these pumps. Ramaswamy et al. address this using molecular dynamics simulations of the centrally important RND-transporters MexB and MexY from *Pseudomonas aeruginosa*. This study characterizes the potential binding pockets of these transporters and their substrates which, by innovative use of electrostatic complementarity analysis, allows the authors to reveal key differences between these transporters. Importantly, this first comparative study of the major *P. aeruginosa* transporters suggests that the deep binding pocket of the tight conformer plays a central role in substrate selectivity.

While the role of RND transporters in efflux and tripartite assemblies has been extensively studied, until recently, much less was known about the structural organization of the ABC-transporter family members participating in tripartite assemblies. A wide-ranging review by Greene et al. synthesizes the recent advances in structure and function of the MacB-family of ABC-transporters, which form unique tripartite assemblies with a role in macrolide efflux and protein export. The authors provide a tantalizing novel model of functional mechanotransmission and discuss the links to homologous tripartite systems from other pathogenic bacteria, which similarly export protein-like signaling molecules, virulence factors, and siderophores.

Genetic regulation of efflux pumps is a key mechanism of resistance, with their associated transcriptional regulators emerging as promising therapeutic targets, and yet, this remains one of least well-understood areas in MDR. Bridging this gap, Issa et al., provide a comprehensive review of the recent progress in the structural biology of regulator families in *P. aeruginosa*, including the one-component system regulators of the TetR, LysR, MarR, AraC families, and two-component systems (TCS) families of regulators. In a related work, Milton et al., combine molecular modeling with biochemical and cellular studies to propose a potential mechanism of interaction between TCS response regulators and 2-aminoimidazole compounds which can inhibit bacterial biofilm formation, disperse preformed biofilms, and re-sensitize MDR bacteria to antibiotics. This study focuses on two important pathogens, *Acinetobacter baumannii* and *Francisella tularensis*, and provides promising new insights into this potential new therapeutic avenue.

## CELL WALL ALTERATIONS

The complex role played by the bacterial cell-envelope structure, and particularly the lipid A (endotoxin) component of lipopolysaccharide (LPS) outer membrane layer, in modulating the bacterial susceptibility to host antimicrobials such as cationic antimicrobial peptides, is subject to an in-depth review by Kahler et al.. The role of LPS in bacterial pathogenesis and immunological evasion has recently been the focus of increased attention and this work provides a timely summary of the knowledge of the effects of phosphoethanolamine decoration of lipid A in pathogenic *Neisseria* strains and the potential of targeting the EptA-enzyme responsible for therapeutic purposes.

Another way bacteria protect themselves against external agents is by altering the peptidoglycan (PG) cell wall and a well-known example is replacing the D-Ala moiety of PG to D-lactate to confer vancomycin resistance in enterococci. In their review article, Yadav et al. explain how various chemical modifications to PG help defend bacteria against host-generated antimicrobials, such as lysozyme and other hydrolytic enzymes, as well as antibiotics. Such knowledge can help guide new therapeutic approaches that weaken the bacterial cell wall and increase susceptibility to existing antibiotics.

## RIBOSOME-TARGETING ANTIBIOTICS AND RESISTANCE MECHANISMS

Ribosomes are the essential RNA-protein complexes responsible for protein synthesis in all cells. However, unique aspects of the bacterial ribosome allow for specific antibiotics that interfere with every aspect of ribosome function. These chemically diverse drugs have been a major component of our clinical arsenal for many decades and three articles here focus on their action and associated resistance mechanisms.

Polikanov et al. provide a detailed review of ribosome-targeting peptide antibiotics, with specific emphasis on each drug's interaction with either the small (30S) or large (50S) ribosome subunit and mechanism of action. Accumulating information on these antibiotics, including high-resolution ribosome-drug structures, offers opportunities to develop improved, next generation antibiotics with enhanced activity and, through modification of regions dispensable for ribosome inactivation, improvements in other properties such as uptake/retention or reduced toxicity.

Markley and Wencewicz describe the known mechanisms of resistance to tetracyclines, drugs that have been in clinical use for over 60 years. Resistance via efflux, ribosome modification, and the action of ribosome protection proteins are well-established, but their effects have been successfully countered through the design of more recent generations of tetracyclines such as tigecycline. However, these drugs are also now threatened by the emergence of the tetracycline-inactivating enzymes, which are the main focus of this review. Similarly, Golkar et al. describe the chemical structures, mechanisms of action, and resistance for a second major class of drugs, the macrolides, which bind in the peptide exit tunnel. Like tetracyclines, macrolides are subject to resistance via efflux, ribosome modification or mutation, and protection proteins. Additionally, their efficacy is also threatened by macrolide modifying phosphotransferase and esterase enzymes, the structures, and activities of which are the major focus of this comprehensive review.

## SULFONAMIDES AND $\beta$ -LACTAMASES: RESISTANCE AND FRONTIERS IN DRUG DEVELOPMENT

Sulfa drugs (sulfonamides) were first introduced in the 1930s and have a long history of efficacy against bacterial disease. These drugs inhibit bacterial dihydropteroate synthase (DHPS)

by mimicking one of its substrates, *para*-aminobenzoic acid (PABA). Mutations in DHPS cause resistance to sulfonamides but their mechanism is often unknown. Griffith et al. identify five mutations of DHPS associated with sulfonamide resistance in *Staphylococcus aureus* and investigate their impacts on strain susceptibility and fitness, and enzyme kinetics. Three of the mutations contribute to resistance by sterically blocking the outer ring moiety of sulfonamides, whereas the other two increase fitness of the strain. The work reveals a critical weakness of sulfonamides with implications for drug design: resistance mutations target the part of the antimicrobial that is most important for its efficacy.

Discussion of antimicrobial resistance would not be complete without mention of  $\beta$ -lactamases, a common mechanism of resistance in bacteria, including the ESKAPE pathogens. These enzymes hydrolyze  $\beta$ -lactam antibiotics before they reach their molecular targets, the so-called penicillin-binding proteins. In his review, Palzkill explains the molecular basis for the differing specificities of three important groups of Class A  $\beta$ -lactamases (the TEM, CTX-M, and KPC enzymes) for oxyaminocephalosporins. He highlights mutations that increase the conformational heterogeneity within the active sites of these enzymes to accommodate cephalosporins and the existence of global suppressor mutations elsewhere in the protein to

compensate for loss of stability. Finally, in their review, van den Akker and Bonomo describe extensive efforts by a number of groups to develop  $\beta$ -lactamase inhibitors, including five approved for clinical use. They emphasize the success of strategies that exploit specific aspects of enzyme mechanism in the design of these critical antimicrobial agents.

## AUTHOR CONTRIBUTIONS

All authors listed have made a substantial, direct and intellectual contribution to the work, and approved it for publication.

## FUNDING

Related research in the authors' labs is supported by the National Institutes of Health grants R01-GM066861 (to CD) and R01-AI088025 (to GC), and BBSRC grant BB/N002776/1 and Wellcome Trust grant 108372/A/15/Z (to VB).

## ACKNOWLEDGMENTS

We wish to convey our appreciation to all the authors who participated in this Research Topic, as well as the many reviewers for their insightful comments.

## REFERENCES

Vargiu, A. V., Pos, K. M., Poole, K., and Nikaido, H. (2016). Editorial: bad bugs in the XXIst century: resistance mediated by multi-drug efflux pumps in gram-negative bacteria. *Front. Microbiol.* 7:833. doi: 10.3389/fmicb.2016.00833

**Conflict of Interest Statement:** The authors declare that the research was conducted in the absence of any commercial or financial relationships that could be construed as a potential conflict of interest.

Copyright © 2019 Conn, Bavro and Davies. This is an open-access article distributed under the terms of the Creative Commons Attribution License (CC BY). The use, distribution or reproduction in other forums is permitted, provided the original author(s) and the copyright owner(s) are credited and that the original publication in this journal is cited, in accordance with accepted academic practice. No use, distribution or reproduction is permitted which does not comply with these terms.





# Hoisting-Loop in Bacterial Multidrug Exporter AcrB Is a Highly Flexible Hinge That Enables the Large Motion of the Subdomains

Martijn Zwama<sup>1,2,3</sup>, Katsuhiko Hayashi<sup>1,2</sup>, Keisuke Sakurai<sup>1</sup>, Ryosuke Nakashima<sup>1</sup>, Kimie Kitagawa<sup>1</sup>, Kunihiro Nishino<sup>2\*</sup> and Akihito Yamaguchi<sup>1\*</sup>

<sup>1</sup> Department of Cell Membrane Structural Biology, Institute of Scientific and Industrial Research, Osaka University, Osaka, Japan, <sup>2</sup> Department of Biomolecular Science and Regulation, Institute of Scientific and Industrial Research, Osaka University, Osaka, Japan, <sup>3</sup> Graduate School of Pharmaceutical Sciences, Osaka University, Osaka, Japan

## OPEN ACCESS

### Edited by:

Vassily Bavo,  
University of Essex, United Kingdom

### Reviewed by:

Klaas Martinus Pos,  
Goethe University Frankfurt, Germany  
Jessica M. A. Blair,  
University of Birmingham,  
United Kingdom  
Attilio Vittorio Vargiu,  
Università degli studi di Cagliari, Italy

### \*Correspondence:

Kunihiro Nishino  
nishino@sanken.osaka-u.ac.jp  
Akihito Yamaguchi  
akihito@sanken.osaka-u.ac.jp

### Specialty section:

This article was submitted to  
Antimicrobials, Resistance and  
Chemotherapy,  
a section of the journal  
Frontiers in Microbiology

**Received:** 21 August 2017

**Accepted:** 12 October 2017

**Published:** 25 October 2017

### Citation:

Zwama M, Hayashi K, Sakurai K,  
Nakashima R, Kitagawa K, Nishino K  
and Yamaguchi A (2017)  
Hoisting-Loop in Bacterial Multidrug  
Exporter AcrB Is a Highly Flexible  
Hinge That Enables the Large Motion  
of the Subdomains.  
Front. Microbiol. 8:2095.  
doi: 10.3389/fmicb.2017.02095

The overexpression of RND-type exporters is one of the main causes of multidrug resistance (MDR) in Gram-negative pathogens. In RND transporters, such as *Escherichia coli*'s main efflux pump AcrB, drug efflux occurs in the porter domain, while protons flow through the transmembrane domain: remote conformational coupling. At the border of a transmembrane helix (TM8) and subdomain PC2, there is a loop which makes a hoisting movement by a random-coil-to- $\alpha$ -helix change, and opens and closes a drug channel entrance. This loop is supposed to play a key role in the allosteric conformational coupling between the transmembrane and porter domain. Here we show the results of a series of flexibility loop-mutants of AcrB. We determined the crystal structure of a three amino acid truncated loop mutant, which is still a functional transporter, and show that the short  $\alpha$ -helix between C $\beta$ 15 and the loop unwinds to a random coil in the access and binding monomers and in the extrusion monomer it makes a partially stretched coil-to-helix change. The loop has undergone compensatory conformational changes and still facilitates the opening and closing of the channel. In addition, more flexible mutated loops (proline mutated and significantly elongated) can still function during export. The flexibility in this region is however limited, as an even more truncated mutant (six amino acid deletion) becomes mostly inactive. We found that the hoisting-loop is a highly flexible hinge that enables the conformational energy transmission passively.

**Keywords:** multidrug resistance, antimicrobial resistance, RND, AcrB, mechanism, pathogens, transporters, crystal structure

## INTRODUCTION

Multidrug resistance (MDR) is a serious problem in global health we face today (World Health Organization, 2014). Antimicrobial resistance in gram-negative bacterial pathogens is one of the main challenges (Poole, 2004; Li et al., 2015). The overexpression of tripartite efflux systems is a major cause of MDR in these gram-negative pathogens (Poole et al., 1993; Nikaido, 1998; Blair et al., 2014). These complexes can facilitate efflux directly across the outer membrane as they consist of a Resistance-Nodulation-Division (RND) efflux pump and an outer membrane protein, bridged together by an adapter protein (Zgurskaya and Nikaido, 2000; Lomovskaya and Totrov, 2005). In

*Escherichia coli*, the main RND transporter is AcrB, part of the AcrAB-TolC complex (Nishino and Yamaguchi, 2001). This secondary efflux pump facilitates efflux by using the electrochemical proton gradient (Zgurskaya and Nikaido, 1999) and besides being the main cause of MDR when overexpressed, its physiological function in bacterial cells is to export naturally occurring toxic compounds, such as bile salts (Thanassi et al., 1997; Nishino et al., 2009). RND transporters also play a major role in virulence and in MDR in other organisms, such as the MexAB-OprM efflux system in *Pseudomonas aeruginosa*. Overexpression of RND transporters cause MDR as they recognize and transport a wide range of structurally unrelated compounds, ranging from dyes to antibiotics and from small compounds to large compounds (Nikaido and Pagès, 2012). The physiologically active form of AcrB is a homotrimer consisting of three protomers, each representing one step in the drug-extrusion cycle. This functionally rotating mechanism is shown by each of the three monomers in the asymmetrical crystal structure of AcrB: access, binding and extrusion (Murakami et al., 2006; Seeger et al., 2006). During this cycle, conformational changes take place in both the transmembrane (TM) and the porter region, which are about 50 Å apart. These regions therefore have to be energy-coupled with each other in a remote conformational way.

In the transmembrane domain, several helix bundles and amino acids change their conformation upon protonation and deprotonation of crucial amino acids and the interaction with the conformational changes in the porter domain of AcrB. In the binding monomer, Asp407 is exposed to the periplasm by a water-void and a proton can bind. Now the transition to the extrusion state can occur. During this transition from the binding to the extrusion state, six N-terminal TM-helices (TM1-TM6) and six C-terminal TM-helices (TM7-TM12) are twisted relatively to each other as a result of the ion-pair breakage between Asp407, Asp408 and Lys940. During this transition to the extrusion monomer, residue Arg971 extends and bends downwards to TM10 and the phenyl-ring of Phe948 is tilted downwards and Met970 bent away. In this way, Arg971 is exposed to a water-void open to the cytoplasm and can release a proton. Now, in the extrusion monomer, the loop at the N-terminal end of TM8 performed a hoisting-like motion by its conformational change from a random coil to an  $\alpha$ -helix (to make an extended TM8), presumably playing a key role in conformational transmission and facilitating the motion of PN1/PC2 during the transition to the extrusion monomer (Eicher et al., 2012; Yamaguchi et al., 2015).

At the interface of the transmembrane and porter domain, this most significant conformational change during this extrusion cycle occurs at the region between the  $\beta$ -strand (C $\beta$ 15) of the PC2 subdomain and TM8 (Figure 1). This segment comprises 13 amino acid residues (<sup>860</sup>TGMSYQERLSGNQ<sup>872</sup>). In the extrusion monomer, this segment forms three turns of the  $\alpha$ -helix which extends the top of TM8. On the other hand, in the access and binding monomer, a part of this helix (<sup>868</sup>LSGNQ<sup>872</sup>) unwinds to a random coil, enabling the upward swinging motion of PC2 by extending the distance from TM8 to C $\beta$ 5. This random-coil-to- $\alpha$ -helix change also opens and closes the

membrane surface channel (CH1) during the drug extrusion cycle (Murakami et al., 2006; Figure 1B). Considering the location of the loop and the significant conformational change during the export cycle, the loop is assumed to be implicated in the mechanism of the energy transduction in AcrB (Murakami et al., 2006; Su et al., 2006; Sennhauser et al., 2007; Seeger et al., 2008; Pos, 2009; Eicher et al., 2012, 2014; Long et al., 2012; Yamane et al., 2013; Yu et al., 2013; Du et al., 2015; Yamaguchi et al., 2015). We created a series of loop-flexibility mutants of AcrB, ranging from low flexibility (truncated mutants) to high flexibility [proline (which break the helix) and significantly elongated (flexible gly/ser linkers) mutants] and checked the export activity of all of these mutants. Additionally, we solved the crystal structure of a truncated mutant at 3.0 Å to elucidate the role of this segment of AcrB and to better understand the remote conformation coupling mechanism of RND multidrug exporters.

## MATERIALS AND METHODS

### Bacterial Strains and Growth Conditions

The *E. coli* MG1655 strain (Blattner et al., 1997) was used as the wild-type strain in this study. The  $\Delta$ acrB (NKE96) (Nishino et al., 2008) and  $\Delta$ tolC (NKE95) (Horiyama and Nishino, 2014) deleted mutants were derived from MG1655. Gene deletion was performed according to the method of Datsenko and Wanner, with recombination between short homologous DNA regions catalyzed by phage  $\lambda$  Red recombinase (Datsenko and Wanner, 2000). The drug resistance markers were eliminated using plasmid pCP20, as previously described (Datsenko and Wanner, 2000). The Bacterial strains were grown at 37°C in Luria-Bertani broth (Sambrook et al., 1989).

### Drug Susceptibility by MIC

The minimal inhibitory concentrations (MIC) for wild-type and mutant AcrB were determined using LB-agar plates supplemented with substrates. The substrates were added in a series of dilutions. Agar plates were stamped with the desired strains and grown at 37°C overnight. The MIC values are the concentration of drugs in the agar plates at which no cells were viable anymore. For growth curves, cells were grown from diluted exponentially growing cells in 96-well plates for 8 h at 37°C. OD<sub>600 nm</sub> readings were performed by using the Infinite M200 Pro (Tecan).

### Drug Exclusion Assay

For ethidium bromide exclusion efflux determination, BL21 $\Delta$ acrB *E. coli* cells were used. Overnight cultures of the *E. coli* cells were diluted and grown at 37°C until OD<sub>600 nm</sub> 0.5–0.6 was reached. Cells were harvested and washed twice with Efflux Buffer (100 mM potassium phosphate (pH 7.5) and 5 mM MgSO<sub>4</sub>) and diluted to final OD<sub>600 nm</sub> of 18. 10  $\mu$ M of ethidium bromide and 10 mM arabinose was added. Ethidium bromide fluorescence was measured by SH-8100 reader (Corona Electric Co.) using  $\lambda_{ex}$  = 530 nm and  $\lambda_{em}$  = 600 nm. Exclusion assays were repeated at least four times providing the error envelopes.

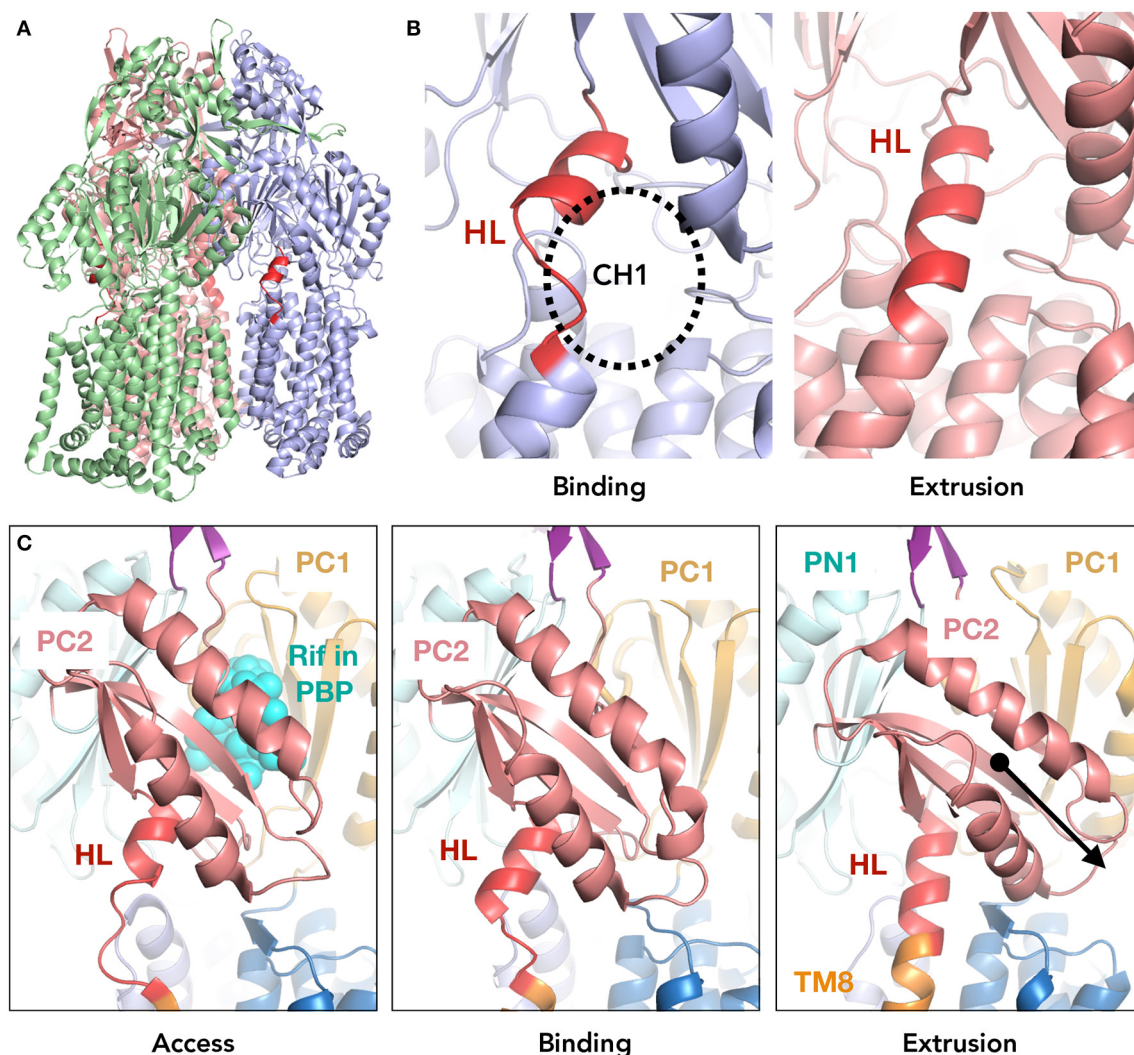


**FIGURE 1 |** The location of the hoisting-loop in the AcrB drug transporter. **(A)** A side view of the AcrB trimer. Each protomer representing one step in the drug extrusion cycle is depicted in green, blue and light red for access, binding and extrusion, respectively. The hoisting-loop is shown in dark red. **(B)** A close-up view of the hoisting-loop in the binding and extrusion monomers. Dark red indicated the residues <sup>860</sup>TGMSYQERLSGNQ<sup>872</sup>. The open and closed channel 1 (CH1) can be seen. **(C)** A close-up of the hoisting-loop region including TM8 and PC2 for the access, binding and extrusion monomers of AcrB. In the extrusion monomer, the PC2 domain (light red) is shifted downwards significantly along with the elongation of TM8 (altering the hoisting-loop from a random coil to an  $\alpha$ -helix). Abbreviations: TM8, transmembrane 8; HL, hoisting-loop; CH1, channel 1; Rif, rifampicin; PBP, proximal binding pocket.

## Protein Expression and Crystallization

C-terminally His6-tagged mutant AcrB (hoisting-loop truncated mutant) were expressed in JM109 $\Delta$ *acrB* *E. coli* cells harboring the pAcBH plasmid. The final mutant AcrB buffer condition was 20 mM sodium phosphate pH6.2, 10% (v/v) glycerol, 0.05% (w/v) n-Dodecyl- $\beta$ -D-maltoside and the final protein concentration was 20 mg/ml. Crystals of AcrB variants were made by the hanging drop vapor diffusion method at 25°C. The protein solution was mixed with an equal volume of reservoir solution. The reservoir solution contained 100 mM SPG (succinic acid, sodium phosphate monobasic monohydrate and glycine) buffer at pH5.0 and 20% (w/v) PEG1500.

## Crystallographic Analysis

X-ray diffraction data were collected at 100 K on beamline BL44XU at SPring-8 (Hyogo, Japan). X-ray data set was indexed, integrated and scaled using *iMosflm* (Battye et al., 2011) and *Scala* (Evans, 2006) from *CCP4* program suite (Lebedev et al., 2012). The initial structure was solved by molecular replacement using *MOLREP* (Vagin and Teplyakov, 2000) with wild-type AcrB (3AOA with manual truncation of hoisting-loop) as a search model. The model refinement was performed through multiple cycles of manual rebuilding using the program *COOT* (Emsley et al., 2010) and refinement using *REFMAC5* (Murshudov et al., 2011) with jelly-body option.



## RESULTS

### Truncated Hoisting-Loop

To check the role of the hoisting-loop segment, <sup>860</sup>TGMSYQERLSGNQ<sup>872</sup> located at the N-terminal end of TM8 (Figure 1), we created a shortened (truncated) hoisting-loop mutant by deleting the three amino acids Leu868, Asn871 and Gln872 (one turn of the  $\alpha$ -helix, Figure 4). We tested the efflux ability of the mutated pump by determining the growth ability of AcrB-expressing *E. coli* cells (both wild-type and mutant) in the presence of various structurally unrelated compounds: minocycline, erythromycin, ethidium bromide, cloxacillin, acriflavine, benzalkonium, crystal violet and rhodamine 6G. We also tested the truncated mutant on ethidium bromide exclusion ability in *E. coli* cells, compared to wild-type AcrB expressing and *acrB*-knockout cells. When ethidium enters the cell, it binds to DNA and becomes fluorescent. Active AcrB transporters export ethidium out of the cell from the periplasm or outer leaflet of the inner membrane before it enters the cytoplasm and the fluorescence is kept significantly low, hence *acrB*-knockout cells give a high fluorescent signal. The mutant was expressed equally to wild-type AcrB (Supplementary Figure 1). Figure 2A shows the growth curves panels for a selected concentration of the compounds (all concentrations can be seen in Supplementary Figure 2) and Figure 2B shows the ethidium bromide accumulation in wild-type and mutant AcrB. We found that the truncated mutant is a transporter which retains its exclusion ability for all tested compounds. The growth curves showing the vitality of the cells are in some concentrations (especially higher ones) just slightly lower than for wild-type AcrB (Supplementary Figure 2), but the mutant basically retains complete efflux efficiency compared to wild-type AcrB. The ethidium bromide exclusion assay also indicates that the truncated mutant is a functional transporter, able to pump ethidium out of the periplasm, with a fluorescent signal very close to wild-type AcrB. The deletion of three amino acids in this hoisting-loop segment of AcrB seems to have no effect on the function of the transporter.

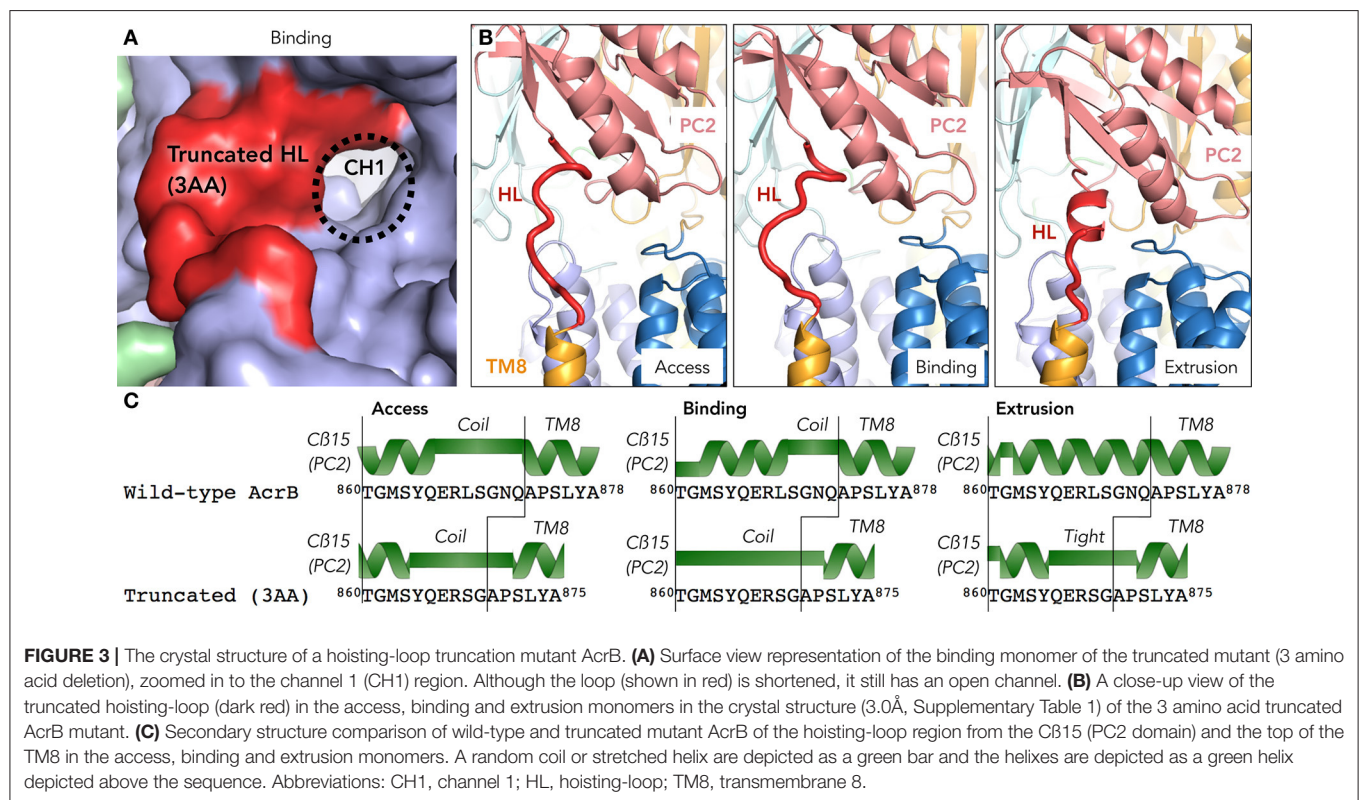
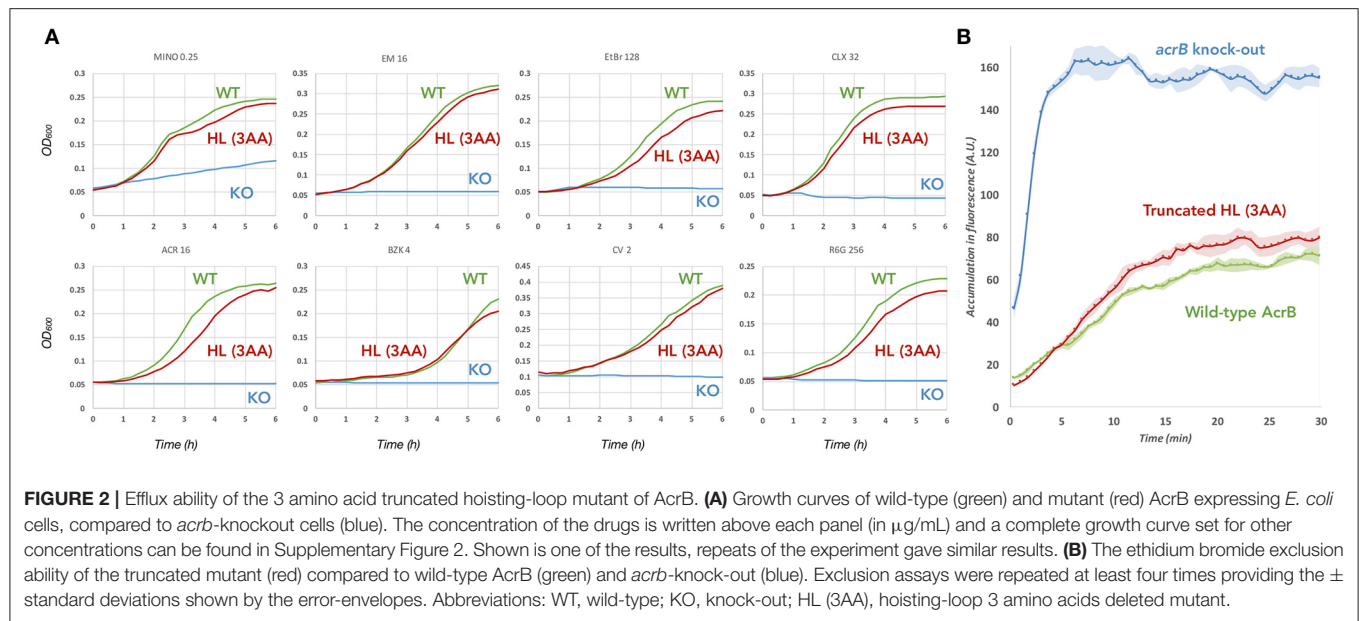
### Crystal Structure of the Hoisting-Loop Truncation Mutant AcrB

As the truncated mutant was a functional transporter, it raised the question how a loop-deletion mutant AcrB can still make the required conformational changes for the drug extrusion cycle. We were also speculating if the entrance of the surface channel CH1 was open or closed and thus whether or not the truncated loop would still be able to have a gating function for CH1. In order to address these questions, we solved the crystal structure of the hoisting-loop-truncated mutant AcrB at 3.0 Å. The crystal was formed by hanging drop vapor diffusion at 25°C at reservoir pH 5.0 (see section Materials and Methods). In general, the structure is almost identical to wild-type AcrB (RMSD 0.70, 0.67 and 0.78 Å for access, binding and extrusion monomers, respectively). Surprisingly, the structure shows that the entrance of CH1 to the proximal binding pocket is still completely open in the access and binding monomers (Figure 3A), similar to wild-type AcrB (Figure 3). The shortened loop flexibly retains the

same length between C $\beta$ 5 and TM8 as in wild-type during the export cycle by unwinding a part of the  $\alpha$ -helix (Figure 3C). Now, the random coil region is <sup>864</sup>YQERSGAP<sup>871</sup> in the access and binding monomers of the truncated mutant. Although the channel is completely open in the binding monomer, in the extrusion monomer, we found that the loop was tightened and stretched compared to wild-type AcrB. In contrast to wild-type AcrB, the loop was not an  $\alpha$ -helix extending the top of TM8, but a stretched coil from the top of TM8 to the bottom of PC2 (Figures 3B,C). As seen in Figure 3C (which compares the secondary structure of wild-type and truncated AcrB), the top region of the TM8 helix became a coil rather than a helix in all monomers, indicating a shift: the random coil became slightly longer in the access and binding monomer and became a tight stretch in the extrusion monomer. The rest of the protein domains were unchanged compared to wild-type AcrB, indicating that the truncated loop was still able to act as a gate for CH1, facilitating efflux for certain compounds by opening the channel completely (Figure 3A), although the truncation of the loop did cause a significant tightening of the loop (Figure 3B). It also shows that this significantly moving region of AcrB is very flexible and that the deletion of three residues (about one turn of the  $\alpha$ -helix) does not limit the ability of movement of the porter-region sub-domains, nor the energy transduction from the TM-domain to the porter-domain. A full comparison of the wild-type and truncated (3AA deletion) AcrB movement throughout the drug extrusion cycle can be seen in Supplementary Videos 1, 2 (cartoon and surface representation, respectively).

### Flexibility of the Hoisting-Loop Segment

The previous results indicate that a truncated mutant of AcrB is an active transporter and the protein adapts to a slightly different structural arrangement by undergoing compensatory conformational changes while maintaining full efflux ability. Now, we wanted to test the flexibility of this region more extensively. We created several more flexible and less flexible hoisting-loop mutants. First, we replaced the amino acid residues at both ends of this loop by proline residues (L868P and Q872P), as depicted in Figure 4. The proline mutations break the helix-formation and, as a result, the random coil structure would be fixed in the extrusion state. We created single and double mutants of these residue mutations. Furthermore, we created even more flexible mutants, by the introduction of repeats of GGS-residues: elongated mutant AcrB. The three elongated mutations were <sup>868</sup>LSGGSGNQ, <sup>868</sup>LSGGSGGSGNQ, and <sup>868</sup>LSGGSGGSGGSGNQ (Figure 4). In addition, we constructed a hoisting-loop 6 amino acid truncated mutant, 3 amino acids more than the truncated mutant discussed previously, by deleting the six residues <sup>863</sup>SYQERL<sup>868</sup> from the loop (Figure 4). We tested all mutants (including the previously discussed truncated mutant) on efflux activity by determining the agar plate Minimal Inhibitory Concentration (MIC) values for nine compounds, which are shown in Table 1. We found that all proline mutants and the hoisting-loop (3AA deleted)-truncated mutant were fully functional. Also, the very flexible significantly elongated mutants with GGS-repeats were completely active. Even the 9AA elongated mutant



is an active transporter, showing that the loop does not play an active role in the energy transduction. However, when the flexibility of the hoisting-loop was decreased too much (the 6AA deleted hoisting-loop mutant), the protein become mostly (but not entirely) inactive for all tested compounds. This shows that the flexibility of this region is a very important factor for the activity of the transporter. There

is a limit in shortening the length of the hoisting-loop of about one turn of the helix (as discussed previously, see **Figures 2, 3**) and removing about two turns makes the efflux of compounds out of the cell very inefficient, probably by limiting the required movement of the PC2 domain. All mutants were expressed equally to wild-type AcrB (Supplementary Figure 1).

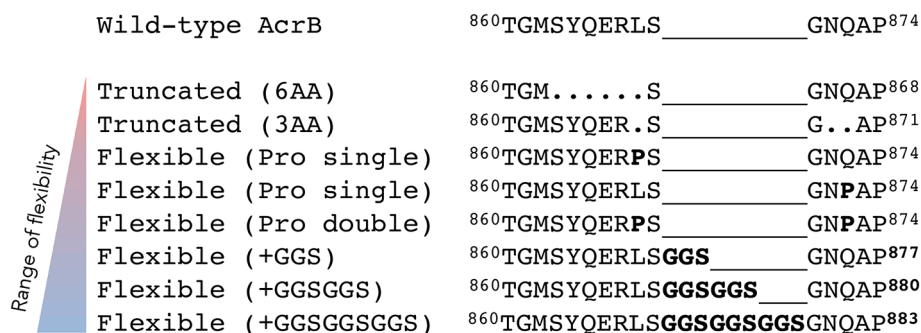


**FIGURE 4 |** The range of flexibility of the hoisting-loop mutants. Sequence alignment of wild-type and hoisting-loop mutants of AcrB (here written as <sup>860</sup>TGMSYQERLSGNQAP<sup>874</sup>). The triangle on the left indicates the degree of flexibility from low (red) to high (blue). “Truncated (6AA)” is the 6 amino acid deletion-mutant and “Truncated (3AA)” is the 3 amino acid deletion-mutant. Each “Pro Single” is either mutation L868P or Q872P, and “Pro Double” represents both mutations. The flexible elongated mutations are shown as “Flexible (+GGS),” “Flexible (+GGSGGS),” and “Flexible (+GGSGSGGS).” A dot shows a deletion mutation and a line simply represents the relative difference compared to the most elongated flexible mutant in order to align all mutants.

**TABLE 1 |** Minimal Inhibitory Concentration (MIC) values for several structurally unrelated drugs.

Strain	Flexibility	Minimal Inhibitory Concentration (MIC, $\mu$ g/mL)								
		CLX	BZK	EtBr	CV	NB	R6G	MINO	ACR	EM
$\Delta$ tolC		0.25	4	8	2	2	32	0.5	8	2
acrB-KO		2	4	16	2	16	32	0.5	16	4
Wild-type AcrB		256	512	1,024	16	1,024	8,192	>2	1,024	128
Truncated (6 amino acids)	Lowest	16	32	256	8	128	256	0.5	32	32
Truncated (3 amino acids)		256	128	1,024	16	1,024	8,192	>2	1,024	128
Pro single (L868P)		256	128	1,024	16	1,024	8,192	>2	512	128
Pro single (Q872P)		256	256	1,024	16	1,024	8,192	>2	1,024	128
Pro double (L868P+Q872P)		256	512	1,024	16	1,024	8,192	>2	1,024	128
Elongated (+GGS)		512	512	>1,024	16	1,024	>8,192	>2	1,024	128
Elongated (+GGSGGS)		256	512	1,024	16	1,024	8,192	>2	1,024	128
Elongated (+GGSGSGGS)	Highest	512	512	1,024	16	1,024	8,192	>2	1,024	128

MIC concentrations were determined by step-wise dilutions gradients of the compounds in agar plates and the growth ability of MG1655  $\Delta$ acrB *E. coli* cells (expressing the proteins from the plasmid) was determined. Values are in  $\mu$ g/mL. The colors indicate the degree of flexibility from low (red) to high (blue). Abbreviations: CLX, cloxacillin; BZK, benzalkonium; EtBr, ethidium bromide; CV, crystal violet; NB, novobiocin; R6G, rhodamine 6G; MINO, minocycline; ACR, acriflavine; EM, erythromycin.

## DISCUSSION

We show that the hoisting-loop is a highly flexible hinge that enables the large conformational changes of the subdomains of AcrB. Helix-breaking proline mutants, elongated loop mutants and truncated mutants show that this loop is extremely flexible. These protein mutants are still able to execute the required drug extrusion cycle (Table 1). The results of the truncated mutant indicate that the loop's conformational changes are a result of the movement of the protein during its extrusion process, and its flexibility enables these significant conformational changes in the AcrB drug transporter. The flexibility is indeed important for the protein function, as the 6 amino acid truncated mutant becomes mostly inactive (Table 1).

Crystal structures of AcrB TM-mutants by Eicher et al. (2012) support the hypothesis that there is a relationship between the TM-region and porter domain and between the conformational changes within the TM-domain and the configuration of certain

amino acids within the proton relay pathway (Guan and Nakae, 2001; Su et al., 2006; Takatsuka and Nikaido, 2006; Eicher et al., 2014). In the access and binding monomers, Asp407, Asp408 (both TM4) and Lys940 (TM10) form ion pairs. In the extrusion monomer, the Lys940 is tilted about 45° and the ion pairs are broken. In addition, residue Arg971 (TM11) changes its conformation significantly in the extrusion monomer compared to the other monomers (Murakami et al., 2006; Seeger et al., 2006; Sennhauser et al., 2007; Yamaguchi et al., 2015). In the binding monomer, Arg971 is separated from the cytoplasm by the residues Phe948, Met970 and Gln437, but open to the periplasm by a water channel (a center void). On the other hand, in the extrusion monomer, Arg971 is extended and exposed to a water channel connected to the cytoplasm, where it can supposedly release a proton to the interior of the cell. It is postulated that after the release of the proton from Arg971 to the cytoplasm, the residue takes a new proton from Asp408 and as a consequence, protonated Lys940 can restore its ion bond with Asp408, to



form the access monomer. From this point, the proton of Lys940 is able to translocate to the deprotonated Asp408 and the proton from Asp407 can subsequently bind to Lys940, to form the binding monomer (Fischer and Kandt, 2011; Yamaguchi et al., 2015). Although the movements of the different regions and subdomains (such as TM2, TM8, 1 $\alpha$ , the two TM-helix repeats, PN1/PC2 and PN2/PC2 and amino acids such as Lys940 and Arg971), as well as the protonation and deprotonation in the different stages of transport is well defined (Eicher et al., 2014) and possible mechanisms hypothesized (Eicher et al., 2014; Yamaguchi et al., 2015), it remains unclear how exactly the conformational coupling across the transmembrane and the porter domains occurs.

We found that the flexible hinge of the hoisting-loop helps facilitating the radical movements of the subdomains passively, as the elongated loop mutants (even the 9AA elongated mutant) exhibit the same phenotype as wild-type AcrB. As there are no other significant conformational changes in loops and regions linking the TM- and porter-domains directly during the drug extrusion cycle (e.g., similar to the hoisting-loop discussed in this study), another hypothesis needs to explain remote energy coupling mechanism of RND transporters. Computer simulations may shed a light on the complex mechanism of the exporter. Energy transduction might be due to the subtle changes in the TM-domain, explained by packing efficiency through the solvent-entropy effect translated to the porter domain, described by thermodynamics by computer simulations (Mishima et al., 2015) rather than a direct allosteric energy coupling. The structure of the AcrB trimer has often been compared to the  $\alpha\beta$ -subunits of bovine F<sub>1</sub>-ATPase, which also comprises similar functional access, binding and extrusion states by its monomers. Perhaps similar to F<sub>1</sub>-ATPase (Abrahams et al., 1994), the most stable conformation is disturbed (in this case by the binding of ATP instead of a proton) and the adjacent subunits react accordingly to these changes (compensating for energy loss) (Ito and Ikeguchi, 2015). This may be compared to the trimer reorganization of both the TM- and the porter-domain (the functionally rotating mechanism) and the interaction of the monomers with each other within the homotrimer (the entropy loss in one monomer due to the conformational changes during the export cycle is balanced by the entropy-gain of the other two monomers), facilitated by the necessary compensation of the protonation and deprotonation of AcrB (the proton-motive-force is necessary to energize the energy-unfavorable transitions during the export cycle) (Mishima et al., 2015). Although computer simulations can show the thermodynamic properties of the transporter during transport, they have their limitations

and more biochemical and biophysical studies need to be done in order to elucidate the remote energy coupling mechanism of RND transporters. From our study, it is clear that the hoisting-loop region of AcrB plays an important role as facilitator between the transmembrane and porter domains, acting as a flexible hinge.

In summary, we show that the hoisting-loop is extremely flexible and necessary. Even a truncated loop mutant is able to have a functional gating mechanism with an open CH1 channel, although additional truncation significantly inhibits the function of the exporter. Fully active elongated mutants show us that this region of AcrB is extremely flexible and that an increase of flexibility does not inhibit the energy transduction nor the function of the protein. The flexible loop can facilitate the significant changes in the porter subdomains PC1 and PC2. Our knowledge and understanding of RND transporters is crucial for the development of new antibiotic therapeutics.

## AUTHOR CONTRIBUTIONS

MZ and KH performed the molecular biological and biochemical experiments. KK, MZ, KH, RN, and KS performed the protein crystallization and structure analysis. KH and MZ designed the research. MZ, KN, and AY wrote the manuscript. The coordinates for the hoisting-loop mutant of AcrB have been deposited in the Protein Data Bank under accession number 5YIL.

## ACKNOWLEDGMENTS

This work was supported by CREST and the Center of Innovation Program (COI) from the Japan Science and Technology Agency (JST), the Program for the Promotion of Fundamental Studies in Health Sciences of the National Institute of Biomedical Innovation, Grants-in-Aid, Network Joint Research Center for Materials and Devices, and Dynamic Alliance for Open Innovation Bridging Human, Environment and Materials from the Ministry of Education, Culture, Sports, Science and Technology of Japan (MEXT), Grant-in-Aid for Scientific Research (B) (Kakenhi 17H03983) from Japan Society for the Promotion of Science (JSPS), and Japan Agency for Medical Research and Development (AMED).

## SUPPLEMENTARY MATERIAL

The Supplementary Material for this article can be found online at: <https://www.frontiersin.org/articles/10.3389/fmicb.2017.02095/full#supplementary-material>

## REFERENCES

- Abrahams, J. P., Leslie, A. G., Lutter, R., and Walker, J. E. (1994). Structure at 2.8 Å resolution of F<sub>1</sub>-ATPase from bovine heart mitochondria. *Nature* 370, 621–628. doi: 10.1038/370621a0
- Battye, T. G., Kontogiannis, L., Johnson, O., Powell, H. R., and Leslie, A. G. (2011). iMOSFLM: a new graphical interface for diffraction-image processing with MOSFLM. *Acta. Cryst. D* 67, 271–281. doi: 10.1107/S0907444910048675
- Blair, J. M. A., Richmond, G. E., and Piddock, L. J. V. (2014). Multidrug efflux pumps in Gram-negative bacteria and their role in antibiotic resistance. *Future Microbiol.* 9, 1165–1177. doi: 10.2217/fmb.14.66
- Blattner, F. R., Plunkett, G., Bloch, C. A., Perna, N. T., Burland, V., Riley, M., et al. (1997). The complete genome sequence of *Escherichia coli* K-12. *Science* 277, 1453–1462. doi: 10.1126/science.277.5331.1453
- Datsenko, K. A., and Wanner, B. L. (2000). One-step inactivation of chromosomal genes in *Escherichia coli* K-12 using PCR products.

- Proc. Natl. Acad. Sci. U.S.A. 97, 6640–6645. doi: 10.1073/pnas.120163297
- Du, D., van Veen, H. W., Murakami, S., Pos, K. M., and Luisi B. F. (2015). Structure, mechanism and cooperation of bacterial multidrug transporters. *Curr. Opin. Struct. Biol.* 33, 76–91. doi: 10.1016/j.sbi.2015.07.015
- Eicher, T., Cha, H., Seeger, M. A., Brandstätter, L., El-Delik, J., Bohnert, J. A., et al. (2012). Transport of drugs by the multidrug transporter AcrB involves an access and a deep binding pocket that are separated by a switch-loop. *Proc. Natl. Acad. Sci. U.S.A.* 109, 5687–5692. doi: 10.1073/pnas.1114944109
- Eicher, T., Seeger, M. A., Anselmi, C., Zhou, W., Brandstätter, L., Verrey, F., et al. (2014). Coupling of remote alternating-access transport mechanisms for protons and substrates in the multidrug efflux pump AcrB. *eLife* 3:e03145. doi: 10.7554/eLife.03145
- Emsley, P., Lohkamp, B., Scott, W. G., and Cowtan, K. (2010). Features and development of Coot. *Acta. Cryst. D* 66, 486–501. doi: 10.1107/S0907444910007493
- Evans, P. (2006). Scaling and assessment of data quality. *Acta. Cryst. D* 62, 72–82. doi: 10.1107/S0907444905036693
- Fischer, N., and Kandt, C. (2011). Three ways in, one way out: water dynamics in the transmembrane domains of the inner membrane translocase AcrB. *Proteins* 79, 2871–2885. doi: 10.1002/prot.23122
- Guan, L., and Nakae, T. (2001). Identification of essential charged residues in transmembrane segments of the multidrug transporter MexB of *Pseudomonas aeruginosa*. *J. Bacteriol.* 183, 1734–1739. doi: 10.1128/JB.183.5.1734-1739.2001
- Horiyama, T., and Nishino, K. (2014). AcrB, AcrD, and MdtABC multidrug efflux systems are involved in enterobactin export in *Escherichia coli*. *PLoS ONE* 9:e108642. doi: 10.1371/journal.pone.0108642
- Ito, Y., and Ikeguchi, M. (2015). Mechanism of the  $\alpha\beta$  conformational change in F1-ATPase after ATP hydrolysis: free-energy simulations. *Biophys. J.* 108, 85–97. doi: 10.1016/j.bpj.2014.11.1853
- Lebedev, A. A., Young, P., Isupov, M. N., Moroz, O. V., Vagin, A. A., and Murshudov, G. N. (2012). JLigand: a graphical tool for the CCP4 template-restraint library. *Acta. Cryst. D* 68, 431–440. doi: 10.1107/S090744491200251X
- Li, X. Z., Plésiat, P., and Nikaido, H. (2015). The challenge of efflux-mediated antibiotic resistance in Gram-negative bacteria. *Clin. Microbiol. Rev.* 28, 337–418. doi: 10.1128/CMR.00117-14
- Lomovskaya, O., and Totrov, M. (2005). Vacuuming the periplasm. *J. Bacteriol.* 187, 1879–1883. doi: 10.1128/JB.187.6.1879-1883.2005
- Long, F., Su, C. C., Lei, H. T., Bolla, J. R., Do, S. V., and Yu, E. W. (2012). Structure and mechanism of the tripartite CusCBA heavy-metal efflux complex. *Philos. Trans. R. Soc. Lond. B. Biol. Sci.* 367, 1047–1058. doi: 10.1098/rstb.2011.0203
- Mishima, H., Oshima, H., Yasuda, S., and Kinoshita, M. (2015). Statistical thermodynamics for functionally rotating mechanism of the multidrug efflux transporter AcrB. *J. Phys. Chem. B* 119, 3423–3433. doi: 10.1021/jp5120724
- Murakami, S., Nakashima, R., Yamashita, E., Matsumoto, T., and Yamaguchi, A. (2006). Crystal structures of a multidrug transporter reveal a functionally rotating mechanism. *Nature* 443, 173–179. doi: 10.1038/nature05076
- Murshudov, G. N., Shubák, P., Lebedev, A. A., Pannu, N. S., Steiner, R. A., Nicholis, R. A., et al. (2011). REFMAC5 for the refinement of macromolecular crystal structures. *Acta Cryst. D* 67, 355–367. doi: 10.1107/S0907444911001314
- Nikaido, H. (1998). Antibiotic resistance caused by gram-negative multidrug efflux pumps. *Clin. Infect. Dis.* 27, S32–S41. doi: 10.1086/514920
- Nikaido, H., and Pagès, J. M. (2012). Broad-specificity efflux pumps and their role in multidrug resistance of Gram-negative bacteria. *FEMS Microbiol. Rev.* 36, 340–363. doi: 10.1111/j.1574-6976.2011.00290.x
- Nishino, K., Nikaido, E., and Yamaguchi, A. (2009). Regulation and physiological function of multidrug efflux pumps in *Escherichia coli* and *Salmonella*. *Biochim. Biophys. Acta* 1794, 834–843. doi: 10.1016/j.bbapap.2009.02.002
- Nishino, K., Senda, Y., and Yamaguchi, A. (2008). The AraC-family regulator GadX enhances multidrug resistance in *Escherichia coli* by activating expression of *mdtEF* multidrug efflux genes. *J. Infect. Chemother.* 14, 23–29. doi: 10.1007/s10156-007-0575-Y
- Nishino, K., and Yamaguchi, A. (2001). Analysis of a complete library of putative drug transporter genes in *Escherichia coli*. *J. Bacteriol.* 183, 5803–5812. doi: 10.1128/JB.183.20.5803-5812.2001
- Poole, K. (2004). Efflux-mediated multidrug resistance in Gram-negative bacteria. *Clin. Microbiol. Infect.* 10, 12–26. doi: 10.1111/j.1469-0691.2004.00763.x
- Poole, K., Krebes, K., McNally, and, C., and Neshat, S. (1993). Multiple antibiotic resistance in *Pseudomonas aeruginosa*: evidence for involvement of an efflux operon. *J. Bacteriol.* 175, 7363–7372. doi: 10.1128/jb.175.22.7363-7372.1993
- Pos, K. M. (2009). Drug transport mechanism of the AcrB efflux pump. *Biochim. Biophys. Acta* 1794, 782–793. doi: 10.1016/j.bbapap.2008.12.015
- Sambrook, J., Fritsch, E. F., and Maniatis, T. (1989). *Molecular Cloning: A Laboratory Manual, 2nd Edn.* New York, NY: Cold Spring Laboratory Press.
- Seeger, M. A., Diederichs, K., Eicher, T., Brandstätter, L., Schiefner, A., Verrey, F., et al. (2008). The AcrB efflux pump: conformational cycling and peristalsis lead to multidrug resistance. *Curr. Drug. Targets.* 9, 729–749. doi: 10.2174/138945008785747789
- Seeger, M. A., Schiefner, A., Eicher, T., Verrey, F., Diederichs, K., and Pos, M. (2006). Structural asymmetry of AcrB trimer suggests a peristaltic pump mechanism. *Science* 313, 1295–1298. doi: 10.1126/science.1131542
- Sennhauser, G., Amstutz, P., Briand, C., Storchenegger, O., and Grütter, M. G. (2007). Drug export pathway of multidrug exporter AcrB revealed by DARPIn inhibitors. *PLoS Biol.* 5:e7. doi: 10.1371/journal.pbio.0050007
- Su, C. C., Li, M., Gu, R., Takatsuka, Y., McDermott, G., Nikaido, H., et al. (2006). Conformation of the AcrB multidrug efflux pump in mutants of the putative proton relay pathway. *J. Bacteriol.* 188, 7290–7296. doi: 10.1128/JB.00684-06
- Takatsuka, Y., and Nikaido, H. (2006). Threonine-978 in the transmembrane segment of the multidrug efflux pump AcrB of *Escherichia coli* is crucial for drug transport as a probable component of the proton relay network. *J. Bacteriol.* 188, 7284–7289. doi: 10.1128/JB.00683-06
- Thanassi, D. G., Cheng, L. W., and Nikaido, H. (1997). Active efflux of bile salts by *Escherichia coli*. *J. Bacteriol.* 179, 2512–2518. doi: 10.1128/jb.179.8.2512-2518.1997
- Vagin, A., and Teplyakov, A. (2000). An approach to multi-copy search in molecular replacement. *Acta. Cryst. D* 56, 1622–1624. doi: 10.1107/S0907444900013780
- World Health Organization (WHO) (2014). *Antimicrobial Resistance Global Report on Surveillance: 2014 Summary*. Geneva: WHO.
- Yamaguchi, A., Nakashima, R., and Sakurai, K. (2015). Structural basis of RND-type multidrug exporters. *Front. Microbiol.* 6:327. doi: 10.3389/fmicb.2015.00327
- Yamane, T., Murakami, S., and Ikeguchi, M. (2013). Functional rotation induced by alternating protonation states in the multidrug transporter AcrB: all-atom molecular dynamics simulations. *Biochemistry* 52, 7648–7658. doi: 10.1021/bi400119v
- Yu, E. W., Zhang, Q., Brown, M. H., and Baugh, S. (2013). *Microbial Efflux Pumps: Current Research*. Norfolk: Horizon Scientific Press.
- Zgurskaya, H. I., and Nikaido, H. (1999). Bypassing the periplasm: reconstitution of the AcrAB multidrug efflux pump of *Escherichia coli*. *Proc. Natl. Acad. Sci. U.S.A.* 96, 7190–7195. doi: 10.1073/pnas.96.13.7190
- Zgurskaya, H. I., and Nikaido, H. (2000). Multidrug resistance mechanisms: drug efflux across two membranes. *Mol. Microbiol.* 37, 219–225. doi: 10.1046/j.1365-2958.2000.01926.x

**Conflict of Interest Statement:** The authors declare that the research was conducted in the absence of any commercial or financial relationships that could be construed as a potential conflict of interest.

Copyright © 2017 Zwama, Hayashi, Sakurai, Nakashima, Kitagawa, Nishino and Yamaguchi. This is an open-access article distributed under the terms of the Creative Commons Attribution License (CC BY). The use, distribution or reproduction in other forums is permitted, provided the original author(s) or licensor are credited and that the original publication in this journal is cited, in accordance with accepted academic practice. No use, distribution or reproduction is permitted which does not comply with these terms.



# Molecular Determinants of the Promiscuity of MexB and MexY Multidrug Transporters of *Pseudomonas aeruginosa*

Venkata K. Ramaswamy<sup>1</sup>, Attilio V. Vargiu<sup>1</sup>, Giuliano Mallocci<sup>1</sup>, Jürg Dreier<sup>2</sup> and Paolo Ruggerone<sup>1\*</sup>

<sup>1</sup> Department of Physics, University of Cagliari, Monserrato, Italy, <sup>2</sup> Basilea Pharmaceutica International Ltd., Basel, Switzerland

## OPEN ACCESS

### Edited by:

Vassily Bavro,  
University of Essex, United Kingdom

### Reviewed by:

J. C. Gumbart,  
Georgia Institute of Technology,  
United States  
Martin Picard,  
University Paris Diderot, France

Jon William Weeks,  
United States Food and Drug  
Administration, United States

### \*Correspondence:

Paolo Ruggerone  
paolo.ruggerone@dsf.unica.it

### Specialty section:

This article was submitted to  
Antimicrobials, Resistance  
and Chemotherapy,  
a section of the journal  
Frontiers in Microbiology

Received: 16 February 2018

Accepted: 14 May 2018

Published: 01 June 2018

### Citation:

Ramaswamy VK, Vargiu AV,  
Mallocci G, Dreier J and Ruggerone P  
(2018) Molecular Determinants of the  
Promiscuity of MexB and MexY  
Multidrug Transporters  
of *Pseudomonas aeruginosa*.  
Front. Microbiol. 9:1144.  
doi: 10.3389/fmicb.2018.01144

Secondary multidrug transporters of the resistance-nodulation-cell division (RND) superfamily contribute crucially to antibiotic resistance in Gram-negative bacteria. Compared to the most studied transporter AcrB of *Escherichia coli*, little is known about the molecular determinants of distinct polyspecificities of the most important RND transporters MexB and MexY of *Pseudomonas aeruginosa*. In an effort to add knowledge on this topic, we performed an exhaustive atomic-level comparison of the main putative recognition sites (access and deep binding pockets) in these two Mex transporters. We identified an underlying link between some structural, chemical and dynamical features of the binding pockets and the physicochemical nature of the corresponding substrates recognized by either one or both pumps. In particular, mosaic-like lipophilic and electrostatic surfaces of the binding pockets provide for both proteins several multifunctional sites for diffuse binding of diverse substrates. Specific lipophilicity signatures of the weakly conserved deep pocket suggest a key role of this site as a selectivity filter as in Acr transporters. Finally, the different dynamics of the bottom-loop in MexB and MexY support its possible role in binding of large substrates. Our work represents the first comparative study of the major RND transporters in *P. aeruginosa* and also the first structure-based study of MexY, for which no experimental structure is available yet.

**Keywords:** RND efflux pumps, multidrug transporter, *Pseudomonas aeruginosa*, antibiotic resistance, molecular dynamics, molecular modeling

## INTRODUCTION

*Pseudomonas aeruginosa* is an opportunistic human pathogen and a leading cause of nosocomial infections worldwide due to the emergence and spread of multi, extensive, and pan-drug resistant isolates susceptible to very few antimicrobial agents (Fischbach and Walsh, 2009; Poole, 2011). The intrinsic resistance of *P. aeruginosa* to multiple antibiotics results from the synergy between its low permeable outer membrane and the action of (chromosomally encoded) multidrug efflux systems like the ones constituted by the resistance-nodulation-cell division (RND) superfamily of secondary transporters (Hancock, 1998; Li et al., 2015), which contribute to both intrinsic and acquired resistance (Poole, 2001; Poole and Srikumar, 2001; Dreier and Ruggerone, 2015).

Several RND type efflux systems have been identified in *P. aeruginosa* PAO1 (Webber and Piddock, 2003; Poole, 2005; Lister et al., 2009; Zechini and Versace, 2009; Fernández and Hancock, 2012; Blair et al., 2014; Delmar et al., 2014; Sun et al., 2014), with the most significant for multidrug resistance being MexAB-OprM (Poole et al., 1993; Gotoh et al., 1995) and MexXY-OprM (Aires et al., 1999; Mine et al., 1999; Westbrook-Wadman et al., 1999). These two machineries contribute additively to the resistance to common substrate antibiotics (Lee et al., 2000; Llanes et al., 2004); moreover, their different specificities (viz. MexB for  $\beta$ -lactams and MexY for aminoglycosides) drastically reduce the susceptibility of infectious strains to numerous classes of antibiotics (Llanes et al., 2004).

The MexAB-OprM tripartite system was the first RND-type multidrug efflux system to be discovered in *P. aeruginosa* at approximately the same time as the AcrAB-TolC system of *E. coli* (Poole et al., 1993). MexB resembles AcrB with a jellyfish-like structural topology formed by an asymmetric trimer with each protomer comprising three domains (Ruggerone et al., 2013) (**Figure 1A**): (i) a trans-membrane domain (TMD) of 12  $\alpha$ -helices embedded in the inner membrane (IM), where the chemical-to-mechanical energy conversion takes place; (ii) a pore (porter) domain (PD) located in the periplasm, where substrate recruitment and transport occur; and (iii) a periplasmic funnel domain (FD), which connects the RND transporter to the outer membrane protein (OMP) via the assembly of membrane fusion proteins (MFPs) (Symmons et al., 2015) in the constituted pump. Substrate transport is characterized by the typical “functional rotation mechanism” (Supplementary Figure 1) in which concerted (but not necessarily synchronous) cycling of the protomers occurs through all of the so far identified asymmetric states: *Loose* (*L*) (a.k.a. *Access*) in which a substrate binds to a peripheral site termed access pocket ( $AP_L$ ); *Tight* (*T*) (a.k.a. *Binding*) in which the substrate binds to a deeper pocket ( $DP_T$ ); and *Open* (*O*) (a.k.a. *Extrusion*) in which the substrate is released into the central funnel leading toward the OMP (Murakami et al., 2006; Seeger et al., 2006; Pos, 2009). The two pockets,  $AP_L$  and  $DP_T$  (**Figure 1B** and Supplementary Figure 1), were previously identified in AcrB [and the latter also in MexB (Nakashima et al., 2013)] as the binding sites responsible for the recognition and selectivity of different types of substrate molecules based on their molecular weight or chemical type (Nakashima et al., 2011; Kobayashi et al., 2014; Iyer et al., 2015; Schuster et al., 2016). The pockets are separated by a G-rich (a.k.a. switch) loop whose flexibility has been shown to be important for the transport of high-molecular mass compounds (Nakashima et al., 2011; Eicher et al., 2012).

The MexY system, identified later, shares an overall sequence identity (similarity) of nearly 47% (66%) with MexB and nearly 48% (67%) with AcrB and AcrD (Supplementary Table 1). Thus, MexY is expected to resemble them in global features like structural fold, location of main ligand binding pockets and functional rotation mechanism (Srikumar et al., 1997; Murata et al., 2002; Eda et al., 2003a). However, MexB and MexY display relevant differences in their substrate specificities (**Table 1** and Supplementary Figures 2, 3). For instance, the substrate specificity of MexB is very similar to that of AcrB

(e.g., both proteins transport macrolides such as erythromycin, most  $\beta$ -lactams, chloramphenicol, etc.) and slightly yet significantly different from that of MexY (aminoglycosides such as gentamicin, tobramycin, amikacin, and isepamycin are transported only by MexY but not by MexB and AcrB) (Krahn et al., 2012; Dreier and Ruggerone, 2015).

Previous studies on these Mex pumps focused on identifying domains responsible for substrate recognition by means of chimeric domain swapping (Tikhonova et al., 2002; Eda et al., 2003b). A few investigations attempted to identify the substrates of Mex pumps (Masuda et al., 2000b; Collu et al., 2012), the residues involved in substrate selectivity (Middlemiss and Poole, 2004; Wehmeier et al., 2009) and also to explain the structural basis for the differential binding of inhibitors to MexB and MexY (Nakashima et al., 2013). However, the molecular basis for the diversity in the substrate profile of these Mex pumps remains largely unknown. One of the key steps to bridge this gap would be to map the differences in substrate specificities between these proteins to distinct structural, chemical and dynamic features of their main putative substrate-binding pockets. Unfortunately, the absence of an experimental structure of MexY and the availability of only one structure of MexB bound to compounds [the ABI-PP inhibitor D13-9001 within  $DP_T$  (Nakashima et al., 2013)] have made it hard to reach this goal. However, given the overall good sequence identity and similarity of MexY with MexB of *P. aeruginosa* and with AcrB of *E. coli* for which high resolution X-ray structures are available, reliable computational modeling of MexY and related structure-based studies are possible.

In addition, as these biological systems are not static *in vivo*, understanding their dynamics in terms of statistically relevant conformations, interactions with solvent, and physicochemical nature of the putative binding pockets is essential for a more robust comparison. In this regard, computational modeling, in particular all-atom molecular dynamics (MD) simulations, have already proven to be valuable in addressing the molecular mechanisms of RND transporters (Schulz et al., 2010; Vargiu et al., 2011, 2014, 2018; Collu et al., 2012; Fischer and Kandt, 2013; Ruggerone et al., 2013; Zuo et al., 2015, 2016; Ramaswamy et al., 2017a,b; Matsunaga et al., 2018). By employing homology modeling and extensive multi-copy  $\mu$ s-long MD simulations, we recently identified the underlying link between the microscopic environment of the dynamic binding pockets and drug properties that governs and regulates substrate recognition and transport in AcrB and AcrD transporters of *E. coli* (Ramaswamy et al., 2017b). Very little is known of the physicochemical and dynamic features of the corresponding binding pockets in MexB and hardly anything for MexY.

In this work, we characterized and compared the main putative binding pockets ( $AP_L$  and  $DP_T$ ) of MexB and MexY in terms of molecular descriptors like accessible volume, lipophilic index, electrostatic potential, hydration profile and distribution of multi-functional sites (MFSs). These descriptors depend on the sequence, structure and dynamics of the pockets, and clearly affect the molecular recognition of substrates. We identified features that potentially explain the highly multifunctional nature of these pockets in MexB and MexY. In particular, the ability of



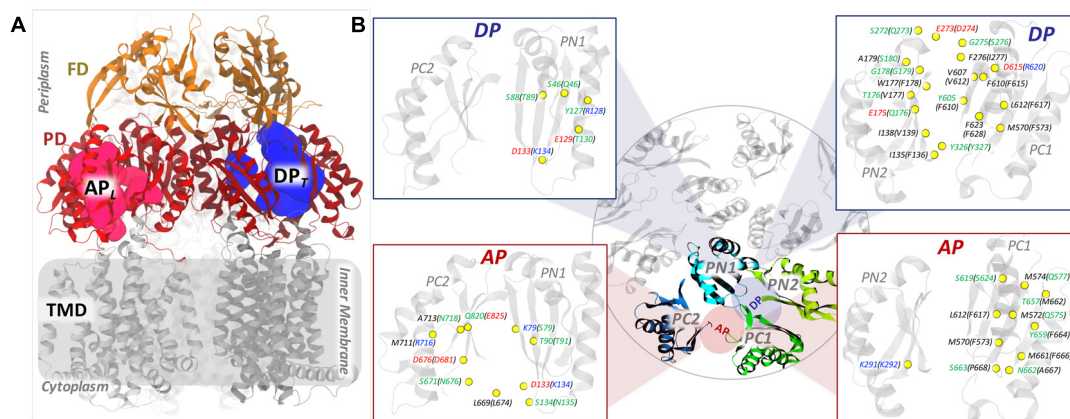


**FIGURE 1 |** General structure of an RND transporter and comparison of the putative binding pockets (AP and DP) between MexY and MexB. **(A)** The general structure of an RND transporter highlighting the three main domains (TMD, PD, and FD) with different colors. **(B)** The figure in the middle shows the top view of the four main domains (colored differently) enclosing the AP and DP. The locations of the pockets are schematically shown as red and blue colored circles for AP and DP, respectively. The insets highlight the mismatched residues of MexY and MexB as yellow-colored beads with the residue labels colored by residue type (non-polar residues in black, polar residues in green, basic residues in blue, and acidic residues in red). The residue labeling follows the notation "MexY (MexB)."

MexY to accommodate a very diverse set of substrates ranging from hydrophobic macrolides to hydrophilic aminoglycosides, can be explained by the intermediate lipophilic profile (scaling between that of AcrB and AcrD) in synergy with the mosaic-like electrostatic environment of its main putative binding pockets. Furthermore, correlating our previous findings on the structure-function relation of Acr transporters (Ramaswamy et al., 2017b) with those of Mex transporters could be informative to new drug design attempts addressing efflux pumps-based antibiotic resistance (Ruggerone et al., 2013).

## RESULTS AND DISCUSSION

### Sequence Comparison

Since bacteria respond to adverse environmental stress by altering their genetic makeup, we first analyzed the sequences of MexB and MexY from all available bacterial strains of *P. aeruginosa*. Both these protein sequences were found to be well conserved across the strains deposited in UniProtKB<sup>1</sup> (accessed November 2017). MexB of *P. aeruginosa* and AcrB of *E. coli* showed a

comparable sequence identity (~47 and ~48%, respectively) and similarity (~66 and ~67%, respectively) with MexY having least gaps (none in the binding pockets) over maximum sequence coverage (Supplementary Table 1). Further, on comparing MexY to MexB (Figure 1B and Supplementary Figure 3), we noticed that both AP and DP were less conserved than the overall proteins, sharing only around 35 and 34% identities, respectively. However, in terms of chemical composition of the pockets, the DP of both MexB and MexY showed an equal proportion of hydrophobic residues (~50%), but different proportions of polar and charged residues (32 and 11% in MexB vs. 23 and 16% in MexY, respectively). The AP exhibited a slightly higher proportion of hydrophobic residues and a lower proportion of polar and charged residues in MexB than in MexY (56% vs. 50%, 21% vs. 27%, and 13% vs. 15%, respectively). Most of the residues identified as essential to establish interactions with the substrates and/or the inhibitors in AcrB (Elkins and Nikaido, 2002; Nakashima et al., 2011; Vargiu et al., 2011; Eicher et al., 2012; Yao et al., 2013; Kobayashi et al., 2014; Blair et al., 2015; Opperman and Nguyen, 2015) were well conserved in MexB. The characteristic hydrophobic trap (HP-trap) sitting within the DP and rich in phenylalanine residues was completely conserved in MexB but not in MexY. The

<sup>1</sup><http://www.uniprot.org/blast>

**TABLE 1 |** Antibiotic substrate specificities of the paralog RND transporters MexB and MexY from *P. aeruginosa* (Li et al., 1995; Köhler et al., 1996; Zhao et al., 1998; Zihra-Zarifi et al., 1999; Masuda et al., 2000a; Chuanchuen et al., 2001; Okamoto et al., 2001; Hocquet et al., 2003; Llanes et al., 2004; Mesaros et al., 2007; Nakashima et al., 2013).

Transporter(s)	MexB	MexY	MexB and MexY
Substrates	Most beta-lactams (except imipenem), novobiocin, trimethoprim and triclosan	Aminoglycosides (gentamicin, tobramycin, amikacin), Penicillins (except carbenicillin and sulbenicillin), Cepheids (except cefsulodin and ceftazidime)	Macrolides (erythromycin, spiramycin), Fluoroquinolones, chloramphenicol, Tetracyclines
Substrate type	Hydrophobic	Hydrophilic	Amphiphilic

Classes of compounds are indicated, with examples of specific compounds within parentheses (2D chemical structures of these compounds are shown in Supplementary Figure 2). General physicochemical property of antibiotic substrates of MexB and MexY are also specified.

HP-trap does interact only smoothly with the transported drugs (Kinana et al., 2016) but it is likely a preferred target site for inhibitor design in AcrB (Bohnert et al., 2008; Vargiu et al., 2011, 2014; Ruggerone et al., 2013; Opperman and Nguyen, 2015; Ramaswamy et al., 2016). The corresponding HP-trap region in MexY though mostly hydrophobic contains the hydroxyl group of Y605 (corresponding to F610 in MexB and AcrB) and the nitrogen atom of the indole ring of W177 (corresponding to F178 in MexB and AcrB) (Nakashima et al., 2013).

## MD Simulations of MexB and MexY

The all-atom MD simulations of apo-form of MexB were started from the crystallographic structure with PDB code 3W9I (pre-MD of MexB). As no experimental structure of MexY is available to date, we generated a reliable multi-template homology model of this transporter using the crystal structures of MexB (PDB code 3W9I) and AcrB (PDB code 4DX5). Details of the rigorous validation of this model (pre-MD of MexY) are reported in Supplementary Material (Supplementary Table 2). The stability of the MexY model and its suitability for subsequent quantitative analyses were further validated by performing 4 independent  $\mu$ s-long MD simulations.

Considering the root mean square deviation of the whole protein backbone and of each protomer with reference to the initial structure (Supplementary Figure 4), we established the equilibration time of  $\sim 0.2 \mu$ s to be the most suitable for both MexB and MexY simulations. On the remaining  $\sim 4 \mu$ s-long ( $4 \times 1 \mu$ s) cumulative MD trajectory of each protein, we performed a cluster analysis to extract statistically relevant conformations sampled by the proteins (Supplementary Figures 5, 6). The most populated clusters were used to characterize the distribution of accessible binding volumes, molecular lipophilicity, electrostatic potential and MFSSs. The trajectories themselves were further analyzed for hydration patterns within the  $AP_L$  and  $DP_T$  of both proteins. In the following, we discuss separately the results of these characterizations.

## Access Pocket of the Loose Protomer

### Pocket Volume and Essential Dynamics

The accessible volume at the recognition pocket is the first of the many factors governing optimal ligand binding in addition to shape and electrostatic complementarity (Ruiz-Carmona et al., 2014). Promiscuous RND transporters were earlier identified to have a large binding site with a reasonable degree of plasticity to facilitate binding of molecules of a wide range of sizes (Edward et al., 2003; Nikaido and Takatsuka, 2009; Marsh, 2015).

The  $AP_L$  of MexB featured an average value of  $\sim 1120 \text{ \AA}^3$  with the most populated cluster (about 28% of the simulation time) showing a pocket volume of around  $1440 \text{ \AA}^3$ . In the case of MexY, the  $AP_L$  showed a larger average volume of  $\sim 1590 \text{ \AA}^3$  with the most populated cluster (covering  $\sim 19\%$  of the simulation time) showing around  $2180 \text{ \AA}^3$  (Figure 2 and Table 2). Interestingly, while in MexB the volume of  $AP_L$

diminished significantly from that in the pre-MD structure ( $3350 \text{ \AA}^3$ ), the values calculated in MexY were overall in line with the initial volume of  $\sim 1600 \text{ \AA}^3$  (Table 2). The opening of this site in the crystal structures 2V50 (Sennhauser et al., 2009) and 3W9I (Nakashima et al., 2013) of MexB with respect to the MD-based structures could, for instance, have been induced by the presence of other (perhaps unresolved) molecules, as suggested earlier for the  $DP_T$  of AcrB (Seeger et al., 2006; Sennhauser et al., 2007; Fischer and Kandt, 2013).

It is also worth pointing out that both Mex transporters display smaller  $AP_L$  average volumes compared to AcrB and AcrD (about  $2510 \pm 440 \text{ \AA}^3$  and  $3010 \pm 380 \text{ \AA}^3$ , respectively). In particular, during MD we observed a compression of the  $AP_L$  volume of nearly 66% in MexB vs. 30% in AcrB. It is to be noted that a constricted state of MexB (PDB code 2V50) with respect to AcrB was previously reported by Sennhauser et al. (2009) from their crystallographic studies. Nonetheless, the volumes of  $AP_L$  in MexB and MexY (Table 2) are much larger than those of the largest substrates [e.g., erythromycin having a volume of  $727 \pm 2 \text{ \AA}^3$  (Mallocci et al., 2015)] transported by these pumps. This indicates the possibility of a substrate to bind in different orientations and/or at different sub-pockets, a hypothesis compatible with the multisite-drug-oscillation (Yamaguchi et al., 2015) and diffuse binding (Marsh, 2015) in these proteins.

In addition to pocket volume calculations, we performed principal component analysis (PCA) of equilibrium MD trajectories in order to identify the essential dynamics of regions lining the putative main binding pockets. Porcupine plots of the top three principal components (Figures 2B,D) show the entire  $AP_L$  of MexB and MexY exhibiting almost a coherent motion with slightly larger magnitude (depicted by length of the arrows) in the case of MexB. The dynamicity of the bottom-loop lining the base of  $AP_L$  and earlier identified as a peculiar feature of AcrB but not AcrD (Ramaswamy et al., 2017b) appeared to be different even in Mex transporters (Figure 3). The most populated cluster in MexB and in fact all cluster representatives were characterized by an “up” conformation, comparable to the pre-MD or the crystal structure of MexB (PDB code 3W9I). In the case of MexY, the corresponding bottom-loop showed an intermediate state between the “up” state of its pre-MD and its MexB template structure and the “down” state seen in the AcrB template structure (PDB code 4DX5). The magnitude of  $C\alpha$  displacements of the bottom-loop was different in Mex ( $<6.4 \text{ \AA}$  in MexB and  $<8.9 \text{ \AA}$  in MexY) and Acr ( $<12.5 \text{ \AA}$  in AcrB and  $<6.7 \text{ \AA}$  in AcrD) transporters (Ramaswamy et al., 2017b). On comparing the amino acid sequence among these different transporters, we found it interesting that this loop is poorly conserved across the Mex (MexB: LELGNA, MexY: PDLGST) and Acr (AcrB: VELGTA, AcrD: SGLGSS) transporters, with only residues LG being fully preserved across the four proteins. This could partly explain the differential dynamicity of the bottom-loop observed in our simulations. Further studies are needed to investigate the role of this loop in synergy with the G-loop in regulating substrate access and transport in these RND transporters.



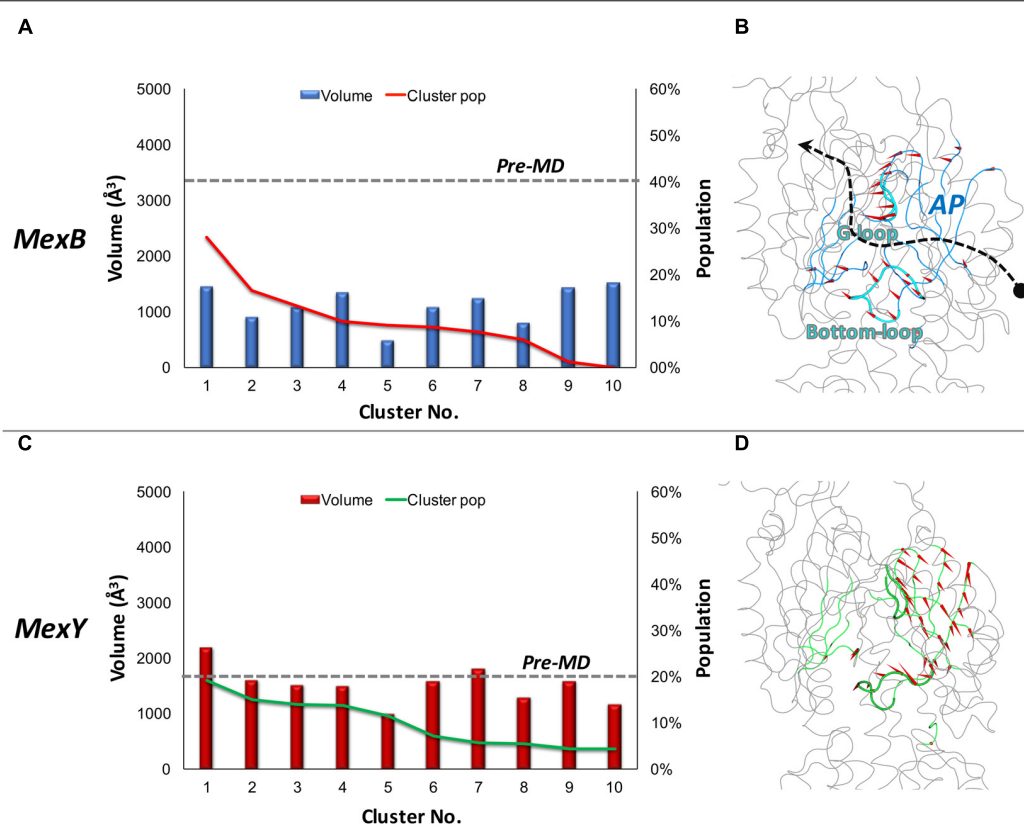


**FIGURE 2 |** Volume dynamics of AP<sub>L</sub> of MexB and MexY. (Left panel) Distribution of the volume of AP<sub>L</sub> of MexB (A) and MexY (C), calculated for the 10 top cluster representatives extracted from equilibrium MD trajectories. Histograms refer to the volumes, lines to the relative population of the corresponding clusters. The volumes calculated for the pre-MD structures of MexB and MexY are shown as dashed lines. (Right panel with side view of the protomer) Porcupine plots representing collective motions along the PC eigenvector for AP<sub>L</sub> in MexB (B) and MexY (D) simulations shown as arrows (>2Å) attached to C $\alpha$  atoms indicating the magnitude of the corresponding eigenvalues. Features of AP<sub>L</sub> are colored blue and green in MexB and MexY, respectively. The G-loop and bottom-loop are shown as thicker tubes. The substrate path from the periplasmic entrance (dot) to the exit gate (arrow head) is shown with a dashed arrow passing between the two main loops likely governing substrate access and transport in RND pumps.

## Lipophilic Index (LI) and Molecular Lipophilicity Potential (MLP)

In addition to steric features, an adequate lipophilic profile is essential for suitable binding of hydrophobic or amphipathic molecules such as macrolides (e.g., erythromycin and

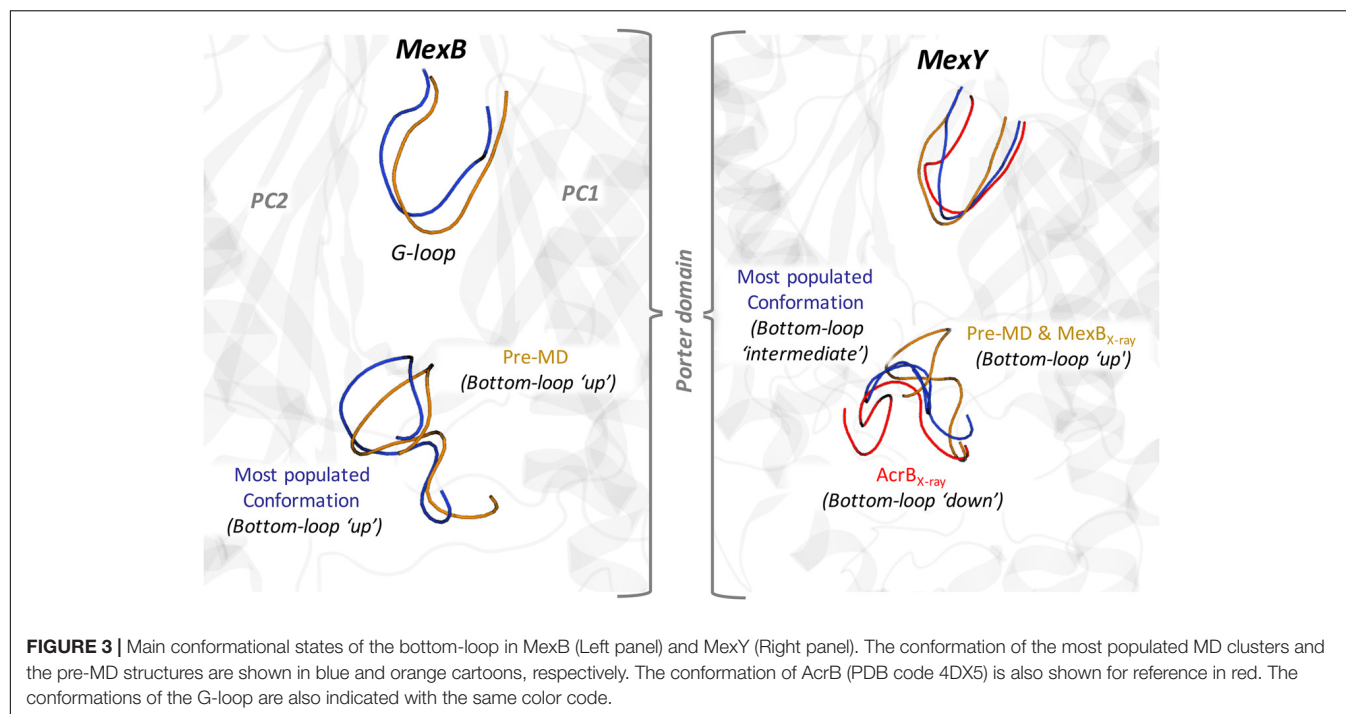
spiramycin) transported by both Mex proteins. In order to characterize the lipophilicity of the pocket, estimate its dependence on the conformation of the protein, and compare closely related RND transporters, we calculated the LI of AP<sub>L</sub> for the pre-MD structures and for representative structures of all clusters. There was no remarkable difference in LI of AP<sub>L</sub> between pre-MD and MD values of MexB and MexY in our case [Table 3 and Supplementary Figure 7 (Upper panel)], as observed also for the LIs of Acr proteins (Ramaswamy et al., 2017b) [AcrB: 7.2 vs. 7.0 ( $\pm 1.0$ ) and AcrD: 1.2 vs. 1.6 ( $\pm 0.6$ ) for pre-MD and MD, respectively].

Considering the four RND transporters, we found that MexB and MexY featured intermediate LIs between those of AcrB (highest) and AcrD (lowest). Specifically, for the Mex transporters, the LIs were slightly higher for MexY than for MexB, despite the higher percentage of hydrophobic residues at this site in the latter protein. This is due to the reduced exposed lipophilic surface (Oberhauser et al., 2014) associated with the aforementioned closure of the pocket in MexB during MD simulations. To verify this aspect we considered open structures of MexB [both crystal structures with PDB

**TABLE 2 |** Volumes of AP<sub>L</sub> and DP<sub>T</sub> of MexB and MexY.

System	Volume (Å <sup>3</sup> )	
	Pre-MD	MD clusters
<b>AP<sub>L</sub></b>		
MexB	3350	1120 $\pm$ 290
MexY	1600	1590 $\pm$ 350
<b>DP<sub>T</sub></b>		
MexB	5120	2310 $\pm$ 200
MexY	3840	2400 $\pm$ 210

For MexB, the pre-MD structure corresponds to the crystal structure identified by PDB code 3W9I while for MexY it is the final optimized model used as starting configuration for MD simulations.



codes 2V50 (Sennhauser et al., 2009) and 3W9J (Nakashima et al., 2013), and homology models built using AcrB with PDB code 4DX5 (Eicher et al., 2012) as template] and top five models of MexY built using 2V50 as template. The average LI values computed were  $6.4 \pm 2.5$  and  $5.5 \pm 1.0$  for MexB and MexY, respectively, in line with the features of the residues lining the pocket. Overall, the intermediate values of the Mex transporters reveal that the specific chemical environment of their APs is neither entirely hydrophobic nor entirely polar in both proteins as noticeable from their molecular lipophilic surfaces (Figures 4A,B), thereby giving rise to weak binding with dispersed interactions, possibly facilitating substrate transport (Marsh, 2015; Yamaguchi et al., 2015).

### Electrostatic Potential

The recognition of charged substrates (viz. polycationic aminoglycosides by MexY and zwitterionic or anionic  $\beta$ -lactams

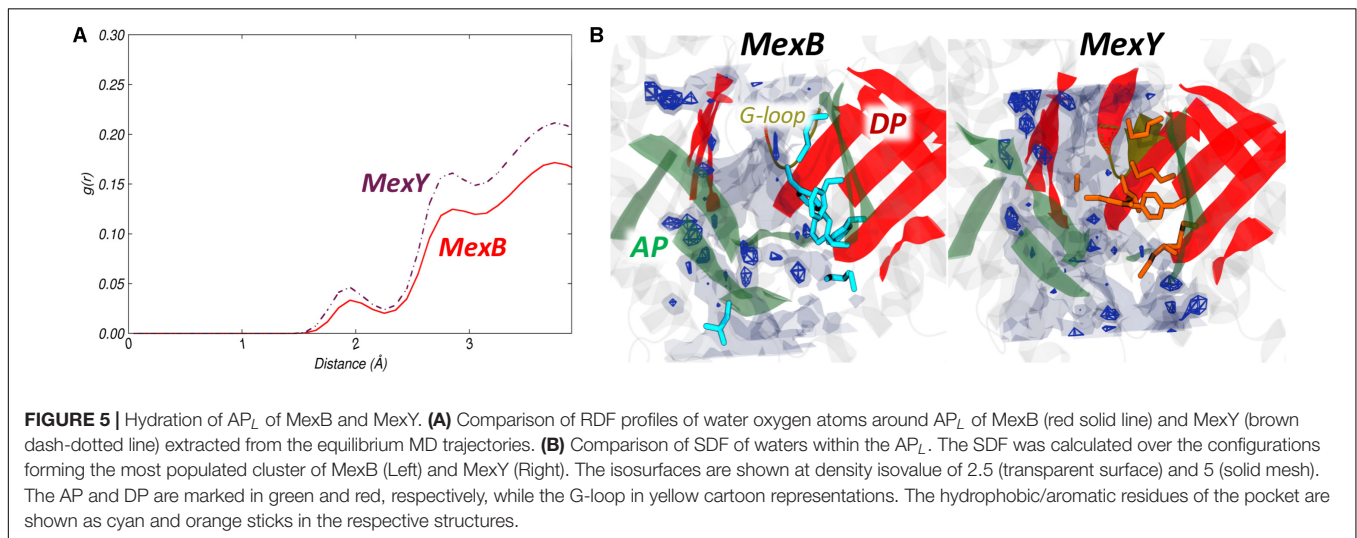
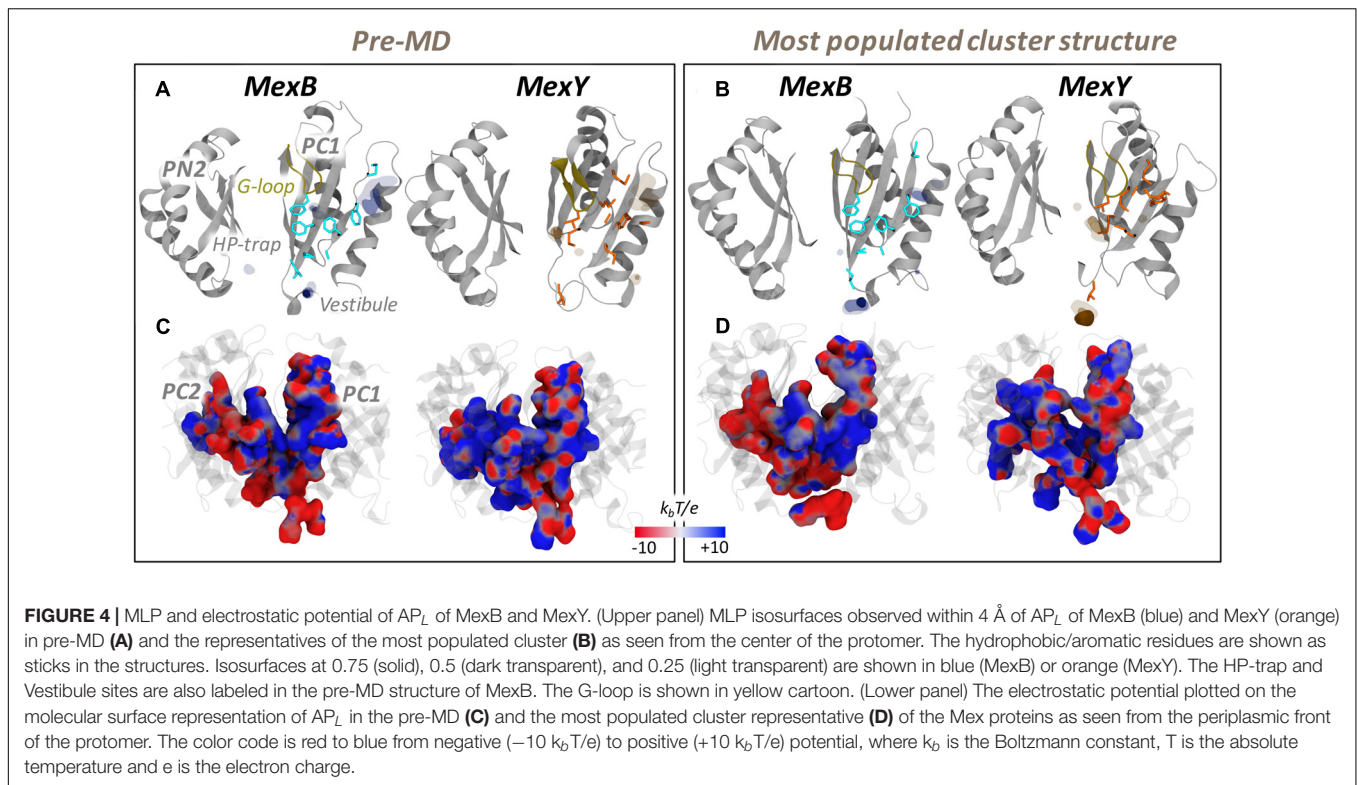
by MexB) is mediated by electrostatic complementarity, which is essential for initial substrate recruitment and augmentation of their association rate (Selzer et al., 2000; Levy et al., 2007). The AP<sub>L</sub> of MexY has a slightly greater number of polar and charged residues compared to that of MexB. This difference was mirrored in the different electrostatic potentials of the two transporters, as can be seen from their projection onto the solvent accessible surface areas in Figures 4C,D. In particular, two main regions are clearly visible in MexB: a negative patch near the base of AP<sub>L</sub> and on the PC2 domain, and positive patches near the zone exposed to the periplasmic cleft entrance (mostly on PC1). This separation was less intense in MexY, which compared to MexB also featured an overall greater distribution of positive patches within the AP<sub>L</sub>. The marked influence of electrostatics on substrate recognition and transport in MexY was already highlighted in an experimental mutation study reported by Poole and co-workers (Lau et al., 2014). In particular, three residues (D133, Y613, and K79) principally lining the AP compromised (D133, Y613) or enhanced (K79) aminoglycoside resistance upon substitution. These effects are in agreement with our findings, as the removal of the positive charge on K79 along the transport path likely enables a more efficient transport of molecules such as polycationic aminoglycosides, while substituting D133 with S or A, thus removing a negative patch in that pocket, probably has a negative effect on the recognition/binding of positively charged molecules.

It is interesting to note that the electrostatic nature of MexB and MexY seen here are comparable to that of AcrB (more negative) and AcrD (more positive), respectively. However, based on the homology to Acr transporters of *E. coli* in which residues essential for specificity to anionic  $\beta$ -lactams in AcrD

**TABLE 3 |** Lipophilic indexes of AP<sub>L</sub> and DP<sub>T</sub> of MexB and MexY.

System	Lipophilic Index	
	Pre-MD	MD clusters
<b>AP<sub>L</sub></b>		
MexB	2.7	$2.7 \pm 0.9$
MexY	4.2	$4.5 \pm 1.2$
<b>DP<sub>T</sub></b>		
MexB	20.1	$4.1 \pm 2.3$
MexY	15.9	$8.9 \pm 2.2$

See Table 2 for further details.



were recently identified (Kobayashi et al., 2014), we found the corresponding residues (Q in MexB/MexY at position of R568 in AcrD; M in MexB/MexY at position of R625 in AcrD; E in MexB and D in MexY at position of G672 in AcrD) to differ in MexB and MexY. This lack of sequence identity may indicate a different selection filter for charged substrates in these Mex transporters.

### Hydration Analysis

The radial distribution function (RDF) and spatial distribution function (SDF) profiles of water oxygen atoms around the AP<sub>L</sub>

residues in MexB and MexY were assessed for any possible difference in the density of hydration. The first solvation shell was found at around 2 Å from any residue lining the pocket in both proteins, displaying a slightly lower intensity in MexB (Figure 5A). The SDF was calculated on the trajectory of the most populated cluster extracted from MD simulations of MexB and MexY to get more insights into the spatial distribution of water in the pocket (Figure 5B). The SDF profiles featured no water density spots near the hydrophobic residues in AP<sub>L</sub> of both MexB and MexY but showed a slightly higher number of dense regions in MexY at identical density isovalues (Figure 5B). The

other lesser populated clusters showed no water dense regions at similar isovalue in both proteins.

From visual inspection, the RDF plots of MexB and MexY are comparable to those of AcrB and AcrD, respectively, which can be related to the similarity in the overall physicochemical makeup of their putative binding pockets. However, MexB featured much less water dense regions than MexY at density isovalues corresponding to the spots found earlier in AcrB and AcrD (Ramaswamy et al., 2017b).

## Deep Pocket of the *Tight* Protomer

The DP was earlier suggested to be the recognition site for low molecular mass compounds and inhibitors (the latter interacting strongly with the HP-trap within this site) (Murakami et al., 2006; Nakashima et al., 2011, 2013; Eicher et al., 2012; Vargiu and Nikaido, 2012; Vargiu et al., 2014; Sjuts et al., 2016; Wang et al., 2017). According to the available X-ray structures of AcrB (Murakami et al., 2006; Seeger et al., 2006; Sennhauser et al., 2007; Eicher et al., 2012) and MexB (Sennhauser et al., 2009; Nakashima et al., 2013), this pocket is open only in the *Tight* protomer; therefore, all the analyses concerning this site were performed on the *Tight* protomer of MexB and MexY.

## Pocket Volume and Essential Dynamics

The volume of the DP<sub>T</sub> ranged from 2000 to 2800 Å<sup>3</sup> in both proteins (average values around 2310 and 2400 Å<sup>3</sup> for MexB and MexY, respectively), and also the most populated clusters featured a very similar volume of ~2500 Å<sup>3</sup> (Figures 6A,C). The pre-MD structures showed a much larger DP<sub>T</sub> in both proteins (5120 and 3840 Å<sup>3</sup> in MexB and MexY, respectively) (Table 2). This result resembled our previous findings for the major RND transporters of *E. coli* (Ramaswamy et al., 2017b), where the average volumes of the DP<sub>T</sub> of AcrB and AcrD were around 2610 and 2770 Å<sup>3</sup>, respectively, during MD, and 3710 and 3850 Å<sup>3</sup>, respectively, in their pre-MD structures. As concluded in that study, despite a large collapse of the pocket (55% in MexB and 37% in MexY) with respect to the conformations in the initial (pre-MD) structures, the DP<sub>T</sub> remained large enough to accommodate ligands even in these Mex proteins. A marked dynamical behavior of the DP<sub>T</sub> was evident in both transporters as seen from the PCA analysis, the switch-loop and the PN2 (bottom-right region in Figure 6D) being the most flexible regions in MexB and MexY, respectively (Figures 6B,D).

In MexY, the sterically bulky side chain of W177 (corresponding to F178 in MexB) oriented into the DP<sub>T</sub> reduced the volumes in both pre-MD and MD-derived conformations. Also, the populations of the identified clusters indicate a non-preferential distribution of conformations adopted by DP<sub>T</sub> in contrast to what we found in Acr transporters (Ramaswamy et al., 2017b), where specific conformations were predominant.

## Lipophilic Index (LI) and Molecular Lipophilicity Potential (MLP)

The difference between the DP<sub>T</sub> of MexB and MexY became more noticeable from their MLP surfaces (Figures 7A,B) and LI

values (Table 3). With its phenylalanine-rich hydrophobic region wide open in MexB, the MLP features high-value isosurfaces over the whole bottom of the DP<sub>T</sub>; interestingly, MexY also features a relatively wide and strong MLP in the same region. This result is consistent with the observed higher LI in the pre-MD structure of MexB compared to that of MexY. The differences observed in Figures 7A,B and Table 3 are less marked as compared to that seen for AcrB and AcrD (Ramaswamy et al., 2017b).

An evident reduction in the MLP isosurfaces and in the LI values (for the latter, 80 and 44% in MexB and MexY, respectively) was observed when considering the weighted average computed for the cluster representatives extracted from MD trajectories. This is partly attributed to the larger shrinkage of the DP<sub>T</sub> in MexB (55% in volume) than in MexY (37%) thereby influencing the calculation of the LIs as shown for AP<sub>L</sub> (see Table 3 and Supplementary Figure 7).

In the case of DP<sub>T</sub>, even though the corresponding HP-trap region is conserved in its overall hydrophobic nature, the residues W177 and Y605 in MexY are less hydrophobic than their phenylalanine counterparts in MexB. Nevertheless, the values of the LI as well as their difference between MexB and MexY are greater in the lesser-conserved DP<sub>T</sub> than in the AP<sub>L</sub>, as observed for the homologous Acr transporters (Ramaswamy et al., 2017b). This suggests that the DP<sub>T</sub> might act even in this case as a lipophilicity-based selectivity filter.

## Electrostatic Potential

The differences in the electrostatic potential between the DP<sub>T</sub> of MexB and MexY appear to be strikingly distinctive like that of the lipophilic potential in these Mex transporters. The electrostatic potential projected onto the surfaces of the DP<sub>T</sub> indicated a significantly greater positively charged environment in MexB compared to the more negative pocket of MexY (Figures 7C,D). This is consistent with the sequence analysis showing that the DP<sub>T</sub> of MexY and MexB are, respectively, composed of around 14 and 5% (2 and 7%) negatively (positively) charged residues. Moreover, these electrostatic features are in good agreement with the desired complementarity needed to accommodate the charged substrates transported by these proteins. The greater negative charge in the DP<sub>T</sub> of MexY favors positively charged aminoglycosides and disfavors negatively charged molecules; however, along with the scattered positive charges, the DP<sub>T</sub> in MexY may feebly favor binding of β-lactams (especially zwitterionic). Likewise, MexB with its predominant positive electrostatic potential surface in the DP<sub>T</sub> may attract negatively charged as well as zwitterionic β-lactams, and extrude them with greater efficiency along with weakly acidic quinolones such as cinoxacin and nalidixic acid, in comparison to its lower efficiency in pumping out cationic antibiotics (oleandomycin, erythromycin, and puromycin) (Table 1).

## Hydration Analysis

The overall hydration of the DP<sub>T</sub> and HP-trap as reflected by the RDF plot was not very different between the Mex proteins (Figure 8A). In contrast, the spatial positions of water dense regions as seen from the SDF (Figure 8B) showed the DP<sub>T</sub> of



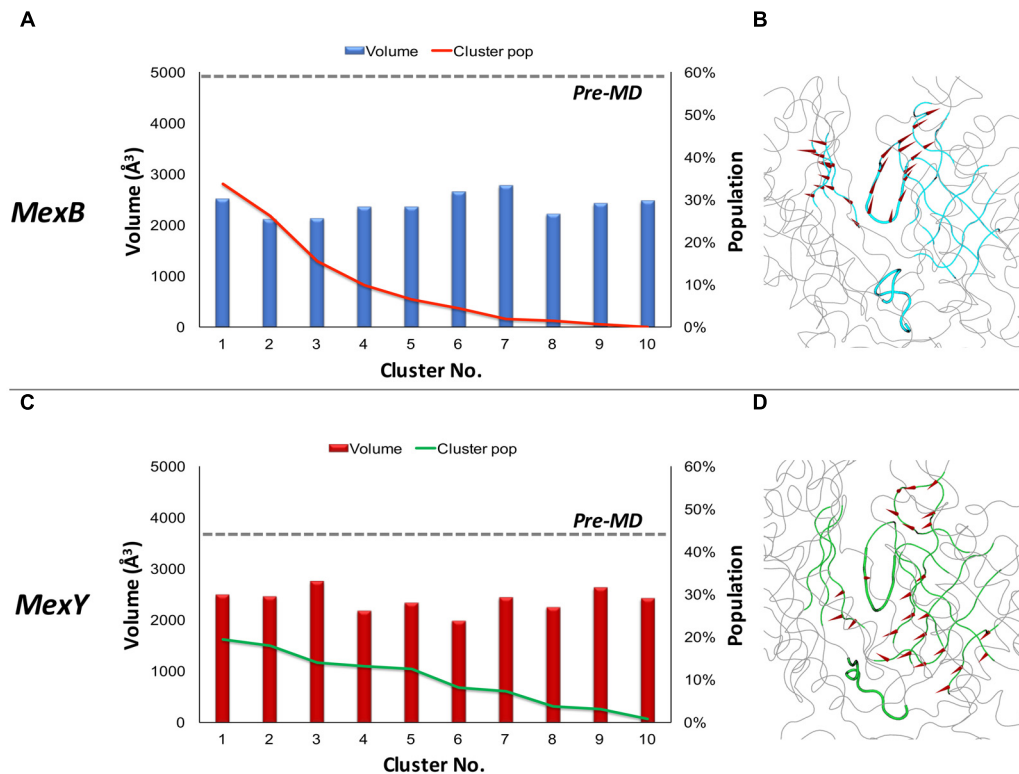


**FIGURE 6 |** Volume dynamics of DP<sub>T</sub> of MexB and MexY. (Left panel) Volume distribution of DP<sub>T</sub> of MexB (A) and MexY (C). (Right panel) Porcupine plots of the PC eigenvector for DP<sub>T</sub> of MexB (B) and MexY (D) simulations shown as arrows (>2Å) attached to C $\alpha$  atoms indicating the magnitude of the corresponding eigenvalues. The DP<sub>T</sub> is highlighted in cyan and green in MexB and MexY, respectively. The G-loop and bottom-loop are shown as thicker tubes.

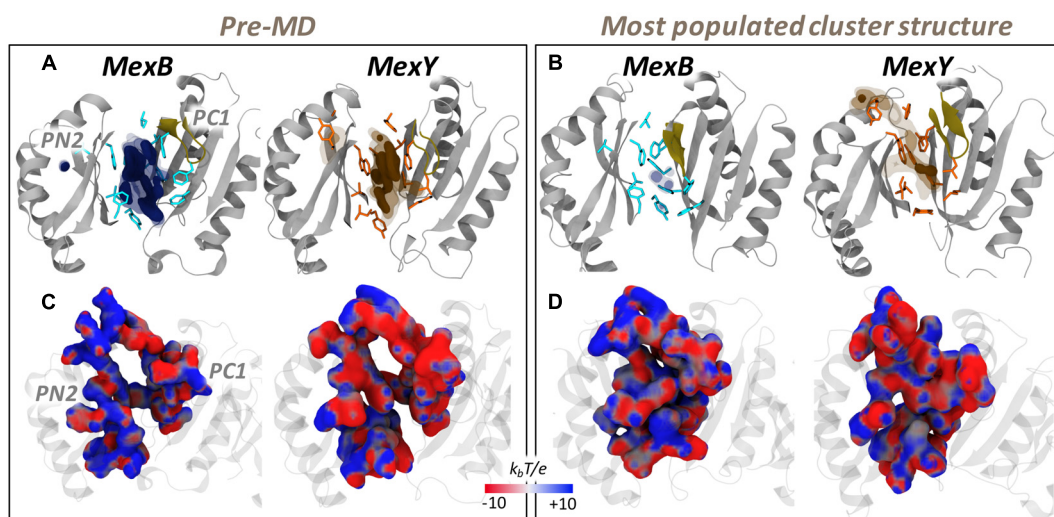
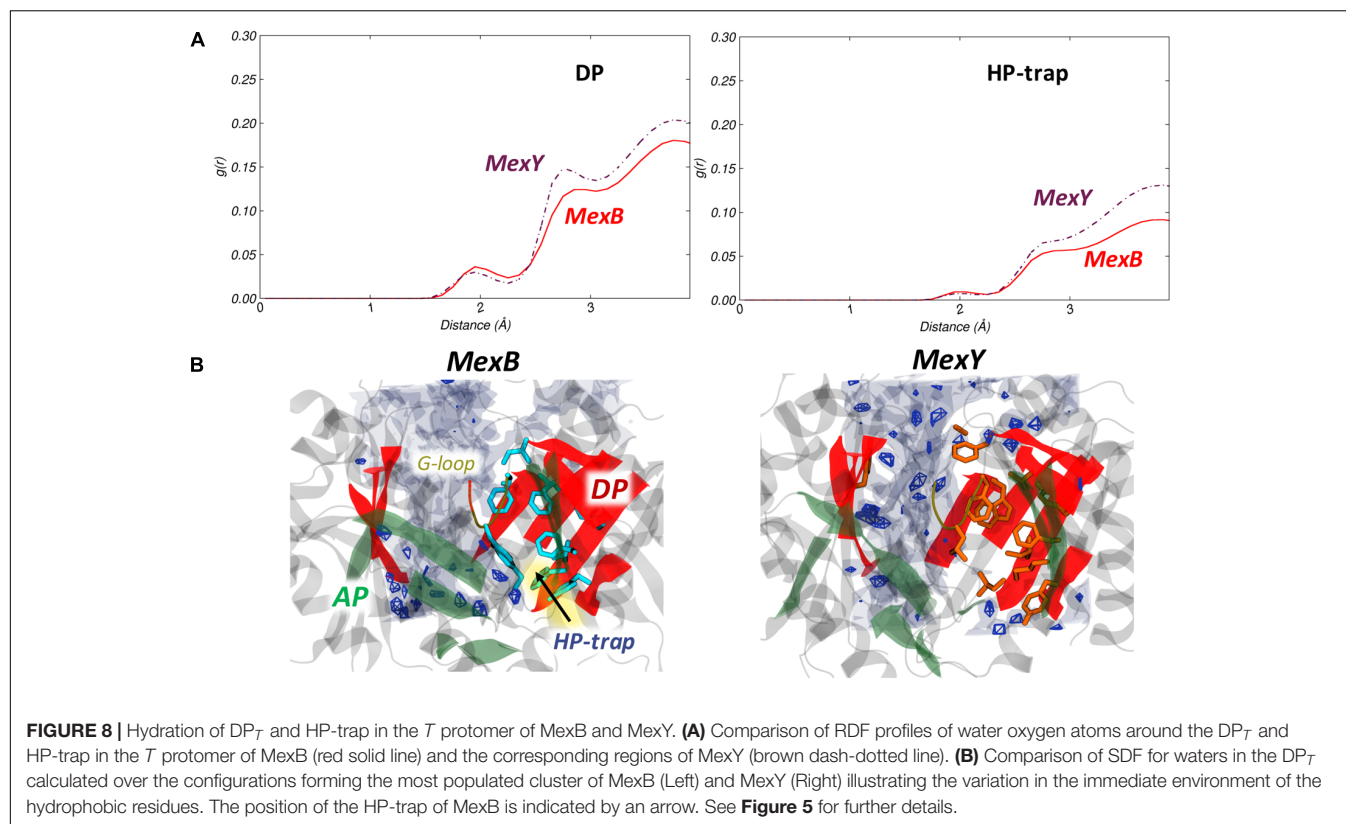


**FIGURE 7 |** MLP (Upper panel) and electrostatic potential (Lower panel) surfaces of DP<sub>T</sub> of MexB and MexY as seen from PC2-PN1 side. (A,C) and (B,D) correspond to the results from pre-MD and the representative of the most populated cluster, respectively. See Figure 4 for further details.

MexY with more high-density regions than that of MexB, possibly due to a greater number of charged residues in the translocation channel part of the DP<sub>T</sub>. The HP-trap region was devoid of water in both proteins due to the shrinkage of the pockets during MD.

The presence of a polar residue (Y605) might have had a minor influence on the hydration of the corresponding HP-trap region in MexY, provided it was less buried by the hydrophobic bulky side chain of W177.



## Fragment-Based Binding Site Characterization

MDR transporters like the Mex pumps investigated here often feature recognition sites endowed with several binding hotspots (Vargiu and Nikaido, 2012; Ruggerone et al., 2013; Yamaguchi et al., 2015) whose number, strength and spatial distribution determine the level of promiscuity of their interactions (Ciulli et al., 2006). Therefore, by using fragment moieties (Supplementary Figure 8) characterized by different physicochemical features, we probed the AP<sub>L</sub> and DP<sub>T</sub> of the two proteins to map their possible MFSs (Imai et al., 2011; Ramaswamy et al., 2017b).

As expected, several MFSs were identified within the AP<sub>L</sub> and DP<sub>T</sub> of both transporters (Figure 9 and Supplementary Table 3). In particular, MexY had a larger (lower) number of MFSs in the AP<sub>L</sub> (DP<sub>T</sub>) than MexB. Considering the pre-MD and the top 5 clusters extracted from MD trajectories, the AP<sub>L</sub> and the interface/G-loop region almost always showed the presence of at least 1 MFS in both proteins. For the DP<sub>T</sub>, however, a marginal difference was found, with MexB housing an average of 1 MFS compared to 0.7 in MexY. This difference was greater in the DP<sub>T</sub> of Acr transporters (AcrB with 1.3 and AcrD with 0.3 MFSs on average) (Ramaswamy et al., 2017b), which feature greater diversity in their substrate profile as compared to MexB and MexY. Note that the MFS identified in the DP<sub>T</sub> of the pre-MD structure in MexB is located exactly where the inhibitor D13-9001 (Nakashima et al., 2013) was experimentally resolved. In comparison to AcrB crystal structures, this is the

site where several substrates like minocycline (Murakami et al., 2006; Nakashima et al., 2011; Eicher et al., 2012), doxorubicin (Murakami et al., 2006; Eicher et al., 2012), and inhibitors like D13-9001 (Nakashima et al., 2013) and MBX compounds (Sjuts et al., 2016) were resolved. Conformational changes during the MD simulation impacted the number and location of MFS compared to their pre-MD structures, nevertheless retaining the promiscuity in both transporters (Supplementary Figure 9 and Supplementary Table 3). An interesting feature was that though several consensus sites (CSs) populated with hydrogen bond donors and acceptors were observable in both proteins, those of MexB had many more aromatic-preferred sites than MexY.

The position of the MFSs was not the same for all MD-derived clusters (Supplementary Figure 9 and Supplementary Table 3) and this dynamicity (in addition to the scattered profile) in the distribution of MFSs results from the exposure of different weak binding sites during conformational changes in the protein. Presence of such MFSs is likely very important to avoid the substrate from being trapped in a single site and to facilitate its efflux by multisite-drug-oscillation (Yamaguchi et al., 2015).

## CONCLUSION AND PERSPECTIVES

We presented here an extensive comparative investigation of the structural and dynamic features of the two major RND multidrug transporters in *P. aeruginosa*, MexB and



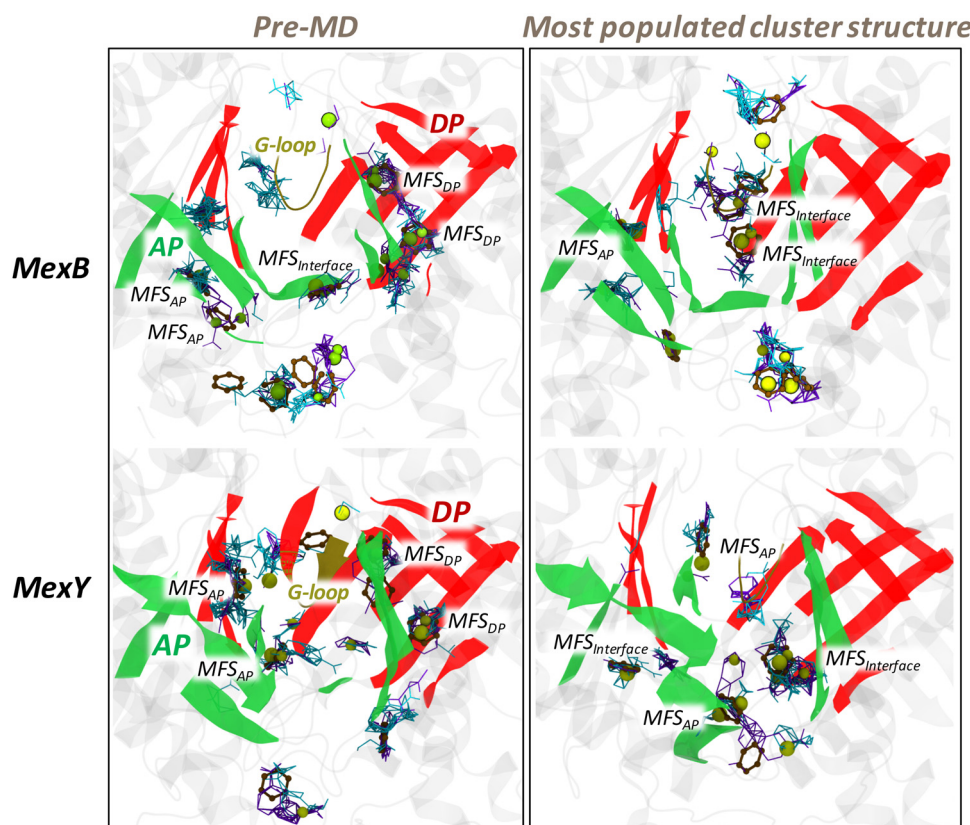


**FIGURE 9 |** The various MFSs identified in the AP<sub>L</sub> and DP<sub>T</sub> of MexB and MexY. The binding modes of the different probes are shown as lines for hydrogen-bond donor (cyan) and hydrogen-bond acceptor (violet), as beads for aliphatic (yellow), and as CPK for aromatic (ochre) ligands. The AP and DP are marked in green and red, respectively, while the G-loop in yellow cartoon representations. (Note: The categorizing of MFSs here is arbitrary due to indistinct boundaries between the pockets. The sites not labeled as MFS here are all CSSs; for further details see section “Materials and Methods”).

MexY. To the best of our knowledge this is the first structure-based study of MexY and also the first thorough quantitative comparison of the main putative binding pockets of the two transporters. We identified specific features of their multidrug binding pockets that partly explain the similarities and differences in their substrate selectivity profiles. Both proteins feature dispersed (mosaic-like) profiles of lipophilic and electrostatic surfaces within their access and deep binding pockets, which provide several multifunctional sites for diffuse binding of chemically dissimilar compounds. Several differences spotted in the molecular descriptors of the binding sites of MexB and MexY can be related to their different specificity profiles. Our results point out that the lesser conserved DP<sub>T</sub> could likely be the major substrate selection site in both proteins. In addition, the observed dynamics of the bottom-loop support our earlier hypothesis for Acr pumps of *E. coli* (Ramaswamy et al., 2017b) that their different dynamics contributes to the binding of substrates of different sizes. Collectively, our findings add a valuable piece to fill in the knowledge gap in molecular recognition and transport by bacterial RND transporters, an issue of importance in addressing antibiotic resistance.

## MATERIALS AND METHODS

The protocol followed in this study is the same as that we used in our previous work for Acr transporters of *E. coli* (Ramaswamy et al., 2017b).

### Homology Modeling of MexY

Since no experimental structure of MexY has been solved yet, we built a model of its asymmetric trimer structure by multiple template-based homology modeling using Modeler 9.13 (Šali and Blundell, 1993). The amino acid sequence of full length MexY transporter protein from *P. aeruginosa* PAO1 was retrieved from the UniProt database (The UniProt Consortium, 2015) (UNIPROT ID: Q9ZNG8), and subsequently searched for the best available template structures bearing homologous relationship to the query sequence using the NCBI-BLAST tool (Madden, 2013) against the Protein Data Bank (PDB)<sup>2</sup>. The high-resolution crystal structure of AcrB at 1.9 Å [PDB code 4DX5 (Eicher et al., 2012)] and MexB at 2.7 Å [PDB code 3W9I (Nakashima et al., 2013)] were chosen as templates for multiple-template based modeling of MexY. The protein

<sup>2</sup>www.rcsb.org

sequences were optimally aligned by ClustalOmega (Sievers et al., 2011) and the results were visually inspected to ensure the absence of gaps in important secondary structure regions. Modeler 9.13 (Šali and Blundell, 1993) was used to generate a total of 100 asymmetric models of MexY based on AcrB and MexB templates using an optimization method combining slow MD with very thorough variable target function method through 300 iterations, and this whole cycle was repeated twice unless the objective function MOLPDF was greater than  $10^6$ . The resulting models were ranked using discrete optimized protein energy (DOPE) (Shen and Sali, 2006) score values, and the top 5 models (with the lowest DOPE score) were selected for individual structure quality checks. Each model was further subjected to loop refinement using Modeler, and to overall structure relaxation by energy minimizations using AMBER14 (Case et al., 2014). The most reliable model was then selected based on various geometric and stereochemical quality factors evaluated for backbone angles, side chains flips, rotamers, steric clashes etc. using PROCHECK (Laskowski et al., 1993), ERRAT (Colovos and Yeates, 1993), ProSA (Wiederstein and Sippl, 2007), Verify3D (Eisenberg et al., 1997) programs available in MolProbity (Chen et al., 2010) and Structure Analysis and Verification Server<sup>3</sup>.

We performed comparative structural evaluation by superimposition of the modeled MexY structures over experimentally determined X-ray crystal structures of AcrB and MexB used as templates. Likewise, the template structures were also evaluated with the same programs to serve as reference for the results obtained for the MexY models. Visual inspections were performed with VMD1.9.1 (Humphrey et al., 1996) and PyMOL (Schrödinger, 2015).

## Molecular Dynamics Simulations of MexB and MexY

Molecular dynamics simulations of the crystal structure of MexB (PDB code 3W9I) and of the most reliable homology model of MexY were carried out using the AMBER14 (Case et al., 2014) program. Protomer specific protonation states (Eicher et al., 2014) were adopted with E346 (E345) and D923 (D919) protonated in both *Loose* and *Tight* protomers while deprotonated in the *Open* protomer of MexB (MexY). The residues D407 (D406), D408 (D407), D566 (E563) were protonated only in the *Open* protomer of MexB (MexY). The proteins were successively embedded in 1-palmitoyl-2-oleoyl-sn-glycero-3-phosphoethanolamine (POPE) bilayer patches, solvated with explicit TIP3P water model. The residual charge of the systems was neutralized by appropriate numbers of randomly placed  $K^+/Cl^-$  ions (Schulz et al., 2010, 2011, 2015; Vargiu et al., 2011). The ions count was suitably adjusted to account for an osmolarity of 0.15 M KCl. Embedding of the protein into a pre-equilibrated POPE bilayer patch was done using the PPM server (Lomize et al., 2012) and subsequently the CharmmGUI tool (Jo et al., 2008). The lipid residue nomenclature was converted from the CHARMM to AMBER format using the *charmm2lipid2amber.py* python script

provided with AmberTools. The central pore lipids were added after calculating the number of lipids to be added to each leaflet by dividing the approximate area of the central pore by the standard area per lipid of POPE molecules (Dickson et al., 2014). The topology and the initial coordinate files were created using the *LEaP* module of AmberTools14. Periodic boundary conditions were used and the distance between the protein and the edge of the box was set to be at least 30 Å in each direction.

Multi-step energy minimization with a combination of steepest descent and conjugate gradient methods was carried out using the *pmemd* program implemented in AMBER14 to relax internal constraints of the systems by gradually releasing positional restraints. Following this, the systems were heated from 0 to 310 K by a 1 ns heating (0–100 K) under constant volume (NVT) followed by 5 ns of constant pressure heating (NPT) (100–310 K) with the phosphorous heads of lipids restrained along the z-axis to allow membrane merging and to bring the atmospheric pressure of the system to 1 bar. Langevin thermostat (collision frequency of  $1\text{ ps}^{-1}$ ) was used to maintain a constant temperature, and multiple short equilibration steps of 500 ps under anisotropic pressure scaling (Berendsen barostat) in NPT conditions were performed to equilibrate the box dimensions. A time step of 2 fs was used during all these runs, while post-equilibrium MD simulations were performed with a time step of 4 fs under constant volume conditions after hydrogen mass repartitioning (Hopkins et al., 2015). The particle-mesh Ewald (PME) algorithm was used to evaluate long-range electrostatic forces with a non-bonded cutoff of 9 Å. During the MD simulations, the length of all R-H bonds was constrained with SHAKE algorithm. Coordinates were saved every 100 ps. The ff14SB (Maier et al., 2015) version of the all-atom Amber force field was used to represent the protein systems while lipid14 (Dickson et al., 2014) parameters were used for the POPE bilayer. After equilibration, multi-copy  $\mu\text{s}$ -long MD simulations were performed for each system, namely four  $\sim 1\text{ }\mu\text{s}$ -long production simulations for each transporter (for a total simulation time of  $\sim 8\text{ }\mu\text{s}$ ). Trajectory analysis was done using *cptraj* module of AmberTools14 and VMD1.9.1, and graphs were plotted using the *xmgrace* tool.

## Principal Component Analysis

To characterize and highlight possible similarities and differences in the collective motions of the binding pockets, we calculated the covariance matrices from the equilibrium trajectory and performed a PCA (García, 1992; Daidone and Amadei, 2012). As customary in PCA analysis, the covariance matrix was constructed taking the three-dimensional positional fluctuations of C $\alpha$  atoms from their ensemble average position (after least-squares fitting to remove rotational and translational motion). Diagonalization of the covariance matrix yields a set of eigenvectors and corresponding eigenvalues, which represent the direction and amplitude of the motion, respectively. The eigenvectors are then ranked according to the decreasing order of their associated eigenvalues, such that the first eigenvector represents the largest contribution to the total fluctuation of the system. To visualize the motions represented by the eigenvectors,

<sup>3</sup><http://services.mbi.ucla.edu/SAVES/>

the structures from the trajectories can be projected onto each eigenvector of interest [principal component (PC)] and transformed back into Cartesian coordinates. The two extreme projections along each eigenvector can then be interpolated to create an animation or compared to understand which parts of the protein are moving according to that specific eigenvector and to what extent. Usually (a combination of), the first few principal components are able to represent most of the collective motions [the “essential dynamics” (Daidone and Amadei, 2012)] occurring in an MD simulation among the different regions of a protein.

## Clustering of MD Trajectories

A cluster analysis of the MD trajectories was performed using the average-linkage hierarchical agglomerative clustering method implemented in *cptraj* module of AMBER. Such clustering helps to reduce the number of structures for analysis yet retaining the large conformational space sampled during the MD runs. In this approach, we clustered in two separate instances the trajectory based on root mean square deviation (RMSD) (cutoff set to 3 Å) of the AP in *L* protomer and of the DP in *T* protomer. For each protein, the representative structures from each of the 10 top clusters generated in each of the two cases considered (AP in *L*, DP in *T*) were used to perform quantitative analyses in order to account for dynamical behavior. All non-protein molecules were stripped from the trajectory during post-processing to reduce additional memory usage and to speed up file processing.

## Pocket Descriptors

The list of the pocket descriptors identified for the present study includes: (i) cavity volume; (ii) molecular lipophilicity potential; (iii) electrostatic potential; (iv) site hydration; and (v) fragment-based binding site characterization. The various pocket descriptors used to characterize the binding site were calculated using specific programs after validating their applicability to RND systems by assessing results against available crystal structures and experimental data, as well as previous computational reports (Imai et al., 2011; Schulz et al., 2011; Vargiu et al., 2011, 2014; Vargiu and Nikaido, 2012; Fischer and Kandt, 2013; Ramaswamy et al., 2017b).

## Cavity Volume

Evolution of size and shape of the AP and DP during MD simulations was examined using the two-probe sphere method of *rbccavity* program bundled in the rDock suite (Ruiz-Carmona et al., 2014). This allows obtaining detailed information on the pocket volume and plasticity of the site. In this method, the binding site volume was identified by a fast grid-based cavity detection algorithm (Morley and Afshar, 2004) within a sphere of radius 13 Å for AP<sub>L</sub> and 14 Å for DP<sub>T</sub>, centered over the pockets, using large and small probe radii of 6.0 and 1.5 Å, respectively. These radii were found to be optimal for our case after evaluating different combinations and checking through visual inspection their accuracy in predicting volume of the pocket space by keeping the possible inclusion of regions extending outside the pocket of interest at its least.

## Molecular Lipophilicity Potential

The three-dimensional distribution of lipophilicity in space or on a molecular surface can be described using molecular lipophilicity potential (MLP), which represents the influence of all lipophilic fragmental contributions of a molecule on its environment. The MLP value of a point in space (*k*) is generated as the result of intermolecular interactions between all fragments in the molecule and the solvent system, at that given point. Thus, MLP can be calculated from the fragmental system of logP and a distance function as shown in the following equation (Gaillard et al., 1994):

$$MLP_k = \sum_{i=1}^N F_i \cdot f(d_{ik})$$

where *N* is the number of fragments, *F<sub>i</sub>* is the lipophilic contribution of fragment *i* of the molecule and *f(d<sub>ik</sub>)* is a function based on the distance of the measured point in space *k* to fragment *i*.

In this way, summing up all positive and all negative MLP values associated to each point on the binding pocket yields the lipophilic index (LI) as:

$$LI = \frac{\sum MLP^+}{\sum MLP^+ + |\sum MLP^-|} \cdot 100$$

The lipophilicity of AP in *L* protomer and of DP in *T* protomer were qualitatively and quantitatively estimated in this way using MLP Tools (Oberhauser et al., 2014) plugin available for PyMOL.

## Electrostatic Potential

The electrostatic potential surface maps were computed by APBS (Baker et al., 2001), after pre-processing structures of MexB and MexY to assign charges and atomic radii using the PDB2PQR server (Dolinsky et al., 2004). All electrostatic potential calculations were performed at 0.15 M physiological salt concentration, with a solvent probe of radius 1.4 Å, a solvent dielectric constant of 78.5, a biomolecular dielectric constant of 2.0, a temperature of 310 K, a minimum grid spacing of 0.5 Å and keeping the other Poisson–Boltzmann parameters at default.

## Hydration Analysis

The RDF indicates the probability of finding water molecules at a certain distance from a region or residue of interest and is commonly used to analyse the solution structure revealed from either experimental or computer simulations data.

The RDF analysis of water oxygen atoms was performed using *cptraj* module of AMBER14, in which the RDF is computed from the histogram of the number of solvent particles found as a function of the distance *R* from an (ensemble of) atom(s), normalized by the expected number of solvent particles at that distance in bulk. The normalization is estimated from:

$$Density^* \left( \left[ \frac{4\pi}{3} (R + dR)^3 \right] - \left[ \frac{4\pi}{3} dR^3 \right] \right)$$

where *dR* is equal to the bin spacing, the default *density* value is 0.033456 molecules Å<sup>-3</sup>, which corresponds to density of water approximately equal to 1.0 g mL<sup>-1</sup>. Bin spacing of 0.1 and



a maximum bin value of 4.0 was used in this case to calculate the RDF of all water oxygen atoms to each atom of AP in *L* protomer and of DP in *T* protomer over the entire length of the simulation.

Though RDF clearly shows a difference in the water distribution around the desired regions, it lacks the ability to present the information about the spatial positions of these differences. Hence, SDF of waters around the whole protein was calculated using the Gromacs utility *g\_spatial* (Abraham et al., 2015) on the trajectory frames grouped into the most populated conformational clusters extracted from MD simulations. SDF allows determining the three-dimensional density distribution of aqueous solution around the binding pockets of the transporters. RDF and SDF together highlight the hydration around the binding pockets of these proteins, which can be effectively used to understand the molecular mechanism of interaction of water molecules penetrating the pocket in a dynamic manner.

### Fragment-Based Binding Site Characterization

The FTMap server (Kozakov et al., 2015) implementing the FTSite algorithm is a tool helpful in the identification of binding sites and of the fragments that could be possible source of structure- and fragment-based drug design attempts. The main aim of such fragment-based binding site analysis is to obtain a measure of the ability of the protein (and in particular the pockets under study) to bind a drug-like molecule.

FTMap identifies the important hot spots based on the consensus clusters of 16 standard probes which include molecules varying in size, shape and polarity (Supplementary Figure 8). Such a diverse library of probes is useful to capture a range of interaction types that include hydrophilic, hydrophobic, hydrogen-bonding and aromatic interactions. The regions where clusters of different probes of the same or different type overlap are marked as CSs and MFSSs, respectively, and are ranked based

on the number of their clusters. Clusters in close proximity to a top ranked cluster are merged with it and the protein residues within this region become the top ranked putative ligand binding site.

## AUTHOR CONTRIBUTIONS

VR performed homology modeling, MD simulations and analysis. VR, AV, GM, and PR analyzed the results. VR, AV, GM, JD, and PR designed the experiments, discussed the results, and wrote the manuscript. All authors contributed to manuscript revision, read and approved the submitted version.

## FUNDING

The research leading to the results discussed here was partly conducted as part of the Translocation Consortium (<http://www.translocation.eu>) and has received support from the Innovative Medicines Initiative Joint Undertaking under Grant Agreement No. 115525, resources that are composed of financial contribution from the European Union's Seventh Framework Programme (FP7/2007-2013) and EFPIA companies in kind contribution. VR is a Marie Skłodowska-Curie fellow within the "Translocation" Network, project No. 607694.

## SUPPLEMENTARY MATERIAL

The Supplementary Material for this article can be found online at: <https://www.frontiersin.org/articles/10.3389/fmicb.2018.01144/full#supplementary-material>

## REFERENCES

- Abraham, M. J., Murtola, T., Schulz, R., Páll, S., Smith, J. C., Hess, B., et al. (2015). GROMACS: high performance molecular simulations through multi-level parallelism from laptops to supercomputers. *SoftwareX* 1–2, 19–25. doi: 10.1016/j.softx.2015.06.001
- Aires, J. R., Köhler, T., Nikaido, H., and Plésiat, P. (1999). Involvement of an active efflux system in the natural resistance of *Pseudomonas aeruginosa* to aminoglycosides. *Antimicrob. Agents Chemother.* 43, 2624–2628.
- Baker, N. A., Sept, D., Joseph, S., Holst, M. J., and McCammon, J. A. (2001). Electrostatics of nanosystems: application to microtubules and the ribosome. *Proc. Natl. Acad. Sci. U.S.A.* 98, 10037–10041. doi: 10.1073/pnas.181342398
- Blair, J. M., Bavro, V. N., Ricci, V., Modi, N., Cacciottolo, P., Kleinekathöfer, U., et al. (2015). AcrB drug-binding pocket substitution confers clinically relevant resistance and altered substrate specificity. *Proc. Natl. Acad. Sci. U.S.A.* 112, 3511–3516. doi: 10.1073/pnas.1419939112
- Blair, J. M., Richmond, G. E., and Piddock, L. J. (2014). Multidrug efflux pumps in Gram-negative bacteria and their role in antibiotic resistance. *Future Microbiol.* 9, 1165–1177. doi: 10.2217/fmb.14.66
- Bohnert, J. A., Schuster, S., Seeger, M. A., Fähnrich, E., Pos, K. M., and Kern, W. V. (2008). Site-directed mutagenesis reveals putative substrate binding residues in the *Escherichia coli* RND efflux pump AcrB. *J. Bacteriol.* 190, 8225–8229. doi: 10.1128/JB.00912-08
- Case, D., Babin, V., Berryman, J., Betz, R., Cai, Q., Cerutti, D., et al. (2014). Data for molecular dynamics simulations of B-type cytochrome c oxidase with the Amber force field. *Data Brief* 8, 1209–1214. doi: 10.1016/j.dib.2016.07.043
- Chen, V. B., Arendall, W. B., Headd, J. J., Keedy, D. A., Immormino, R. M., Kapral, G. J., et al. (2010). MolProbity: all-atom structure validation for macromolecular crystallography. *Acta Crystallogr. D Biol. Crystallogr.* 66, 12–21. doi: 10.1107/S0907444909042073
- Chuanchnen, R., Beinlich, K., Hoang, T. T., Becher, A., Karkhoff-Schweizer, R. R., and Schweizer, H. P. (2001). Cross-resistance between triclosan and antibiotics in *Pseudomonas aeruginosa* is mediated by multidrug efflux pumps: exposure of a susceptible mutant strain to triclosan selects nfxB mutants overexpressing MexCD-OprJ. *Antimicrob. Agents Chemother.* 45, 428–432. doi: 10.1128/AAC.45.2.428-432.2001
- Ciulli, A., Williams, G., Smith, A. G., Blundell, T. L., and Abell, C. (2006). Probing hot spots at protein-ligand binding sites: a fragment-based approach using biophysical methods. *J. Med. Chem.* 49, 4992–5000. doi: 10.1021/jm060490r
- Collu, F., Vargiu, A. V., Dreier, J., Cascella, M., and Ruggerone, P. (2012). Recognition of imipenem and meropenem by the RND-transporter MexB studied by computer simulations. *J. Am. Chem. Soc.* 134, 19146–19158. doi: 10.1021/ja307803m
- Colovos, C., and Yeates, T. (1993). Verification of protein structures: patterns of nonbonded atomic interactions. *Protein Sci.* 2, 1511–1519. doi: 10.1002/pro.5560020916
- Daidone, I., and Amadei, A. (2012). Essential dynamics: foundation and applications. *Wiley Interdiscip. Rev. Comput. Mol. Sci.* 2, 762–770. doi: 10.1002/wcms.1099
- Delmar, J. A., Su, C.-C., and Edward, W. Y. (2014). Bacterial multi-drug efflux transporters. *Annu. Rev. Biophys.* 43, 93–117. doi: 10.1146/annurev-biophys-051013-022855

- Dickson, C. J., Madej, B. D., Skjevik, Å.A., Betz, R. M., Teigen, K., Gould, I. R., et al. (2014). Lipid14: the amber lipid force field. *J. Chem. Theory Comput.* 10, 865–879. doi: 10.1021/ct4010307
- Dolinsky, T. J., Nielsen, J. E., McCammon, J. A., and Baker, N. A. (2004). PDB2PQR: an automated pipeline for the setup of Poisson–Boltzmann electrostatics calculations. *Nucleic Acids Res.* 32(Suppl. 2), W665–W667. doi: 10.1093/nar/gkh381
- Dreier, J., and Ruggerone, P. (2015). Interaction of antibacterial compounds with RND efflux pumps in *Pseudomonas aeruginosa*. *Front. Microbiol.* 6:660. doi: 10.3389/fmicb.2015.00660
- Eda, S., Maseda, H., and Nakae, T. (2003a). An elegant means of self-protection in gram-negative bacteria by recognizing and extruding xenobiotics from the periplasmic space. *J. Biol. Chem.* 278, 2085–2088. doi: 10.1074/jbc.C200661200
- Eda, S., Yoneyama, H., and Nakae, T. (2003b). Function of the MexB efflux-transporter divided into two halves. *Biochemistry* 42, 7238–7244. doi: 10.1021/bi0300074
- Edward, W. Y., Aires, J. R., and Nikaido, H. (2003). AcrB multidrug efflux pump of *Escherichia coli*: composite substrate-binding cavity of exceptional flexibility generates its extremely wide substrate specificity. *J. Bacteriol.* 185, 5657–5664. doi: 10.1128/JB.185.19.5657-5664.2003
- Eicher, T., Cha, H.-J., Seeger, M. A., Brandstätter, L., El-Delik, J., Bohnert, J. A., et al. (2012). Transport of drugs by the multidrug transporter AcrB involves an access and a deep binding pocket that are separated by a switch-loop. *Proc. Natl. Acad. Sci. U.S.A.* 109, 5687–5692. doi: 10.1073/pnas.1114944109
- Eicher, T., Seeger, M. A., Anselmi, C., Zhou, W., Brandstätter, L., Verrey, F., et al. (2014). Coupling of remote alternating-access transport mechanisms for protons and substrates in the multidrug efflux pump AcrB. *eLife* 3:e03145. doi: 10.7554/eLife.03145
- Eisenberg, D., Lüthy, R., and Bowie, J. U. (1997). VERIFY3D: assessment of protein models with three-dimensional profiles. *Methods Enzymol.* 277, 396–404. doi: 10.1016/S0076-6879(97)77022-8
- Elkins, C. A., and Nikaido, H. (2002). Substrate specificity of the RND-type multidrug efflux pumps AcrB and AcrD of *Escherichia coli* is determined predominately by two large periplasmic loops. *J. Bacteriol.* 184, 6490–6498. doi: 10.1128/JB.184.23.6490-6499.2002
- Fernández, L., and Hancock, R. E. (2012). Adaptive and mutational resistance: role of porins and efflux pumps in drug resistance. *Clin. Microbiol. Rev.* 25, 661–681. doi: 10.1128/CMR.00043-12
- Fischbach, M. A., and Walsh, C. T. (2009). Antibiotics for emerging pathogens. *Science* 325, 1089–1093. doi: 10.1126/science.1176667
- Fischer, N., and Kandt, C. (2013). Porter domain opening and closing motions in the multi-drug efflux transporter AcrB. *Biochim. Biophys. Acta* 1828, 632–641. doi: 10.1016/j.bbame.2012.10.016
- Gaillard, P., Carrupt, P.-A., Testa, B., and Boudon, A. (1994). Molecular lipophilicity potential, a tool in 3D QSAR: method and applications. *J. Comput. Aided Mol. Des.* 8, 83–96. doi: 10.1007/BF00119860
- García, A. E. (1992). Large-amplitude nonlinear motions in proteins. *Phys. Rev. Lett.* 68, 2696–2699. doi: 10.1103/PhysRevLett.68.2696
- Gotoh, N., Tsujimoto, H., Poole, K., Yamagishi, J., and Nishino, T. (1995). The outer membrane protein OprM of *Pseudomonas aeruginosa* is encoded by oprK of the mexA-mexB-oprK multidrug resistance operon. *Antimicrob. Agents Chemother.* 39, 2567–2569. doi: 10.1128/AAC.39.11.2567
- Hancock, R. E. (1998). Resistance mechanisms in *Pseudomonas aeruginosa* and other nonfermentative gram-negative bacteria. *Clin. Infect. Dis.* 27(Suppl. 1), S93–S99. doi: 10.1086/514909
- Hocquet, D., Vogne, C., El Garch, F., Vejux, A., Gotoh, N., Lee, A., et al. (2003). MexXY-OprM efflux pump is necessary for adaptive resistance of *Pseudomonas aeruginosa* to aminoglycosides. *Antimicrob. Agents Chemother.* 47, 1371–1375. doi: 10.1128/AAC.47.4.1371-1375.2003
- Hopkins, C. W., Le Grand, S., Walker, R. C., and Roitberg, A. E. (2015). Long-time-step molecular dynamics through hydrogen mass repartitioning. *J. Chem. Theory Comput.* 11, 1864–1874. doi: 10.1021/ct5010406
- Humphrey, W., Dalke, A., and Schulten, K. (1996). VMD: visual molecular dynamics. *J. Mol. Graph.* 14, 33–38. doi: 10.1016/0263-7855(96)00018-5
- Imai, T., Miyashita, N., Sugita, Y., Kovalenko, A., Hirata, F., and Kidera, A. (2011). Functionality mapping on internal surfaces of multidrug transporter AcrB based on molecular theory of solvation: implications for drug efflux pathway. *J. Phys. Chem. B* 115, 8288–8295. doi: 10.1021/jp2015758
- Iyer, R., Ferrari, A., Rijnbrand, R., and Erwin, A. L. (2015). A fluorescent microplate assay quantifies bacterial efflux and demonstrates two distinct compound binding sites in AcrB. *Antimicrob. Agents Chemother.* 59, 2388–2397. doi: 10.1128/AAC.05112-14
- Jo, S., Kim, T., Iyer, V. G., and Im, W. (2008). CHARMM-GUI: a web-based graphical user interface for CHARMM. *J. Comput. Chem.* 29, 1859–1865. doi: 10.1002/jcc.20945
- Kinana, A. D., Vargiu, A. V., and Nikaido, H. (2016). Effect of site-directed mutations in multidrug efflux pump AcrB examined by quantitative efflux assays. *Biochem. Biophys. Res. Commun.* 480, 552–557. doi: 10.1016/j.bbrc.2016.10.083
- Kobayashi, N., Tamura, N., van Veen, H. W., Yamaguchi, A., and Murakami, S. (2014).  $\beta$ -Lactam selectivity of multidrug transporters AcrB and AcrD resides in the proximal binding pocket. *J. Biol. Chem.* 289, 10680–10690. doi: 10.1074/jbc.M114.547794
- Köhler, T., Kok, M., Michea-Hamzehpour, M., Plesiat, P., Gotoh, N., Nishino, T., et al. (1996). Multidrug efflux in intrinsic resistance to trimethoprim and sulfamethoxazole in *Pseudomonas aeruginosa*. *Antimicrob. Agents Chemother.* 40, 2288–2290.
- Kozakov, D., Grove, L. E., Hall, D. R., Bohnuud, T., Mottarella, S. E., Luo, L., et al. (2015). The FTMap family of web servers for determining and characterizing ligand-binding hot spots of proteins. *Nat. Protoc.* 10, 733–755. doi: 10.1038/nprot.2015.043
- Krahn, T., Gilmour, C., Tilak, J., Fraud, S., Kerr, N., Lau, C. H., et al. (2012). Determinants of intrinsic aminoglycoside resistance in *Pseudomonas aeruginosa*. *Antimicrob. Agents Chemother.* 56, 5591–5602. doi: 10.1128/AAC.01446-12
- Laskowski, R. A., MacArthur, M. W., Moss, D. S., and Thornton, J. M. (1993). PROCHECK: a program to check the stereochemical quality of protein structures. *J. Appl. Crystallogr.* 26, 283–291. doi: 10.1107/S0021889892009944
- Lau, C. H., Hughes, D., and Poole, K. (2014). MexY-promoted aminoglycoside resistance in *Pseudomonas aeruginosa*: involvement of a putative proximal binding pocket in aminoglycoside recognition. *mBio* 5:e01068. doi: 10.1128/mBio.01068-14
- Lee, A., Mao, W., Warren, M. S., Mistry, A., Hoshino, K., Okumura, R., et al. (2000). Interplay between efflux pumps may provide either additive or multiplicative effects on drug resistance. *J. Bacteriol.* 182, 3142–3150. doi: 10.1128/JB.182.11.3142-3150.2000
- Levy, Y., Onuchic, J. N., and Wolynes, P. G. (2007). Fly-casting in protein-DNA binding: frustration between protein folding and electrostatics facilitates target recognition. *J. Am. Chem. Soc.* 129, 738–739. doi: 10.1021/ja065531n
- Li, X.-Z., Nikaido, H., and Poole, K. (1995). Role of mexA-mexB-oprM in antibiotic efflux in *Pseudomonas aeruginosa*. *Antimicrob. Agents Chemother.* 39, 1948–1953. doi: 10.1128/AAC.39.9.1948
- Li, X.-Z., Plésiat, P., and Nikaido, H. (2015). The challenge of efflux-mediated antibiotic resistance in Gram-negative bacteria. *Clin. Microbiol. Rev.* 28, 337–418. doi: 10.1128/CMR.00117-14
- Lister, P. D., Wolter, D. J., and Hanson, N. D. (2009). Antibacterial-resistant *Pseudomonas aeruginosa*: clinical impact and complex regulation of chromosomally encoded resistance mechanisms. *Clin. Microbiol. Rev.* 22, 582–610. doi: 10.1128/CMR.00040-09
- Llanes, C., Hocquet, D., Vogne, C., Benali-Baitich, D., Neuwirth, C., and Plésiat, P. (2004). Clinical strains of *Pseudomonas aeruginosa* overproducing MexAB-OprM and MexXY efflux pumps simultaneously. *Antimicrob. Agents Chemother.* 48, 1797–1802. doi: 10.1128/AAC.48.5.1797-1802.2004
- Lomize, M. A., Pogozheva, I. D., Joo, H., Mosberg, H. I., and Lomize, A. L. (2012). OPM database and PPM web server: resources for positioning of proteins in membranes. *Nucleic Acids Res.* 40, D370–D376. doi: 10.1093/nar/gkr703
- Madden, T. (2013). “The BLAST sequence analysis tool,” in *The NCBI Handbook*, 2 Edn, eds M. Jo and O. Jim (Bethesda, MD: National Center for Biotechnology Information).
- Maier, J. A., Martinez, C., Kasavajhala, K., Wickstrom, L., Hauser, K. E., and Simmerling, C. (2015). ff14SB: improving the accuracy of protein side chain and backbone parameters from ff99SB. *J. Chem. Theory Comput.* 11, 3696–3713. doi: 10.1021/acs.jctc.5b00255
- Mallocci, G., Vargiu, A. V., Serra, G., Bosin, A., Ruggerone, P., and Ceccarelli, M. (2015). A database of force-field parameters, dynamics, and properties



- of antimicrobial compounds. *Molecules* 20, 13997–14021. doi: 10.3390/molecules200813997
- Marsh, L. (2015). Strong ligand-protein interactions derived from diffuse ligand interactions with loose binding sites. *Biomed Res. Int.* 2015:746980. doi: 10.1155/2015/746980
- Masuda, N., Sakagawa, E., Ohya, S., Gotoh, N., Tsujimoto, H., and Nishino, T. (2000a). Contribution of the MexX-MexY-OprM efflux system to intrinsic resistance in *Pseudomonas aeruginosa*. *Antimicrob. Agents Chemother.* 44, 2242–2246. doi: 10.1128/AAC.44.9.2242-2246.2000
- Masuda, N., Sakagawa, E., Ohya, S., Gotoh, N., Tsujimoto, H., and Nishino, T. (2000b). Substrate specificities of MexAB-OprM, MexCD-OprJ, and MexXY-oprM efflux pumps in *Pseudomonas aeruginosa*. *Antimicrob. Agents Chemother.* 44, 3322–3327. doi: 10.1128/AAC.44.12.3322-3327.2000
- Matsunaga, Y., Yamane, T., Terada, T., Moritsugu, K., Fujisaki, H., Murakami, S., et al. (2018). Energetics and conformational pathways of functional rotation in the multidrug transporter AcrB. *Elife* 7:e31715. doi: 10.7554/eLife.31715
- Mesaros, N., Nordmann, P., Plésiat, P., Roussel-Delvallez, M., Van Eldere, J., Glupczynski, Y., et al. (2007). *Pseudomonas aeruginosa*: resistance and therapeutic options at the turn of the new millennium. *Clin. Microbiol. Infect.* 13, 560–578. doi: 10.1111/j.1469-0691.2007.01681.x
- Middlemiss, J. K., and Poole, K. (2004). Differential impact of MexB mutations on substrate selectivity of the MexAB-OprM multidrug efflux pump of *Pseudomonas aeruginosa*. *J. Bacteriol.* 186, 1258–1269. doi: 10.1128/JB.186.5.1258-1269.2004
- Mine, T., Morita, Y., Kataoka, A., Mizushima, T., and Tsuchiya, T. (1999). Expression in *Escherichia coli* of a new multidrug efflux pump, MexXY, from *Pseudomonas aeruginosa*. *Antimicrob. Agents Chemother.* 43, 415–417.
- Morley, S. D., and Afshar, M. (2004). Validation of an empirical RNA-ligand scoring function for fast flexible docking using RiboDock®. *J. Comput. Aided Mol. Des.* 18, 189–208. doi: 10.1023/B:JCAM.0000035199.48747.1e
- Murakami, S., Nakashima, R., Yamashita, E., Matsumoto, T., and Yamaguchi, A. (2006). Crystal structures of a multidrug transporter reveal a functionally rotating mechanism. *Nature* 443, 173–179. doi: 10.1038/nature05076
- Murata, T., Kuwagaki, M., Shin, T., Gotoh, N., and Nishino, T. (2002). The substrate specificity of tripartite efflux systems of *Pseudomonas aeruginosa* is determined by the RND component. *Biochem. Biophys. Res. Commun.* 299, 247–251. doi: 10.1016/S0006-291X(02)02626-8
- Nakashima, R., Sakurai, K., Yamasaki, S., Hayashi, K., Nagata, C., Hoshino, K., et al. (2013). Structural basis for the inhibition of bacterial multidrug exporters. *Nature* 500, 102–106. doi: 10.1038/nature12300
- Nakashima, R., Sakurai, K., Yamasaki, S., Nishino, K., and Yamaguchi, A. (2011). Structures of the multidrug exporter AcrB reveal a proximal multisite drug-binding pocket. *Nature* 480, 565–569. doi: 10.1038/nature10641
- Nikaido, H., and Takatsuka, Y. (2009). Mechanisms of RND multidrug efflux pumps. *Biochim. Biophys. Acta* 1794, 769–781. doi: 10.1016/j.bbapap.2008.10.004
- Oberhauser, N., Nurisso, A., and Carrupt, P.-A. (2014). MLP Tools: a PyMOL plugin for using the molecular lipophilicity potential in computer-aided drug design. *J. Comput. Aided Mol. Des.* 28, 587–596. doi: 10.1007/s10822-014-9744-0
- Okamoto, K., Gotoh, N., and Nishino, T. (2001). *Pseudomonas aeruginosa* reveals high intrinsic resistance to penem antibiotics: penem resistance mechanisms and their interplay. *Antimicrob. Agents Chemother.* 45, 1964–1971. doi: 10.1128/AAC.45.7.1964-1971.2001
- Opperman, T. J., and Nguyen, S. T. (2015). Recent advances toward a molecular mechanism of efflux pump inhibition. *Front. Microbiol.* 6:421. doi: 10.3389/fmicb.2015.00421
- Poole, K. (2001). Multidrug efflux pumps and antimicrobial resistance in *Pseudomonas aeruginosa* and related organisms. *J. Mol. Microbiol. Biotechnol.* 3, 255–264.
- Poole, K. (2005). Efflux-mediated antimicrobial resistance. *J. Antimicrob. Chemother.* 56, 20–51. doi: 10.1093/jac/dki171
- Poole, K. (2011). *Pseudomonas aeruginosa*: resistance to the Max. *Front. Microbiol.* 2:65. doi: 10.3389/fmicb.2011.00065
- Poole, K., Krebs, K., McNally, C., and Neshat, S. (1993). Multiple antibiotic resistance in *Pseudomonas aeruginosa*: evidence for involvement of an efflux operon. *J. Bacteriol.* 175, 7363–7372. doi: 10.1128/jb.175.22.7363-7372.1993
- Poole, K., and Srikumar, R. (2001). Multidrug efflux in *Pseudomonas aeruginosa* components, mechanisms and clinical significance. *Curr. Top. Med. Chem.* 1, 59–71. doi: 10.2174/1568026013395605
- Pos, K. M. (2009). Drug transport mechanism of the AcrB efflux pump. *Biochim. Biophys. Acta* 1794, 782–793. doi: 10.1016/j.bbapap.2008.12.015
- Ramaswamy, V. K., Caccioto, P., Mallocci, G., Ruggerone, P., and Vargiu, A. V. (2016). “Multidrug efflux pumps and their inhibitors characterized by computational modeling,” in *Efflux-Mediated Antimicrobial Resistance in Bacteria: Mechanisms, Regulation and Clinical Implications*, eds X.-Z. Li, C. A. Elkins, and H. I. Zgurskaya (Cham: Springer), 797–831. doi: 10.1007/978-3-319-39658-3\_30
- Ramaswamy, V. K., Caccioto, P., Mallocci, G., Vargiu, A. V., and Ruggerone, P. (2017a). Computational modelling of efflux pumps and their inhibitors. *Essays Biochem.* 61, 141–156. doi: 10.1042/EBC20160065
- Ramaswamy, V. K., Vargiu, A. V., Mallocci, G., Dreier, J., and Ruggerone, P. (2017b). Molecular rationale behind the differential substrate specificity of bacterial RND multi-drug transporters. *Sci. Rep.* 7:8075. doi: 10.1038/s41598-017-08747-8
- Ruggerone, P., Murakami, S., Pos, K. M., and Vargiu, A. V. (2013). RND efflux pumps: structural information translated into function and inhibition mechanisms. *Curr. Top. Med. Chem.* 13, 3079–3100. doi: 10.2174/15680266113136660220
- Ruiz-Carmona, S., Alvarez-Garcia, D., Foloppe, N., Garmendia-Doval, A. B., Juhos, S., Schmidtke, P., et al. (2014). rDock: a fast, versatile and open source program for docking ligands to proteins and nucleic acids. *PLoS Comput. Biol.* 10:e1003571. doi: 10.1371/journal.pcbi.1003571
- Šali, A., and Blundell, T. L. (1993). Comparative protein modelling by satisfaction of spatial restraints. *J. Mol. Biol.* 234, 779–815. doi: 10.1006/jmbi.1993.1626
- Schrödinger (2015). *The PyMOL Molecular Graphics System, Version 1.5 LLC*. New York, NY: Schrödinger.
- Schulz, R., Vargiu, A. V., Collu, F., Kleinekathöfer, U., and Ruggerone, P. (2010). Functional rotation of the transporter AcrB: insights into drug extrusion from simulations. *PLoS Comput. Biol.* 6:e1000806. doi: 10.1371/journal.pcbi.1000806
- Schulz, R., Vargiu, A. V., Ruggerone, P., and Kleinekathöfer, U. (2015). Computational study of correlated domain motions in the AcrB efflux transporter. *Biomed Res. Int.* 2015:487298. doi: 10.1155/2015/487298
- Schulz, R., Vargiu, A. V., Ruggerone, P., and Kleinekathöfer, U. (2011). Role of water during the extrusion of substrates by the efflux transporter AcrB. *J. Phys. Chem. B* 115, 8278–8287. doi: 10.1021/jp200996x
- Schuster, S., Vavra, M., and Kern, W. V. (2016). Evidence of a substrate discriminating entrance channel in the lower porter domain of the multidrug resistance efflux pump AcrB. *Antimicrob. Agents Chemother.* 60, 4315–4323. doi: 10.1128/AAC.00314-16
- Seeger, M. A., Schiefner, A., Eicher, T., Verrey, F., Diederichs, K., and Pos, K. M. (2006). Structural asymmetry of AcrB trimer suggests a peristaltic pump mechanism. *Science* 313, 1295–1298. doi: 10.1126/science.1131542
- Selzer, T., Albeck, S., and Schreiber, G. (2000). Rational design of faster associating and tighter binding protein complexes. *Nat. Struct. Mol. Biol.* 7, 537–541. doi: 10.1038/76744
- Sennhauser, G., Amstutz, P., Briand, C., Storchenegger, O., and Grütter, M. (2007). Drug export pathway of multidrug exporter AcrB revealed by DARPIn inhibitors. *PLoS Biol.* 5:e7. doi: 10.1371/journal.pbio.0050007
- Sennhauser, G., Bukowska, M. A., Briand, C., and Grütter, M. G. (2009). Crystal structure of the multidrug exporter MexB from *Pseudomonas aeruginosa*. *J. Mol. Biol.* 389, 134–145. doi: 10.1016/j.jmb.2009.04.001
- Shen, M.-Y., and Sali, A. (2006). Statistical potential for assessment and prediction of protein structures. *Protein Sci.* 15, 2507–2524. doi: 10.1110/ps.062416606
- Sievers, F., Wilm, A., Dineen, D., Gibson, T. J., Karplus, K., Li, W., et al. (2011). Fast, scalable generation of high-quality protein multiple sequence alignments using Clustal Omega. *Mol. Syst. Biol.* 7:539. doi: 10.1038/msb.2011.75
- Sjuts, H., Vargiu, A. V., Kwasny, S. M., Nguyen, S. T., Kim, H.-S., Ding, X., et al. (2016). Molecular basis for inhibition of AcrB multidrug efflux pump by novel and powerful pyranopyridine derivatives. *Proc. Natl. Acad. Sci. U.S.A.* 113, 3509–3514. doi: 10.1073/pnas.1602472113
- Srikumar, R., Li, X.-Z., and Poole, K. (1997). Inner membrane efflux components are responsible for beta-lactam specificity of multidrug efflux pumps in *Pseudomonas aeruginosa*. *J. Bacteriol.* 179, 7875–7881. doi: 10.1128/jb.179.24.7875-7881.1997

- Sun, J., Deng, Z., and Yan, A. (2014). Bacterial multidrug efflux pumps: mechanisms, physiology and pharmacological exploitations. *Biochem. Biophys. Res. Commun.* 453, 254–267. doi: 10.1016/j.bbrc.2014.05.090
- Symmons, M. F., Marshall, R. L., and Bavro, V. N. (2015). Architecture and roles of periplasmic adaptor proteins in tripartite efflux assemblies. *Front. Microbiol.* 6:513. doi: 10.3389/fmicb.2015.00513
- The UniProt Consortium (2015). UniProt: a hub for protein information. *Nucleic Acids Res.* 43, D204–D212. doi: 10.1093/nar/gku989
- Tikhonova, E. B., Wang, Q., and Zgurskaya, H. I. (2002). Chimeric analysis of the multicomponent multidrug efflux transporters from gram-negative bacteria. *J. Bacteriol.* 184, 6499–6507. doi: 10.1128/JB.184.23.6499-6507.2002
- Vargiu, A. V., Collu, F., Schulz, R., Pos, K. M., Zacharias, M., Kleinekathöfer, U., et al. (2011). Effect of the F610A mutation on substrate extrusion in the AcrB transporter: explanation and rationale by molecular dynamics simulations. *J. Am. Chem. Soc.* 133, 10704–10707. doi: 10.1021/ja202666x
- Vargiu, A. V., and Nikaido, H. (2012). Multidrug binding properties of the AcrB efflux pump characterized by molecular dynamics simulations. *Proc. Natl. Acad. Sci. U.S.A.* 109, 20637–20642. doi: 10.1073/pnas.1218348109
- Vargiu, A. V., Ramaswamy, V. K., Malvacio, I., Mallocci, G., Kleinekathöfer, U., and Ruggerone, P. (2018). Water-mediated interactions enable smooth substrate transport in a bacterial efflux pump. *Biochim. Biophys. Acta* 1862, 836–845. doi: 10.1016/j.bbagen.2018.01.010
- Vargiu, A. V., Ruggerone, P., Opperman, T. J., Nguyen, S. T., and Nikaido, H. (2014). Molecular mechanism of MBX2319 inhibition of *Escherichia coli* AcrB multidrug efflux pump and comparison with other inhibitors. *Antimicrob. Agents Chemother.* 58, 6224–6234. doi: 10.1128/AAC.03283-14
- Wang, Z., Fan, G., Hryc, C. F., Blaza, J. N., Serysheva, I. I., Schmid, M. F., et al. (2017). An allosteric transport mechanism for the AcrAB-TolC multidrug efflux pump. *eLife* 6:e24905. doi: 10.7554/eLife.24905
- Webber, M., and Piddock, L. (2003). The importance of efflux pumps in bacterial antibiotic resistance. *J. Antimicrob. Chemother.* 51, 9–11. doi: 10.1093/jac/dkg050
- Wehmeier, C., Schuster, S., Fährnich, E., Kern, W. V., and Bohnert, J. A. (2009). Site-directed mutagenesis reveals amino acid residues in the *Escherichia coli* RND efflux pump AcrB that confer macrolide resistance. *Antimicrob. Agents Chemother.* 53, 329–330. doi: 10.1128/AAC.00921-08
- Westbrock-Wadman, S., Sherman, D. R., Hickey, M. J., Coulter, S. N., Zhu, Y. Q., Warrenner, P., et al. (1999). Characterization of a *Pseudomonas aeruginosa* efflux pump contributing to aminoglycoside impermeability. *Antimicrob. Agents Chemother.* 43, 2975–2983.
- Wiederstein, M., and Sippl, M. J. (2007). ProSA-web: interactive web service for the recognition of errors in three-dimensional structures of proteins. *Nucleic Acids Res.* 35(Suppl. 2), W407–W410. doi: 10.1093/nar/gkm290
- Yamaguchi, A., Nakashima, R., and Sakurai, K. (2015). Structural basis of RND-type multidrug exporters. *Front. Microbiol.* 6:327. doi: 10.3389/fmicb.2015.00327
- Yao, X.-Q., Kimura, N., Murakami, S., and Takada, S. (2013). Drug uptake pathways of multidrug transporter AcrB studied by molecular simulations and site-directed mutagenesis experiments. *J. Am. Chem. Soc.* 135, 7474–7485. doi: 10.1021/ja310548h
- Zechini, B., and Versace, I. (2009). Inhibitors of multidrug resistant efflux systems in bacteria. *Recent Pat. AntiInfect. Drug Discov.* 4, 37–50. doi: 10.2174/157489109787236256
- Zhao, Q., Li, X.-Z., Mistry, A., Srikumar, R., Zhang, L., Lomovskaya, O., et al. (1998). Influence of the TonB energy-coupling protein on efflux-mediated multidrug resistance in *Pseudomonas aeruginosa*. *Antimicrob. Agents Chemother.* 42, 2225–2231.
- Ziha-Zarif, I., Llanes, C., Köhler, T., Pechere, J.-C., and Plesiat, P. (1999). In vivo emergence of multidrug-resistant mutants of *Pseudomonas aeruginosa* overexpressing the active efflux system MexA-MexB-OprM. *Antimicrob. Agents Chemother.* 43, 287–291.
- Zuo, Z., Wang, B., Weng, J., and Wang, W. (2015). Stepwise substrate translocation mechanism revealed by free energy calculations of doxorubicin in the multidrug transporter AcrB. *Sci. Rep.* 5:13905. doi: 10.1038/srep13905
- Zuo, Z., Weng, J., and Wang, W. (2016). Insights into the inhibitory mechanism of D13-9001 to the multidrug transporter AcrB through molecular dynamics simulations. *J. Phys. Chem. B* 120, 2145–2154. doi: 10.1021/acs.jpcc.5b11942

**Conflict of Interest Statement:** The authors declare that the research was conducted in the absence of any commercial or financial relationships that could be construed as a potential conflict of interest.

Copyright © 2018 Ramaswamy, Vargiu, Mallocci, Dreier and Ruggerone. This is an open-access article distributed under the terms of the Creative Commons Attribution License (CC BY). The use, distribution or reproduction in other forums is permitted, provided the original author(s) and the copyright owner are credited and that the original publication in this journal is cited, in accordance with accepted academic practice. No use, distribution or reproduction is permitted which does not comply with these terms.



# Antibiotic Resistance Mediated by the MacB ABC Transporter Family: A Structural and Functional Perspective

Nicholas P. Greene<sup>1</sup>, Elise Kaplan<sup>1</sup>, Allister Crow<sup>2</sup> and Vassilis Koronakis<sup>1\*</sup>

<sup>1</sup> Department of Pathology, University of Cambridge, Cambridge, United Kingdom, <sup>2</sup> School of Life Sciences, University of Warwick, Coventry, United Kingdom

## OPEN ACCESS

### Edited by:

Vassily Bavro,  
University of Essex, United Kingdom

### Reviewed by:

Helen Zgurskaya,  
University of Oklahoma, United States  
Arthur Neuberger,  
University of Cambridge,  
United Kingdom  
Satoshi Murakami,  
Tokyo Institute of Technology, Japan

### \*Correspondence:

Vassilis Koronakis  
vk103@cam.ac.uk

### Specialty section:

This article was submitted to  
Antimicrobials, Resistance and  
Chemotherapy,  
a section of the journal  
Frontiers in Microbiology

**Received:** 01 March 2018

**Accepted:** 24 April 2018

**Published:** 28 May 2018

### Citation:

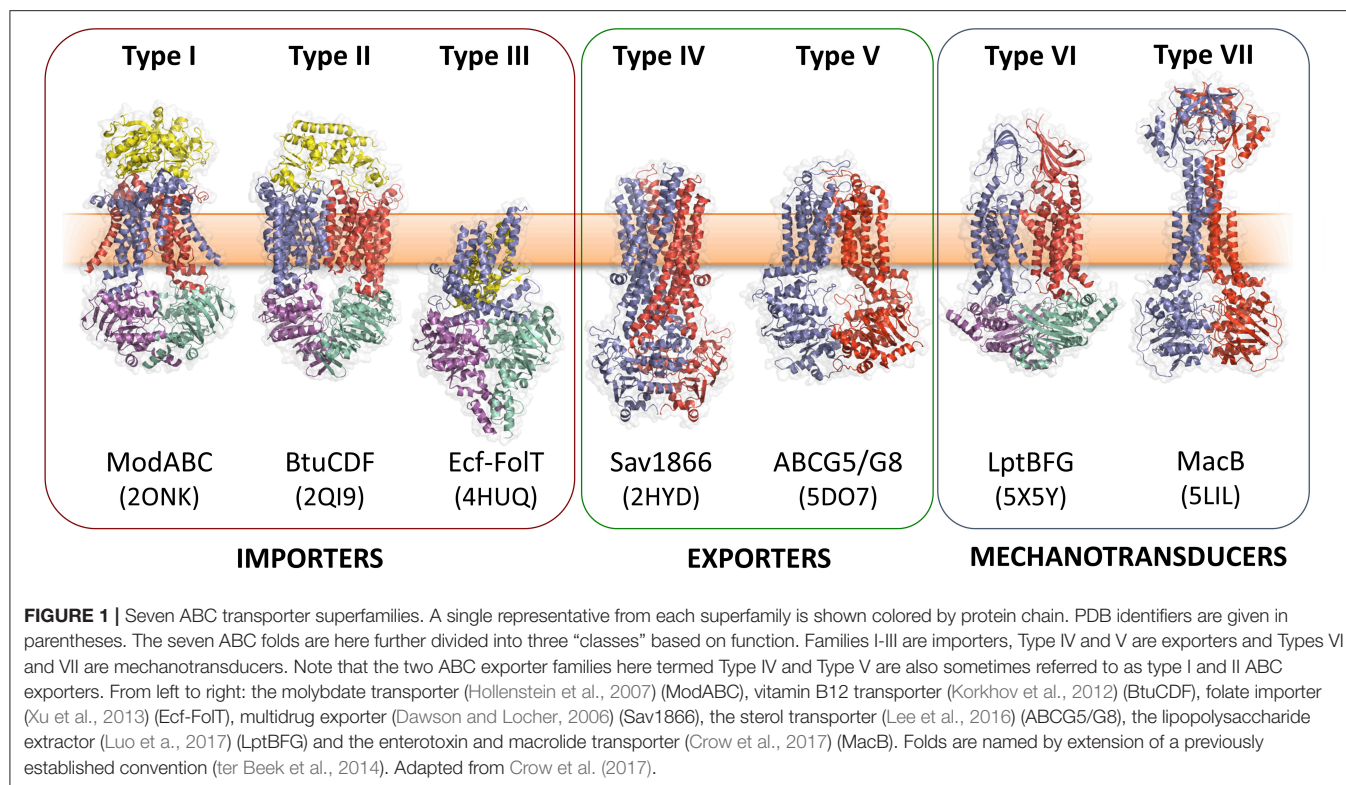
Greene NP, Kaplan E, Crow A and  
Koronakis V (2018) Antibiotic  
Resistance Mediated by the MacB  
ABC Transporter Family: A Structural  
and Functional Perspective.  
*Front. Microbiol.* 9:950.  
doi: 10.3389/fmicb.2018.00950

The MacB ABC transporter forms a tripartite efflux pump with the MacA adaptor protein and TolC outer membrane exit duct to expel antibiotics and export virulence factors from Gram-negative bacteria. Here, we review recent structural and functional data on MacB and its homologs. MacB has a fold that is distinct from other structurally characterized ABC transporters and uses a unique molecular mechanism termed mechanotransmission. Unlike other bacterial ABC transporters, MacB does not transport substrates across the inner membrane in which it is based, but instead couples cytoplasmic ATP hydrolysis with transmembrane conformational changes that are used to perform work in the extra-cytoplasmic space. In the MacAB-TolC tripartite pump, mechanotransmission drives efflux of antibiotics and export of a protein toxin from the periplasmic space via the TolC exit duct. Homologous tripartite systems from pathogenic bacteria similarly export protein-like signaling molecules, virulence factors and siderophores. In addition, many MacB-like ABC transporters do not form tripartite pumps, but instead operate in diverse cellular processes including antibiotic sensing, cell division and lipoprotein trafficking.

**Keywords:** antibiotic resistance, tripartite efflux pump, MacB, mechanotransmission, ABC transporter, lantibiotic, membrane protein, antimicrobial resistance

## INTRODUCTION

ABC (ATP-binding cassette) transporters are present in all three domains of life, and mediate transmembrane transport of a diverse array of substrates including drugs, sugars, ions, amino acids and proteins (ter Beek et al., 2014; Locher, 2016). All ABC transporters possess conserved nucleotide binding domains (NBDs) that facilitate power generation through ATP hydrolysis, and transmembrane domains (TMDs) that determine transporter function. The NBDs at the core of all ABC transporters are homologous, while the TMDs are structurally heterogeneous and proposed to have discrete evolutionary origins (Wang et al., 2009; ter Beek et al., 2014; Locher, 2016). Analysis of available ABC transporter crystal structures shows that there are at least seven structurally distinct ABC transporter folds, of which MacB is the most-recently determined representative (**Figure 1**). MacB is therefore the “holotype” for the Type VII ABC transporter superfamily (Crow et al., 2017), and the first structurally-characterized member of a clade of ABC transporters classified by Saier as the ABC3 superfamily (Wang et al., 2009).



ABC transporters with roles in antibiotic resistance are typically exporters, and operate by some variation of an alternating access mechanism (see below) (ter Beek et al., 2014; Locher, 2016). In bacteria, ABC exporters possess six transmembrane helices (TMHs) and operate as dimers. In eukaryotes, they typically exist as apparent fusions of two half transporters, that are otherwise structurally similar to their bacterial counterparts (Locher, 2016). Key examples of ABC exporters include Sav1866 from *Staphylococcus aureus* (Dawson and Locher, 2006), *Bacillus subtilis* LmrA (van Veen et al., 1996) and P-glycoprotein from humans (Aller et al., 2009).

Structures of ABC transporters in the presence and absence of ATP reveal different conformations which led to the proposal of an alternating access mechanism for transport (ter Beek et al., 2014; Locher, 2016). ATP-dependent conformational changes in the NBDs cause the TMDs to cycle between “inward open” and “outward open” states allowing substrate to be bound at one side of the membrane and released on the other. In the inward open state, the NBDs are parted and substrates can bind to a site at the interface of the TMDs, exposed to the cytoplasmic side of the membrane (Johnson and Chen, 2017). ATP binding promotes tight association of the NBDs and is communicated to the TMDs through a conserved coupling helix (Dawson and Locher, 2006). The resultant reorganization of the TMD results in an “outward-open” state with a reduced affinity for substrate allowing release on the distal side of the membrane (Ramachandra et al., 1998; Johnson and Chen, 2018). ATP hydrolysis then resets the transporter to an inward facing conformation. The stoichiometry of ATP hydrolysis per translocation event is unclear since

heterodimeric transporters with only one functional NBD are translocation competent (Zutz et al., 2011). Transport may be further aided by the transmembrane proton electrochemical gradient (Singh et al., 2016). Structures of occluded states, in which the binding site is not accessible to either side of the membrane, lack substrate but represent plausible intermediates on the pathway between inward and outward open states (Choudhury et al., 2014; Lin et al., 2015a; Bountra et al., 2017). Variations of the mechanism in which only the outward facing state takes part in transport have been proposed (Perez et al., 2015; Locher, 2016). Indeed, it has been suggested that the diverse structures and substrates of ABC transporters are incompatible with a single unified transport mechanism (Locher, 2016).

In Gram-positive bacteria, ABC transporters are widely used to expel xenobiotics (Lubelski et al., 2007). Antibiotic efflux by Gram-negative ABC transporters has been less well studied although expression of *Stenotrophomonas maltophilia* SmrA (Al-Hamad et al., 2009) or *Serratia marcescens* SmdAB (Matsuo et al., 2008), in hypersusceptible *E. coli*, provides resistance to multiple drugs including norfloxacin and tetracycline. Overexpression of *E. coli* MsbA confers resistance to multiple drugs in *E. coli* and *Lactococcus lactis* (Reuter et al., 2003; Woecking et al., 2005).

Most ABC exporters operate independently to transport substrates across the cytoplasmic membrane in which they are embedded. However, in Gram-negative bacteria specific ABC transporters can form part of tripartite efflux pumps, larger assemblies that span the entire cell envelope and mediate transport across the outer membrane.



## TRIPARTITE EFFLUX PUMPS (TEPs): BACTERIAL NANOMACHINES DRIVING ANTIBIOTIC EFFLUX

Gram-negative bacteria use tripartite efflux pumps that span both inner and outer membranes to export and efflux noxious molecules including antibiotics. They are a major determinant of multidrug resistance (Hinchliffe et al., 2013). The pumps consist of an outer membrane exit duct exemplified by *E. coli* TolC (Koronakis et al., 2000), a periplasmic adaptor protein and an inner membrane transporter. The periplasmic adaptors have a conserved, multi-domain, architecture consisting of membrane proximal (MP),  $\beta$ -barrel, lipoyl and hairpin domains, although some adaptors lack one of these domains (Greene et al., 2013; Hinchliffe et al., 2014). The energy-transducing inner membrane transporter comes from one of four distinct classes. The Resistance-Nodulation-Cell Division (RND) e.g., AcrB and Major Facilitator Superfamily (MFS) transporters e.g., EmrB both couple export to dissipation of the transmembrane electrochemical ion gradient. Conversely, ATP hydrolysis is used by two distinct ABC transporters, HlyB and MacB, that account for the third and fourth TEP types (Figure 2). In *E. coli*, all four TEP classes use one outer membrane efflux protein, TolC (Hinchliffe et al., 2013).

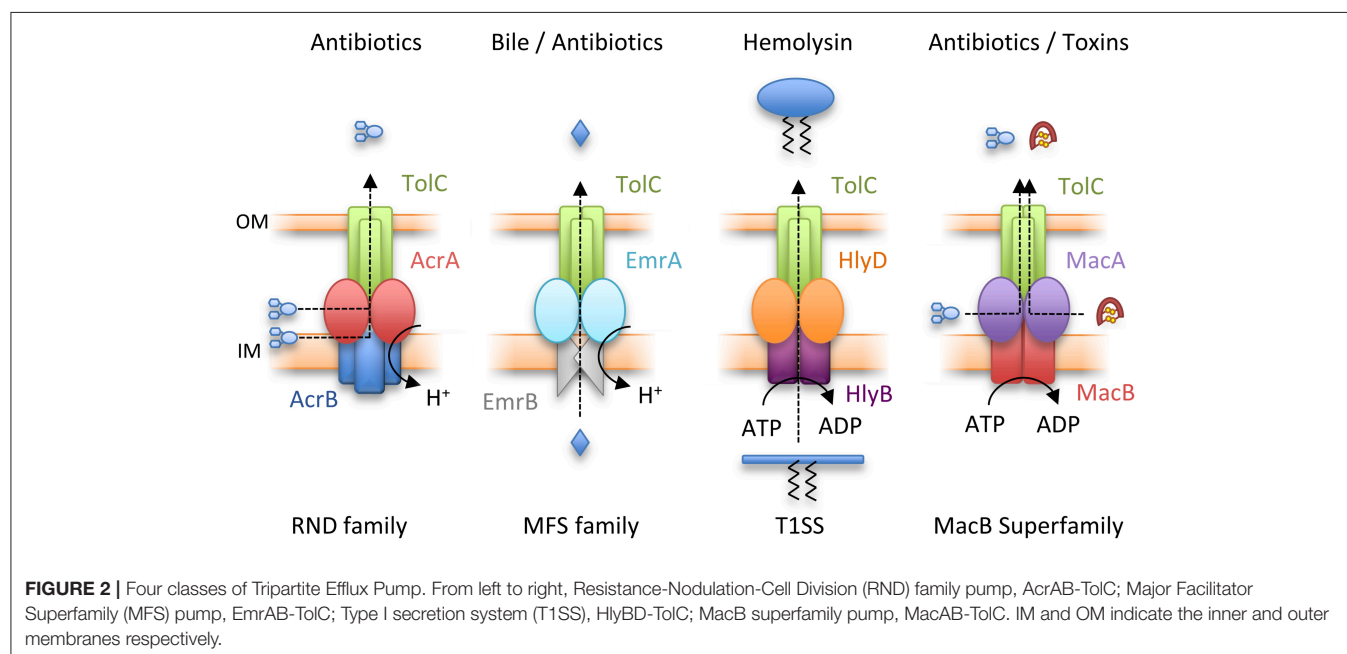
### The Different Classes of Transporter Powering TEPs

Structures of the best characterized RND inner membrane component, AcrB, were first determined over 15 years ago. AcrB functions as a homotrimer, with each monomer containing 12 TMHs and an extensive periplasmic domain projecting 70 Å into the periplasm (Murakami et al., 2002). Subsequent structures

revealed asymmetric AcrB trimers in which individual AcrB monomers adopted different conformational states (Murakami et al., 2006; Seeger et al., 2006). This led to the proposal of a transport mechanism in which each monomer cycles between open, loose and tight substrate-binding states to effect transport. The broad substrate specificity of AcrB is explained by multiple binding sites for drugs and entry routes from both the outer leaflet of the inner membrane and the periplasm (Nakashima et al., 2011; Eicher et al., 2012; Zwama et al., 2018). More recently, structures of the assembled AcrAB-TolC complex have been obtained using negative-stain and cryo-electron microscopy (cryo-EM) (Du et al., 2014; Daury et al., 2016; Wang et al., 2017).

MFS transporters associating with TEPs have been less well studied. In *E. coli*, the exemplar is EmrB which, with its cognate adaptor EmrA, confers resistance to hydrophobic compounds including the proton-motive force uncoupler, CCCP, and nalidixic acid (Lomovskaya and Lewis, 1992). EmrB is predicted to have 14 TMHs and, unlike other TEP transporters, lacks a substantial periplasmic domain (Tanabe et al., 2009). Consistent with this, EmrA does not have an MP domain (Hinchliffe et al., 2014) that in other transporters forms extensive interactions with the transporter periplasmic domain (Du et al., 2014). MFS transporters have been reported to operate either as monomers or dimers (Quistgaard et al., 2016). Purified EmrB was reported to form dimers (Tanabe et al., 2009) whereas the diameter of a modeled EmrA hexamer was compatible with monomeric EmrB (Hinchliffe et al., 2014). Further studies are required to understand the EmrB stoichiometry *in vivo* and the EmrA-EmrB interactions underpinning pump assembly.

In *E. coli*, two very different ABC transporters form TolC-dependent TEPs; HlyB and MacB. HlyB acts in concert with the adaptor HlyD to export the large protein toxin, hemolysin



A (HlyA), from the cytoplasm across both membranes in a concerted step (Thanabalu et al., 1998). Topological analysis, and the crystal structure of a peptide exporting homolog (PCAT1), demonstrate HlyB has a classic 6-TMH topology with the NBD fused to the C-terminus (Lin et al., 2015a). Conversely, sequence analysis of *E. coli* MacB suggested that it has an atypical topology. An N-terminal cytoplasmic NBD is followed by four TMHs, with a large periplasmic domain of approximately 200 amino acids situated between TMH1 and TMH2. The 4-TMH topology predicted from amino acid sequence was experimentally confirmed by site-specific chemical modification of single cysteine residues (Kobayashi et al., 2003). Subsequent bioinformatic analysis revealed the MacB architecture is widespread throughout bacterial genomes (Khwaja et al., 2005; Wang et al., 2009).

### The MacAB-TolC TEP Mediates Antibiotic Resistance and Export of Virulence Factors

MacB, along with its periplasmic adaptor protein MacA, was first identified in a screen of *E. coli* transporter genes as providing resistance to macrolide drugs in a strain lacking the major RND efflux pump AcrAB (Kobayashi et al., 2001). Further studies demonstrated that expression of MacAB increases *E. coli* resistance to colistin and bacitracin (Crow et al., 2017). Additionally, the MacAB-TolC TEP supports the export of small proteins such as enterotoxin STII (Yamanaka et al., 2008), and is suggested to export the heme-precursor protoporphyrin (Turlin et al., 2014).

The role of the MacAB-TolC TEP has been investigated in other Gram-negative species. *S. maltophilia* MacAB confers resistance to a variety of macrolides, aminoglycosides and polymyxins (Lin et al., 2014). In *Neisseria gonorrhoeae*, mutations in the *macAB* promoter increase macrolide resistance in a strain lacking the RND pump MtrCDE (Rouquette-Loughlin et al., 2005). *Acinetobacter baumannii* MacAB expression is significantly upregulated in both multidrug-resistant clinical strains (Lin et al., 2015b), and colistin-resistant strains devoid of LPS (Henry et al., 2012). Expression of the *Vibrio cholerae* MacAB homolog VarDEF increases resistance to four different macrolides by 8-fold or greater (Lin et al., 2017), and these genes were upregulated in presence of polymyxin B (Matson et al., 2017). In *Pseudomonas* species, homologs of MacB secrete toxins (Balibar et al., 2005; Dubern et al., 2008; Lim et al., 2009; Cho and Kang, 2012; Li et al., 2013), and siderophores such as pyoverdine (Imperi et al., 2009; Hannauer et al., 2010). Deletion of MacB impacts virulence of *Salmonella* in a mouse model (Nishino et al., 2006), possibly by promoting survival within macrophages (Bogomolnaya et al., 2013). Taken together, MacB, in concert with the adaptor MacA and the outer membrane exit duct, TolC, can underpin efflux of a variety of drugs and export of virulence factors from multiple Gram-negative bacterial species. While TolC expression is constitutive, expression of MacAB in *Salmonella* and *E. coli* is regulated by the PhoPQ two-component system (Nishino et al., 2006). Among other stimuli, PhoPQ senses and responds to host antimicrobial peptides and peptide antibiotics (Bader

et al., 2005; Prost et al., 2007). Thus, MacAB production is likely to be induced in response to challenge with these agents.

## STRUCTURAL BIOLOGY OF THE MacAB-TolC SYSTEM

Studies by the Zgurskaya lab demonstrate that the ATPase activity of reconstituted MacB is dependent on intact MacA. Furthermore, MacAB mediated antibiotic resistance *in vivo* requires the presence of the outer membrane efflux channel TolC (Tikhonova et al., 2007). Taken together, these data confirm that MacAB-TolC forms a functional TEP. Recently, crystal structures of the individual components, and a cryo-EM structure of the entire pump, have been elucidated, providing substantive insight into the assembly and function of the MacB-powered TEP (Table 1, Figure 3).

### The Outer Membrane Exit Duct, TolC

The first structural component of a TEP solved was the TolC outer membrane channel (Koronakis et al., 2000; Figure 3). Three TolC monomers trimerise to form a 12-stranded  $\beta$ -barrel and a 100 Å long  $\alpha$ -helical tunnel extending down into the periplasm. An equatorial domain comprising the N- and C-termini forms a belt around the middle of the  $\alpha$ -helical domain. This  $\alpha$ -tunnel is composed of six pairs of coiled coils packing together, and has an approximate diameter of 35 Å for almost its entire length. At the bottom of the channel, three aspartate residues, one from each monomer, form a constriction of ~4 Å effectively closing the channel at the periplasmic side of the membrane. This closed conformation of the tunnel is constrained by an inter- and intra-monomer network of hydrogen bonds and salt bridges. Crystal structures of TolC variants, in which this stabilizing network was disrupted by one or more point mutations, suggested how the duct opens to allow passage of substrate (Bavro et al., 2008; Pei et al., 2011). Subsequently, pseudoatomic cryo-EM structures of the AcrAB-TolC pump, in the presence and absence of substrate, revealed the iris-like opening of the periplasmic constriction of wild-type TolC (Wang et al., 2017). TolC homologs from other organisms are divergent in sequence and exhibit variation in the structure of the equatorial domain (Akama et al., 2004; Federici et al., 2005; Kulathila et al., 2011; Su et al., 2014; Guan et al., 2015; Yonehara et al., 2016). However, the same  $\beta$ -barrel and  $\alpha$ -tunnel structure is evident suggesting the gross topology is likely to be conserved in all outer membrane efflux channels from Gram-negative bacteria.

### The Periplasmic Adaptor Protein, MacA

Structures of *E. coli* and *Aggregatibacter actinomycetemcomitans* MacA have both been solved by X-ray crystallography (Yum et al., 2009; Xu et al., 2012). Like the RND pump adaptors, AcrA (Mikolosko et al., 2006) and MexA (Higgins et al., 2004), the MacA adaptor comprises helical hairpin, lipoyl,  $\beta$ -barrel and MP domains. The native MacA protein also has an N-terminal TMH, which distinguishes it from other adaptors, including AcrA and MexA, typically anchored to the inner membrane by an N-terminal lipoyl group (Hinchliffe et al., 2013).

**TABLE 1** | Structures in the Protein Data Bank associated with MacAB-TolC.

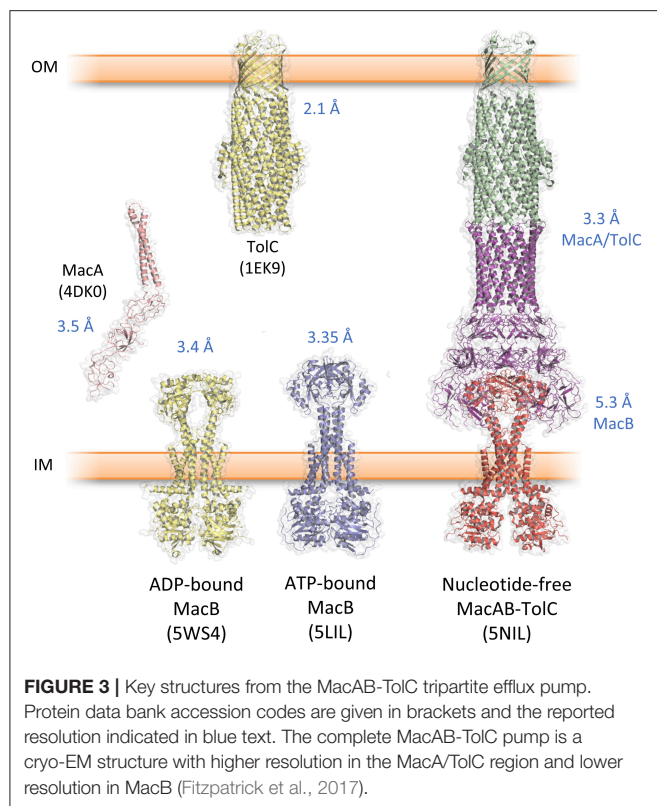
Protein	Organism	PDB	Details	Resolution (Å)	Publication
TolC	<i>E. coli</i>	1EK9	Trimer, closed state. C-terminal 43 amino acids removed.	2.1	Koronakis et al., 2000
MacA	<i>A. actino</i>	4DK0	Functions as a hexamer, TMH removed.	3.5	Xu et al., 2012
	<i>E. coli</i>	3FPP	Functions as a hexamer, TMH removed. MP present but not resolved.	2.99	Yum et al., 2009
MacB	<i>S. pneu</i>	5XU0	SeMet, functions as a hexamer, MP domain and TMH removed.	2.95	Yang et al., 2018
	<i>A. actino</i>	5LIL	ATP $\gamma$ S-bound dimer (P2 <sub>1</sub> ).	3.35	Crow et al., 2017
		5LJ6	ATP-bound dimer (P6 <sub>5</sub> 22).	3.9	Crow et al., 2017
		5LJ7	ATP-bound dimer (P2 <sub>1</sub> ).	3.25	Crow et al., 2017
	<i>A. baumannii</i>	5GKO	SeMet labeled, nucleotide-free dimer.	3.39	Okada et al., 2017
		5WS4	ADP $\beta$ S-bound dimer.	3.4	Okada et al., 2017
MacAB-TolC	<i>S. pneu</i>	5XU1	Nucleotide-free dimer.	3.3	Yang et al., 2018
	<i>E. coli</i>	5NIL	Nucleotide-free MacA <sub>6</sub> MacB <sub>2</sub> TolC <sub>3</sub> assembly Cryo-EM (MacB region).	5.3	Fitzpatrick et al., 2017
		5NIK	Nucleotide-free MacA <sub>6</sub> MacB <sub>2</sub> TolC <sub>3</sub> assembly. Cryo-EM (MacA-TolC region). TolC in the open state.	3.3	Fitzpatrick et al., 2017
MacB periplasmic domains	<i>A. actino</i>	3FTJ	Monomer, functions as dimer in full-length protein.	2.0	Xu et al., 2009
		5C59	SeMet monomer (P2 <sub>1</sub> $\beta$ = 99.7°). Functions as a dimer in full-length protein.	3.0	Ha and Kim, unpublished
	<i>E. coli</i>	5LJ8	Monomer, extended conformation (P2 <sub>1</sub> $\beta$ = 92.9°). Functions as a dimer in full-length protein.	1.95	Crow et al., 2017
		5LJ9	Nucleotide-free monomer. (C222 <sub>1</sub> ), functions as a dimer in full-length protein.	2.3	Crow et al., 2017
MacB cytoplasmic NBD	<i>E. coli</i>	5LJA	Nucleotide-free monomer (P6 <sub>1</sub> 22), functions as a dimer in full-length protein.	2.4	Crow et al., 2017

*A. actino*, *Aggregatibacter actinomycetemcomitans*; *S. pneu*, *Streptococcus pneumoniae*; SeMet, selenomethionine labeled; MP, Membrane proximal; TMH, Transmembrane helix.

However, the MacA crystal structures were determined using protein constructs lacking this N-terminal TMH. Both *E. coli* and *A. actinomycetemcomitans* MacA crystallized as hexamers without additional stabilization using chemical cross-linking reagents or engineered disulfide bonds (Yum et al., 2009; Xu et al., 2012). The MacA hexamer resembles an inverted funnel with the 70 Å stem formed by the hairpin domains and a wider mouth formed by association of the lipoyl and  $\beta$ -barrel domains. The cryo-EM structure of *E. coli* MacA within the context of the assembled pump revealed a similar hexameric organization (Fitzpatrick et al., 2017). Notably, six lipoyl domain loops, one from each monomer, project into the center of the MacA channel. The resulting constriction is stabilized by inter-protomer hydrogen bonds between glutamine residues at the tip of the loop (Fitzpatrick et al., 2017). These glutamine residues are conserved in MacA proteins (Yum et al., 2009; Fitzpatrick et al., 2017) but replacement with alanine did not affect MacAB conferred erythromycin resistance (Fitzpatrick et al., 2017). Instead, steered molecular dynamics simulations suggested that the lipoyl domain loops favor unidirectional movement of erythromycin through the MacA channel. The construction in the MacA hexamer could therefore act as a gate to regulate flow of substrates through the assembled efflux pump (Fitzpatrick et al., 2017).

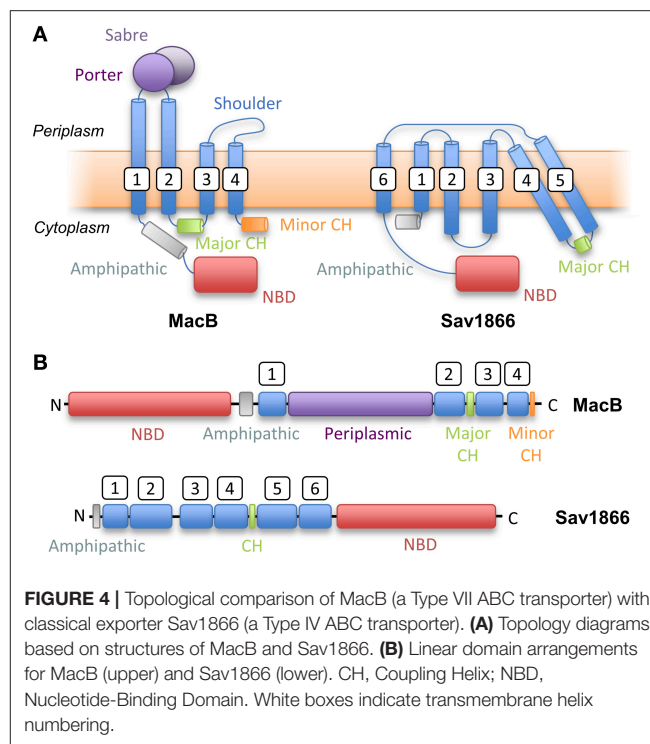
## The Inner Membrane ABC Transporter, MacB

The structure of the isolated periplasmic domain of the monomeric MacB periplasmic domain was solved almost 10 years ago revealing the presence of two subdomains (Xu et al., 2009). However, without the context of the membrane, it was difficult to infer details of the transport mechanism. Now, a series of structures of full-length MacB have helped reveal molecular details of its operation. MacB from *A. actinomycetemcomitans* and *A. baumannii* were crystallized in ATP- and ADP-bound forms, respectively (Crow et al., 2017; Okada et al., 2017; Figure 3). MacB crystallized as a dimer consistent with analytical ultracentrifugation and atomic force microscopy studies (Lin et al., 2009). Each MacB monomer comprises an N-terminal NBD, four TMHs and a large periplasmic domain between TMH1 and TMH2. Helical extensions of TMH1 and TMH2 from each monomer form a four helix bundle that elevates the periplasmic domain above the plane of the membrane, giving a mushroom-like appearance. TMH3 and TMH4 pack on the outside of the helical bundle and are linked by a short extracytoplasmic loop which has been referred to as the “shoulder” (Crow et al., 2017). The cytoplasmic N-terminus of TM1 is connected to the NBDs by an amphipathic helix running parallel to the membrane surface and a “skirting loop.” The



major coupling helix is located on the cytoplasmic side of the membrane between TM2 and TM3, and provides a means of communicating conformational changes from the NBDs to the TMDs, as suggested for other ABC transporters. A second helix at the C-terminus, the minor coupling helix, also makes contact with the NBD. Deletion of the minor coupling helix had a modest impact on activity of *E. coli* MacB (Crow et al., 2017) but a greater effect on *A. baumannii* MacB mediated macrolide resistance (Okada et al., 2017), which may reflect differences in the assays used.

The two subdomains of the MacB periplasmic domain are the Porter, named for structural similarity to a domain of AcrB, and the Sabre named for the acronym: Small, alpha/beta rich, extracytoplasmic. The Sabre domain is formed from a contiguous stretch of residues (347–465 in *A. actinomycetemcomitans* MacB) while the Porter domain is formed from two  $\beta$ - $\alpha$ - $\beta$  motifs found on either side of the Sabre domain (residues 306–346 and 466–503). The Porter domain is directly connected to both stalk helices of the MacB monomer. The same fold is evident in the ADP-bound *A. baumannii* MacB structure although there are striking differences in conformation (see mechanotransmission section below). The crystal structures reveal that the architecture of MacB is clearly distinct from classic ABC exporters such as Sav1866 (Figure 4). Like other multidrug exporters, Sav1866 is characterized by a 6-TMH topology, C-terminally fused NBD, and a coupling helix located between TMH4 and TMH5 of each monomer that reciprocally “cross-over” to engage the NBDs. MacB, in contrast, has four TMHs, an N-terminally fused NBD, a



large periplasmic domain and a major coupling helix that engages the NBDs in intra-molecular fashion.

## The Assembled MacAB-TolC Tripartite Pump

The significant technical challenge of isolating an assembled MacAB-TolC pump and maintaining it through the purification procedure was achieved by creating a fusion of MacA to the C-terminus of MacB, and subsequently by introducing specific cysteine residues into MacA and MacB to stabilize their interaction with disulfide bonds (Fitzpatrick et al., 2017). Crystal structures of *E. coli* MacA (Yum et al., 2009), *E. coli* TolC (Koronakis et al., 2000) were already available. Docking these, and a homology model of *E. coli* MacB based on the *A. baumannii* MacB structure (Okada et al., 2017), into a cryo-EM map enabled the structure of the *E. coli* MacAB-TolC assembly to be solved (Fitzpatrick et al., 2017) (Figure 3). The assembled tripartite pump comprises a single MacB dimer, MacA hexamer and the trimeric TolC exit duct. The complete MacAB-TolC assembly is approximately 320 Å long, comparable to the size of the AcrAB-TolC pump (Du et al., 2014; Daury et al., 2016).

The structure reveals how the three components interact in the context of an assembled pump (Fitzpatrick et al., 2017). The tips of the MacA hairpin domains intermesh with the periplasmic ends of the TolC coiled coils. These “tip to tip” interactions were first suggested on the basis of *in vitro* binding experiments (Xu et al., 2010), and EM analysis of a complex of *E. coli* MacA and a hybrid protein bearing the tip regions of the TolC helical barrel (Xu et al., 2011). Association with MacA stabilizes the TolC trimer in an open state in which the aspartates at the



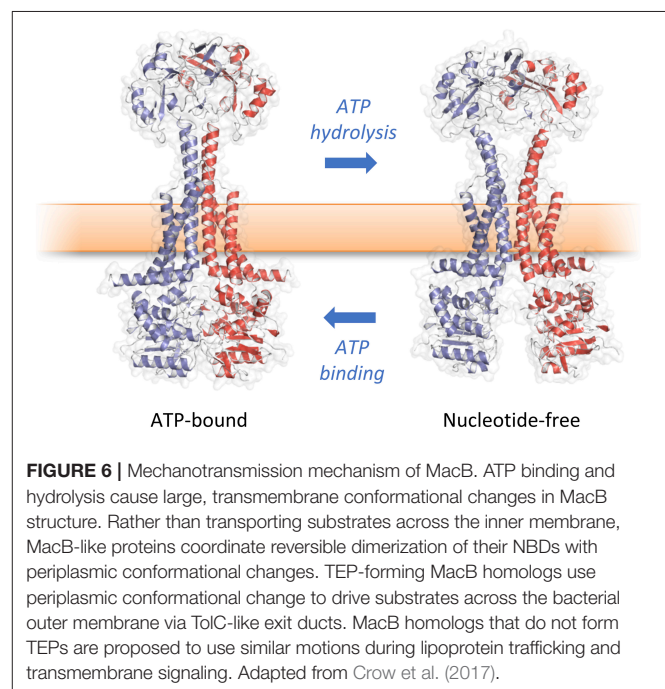
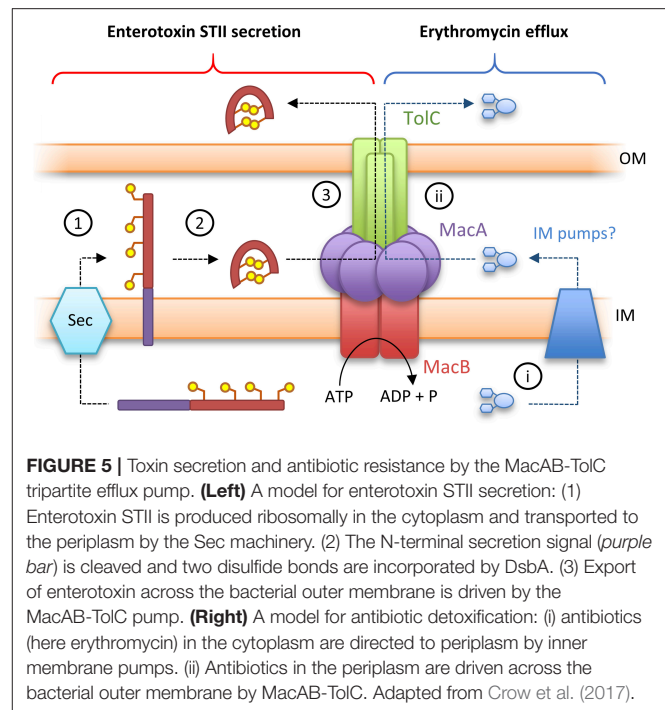
periplasmic constriction are almost 30 Å apart. This results in a continuous channel from the top of TolC down to the lipoyl loop constriction in MacA. Adaptor interactions with the periplasmic domain of MacB are mediated by the MacA β-barrel and MP domains. The annulus of MacA β-barrel domains sit on top of MacB with three MacA monomers contacting each MacB. The ring of MacA MP domains makes extensive contacts with the MacB periplasmic domain consistent with previous biochemical studies (Modali and Zgurskaya, 2011). Two MacA MP domains contact the Sabre, and one interacts with the Porter subdomain of each MacB monomer. The MacA hairpin and lipoyl domains do not contact MacB (Fitzpatrick et al., 2017).

The MacB structure within the assembled complex resembles that of the ADP-bound *A. baumannii* structure. The NBDs are separated and the MacB stalk helices bend away from each other leading to a separation of the periplasmic domains and formation of a periplasmically accessible cavity between MacB and MacA (Fitzpatrick et al., 2017).

## THE MECHANOTRANSMISSION MECHANISM OF MacB

Canonical ABC transporters provide a transmembrane substrate pathway in the form of a vestibule or cavity located between the two halves of the dimer interface (Choudhury et al., 2014). Analysis of the MacB structures described above indicate there is not a sufficient channel to provide a transmembrane pathway for substrate in either the ATP or nucleotide-free state (Crow et al., 2017). Furthermore, a functional MacAB-TolC pump is required to export peptide substrate enterotoxin STII (Yamanaka et al., 2008; Crow et al., 2017). STII is exported to the periplasm by the Sec system, and requires the action of the periplasmically located Dsb system to catalyze the formation of its two disulfide bonds (Foreman et al., 1995). Taken together, these data suggest MacB does not transport substrates across the inner membrane but instead accepts substrates in the periplasm and, in concert with MacA, ejects them across the outer membrane via the TolC exit duct (Figure 5). This mechanism is functionally akin to the “periplasmic vacuum cleaner” model, proposed for RND-type transport pumps, in which substrates are bound in the periplasm and ejected across the outer membrane (Aires and Nikaido, 2005). The network is completed by standalone transporters in the inner membrane which remove substrates from the cytoplasm (Tal and Schuldiner, 2009).

How then do ATP-induced changes in the cytoplasmic NBDs affect the periplasmic domains of MacB? Comparison of the ATP-bound and free forms of MacB reveal long-range conformational changes in the transmembrane helices, stalk and periplasmic domains (Crow et al., 2017; Fitzpatrick et al., 2017; Okada et al., 2017). In the nucleotide-free form, ATP binding induces dimerization of the NBDs causing the major coupling helix to push upwards on TM2. The resultant “zipping up” of the transmembrane helices into a rigid 4-helix bundle brings the periplasmic domains of each monomer together, eliminating the cavity between them (Figure 6). We term these long-range movements mechanotransmission, as ATP hydrolysis is not used to transport a substrate across the membrane in which the ABC



protein resides, but instead to transmit conformational changes from cytoplasmic NBDs to achieve useful work in the periplasm. The importance of the relative movements of the stalk helices was underlined by a severe reduction in MacB function *in vivo* when the helices were locked together with a disulfide bond (Crow et al., 2017).

Docking of the ATP-bound MacB form into the cryo-EM MacAB-TolC structure has led to the suggestion that MacB

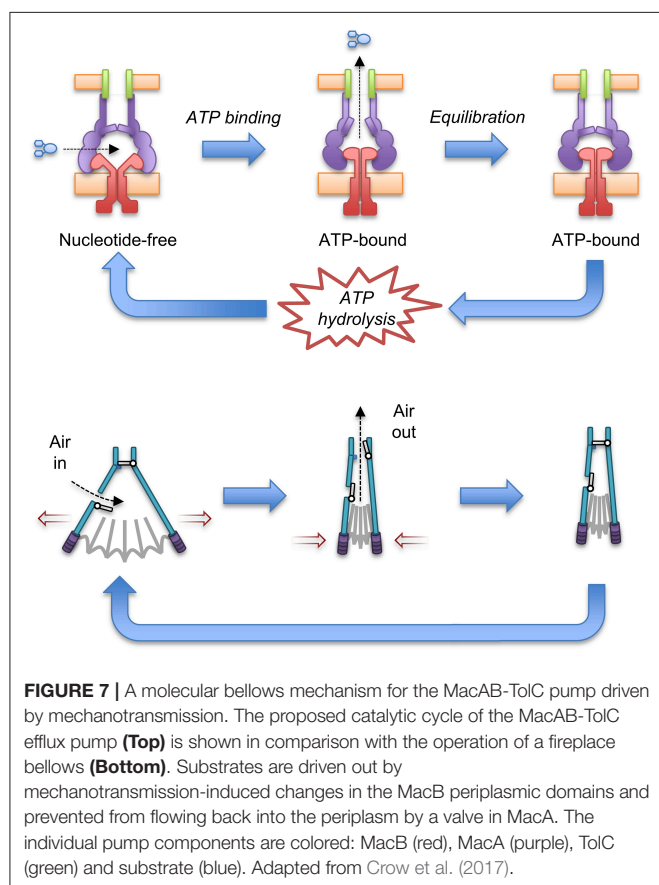
could harness mechanotransmission to operate the assembled pump as a molecular bellows (Crow et al., 2017; **Figure 7**). The MacA hexamer accommodates the MacB periplasmic domain in both open (ATP-free) and closed (ATP-bound) conformations. Initially, the pump is in a nucleotide-free state in which the stalk helices and periplasmic domains of MacB are separated. Consequently, substrates can enter the cavity at the interface of MacB and MacA. ATP binding brings the NBDs together and the mechanotransmission mechanism results in tight association of the stalk helices and MacB periplasmic domains. The ensuing reduction in the cavity volume creates pressure which forces the substrates upwards into the MacA channel and through the MacA gate described above. Once the pressure is equalized, the gate closes, preventing backflow of substrates. ATP hydrolysis then resets the pump, with the MacB stalk helices moving apart allowing substrates to bind and another round of efflux to proceed. The proposed model requires a mechanism to prevent substrate egress back through MacB. Cryo-EM analysis of the assembled AcrAB-TolC TEP revealed a  $\sim 10$  Å contraction along the long axis of the pump in the substrate-bound state (Wang et al., 2017). A similar contraction of the MacAB-TolC TEP could ensure that MacA packs more tightly around MacB to ensure substrates are driven out through MacA/TolC rather than escaping into the periplasm. Clearly, structures of a substrate-bound state of the MacB-driven TEP will be invaluable in determining the precise details of its mechanism.

Little is known about how substrates are recognized by MacB. Unexplained electron density at the cleft between the MacB periplasmic domains in the assembled pump could represent an endogenous substrate (Fitzpatrick et al., 2017), but details remain obscure. Mutagenesis of a patch of predominantly hydrophobic residues, on the interior surface of the periplasmic domain, reduced MacB conferred resistance to erythromycin, bacitracin and colistin. This patch constitutes a plausible substrate binding domain (Crow et al., 2017). However, it is still unclear whether antibiotics are directly effluxed or resistance is mediated as an indirect effect of transport of another substrate. Zgurskaya and colleagues demonstrated *E. coli* MacA co-purified with lipopolysaccharide and suggested the native substrate could be a glycolipid (Lu and Zgurskaya, 2013).

Biochemical data suggests that MacA is able to influence the ATPase activity of MacB and may have a role in communicating the presence or absence of substrate in the periplasm to the cytoplasmic NBDs (Tikhonova et al., 2007; Modali and Zgurskaya, 2011; Lu and Zgurskaya, 2012). Deletion of the cytoplasmic region, or N-terminal MacA TMH, compromised the MacA-mediated stimulation of MacB ATPase activity *in vitro* and prevented MacAB mediated macrolide resistance *in vivo* (Tikhonova et al., 2007). The structural basis for ATPase stimulation remains unclear, because the MacA TMH was not resolved in the MacAB-TolC cryo-EM structure (Fitzpatrick et al., 2017).

## MacB FAMILY MEDIATED ANTIBIOTIC RESISTANCE IN GRAM-POSITIVE BACTERIA

The classic view of adaptor proteins is that they serve to bridge the inner and outer membrane components of TEPs. Bioinformatic analysis suggesting the widespread presence of adaptor proteins in Gram-positive bacteria was therefore somewhat unanticipated (Harley et al., 2000; Zgurskaya et al., 2009). Many of the genes encoding these Gram-positive adaptor proteins are found in operons with homologs of *macB*. The first of these systems to be characterized, YknXYZ, is responsible for protection from the endogenous toxin, sporulation delaying peptide (SDP). The release of SDP causes lysis of nearby cells to provide nutrients for producing cells to complete sporulation – a process that has been described as bacterial cannibalism. Mature SDP is a 42 amino acid peptide with one disulfide bond (Liu et al., 2010). Structures of the adaptor protein YknX (Xu et al., 2017) reveal that it has the same fold and hexameric arrangement as *E. coli* MacA (Yum et al., 2009; Fitzpatrick et al., 2017). Similarly, the permease component YknZ is clearly homologous to the transmembrane and periplasmic domain of MacB (Xu et al., 2016; Fitzpatrick et al., 2017), while YknY encodes a cytoplasmic NBD. Sec-dependence of SDP export suggests that like MacB, YknXYZ probably mediates its protective effect from the extracytoplasmic side of the membrane—perhaps by keeping SDP away from the bilayer. Interestingly, a co-transcribed membrane protein, YknW, may influence the oligomerisation



and/or conformational state of the adaptor YknX, but its role remains enigmatic (Yamada et al., 2012).

In *Enterococcus faecalis*, a MacB-type transporter and cognate adaptor are required for protection against endogenously produced AS-48, a 70 amino acid cyclic peptide antibiotic (González et al., 2000). A 10 gene cluster organized into two operons is associated with AS-48 biosynthesis. The first operon encodes genes responsible for AS-48 production and export across the cytoplasmic membrane while the second operon, AS-48EFGH, is important for resistance to exogenous AS-48 (Diaz et al., 2003). Together, AS-48G (NBD) and AS-48H (TMD) encode a MacB-like ABC transporter with an extracytoplasmic domain of approximately 230 amino acids. AS-48E is predicted to contain four TMHs and cytoplasmic N- and C-termini. Further investigation is required to establish the role of AS-48E and whether it influences the AS48-FGH pump activity in a similar manner to YknW in the SDP-exporting pump described above.

A global analysis of *Streptococcus pneumoniae* D39 gene expression showed upregulation of an operon (Sp0785-0787) in response to bacitracin and the human defensin LL-37. Deletion of this operon increased susceptibility to LL-37 and lincomycin (Majchrzykiewicz et al., 2010). Analysis of these genes suggest they encode a periplasmic adaptor protein and transporter homologous to MacB. Very recently, structures of the equivalent proteins from *S. pneumoniae* R6 (Spr0693-0695) were obtained (Yang et al., 2018). These structures reveal remarkable structural similarity to the Gram-negative proteins already crystallized. *S. pneumoniae* MacA (hereafter SpMacA) was crystallized in the absence of the MP domain and is made up of characteristic  $\beta$ -barrel, lipoyl and  $\alpha$ -helical hairpin domains. A lipoyl domain loop from each monomer projects into the SpMacA channel in a similar fashion observed in the *E. coli* MacA structure (Fitzpatrick et al., 2017). However, the residue at the tip is not conserved and the physiological role of the SpMacA loop was not tested (Yang et al., 2018). SpMacB is remarkably similar to the Gram-negative MacB structures (Crow et al., 2017; Fitzpatrick et al., 2017; Okada et al., 2017; Yang et al., 2018). It was crystallized in the presence of the non-hydrolysable ATP analog AMP-PNP although this was not resolved in the structure, and the arrangement of the stalk helices is more similar to the ADP-bound or nucleotide-free form (Fitzpatrick et al., 2017; Okada et al., 2017; Yang et al., 2018). As with *E. coli* MacAB (Tikhonova et al., 2007), the ATPase activity of SpMacB reconstituted in proteoliposomes was stimulated by co-reconstitution with full-length SpMacA, but not by variants lacking the cytoplasmic region and N-terminal TMH (Yang et al., 2018).

In these Gram-positive systems, an adaptor protein is present but in the absence of an outer membrane, what is its role? Cryo-EM studies of vitrified cell samples reveal a discrete zone between the inner membrane and peptidoglycan akin to a Gram-positive “periplasm” (Matias and Beveridge, 2006; Zuber et al., 2006). The presence of these adaptors could therefore form channels to remove xenobiotics from this space, and prevent their immediate re-association with the membrane. The height of the SpMacA channel is consistent with the dimensions of this periplasm-like zone (Yang et al., 2018) and purified YknX adaptor is able to bind peptidoglycan (Xu et al., 2017). Further analysis of Gram-positive

MacAB-like assemblies is vital to understand their roles *in vivo*.

## SENSING AND RESISTING THE THREAT OF LANTIBIOTICS USING THE MacB ARCHITECTURE

Lantibiotics are post-translationally modified peptides containing the polycyclic thioether amino acids lanthionine or methyllanthionine e.g., bacitracin and nisin (Draper et al., 2015). They are produced by low G+C Gram-positive bacteria and typically interfere with cell wall/peptidoglycan biosynthesis by binding to precursors such as undecaprenyl-pyrophosphate (UPP) and Lipid II (Draper et al., 2015). Multiple methods of resistance to lantibiotics exist, but intriguingly one class of resistance proteins are ABC transporters homologous to MacB proteins. These systems are exemplified by BceAB of *B. subtilis* but multiple homologs in other Gram-positive bacteria have been characterized including *Streptococcus mutans* MbrAB (Tsuda et al., 2002), *Listeria monocytogenes* AnrAB (Collins et al., 2010), *S. aureus* VraFG (Meehl et al., 2007), and *Streptococcus agalactiae* NsrFP (Khosa et al., 2013).

BceA encodes an ATPase domain, while BceB is a membrane permease with ten TMHs and a large extracellular domain between TMH7 and TMH8. The final four TMHs and intervening periplasmic domain are topologically similar to MacB. Intriguingly, the BceAB-type transporters appear to have coevolved with a two-component system (TCS) that works with BceAB to sense and respond to extracellular antibiotics (Coumes-Florens et al., 2011; Dintner et al., 2011). Typically, TCSs consist of a membrane intrinsic histidine kinase that phosphorylates a response regulator to control gene expression in response to an external stimulus. Two-hybrid analysis of the proteins suggest that BceB and BceS directly interact (Kallenberg et al., 2013; Dintner et al., 2014). However, unlike in classical TCS systems, the histidine kinase (BceS) cannot directly sense antibiotics and requires the presence of BceB and an active BceA ATPase domain to respond to bacitracin (Rietkötter et al., 2008). Two different mechanisms for BceB mediated detoxification have been suggested. Kingston and colleagues proposed that BceAB induces resistance by flipping UPP into the inner leaflet of the cytoplasmic membrane, thereby protecting it from bacitracin (Kingston et al., 2014). Conversely, Dintner and coworkers demonstrated purified BceAB complex could directly bind bacitracin-Zn<sup>2+</sup>, the active form of the peptide, with nanomolar affinity. They therefore suggested that BceAB mediates resistance by direct efflux of bacitracin itself (Dintner et al., 2014). Though the nature of the substrate *in vivo* remains unclear, BceAB is active in both the sensing and detoxification of bacitracin.

Analysis of the BceB sequence suggests a possible fusion of two MacB architectures in which the first periplasmic domain has been lost (Dintner et al., 2014). Consistent with this idea, bacterial two-hybrid analysis suggests BceB monomers do not interact. Furthermore, size-exclusion chromatography analysis of detergent-purified BceA:BceB complex suggested a 2:1 stoichiometry, although the purified complex did not



have ATPase activity (Dintner et al., 2014). Mutations affecting both sensing, and detoxification, of bacitracin map to the C-terminal half of BceB, including TMH8 (Kallenberg et al., 2013). This helix is equivalent to TMH2 in MacB, suggesting a mechanotransmission-like mechanism could also underpin BceB action.

Unlike YknYZ and SpMacB discussed in the previous section, BceAB is not associated with an adaptor protein. However, interestingly, the activity of a BceAB homolog from *S. aureus* (VraDE) is modulated by a two-TMH membrane protein (VraH) that has cytoplasmic N- and C-termini. Two-hybrid analysis demonstrated VraH interacts with VraE and increases resistance to daptomycin and gallidermin but the mechanism of this modulation is not clear (Popella et al., 2016).

## INSIGHTS INTO THE WIDER MacB FAMILY OF ABC TRANSPORTERS

### TEP-Forming MacB Homologs

The structures and mechanisms detailed here are also likely to apply to MacB homologs operating as part of tripartite efflux pumps to export substrates other than antibiotics (Table 2). One such example is export of the siderophore pyoverdine by *Pseudomonas aeruginosa* PvdRT-OpmQ. Pyoverdine is matured by periplasmic enzymes, and mutants lacking PvdRT accumulate pyoverdine in the periplasm. These observations suggest that the MacB homolog PvdT mediates transport from the periplasm, not the cytoplasm (Hannauer et al., 2010). In other *Pseudomonas* species, homologs of MacAB are required for phytotoxin secretion (Cho and Kang, 2012). In these systems, the toxin biosynthetic operons include homologs of MacAB. By analogy with MacB, another pump would be required to export the non-ribosomally synthesized peptide across the cytoplasmic membrane into the periplasm, a role which could be fulfilled by SyrD-type ABC transporters (Quigley et al., 1993).

The MacB-type ABC transporter DevCA, adaptor protein DevB and TolC homolog HgD form a TEP responsible for glycolipid export underpinning heterocyst formation in the nitrogen fixing cyanobacterium *Anabaena*. Deletion of the N-terminus of DevB prevents substrate export, but not association with DevCA, suggesting the cytoplasmic region of the adaptor protein can control the activity of the pump as proposed for *E. coli* MacAB-TolC (Staron et al., 2011, 2014).

Enteraggregative *E. coli* express a virulence plasmid-encoded MacB based TEP dedicated to the export of dispersin, a positively-charged, surface-associated protein, that prevents bacterial aggregation (Nishi et al., 2003). A similar TEP exports the dispersin homolog, CexE, from enterotoxigenic *E. coli* (Pilonieta et al., 2007). The structure of 10 kDa dispersin is made up of two antiparallel 3-stranded beta-sheets with decorating  $\alpha$ -helices at either end, resulting in a 20 Å diameter, 50 Å long “bullet” shape (Velarde et al., 2007). The narrowest dimension is consistent with transport through the periplasmic cavity of MacB (and the lumen of the TolC exit duct) but may represent the upper size-bound for folded substrates that are transported by MacB-dependent TEPs.

### TEP-Independent MacB Homologs

The MacB architecture is also found in proteins that operate independently of adaptor proteins/TEPs (Table 3). For example, LolCDE, an ABC transporter with the same topological organization as MacB, underpins lipoprotein trafficking in Gram-negative bacteria. Lipoproteins destined for the outer membrane are first transported across the cytoplasmic membrane by the Sec system, and then successively acylated by membrane intrinsic machineries (Narita and Tokuda, 2017). LolCDE then extracts the lipid moiety of lipoproteins from the outer leaflet of the inner membrane and passes it to the periplasmic chaperone LolA for delivery to the outer membrane. LolD encodes an NBD, while LolC and LolE both have the 4-TM helix MacB type architecture (Yakushi et al., 2000; Narita and Tokuda, 2017). The structure of the periplasmic domain of LolC revealed a fold homologous to MacB, suggesting that lipoprotein extraction could be performed by the LolCDE complex using a mechanotransmission mechanism (Crow et al., 2017).

The MacB architecture is also found in FtsEX which is required for efficient cell division in Gram-negative bacteria (Schmidt et al., 2004; Yang et al., 2011; Du et al., 2016), sporulation in *Bacillus* (Garti-Levi et al., 2008) and survival of mycobacteria (Mavrici et al., 2014) and *Streptococcus* (Sham et al., 2011). In these organisms, the FtsEX complex is proposed to regulate the activity of extracytoplasmic cell wall amidases in the final stages of cell division. The periplasmic domain of *Mycobacterium tuberculosis* FtsX lacks a significant Sabre subdomain, but the Porter subdomain is remarkably similar to that of *E. coli* MacB (Mavrici et al., 2014; Crow et al., 2017). The absence of the Sabre and conservation of the Porter subdomain in FtsEX raises interesting questions regarding the role of these subdomains in MacB and other Type VII ABC transporters, including LolCDE and FtsEX. As far as we are aware, the Porter subdomain is present in all members of the Type VII ABC superfamily and is likely an intrinsic part of the mechanotransmission apparatus. The role of the Sabre subdomain is less obvious but it may be adapted to carry out specific tasks in different proteins.

HrtAB is another ABC transporter homologous to MacB found throughout Gram-positive bacteria. The HrtAB pair were initially proposed to protect cells from the toxic effect of high concentrations of heme by removing it from the cytoplasm (Stauff et al., 2008; Bibb and Schmitt, 2010). Direct transfer of substrates from the cytoplasm to the extracellular space has not yet been demonstrated, and more recent studies suggest HrtAB removes heme from the membrane in *S. aureus* (Wakeman et al., 2012) and *L. lactis* (Joubert et al., 2014). Consistent with this idea, mutation of two conserved tyrosine residues in the periplasmic domain abrogated HrtAB mediated tolerance of heme stress. Comparison of HrtB with MacB suggests these residues map to the top of the stalk, and so it is tempting to speculate that they could co-ordinate heme during transport. Further study of HrtAB is essential to assess whether this assembly receives substrates from the cytoplasm or not, and whether it can transport such substrates across the inner membrane.



**TABLE 2** | Representative MacB superfamily TEPs.

Protein	Organism(s)	Complex	Substrate(s)	Function(s)	References
MacB	Gram-negative bacteria	MacAB-ToIC (TEP)	Enterotoxin STII, Erythromycin, Colistin, Bacitracin, Kanamycin, Glycolipids, Protoporphyrin	Toxin secretion Antibiotic resistance Cell envelope biogenesis? Detoxification?	Kobayashi et al., 2001; Yamanaka et al., 2008; Lu and Zgurskaya, 2013; Turlin et al., 2014; Crow et al., 2017
PvdT	<i>Pseudomonas aeruginosa</i>	PvdRT-OpmQ (TEP)	Pyoverdine	Siderophore export Virulence?	Imperi et al., 2009; Hannauer et al., 2012
AatP	Enteroaggregative <i>E. coli</i> (EAEC)	AatABCP (TEP)	Dispersin	Biofilm dispersal signaling	Nishi et al., 2003; Velarde et al., 2007
DevC	<i>Anabaena</i> sp.	DevABC-ToIC	Glycolipids	Heterocyst envelope biogenesis	Staron et al., 2011, 2014
CexP	Enterotoxigenic <i>E. coli</i> (ETEC)	CexPABC	CexE?	CexE secretion?	Pilonieta et al., 2007

**TABLE 3** | Representative non-TEP forming homologs of the MacB ABC transporter.

Protein	Organism(s)	Complex	Substrate(s)	Function(s)	References
LolC, LolE, LolF	Gram-negative bacteria	LolCDE or LolDF	Lipoproteins	Lipoprotein extraction and trafficking	Yakushi et al., 2000; Narita and Tokuda, 2017
FtsX	Gram-positive and Gram-negative bacteria	FtsEX	–	Cell division	Yang et al., 2011; Mavrici et al., 2014; Du et al., 2016
YknZ	<i>Bacillus amyloliquefaciens</i>	YknXYZ	Antimicrobial peptide?	Detoxification?	Yamada et al., 2012; Xu et al., 2017
BceB	<i>Bacillus subtilis</i>	BceABS	Bacitracin,	Sensing & detoxification	Dintner et al., 2014
HrtB	Gram-positives	HrtAB	Heme?	Detoxification?	Stauff et al., 2008; Bibb and Schmitt, 2010
AS-48H	<i>Enterococcus faecalis</i>	AS-48EFGH	Mature AS-48?	Bacteriocin AS-48 export?	Diaz et al., 2003

YbbP is an *E. coli* protein of unknown function that appears to represent a fusion of two MacB permease units with two linking TMHs. Surveying this, and other homologs, reveals that the MacB 4-TMH architecture may be organized in different ways. The NBDs may be fused to the TMDs or encoded in a separate polypeptide. Similarly, the transmembrane domains may organize as homodimer (MacB and FtsX) or heterodimer of individual units (LolCE). Alternatively, the two permease domains may be fused into a single polypeptide with two interceding TMHs, and either one (BceB) or two periplasmic domains (YbbP; **Figure 8**). As previously noted by Milton Saier, one permutation that appears to be absent in this ABC superfamily is the fusion of two permease domains and two NBDs into a single polypeptide (Khwaja et al., 2005). In cases where the TMDs represent an apparent fusion of two monomers, the NBD is always encoded as a separate protein (Khwaja et al., 2005).

## CONCLUSIONS AND FUTURE DIRECTIONS

MacB and its homologs confer resistance to antibiotics, but the current evidence suggests they do not transport substrates across the cytoplasmic membrane. Crystal and cryo-EM structures demonstrate how the distinctive MacB architecture uses a mechanotransmission mechanism in which the energy

from cytoplasmic ATP hydrolysis is communicated through transmembrane movements to perform useful work in the extracytoplasmic space. Despite recent advances, many questions remain. The absence of a substrate-bound structure is one of the biggest barriers to our collective understanding of MacB-type ABC transporters. Substrate-bound structures of other ABC exporters are the exception, not the rule (Johnson and Chen, 2017; Mi et al., 2017), but they would demonstrate how substrate is recognized by the MacB periplasmic domain. The N-terminus of MacA affects the ATPase activity of MacB but this region has not been resolved in any of the current structures; clearly structural information demonstrating how this region of MacA can affect MacB is vital to completely understand the mechanism.

All the available structures have been determined using detergent-solubilised proteins but the presence of a membrane environment dramatically alters the ATPase activity of MacB and its response to MacA (Tikhonova et al., 2007; Picard et al., 2018). Mass spectrometry analysis of purified MacB suggested it specifically binds phosphatidylethanolamine molecules (Barrera et al., 2009) while different phospholipids were found to differentially affect the activity of the MacB homolog LolCDE (Miyamoto and Tokuda, 2007). Structures of MacB within the context of a lipid bilayer may help reveal how specific phospholipids can modulate transporter activity.

Another important line of enquiry will be to better understand the range of substrates that MacB-like proteins interact

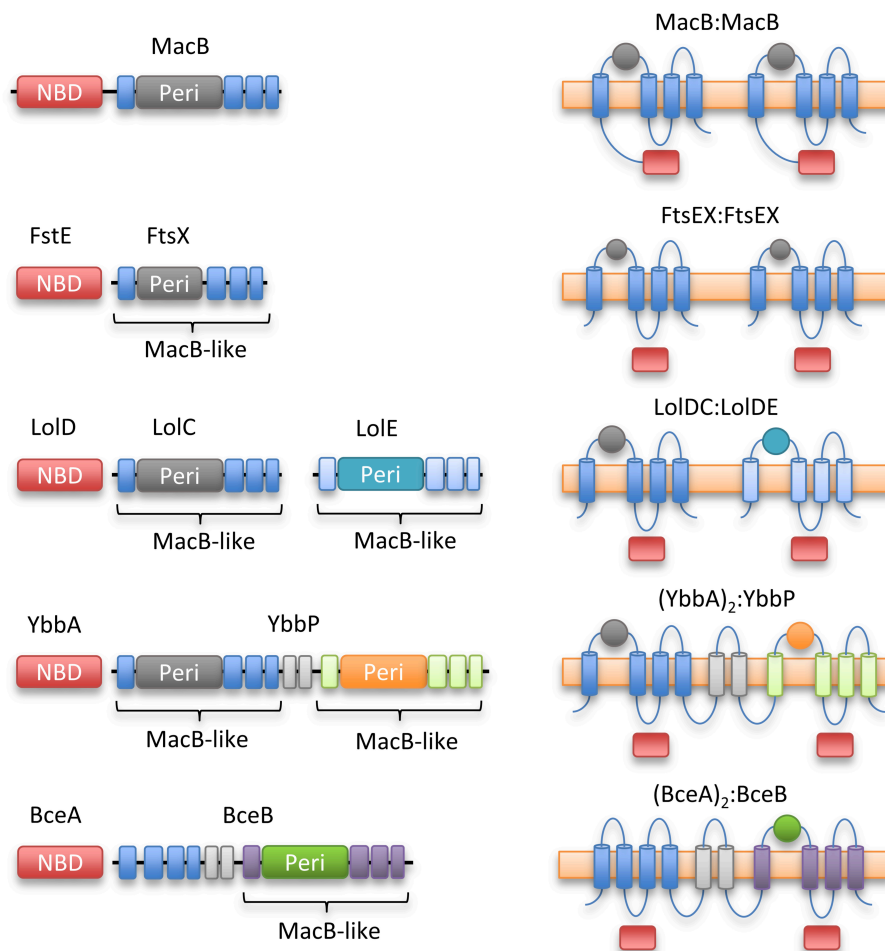


**FIGURE 8 |** Topological organization of MacB family members. Linear domain arrangement (**Left**) and transmembrane topologies (**Right**) are shown for MacB and four representative homologs. From top to bottom, macrolide and toxin transporter MacB, cell division protein FtsEX, lipoprotein trafficking LolCDE, YbbAP (unknown function), bacitracin sensing and efflux protein BceAB. MacB type ABC transporters share a distinctive transmembrane topology although NBDs are not always fused to transmembrane encoding domain and some families exist as apparent fusions of two half-transporters. Sequence identity between the periplasmic domains of each Type VII motif is low, but the extracellular domain of *Mycobacterium tuberculosis* FtsEX (Mavrici et al., 2014) also contains a Porter subdomain suggesting this could be a common element of Type VII ABC proteins.

with. The peptide substrates of MacB and its homologs are commonly small disulfide bonded peptides reminiscent of some antimicrobial peptides such as mammalian defensins. Expression of MacB-like proteins influences survival of *Salmonella* and *Streptococcus pyogenes* in macrophages (Phelps and Neely, 2007; Bogomolnaya et al., 2013). Whether MacB can protect pathogenic bacteria within host systems by efflux of defensins or other substrates bears further investigation. Moreover, the sheer structural diversity and size-range of the MacB substrate repertoire (ranging from ~0.5 kDa macrolides to 10 kDa proteins such as dispersin) requires explanation.

In *Bacillus*, an additional membrane protein that is not found in conventional tripartite systems from Gram-negative bacteria, YknW, associates with and affects the activity of the Gram-positive MacAB homolog YknXYZ. Furthermore, a small

membrane protein, AcrZ, modulates the action of the *E. coli* AcrAB-TolC TEP (Hobbs et al., 2012). Many small membrane proteins in *E. coli* remain uncharacterized (Storz et al., 2014), and so the possibility of other proteins affecting the activity of MacB cannot be excluded.

MacB mediated antibiotic resistance, and the involvement of its homologs in different facets of bacterial physiology make Type VII ABC transporters an attractive target for antibiotic therapy. Inhibitors of MacAB have not been isolated, but screening of chemical libraries identified two different inhibitors that target the MacB homolog LolCDE (McLeod et al., 2015; Nayar et al., 2015; Nickerson et al., 2018). Mutations conferring resistance map to the stalk helices, and interestingly, one of these inhibitors stimulated the ATPase activity of LolCDE *in vitro* (Nickerson et al., 2018). These inhibitors may therefore function by uncoupling ATP

hydrolysis from the mechanotransmissive movement of the extracytoplasmic domains. Clearly, a general class of inhibitors that could interrupt mechanotransmission would be immediately useful as tools to study MacB-like transporters and, in the longer term, as potential new antibiotics. Indeed, targeting MacB-like ABC transporters for inhibition is particularly attractive, not only because FtsEX and LolCDE are essential, but also because this class of transporters is absent in humans.

The importance of the MacB architecture in bacterial physiology is becoming increasingly apparent. The recent structures now provide a template to understand its action not only in antibiotic resistance but in underpinning a variety of

fundamental bacterial cell processes which are themselves targets for antimicrobial therapy.

## AUTHOR CONTRIBUTIONS

NG wrote the draft manuscript. AC and EK prepared the figures. All authors read and revised the final manuscript.

## FUNDING

The authors gratefully acknowledge grants from the Medical Research Council (MR/N000994/1) and the Wellcome Trust (101828/Z/13/Z).

## REFERENCES

- Aires, J. R., and Nikaido, H. (2005). Aminoglycosides are captured from both periplasm and cytoplasm by the AcrD multidrug efflux transporter of *Escherichia coli*. *J. Bacteriol.* 187, 1923–1929. doi: 10.1128/JB.187.6.1923-1929.2005
- Akama, H., Kanemaki, M., Yoshimura, M., Tsukihara, T., Kashiwagi, T., Yoneyama, H., et al. (2004). Crystal structure of the drug discharge outer membrane protein, OprM, of *Pseudomonas aeruginosa*: dual modes of membrane anchoring and occluded cavity end. *J. Biol. Chem.* 279, 52816–52819. doi: 10.1074/jbc.C400445200
- Al-Hamad, A., Upton, M., and Burnie, J. (2009). Molecular cloning and characterization of SmrA, a novel ABC multidrug efflux pump from *Stenotrophomonas maltophilia*. *J. Antimicrob. Chemother.* 64, 731–734. doi: 10.1093/jac/dkp271
- Aller, S. G., Yu, J., Ward, A., Weng, Y., Chittaboina, S., Zhuo, R., et al. (2009). Structure of P-glycoprotein reveals a molecular basis for poly-specific drug binding. *Science* 323, 1718–1722. doi: 10.1126/science.1168750
- Bader, M. W., Sanowar, S., Daley, M. E., Schneider, A. R., Cho, U., Xu, W., et al. (2005). Recognition of antimicrobial peptides by a bacterial sensor kinase. *Cell* 122, 461–472. doi: 10.1016/j.cell.2005.05.030
- Balibar, C. J., Vaillancourt, F. H., and Walsh, C. T. (2005). Generation of D amino acid residues in assembly of arthorfactin by dual condensation/epimerization domains. *Chem. Biol.* 12, 1189–1200. doi: 10.1016/j.chembiol.2005.08.010
- Barrera, N. P., Isaacson, S. C., Zhou, M., Bavro, V. N., Welch, A., Schaedler, T. A., et al. (2009). Mass spectrometry of membrane transporters reveals subunit stoichiometry and interactions. *Nat. Methods* 6, 585–587. doi: 10.1038/nmeth.1347
- Bavro, V. N., Pietras, Z., Furnham, N., Pérez-Cano, L., Fernández-Recio, J., Pei, X. Y., et al. (2008). Assembly and channel opening in a bacterial drug efflux machine. *Mol. Cell* 30, 114–121. doi: 10.1016/j.molcel.2008.02.015
- Bibb, L. A., and Schmitt, M. P. (2010). The ABC transporter HrtAB confers resistance to hemin toxicity and is regulated in a hemin-dependent manner by the ChrAS two-component system in *Corynebacterium diphtheriae*. *J. Bacteriol.* 192, 4606–4617. doi: 10.1128/JB.00525-10
- Bogomolnaya, L. M., Andrews, K. D., Talamantes, M., Maple, A., Ragoza, Y., Vazquez-Torres, A., et al. (2013). The ABC-type efflux pump MacAB protects *Salmonella enterica* serovar typhimurium from oxidative stress. *MBio* 4, e00630–e00613. doi: 10.1128/mBio.00630-13
- Bountra, K., Hagelueken, G., Choudhury, H. G., Corradi, V., El Omari, K., Wagner, A., et al. (2017). Structural basis for antibacterial peptide self-immunity by the bacterial ABC transporter McjD. *EMBO J.* 36, 3062–3079. doi: 10.15252/embj.201797278
- Cho, H., and Kang, H. (2012). The PseEF efflux system is a virulence factor of *Pseudomonas syringae* pv. *syringae*. *J. Microbiol.* 50, 79–90. doi: 10.1007/s12275-012-1353-9
- Choudhury, H. G., Tong, Z., Mathavan, I., Li, Y., Iwata, S., Zirah, S., et al. (2014). Structure of an antibacterial peptide ATP-binding cassette transporter in a novel outward occluded state. *Proc. Natl. Acad. Sci. U.S.A.* 111, 9145–9150. doi: 10.1073/pnas.1320506111
- Collins, B., Curtis, N., Cotter, P. D., Hill, C., and Ross, R. P. (2010). The ABC transporter AnrAB contributes to the innate resistance of *Listeria monocytogenes* to nisin, bacitracin, and various beta-lactam antibiotics. *Antimicrob. Agents Chemother.* 54, 4416–4423. doi: 10.1128/AAC.00503-10
- Coumes-Florens, S., Brochier-Armanet, C., Guiseppe, A., Denizot, F., and Foglino, M. (2011). A new highly conserved antibiotic sensing/resistance pathway in firmicutes involves an ABC transporter interplaying with a signal transduction system. *PLoS ONE* 6:e15951. doi: 10.1371/journal.pone.0015951
- Crow, A., Greene, N. P., Kaplan, E., and Koronakis, V. (2017). Structure and mechanotransmission mechanism of the MacB ABC transporter superfamily. *Proc. Natl. Acad. Sci. U.S.A.* 114, 12572–12577. doi: 10.1073/pnas.1712153114
- Daur, L., Orange, F., Taveau, J.-C., Verchère, A., Monlezun, L., Gounou, C., et al. (2016). Tripartite assembly of RND multidrug efflux pumps. *Nat. Commun.* 7:10731. doi: 10.1038/ncomms10731
- Dawson, R. J., and Locher, K. P. (2006). Structure of a bacterial multidrug ABC transporter. *Nature* 443, 180–185. doi: 10.1038/nature05155
- Diaz, M., Valdivia, E., Martínez-Bueno, M., Fernández, M., Soler-González, A. S., Ramírez-Rodrigo, H., et al. (2003). Characterization of a new operon, as-48EFGH, from the as-48 gene cluster involved in immunity to enterocin AS-48. *Appl. Environ. Microbiol.* 69, 1229–1236. doi: 10.1128/AEM.69.2.1229-1236.2003
- Dintner, S., Heermann, R., Fang, C., Jung, K., and Gebhard, S. (2014). A sensory complex consisting of an ATP-binding cassette transporter and a two-component regulatory system controls bacitracin resistance in *Bacillus subtilis*. *J. Biol. Chem.* 289, 27899–27910. doi: 10.1074/jbc.M114.596221
- Dintner, S., Staron, A., Berchtold, E., Petri, T., Mascher, T., and Gebhard, S. (2011). Coevolution of ABC transporters and two-component regulatory systems as resistance modules against antimicrobial peptides in Firmicutes Bacteria. *J. Bacteriol.* 193, 3851–3862. doi: 10.1128/JB.05175-11
- Draper, L. A., Cotter, P. D., Hill, C., and Ross, R. P. (2015). Antibiotic resistance. *Microbiol. Mol. Biol. Rev.* 79, 171–191. doi: 10.1128/MMBR.00051-14
- Dubern, J.-F., Coppoolse, E. R., Stiekema, W. J., and Bloemberg, G. V. (2008). Genetic and functional characterization of the gene cluster directing the biosynthesis of putisolvin I and II in *Pseudomonas putida* strain PCL1445. *Microbiology* 154, 2070–2083. doi: 10.1099/mic.0.2008/016444-0
- Du, D., Wang, Z., James, N. R., Voss, J. E., Klimont, E., Ohene-Agyei, T., et al. (2014). Structure of the AcrAB-TolC multidrug efflux pump. *Nature* 509, 512–515. doi: 10.1038/nature13205
- Du, S., Pichoff, S., and Lutkenhaus, J. (2016). FtsEX acts on FtsA to regulate divisome assembly and activity. *Proc. Natl. Acad. Sci. U.S.A.* 113, E5052–E5061. doi: 10.1073/pnas.1606656113
- Eicher, T., Cha, H., Seeger, M. A., Brandstätter, L., El-Delik, J., Bohnert, J. A., et al. (2012). Transport of drugs by the multidrug transporter AcrB involves an access and a deep binding pocket that are separated by a switch-loop. *Proc. Natl. Acad. Sci. U.S.A.* 109, 5687–5692. doi: 10.1073/pnas.1114944109

- Federici, L., Du, D., Walas, F., Matsumura, H., Fernandez-Recio, J., McKeegan, K. S., et al. (2005). The crystal structure of the outer membrane protein VceC from the bacterial pathogen *Vibrio cholerae* at 1.8 Å resolution. *J. Biol. Chem.* 280, 15307–15314. doi: 10.1074/jbc.M500410200
- Fitzpatrick, A. W. P., Llabrés, S., Neuberger, A., Blaza, J. N., Bai, X.-C., Okada, U., et al. (2017). Structure of the MacAB–TolC ABC-type tripartite multidrug efflux pump. *Nat. Microbiol.* 2:17070. doi: 10.1038/nmicrobiol.2017.70
- Foreman, D. T., Martinez, Y., Coombs, G., Torres, A., and Kupersztoch, Y. M. (1995). TolC and DsbA are needed for the secretion of STB, a heat-stable enterotoxin of *Escherichia coli*. *Mol. Microbiol.* 18, 237–245. doi: 10.1111/j.1365-2958.1995.mmi\_18020237.x
- Garti-Levi, S., Hazan, R., Kain, J., Fujita, M., and Ben-Yehuda, S. (2008). The FtsEX ABC transporter directs cellular differentiation in *Bacillus subtilis*. *Mol. Microbiol.* 69, 1018–1028. doi: 10.1111/j.1365-2958.2008.06340.x
- González, C., Langdon, G. M., Bruix, M., Gálvez, A., Valdivia, E., Maqueda, M., et al. (2000). Bacteriocin AS-48, a microbial cyclic polypeptide structurally and functionally related to mammalian NK-lysin. *Proc. Natl. Acad. Sci. U.S.A.* 97, 11221–11226. doi: 10.1073/pnas.210301097
- Greene, N. P., Hinchliffe, P., Crow, A., Ababou, A., Hughes, C., and Koronakis, V. (2013). Structure of an atypical periplasmic adaptor from a multidrug efflux pump of the spirochete *Borrelia burgdorferi*. *FEBS Lett.* 587, 2984–2988. doi: 10.1016/j.febslet.2013.06.056
- Guan, H.-H., Yoshimura, M., Chuankhayan, P., Lin, C.-C., Chen, N.-C., Yang, M.-C., et al. (2015). Crystal structure of an antigenic outer-membrane protein from *Salmonella Typhi* suggests a potential antigenic loop and an efflux mechanism. *Sci. Rep.* 5:16441. doi: 10.1038/srep16441
- Hannauer, M., Schäfer, M., Hoegy, F., Gizzi, P., Wehrung, P., Mislin, G. L. A., et al. (2012). Biosynthesis of the pyoverdine siderophore of *Pseudomonas aeruginosa* involves precursors with a myristic or a myristoleic acid chain. *FEBS Lett.* 586, 96–101. doi: 10.1016/j.febslet.2011.12.004
- Hannauer, M., Yeterian, E., Martin, L. W., Lamont, I. L., and Schalk, I. J. (2010). An efflux pump is involved in secretion of newly synthesized siderophore by *Pseudomonas aeruginosa*. *FEBS Lett.* 584, 4751–4755. doi: 10.1016/j.febslet.2010.10.051
- Harley, K. T., Djordjevic, G. M., Tseng, T.-T., and Saier, M. H. (2000). Membrane-fusion protein homologues in Gram-positive bacteria. *Mol. Microbiol.* 36, 516–517. doi: 10.1046/j.1365-2958.2000.01866.x
- Henry, R., Vithanage, N., Harrison, P., Seemann, T., Coutts, S., Moffatt, J. H., et al. (2012). Colistin-resistant, lipopolysaccharide-deficient *Acinetobacter baumannii* responds to lipopolysaccharide loss through increased expression of genes involved in the synthesis and transport of lipoproteins, phospholipids, and poly- $\beta$ -1,6-N-acetylglucos. *Antimicrob. Agents Chemother.* 56, 59–69. doi: 10.1128/AAC.05191-11
- Higgins, M. K., Bokma, E., Koronakis, E., Hughes, C., and Koronakis, V. (2004). Structure of the periplasmic component of a bacterial drug efflux pump. *Proc. Natl. Acad. Sci. U.S.A.* 101, 9994–9999. doi: 10.1073/pnas.0400375101
- Hinchliffe, P., Greene, N. P., Paterson, N. G., Crow, A., Hughes, C., and Koronakis, V. (2014). Structure of the periplasmic adaptor protein from a major facilitator superfamily (MFS) multidrug efflux pump. *FEBS Lett.* 588, 3147–3153. doi: 10.1016/j.febslet.2014.06.055
- Hinchliffe, P., Symmons, M. F., Hughes, C., and Koronakis, V. (2013). Structure and operation of bacterial tripartite pumps. *Annu. Rev. Microbiol.* 67, 221–242. doi: 10.1146/annurev-micro-092412-155718
- Hobbs, E. C., Yin, X., Paul, B. J., Astarita, J. L., and Storz, G. (2012). Conserved small protein associates with the multidrug efflux pump AcrB and differentially affects antibiotic resistance. *Proc. Natl. Acad. Sci. U.S.A.* 109, 16696–16701. doi: 10.1073/pnas.1210093109
- Hollenstein, K., Frei, D. C., and Locher, K. P. (2007). Structure of an ABC transporter in complex with its binding protein. *Nature* 446, 213–216. doi: 10.1038/nature05626
- Imperi, F., Tiburzi, F., and Visca, P. (2009). Molecular basis of pyoverdine siderophore recycling in *Pseudomonas aeruginosa*. *Proc. Natl. Acad. Sci. U.S.A.* 106, 20440–20445. doi: 10.1073/pnas.0908760106
- Johnson, Z. L., and Chen, J. (2017). Structural basis of substrate recognition by the multidrug resistance protein MRP1. *Cell* 168, 1075.e9–1085.e9. doi: 10.1016/j.cell.2017.01.041
- Johnson, Z. L., and Chen, J. (2018). ATP binding enables substrate release from multidrug resistance protein 1. *Cell* 172, 81.e10–83.e10. doi: 10.1016/j.cell.2017.12.005
- Joubert, L., Derré-Bobillot, A., Gaudu, P., Gruss, A., and Lechardeur, D. (2014). HrtBA and menaquinones control haem homeostasis in *Lactococcus lactis*. *Mol. Microbiol.* 93, 823–833. doi: 10.1111/mmi.12705
- Kallenberg, F., Dintner, S., Schmitz, R., and Gebhard, S. (2013). Identification of regions important for resistance and signalling within the antimicrobial peptide transporter BceAB of *Bacillus subtilis*. *J. Bacteriol.* 195, 3287–3297. doi: 10.1128/JB.00419-13
- Khwaja, M., Ma, Q., and Saier, M. H. (2005). Topological analysis of integral membrane constituents of prokaryotic ABC efflux systems. *Res. Microbiol.* 156, 270–277. doi: 10.1016/j.resmic.2004.07.010
- Kingston, A. W., Zhao, H., Cook, G. M., and Helmann, J. D. (2014). Accumulation of heptaprenyl diphosphate sensitizes *Bacillus subtilis* to bacitracin: implications for the mechanism of resistance mediated by the BceAB transporter. *Mol. Microbiol.* 93, 37–49. doi: 10.1111/mmi.12637
- Khosa, S., AlKhatib, Z., and Smits, S. H. J. (2013). NSR from *Streptococcus agalactiae* confers resistance against nisin and is encoded by a conserved nsr operon. *Biol. Chem.* 394, 1543–1549. doi: 10.1515/hsz-2013-0167
- Kobayashi, N., Nishino, K., Hirata, T., and Yamaguchi, A. (2003). Membrane topology of ABC-type macrolide antibiotic exporter MacB in *Escherichia coli*. *FEBS Lett.* 546, 241–246. doi: 10.1016/S0014-5793(03)00579-9
- Kobayashi, N., Nishino, K., and Yamaguchi, A. (2001). Novel macrolide-specific ABC-type efflux transporter in *Escherichia coli*. *J. Bacteriol.* 183, 5639–5644. doi: 10.1128/JB.183.19.5639-5644.2001
- Korkhov, V. M., Mireku, S. A., and Locher, K. P. (2012). Structure of AMP-PNP-bound vitamin B12 transporter BtuCD–F. *Nature* 490, 367–372. doi: 10.1038/nature11442
- Koronakis, V., Sharff, A., Koronakis, E., Luisi, B., and Hughes, C. (2000). Crystal structure of the bacterial membrane protein TolC central to multidrug efflux and protein export. *Nature* 405, 914–919. doi: 10.1038/35016007
- Kulathila, R., Kulathila, R., Indic, M., and van den Berg, B. (2011). Crystal structure of *Escherichia coli* CusC, the outer membrane component of a heavy metal efflux pump. *PLoS ONE* 6:e15610. doi: 10.1371/journal.pone.0015610
- Lee, J.-Y., Kinch, L. N., Borek, D. M., Wang, J., Wang, J., Urbatsch, I. L., et al. (2016). Crystal structure of the human sterol transporter ABCG5/ABCG8. *Nature* 533, 561–564. doi: 10.1038/nature17666
- Lim, S. P., Roongsawang, N., Washio, K., and Morikawa, M. (2009). Flexible exportation mechanisms of arthofactin in *Pseudomonas* sp. MIS38. *J. Appl. Microbiol.* 107, 157–166. doi: 10.1111/j.1365-2672.2009.04189.x
- Lin, D. Y., Huang, S., and Chen, J. (2015a). Crystal structures of a polypeptide processing and secretion transporter. *Nature* 523, 425–430. doi: 10.1038/nature14623
- Lin, H. T., Bavro, V. N., Barrera, N. P., Frankish, H. M., Velamakanni, S., Van Veen, H. W., et al. (2009). MacB ABC transporter is a dimer whose ATPase activity and macrolide-binding capacity are regulated by the membrane fusion protein MacA. *J. Biol. Chem.* 284, 1145–1154. doi: 10.1074/jbc.M806964200
- Lin, H.-T. V., Massam-Wu, T., Lin, C.-P., Wang, Y.-J. A., Shen, Y.-C., Lu, W.-J., et al. (2017). The *Vibrio cholerae* var regulon encodes a metallo- $\beta$ -lactamase and an antibiotic efflux pump, which are regulated by VarR, a LysR-type transcription factor. *PLoS ONE* 12:e0184255. doi: 10.1371/journal.pone.0184255
- Lin, M.-F., Lin, Y.-Y., Tu, C.-C., and Lan, C.-Y. (2015b). Distribution of different efflux pump genes in clinical isolates of multidrug-resistant *Acinetobacter baumannii* and their correlation with antimicrobial resistance. *J. Microbiol. Immunol. Infect.* 50, 224–231. doi: 10.1016/j.jmii.2015.04.004
- Lin, Y. T., Huang, Y. W., Liou, R. S., Chang, Y. C., and Yang, T. C. (2014). MacABCsm, an ABC-type tripartite efflux pump of *Stenotrophomonas maltophilia* involved in drug resistance, oxidative and envelope stress tolerances and biofilm formation. *J. Antimicrob. Chemother.* 69, 3221–3226. doi: 10.1093/jac/dku317
- Liu, W.-T., Yang, Y.-L., Xu, Y., Lamsa, A., Haste, N. M., Yang, J. Y., et al. (2010). Imaging mass spectrometry of intraspecies metabolic exchange revealed the cannibalistic factors of *Bacillus subtilis*. *Proc. Natl. Acad. Sci. U.S.A.* 107, 16286–16290. doi: 10.1073/pnas.1008368107



- Li, W., Rokni-Zadeh, H., De Vleeschouwer, M., Ghequire, M. G. K., Sinnaeve, D., Xie, G.-L., et al. (2013). The antimicrobial compound xantholysin defines a new group of *Pseudomonas* cyclic lipopeptides. *PLoS ONE* 8:e62946. doi: 10.1371/journal.pone.0062946
- Locher, K. P. (2016). Mechanistic diversity in ATP-binding cassette (ABC) transporters. *Nat. Struct. Mol. Biol.* 23, 487–493. doi: 10.1038/nsmb.3216
- Lomovskaya, O., and Lewis, K. (1992). Emr, an *Escherichia coli* locus for multidrug resistance. *Proc. Natl. Acad. Sci. U.S.A.* 89, 8938–8942. doi: 10.1073/pnas.89.19.8938
- Lubelski, J., Konings, W. N., and Driessen, A. J. M. (2007). Distribution and physiology of ABC-Type transporters contributing to multidrug resistance in bacteria. *Microbiol. Mol. Biol. Rev.* 71, 463–476. doi: 10.1128/MMBR.00001-07
- Lu, S., and Zgurskaya, H. I. (2012). Role of ATP binding and hydrolysis in assembly of MacAB-TolC macrolide transporter. *Mol. Microbiol.* 86, 1132–1143. doi: 10.1111/mmi.12046
- Lu, S., and Zgurskaya, H. I. (2013). MacA, a periplasmic membrane fusion protein of the macrolide transporter MacAB-TolC, binds lipopolysaccharide core specifically and with high affinity. *J. Bacteriol.* 195, 4865–4872. doi: 10.1128/JB.00756-13
- Luo, Q., Yang, X., Yu, S., Shi, H., Wang, K., Xiao, L., et al. (2017). Structural basis for lipopolysaccharide extraction by ABC transporter LptB2FG. *Nat. Struct. Mol. Biol.* 24, 469–474. doi: 10.1038/nsmb.3399
- Majchrzykiewicz, J. A., Kuipers, O. P., and Bijlsma, J. J. E. (2010). Generic and specific adaptive responses of *Streptococcus pneumoniae* to challenge with three distinct antimicrobial peptides, bacitracin, LL-37, and nisin. *Antimicrob. Agents Chemother.* 54, 440–451. doi: 10.1128/AAC.00769-09
- Matias, V. R., and Beveridge, T. J. (2006). Native cell wall organization shown by cryo-electron microscopy confirms the existence of a periplasmic space in *Staphylococcus aureus*. *J. Bacteriol.* 188, 1011–1021. doi: 10.1128/JB.188.3.1011-1021.2006
- Matson, J. S., Livny, J., and DiRita, V. J. (2017). A putative *Vibrio cholerae* two-component system controls a conserved periplasmic protein in response to the antimicrobial peptide polymyxin B. *PLoS ONE* 12:e0186199. doi: 10.1371/journal.pone.0186199
- Matsuo, T., Chen, J., Minato, Y., Ogawa, W., Mizushima, T., Kuroda, T., et al. (2008). SmdAB, a heterodimeric ABC-Type multidrug efflux pump, in *Serratia marcescens*. *J. Bacteriol.* 190, 648–654. doi: 10.1128/JB.01513-07
- Mavrici, D., Marakalala, M. J., Holton, J. M., Prigozhin, D. M., Gee, C. L., Zhang, Y. J., et al. (2014). *Mycobacterium tuberculosis* FtsX extracellular domain activates the peptidoglycan hydrolase, RipC. *Proc. Natl. Acad. Sci. U.S.A.* 111, 8037–8042. doi: 10.1073/pnas.1321812111
- McLeod, S. M., Fleming, P. R., MacCormack, K., McLaughlin, R. E., Whiteaker, J. D., Narita, S.-I., et al. (2015). Small-molecule inhibitors of gram-negative lipoprotein trafficking discovered by phenotypic screening. *J. Bacteriol.* 197, 1075–1082. doi: 10.1128/JB.02352-14
- Meehl, M., Herbert, S., Götz, F., and Cheung, A. (2007). Interaction of the GraRS two-component system with the VraFG ABC transporter to support vancomycin-intermediate resistance in *Staphylococcus aureus*. *Antimicrob. Agents Chemother.* 51, 2679–2689. doi: 10.1128/AAC.00209-07
- Mikolosko, J., Bobyk, K., Zgurskaya, H. I., and Ghosh, P. (2006). Conformational flexibility in the multidrug efflux system protein AcrA. *Structure* 14, 577–587. doi: 10.1016/j.str.2005.11.015
- Mi, W., Li, Y., Yoon, S. H., Ernst, R. K., Walz, T., and Liao, M. (2017). Structural basis of MsbA-mediated lipopolysaccharide transport. *Nature* 549, 233–237. doi: 10.1038/nature23649
- Miyamoto, S., and Tokuda, H. (2007). Diverse effects of phospholipids on lipoprotein sorting and ATP hydrolysis by the ABC transporter LolCDE complex. *Biochim. Biophys. Acta* 1768, 1848–1854. doi: 10.1016/j.bbame.2007.04.005
- Modali, S. D., and Zgurskaya, H. I. (2011). The periplasmic membrane proximal domain of MacA acts as a switch in stimulation of ATP hydrolysis by MacB transporter. *Mol. Microbiol.* 81, 937–951. doi: 10.1111/j.1365-2958.2011.07744.x
- Murakami, S., Nakashima, R., Yamashita, E., Matsumoto, T., and Yamaguchi, A. (2006). Crystal structures of a multidrug transporter reveal a functionally rotating mechanism. *Nature* 443, 173–179. doi: 10.1038/nature05076
- Murakami, S., Nakashima, R., Yamashita, E., and Yamaguchi, A. (2002). Crystal structure of bacterial multidrug efflux transporter AcrB. *Nature* 419, 587–593. doi: 10.1038/nature01050
- Nakashima, R., Sakurai, K., Yamasaki, S., Nishino, K., and Yamaguchi, A. (2011). Structures of the multidrug exporter AcrB reveal a proximal multisite drug-binding pocket. *Nature* 480, 565–569. doi: 10.1038/nature10641
- Narita, S. I., and Tokuda, H. (2017). Bacterial lipoproteins; biogenesis, sorting and quality control. *Biochim. Biophys. Acta* 1862, 1414–1423. doi: 10.1016/j.bbali.2016.11.009
- Nayar, A. S., Dougherty, T. J., Ferguson, K. E., Granger, B. A., McWilliams, L., Stacey, C., et al. (2015). Novel antibacterial targets and compounds revealed by a high-throughput cell wall reporter assay. *J. Bacteriol.* 197, 1726–1734. doi: 10.1128/JB.02552-14
- Nickerson, N. N., Jao, C. C., Xu, Y., Quinn, J., Skippington, E., Alexander, M. K., et al. (2018). A novel inhibitor of the LolCDE ABC transporter essential for lipoprotein trafficking in Gram-negative bacteria. *Antimicrob. Agents Chemother.* 62:e02151-17. doi: 10.1128/AAC.02151-17
- Nishi, J., Sheikh, J., Mizuguchi, K., Luisi, B., Burland, V., Boutin, A., et al. (2003). The export of coat protein from enteroaggregative *Escherichia coli* by a specific ATP-binding cassette transporter system. *J. Biol. Chem.* 278, 45680–45689. doi: 10.1074/jbc.M306413200
- Nishino, K., Latifi, T., and Groisman, E. A. (2006). Virulence and drug resistance roles of multidrug efflux systems of *Salmonella enterica* serovar Typhimurium. *Mol. Microbiol.* 59, 126–141. doi: 10.1111/j.1365-2958.2005.04940.x
- Okada, U., Yamashita, E., Neuberger, A., Morimoto, M., van Veen, H. W., and Murakami, S. (2017). Crystal structure of tripartite-type ABC transporter MacB from *Acinetobacter baumannii*. *Nat. Commun.* 8:1336. doi: 10.1038/s41467-017-01399-2
- Pei, X.-Y., Hinchliffe, P., Symmons, M. F., Koronakis, E., Benz, R., Hughes, C., et al. (2011). Structures of sequential open states in a symmetrical opening transition of the TolC exit duct. *Proc. Natl. Acad. Sci. U.S.A.* 108, 2112–2117. doi: 10.1073/pnas.1012588108
- Perez, C., Gerber, S., Boilevin, J., Bucher, M., Darbre, T., Aebi, M., et al. (2015). Structure and mechanism of an active lipid-linked oligosaccharide flippase. *Nature* 524, 433–438. doi: 10.1038/nature14953
- Phelps, H. A., and Neely, M. N. (2007). SalY of the *Streptococcus pyogenes* lantibiotic locus is required for full virulence and intracellular survival in macrophages. *Infect. Immun.* 75, 4541–4551. doi: 10.1128/IAI.00518-07
- Picard, M., Tikhonova, E. B., Broutin, I., Lu, S., Verchère, A., and Zgurskaya, H. I. (2018). Biochemical reconstitution and characterization of multicomponent drug efflux transporters *Methods Mol. Biol.* 1700, 113–145. doi: 10.1007/978-1-4939-7454-2\_8
- Pilonieta, M. C., Boder, M. D., and Munson, G. P. (2007). CfaD-dependent expression of a novel extracytoplasmic protein from enterotoxigenic *Escherichia coli*. *J. Bacteriol.* 189, 5060–5067. doi: 10.1128/JB.00131-07
- Popella, P., Krauss, S., Ebner, P., Nega, M., Deibert, J., and Götz, F. (2016). VraH Is the Third component of the *Staphylococcus aureus* VraDEH system involved in gallidermin and daptomycin resistance and pathogenicity. *Antimicrob. Agents Chemother.* 60, 2391–2401. doi: 10.1128/AAC.02865-15
- Prost, L. R., Sanowar, S., and Miller, S. I. (2007). Salmonella sensing of antimicrobial mechanisms to promote survival within macrophages. *Immunol. Rev.* 219, 55–65. doi: 10.1111/j.1600-065X.2007.00557.x
- Quigley, N. B., Mo, Y.-Y., and Gross, D. C. (1993). SyrD is required for syringomycin production by *Pseudomonas syringae* pathovar syringae and is related to a family of ATP-binding secretion proteins. *Mol. Microbiol.* 9, 787–801. doi: 10.1111/j.1365-2958.1993.tb01738.x
- Quistgaard, E. M., Löw, C., Guettou, F., and Nordlund, P. (2016). Understanding transport by the major facilitator superfamily (MFS): structures pave the way. *Nat. Rev. Mol. Cell Biol.* 17, 123–132. doi: 10.1038/nrm.2015.25
- Ramachandra, M., Ambudkar, S. V., Chen, D., Hrycyna, C. A., Dey, S., Gottesman, M. M., et al. (1998). Human P-Glycoprotein exhibits reduced affinity for substrates during a catalytic transition state †. *Biochemistry* 37, 5010–5019. doi: 10.1021/bi973045u
- Reuter, G., Janvilisri, T., Venter, H., Shahi, S., Balakrishnan, L., and van Veen, H. W. (2003). The ATP binding cassette multidrug transporter LmrA and lipid transporter MsbA have overlapping substrate specificities. *J. Biol. Chem.* 278, 35193–35198. doi: 10.1074/jbc.M306226200

- Rietkötter, E., Hoyer, D., and Mascher, T. (2008). Bacitracin sensing in *Bacillus subtilis*. *Mol. Microbiol.* 68, 768–785. doi: 10.1111/j.1365-2958.2008.06194.x
- Rouquette-Loughlin, C. E., Balthazar, J. T., and Shafer, W. M. (2005). Characterization of the MacA-MacB efflux system in *Neisseria gonorrhoeae*. *J. Antimicrob. Chemother.* 56, 856–860. doi: 10.1093/jac/dki333
- Schmidt, K. L., Peterson, N. D., Kustus, R. J., Wissel, M. C., Graham, B., Phillips, G. J., et al. (2004). A predicted ABC transporter, FtsEX, is needed for cell division in *Escherichia coli*. *J. Bacteriol.* 186, 785–793. doi: 10.1128/JB.186.3.785-793.2004
- Seeger, M. A., Schiefner, A., Eicher, T., Verrey, F., Diederichs, K., and Pos, K. M. (2006). Structural asymmetry of AcrB trimer suggests a peristaltic pump mechanism. *Science* 313, 1295–1298. doi: 10.1126/science.1131542
- Sham, L.-T., Barendt, S. M., Kopecky, K. E., and Winkler, M. E. (2011). Essential PcsB putative peptidoglycan hydrolase interacts with the essential FtsXSpn cell division protein in *Streptococcus pneumoniae* D39. *Proc. Natl. Acad. Sci. U.S.A.* 108, E1061–E1069. doi: 10.1073/pnas.1108323108
- Singh, H., Velamakanni, S., Deery, M. J., Howard, J., Wei, S. L., and van Veen, H. W. (2016). ATP-dependent substrate transport by the ABC transporter MsbA is proton-coupled. *Nat. Commun.* 7:12387. doi: 10.1038/ncomms12387
- Staron, P., Forchhammer, K., and Maldener, I. (2011). Novel ATP-driven pathway of glycolipid export involving TolC protein. *J. Biol. Chem.* 286, 38202–38210. doi: 10.1074/jbc.M111.269332
- Staron, P., Forchhammer, K., and Maldener, I. (2014). Structure-function analysis of the ATP-driven glycolipid efflux pump DevBCA reveals complex organization with TolC/HgdD. *FEBS Lett.* 588, 395–400. doi: 10.1016/j.febslet.2013.12.004
- Stauff, D. L., Bagaley, D., Torres, V. J., Joyce, R., Anderson, K. L., Kuechenmeister, L., et al. (2008). *Staphylococcus aureus* HrtA Is an ATPase required for protection against heme toxicity and prevention of a transcriptional heme stress response. *J. Bacteriol.* 190, 3588–3596. doi: 10.1128/JB.01921-07
- Storz, G., Wolf, Y. I., and Ramamurthi, K. S. (2014). Small proteins can no longer be ignored. *Annu. Rev. Biochem.* 83, 753–777. doi: 10.1146/annurev-biochem-070611-102400
- Su, C.-C., Radhakrishnan, A., Kumar, N., Long, F., Bolla, J. R., Lei, H.-T., et al. (2014). Crystal structure of the *Campylobacter jejuni* CmeC outer membrane channel. *Protein Sci.* 23, 954–961. doi: 10.1002/pro.2478
- Tal, N., and Schuldiner, S. (2009). A coordinated network of transporters with overlapping specificities provides a robust survival strategy. *Proc. Natl. Acad. Sci. U.S.A.* 106, 9051–9056. doi: 10.1073/pnas.0902400106
- Tanabe, M., Szakonyi, G., Brown, K. A., Henderson, P. J. F., Nield, J., and Byrne, B. (2009). The multidrug resistance efflux complex, EmrAB from *Escherichia coli* forms a dimer *in vitro*. *Biochem. Biophys. Res. Commun.* 380, 338–342. doi: 10.1016/j.bbrc.2009.01.081
- ter Beek, J., Guskov, A., and Slotboom, D. J. (2014). Structural diversity of ABC transporters. *J. Gen. Physiol.* 143, 419–435. doi: 10.1085/jgp.201411164
- Thanabalu, T., Koronakis, E., Hughes, C., and Koronakis, V. (1998). Substrate-induced assembly of a contiguous channel for protein export from *E. coli*: reversible bridging of an inner-membrane translocase to an outer membrane exit pore. *EMBO J.* 17, 6487–6496.
- Tikhonova, E. B., Devroy, V. K., Lau, S. Y., and Zgurskaya, H. I. (2007). Reconstitution of the *Escherichia coli* macrolide transporter: the periplasmic membrane fusion protein MacA stimulates the ATPase activity of MacB. *Mol. Microbiol.* 63, 895–910. doi: 10.1111/j.1365-2958.2006.05549.x
- Tsuda, H., Yamashita, Y., Shibata, Y., Nakano, Y., and Koga, T. (2002). Genes involved in bacitracin resistance in *Streptococcus mutans*. *Antimicrob. Agents Chemother.* 46, 3756–3764. doi: 10.1128/AAC.46.12.3756-3764.2002
- Turlin, E., Heuck, G., Simões Brandão, M. I., Szili, N., Mellin, J. R., Lange, N., et al. (2014). Protoporphyrin (PPIX) efflux by the MacAB-TolC pump in *Escherichia coli*. *Microbiologyopen* 3, 849–859. doi: 10.1002/mbo3.203
- van Veen, H. W., Venema, K., Bolhuis, H., Oussenko, I., Kok, J., Poolman, B., et al. (1996). Multidrug resistance mediated by a bacterial homolog of the human multidrug transporter MDRI. *Proc. Natl. Acad. Sci. U.S.A.* 93, 10668–10672. doi: 10.1073/pnas.93.20.10668
- Velarde, J. J., Varney, K. M., Inman, K. G., Farfan, M., Dudley, E., Fletcher, J., et al. (2007). Solution structure of the novel dispersin protein of enteroaggregative *Escherichia coli*. *Mol. Microbiol.* 66, 1123–1135. doi: 10.1111/j.1365-2958.2007.05985.x
- Wakeman, C. A., Hammer, N. D., Stauff, D. L., Attia, A. S., Anzaldi, L. L., Dikalov, S. I., et al. (2012). Menaquinone biosynthesis potentiates haem toxicity in *Staphylococcus aureus*. *Mol. Microbiol.* 86, 1376–1392. doi: 10.1111/mmi.12063
- Wang, B., Dukarevich, M., Sun, E. I., Yen, M. R., and Saier, M. H. (2009). Membrane porters of ATP-binding cassette transport systems are polyphyletic. *J. Membr. Biol.* 231, 1–10. doi: 10.1007/s00232-009-9200-6
- Wang, Z., Fan, G., Hryc, C. F., Blaza, J. N., Serysheva, I. I., Schmid, M. F., et al. (2017). An allosteric transport mechanism for the AcrAB-TolC multidrug efflux pump. *Elife* 6, 1–19. doi: 10.7554/eLife.24905
- Woecking, B., Reuter, G., Shilling, R. A., Velamakanni, S., Shahi, S., Venter, H., et al. (2005). Drug-lipid A interactions on the *Escherichia coli* ABC transporter MsbA. *J. Bacteriol.* 187, 6363–6369. doi: 10.1128/JB.187.18.6363-6369.2005
- Xu, K., Zhang, M., Zhao, Q., Yu, F., Guo, H., Wang, C., et al. (2013). Crystal structure of a folate energy-coupling factor transporter from *Lactobacillus brevis*. *Nature* 497, 268–271. doi: 10.1038/nature12046
- Xu, Y., Guo, J., Wang, L., Jiang, R., Jin, X., Liu, J., et al. (2016). The crystal structure of the YknZ extracellular domain of ABC transporter YknWXYZ from *Bacillus amyloliquefaciens*. *PLoS ONE* 11:e0155846. doi: 10.1371/journal.pone.0155846
- Xu, Y., Jo, I., Wang, L., Chen, J., Fan, S., Dong, Y., et al. (2017). Hexameric assembly of membrane fusion protein YknX of the sporulation delaying efflux pump from *Bacillus amyloliquefaciens*. *Biochem. Biophys. Res. Commun.* 493, 152–157. doi: 10.1016/j.bbrc.2017.09.059
- Xu, Y., Moeller, A., Jun, S.-Y., Le, M., Yoon, B.-Y., Kim, J.-S., et al. (2012). Assembly and channel opening of outer membrane protein in tripartite drug efflux pumps of Gram-negative bacteria. *J. Biol. Chem.* 287, 11740–11750. doi: 10.1074/jbc.M111.329375
- Xu, Y., Sim, S. H., Ki, H. N., Xiao, L. J., Kim, H. M., Kwang, Y. H., et al. (2009). Crystal structure of the periplasmic region of MacB, a noncanonical ABC transporter. *Biochemistry* 48, 5218–5225. doi: 10.1021/bi900415t
- Xu, Y., Sim, S. H., Song, S., Piao, S., Kim, H. M., Jin, X. L., et al. (2010). The tip region of the MacA alpha-hairpin is important for the binding to TolC to the *Escherichia coli* MacAB-TolC pump. *Biochem. Biophys. Res. Commun.* 394, 962–965. doi: 10.1016/j.bbrc.2010.03.097
- Xu, Y., Song, S., Moeller, A., Kim, N., Piao, S., Sim, S. H., et al. (2011). Functional implications of an intermeshing cogwheel-like interaction between TolC and MacA in the action of macrolide-specific efflux pump MacAB-TolC. *J. Biol. Chem.* 286, 13541–13549. doi: 10.1074/jbc.M110.202598
- Yakushi, T., Masuda, K., Narita, S., Matsuyama, S., and Tokuda, H. (2000). A new ABC transporter mediating the detachment of lipid-modified proteins from membranes. *Nat. Cell Biol.* 2, 212–218. doi: 10.1038/35008635
- Yamada, Y., Tikhonova, E. B., and Zgurskaya, H. I. (2012). YknWXYZ is an unusual four-component transporter with a role in protection against sporulation-delaying-protein-induced killing of *Bacillus subtilis*. *J. Bacteriol.* 194, 4386–4394. doi: 10.1128/JB.00223-12
- Yamanaka, H., Kobayashi, H., Takahashi, E., and Okamoto, K. (2008). MacAB is involved in the secretion of *Escherichia coli* heat-stable enterotoxin II. *J. Bacteriol.* 190, 7693–7698. doi: 10.1128/JB.00853-08
- Yang, D. C., Peters, N. T., Parzych, K. R., Uehara, T., Markovski, M., and Bernhardt, T. G. (2011). An ATP-binding cassette transporter-like complex governs cell-wall hydrolysis at the bacterial cytokinetic ring. *Proc. Natl. Acad. Sci. U.S.A.* 108, E1052–E1060. doi: 10.1073/pnas.1107780108
- Yang, H.-B., Hou, W.-T., Cheng, M.-T., Jiang, Y.-L., Chen, Y., and Zhou, C.-Z. (2018). Structure of a MacAB-like efflux pump from *Streptococcus pneumoniae*. *Nat. Commun.* 9:196. doi: 10.1038/s41467-017-02741-4
- Yonehara, R., Yamashita, E., and Nakagawa, A. (2016). Crystal structures of OprN and OprJ, outer membrane factors of multidrug tripartite efflux pumps of *Pseudomonas aeruginosa*. *Proteins* 84, 759–769. doi: 10.1002/prot.25022
- Yum, S., Xu, Y., Piao, S., Sim, S. H., Kim, H. M., Jo, W. S., et al. (2009). Crystal structure of the periplasmic component of a tripartite macrolide-specific efflux pump. *J. Mol. Biol.* 387, 1286–1297. doi: 10.1016/j.jmb.2009.02.048
- Zgurskaya, H. I., Yamada, Y., Tikhonova, E. B., Ge, Q., and Krishnamoorthy, G. (2009). Structural and functional diversity of bacterial membrane fusion proteins. *Biochim. Biophys. Acta* 1794, 794–807. doi: 10.1016/j.bbapap.2008.10.010

- Zuber, B., Haenni, M., Ribeiro, T., Minnig, K., Lopes, F., Moreillon, P., et al. (2006). Granular layer in the periplasmic space of Gram-positive bacteria and fine structures of *Enterococcus gallinarum* and *Streptococcus gordonii* septa revealed by cryo-electron microscopy of vitreous sections. *J. Bacteriol.* 188, 6652–6660. doi: 10.1128/JB.00391-06
- Zutz, A., Hoffmann, J., Hellmich, U. A., Glaubitz, C., Ludwig, B., Brutschy, B., et al. (2011). Asymmetric ATP hydrolysis cycle of the heterodimeric multidrug ABC transport complex TmrAB from *thermus thermophilus*. *J. Biol. Chem.* 286, 7104–7115. doi: 10.1074/jbc.M110.201178
- Zwama, M., Yamasaki, S., Nakashima, R., Sakurai, K., Nishino, K., and Yamaguchi, A. (2018). Multiple entry pathways within the efflux transporter AcrB contribute to multidrug recognition. *Nat. Commun.* 9:124. doi: 10.1038/s41467-017-02493-1

**Conflict of Interest Statement:** The authors declare that the research was conducted in the absence of any commercial or financial relationships that could be construed as a potential conflict of interest.

The reviewer AN declared a shared affiliation, with no collaboration, with several of the authors, NG, EK, VK, to the handling Editor.

Copyright © 2018 Greene, Kaplan, Crow and Koronakis. This is an open-access article distributed under the terms of the Creative Commons Attribution License (CC BY). The use, distribution or reproduction in other forums is permitted, provided the original author(s) and the copyright owner(s) are credited and that the original publication in this journal is cited, in accordance with accepted academic practice. No use, distribution or reproduction is permitted which does not comply with these terms.



# Functional Mechanism of the Efflux Pumps Transcription Regulators From *Pseudomonas aeruginosa* Based on 3D Structures

Karim Housseini B Issa, Gilles Phan and Isabelle Broutin\*

Laboratoire de Cristallographie et RMN Biologiques (UMR 8015), Centre National de la Recherche Scientifique, Faculté de Pharmacie, Université Paris Descartes, Université Sorbonne Paris Cité, Paris, France

## OPEN ACCESS

### Edited by:

Vassiliy Bavro,  
University of Essex, United Kingdom

### Reviewed by:

Zhao Wang,  
Baylor College of Medicine,  
United States  
Anastassios C. Papageorgiou,  
University of Turku, Finland

### \*Correspondence:

Isabelle Broutin  
isabelle.broutin@parisdescartes.fr

### Specialty section:

This article was submitted to  
Structural Biology,  
a section of the journal  
Frontiers in Molecular Biosciences

**Received:** 28 February 2018

**Accepted:** 31 May 2018

**Published:** 19 June 2018

### Citation:

Housseini B Issa K, Phan G and  
Broutin I (2018) Functional Mechanism  
of the Efflux Pumps Transcription  
Regulators From *Pseudomonas*  
*aeruginosa* Based on 3D Structures.  
Front. Mol. Biosci. 5:57.  
doi: 10.3389/fmolb.2018.00057

Bacterial antibiotic resistance is a worldwide health problem that deserves important research attention in order to develop new therapeutic strategies. Recently, the World Health Organization (WHO) classified *Pseudomonas aeruginosa* as one of the priority bacteria for which new antibiotics are urgently needed. In this opportunistic pathogen, antibiotics efflux is one of the most prevalent mechanisms where the drug is efficiently expelled through the cell-wall. This resistance mechanism is highly correlated to the expression level of efflux pumps of the resistance-nodulation-cell division (RND) family, which is finely tuned by gene regulators. Thus, it is worthwhile considering the efflux pump regulators of *P. aeruginosa* as promising therapeutic targets alternative. Several families of regulators have been identified, including activators and repressors that control the genetic expression of the pumps in response to an extracellular signal, such as the presence of the antibiotic or other environmental modifications. In this review, based on different crystallographic structures solved from archetypal bacteria, we will first focus on the molecular mechanism of the regulator families involved in the RND efflux pump expression in *P. aeruginosa*, which are TetR, LysR, MarR, AraC, and the two-components system (TCS). Finally, the regulators of known structure from *P. aeruginosa* will be presented.

**Keywords:** multidrug resistance, efflux pumps regulators, activator, repressor, X-ray structures

## INTRODUCTION

Just after the introduction of antibiotics on the market in the mid-twentieth century, bacterial resistance was recognized as a natural but worrisome phenomenon (McDermott et al., 2003; Hede, 2014). More than 60 years later, the resistance is still a worldwide health concern (Frieri et al., 2017), threatening the effectiveness of antibacterial therapy, and challenging the efforts of developing novel antibiotics (Li et al., 2015), but fortunately some studies tend to give hope in this research area (D'Costa et al., 2011; Rolain et al., 2016).

To survive, bacteria have developed an inexhaustible range of antibiotic resistance mechanisms (Coates et al., 2002; Levy and Marshall, 2004). One of them involves the efflux of toxic compounds through bacterial cell-wall by membrane-bound protein transporters called multidrug efflux pumps (Poole and Srikumar, 2001; Rahman et al., 2017). These multidrug efflux systems (MES) existed in



bacterial genomes long before the use of antibiotics by human to cure infection (Davies and Davies, 2010). MES are essential in bacterial physiology and natural defenses (Poole, 2008; Li and Nikaido, 2009; Alvarez-Ortega et al., 2013; Blanco et al., 2016), including export of organic solvent, detergents, fatty acids, toxic lipids and quorum sensing molecules. Because many structurally unrelated compounds are extruded by the same system, MES are also responsible for the multidrug resistance (MDR) phenotype (Nikaido, 2009). Efflux pumps have been categorized into five different families (Li and Nikaido, 2009), based on three criteria: the amino acid sequence identity, the energy source required to drive export and the substrate specificities (Li et al., 2015). The five major known families are the ATP-binding cassette (ABC) (Szakács et al., 2008; Locher, 2009), the small multidrug resistance (SMR) (Schuldiner, 2009), the major facilitator superfamily (MFS) (Kumar et al., 2013; Yan, 2015), the resistance-nodulation-cell division (RND) (Du et al., 2014; Yamaguchi et al., 2015; Daury et al., 2016; Vargiu et al., 2016) and the multidrug and toxic compound extrusion (MATE) (Hvorup et al., 2003; Kuroda and Tsuchiya, 2009). ABC superfamily belongs to the primary active transporters class which function depends on ATP hydrolysis, whereas the other pumps are secondary active transporters (symporters, antiporters, and uniporters) using energy from proton and/or sodium gradient (Mousa and Bruner, 2016).

Multidrug efflux transporters overexpression is tightly regulated by transcriptional activators and/or repressors upon the presence of toxic compounds (Sun et al., 2014). Interestingly, the regulators themselves are potentially triggered by the substrate that will be transported in turn by the regulated pumps (Schumacher and Brennan, 2002). A very specific and imbricated regulation system seems to link the transcriptional regulators to the cognate efflux pumps expression. In order to combat antibiotic resistance, all the different resistance mechanisms must be targeted, and despite recent encouraging results (Fair and Tor, 2014; Khameneh et al., 2016; Cheesman et al., 2017), multidrug transporters remain largely responsible for antibiotherapy failures (Sun et al., 2014). Because the last discovered antibiotic is specific to Gram positive (Gram+) bacteria (Ling et al., 2015), it is urgent to find new drugs targeting the Gram negative (Gram-). This is also supported by the fact that most of the main problematic multiresistant pathogens in hospitals or “ESKAPE”

bacteria are Gram- (Tacconelli et al., 2017). This acronym comes from the initials of six superbugs which are *Enterococcus faecium* and *Staphylococcus aureus*, both Gram+, and the Gram- *Klebsiella pneumoniae*, *Acinetobacter baumannii*, *Pseudomonas aeruginosa* and *Enterobacter*. The particularity of Gram- bacteria is the presence of two membranes and a soluble space in between called the periplasm. Consequently, the efflux pumps must cross two lipidic barriers and the periplasm to transport the molecules out of the cell. This can be achieved by RND transporters that represent the major drug efflux pumps in Gram- bacteria, and more specifically by the hydrophobe/amphiphile efflux 1 (HAE1) sub-family (Nikaido, 2018) in which the transporter is a homotrimer that belongs to a tripartite complex. These efflux pumps are constituted of three different proteins forming an elongated nanomachine. The transporter itself, called RND, is localized in the inner membrane. It is the motor of the pump activated by the proton motive force. Another partner protein called Outer Membrane Factor (OMF) is embedded in the outer membrane. The third protein called Membrane Fusion Protein (MFP) is localized at the periplasm with a lipidic anchor inserted in the inner membrane. The 3D structure of the whole assembly has been solved recently by cryo-EM (Du et al., 2014; Daury et al., 2016; Wang Z. et al., 2017) highlighting how the different protein partners interact. Similar assembly architecture is also observed in the ABC family despite a different oligomeric organization of the transporter (Fitzpatrick et al., 2017). The fact that the HAE1-RND efflux system is only found in Gram- makes them interesting and specific target. Nevertheless, more than 10 years of research on this transporter family has not provided active and non-toxic drug yet. Thus, targeting the efflux pump expression regulation appears as an attractive alternative. Prokaryotic transcriptional regulators are classified into two groups: the one-component system and the two-components system. The gene expression regulation of the same HAE1-RND could involve both systems. A better comprehension of the molecular basis of efflux pumps genes expression is highly needed to pave the way for the design of new drugs toward multidrug resistance by efflux pump.

This review will focus on the regulators of the HAE1-RND efflux pumps (later called RND for simplification) involved in drug-resistance, with a particular focus on the regulator families controlling the pumps of *P. aeruginosa*, one of the most difficult bacteria to treat in clinic. For each family of the two-component and one-component regulators, a description of the molecular mechanism will be given based on structural knowledge obtained from archetypal organisms.

## THE REGULATION OUTLINE OF *P. AERUGINOSA* RND EFFLUX PUMPS

*Pseudomonas aeruginosa* is an opportunistic bacterium that has the ability to rapidly grow in diverse environmental niches, from different soils to human respiratory tract. It is involved in severe human diseases like meningitis, septicaemia or cystic fibrosis and is also a major cause of nosocomial infections due to its high capacity to develop resistances (Poole, 2011). One of

**Abbreviations:** ABS, Activation binding site; ABC, ATP-binding cassette; CA, Catalytic and ATP binding domain; DBD, DNA-Binding Domain; DHP, Dimerization and histidine phosphotransfer domain; GAF, cGMP-specific phosphodiesterases, Adenyl cyclases, FhlA domain; HAE1, hydrophobe/amphiphile efflux 1; HAMP, Histidine kinases, Adenyl cyclases, Methylaccepting proteins, Phosphatases domains; HK, Histidine kinase domain; HTH, Helix-turn-helix; LBD, Ligand binding domain; LTTR, LysR-type transcription regulators; MATE, Multidrug and toxic compound extrusion; MDR, Multidrug resistance; MES, Multidrug efflux systems; MFS, Major facilitator superfamily; PAS, Per arnt sim domain; PDB, Protein data bank; RBS, Regulatory binding site; RD, Regulatory domain; REC, N-terminal receiver domain; RND, Resistance-nodulation-cell division; ROS, Reactive oxygen species; RR, Response regulator; SD, Sensor domain; SK, Sensor kinase receptor; SMR, Small multidrug resistance; TCS, Two-component system; TetR, Tetracycline repressor; TF, Transcription factor; TFBS, Transcription factor binding site; TG, Target gene; TM, Trans-membrane domain; TSA, paratoluene sulfonate.

the most efficient resistance mechanisms is the overexpression of the tripartite RND-MFP-OMF efflux pumps. Up to twelve genes coding for the efflux pumps were identified in PAO1 genome, each of them showing substrates specificity (Stover et al., 2000). Nevertheless, only five of the efflux pumps are involved in resistance in clinical strains, i.e., MexA<sup>MFP</sup>-MexB<sup>RND</sup>-OprM<sup>OMF</sup>, MexX<sup>MFP</sup>-MexY<sup>RND</sup>-OprM<sup>OMF</sup>, MexC<sup>MFP</sup>-MexD<sup>RND</sup>-OprJ<sup>OMF</sup>, MexE<sup>MFP</sup>-MexF<sup>RND</sup>-OprN<sup>OMF</sup>, and MexJ<sup>MFP</sup>-MexK<sup>RND</sup>-OprM<sup>OMF</sup> (Lister et al., 2009; Li et al., 2015). These tripartite pumps are encoded in operon, but some of them do not bear their own OMF gene, such as MexXY, MexJK, MexVW, and MexMN. In that case, they usually assemble with OprM, the versatile OMF of *P. aeruginosa*, which structure has been extensively studied (Phan et al., 2010, 2015; Monlezun et al., 2015). MexAB-OprM is the only pump that is constitutively expressed and is able to transport most of the antibiotic families whereas the others are more selective and are induced under specific conditions. Dedicated activators or repressors regulate the efflux pumps expression, but complementary regulators, including the two-components system, could intervene to finely orchestrate the operons transcription. A blast analysis (<https://blast.ncbi.nlm.nih.gov/>) of the regulators based on *P. aeruginosa* amino acid sequences and known 3D structure homologs allows us to identify the main families of regulators in *P. aeruginosa* as illustrated in **Figure 1**. A majority of them belongs to the TetR family. We will first describe the regulators function of each family from archetypal structures. We will start with the two-component system (TCS) and then the one-component systems, i.e., TetR, LysR, MarR, and AraC. Finally, we will present MexR, NalD and MexZ, the only 3D structures solved from *P. aeruginosa* one-component regulators so far.

## THE TWO-COMPONENT SYSTEM REGULATORS IN *P. AERUGINOSA*

In bacteria, efficient adaptation to environmental changes is very often orchestrated by the two-component systems (TCS) (Stock et al., 2000). As such, TCS is one of the most abundant bacterial molecular devices to cope the variety of environmental signals (Krell et al., 2010; Capra and Laub, 2012; Jung et al., 2012). In particular, according to the whole genome prediction, *P. aeruginosa* owns around 130 different TCS (Rodrigue et al., 2000) and uses more than 60 TCS to regulate virulence and antibiotic resistance (Gooderham and Hancock, 2009; Muller et al., 2011; Li et al., 2015). All the TCSs regulating *P. aeruginosa* efflux pumps belong to the prototypical system, which mechanism will be described here.

Regarding the specific genes regulation of the RND efflux pumps, five TCSs were identified so far (see **Figure 1** for those involved in resistance in clinical strains) (Li et al., 2015). The RocS2-RocA2 system was shown to downregulate the expression of the constitutive efflux pump MexAB-OprM in order to favor biofilm set up (Sivaneson et al., 2011). The TCSs ParR-ParS and AmgR-AmgS switch on the expression of the efflux pump MexXY following bacterial envelope stress and membrane perturbation by either colistin or polymyxin B (Fernández et al., 2010;

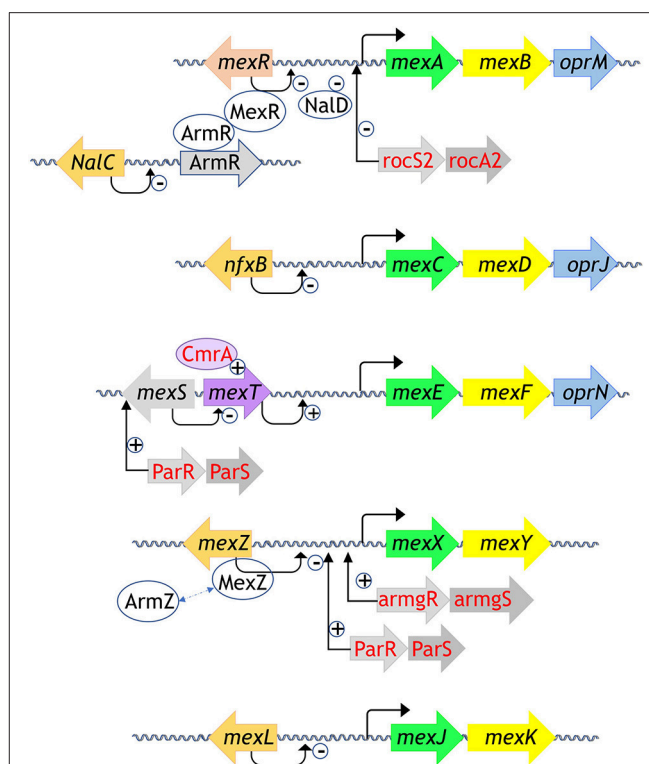


**FIGURE 1** | Regulation systems of the RND efflux pumps involved in antibiotic resistance from *P. aeruginosa*. Genes are schemed as arrows, proteins are oval shaped. The MFP are in yellow, the RND in green, the OMF in blue. The regulators from the TetR family are in orange, the MexR regulator from the MarR family is in salmon, MexT from the LysR family is in purple, CmrA coded by an AraC regulator is in light purple written in red, TCS are in gray written in red, all the other partners are in gray, written in black. Repression is indicated by “-” sign and activation is indicated by “+” sign. All the 3D structures are generated with PyMol (<http://www.pymol.org>; DeLano, 2009).

Muller et al., 2011; Lau et al., 2015). Besides, ParR-ParS also upregulates the efflux pump MexEF-OprN operon by enhancing the expression of the activator MexS (Wang D. et al., 2013). Finally, both systems CzcR-CzcS and CopR-CopS stimulate the expression of the heavy-metal efflux pump CzcABC (Perron et al., 2004; Caille et al., 2007). This pump is not involved in antibiotic resistance but it is mentioned here as the only TCS crystal structure solved so far in *P. aeruginosa*. Indeed, the sensor domain of the zinc-responsive histidine kinase CzcS shows the typical mixed  $\alpha/\beta$ -fold of the PhoQ family (Wang D. et al., 2017).

Most of these TCS targeting the efflux pump genes of *P. aeruginosa* belong to the OmpR/PhoB family, except RocS2-RocA2, which is part of the CheY family. The architecture of the OmpR/PhoB and CheY families corresponds to the typical TCS which is a duet of phosphor-relay proteins (**Figure 2**): (1) a receptor Histidine-Kinase (HK), also named Sensor Kinase (SK), receives the extra-cytoplasmic (or periplasmic) signal and then activates (3) a cognate intracellular response regulator (RR) through a concerted trans-phosphorylation process (2). Subsequently, activated RR displays generally a DBD domain that targets a repeated sequence (4) upstream or within the promoter,

in order to up-regulate or to repress the expression of specific genes (Krell et al., 2010; Capra and Laub, 2012; Zschiedrich et al., 2016).

Despite the lack of the full-length structure of HK, more than 100 structures of the different domains and fragments from different bacterial species shed light on the transduction mechanism upon ligand binding (Bhate et al., 2015; Zschiedrich et al., 2016). HK are membrane proteins and function as homodimeric receptors. The canonical monomer is made of 4 domains: (i) a sensor domain (SD) that recognizes various signals (gas, ions, osmotic change, temperature, light or variable organic compounds including antibiotics (Krell et al., 2010), (ii) a transmembrane domain (TM), (iii) one or several signal transduction domains (i.e., the domains HAMP - *histidine kinases*, *adenyl cyclases*, *methylaccepting proteins*, *phosphatases*, PAS—*per arnt sim* or GAF—*cGMP-specific phosphodiesterases*, *adenylyl cyclases*, *FhlA*) and (iv) an autokinase domain made of two subdomains DHP (*dimerization and histidine phosphotransfer*) and CA (*catalytic and ATP binding*). Thus, HK are multi-domains receptors with variable and complex architectures, but the structure of the transmembrane and the cytosolic domains tend to be more conserved than the sensor domains across the receptor family (Krell et al., 2010; Bhate et al., 2015; Zschiedrich et al., 2016).

The different domains of HK show diverse folds, mainly from  $\alpha/\beta$  to all- $\alpha$  classes. Behind the variety of stimuli and domain structures, signal transduction mechanism tends to be well conserved, driven by key  $\alpha$ -helices connecting the different domains along the receptor. Signal transduction mechanism starts at the sensor domain by the p-helices (*periplasmic helices*) which are localized at the dimer interface of the sensor domain. Upon binding of the ligand, helices rearrangements, described as a piston-like shift, are transmitted to the TM domain across a bundle of two pairs of anti-parallel  $\alpha$ -helices connected to the cytosolic domain, mainly HAMP, PAS, or GAF domains. As for the sensor domain, cytosolic domain folds are variable but the signal transduction is again driven by specific  $\alpha$ -helices, in particular a tandem of input and output helices. Through dynamic scissoring and rotation of the  $\alpha$ -helices bundle, a major structural event is the transition from a symmetrical apo-conformation (ligand-free) to an asymmetric holo-conformation (ligand-bound) and then active state. To summarize the complex signal transduction within the receptor structure, a global  $\alpha$ -helices coiled-coil disturbance mediated by the key helices stretching and rotation leads to an asymmetric kinase-competent state (Wang C. et al., 2013; Mechaly et al., 2014; Molnar et al., 2014; Gushchin et al., 2017).

The catalytic event of HK takes place at the DHP and CA domains. It starts with the auto-phosphorylation of the conserved histidine of DHP domain which is a symmetrical dimer of helix-turn-helix. The CA domain binds to the upper region of the DHP and captures the phosphoryl group from one ATP to phosphorylate the histidine of DHP. Depending of the orientation of the helices, histidine phosphorylation could be within the same protomer (*cis*-phosphorylation) or between (*trans*-phosphorylation) the subunits of the homodimer receptor (Casino et al., 2009, 2010). The lower part of DHP receives the

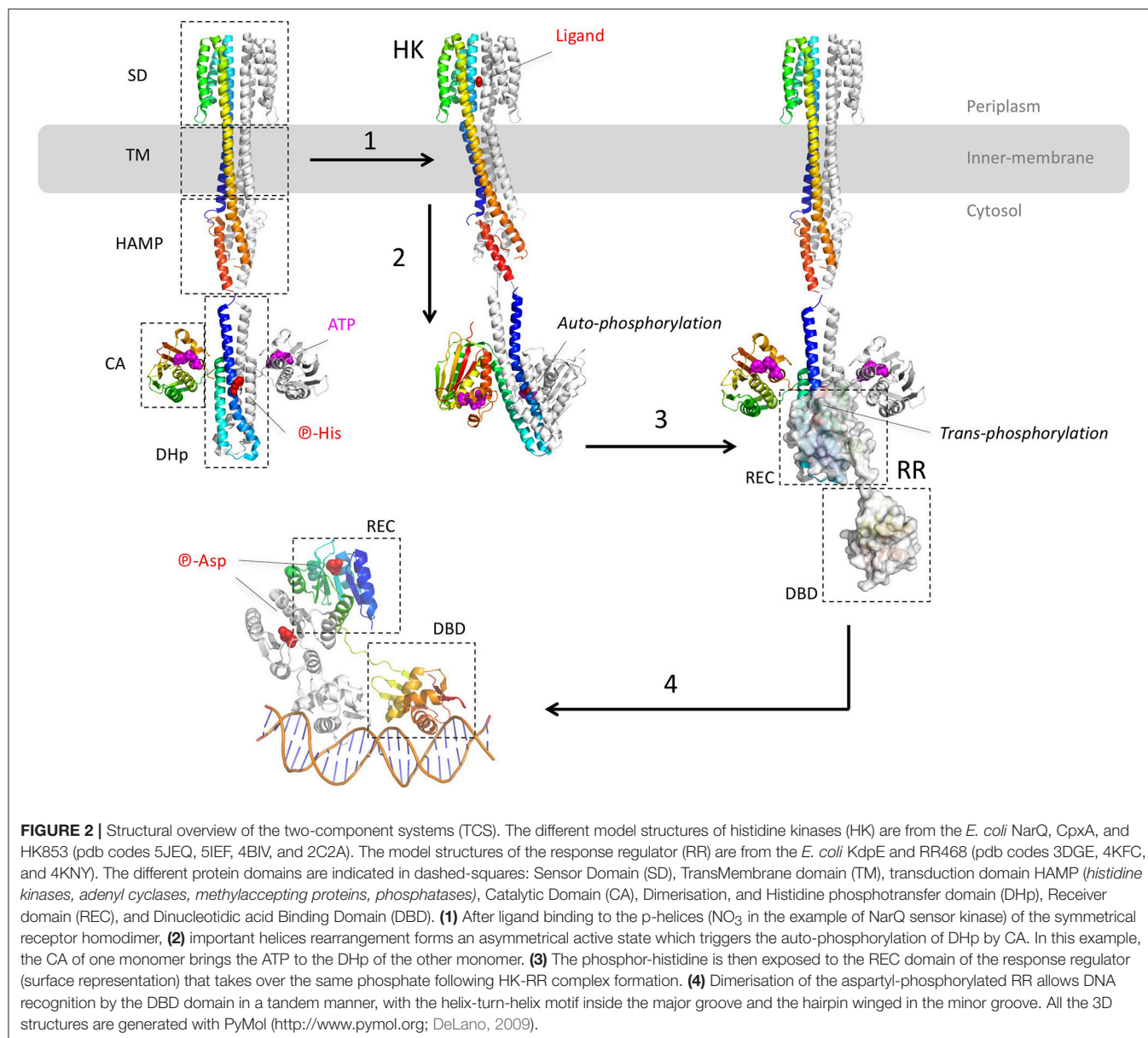
response regulator RR. Again, a critical switch to an asymmetric conformation of the DHP correlates with the active kinase state. The formed phosphor-histidine is then available for the trans-phosphorylation to the RR.

Actually, the RR protein is a kinase itself and catalyzes its own phosphorylation on a conserved aspartate. The prototypical RR of the OmpR/PhoB superfamily presents two domains: a conserved N-terminal *receiver* (REC) domain linked to a more variable C-terminal domain, mainly a DBD. The typical REC domain consists of a typical  $\alpha/\beta$  fold with five parallel  $\beta$ -strands surrounded by five  $\alpha$ -helices. The REC domain docks onto the lower part of the DHP domain and catalyzes its own aspartyl-phosphorylation from the phospho-histidine donor. This phosphor-relay disturbs the molecular surface of REC and triggered the switch of two conserved residues T/S and F/Y localized between the strands  $\beta 4$ - $\beta 5$  of REC, nearby the phosphor-aspartate. This event induces the symmetric dimerization of the REC domain (Gao and Stock, 2009) and brings in close proximity the C-terminal DBDs each other. Thus, the DBD tandem is able to recognize and to interact with the DNA repeat sequence. Remarkably both REC domains of the RR dimer form a symmetrical head-to-head complex, whereas the associated DBD are poised asymmetrically on the cognate DNA, in a head-to-tail manner (Narayanan et al., 2014; Lou et al., 2015; He et al., 2016). Structural determination of the DNA-RR complexes revealed that the DBD-DNA interface is conserved, described as a winged-helix fold where the recognition  $\alpha 3$  penetrates the major groove whereas the  $\alpha$ - $\beta$  hairpin wings interacts with the minor groove, motif found in the LysR and MarR of the one-component system (see below) (Blanco et al., 2002; Narayanan et al., 2014; Lou et al., 2015; He et al., 2016). The surface contact of the DBD-DNA complex covers around 1,800 Å<sup>2</sup> with mainly van der Waals interactions toward the ribose groups and electrostatic attractions to the phosphates backbone.

## THE ONE-COMPONENT SYSTEM REGULATORS

The one-component regulator system comprises both activators and repressors depending on the location of their binding site (TFBS) with the one of the RNA polymerase (RNAP). If the TFBS interferes with RNAP binding, the transcription factor will act as a repressor. When located upstream, the transcription factor helps RNAP recruitment as an activator or by competing with a repressor. One-component regulators can either act locally, interfering directly with the regulated operon, or remotely through general signaling events. These regulatory proteins are composed of two domains, one DNA-binding domain (DBD) comprising a Helix-Turn-Helix (HTH) motif, and one sensory domain involved in the oligomerization of the protein, often triggered by the binding of the sensor molecule. The one-component regulators are implicated in most of the essential signaling events in prokaryotic cells that is why a majority of bacterial regulators belong to this system. They are classified into more than 20 families (Cuthbertson and Nodwell, 2013) mainly based on sequence similarity of the DBD (Grkovic et al.,





2002), and most of them belong to six major families: TetR, MarR, LacI, LysR, AraC and MerR (Spengler et al., 2017). Four of them are involved in *P. aeruginosa* RND efflux pumps regulation (TetR, MarR, LysR, AraC) and they will be described here.

## The TetR Family

The tremendous amount of sequences deposited in the UniProtKB databank (>2,300 verified TetR family assigned sequences in 2005; Ramos et al., 2005) supports the fact that most of bacterial genomes carries several TetR regulators to control vital and diverse functions. Interestingly, more than 15% of them regulate membrane-associated proteins, which are transporters in majority. As expected, the number of solved structures deposited in the protein data bank (PDB) is still low

with hardly more than 280 entries (December 2017). The first solved 3D structure of a member of this family corresponds to the tetracycline repressor (TetR) from *E. coli* [2TCT (Kisker et al., 1995); 2TRT (Hinrichs et al., 1994)] repressing the expression of TetA, a MFS efflux pump expelling the tetracycline antibiotic. Surprisingly, structural alignment of the known structures of this family did not provide conserved motif because of a low sequence identity (as low as 7%), despite the well conserved fold of the N-terminal DBD domain (≈50 amino acids). Nevertheless, this analysis highlights the fact that most of the studied regulators are frequently involved in antibiotic resistance or virulence of pathogenic bacteria. The larger group of solved structures corresponds to EthR from *Mycobacterium tuberculosis* with 57 entries (Carette et al., 2012; Blondiaux et al., 2017; Nikiforov et al., 2017). It negatively regulates the expression of EthA



monooxygenase implicated in the inactivation of the anti-tuberculosis drug ethionamide.

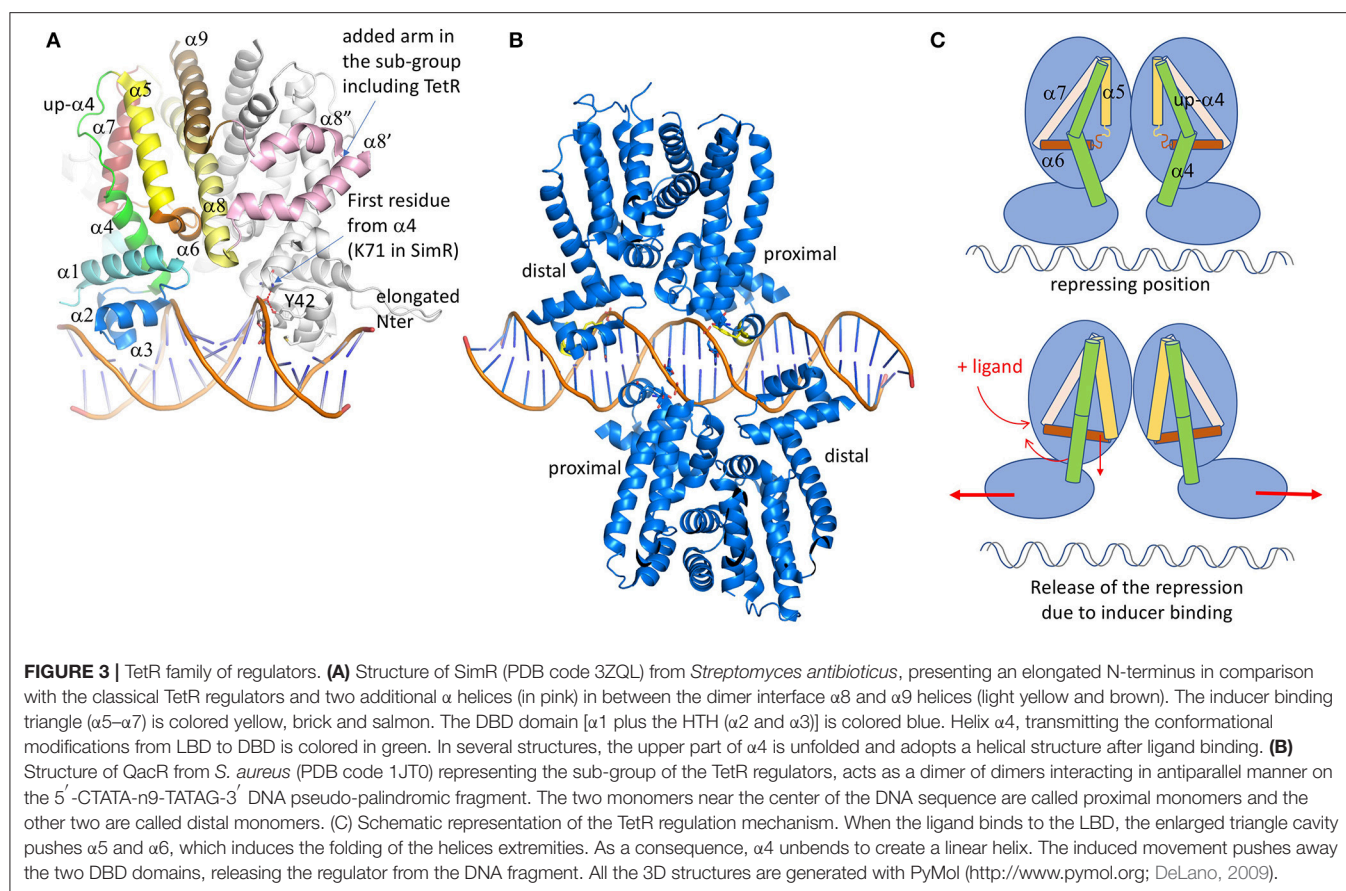
In spite of low sequence identity, the 3D structure of these regulators is conserved (**Figure 3A**). It is formed of 9  $\alpha$ -helices, with  $\alpha$ 1- $\alpha$ 3 corresponding to the DBD and  $\alpha$ 4- $\alpha$ 9 to the ligand-binding domain (LBD) (Deng et al., 2013). The contacts between the two domains involve  $\alpha$ 1 with  $\alpha$ 4 and  $\alpha$ 6, the latter being perpendicular to the dimer interface formed by  $\alpha$ 8 and  $\alpha$ 9 of each subunit (**Figure 3**). These inter-domain helices play a key role in the regulator activation through conformational modifications induced by the ligand binding. Among the 280 structures of TetR deposited in the PDB, more than 80 are declared to be associated with ligands. The chemical nature of these ligands is diverse, from a simple benzenediol such as resorcinol interacting with RolR, regulator of the aromatic catabolism from *Corynebacterium glutamicum* (3AQT; Li et al., 2011), to a more complex nucleotide derivative compound like isovaleryl coenzyme A (IV-CoA), an important building block in the formation of iso-fatty acids, interacting with AibR from *Myxococcus xanthus* (5K7H, 5K7Z; Bock et al., 2017). Most of the regulators classically repress the transcription in their apo-form, except for the AibR which is a repressor in a ligand-bound form of a whole operon bearing five genes involved in the biosynthesis process of IV-CoA, once bound to the same ligand. Besides, protein partners instead of chemicals also modulate some regulators. For instance, the SlmA regulator involved in cell-division of *E. coli* (Schumacher and Zeng, 2016) or AmtR, the nitrogen regulator of *Corynebacterium glutamicum* (Palanca and Rubio, 2016), both have to bind to DNA and another cognate protein at the same time to act. The diversity of the TetR regulator/ligand complexes is not limited to the ligand nature, but also depends on the localization of the binding regions which could be at the protein surface, close to the dimer or the domain interfaces, or in a deeply buried cavity that could even cross the entire protein like ActR (see Figure 8 from Cuthbertson and Nodwell, 2013 for a graphical representation). It differs also by the stoichiometry of the binding molecules, perfectly exemplified with TtgR (Alguel et al., 2007), a repressor of the key efflux pump TtgABC in *Pseudomonas putida*. Unlike TetR, which is only activated by tetracycline, TtgR can accommodate different molecules in the same ligand-binding site. Five structures have been solved of TtgR in complex with different antimicrobial molecules (2UXH, 2UXI, 2UXO, 2UXP, and 2UXU). In three different structures, the ligand occupies a large cavity formed by helices  $\alpha$ 5- $\alpha$ 8, within each monomer (quercetin in 2UXH, chloramphenicol in 2UXP and naringenin in 2UXU). In the complex with tetracycline (2UXO), a single monomer site is occupied despite the structural similarity with quercetin or naringenin. On the contrary, the structure of TtgR with phloretin shows both cavities occupied with an additional molecule close to  $\alpha$ 6 but in one monomer only. Using isothermal calorimetry to measure the binding of the different molecules, it has been shown that the affinity of phloretin for the different binding sites differs by two orders of magnitude, suggesting the existence of a positive cooperativity between the two sites.

Because of the important diversity of the ligands and the binding sites, it will not be possible to bring out a prototypical interaction mechanism. Nevertheless, the global structural

analysis of the LBD shows a conserved helical architecture built around helices  $\alpha$ 5- $\alpha$ 7 forming the so-called triangle that can be superimposed easily despite a root-mean-square deviation (rmsd) of more than 15 Å. This long atomic distance is due to differences in helices length and curvature.  $\alpha$ 8 is parallel to  $\alpha$ 5, stabilizing the triangle. Even if most of LBD domains are formed by 6 helices ( $\alpha$ 4 to  $\alpha$ 9), TetR belongs to a subclass itself, together with some minority proteins like the ActR regulator of actinorhodin efflux pump from *Streptomyces coelicolor* (Willems et al., 2008). We notice that the family name TetR was historically given because it was the first structure solved, but it is actually not representative since the folds are quite variable. For instance, in a sub-class of the TetR family, two additional helices are inserted between the classical  $\alpha$ 8 and  $\alpha$ 9, keeping the C-terminal helix at the conserved dimer interface. The two extra helices adopt a coiled-coil structure forming an arm that shell the second monomer, thus stabilizing the dimer. This is not the only difference in this sub-family. They also present a shorter helix  $\alpha$ 4 at the interface between the LBD and the DBD, the upper part of the traditionally curved  $\alpha$ 4 being unstructured but still parallel to  $\alpha$ 5.

In all the TetR family regulators, the dimer interface is formed by two antiparallel coiled-coil helices from each monomer ( $\alpha$ 8 and  $\alpha$ 9), forming a symmetrical four-helices bundle with the other monomer. The dimer is not always symmetrical, that is why ligands are not always present in both cavities of the complex structures. This is the case of QacR (Schumacher et al., 2004), which presents a much smaller cavity in one of the two monomers due to the flexibility of the last turn of  $\alpha$ 5, giving more freedom to  $\alpha$ 6 that can move upper then reducing the triangle cavity. The binding of the ligand in only one cavity is sufficient to release the transcription repression, but two dimers of QacR must interact with DNA (Schumacher et al., 2002), so at the end two ligand-bound cavities are necessary for the DNA recognition. In QacR the enlarged cavity can accept two different molecules (ethidium and proflavin), even if proflavin displaces ethidium from the binding site. Ligand binding pushes  $\alpha$ 6 in an allosteric way, which is transmitted to  $\alpha$ 4 that adopts a pendulum-like movement as described in Resch et al. (2008), driving away the two DNA binding sites (**Figure 3C**). It has also been described in HrtR, the heme homeostasis regulator in *Lactococcus lactis* (Sawai et al., 2012), an induced structural modification of this  $\alpha$ 4 from a partial random-coil to stable  $\alpha$ -helical structure once associated to the cognate DNA. In the case of QacR, the distance between the two sites increases from 37 to 45 Å, causing the detachment of the regulator from the DNA fragment (Schumacher et al., 2001). It has been suggested by Reichheld et al. (2009) that the rigidification of the structure drives the DNA release. This hypothesis is based on far-UV circular dichroism experiments on TetR wild-type and mutants in the presence of increasing concentration of urea, with and without ligands. In the absence of the ligand, the DBD unfolds first followed by the LBD. In presence of the ligand, the two domains unfold at the same time, suggesting cooperativity. The instability of DBD domain without the ligand would be a clue for its DNA adaptation.

The DBD, generally localized at the N-terminus of the protein, is composed of  $\alpha$ 1, HTH domain, and the beginning of  $\alpha$ 4.



Among the 280 deposited TetR structures, only 19 are associated with the cognate DNA fragments, highlighting the difficulty to stabilize these protein/DNA complexes. These regulator-DNA complex structures were crucial to understand the functional mechanism of this regulator family. There are two sub-classes of DNA-binding mode: one represents DNA promoters interacting with a dimer (1QPI: TetR; 3ZQL: SimR; 3LSP and 3LSR: DesT; 3VOK: HrtR; 5UA2 and 5UA1: KstR; 5DY0: AmtR; 4I6Z: Tm1030; 5K7Z: AibR). The second involves two dimers interaction (1JT0: QacR; 5HAW, 5HBU and 5k58: SImA; 4PXI and 5H58: CprB; 2YVH: CgmR; 4JL3: Ms6564; 5GPC: FadR) (**Figure 3B**). The first DNA complex was determined 5 years after the first structures of TetR by the same research group (1QPI; Orth et al., 2000). The main interacting region corresponds to the HTH domain formed by  $\alpha 2$  and  $\alpha 3$ , which is also the most conserved sequence region used to create an identification profile of the TetR family (Ramos et al., 2005). The two helices deeply enter the DNA major groove but most of the contacts involve  $\alpha 3$  only. In DesT, a regulator that controls the fatty acid saturation ratio in membrane lipid biogenesis, additional interactions were described with the DNA minor groove involving the elongated N-terminus of the protein (Miller et al., 2010). This is also the case for SimR, an exporter of a potent DNA gyrase inhibitor from *Streptomyces antibioticus*, which presents an even longer N-terminus that turns back to the added “arm” between  $\alpha 8$  and  $\alpha 9$

of the second monomer (Le et al., 2011). CprB from *S. coelicolor*, a receptor of c-butyrolactones, a class of quorum sensing molecules (Bhukya et al., 2017), also takes part of this N-terminal extended sub-family. AmtR, the global nitrogen regulator of *C. glutamicum* that is activated by a protein instead of a small molecule (Palanca and Rubio, 2016), also shows an additional C-terminal helix of unclear function. The recognized DNA operator is often formed by one central base pair (bp) surrounded by a palindromic sequence of a minimum of 6 bp in each opposite direction from the center (Yu et al., 2010). So, the complex is formed by a symmetrical protein dimer bound to a symmetric DNA fragment. Among the sub-class acting as a dimer of dimers, the regulators bind two overlapping DNA palindromic sequences instead of one in a cooperative manner. It is the case of QacR (Grkovic et al., 2001; Schumacher et al., 2002), which represses the expression of the MFS efflux pump QacA, transporting toxic organic compounds like the quaternary ammonium compounds. In this case, the palindromic DNA fragment is elongated by 28 bp with a longer central non-palindromic sequence (6 instead of 1) in order to accommodate the two dimers. For this class of regulators, the following nomenclature has been adopted: depending on the distance of the dimer from the central DNA sequence, there are the proximal and the distal subunits. Both dimers bind on opposite side of the promoter sequence, the two proximal monomers being very close to each other, sharing

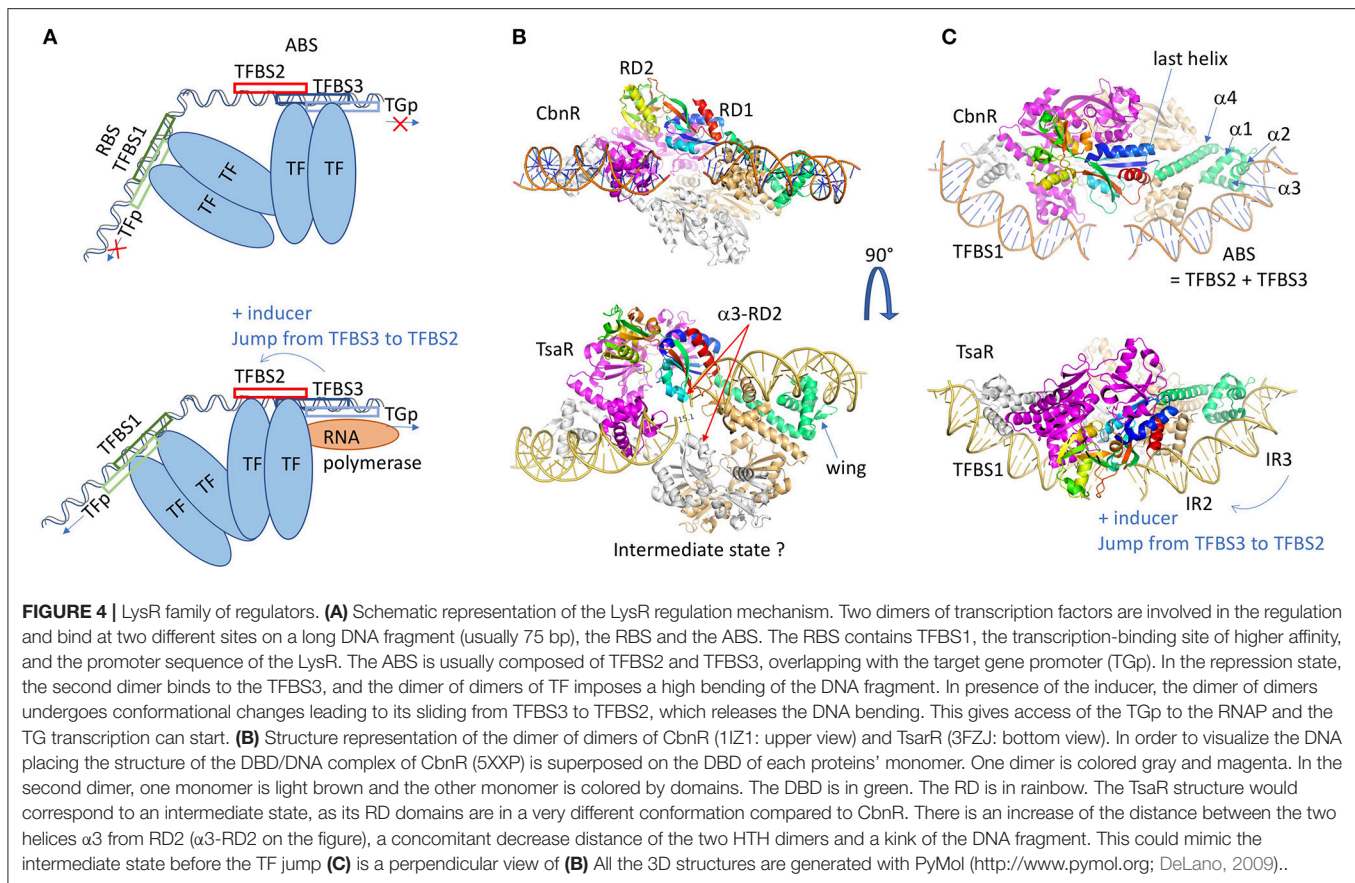
several DNA base pairs in their binding site. With the opposite binding mode, the two dimers axis form an angle of  $<180^\circ$  except Ms6564 (Yang et al., 2013), a broad regulator in *Mycobacterium smegmatis* that presents a smooth interaction involving water molecules which allow a sliding motion of the regulator along the genome to target several genes. For instance, the measured angles are  $130^\circ$  for both QacR and SlmA (the smallest ones),  $142^\circ$  for CprB and  $145^\circ$  for CgmR (Itou et al., 2010; Bhukya et al., 2014). In spite of this particularity, the interaction of two dimers with the DNA is very similar to that of one dimer. The main difference is a larger spacing between the two DNA binding sites within a dimer (3 bp for TetR-like regulators and 4 bp for QacR-like), reducing the induced bending of the DNA fragment ( $\approx 3^\circ$  compared to  $\approx 16^\circ$  for the one-dimer class) and increasing the  $\alpha 3$ - $\alpha 3'$  distance from  $\approx 34$  to  $\approx 37$  Å. This distance is comparable to one turn of DNA-B form and was questionable for a long time. The numerous unbound and ligand-bound structures show very variable distances between these two  $\alpha 3$  helices, ranging from 37.4 to 48.1 Å (Yu et al., 2010). This was confusing for scientists in their interpretation of the regulation mechanism, as discussed by Frénois et al. (2004) when they compared the structure of EthR solved with hexadecyl octanoate in LBD, and that of QacR solved in different forms (free, complexed with a ligand and complexed with DNA).

When superposing the DBD from the solved TetR structures in complex with DNA, it clearly appears that the HTH and the N-terminus of  $\alpha 4$  of the DNA binding site match perfectly without any amino acid insertion. There are eight important residues for the binding: the two first correspond to the first residues of  $\alpha 2$  and  $\alpha 4$  that are not conserved since the interaction involve the protein backbone only with the phosphates of the DNA. The six other residues correspond to the whole  $\alpha 3$  helix except the central residue oriented toward  $\alpha 2$  (T41 in TetR). The nature of these amino acids varies with the cognate DNA sequence, even though most of the protein/DNA interactions involve the DNA backbone and not the nucleic base. This is the case for AibR presenting seven residues interacting with phosphates backbone and only two involving specific contacts with the base (Bock et al., 2017). Nevertheless, one residue is particularly well conserved, a tyrosine (Y42 in TetR and Y40 in QacR) that interacts with the same DNA phosphate as the amine group of the N-terminal residue of  $\alpha 4$ , reinforcing the DNA binding. This phosphate corresponds to the center of the DNA palindromic sequence. The amino acid the most deeply buried into the DNA major groove is positioned four residues before the conserved tyrosine (Y-4), in the turn preceding helix  $\alpha 3$ . This amino acid is often a short one (Ramos et al., 2005). In the case of FadR, a regulator involved in the fatty-acid degradation and synthesis pathways, mutation of each of these two conserved residues led to a significant reduction of DNA binding as proved by electrophoretic mobility shift assays (Yeo et al., 2017). It seems that the regulator could slide on the DNA until the  $\alpha 3$  helix recognizes the cognate sequence, using a short residue at position Y-4 to enter more deeply into the groove. Then the clamp formed by the tyrosine and the first residue of  $\alpha 4$  lock the interaction.

## The LysR Family

The transcription factors (TF) belonging to the LysR family (LysR-Type Transcription Regulators: LTTR) are the most abundant in prokaryotes. This is due to the fact they regulate the expression of genes coding for proteins involved in very diverse functions like  $\beta$ -lactamase, transporter, amino acids biosynthesis, metabolic signaling, secretion, oxidative-stress response, cell division, quorum sensing, virulence, motility, detoxification, attachment (Schell, 1993; Maddocks and Oyston, 2008; Jiang et al., 2018). The family was named after the extensively studied transcription regulator of *lysA* implicated in lysine biosynthesis (Stragier et al., 1983) and is composed of both activators and repressors (Maddocks and Oyston, 2008) depending on the location of the transcription factor binding site (TFBS). The genetic organization of LTTRs targeted promoters and TFBSs has been studied by a computational protocol termed Phylogenetic Profile of Consensus Motifs issued by the analysis of Phylogenetic Footprinting techniques (Oliver et al., 2016). In the LysR family, the gene coding for the TF is divergently oriented from its target gene (TG) and located  $<100$  nucleotides upstream the beginning of the TG, and sometimes up to 500 bp from the initiation codon (Heroven and Dersch, 2006). Two to three different TFBSs are found in the intergenic region, the inter-motif length between the two first is generally seven nucleotides, except for the LyrR which is six. When the third motif exists, it very often overlaps with the second one, the global site being called the ABS (activation binding site) (Figure 4A). LysR also differs for this rule, because it presents 19 bp intermotif length between TFBSs 2 and 3. In each case, the transcription activation involves the binding, with different affinities, of two activated TF dimers in a cooperative manner, triggered by one or several inducers. An overlap of TF promoter and TFBSs causes an auto-repression by the TF when bound to the TFBS on the opposite strand of the DNA. The global site is called the RBS (regulatory binding site). Depending on the affinity of the TF for one of the different TFBSs, the TF will be an activator or a repressor. The mean length of the TFBSs is 15 bp and the consensus sequence, originally described as 5'-T-n11-A-3' (Goethals et al., 1992), has been extended to 5'-CTATA-n9-TATAG-3' (Oliver et al., 2016). Based on DNaseI protection assays combined with structural analysis (Wang and Winans, 1995; Muraoka et al., 2003; Picossi et al., 2007), a model has been proposed for the molecular mechanism of the LysR-type transcription regulators when three TFBSs are present, which is the majority of the LysR-type intergenic organization (Figure 4A). The affinity of the TF for the first and last TFBSs is greater than for the second one. Then in absence of the co-inducer, the formation of the dimer imposes a large bending of the DNA from  $50$  to  $100^\circ$ . With the inducer, the dimer interacts with the second TFBS which releases the third TFBS and unbends the DNA of  $9^\circ$  up to  $50^\circ$ . From this conformation, the TF will interact with the  $\alpha$ -subunit of the RNAP so that the transcription of the TG can start. This mechanism model was reinforced by DNA-binding studies performed on modified DNA sequences, and is known as the "sliding dimer" (Porrúa et al., 2007). To get insights into the molecular details of this model, several 3D





structures were necessary and several examples will be described below.

The LysR-type genes code for proteins of around 330 amino acids. When searching for LysR transcription regulator in the PDB, it issues 87 entries corresponding to 27 different proteins, the majority corresponds to BenM from *Acinetobacter baylyi* or *sp.*, DntR from *Burkholderia sp.* or *cepacia*, OxyR from *Vibrio vulnificus*, CysB from *Salmonella typhimurium*, TsaR from *Comamonas testosteroni* and AphB from *Vibrio vulnificus*. Their structure shows a HTH motif in the DBD at the N-terminus like the TetR family, and a regulatory domain (RD) receiving an inducer (Henikoff et al., 1988). A long helical linker separated the two domains. The HTH is the most conserved region and is used to identify the members of this family in genome analysis (Schell, 1993). In contrary to the TetR HTH motif, there are two additional  $\beta$ -strands between  $\alpha 3$  and  $\alpha 4$ , a particular topology called winged-HTH. It also differs by the relative orientation of the three helices forming the DBD domain. Unlike the TetR family, the N-terminus of LTTR is localized at the dimer interface. As a consequence, all the helix axes are reverted as we can see by comparing **Figure 3A** with the DBDs on the ABS site of **Figure 4C**. The rest of the sequence is not very conserved except the C-terminal fragment of about 15 residues. Mutational analysis indicated implication in DNA binding or oligomerization (Schell et al., 1990; Bartowsky and Normark, 1991) which was partially confirmed with the

first crystal structure of the RD of CysB from *Salmonella typhimurium*, the regulator of the cysteine regulon expression (1AL3, Tyrrell et al., 1997). The co-inducer binding domain is composed of two  $\alpha/\beta$  Rossmann fold-like subdomains RD1 and RD2 (**Figure 4B**) with a long  $\beta$ -sheet in between. The RD architecture forms a bend where the co-inducer interacts. Punctual mutations introduced in the co-inducer binding site of CysB led to an uncontrolled activation phenotype in spite of a proper interaction with the TFBS according to gel-shift assays (Colyer and Kredich, 1996). The nature of the replacing residue was important since the mutant T149M is comparable to the wild type, whereas T149P shows only a 10% activity, which suggests that the conformational flexibility of the protein is required for the co-activator effect.

Several structures of the isolated RD domain were solved with a monomer or a dimer in the asymmetric unit of the crystal, but none of them reveals the functional mechanism by a tetramer. The first structure of a full-length LTTR corresponds to the one of CbnR from *Cupriavidus necator*, involved in the degradation of chlorocatechol converted from 3-chlorobenzoate, using cis,cis-muconate as inducer (1IXC and 1IZL: Muraoka et al., 2003). The structure shows a tetramer that can be considered as a dimer of dimer, composed of two types of subunits with different conformations (**Figures 4B,C** upper panel), either compact or extended forms. Within one dimer, the main interacting region corresponds to the helical linker  $\alpha 4$  localized between the DBD



and the RD. The two  $\alpha 4$  helices bind in an anti-parallel manner, imposing the head-to-head orientation of both DBD interacting by their N-termini. In this architecture, the distance between the two  $\alpha 3$  helices is compatible with an interaction with the major groove of the B-form DNA. The angle between  $\alpha 4$  and the RD axis is about  $50^\circ$  in the compact form and  $130^\circ$  in the extended form. Contacts between two RD domains appear through the interaction of the tetramer, i.e., two LTTRs dimers. It has to be noticed that the so-formed RD dimer interface is similar to those described in the structures of the isolated domain from several LTTRs, such as BenM from *Acinetobacter baylyi* regulating aromatic compound degradation (2F8D: Ezezika et al., 2007a). The two dimers are properly superimposed without showing any hinge movement between RD1 and RD2, with the exception of the C-terminal  $\alpha/\beta$  domain of RD1 that is more divergent. Because the last helix is localized in the continuity of the linker  $\alpha 4$  in the extended form of CbnR (see **Figure 4C** upper panel), this swapping domain could be involved in the conformational changes necessary for proper function of this family of regulators. The global quaternary structure of CbnR is compatible with an interaction with two DNA binding sites on a bended DNA fragment, supporting that the crystal structure is biologically relevant. Among the different full-length structures solved later, the one of TsaR (3FXU and 3FZJ: Monferrer et al., 2010) from the soil bacteria *Comamonas testosteroni* brought interesting insights in the regulation mechanism of the LTTRs. TsaR regulates the degradation of paratoluenesulfonate (TSA), a commonly found industrial pollutant, that also induces the regulator transcription itself. The tetrameric structure solved in complex with TSA is flatter than CbnR and presents less contacts between the different RD domains as they swing almost perpendicular to the tetramer plane, which yields a different interface (**Figures 4B,C** lower panel). In this conformation, the hinge between the DBD and the RD reaches  $153^\circ$  whereas  $130^\circ$  was measured for CbnR. On the contrary, for the compact form, the angle of  $50^\circ$  is conserved. The distance between the two pairs of  $\alpha 3$  helices of the DBD domain varies largely because of the surface convexity between two pairs of DBDs. It has been suggested that the open form structure of TsaR could represent the active tetramer whereas the more compact form of CbnR tetramer, through contacts between the third helix from the RD2 domains ( $\alpha 3$ -RD2) (see **Figure 4B** lower panel), would represent the inactive form. The transit to the active form could be induced by the binding of the TSA inducer in the cleft formed by two RD domains: in the structure of TsaR, the crossing  $\beta$ -sheet is broken in the middle when compared to CbnR. The hypothesis of a switch from a compact to an extended conformation of the tetramer once activated by the inducer in the RD cleft was confirmed by several LTTRs structures, i.e., ArgP regulating chromosome replication in *Mycobacterium tuberculosis* (Zhou et al., 2010), NdhR from *Synechocystis* involved in the control of carbon metabolism (Jiang et al., 2018), many of BenM (Ezezika et al., 2007b), and the SAXS experiments performed on DntR (Lerche et al., 2016). Nevertheless, the activation does not always depend on an inducer binding. For instance, a redox switch activates the oxidative stress regulator OxyR (Jo et al., 2015, 2017). Two cysteines (C199 and C208) from the helix  $\alpha 3$ -RD2

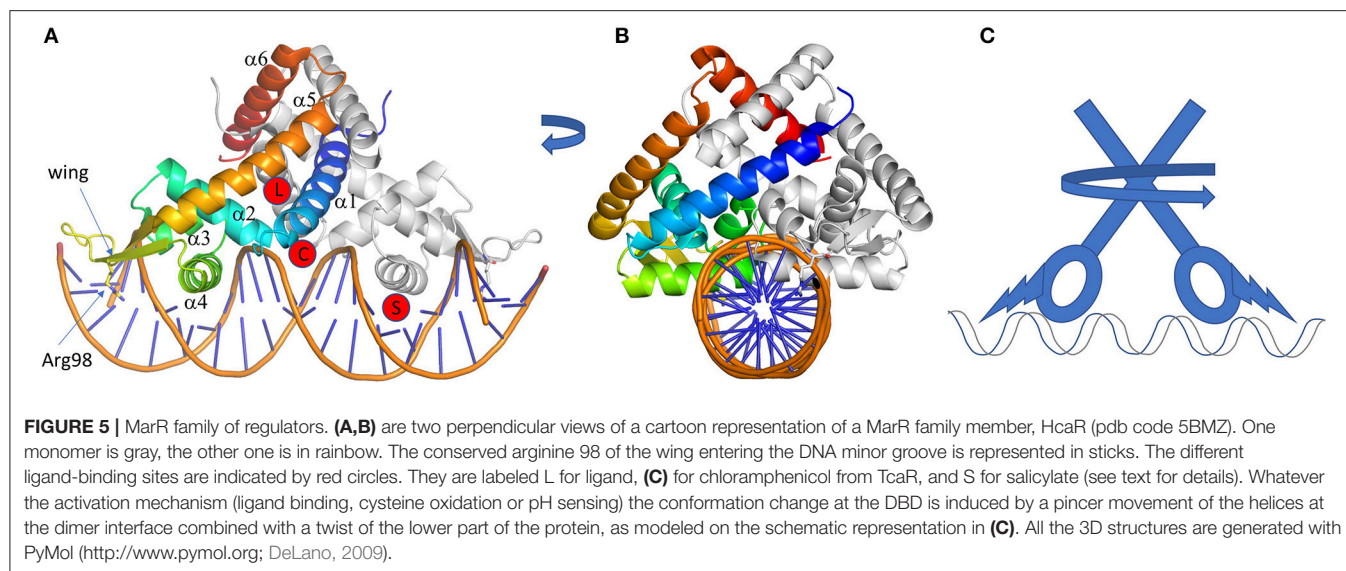
form a disulfide bond in the presence of  $H_2O_2$ , which results in the unfolding of the helix and subsequent conformation modifications.

Only three structures of LTTR were solved in complex with DNA [two of BenM (4IHT, 4IHS) and one of CbnR (5XXP)] and all of them concern only the N-terminus DBD, including the HTH and the  $\alpha 4$  in order to stabilize the dimer (Alanazi et al., 2013; Koentjoro et al., 2018). As already mentioned, the antiparallel  $\alpha 4$  helices coiled-coil and the N-terminus are at the proximity of the pseudo-palindromic DNA center. Helix  $\alpha 3$  enters deeply in the DNA major groove and brings most of the specific contacts with the DNA bases. The winged  $\beta$ -strand between the HTH and  $\alpha 4$  makes contacts with the DNA minor groove, mainly through the phosphates, and one residue (R53) makes selective contact in BenM, which is absent in CbnR. Nevertheless, most of the selective residues are located in  $\alpha 3$ . Among these residues (A28, Q29, P30, P31, and R34 in CbnR), the remarkable mutation Q29A did not modify the interaction with DNA as proved by EMSA. Nevertheless, the mutant does not activate the transcription of the TG. This supports the importance of residues of the ABS site instead of the RBS. A plausible hypothesis is the involvement of Q29 in the RNA polymerase recruitment, since it is highly conserved among the LTTR family.

## The MarR Family

The members of the Multiple Antibiotic Resistance Regulator (MarR) family are usually repressors found in bacteria and Archaea genomes (Wilkinson and Grove, 2006). They are mainly activated by sensors of environmental changes, like the presence of nutrients or toxins. Logically they often regulate genes coding for exporters of antibiotics, but they are also implicated in virulence, degradation processes, stress response and metabolic pathway (Aleksun and Levy, 1997; Perera and Grove, 2010). MarR family are also involved in aromatic compounds metabolism which is one of the attractive field in industrial research of renewable energy (Davis and Sello, 2010; Fuchs et al., 2011; Bugg and Rahmanpour, 2015; Kallscheuer et al., 2016; Grove, 2017). Due to the essential role, MarR family is widely spread in bacterial genomes, up to 24 in *Bacillus subtilis* according to UniProt data bank.

The MarR transcription regulators are small proteins of <150 residues containing a winged HTH domain at the N-terminus similar to the LTTR family but acting in a dimeric form like TetR family. About 120 structure entries are in the PDB and the first one (1JGS) corresponds to MarR regulator from *E. coli* (Aleksun et al., 2001). Compare to the other regulator families, the structure of MarR is quite simple, made of a DBD domain with an extension  $\alpha$ -helix at each extremity (**Figure 5**). Those additional helices ( $\alpha 1$  and  $\alpha 6$ ) are the dimer interface. Besides, some MarR regulators present additional elements, for instance the regulator PcaV, involved in protocatechuate metabolism, an intermediary product of lignin degradation from *Streptomyces coelicolor*, possesses an additional  $\beta$ -strand between  $\alpha 2$  and  $\alpha 3$ , forming a  $\beta$ -sheet wing (strands  $\beta 1$  and  $\beta 2$ ) (Davis et al., 2013). Another additional secondary structure is found in HucR from *Deinococcus radiodurans* (2fbk, Bordelon et al., 2006) involved



in oxidative stress response to uric acid. HucR possesses an additional helix at its N-terminus that stabilizes the dimer in the absence of DNA by pinching the helices of the dimer interface.

TF from the MarR family recognizes one or two types of intergenic region among the different regulated genes. The TFBSs are 16 to 20 bp long and are not always perfectly palindromic (Martin and Rosner, 1995; Perera and Grove, 2010). Like the LysR family, the HTH motif (here  $\alpha 3$  and  $\alpha 4$ ) enters in the DNA major groove and the supplementary  $\beta$ -strand wing interacts with the minor groove. This wing extension is essential for DNA binding, especially the arginine of the loop connecting the  $\beta$ -strands (Kumarevel, 2012), which deeply enters the DNA minor groove (**Figure 5A**). The importance of this basic amino acid for the regulation mechanism was analyzed for the ST1710 regulator from *Sulfolobus tokodaii* involved in antibiotic resistance. Several basic residues from this loop were mutated into alanine (R90A), showing a decrease of binding affinity for the cognate DNA sequence by gel-mobility shift assays (Kumarevel et al., 2009). When two TFBSs are necessary for gene regulation, the binding position of two TFs is either on opposite side or adjacent on DNA depending on the intergenic length and of the size of the  $\beta$ -strands wing, even though a dissociation of the wing was reported in the structure of Rv2887 regulator from *Mycobacterium tuberculosis* in complex with two TFBSs of 30 bp (Gao et al., 2017).

Concerning the LBD, it is reduced to a smaller fold so that the “triangle cavity” described previously in the TetR family does not really exist, even if  $\alpha 5$  and  $\alpha 6$  seem to adopt a triangle-like shape (**Figure 5**). This structure is sufficient to create a cavity surrounded by helix  $\alpha 1$  and sometimes a long loop between  $\alpha 1$  and  $\alpha 2$  like in ZitR, a zinc metalloregulator (Zhu et al., 2017). This cavity is a receiving platform for several kinds of molecules, like coumaric acid, ferulic acid, vanillin and 3,4-dihydroxybenzoic acid in the case of HcaR from *Acinetobacter*, a regulator of the hydroxycinnamate degradation pathway (Kim et al., 2016). The binding of a molecule into the cavity will rearrange the dimer

interface conformation by modulating the distance between the two HTH domains and subsequently controlling the regulator release from the DNA. Nevertheless, structural modification of the regulator could be small for a large group of MarR regulators, like in SlyA, a virulence regulator from *Salmonella* (Dolan et al., 2011). The apo-form and ligand-bound structures are already in a conformation favorable to B-DNA interaction, with a distance of around 30 Å between the two DNA recognition helices. In this case, the presence of the inducer simply add stability to the regulator-DNA complex as demonstrated on MexR by thermal unfolding experiment and surface plasmon resonance (Andrésen et al., 2010). This is also supported by the structure of PcaV (4G9Y and 4FHT; Davis et al., 2013) showing the importance of an arginine (R15) in the functional mechanism (**Figure 5A**). By comparing the structure of the apo-form and the regulator complex with the natural ligand 3,4-dihydroxybenzoic acid, the R15 occupies the binding site in the absence of ligand. It is then pushed away by the ligand and forms hydrogen bonds with residues localized in  $\alpha 2$ ,  $\alpha 3$ ,  $\alpha 3$ - $\alpha 4$  loop,  $\alpha 1$  of the other monomer and the ligand itself. This pulls  $\alpha 1$  by 10° toward the second monomer with an allosteric effect on the DBD orientation and a large movement of the  $\beta$ -sheet wing. To sum up, R15 and the ligand make a stable bridge between the DBD and the dimer interface by many hydrogen bonds. This specific mechanism was also described for NadR, the Neisserial Adhesin NadA repressor from *Neisseria meningitidis* studied by HDX-MS and molecular dynamic (Brier et al., 2012). Other binding sites were suggested for this family. In the case of the monomeric MarR (1JGS), two molecules of sodium salicylate bind on each side of the HTH- $\alpha 4$  of the DBD domain (**Figure 5A**). This compound is an inhibitor of MarR that will activate *marA* gene transcription (Cohen et al., 1993). It suggests the possibility of a regulation mechanism directly at the DBD site. Several other possible interacting sites were described, based on the structures of TcaR solved with different compounds (4EJT, 4EJU, 4EJV, 4EJW, Chang et al., 2010, 2013). For instance, kanamycin binds to similar sites as the ligand

of PcaV, but chloramphenicol binds to an unusual large cavity below the dimer interface (see C in **Figure 5A**), as well as a second site close to the  $\alpha 4$ . The latter is similar to that of salicylate in MarR or MTH313, a MarR homolog from *Methanobacterium thermoautotrophicum* (Saridakis et al., 2008).

Nevertheless, ligand binding is not the only activation mode of MarR family regulators. Some of them are sensitive to oxidative stress like AbfR from *Staphylococcus epidermidis* (Liu et al., 2017). The monomer possesses two cysteines, each one in the terminal helices ( $\alpha 1$  and  $\alpha 6$ ). The regulator binds to DNA in a reduced state. Under oxidative environment, sulfenic acid intermediates catalyze disulfide-bridge formation of the cysteines, which results in a large movement of the two monomers and destabilizes DNA interaction. The same regulation mechanism is also found in OhrR, the regulator of a peroxidase that reduces organic hydroperoxides to alcohols (Newberry et al., 2007). Upon oxidation by hydroperoxides, helix  $\alpha 5$  of OhrR is locally unfolded which brings in close proximity the two cysteines to form the disulfide-bond responsible for a rigid-body rotation of the winged-HTH and then DNA release. Another regulation mechanism that depends on the pH was described for HucR regulator (Deochand et al., 2016). As shown by circular dichroism study at different pH, the N-terminal helices from each monomer interact by H51 stacking which protonation results in a molten globule intermediate with a low affinity for DNA. This explains the necessity for an additional helix at N-terminus to maintain the 3D structure of HucR during the conformation changes.

## The AraC/XylS Family

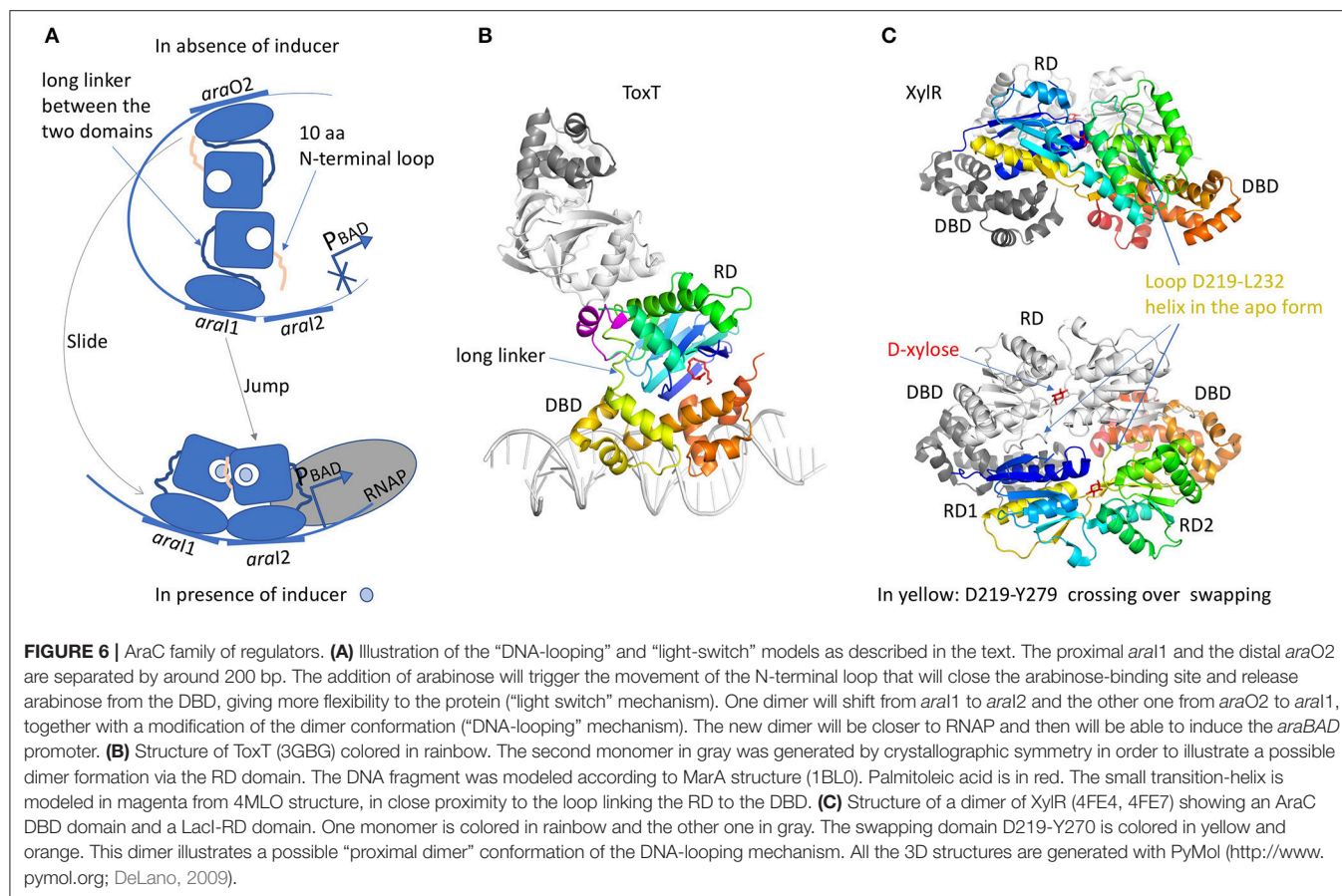
The transcription regulators of AraC family (AFTRs) are generally activators found in all bacterial genomes, except in archaeobacteria (Gallegos et al., 1997). Like most of activators, the main TFBS is located around the  $-35$  region of the promoter, which eases direct interaction with the RNAP (Ptashne and Gann, 1997). The members of the AFTR group are involved in pathogenesis, virulence and environment sensing, responding to oxidative stress, pH, temperature and antibiotics. They are also highly implicated in the regulation of essential metabolism pathways of the carbons, such as sugars, amino acids, alcohols or herbicides degradation (Gallegos et al., 1997; Egan, 2002; Ibarra et al., 2008).

The regulators of this family are generally 300 residues long, with some exceptions such as MarA or SoxS from *E. coli* which are reduced to the sole DBD domain (Rhee et al., 1998). When searching “AraC transcription” in the PDB, only 22 entries are listed which is low compared to the other families. An explanation was published in an essay of Schleif and his group who investigated the AraC regulation mechanism (Schleif, 2003). Because AraC interacts with more than 40 bp, it must be partially unfolded in the absence of DNA to reduce the binding energy for a reversible interaction. Thus, the intrinsically disordered state of this regulator family makes them difficult to handle (Schleif, 2010). Nevertheless, with the constant progress in protein expression and purification methods, several structures were obtained for more than ten different members of the family. Most of the AFTRs are made of two domains: a response domain (RD) involved in protein dimerization and a conserved DBD of

around 100 residues. The HTH motif interacts with the DNA in a similar way to the TetR family with one helix entering the DNA major groove. But unlike TetR, there is no wing interacting with the minor groove and one monomer carries two HTH separated by a long linking-helix. When both HTH interact with two contiguous DNA major grooves (Rhee et al., 1998), the DNA is bended by  $\approx 35^\circ$  (Martin and Rosner, 2001). Besides, some proteins, such as the transcription factor Rob involved in antibiotic resistance and organic solvent tolerance in *E. coli*, makes direct contacts with only one DNA major groove with the first HTH, whereas the second interacts with the RNAP (Bhende and Egan, 2000). The tandem HTHs are generally at the C-terminus but in Rob regulator (PDB code 1D5Y), the HTH motifs are localized at the N-terminus. Even though the interacting configuration of the AraC family is quite specific, HTH motifs are poised from either side of the DNA fragment (Kwon et al., 2000) in a comparable manner to the QacR sub-group of TetR. Affinity measurements and DNA foot-printing experiments show that AraC recognizes DNA sequences as a tandem or inverted repeat orientation with different affinities (Carra and Schleif, 1993; Reeder and Schleif, 1993).

The RD domain is not conserved across the AraC family and it has very different functions. Both RD and DBD domains are independently associated by a long linker. A chimeric construct of the AraC-RD with the LexA-DBD from the LexA repressor (Bustos and Schleif, 1993) results in a protein that was able to dimerize and to repress *lexA* operator in response to L-arabinose. In spite of more than 20 years of work, the full-length structure of AraC is still unsolved. Nevertheless, crystal structures of the RD domain were solved with and without the arabinose ligand (Soisson et al., 1997; Weldon et al., 2007). The domain is a jellyroll that ended by a helix coiled-coil. RD dimer is found in the asymmetric unit only in the presence of arabinose. The dimer interface involves hydrophobic residues from the coiled-coil motif and an additional helix from the region between the jellyroll and the coiled-coil. The arabinose binds in a cavity formed by the jellyroll and locked by N-terminal loop of 10 residues. Without arabinose, this loop was not visible in the electron density. Genetic, biochemical and biophysical characterizations of AraC brought hypothesis on the regulation mechanism by the N-terminal loop (Carra and Schleif, 1993). In *E. coli*, L-arabinose is involved in the regulation of four operons, *araBAD*, *araE*, *araFGH* and *araC*. AraC represses the expression of *araBAD* and *araC* promoters by binding to two different DNA half sites separated by around 200 bp, the proximal site *araI1* and the distal site *araO2*, leading to the formation of a DNA loop (**Figure 6A**). In this configuration, the N-terminal loop makes contacts with the DBD, constraining the monomer in a compact structure. Arabinose binding results in the release of this loop by a “light switch” mechanism, allowing the RDs to form a totally different dimer. Then the DBD shifts from *araO2/araI1* to *araI1/araI2* sites, closer to the RNAP and the induction of the *araBAD* promoter. This mechanism is found in several regulators like ToxT from *Vibrio cholerae* (Lowden et al., 2010) or RegA from *Citrobacter rodentium* (Yang et al., 2009, 2011) respectively regulated by fatty acids or bicarbonate. The structure of the full-length protein ToxT from *Vibrio cholerae*





was solved in the absence of DNA (3GBG; Lowden et al., 2010; **Figure 6B**). The RD domain is very similar to that of the AraC but without the N-terminal loop. Instead, Li et al. (2016) revealed a small  $\alpha$ -helix (D101 to E110) in proximity of the RD to DBD linker. Mutational analysis in ToxT of Met103, Arg105 or Asn106 showed a threefold activation increase of the *ctxA* promoter, pointing out the important role of this small  $\alpha$ -helix (Childers et al., 2007). It could play the same role as the N-terminus loop of AraC by controlling protein flexibility. Another regulator of the AraC family was solved full-length: XylR (4FE4, 4FE7; Ni et al., 2013; **Figure 6C**). It is activated in *E. coli* in the absence of glucose, in order to use D-xylose as an alternative carbon source (Brückner and Titgemeyer, 2002). From structural comparison, the C-terminal DBD domain is very similar to that of AraC, but not the N-terminal RD domains. The XylR-RD domain looks like the periplasmic binding-protein of PurR from the LacI/GalR regulator family. It is composed of two  $\alpha/\beta$  sub-domains linked by a small loop. The ligand-binding cavity is localized at the interface between the two  $\alpha/\beta$  sub-domains. At the beginning of the swapping region between the RD and DBD domains, a flexible loop (D219-L232) in the complex structure with D-xylose changes into  $\alpha$ -helix in the apo-form, which modulates the binding affinity of the DBD toward the cognate DNA operator. XylR forms

antiparallel dimers orienting the DBD domains in a head-to-head manner. Because XylR has to interact with two distant operator sites, a DNA loop must be formed by the DBD dimer, as demonstrated by AFM studies performed on XylR dimer in complex with a 500 bp DNA fragment. Note that unlike AraC, the DNA loop is formed in presence of the inducer ligand D-xylose. Nevertheless, there is a cross talk between the two regulatory mechanisms since AraC binds a DNA region containing the XylR promoter. It gives the possibility to activate one or the other sugar-producing pathway according to the available source of carbon.

All of the AFTRs does not respond to this simple mechanism. For example, InvF from *S. enterica* serovar *Typhimurium* is not able to activate virulence genes without the chaperone protein SicA (Darwin and Miller, 2000). It is suggested that InvF would function as a monomer but associated with SicA. MarA (Rhee et al., 1998; Gillette et al., 2000) and SoxS (Griffith and Wolf, 2002) involved in response to oxidative stress are small proteins of around 100 amino acids, formed by HTH domain only, thus devoid of responsive domain for a signaling ligand. They act as monomers and their regulation depends on the position of the TFBS toward the RNAP.

The tight regulation mechanism of AraC has inspired biotechnology developments and it is largely used as bacterial



expression systems for recombinant protein expression (Brautaset et al., 2009).

## The One-Component Regulators of *P. aeruginosa* RND Efflux Pumps

As mentioned in the introduction, very few structural information is available on *P. aeruginosa* regulators, with only three solved structures to date: MexR, NalD and MexZ. Two of them are involved in the regulation of the MexAB-OprM pump which is considered as constitutive, although mutations in either *mexR*, *nalC* or *nalD* cause an over-expression of the pump (Boutoille et al., 2004; Sobel et al., 2005). MexR is the primary regulator of MexAB-OprM; it belongs to the MarR family and binds to its own promoter and that of the *mexAB-oprM* operon. One MexR regulatory pathway involves the binding of ArmR, a polypeptide of 53 amino acids, which expression is controlled by NalC, another TetR repressor. The structure of NalC has not been solved yet but it shows 31% of similarity with the N-terminal half of MLR\_4833 from *Mesorhizobium loti* (3BHQ), corresponding to a canonical DBD of the TetR family. The LBD structure is not known but pentachlorophenol and other chlorinated phenol molecules have been identified as NalC signaling inducer (Muller et al., 2007; Ghosh et al., 2011). Several structures of MexR were solved: in the apo-form (1LNW, Lim et al., 2002), in complex with the C-terminal part of ArmR (3ECH, Wilke et al., 2008) and a clinical mutant (R21W) that induces overexpression of the pump (4ZZL, Anandapadamanaban et al., 2016). In addition, another apo-form structure was solved upon oxidation of the cysteines (3MEX, Chen et al., 2008), highlighting a new mechanism of regulation by inter-monomer disulfide bond (Chen et al., 2010). The comparison between the four different structures gives some information on the induced conformational changes necessary for the regulation. In the MexR/ArmR complex, ArmR binds into the classical MarR cavity with an oligomeric ratio of 1:2. The C-terminus enters deeply in the protein toward the cavity of the second monomer, labeled as “C” on **Figure 5**. In the mutant R21W structure, the dimer is more packed with a more constricted ligand cavity: the tryptophan mutant is stacked in between four prolines (P37 and P38 from each monomer) at the position normally occupied by G49 of ArmR (**Figure 5C**). This will cause the closure of the pincer formed by helices  $\alpha 1$  and  $\alpha 6$ , and consequently will increase the distance between the two  $\beta$ -wings. The dimer does not fit anymore to a B-DNA conformation, which releases the repression and promotes *Pseudomonas* antibiotic resistance by MexAB-OprM efflux. The structure of the oxidized MexR is comparable to that of mutant R21W despite the 16 Å displacement of the  $\alpha 3$ - $\alpha 4$  loop resulting in the disulfide bond formation between C62 and C30 from each monomer. The distance between the two helices  $\alpha 4$  of the wild-type dimer (29 Å) is more suitable for tandem DNA major grooves interaction (34 Å) compared to the mutant (23.5 Å). These structures have brought important information to understand the regulation mechanisms of MexR.

Another regulator of known structure is NalD, a secondary regulator of MexAB-OprM transcription (Morita et al., 2006).

NalD is a TetR repressor that recognizes a TFBS upstream the operon *mexAB-OprM*. The NalD structure was solved in its apo-form (Chen et al., 2016) and is very similar to that of TtgR, the regulator of TtgABC efflux in *Pseudomonas putida*, which has a less folded  $\alpha 4$  helix. It was proved that NalD is able to bind to novobiocin in a similar pocket to that of TtgR, resulting in resistance increase of *P. aeruginosa* strains.

The repressor NfxB of the MexCD-OprJ efflux pump was first classified in the LacI/GalR family, but the closest sequence homology turns to be the TetR-like regulator LFRR from *Mycobacterium smegmatis*, especially the DBD domain. Besides, MexL also belongs to the TetR family, with sequence identity alignment coverage of 93%. It shares 46.5% sequence identity with the DBD domain of NalD, which suggests a possible competition for the same TFBS. Another TetR repressor is the primary repressor MexZ of the MexXY-OprM efflux pump, which selectively transports aminoglycosides. The structure of MexZ was solved in its apo-form (Alguet et al., 2010). It presents a classical TetR structure, with a partially unfolded  $\alpha 4$  helix. At present, the inducer molecule of MexZ is not known. A novel protein partner ArmZ, classified as a RNA-ligase, is suggested to sequester MexZ which releases the repression of *mexXY* (Hay et al., 2013). The gene of MexZ is the most frequently mutated in *P. aeruginosa* strains from cystic fibrosis patients (Smith et al., 2006). Most of the mutations are found in the DBD or strategic positions such as the dimer interface. One mutation has been reported on the surface of the helix  $\alpha 7$  (L128M, see **Figure 3**; Guénard et al., 2014), which suggests  $\alpha 7$  as part of the recognition site of ArmZ.

Finally, an activator regulates the efflux pump MexEF-OprN this time: MexT, which belongs to the LysR family (Fetar et al., 2011). MexT acts as a primary regulator of the pump together with the repressor of *oprD* porin. A redox mechanism seems to regulate MexT through *mexS* gene which codes for an oxydoreductase that upregulates MexEF-OprN (Morita et al., 2015; Richardot et al., 2016). We modeled the structure of MexT based on that of the DntR regulator from *Burkholderia* and localized in the RD domain the only cysteine that could possibly react to the ROS (Reactive Oxygen Species). Nevertheless, this cysteine can hardly form a disulfide-bond within a dimer of MexT according to the homology model structure. Recently a secondary activator of MexEF-OprN was described to upregulate MexEF-OprN through MexS and MexT (Juarez et al., 2018): it is named CmrA for Chloramphenicol Resistance Activator (Juarez et al., 2017). This regulator belongs to the AraC family and presents several cysteines, which is interesting in the context of the redox regulation mechanism.

## CONCLUSION

As a multidrug-resistant pathogen, *Pseudomonas aeruginosa* possesses many RND efflux pumps. But some of them are functionally redundant, which is *a priori* not needful in term of biological evolution. Surprisingly, efflux pumps that transport similar molecules are not regulated by the same transcriptional systems. This certainly reflects the need to a prompt reactivity of the bacteria upon environment modification. All the 3D

structures of the different regulators solved from different bacteria brought complementary informations to genetic, biochemical and biophysical data, in particular the crystal structures gave important insights in the comprehension of the main regulatory mechanisms. Nevertheless, with the intention of doing specific drug-design, high-resolution structures of regulators from *P. aeruginosa* are still necessary. Recent structures of the virulence factor regulator MvfR, member of the LysR family from *P. aeruginosa*, solved in complex with inducer and inhibitor, illustrate the interest of the structural approach (Kitao et al., 2018). Both molecules bind within the same cavity with subtle interaction differences that are the keystone of the regulation mechanism. Thus, the knowledge of the 3D structures of each specific regulator is mandatory to develop new and specific drugs. From the complex signaling regulation of RND pumps expression illustrated on **Figure 1**, it is clear that

there is a real lack of information concerning the structures of *P. aeruginosa* regulators. As this bacterium belongs to the group of the most problematic clinical pathogens, structural study of the regulators of *P. aeruginosa* are urgently needed.

## AUTHOR CONTRIBUTIONS

All authors listed have made a substantial, direct and intellectual contribution to the work, and approved it for publication.

## FUNDING

Association Vaincre la Mucoviscidose (RF20150501358) and Association Grégory Lemarchal. CNRS. University Paris Descartes. KH was supported by a grant of Vaincre la Mucoviscidose and the Association Grégory Lemarchal.

## REFERENCES

- Alanazi, A. M., Neidle, E. L., and Momany, C. (2013). The DNA-binding domain of BenM reveals the structural basis for the recognition of a T-N11-A sequence motif by LysR-type transcriptional regulators. *Acta Crystallogr. D Biol. Crystallogr.* 69(Pt 10), 1995–2007. doi: 10.1107/S0907444913017320
- Alekshun, M. N., and Levy, S. B. (1997). Regulation of chromosomally mediated multiple antibiotic resistance: the mar regulon. *Antimicrob. Agents Chemother.* 41, 2067–2075.
- Alekshun, M. N., Levy, S. B., Mealy, T. R., Seaton, B. A., and Head, J. F. (2001). The crystal structure of MarR, a regulator of multiple antibiotic resistance, at 2.3 Å resolution. *Nat. Struct. Biol.* 8, 710–714. doi: 10.1038/90429
- Alguel, Y., Lu, D., Quade, N., Sauter, S., and Zhang, X. (2010). Crystal structure of MexZ, a key repressor responsible for antibiotic resistance in *Pseudomonas aeruginosa*. *J. Struct. Biol.* 172, 305–310. doi: 10.1016/j.jsb.2010.07.012
- Alguel, Y., Meng, C., Terán, W., Krell, T., Ramos, J. L., Gallegos, M. T., et al. (2007). Crystal structures of multidrug binding protein TtgR in complex with antibiotics and plant antimicrobials. *J. Mol. Biol.* 369, 829–840. doi: 10.1016/j.jmb.2007.03.062
- Alvarez-Ortega, C., Olivares, J., and Martínez, J. L. (2013). RND multidrug efflux pumps: what are they good for? *Front. Microbiol.* 4:7. doi: 10.3389/fmicb.2013.00007
- Anandapadamanabhan, M., Pilstål, R., Andresen, C., Trehwella, J., Moche, M., Wallner, B., et al. (2016). Mutation-induced population shift in the MexR conformational ensemble disengages DNA binding: a novel mechanism for MarR family derepression. *Structure* 24, 1311–1321. doi: 10.1016/j.str.2016.06.008
- Andrésen, C., Jalal, S., Aili, D., Wang, Y., Islam, S., Jarl, A., et al. (2010). Critical biophysical properties in the *Pseudomonas aeruginosa* efflux gene regulator MexR are targeted by mutations conferring multidrug resistance. *Protein Sci.* 19, 680–692. doi: 10.1002/pro.343
- Bartowsky, E., and Normark, S. (1991). Purification and mutant analysis of *Citrobacter freundii* AmpR, the regulator for chromosomal AmpC beta-lactamase. *Mol. Microbiol.* 5, 1715–1725. doi: 10.1111/j.1365-2958.1991.tb01920.x
- Bhate, M. P., Molnar, K. S., Goulian, M., and DeGrado, W. F. (2015). Signal transduction in histidine kinases: insights from new structures. *Structure* 23, 981–994. doi: 10.1016/j.str.2015.04.002
- Bhende, P. M., and Egan, S. M. (2000). Genetic evidence that transcription activation by RhaS involves specific amino acid contacts with sigma 70. *J. Bacteriol.* 182, 4959–4969. doi: 10.1128/JB.182.17.4959-4969.2000
- Bhukya, H., Bhujbalrao, R., Bitra, A., and Anand, R. (2014). Structural and functional basis of transcriptional regulation by TetR family protein CprB from *S. coelicolor* A3(2). *Nucleic Acids Res.* 42, 10122–10133. doi: 10.1093/nar/gku587
- Bhukya, H., Jana, A. K., Sengupta, N., and Anand, R. (2017). Structural and dynamics studies of the TetR family protein, CprB from *Streptomyces coelicolor* in complex with its biological operator sequence. *J. Struct. Biol.* 198, 134–146. doi: 10.1016/j.jsb.2017.03.006
- Blanco, A. G., Sola, M., Gomis-Rüth, F. X., and Coll, M. (2002). Tandem DNA recognition by PhoB, a two-component signal transduction transcriptional activator. *Structure* 10, 701–713. doi: 10.1016/S0969-2126(02)00761-X
- Blanco, P., Hernando-Amado, S., Reales-Calderon, J. A., Corona, F., Lira, F., Alcalde-Rico, M., et al. (2016). Bacterial multidrug efflux pumps: much more than antibiotic resistance determinants. *Microorganisms* 4:E14. doi: 10.3390/microorganisms4010014
- Blondiaux, N., Moune, M., Desroses, M., Frita, R., Flipo, M., Mathys, V., et al. (2017). Reversion of antibiotic resistance in *Mycobacterium tuberculosis* by spiroisoxazoline SMART-420. *Science* 355, 1206–1211. doi: 10.1126/science.aag1006
- Bock, T., Volz, C., Hering, V., Scrima, A., Müller, R., and Blankenfeldt, W. (2017). The AibR-isovaleryl coenzyme A regulator and its DNA binding site - a model for the regulation of alternative de novo isovaleryl coenzyme A biosynthesis in *Myxococcus xanthus*. *Nucleic Acids Res.* 45, 2166–2178. doi: 10.1093/nar/gkw1238
- Bordelon, T., Wilkinson, S. P., Grove, A., and Newcomer, M. E. (2006). The crystal structure of the transcriptional regulator HucR from *Deinococcus radiodurans* reveals a repressor preconfigured for DNA binding. *J. Mol. Biol.* 360, 168–177. doi: 10.1016/j.jmb.2006.05.005
- Boutoille, D., Corvec, S., Caroff, N., Giraudeau, C., Espaze, E., Caillon, J., et al. (2004). Detection of an IS21 insertion sequence in the mexR gene of *Pseudomonas aeruginosa* increasing beta-lactam resistance. *FEMS Microbiol. Lett.* 230, 143–146. doi: 10.1016/S0378-1097(03)00882-6
- Brautaset, T., Lale, R., and Valla, S. (2009). Positively regulated bacterial expression systems. *Microb. Biotechnol.* 2, 15–30. doi: 10.1111/j.1751-7915.2008.00048.x
- Brier, S., Fagnocchi, L., Donnarumma, D., Scarselli, M., Rappuoli, R., Nisum, M., et al. (2012). Structural insight into the mechanism of DNA-binding attenuation of the Neisseria adhesin repressor NadR by the small natural ligand 4-hydroxyphenylacetic acid. *Biochemistry* 51, 6738–6752. doi: 10.1021/bi300656w
- Brückner, R., and Titgemeyer, F. (2002). Carbon catabolite repression in bacteria: choice of the carbon source and autoregulatory limitation of sugar utilization. *FEMS Microbiol. Lett.* 209, 141–148. doi: 10.1016/S0378-1097(02)00559-1
- Bugg, T. D., and Rahmanpour, R. (2015). Enzymatic conversion of lignin into renewable chemicals. *Curr. Opin. Chem. Biol.* 29, 10–17. doi: 10.1016/j.cbpa.2015.06.009
- Bustos, S. A., and Schleif, R. F. (1993). Functional domains of the AraC protein. *Proc. Natl. Acad. Sci. U.S.A.* 90, 5638–5642. doi: 10.1073/pnas.90.12.5638
- Caille, O., Rossier, C., and Perron, K. (2007). A copper-activated two-component system interacts with zinc and imipenem resistance in *Pseudomonas aeruginosa*. *J. Bacteriol.* 189, 4561–4568. doi: 10.1128/JB.00095-07

- Capra, E. J., and Laub, M. T. (2012). Evolution of two-component signal transduction systems. *Annu. Rev. Microbiol.* 66, 325–347. doi: 10.1146/annurev-micro-092611-150039
- Carette, X., Blondiaux, N., Willery, E., Hoos, S., Lecat-Guillet, N., Lens, Z., et al. (2012). Structural activation of the transcriptional repressor EthR from *Mycobacterium tuberculosis* by single amino acid change mimicking natural and synthetic ligands. *Nucleic Acids Res.* 40, 3018–3030. doi: 10.1093/nar/gkr1113
- Carra, J. H., and Schleif, R. F. (1993). Variation of half-site organization and DNA looping by AraC protein. *EMBO J.* 12, 35–44.
- Casino, P., Rubio, V., and Marina, A. (2009). Structural insight into partner specificity and phosphoryl transfer in two-component signal transduction. *Cell* 139, 325–336. doi: 10.1016/j.cell.2009.08.032
- Casino, P., Rubio, V., and Marina, A. (2010). The mechanism of signal transduction by two-component systems. *Curr. Opin. Struct. Biol.* 20, 763–771. doi: 10.1016/j.sbi.2010.09.010
- Chang, Y. M., Chen, C. K., Ko, T. P., Chang-Chien, M. W., and Wang, A. H. (2013). Structural analysis of the antibiotic-recognition mechanism of MarR proteins. *Acta Crystallogr. D Biol. Crystallogr.* 69(Pt 6), 1138–1149. doi: 10.1107/S0907444913007117
- Chang, Y. M., Jeng, W. Y., Ko, T. P., Yeh, Y. J., Chen, C. K., and Wang, A. H. (2010). Structural study of TcaR and its complexes with multiple antibiotics from *Staphylococcus epidermidis*. *Proc. Natl. Acad. Sci. U.S.A.* 107, 8617–8622. doi: 10.1073/pnas.0913021107
- Cheesman, M. J., Ilanko, A., Blonk, B., and Cock, I. E. (2017). Developing new antimicrobial therapies: are synergistic combinations of plant extracts/compounds with conventional antibiotics the solution? *Pharmacogn. Rev.* 11, 57–72. doi: 10.4103/phrev.phrev\_21\_17
- Chen, H., Hu, J., Chen, P. R., Lan, L., Li, Z., Hicks, L. M., et al. (2008). The *Pseudomonas aeruginosa* multidrug efflux regulator MexR uses an oxidation-sensing mechanism. *Proc. Natl. Acad. Sci. U.S.A.* 105, 13586–13591. doi: 10.1073/pnas.0803391105
- Chen, H., Yi, C., Zhang, J., Zhang, W., Ge, Z., Yang, C. G., et al. (2010). Structural insight into the oxidation-sensing mechanism of the antibiotic resistance of regulator MexR. *EMBO Rep.* 11, 685–690. doi: 10.1038/embor.2010.96
- Chen, W., Wang, D., Zhou, W., Sang, H., Liu, X., Ge, Z., et al. (2016). Novobiocin binding to NalD induces the expression of the MexAB-OprM pump in *Pseudomonas aeruginosa*. *Mol. Microbiol.* 100, 749–758. doi: 10.1111/mmi.13346
- Childers, B. M., Weber, G. G., Prouty, M. G., Castaneda, M. M., Peng, F., and Klose, K. E. (2007). Identification of residues critical for the function of the *Vibrio cholerae* virulence regulator ToxT by scanning alanine mutagenesis. *J. Mol. Biol.* 367, 1413–1430. doi: 10.1016/j.jmb.2007.01.061
- Coates, A., Hu, Y., Bax, R., and Page, C. (2002). The future challenges facing the development of new antimicrobial drugs. *Nat. Rev. Drug Discov.* 1, 895–910. doi: 10.1038/nrd940
- Cohen, S. P., Hächler, H., and Levy, S. B. (1993). Genetic and functional analysis of the multiple antibiotic resistance (mar) locus in *Escherichia coli*. *J. Bacteriol.* 175, 1484–1492. doi: 10.1128/jb.175.5.1484-1492.1993
- Colyer, T. E., and Kredich, N. M. (1996). *In vitro* characterization of constitutive CysB proteins from *Salmonella typhimurium*. *Mol. Microbiol.* 21, 247–256. doi: 10.1046/j.1365-2958.1996.6301347.x
- Cuthbertson, L., and Nodwell, J. R. (2013). The TetR family of regulators. *Microbiol. Mol. Biol. Rev.* 77, 440–475. doi: 10.1128/MMBR.00018-13
- Darwin, K. H., and Miller, V. L. (2000). The putative invasion protein chaperone SicA acts together with InvF to activate the expression of *Salmonella typhimurium* virulence genes. *Mol. Microbiol.* 35, 949–960. doi: 10.1046/j.1365-2958.2000.01772.x
- Dauray, L., Orange, F., Taveau, J. C., Verchère, A., Monlezun, L., Gounou, C., et al. (2016). Tripartite assembly of RND multidrug efflux pumps. *Nat. Commun.* 7:10731. doi: 10.1038/ncomms10731
- Davies, J., and Davies, D. (2010). Origins and evolution of antibiotic resistance. *Microbiol. Mol. Biol. Rev.* 74, 417–433. doi: 10.1128/MMBR.00016-10
- Davis, J. R., Brown, B. L., Page, R., and Sello, J. K. (2013). Study of PcaV from *Streptomyces coelicolor* yields new insights into ligand-responsive MarR family transcription factors. *Nucleic Acids Res.* 41, 3888–3900. doi: 10.1093/nar/gkt009
- Davis, J. R., and Sello, J. K. (2010). Regulation of genes in *Streptomyces* bacteria required for catabolism of lignin-derived aromatic compounds. *Appl. Microbiol. Biotechnol.* 86, 921–929. doi: 10.1007/s00253-009-2358-0
- D'Costa, V. M., King, C. E., Kalan, L., Morar, M., Sung, W. W., Schwarz, C., et al. (2011). Antibiotic resistance is ancient. *Nature* 477, 457–461. doi: 10.1038/nature10388
- DeLano, W. L. (2009). PyMOL molecular viewer: updates and refinements. *Abst. Papers Am. Chem. Soc.* 238.
- Deng, W., Li, C., and Xie, J. (2013). The underlying mechanism of bacterial TetR/AcrR family transcriptional repressors. *Cell. Signal.* 25, 1608–1613. doi: 10.1016/j.cellsig.2013.04.003
- Deochand, D. K., Perera, I. C., Crochet, R. B., Gilbert, N. C., Newcomer, M. E., and A., G. (2016). Histidine switch controlling pH-dependent protein folding and DNA binding in a transcription factor at the core of synthetic network devices. *Mol. Biosyst.* 12, 2417–2426. doi: 10.1039/C6MB00304D
- Dolan, K. T., Duguid, E. M., and He, C. (2011). Crystal structures of SlyA protein, a master virulence regulator of *Salmonella*, in free and DNA-bound states. *J. Biol. Chem.* 286, 22178–22185. doi: 10.1074/jbc.M111.245258
- Du, D., Wang, Z., James, N. R., Voss, J. E., Klimont, E., Ohene-Agyei, T., et al. (2014). Structure of the AcrAB-TolC multidrug efflux pump. *Nature* 509, 512–515. doi: 10.1038/nature13205
- Egan, S. M. (2002). Growing repertoire of AraC/XylS activators. *J. Bacteriol.* 184, 5529–5532. doi: 10.1128/JB.184.20.5529-5532.2002
- Ezeizika, O. C., Haddad, S., Neidle, E. L., and Momany, C. (2007a). Oligomerization of BenM, a LysR-type transcriptional regulator: structural basis for the aggregation of proteins in this family. *Acta Crystallogr. Sect. F Struct. Biol. Cryst. Commun.* 63(Pt 5), 361–368. doi: 10.1107/S1744309107019185
- Ezeizika, O. C., Haddad, S., Clark, T. J., Neidle, E. L., and Momany, C. (2007b). Distinct effector-binding sites enable synergistic transcriptional activation by BenM, a LysR-type regulator. *J. Mol. Biol.* 367, 616–629. doi: 10.1016/j.jmb.2006.09.090
- Fair, R. J., and Tor, Y. (2014). Antibiotics and bacterial resistance in the 21st century. *Perspect. Medicin. Chem.* 6, 25–64. doi: 10.4137/PMC.S14459
- Fernández, L., Gooderham, W. J., Bains, M., McPhee, J. B., Wiegand, I., and Hancock, R. E. (2010). Adaptive resistance to the “last hope” antibiotics polymyxin B and colistin in *Pseudomonas aeruginosa* is mediated by the novel two-component regulatory system ParR-ParS. *Antimicrob. Agents Chemother.* 54, 3372–3382. doi: 10.1128/AAC.00242-10
- Fetar, H., Gilmour, C., Klinoski, R., Daigle, D. M., Dean, C. R., and Poole, K. (2011). mexEF-oprN multidrug efflux operon of *Pseudomonas aeruginosa*: regulation by the MexT activator in response to nitrosative stress and chloramphenicol. *Antimicrob. Agents Chemother.* 55, 508–514. doi: 10.1128/AAC.00830-10
- Fitzpatrick, A. W. P., Llabrés, S., Neuberger, A., Blaza, J. N., Bai, X. C., Okada, U., et al. (2017). Structure of the MacAB-TolC ABC-type tripartite multidrug efflux pump. *Nat. Microbiol.* 2:17070. doi: 10.1038/nmicrobiol.2017.70
- Frénois, F., Engohang-Ndong, J., Loch, C., Baulard, A. R., and Villeret, V. (2004). Structure of EthR in a ligand bound conformation reveals therapeutic perspectives against tuberculosis. *Mol. Cell* 16, 301–307. doi: 10.1016/j.molcel.2004.09.020
- Frieri, M., Kumar, K., and Boutin, A. (2017). Antibiotic resistance. *J. Infect. Public Health* 10, 369–378. doi: 10.1016/j.jiph.2016.08.007
- Fuchs, G., Boll, M., and Heider, J. (2011). Microbial degradation of aromatic compounds - from one strategy to four. *Nat. Rev. Microbiol.* 9, 803–816. doi: 10.1038/nrmicro2652
- Gallegos, M. T., Schleif, R., Bairoch, A., Hofmann, K., and Ramos, J. L. (1997). Arac/XylS family of transcriptional regulators. *Microbiol. Mol. Biol. Rev.* 61, 393–410.
- Gao, R., and Stock, A. M. (2009). Biological insights from structures of two-component proteins. *Annu. Rev. Microbiol.* 63, 133–154. doi: 10.1146/annurev.micro.091208.073214
- Gao, Y. R., Li, D. F., Fleming, J., Zhou, Y. F., Liu, Y., Deng, J. Y., et al. (2017). Structural analysis of the regulatory mechanism of MarR protein Rv2887 in *M. tuberculosis*. *Sci Rep* 7:6471. doi: 10.1038/s41598-017-01705-4
- Ghosh, S., Cremers, C. M., Jakob, U., and Love, N. G. (2011). Chlorinated phenols control the expression of the multidrug resistance efflux pump MexAB-OprM in *Pseudomonas aeruginosa* by interacting with NalC. *Mol. Microbiol.* 79, 1547–1556. doi: 10.1111/j.1365-2958.2011.07544.x



- Gillette, W. K., Martin, R. G., and Rosner, J. L. (2000). Probing the *Escherichia coli* transcriptional activator MarA using alanine-scanning mutagenesis: residues important for DNA binding and activation. *J. Mol. Biol.* 299, 1245–1255. doi: 10.1006/jmbi.2000.3827
- Goethals, K., Van Montagu, M., and Holsters, M. (1992). Conserved motifs in a divergent nod box of *Azorhizobium caulinodans* ORS571 reveal a common structure in promoters regulated by LysR-type proteins. *Proc. Natl. Acad. Sci. U.S.A.* 89, 1646–1650. doi: 10.1073/pnas.89.5.1646
- Gooderham, W. J., and Hancock, R. E. (2009). Regulation of virulence and antibiotic resistance by two-component regulatory systems in *Pseudomonas aeruginosa*. *FEMS Microbiol. Rev.* 33, 279–294. doi: 10.1111/j.1574-6976.2008.00135.x
- Griffith, K. L., and Wolf, R. E. Jr. (2002). A comprehensive alanine scanning mutagenesis of the *Escherichia coli* transcriptional activator SoxS: identifying amino acids important for DNA binding and transcription activation. *J. Mol. Biol.* 322, 237–257. doi: 10.1016/S0022-2836(02)00782-9
- Grkovic, S., Brown, M. H., Schumacher, M. A., Brennan, R. G., and Skurray, R. A. (2001). The staphylococcal QacR multidrug regulator binds a correctly spaced operator as a pair of dimers. *J. Bacteriol.* 183, 7102–7109. doi: 10.1128/JB.183.24.7102-7109.2001
- Grkovic, S., Brown, M. H., and Skurray, R. A. (2002). Regulation of bacterial drug export systems. *Microbiol. Mol. Biol. Rev.* 66, 671–701, table of contents. doi: 10.1128/MMBR.66.4.671-701.2002
- Grove, A. (2017). Regulation of metabolic pathways by MarR family transcription factors. *Comput. Struct. Biotechnol. J.* 15, 366–371. doi: 10.1016/j.csbj.2017.06.001
- Guénard, S., Muller, C., Monlezun, L., Benas, P., Broutin, I., Jeannot, K., et al. (2014). Multiple mutations lead to MexXY-OprM-dependent aminoglycoside resistance in clinical strains of *Pseudomonas aeruginosa*. *Antimicrob. Agents Chemother.* 58, 221–228. doi: 10.1128/AAC.01252-13
- Gushchin, I., Melnikov, I., Polovinkin, V., Ishchenko, A., Yuzhakova, A., Buslaev, P., et al. (2017). Mechanism of transmembrane signaling by sensor histidine kinases. *Science* 356:eaah6345. doi: 10.1126/science.aah6345
- Hay, T., Fraud, S., Lau, C. H., Gilmour, C., and Poole, K. (2013). Antibiotic inducibility of the mexXY multidrug efflux operon of *Pseudomonas aeruginosa*: involvement of the MexZ anti-repressor ArmZ. *PLoS ONE* 8:e56858. doi: 10.1371/journal.pone.0056858
- He, X., Wang, L., and Wang, S. (2016). Structural basis of DNA sequence recognition by the response regulator PhoP in *Mycobacterium tuberculosis*. *Sci. Rep.* 6:24442. doi: 10.1038/srep24442
- Hede, K. (2014). Antibiotic resistance: an infectious arms race. *Nature* 509, S2–S3. doi: 10.1038/509S2a
- Henikoff, S., Haugn, G. W., Calvo, J. M., and Wallace, J. C. (1988). A large family of bacterial activator proteins. *Proc. Natl. Acad. Sci. U.S.A.* 85, 6602–6606. doi: 10.1073/pnas.85.18.6602
- Heroven, A. K., and Dersch, P. (2006). RovM, a novel LysR-type regulator of the virulence activator gene *rovA*, controls cell invasion, virulence and motility of *Yersinia pseudotuberculosis*. *Mol. Microbiol.* 62, 1469–1483. doi: 10.1111/j.1365-2958.2006.05458.x
- Hinrichs, W., Kisker, C., Düvel, M., Müller, A., Tovar, K., Hillen, W., et al. (1994). Structure of the Tet repressor-tetracycline complex and regulation of antibiotic resistance. *Science* 264, 418–420. doi: 10.1126/science.8153629
- Hvorup, R. N., Winnen, B., Chang, A. B., Jiang, Y., Zhou, X. F., and Saier, M. H. Jr. (2003). The multidrug/oligosaccharidyl-lipid/polysaccharide (MOP) exporter superfamily. *Eur. J. Biochem.* 270, 799–813. doi: 10.1046/j.1432-1033.2003.03418.x
- Ibarra, J. A., Pérez-Rueda, E., Segovia, L., and Puente, J. L. (2008). The DNA-binding domain as a functional indicator: the case of the AraC/XylS family of transcription factors. *Genetica* 133, 65–76. doi: 10.1007/s10709-007-9185-y
- Itou, H., Watanabe, N., Yao, M., Shirakihara, Y., and Tanaka, I. (2010). Crystal structures of the multidrug binding repressor *Corynebacterium glutamicum* CgmR in complex with inducers and with an operator. *J. Mol. Biol.* 403, 174–184. doi: 10.1016/j.jmb.2010.07.042
- Jiang, Y. L., Wang, X. P., Sun, H., Han, S. J., Li, W. F., Cui, N., et al. (2018). Coordinating carbon and nitrogen metabolic signaling through the cyanobacterial global repressor NdhR. *Proc. Natl. Acad. Sci. U.S.A.* 115, 403–408. doi: 10.1073/pnas.1716062115
- Jo, I., Chung, I. Y., Bae, H. W., Kim, J. S., Song, S., Cho, Y. H., et al. (2015). Structural details of the OxyR peroxide-sensing mechanism. *Proc. Natl. Acad. Sci. U.S.A.* 112, 6443–6448. doi: 10.1073/pnas.1424495112
- Jo, I., Kim, D., Bang, Y. J., Ahn, J., Choi, S. H., and Ha, N. C. (2017). The hydrogen peroxide hypersensitivity of OxyR2 in *Vibrio vulnificus* depends on conformational constraints. *J. Biol. Chem.* 292, 7223–7232. doi: 10.1074/jbc.M116.743765
- Juarez, P., Broutin, I., Bordin, C., Plésiat, P., and Llanes, C. (2018). Constitutive activation of MexT by amino acid substitutions results in MexEF-OprN overproduction in clinical isolates of *Pseudomonas aeruginosa*. *Antimicrob. Agents Chemother.* 62:e02445–17. doi: 10.1128/AAC.02445-17
- Juarez, P., Jeannot, K., Plésiat, P., and Llanes, C. (2017). Toxic electrophiles induce expression of the multidrug efflux pump MexEF-OprN in *Pseudomonas aeruginosa* through a novel transcriptional regulator, CmrA. *Antimicrob. Agents Chemother.* 61. doi: 10.1128/AAC.00585-17
- Jung, K., Fried, L., Behr, S., and Heermann, R. (2012). Histidine kinases and response regulators in networks. *Curr. Opin. Microbiol.* 15, 118–124. doi: 10.1016/j.mib.2011.11.009
- Kallscheuer, N., Vogt, M., Kappelmann, J., Krumbach, K., Noack, S., Bott, M., et al. (2016). Identification of the phd gene cluster responsible for phenylpropanoid utilization in *Corynebacterium glutamicum*. *Appl. Microbiol. Biotechnol.* 100, 1871–1881. doi: 10.1007/s00253-015-7165-1
- Khameneh, B., Diab, R., Ghazvini, K., and Fazly Bazzaz, B. S. (2016). Breakthroughs in bacterial resistance mechanisms and the potential ways to combat them. *Microb. Pathog.* 95, 32–42. doi: 10.1016/j.micpath.2016.02.009
- Kim, Y., Joachimiak, G., Bigelow, L., Babnigg, G., and Joachimiak, A. (2016). How aromatic compounds block DNA binding of HcaR catabolite regulator. *J. Biol. Chem.* 291, 13243–13256. doi: 10.1074/jbc.M115.712067
- Kisker, C., Hinrichs, W., Tovar, K., Hillen, W., and Saenger, W. (1995). The complex formed between Tet repressor and tetracycline-Mg<sup>2+</sup> reveals mechanism of antibiotic resistance. *J. Mol. Biol.* 247, 260–280. doi: 10.1006/jmbi.1994.0138
- Kitao, T., Lepine, F., Bablouti, S., Walte, F., Steinbacher, S., Maskos, K., et al. (2018). Molecular insights into function and competitive inhibition of *Pseudomonas aeruginosa* multiple virulence factor regulator. *mBio* 9:e02158-17. doi: 10.1128/mBio.02158-17
- Koentjoro, M. P., Adachi, N., Senda, M., Ogawa, N., and Senda, T. (2018). Crystal structure of the DNA-binding domain of the LysR-type transcriptional regulator CbnR in complex with a DNA fragment of the recognition-binding site in the promoter region. *FEBS J.* 285, 977–989. doi: 10.1111/febs.14380
- Krell, T., Lacal, J., Busch, A., Silva-Jiménez, H., Guazzaroni, M. E., and Ramos, J. L. (2010). Bacterial sensor kinases: diversity in the recognition of environmental signals. *Annu. Rev. Microbiol.* 64, 539–559. doi: 10.1146/annurev.micro.112408.134054
- Kumar, S., Mukherjee, M. M., and Varela, M. F. (2013). Modulation of bacterial multidrug resistance efflux pumps of the major facilitator superfamily. *Int. J. Bacteriol.* 2013:204141. doi: 10.1155/2013/204141
- Kumarevel, T. (2012). “The MarR Family of Transcriptional Regulators – A Structural Perspective,” in *Antibiotic Resistant Bacteria – A Continuous Challenge in the New Millennium*, ed M. Pana (London, UK: InTech), 403–418. doi: 10.5772/1058
- Kumarevel, T., Tanaka, T., Umehara, T., and Yokoyama, S. (2009). ST1710-DNA complex crystal structure reveals the DNA binding mechanism of the MarR family of regulators. *Nucleic Acids Res.* 37, 4723–4735. doi: 10.1093/nar/gkp496
- Kuroda, T., and Tsuchiya, T. (2009). Multidrug efflux transporters in the MATE family. *Biochim. Biophys. Acta* 1794, 763–768. doi: 10.1016/j.bbapap.2008.11.012
- Kwon, H. J., Bennis, M. H., Demple, B., and Ellenberger, T. (2000). Crystal structure of the *Escherichia coli* Rob transcription factor in complex with DNA. *Nat. Struct. Biol.* 7, 424–430. doi: 10.1038/75213
- Lau, C. H., Krahn, T., Gilmour, C., Mullen, E., and Poole, K. (2015). AmgRS-mediated envelope stress-inducible expression of the mexXY multidrug efflux operon of *Pseudomonas aeruginosa*. *Microbiologyopen* 4, 121–135. doi: 10.1002/mbo3.226
- Le, T. B., Schumacher, M. A., Lawson, D. M., Brennan, R. G., and Buttner, M. J. (2011). The crystal structure of the TetR family transcriptional repressor SimR bound to DNA and the role of a flexible N-terminal extension in minor groove binding. *Nucleic Acids Res.* 39, 9433–9447. doi: 10.1093/nar/gkr640



- Lerche, M., Dian, C., Round, A., Lönneborg, R., Brzezinski, P., and Leonard, G. A. (2016). The solution configurations of inactive and activated DntR have implications for the sliding dimer mechanism of LysR transcription factors. *Sci. Rep.* 6:19988. doi: 10.1038/srep19988
- Levy, S. B., and Marshall, B. (2004). Antibacterial resistance worldwide: causes, challenges and responses. *Nat. Med.* 10, S122–S129. doi: 10.1038/nm1145
- Li, D. F., Zhang, N., Hou, Y. J., Huang, Y., Hu, Y., Zhang, Y., et al. (2011). Crystal structures of the transcriptional repressor RolR reveals a novel recognition mechanism between inducer and regulator. *PLoS ONE* 6:e19529. doi: 10.1371/journal.pone.0019529
- Li, J., Wehmeyer, G., Lovell, S., Battaile, K. P., and Egan, S. M. (2016). 1.65 Å resolution structure of the AraC-family transcriptional activator ToxT from *Vibrio cholerae*. *Acta Crystallogr. F Struct. Biol. Commun.* 72(Pt 9), 726–731. doi: 10.1107/S2053230X1601298X
- Li, X. Z., and Nikaido, H. (2009). Efflux-mediated drug resistance in bacteria: an update. *Drugs* 69, 1555–1623. doi: 10.2165/11317030-000000000-00000
- Li, X. Z., Plésiat, P., and Nikaido, H. (2015). The challenge of efflux-mediated antibiotic resistance in Gram-negative bacteria. *Clin. Microbiol. Rev.* 28, 337–418. doi: 10.1128/CMR.00117-14
- Lim, D., Poole, K., and Strynadka, N. C. (2002). Crystal structure of the MexR repressor of the mexRAB-oprM multidrug efflux operon of *Pseudomonas aeruginosa*. *J. Biol. Chem.* 277, 29253–29259. doi: 10.1074/jbc.M111381200
- Ling, L. L., Schneider, T., Peoples, A. J., Spoering, A. L., Engels, I., Conlon, B. P., et al. (2015). A new antibiotic kills pathogens without detectable resistance. *Nature* 517, 455–459. doi: 10.1038/nature14098
- Lister, P. D., Wolter, D. J., and Hanson, N. D. (2009). Antibacterial-resistant *Pseudomonas aeruginosa*: clinical impact and complex regulation of chromosomally encoded resistance mechanisms. *Clin. Microbiol. Rev.* 22, 582–610. doi: 10.1128/CMR.00040-09
- Liu, G., Liu, X., Xu, H., Liu, X., Zhou, H., Huang, Z., et al. (2017). Structural insights into the redox-sensing mechanism of MarR-type regulator AbfR. *J. Am. Chem. Soc.* 139, 1598–1608. doi: 10.1021/jacs.6b11438
- Locher, K. P. (2009). Review. Structure and mechanism of ATP-binding cassette transporters. *Philos. Trans. R. Soc. Lond. B Biol. Sci.* 364, 239–245. doi: 10.1098/rstb.2008.0125
- Lou, Y. C., Weng, T. H., Li, Y. C., Kao, Y. F., Lin, W. F., Peng, H. L., et al. (2015). Structure and dynamics of polymyxin-resistance-associated response regulator PmrA in complex with promoter DNA. *Nat. Commun.* 6:8838. doi: 10.1038/ncomms9838
- Lowden, M. J., Skorupski, K., Pellegrini, M., Chiorazzo, M. G., Taylor, R. K., and Kull, F. J. (2010). Structure of *Vibrio cholerae* ToxT reveals a mechanism for fatty acid regulation of virulence genes. *Proc. Natl. Acad. Sci. U.S.A.* 107, 2860–2865. doi: 10.1073/pnas.0915021107
- Maddocks, S. E., and Oyston, P. C. (2008). Structure and function of the LysR-type transcriptional regulator (LTTR) family proteins. *Microbiology* 154(Pt 12), 3609–3623. doi: 10.1099/mic.0.2008/022772-0
- Martin, R. G., and Rosner, J. L. (1995). Binding of purified multiple antibiotic-resistance repressor protein (MarR) to mar operator sequences. *Proc. Natl. Acad. Sci. U.S.A.* 92, 5456–5460. doi: 10.1073/pnas.92.12.5456
- McDermott, P. F., Walker, R. D., and White, D. G. (2003). Antimicrobials: modes of action and mechanisms of resistance. *Int. J. Toxicol.* 22, 135–143. doi: 10.1080/10915810305089
- Martin, R. G., and Rosner, J. L. (2001). The AraC transcriptional activators. *Curr. Opin. Microbiol.* 4, 132–137. doi: 10.1016/S1369-5274(00)00178-8
- Mechaly, A. E., Sassoon, N., Betton, J. M., and Alzari, P. M. (2014). Segmental helical motions and dynamical asymmetry modulate histidine kinase autophosphorylation. *PLoS Biol.* 12:e1001776. doi: 10.1371/journal.pbio.1001776
- Miller, D. J., Zhang, Y. M., Subramanian, C., Rock, C. O., and White, S. W. (2010). Structural basis for the transcriptional regulation of membrane lipid homeostasis. *Nat. Struct. Mol. Biol.* 17, 971–975. doi: 10.1038/nsmb.1847
- Molnar, K. S., Bonomi, M., Pellarin, R., Clinthorne, G. D., Gonzalez, G., Goldberg, S. D., et al. (2014). Cys-scanning disulfide crosslinking and bayesian modeling probe the transmembrane signaling mechanism of the histidine kinase, PhoQ. *Structure* 22, 1239–1251. doi: 10.1016/j.str.2014.04.019
- Monferrer, D., Tralau, T., Kertesz, M. A., Dix, I., Solà, M., and Usón, I. (2010). Structural studies on the full-length LysR-type regulator Tsar from *Comamonas testosteroni* T-2 reveal a novel open conformation of the tetrameric LTTR fold. *Mol. Microbiol.* 75, 1199–1214. doi: 10.1111/j.1365-2958.2010.07043.x
- Monlezun, L., Phan, G., Benabdelhak, H., Lascombe, M. B., Enguéné, V. Y., Picard, M., et al. (2015). New OprM structure highlighting the nature of the N-terminal anchor. *Front. Microbiol.* 6:667. doi: 10.3389/fmicb.2015.00667
- Morita, Y., Cao, L., Gould, V. C., Avison, M. B., and Poole, K. (2006). nalD encodes a second repressor of the mexAB-oprM multidrug efflux operon of *Pseudomonas aeruginosa*. *J. Bacteriol.* 188, 8649–8654. doi: 10.1128/JB.01342-06
- Morita, Y., Tomida, J., and Kawamura, Y. (2015). Efflux-mediated fluoroquinolone resistance in the multidrug-resistant *Pseudomonas aeruginosa* clinical isolate PA7: identification of a novel MexS variant involved in upregulation of the mexEF-oprN multidrug efflux operon. *Front. Microbiol.* 6:8. doi: 10.3389/fmicb.2015.00008
- Mousa, J. J., and Bruner, S. D. (2016). Structural and mechanistic diversity of multidrug transporters. *Nat. Prod. Rep.* 33, 1255–1267. doi: 10.1039/C6NP00006A
- Muller, C., Plésiat, P., and Jeannot, K. (2011). A two-component regulatory system interconnects resistance to polymyxins, aminoglycosides, fluoroquinolones, and beta-lactams in *Pseudomonas aeruginosa*. *Antimicrob. Agents Chemother.* 55, 1211–1221. doi: 10.1128/AAC.01252-10
- Muller, J. F., Stevens, A. M., Craig, J., and Love, N. G. (2007). Transcriptome analysis reveals that multidrug efflux genes are upregulated to protect *Pseudomonas aeruginosa* from pentachlorophenol stress. *Appl. Environ. Microbiol.* 73, 4550–4558. doi: 10.1128/AEM.00169-07
- Muraoka, S., Okumura, R., Ogawa, N., Nonaka, T., Miyashita, K., and Senda, T. (2003). Crystal structure of a full-length LysR-type transcriptional regulator, CbnR: unusual combination of two subunit forms and molecular bases for causing and changing DNA bend. *J. Mol. Biol.* 328, 555–566. doi: 10.1016/S0022-2836(03)00312-7
- Narayanan, A., Kumar, S., Evrard, A. N., Paul, L. N., and Yernool, D. A. (2014). An asymmetric heterodomain interface stabilizes a response regulator-DNA complex. *Nat. Commun.* 5:3282. doi: 10.1038/ncomms4282
- Newberry, K. J., Fuangthong, M., Panmanee, W., Mongkolsuk, S., and Brennan, R. G. (2007). Structural mechanism of organic hydroperoxide induction of the transcription regulator OhrR. *Mol. Cell* 28, 652–664. doi: 10.1016/j.molcel.2007.09.016
- Ni, L., Tonthat, N. K., Chinnam, N., and Schumacher, M. A. (2013). Structures of the *Escherichia coli* transcription activator and regulator of diauxie, XylR: an AraC DNA-binding family member with a LacI/GalR ligand-binding domain. *Nucleic Acids Res.* 41, 1998–2008. doi: 10.1093/nar/gks1207
- Nikaido, H. (2009). Multidrug resistance in bacteria. *Annu. Rev. Biochem.* 78, 119–146. doi: 10.1146/annurev.biochem.78.082907.145923
- Nikaido, H. (2018). RND transporters in the living world. *Res. Microbiol.* doi: 10.1016/j.resmic.2018.03.001. [Epub ahead of print].
- Nikiforov, P. O., Blaszczak, M., Surade, S., Boshoff, H. I., Sajid, A., Delorme, V., et al. (2017). Fragment-sized EthR inhibitors exhibit exceptionally strong ethionamide boosting effect in whole-cell mycobacterium tuberculosis assays. *ACS Chem. Biol.* 12, 1390–1396. doi: 10.1021/acschembio.7b00091
- Oliver, P., Peralta-Gil, M., Tabche, M. L., and Merino, E. (2016). Molecular and structural considerations of TF-DNA binding for the generation of biologically meaningful and accurate phylogenetic footprinting analysis: the LysR-type transcriptional regulator family as a study model. *BMC Genomics* 17:686. doi: 10.1186/s12864-016-3025-3
- Orth, P., Schnappinger, D., Hillen, W., Saenger, W., and Hinrichs, W. (2000). Structural basis of gene regulation by the tetracycline inducible Tet repressor-operator system. *Nat. Struct. Biol.* 7, 215–219. doi: 10.1038/73324
- Palanca, C., and Rubio, V. (2016). Structure of AmtR, the global nitrogen regulator of *Corynebacterium glutamicum*, in free and DNA-bound forms. *FEBS J.* 283, 1039–1059. doi: 10.1111/febs.13643
- Perera, I. C., and Grove, A. (2010). Molecular mechanisms of ligand-mediated attenuation of DNA binding by MarR family transcriptional regulators. *J. Mol. Cell Biol.* 2, 243–254. doi: 10.1093/jmcb/mjq021
- Perron, K., Caille, O., Rossier, C., Van Delden, C., Dumas, J. L., and Köhler, T. (2004). Czcr-CzcS, a two-component system involved in heavy metal and carbapenem resistance in *Pseudomonas aeruginosa*. *J. Biol. Chem.* 279, 8761–8768. doi: 10.1074/jbc.M312080200

- Phan, G., Benabdelhak, H., Lascombe, M. B., Benas, P., Rety, S., Picard, M., et al. (2010). Structural and dynamical insights into the opening mechanism of *P. aeruginosa* OprM channel. *Structure* 18, 507–517. doi: 10.1016/j.str.2010.01.018
- Phan, G., Picard, M., and Broutin, I. (2015). Focus on the outer membrane factor OprM, the forgotten player from efflux pumps assemblies. *Antibiotics* 4, 544–566. doi: 10.3390/antibiotics4040544
- Picossi, S., Belitsky, B. R., and Sonenshein, A. L. (2007). Molecular mechanism of the regulation of *Bacillus subtilis* gltAB expression by GltC. *J. Mol. Biol.* 365, 1298–1313. doi: 10.1016/j.jmb.2006.10.100
- Poole, K. (2008). Bacterial multidrug efflux pumps serve other functions. *Microbe* 3, 179–185. doi: 10.1128/microbe.3.179.1
- Poole, K. (2011). *Pseudomonas aeruginosa*: resistance to the max. *Front. Microbiol.* 2:65. doi: 10.3389/fmicb.2011.00065
- Poole, K., and Srikanth, R. (2001). Multidrug efflux in *Pseudomonas aeruginosa*: components, mechanisms and clinical significance. *Curr. Top. Med. Chem.* 1, 59–71. doi: 10.2174/1568026013395605
- Porriá, O., García-Jaramillo, M., Santero, E., and Govantes, F. (2007). The LysR-type regulator AtzR binding site: DNA sequences involved in activation, repression and cyanuric acid-dependent repositioning. *Mol. Microbiol.* 66, 410–427. doi: 10.1111/j.1365-2958.2007.05927.x
- Ptashne, M., and Gann, A. (1997). Transcriptional activation by recruitment. *Nature* 386, 569–577. doi: 10.1038/386569a0
- Rahman, T., Yarnall, B., and Doyle, D. A. (2017). Efflux drug transporters at the forefront of antimicrobial resistance. *Eur. Biophys. J.* 46, 647–653. doi: 10.1007/s00249-017-1238-2
- Ramos, J. L., Martínez-Bueno, M., Molina-Henares, A. J., Terán, W., Watanabe, K., Zhang, X., et al. (2005). The TetR family of transcriptional repressors. *Microbiol. Mol. Biol. Rev.* 69, 326–356. doi: 10.1128/MMBR.69.2.326-356.2005
- Reeder, T., and Schleif, R. (1993). AraC protein can activate transcription from only one position and when pointed in only one direction. *J. Mol. Biol.* 231, 205–218. doi: 10.1006/jmbi.1993.1276
- Reichheld, S. E., Yu, Z., and Davidson, A. R. (2009). The induction of folding cooperativity by ligand binding drives the allosteric response of tetracycline repressor. *Proc. Natl. Acad. Sci. U.S.A.* 106, 22263–22268. doi: 10.1073/pnas.0911566106
- Resch, M., Striegl, H., Henssler, E. M., Sevana, M., Egerer-Sieber, C., Schiltz, E., et al. (2008). A protein functional leap: how a single mutation reverses the function of the transcription regulator TetR. *Nucleic Acids Res.* 36, 4390–4401. doi: 10.1093/nar/gkn400
- Rhee, S., Martin, R. G., Rosner, J. L., and Davies, D. R. (1998). A novel DNA-binding motif in MarA: the first structure for an AraC family transcriptional activator. *Proc. Natl. Acad. Sci. U.S.A.* 95, 10413–10418. doi: 10.1073/pnas.95.18.10413
- Richardot, C., Juarez, P., Jeannot, K., Patry, I., Plésiat, P., and Llanes, C. (2016). Amino acid substitutions account for most MexS alterations in clinical *nfxC* mutants of *Pseudomonas aeruginosa*. *Antimicrob. Agents Chemother.* 60, 2302–2310. doi: 10.1128/AAC.02622-15
- Rodrigue, A., Quentin, Y., Lazdunski, A., Méjean, V., and Foglino, M. (2000). Two-component systems in *Pseudomonas aeruginosa*: why so many? *Trends Microbiol.* 8, 498–504. doi: 10.1016/S0966-842X(00)01833-3
- Rolain, J. M., Abat, C., Jimeno, M. T., Fournier, P. E., and Raoult, D. (2016). Do we need new antibiotics? *Clin. Microbiol. Infect.* 22, 408–415. doi: 10.1016/j.cmi.2016.03.012
- Saridakis, V., Shahinas, D., Xu, X., and Christendat, D. (2008). Structural insight on the mechanism of regulation of the MarR family of proteins: high-resolution crystal structure of a transcriptional repressor from *Methanobacterium thermoautotrophicum*. *J. Mol. Biol.* 377, 655–667. doi: 10.1016/j.jmb.2008.01.001
- Sawai, H., Yamanaka, M., Sugimoto, H., Shiro, Y., and Aono, S. (2012). Structural basis for the transcriptional regulation of heme homeostasis in *Lactococcus lactis*. *J. Biol. Chem.* 287, 30755–30768. doi: 10.1074/jbc.M112.370916
- Schell, M. A. (1993). Molecular biology of the LysR family of transcriptional regulators. *Annu. Rev. Microbiol.* 47, 597–626. doi: 10.1146/annurev.mi.47.100193.003121
- Schell, M. A., Brown, P. H., and Raju, S. (1990). Use of saturation mutagenesis to localize probable functional domains in the NahR protein, a LysR-type transcription activator. *J. Biol. Chem.* 265, 3844–3850.
- Schleif, R. (2003). AraC protein: a love-hate relationship. *Bioessays* 25, 274–282. doi: 10.1002/bies.10237
- Schleif, R. (2010). AraC protein, regulation of the l-arabinose operon in *Escherichia coli*, and the light switch mechanism of AraC action. *FEMS Microbiol. Rev.* 34, 779–796. doi: 10.1111/j.1574-6976.2010.00226.x
- Schuldiner, S. (2009). EmrE, a model for studying evolution and mechanism of ion-coupled transporters. *Biochim. Biophys. Acta* 1794, 748–762. doi: 10.1016/j.bbapap.2008.12.018
- Schumacher, M. A., and Brennan, R. G. (2002). Structural mechanisms of multidrug recognition and regulation by bacterial multidrug transcription factors. *Mol. Microbiol.* 45, 885–893. doi: 10.1046/j.1365-2958.2002.03039.x
- Schumacher, M. A., Miller, M. C., and Brennan, R. G. (2004). Structural mechanism of the simultaneous binding of two drugs to a multidrug-binding protein. *EMBO J.* 23, 2923–2930. doi: 10.1038/sj.emboj.7600288
- Schumacher, M. A., Miller, M. C., Grkovic, S., Brown, M. H., Skurray, R. A., and Brennan, R. G. (2001). Structural mechanisms of QacR induction and multidrug recognition. *Science* 294, 2158–2163. doi: 10.1126/science.1066020
- Schumacher, M. A., Miller, M. C., Grkovic, S., Brown, M. H., Skurray, R. A., and Brennan, R. G. (2002). Structural basis for cooperative DNA binding by two dimers of the multidrug-binding protein QacR. *EMBO J.* 21, 1210–1218. doi: 10.1093/emboj/21.5.1210
- Schumacher, M. A., and Zeng, W. (2016). Structures of the nucleoid occlusion protein SlmA bound to DNA and the C-terminal domain of the cytoskeletal protein FtsZ. *Proc. Natl. Acad. Sci. U.S.A.* 113, 4988–4993. doi: 10.1073/pnas.1602327113
- Sivaneson, M., Mikkelsen, H., Ventre, I., Bordin, C., and Filloux, A. (2011). Two-component regulatory systems in *Pseudomonas aeruginosa*: an intricate network mediating fimbrial and efflux pump gene expression. *Mol. Microbiol.* 79, 1353–1366. doi: 10.1111/j.1365-2958.2010.07527.x
- Smith, E. E., Buckley, D. G., Wu, Z., Saenphimmachak, C., Hoffman, L. R., D'Argenio, D. A., et al. (2006). Genetic adaptation by *Pseudomonas aeruginosa* to the airways of cystic fibrosis patients. *Proc. Natl. Acad. Sci. U.S.A.* 103, 8487–8492. doi: 10.1073/pnas.0602138103
- Sobel, M. L., Hocquet, D., Cao, L., Plesiat, P., and Poole, K. (2005). Mutations in PA3574 (*nalD*) lead to increased MexAB-OprM expression and multidrug resistance in laboratory and clinical isolates of *Pseudomonas aeruginosa*. *Antimicrob. Agents Chemother.* 49, 1782–1786. doi: 10.1128/AAC.49.5.1782-1786.2005
- Soisson, S. M., MacDougall-Shackleton, B., Schleif, R., and Wolberger, C. (1997). Structural basis for ligand-regulated oligomerization of AraC. *Science* 276, 421–425. doi: 10.1126/science.276.5311.421
- Spengler, G., Kincses, A., Gajdacs, M., and Amaral, L. (2017). New roads leading to old destinations: efflux pumps as targets to reverse multidrug resistance in bacteria. *Molecules* 22:E468. doi: 10.3390/molecules22030468
- Stock, A. M., Robinson, V. L., and Goudreau, P. N. (2000). Two-component signal transduction. *Annu. Rev. Biochem.* 69, 183–215. doi: 10.1146/annurev.biochem.69.1.183
- Stover, C. K., Pham, X. Q., Erwin, A. L., Mizoguchi, S. D., Warriner, P., Hickey, M. J., et al. (2000). Complete genome sequence of *Pseudomonas aeruginosa* PAO1, an opportunistic pathogen. *Nature* 406, 959–964. doi: 10.1038/35023079
- Stragier, P., Richaud, F., Borne, F., and Patte, J. C. (1983). Regulation of diaminopimelate decarboxylase synthesis in *Escherichia coli*. I. Identification of a *lysR* gene encoding an activator of the *lysA* gene. *J. Mol. Biol.* 168, 307–320. doi: 10.1016/S0022-2836(83)80020-5
- Sun, J., Deng, Z., and Yan, A. (2014). Bacterial multidrug efflux pumps: mechanisms, physiology and pharmacological exploitations. *Biochem. Biophys. Res. Commun.* 453, 254–267. doi: 10.1016/j.bbrc.2014.05.090
- Szakács, G., Varadi, A., Ozvegy-Laczka, C., and Sarkadi, B. (2008). The role of ABC transporters in drug absorption, distribution, metabolism, excretion and toxicity (ADME-Tox). *Drug Discov. Today* 13, 379–393. doi: 10.1016/j.drudis.2007.12.010
- Tacconelli, E., Carrara, E., Savoldi, A., Harbarth, S., Mendelson, M., Monnet, D. L., et al. (2017). Discovery, research, and development of new antibiotics: the WHO priority list of antibiotic-resistant bacteria and tuberculosis. *Lancet Infect. Dis.* 18, 318–327. doi: 10.1016/S1473-3099(17)30753-3

- Tyrrell, R., Verschueren, K. H., Dodson, E. J., Murshudov, G. N., Addy, C., and Wilkinson, A. J. (1997). The structure of the cofactor-binding fragment of the LysR family member, CysB: a familiar fold with a surprising subunit arrangement. *Structure* 5, 1017–1032. doi: 10.1016/S0969-2126(97)00254-2
- Vargiu, A. V., Pos, K. M., Poole, K., and Nikaido, H. (2016). Editorial: bad bugs in the XXIst century: resistance mediated by multi-drug efflux pumps in gram-negative bacteria. *Front. Microbiol.* 7:833. doi: 10.3389/fmicb.2016.00833
- Wang, C., Sang, J., Wang, J., Su, M., Downey, J. S., Wu, Q., et al. (2013). Mechanistic insights revealed by the crystal structure of a histidine kinase with signal transducer and sensor domains. *PLoS Biol.* 11:e1001493. doi: 10.1371/journal.pbio.1001493
- Wang, D., Chen, W., Huang, S., He, Y., Liu, X., Hu, Q., et al. (2017). Structural basis of Zn(II) induced metal detoxification and antibiotic resistance by histidine kinase CzcS in *Pseudomonas aeruginosa*. *PLoS Pathog.* 13:e1006533. doi: 10.1371/journal.ppat.1006533
- Wang, D., Seeve, C., Pierson, L. S., and Pierson, E. A. (2013). Transcriptome profiling reveals links between ParS/ParR, MexEF-OprN, and quorum sensing in the regulation of adaptation and virulence in *Pseudomonas aeruginosa*. *BMC Genomics* 14:618. doi: 10.1186/1471-2164-14-618
- Wang, L., and Winans, S. C. (1995). High angle and ligand-induced low angle DNA bends incited by OccR lie in the same plane with OccR bound to the interior angle. *J. Mol. Biol.* 253, 32–38. doi: 10.1006/jmbi.1995.0533
- Wang, Z., Fan, G., Hryc, C. F., Blaza, J. N., Serysheva, I. I., Schmid, M. F., et al. (2017). An allosteric transport mechanism for the AcrAB-TolC multidrug efflux pump. *Elife* 6:e24905. doi: 10.7554/eLife.24905
- Weldon, J. E., Rodgers, M. E., Larkin, C., and Schleif, R. F. (2007). Structure and properties of a truly apo form of AraC dimerization domain. *Proteins* 66, 646–654. doi: 10.1002/prot.21267
- Wilke, M. S., Heller, M., Creagh, A. L., Haynes, C. A., McIntosh, L. P., Poole, K., et al. (2008). The crystal structure of MexR from *Pseudomonas aeruginosa* in complex with its antirepressor ArmR. *Proc. Natl. Acad. Sci. U.S.A.* 105, 14832–14837. doi: 10.1073/pnas.0805489105
- Wilkinson, S. P., and Grove, A. (2006). Ligand-responsive transcriptional regulation by members of the MarR family of winged helix proteins. *Curr. Issues Mol. Biol.* 8, 51–62. Available online at: <http://www.caister.com/cimb/v/v8/51.pdf>
- Willems, A. R., Tahlan, K., Taguchi, T., Zhang, K., Lee, Z. Z., Ichinose, K., et al. (2008). Crystal structures of the Streptomyces coelicolor TetR-like protein ActR alone and in complex with actinorhodin or the actinorhodin biosynthetic precursor (S)-DNPA. *J. Mol. Biol.* 376, 1377–1387. doi: 10.1016/j.jmb.2007.12.061
- Yamaguchi, A., Nakashima, R., and Sakurai, K. (2015). Structural basis of RND-type multidrug exporters. *Front. Microbiol.* 6:327. doi: 10.3389/fmicb.2015.00327
- Yan, N. (2015). Structural Biology of the Major Facilitator Superfamily Transporters. *Annu. Rev. Biophys.* 44, 257–283. doi: 10.1146/annurev-biophys-060414-033901
- Yang, J., Dogovski, C., Hocking, D., Tauschek, M., Perugini, M., and Robins-Browne, R. M. (2009). Bicarbonate-mediated stimulation of RegA, the global virulence regulator from *Citrobacter rodentium*. *J. Mol. Biol.* 394, 591–599. doi: 10.1016/j.jmb.2009.10.033
- Yang, J., Tauschek, M., and Robins-Browne, R. M. (2011). Control of bacterial virulence by AraC-like regulators that respond to chemical signals. *Trends Microbiol.* 19, 128–135. doi: 10.1016/j.tim.2010.12.001
- Yang, S., Gao, Z., Li, T., Yang, M., Zhang, T., Dong, Y., et al. (2013). Structural basis for interaction between Mycobacterium smegmatis Ms6564, a TetR family master regulator, and its target DNA. *J. Biol. Chem.* 288, 23687–23695. doi: 10.1074/jbc.M113.468694
- Yeo, H. K., Park, Y. W., and Lee, J. Y. (2017). Structural basis of operator sites recognition and effector binding in the TetR family transcription regulator FadR. *Nucleic Acids Res.* 45, 4244–4254. doi: 10.1093/nar/gkx009
- Yu, Z., Reichheld, S. E., Savchenko, A., Parkinson, J., and Davidson, A. R. (2010). A comprehensive analysis of structural and sequence conservation in the TetR family transcriptional regulators. *J. Mol. Biol.* 400, 847–864. doi: 10.1016/j.jmb.2010.05.062
- Zhou, X., Lou, Z., Fu, S., Yang, A., Shen, H., Li, Z., et al. (2010). Crystal structure of ArgP from Mycobacterium tuberculosis confirms two distinct conformations of full-length LysR transcriptional regulators and reveals its function in DNA binding and transcriptional regulation. *J. Mol. Biol.* 396, 1012–1024. doi: 10.1016/j.jmb.2009.12.033
- Zhu, R., Song, Y., Liu, H., Yang, Y., Wang, S., Yi, C., et al. (2017). Allosteric histidine switch for regulation of intracellular zinc(II) fluctuation. *Proc. Natl. Acad. Sci. U.S.A.* 114, 13661–13666. doi: 10.1073/pnas.1708563115
- Zschiedrich, C. P., Keidel, V., and Szurmant, H. (2016). Molecular mechanisms of two-component signal transduction. *J. Mol. Biol.* 428, 3752–3775. doi: 10.1016/j.jmb.2016.08.003

**Conflict of Interest Statement:** The authors declare that the research was conducted in the absence of any commercial or financial relationships that could be construed as a potential conflict of interest.

Copyright © 2018 Housseini B Issa, Phan and Broutin. This is an open-access article distributed under the terms of the Creative Commons Attribution License (CC BY). The use, distribution or reproduction in other forums is permitted, provided the original author(s) and the copyright owner are credited and that the original publication in this journal is cited, in accordance with accepted academic practice. No use, distribution or reproduction is permitted which does not comply with these terms.



## OPEN ACCESS

### Edited by:

Vassily Bavro,  
University of Essex, United Kingdom

### Reviewed by:

Doriano Lamba,  
Consiglio Nazionale Delle Ricerche  
(CNR), Italy

Kyeong Kyu Kim,  
Sungkyunkwan University,  
South Korea

### \*Correspondence:

John Cavanagh  
jcavanagh@rti.org

### Specialty section:

This article was submitted to  
Structural Biology,  
a section of the journal  
Frontiers in Molecular Biosciences

**Received:** 07 December 2017

**Accepted:** 30 January 2018

**Published:** 13 February 2018

### Citation:

Milton ME, Minrovic BM, Harris DL,  
Kang B, Jung D, Lewis CP,  
Thompson RJ, Melander RJ, Zeng D,  
Melander C and Cavanagh J (2018)  
Re-sensitizing Multidrug Resistant  
Bacteria to Antibiotics by Targeting  
Bacterial Response Regulators:  
Characterization and Comparison of  
Interactions between  
2-Aminoimidazoles and the Response  
Regulators BfmR from *Acinetobacter*  
*baumannii* and QseB from *Francisella*  
*spp.* *Front. Mol. Biosci.* 5:15.  
doi: 10.3389/fmolb.2018.00015

# Re-sensitizing Multidrug Resistant Bacteria to Antibiotics by Targeting Bacterial Response Regulators: Characterization and Comparison of Interactions between 2-Aminoimidazoles and the Response Regulators BfmR from *Acinetobacter baumannii* and QseB from *Francisella* spp.

Morgan E. Milton<sup>1</sup>, Bradley M. Minrovic<sup>2</sup>, Danni L. Harris<sup>1</sup>, Brian Kang<sup>3</sup>, David Jung<sup>3</sup>, Caleb P. Lewis<sup>1,4</sup>, Richele J. Thompson<sup>1</sup>, Roberta J. Melander<sup>2</sup>, Daina Zeng<sup>3</sup>, Christian Melander<sup>2</sup> and John Cavanagh<sup>1,4\*</sup>

<sup>1</sup> Discovery Sciences, RTI International, NC, United States, <sup>2</sup> Department of Chemistry, North Carolina State University, Raleigh, NC, United States, <sup>3</sup> Agile Sciences, Inc., Raleigh, NC, United States, <sup>4</sup> Department of Molecular and Structural Biochemistry, North Carolina State University, Raleigh, NC, United States

2-aminoimidazole (2-AI) compounds inhibit the formation of bacterial biofilms, disperse preformed biofilms, and re-sensitize multidrug resistant bacteria to antibiotics. 2-AIs have previously been shown to interact with bacterial response regulators, but the mechanism of interaction is still unknown. Response regulators are one part of two-component systems (TCS). TCSs allow cells to respond to changes in their environment, and are used to trigger quorum sensing, virulence factors, and antibiotic resistance. Drugs that target the TCS signaling process can inhibit pathogenic behavior, making this a potent new therapeutic approach that has not yet been fully exploited. We previously laid the groundwork for the interaction of the *Acinetobacter baumannii* response regulator BfmR with an early 2-AI derivative. Here, we further investigate the response regulator/2-AI interaction and look at a wider library of 2-AI compounds. By combining molecular modeling with biochemical and cellular studies, we expand on a potential mechanism for interaction between response regulators and 2-AIs. We also establish that *Francisella tularensis/novicida*, encoding for only three known response regulators, can be a model system to study the interaction between 2-AIs and response regulators. We show that knowledge gained from studying *Francisella* can be applied to the more complex



*A. baumannii* system, which contains over 50 response regulators. Understanding the impact of 2-AIs on response regulators and their mechanism of interaction will lead to the development of more potent compounds that will serve as adjuvant therapies to broad-range antibiotics.

**Keywords:** biofilms, antibiotic resistance, two-component systems, response regulators, *Acinetobacter baumannii*, *Francisella*

## INTRODUCTION

The formation of biofilms contributes to significant bacterial persistence in the environment, pathogenicity, and resistance to antimicrobials (Donlan, 2002). Bacteria spend an estimated 80% of their time in a biofilm state, adhering to surfaces, and one another. A biofilm is composed of an extracellular matrix which provides protection against a variety of physical and chemical assaults. In a biofilm state, bacteria can be up to 1,000-fold more resistant to antibiotics than their planktonic counterparts (Donlan and Costerton, 2002; Rasmussen and Givskov, 2006; Percival et al., 2011). Understanding how biofilms are formed and developing small molecule therapies are vital steps in combating antibiotic resistance.

*Acinetobacter baumannii* and *Francisella* species are of particular interest in studying the impact of biofilms on human health. *A. baumannii* is highly prevalent in hospitals and has shown extensive multi-drug resistance in the clinical setting (Dijkshoorn et al., 2007; Perez et al., 2007). *A. baumannii* belongs to a group of pathogens known as the ESKAPE pathogens, named as such because the bacteria easily “escape” antibiotics through the rapid acquisition of resistance (Rice, 2008). Recently, the World Health Organization has listed *A. baumannii* as a critical priority for combating antibiotic resistant bacteria (World Health Organization, 2017). On the other hand, while infection by *Francisella* species is less common, *Francisella tularensis/tularensis* is listed by the Centers for Disease Control and Prevention as a Category A select agent (Sjöstedt, 2007). Its ease of aerosolization, high infectivity, and ability to quickly incapacitate those infected makes *F. tularensis/tularensis* a highly viable biowarfare agent. Both bacteria utilize biofilms to increase their persistence, pathogenicity, and antibiotic resistance (Durham-Colleran et al., 2010; Imperi et al., 2011; McConnell et al., 2013; Sutura et al., 2014; Kröger et al., 2016).

The response regulator proteins BfmR and QseB are responsible for controlling biofilm formation as well as degrees of antibiotic resistance in *A. baumannii* and *F. tularensis/novicida* (the mouse model of *F. tularensis/tularensis*), respectively. *Francisella* species encode an exceptionally small number of response regulators (Larsson et al., 2005) compared to other bacteria. This reduced complexity makes *F. tularensis/novicida* an excellent system to the cellular effects of targeting response regulators with small molecule therapies. Response regulators work in combination with a sensor kinase to form the ubiquitous communication two component system (TCS) scheme (Stock et al., 2000). Typically, the sensor kinase is a transmembrane histidine kinase that detects an external signal. This response triggers an autophosphorylation event.

The phosphate group is subsequently transferred to a partner response regulator, changing it from an “inactive” to “active” state. The activated response regulator propagates the signal through transcriptional regulation. Response regulators are phosphorylated at a conserved site in the N-terminal receiver domain. A variable C-terminal DNA-binding domain facilitates binding to target DNA promoter sites. A highly flexible linker region of varying length connects these two domains. It is common for response regulators to be monomers in solution until activation triggers dimerization of the receiver domain. This brings the two DNA-binding domains in closer proximity to better bind the two half sites of the cognate promoter (Gao and Stock, 2009).

Derivatives of a cell-permeable, non-toxic family of 2-AIs are known to interact with response regulators (Thompson et al., 2012; Stowe et al., 2015; Milton et al., 2017). This class of compounds has been widely shown to inhibit and disperse biofilms, and also to work as an adjuvant therapy with traditional antibiotics to re-sensitize multidrug-resistant bacteria (Ballard et al., 2008; Richards et al., 2008a,b; Rogers and Melander, 2008; Brackett et al., 2014). Adjuvants act as a complementary therapy to antibiotic treatment. Their use has been proposed to extend the lifespan of antibiotics and reduce further resistance. The potential to re-sensitize bacteria to antibiotics makes adjuvants a powerful tool against the ever increasing antibiotic resistance (Wright, 2016; González-Bello, 2017; Melander and Melander, 2017). Understanding how potential adjuvant compounds function within the cell will aid in the development of more potent therapies. The specific mechanism through which 2-AIs interact with response regulators is still relatively unknown.

We first identified that an early 2-AI derivative could interact with the N-terminal and C-terminal domains of BfmR, as well as with full length protein (Thompson et al., 2012). We probed the interactions between response regulators and 2-AIs by validating QseB as a cellular target for the compounds (Milton et al., 2017). This provided the first direct evidence that QseB was binding to 2-AIs, and that 2-AIs impacted QseB-specific cellular functions, biofilm formation and  $\beta$ -lactam resistance.

Here we provide further evidence that BfmR is a cellular target of 2-AIs. Based on our previous findings with QseB, we propose that *F. tularensis/novicida* can act as a model organism for studying how 2-AIs interact with response regulators within the more complicated *A. baumannii* system. Additionally, understanding the differences between the two systems will aid in the development of organism specific and broad range adjuvant therapies. Here, we combine cellular, biochemical, and molecular dynamics techniques to further elucidate the mechanism of action of 2-AIs and response regulators. These findings will aid

in the development of more potent compounds that can act as broad range or specific adjuvant therapies.

## MATERIALS AND METHODS

### Bacterial Strains, Media, and Antibiotics

*A. baumannii* 19606 and 1605 were obtained from ATCC as 19606 and BAA-1605, respectively. *A. baumannii* strain 5075 was obtained from the Manoil lab at the University of Washington. Cells were grown in LB at 37°C for biofilm assays and Muller Hinton Broth 2 for MIC assays. Antibiotics were purchased from Sigma-Aldrich.

### Cloning, Expression, and Purification

The coding region of *bfmR* from *A. baumannii* strain 19606 was in the expression vector pET28a (Novagen). Protein was over-expressed in BL21(DE3)pLysS cells at 37°C in LB. At an OD<sub>600</sub> of 0.6–0.8, cells were induced with 1 mM isopropyl β-D-thiogalactopyranoside (IPTG) at 30°C, for 4 h. Harvested cell pellets were stored at –80°C for later use.

BfmR pellets were resuspended in lysis buffer (20 mM Tris pH 7.9, 400 mM NaCl, and 5 mM imidazole) at 10 mL g<sup>–1</sup> of pellet. Cells were sonicated and the resulting lysate clarified at 20,400 × g for 15 min. Clarified lysate was loaded onto 10 mL of Ni-NTA resin (QIAGEN) pre-equilibrated in lysis buffer. Bound protein was washed with 10 column volumes of lysis buffer and 10 column volumes of 20 mM Tris pH 7.9, 1 M NaCl, and 15 mM imidazole. The protein was eluted with a linear gradient from lysis buffer to elution buffer (20 mM Tris pH 7.9, 400 mM NaCl, and 300 mM imidazole). Fractions containing protein were pooled and dialyzed into 20 mM Tris pH 7.9 and 200 mM NaCl. The affinity tag was cleaved by 100 units of thrombin for 2 h at room temperature. Cleavage was quenched with 0.1 mM AEBF and sample continued in dialysis of 20 mM Tris pH 7.9 and 200 mM NaCl.

### Thermal Shift Assays (TSA)

The compounds were dissolved in 100% PEG 400 to a final concentration of 1 mM. Reactions were carried out using final concentrations of 5 μM BfmR, 25 μM compound, 10% v/v PEG 400 and 10x SYPRO orange (ThermoFisher Scientific). Samples were prepared in three technical replicates on a CFX384 Touch Real-Time PCR Detection System (BioRad). Samples were heated from 25 to 95°C in 0.5°C increments, holding for 30 s at each step. Fluorescence was detected using the default HEX wavelengths. Data was fit to a Boltzmann curve using SigmaPlot. Assays were repeated in triplicate.

### Biofilm Inhibition Assays

Overnight cultures of *A. baumannii* 19606 in LB were subcultured to an OD<sub>600</sub> of 0.01 in the same media. Compounds were added from stock solutions to give the desired concentrations to be tested. Inoculum with no compound added served as the untreated control. Samples were aliquoted (100 μL) into the wells of the 96-well PVC microtiter plate. Sample plates were then wrapped in plastic and incubated under stationary conditions for 24 h at 37°C. After incubation, the plates were

visually inspected for the presence of consistent bacterial growth. The medium was discarded from the wells and the plates were washed thoroughly with water. Plates were then stained with 110 μL of 0.1% aqueous crystal solution violet (CV) and incubated at ambient temperature for 30 min. Plates were washed with water again. The remaining stain was solubilized with 200 μL of 100% ethanol and incubated again at ambient temperature for 10 min. A sample of 125 μL of solubilized CV stain from each well was transferred to the corresponding wells of a polystyrene microtiter dish. The absorbance of each well was measured at 540 nm and biofilm inhibition was quantified by calculating the 540 nm absorbance of treated wells as a percentage of untreated control wells. The IC<sub>50</sub> value was defined as the concentration of compound at which a 50% reduction in biofilm formation was observed compared to the untreated control. Assays were repeated with between three and eight biological replicates.

### Minimum Inhibitory Concentration (MIC) Assays

MIC assays were performed according to Clinical and Laboratory Standards Institute (CLSI) standards. MIC values of the compounds alone were established prior to studies with antibiotics. *A. baumannii* cells were pre-incubated with 2-AIs for 30 min prior to assessment in the MIC assay. Assays were initially repeated with two biological replicates. Compounds that showed MIC lowering activity were further repeated.

### Docking and MMGBSA Rescoring

Both Autodock Vina (Trott and Olson, 2010) and Schrodinger GLIDE-XP (Friesner et al., 2006) docking approaches were employed in a large region encompassing the N- and C-terminal domains of QseB, PmrA, and BfmR. When employing Autodock Vina, AMBER16 (Case et al., 2016) models of the systems were prepared using TLEAP and the systems energy minimized for 800 steps employing steepest descents followed by 8,000 steps of conjugate gradient minimization using the ff14SB forcefield. In the case of Autodock Vina, potential binding sites were first detected using blind docking. Here we employed large docking region (ca 30 × 30 × 30 Å<sup>3</sup>), completely encompassing the N/C domains. Inhibitor binding pose regions located using this approach were then subsequently re-investigated using smaller docking boxes for finer sampling. In all cases, a Autodock Vina high exhaustiveness setting of 80 was used to sample inhibitor/response-regulator configurations and a total of 20 top-Vina score docking poses saved for subsequent molecular mechanics generalized Born surface area (MMGBSA) rescoring described below. In house test problems, including PDB Bind high quality crystal structures, reveal that this hybrid Vina+MMGBSA approach recovers the crystallographically relevant poses (configurations) as the lowest MMGBSA scored docking pose ca. 75% of the time (with RMSD <2 Å). Additionally, the lowest MMGBSA score has improved affinity correlation compared to docking scores (Hou et al., 2011; Greenidge et al., 2013; Zhang et al., 2014). Parallel exploration using Schrodinger GLIDE-XP first identified potential binding sites in response regulator models using SiteMap on systems prepared with ProteinPrep energy minimized with 2,500 steps

of conjugate gradients and collection of 5–10 top GLIDE-XP scored poses. Predicted inhibitor binding locations for these two (Vina+MMGBSA/GLIDE-XP) distinct approaches were found to be in agreement with small differences in specific residue interaction motifs beyond the scope of the present discussion.

## MMGBSA-Min and MMGBA-SA

Docking poses from Autodock Vina or GLIDE-XP are subjected to MMGBSA rescoring employing a combination of AMBER16 (Case et al., 2016) driven by our own C++ and bash script base. Our automated workflow: (1) collected docking poses of all ligands (in mol2 format), (2) performed ligand formal charge perception (C++/OpenBabel), (3) quantum chemical determination of each of the ligand charges using AM1-BCC, (4) determination of additional internal ligand force field parameters using AMBER-GAFF, (5) energy minimized poses in complexes with the receptor/protein employing a GPU/CPU hybrid MD-simulated annealing (300K MD followed by energy minimization) procedure before computing the MMGBSA/MMPBSA score.

## Molecular Dynamics of Response Regulator Systems

AMBER16 (Case et al., 2016) was used to prepare the coordinates of PmrA. Coordinates were extracted from PDB ID 4S05 with the DNA removed. The initial system, prepared using the TLEAP module along with the ff14SB forcefield, was immersed in boxes of TIPS3P waters. A distance of 15 Å around any protein heavy atom was used as the criterion of choosing the box size. The system was energy minimized for 8,000 steps of conjugate gradient minimization, and then heated to 300K over 200 ps using the NPT ensemble, while harmonically constraining the protein atoms to initially equilibrate the water box density. After energy minimization, the system was allowed 5 ns of unconstrained equilibration at constant volume and temperature (300K). After equilibration, the PmrA system was employed in solvated dynamics in aqueous solution. Dynamics was explored at 300K for 250 ns. The structures were saved every 5 ps. The structural evolution in solution of the initial “extended” conformation in the absence of DNA was examined both in principal component analysis of the dynamics coordinate as well as clustering the backbone coordinates of PmrA over the 250 ns timeframe using the average-linker algorithm to obtain approximate populations of the top 5-clusters as well as representative PDB-snapshots for the clustered families.

## RESULTS AND DISCUSSION

### 2-AIs Bind QseB and BfmR

The formation of a protein-ligand complex is often associated with an increase in protein stability. Complex formation can be determined by measuring the change in the protein's melting temperature ( $T_m$ ), a strategy generally used in drug discovery (Pantoliano et al., 2001; Lo et al., 2004; Niesen et al., 2007). Previously, we developed a high-throughput fluorescence based thermal shift assay to evaluate the binding of 2-AIs to QseB (Milton et al., 2017). This same assay was performed with BfmR

to identify binding interactions (Supplementary Figures 1, 2). As a result, compounds that bind QseB tightly enough to induce a significant change in the  $T_m$  also bind BfmR (**Figure 1**). AGL-726, 778, 793, 802, 753, 777, 811, 810, 756, 833, and 782 increase the  $T_m$  of QseB and BfmR above background. Additionally, AGL-745, 770, and 787 showed binding potential for BfmR. This suggests that compounds may be designed to target a broad range of response regulators or be modified to interact with only a specific response regulator.

We previously observed with QseB that a compound can interact with a response regulator, but the  $\Delta T_m$  upon binding does not change significantly above background levels (Milton et al., 2017). As a result, it is likely that a compound with a moderate to high binding affinity can be confidently detected using the thermal shift assay. This allows for quick identification of leads from a library of compounds.

## Biofilm Inhibition

QseB and BfmR have been shown to play a central role in the regulation of biofilm formation in *F. tularensis/novicida* and *A. baumannii*, respectively (Tomaras et al., 2008; Durham-Colleran et al., 2010; Liou et al., 2014). Since *Francisella* species only encode three known response regulators, *F. tularensis/novicida* has the potential to be an excellent model system to study the effects of 2-AIs on response regulators. We previously demonstrated that AGL-600 and 726 inhibited the formation of *F. tularensis/novicida* biofilms (Milton et al., 2017). Due to the phenotypes associated with QseB knockouts (Durham-Colleran et al., 2010) and our direct evidence that these compounds bound QseB, we concluded that QseB was a target of the 2-AIs *in vitro*. As with QseB, deletion of *bfmR* results in a complete loss of biofilm formation (Tomaras et al., 2008). Since BfmR also directly binds the 2-AIs, we expected the compounds to have similar biofilm inhibition properties in *A. baumannii*.

The library of compounds were screened for their ability to inhibit the formation of *A. baumannii* biofilms using the traditional crystal violet assay (O'Toole, 2011). All compounds inhibited biofilm formation to varying degrees (**Figure 2**). A majority of the compounds identified as BfmR binding partners ranked among the most potent inhibitors, with initial screening  $IC_{50}$  values for biofilm inhibition between 10 and 50  $\mu M$ . This suggests a correlation between compounds that bind BfmR and compounds that reduce *A. baumannii* biofilm growth.

Based on thermal shift data, three compounds were selected for further comparison between *A. baumannii* and *F. tularensis/novicida* biofilm inhibition. AGL-726 significantly increased the  $T_m$  values of QseB (Milton et al., 2017) and BfmR (Supplementary Figure 1) above background, with  $\Delta T_m$  of  $6.77 \pm 1.25$  and  $8.73 \pm 1.26^\circ C$ , respectively. The compound is one of the most potent biofilm inhibitors with an  $IC_{50}$  of  $15.03 \pm 1.99 \mu M$  for *F. tularensis/novicida* and  $17.45 \pm 1.17 \mu M$  for *A. baumannii* (**Figure 3A**). To test a less extreme example, we investigated AGL-833. AGL-833 has a nearly identical  $\Delta T_m$  for QseB and BfmR,  $1.90 \pm 0.26$  and  $1.93 \pm 0.35^\circ C$ , respectively. AGL-833 also proved to be a potent biofilm inhibitor with  $IC_{50}$  values of  $11.56 \pm 0.74$  and  $15.75 \pm 0.87 \mu M$  for *F. tularensis/novicida* and *A. baumannii*, respectively (**Figure 3B**).

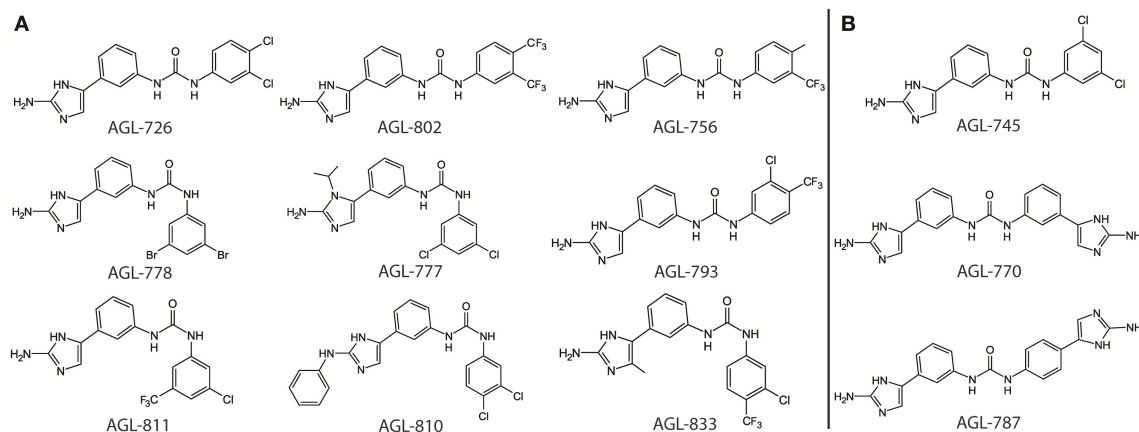


**FIGURE 1 |** Top binding compounds for QseB and BfmR based on protein thermal shift. **(A)** Compounds that significantly increased the  $T_m$  of both QseB and BfmR. Compounds are grouped based on structural similarities. **(B)** Additional compounds that interact with BfmR. 753 and 782 are not shown due to patent pending.

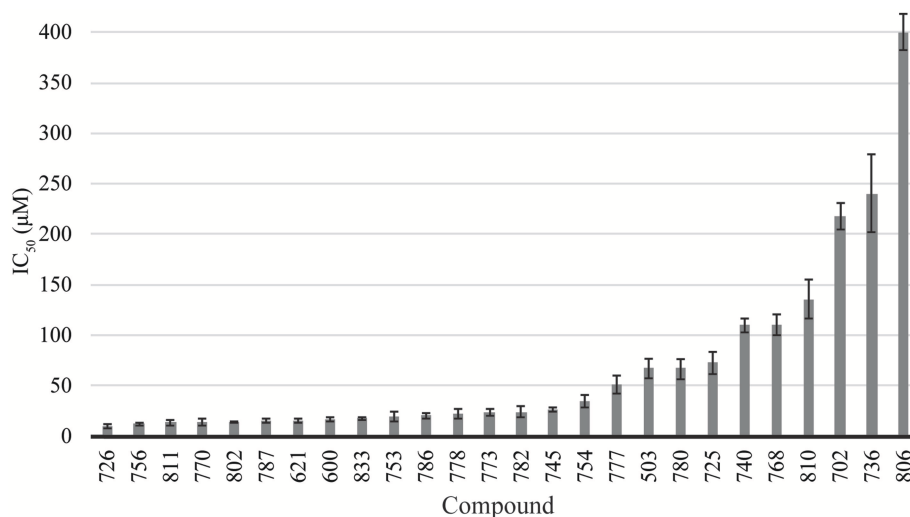


**FIGURE 2 |** Biofilm inhibition by 2-AI compound library. Biofilm inhibition IC<sub>50</sub> rankings for *A. baumannii* 19606 biofilms.

Finally, AGL-600 was investigated. We previously reported that while AGL-600 binds QseB, binding manifested as an insignificant  $\Delta T_m$  (Milton et al., 2017). Likewise, AGL-600 has little impact on the  $\Delta T_m$  of BfmR (Supplementary Figure 1). The lower binding affinity correlates with a decrease in biofilm inhibition. AGL-600 inhibits *F. tularensis/novicida* with an IC<sub>50</sub> of  $57.64 \pm 15.12 \mu\text{M}$  and *A. baumannii* with an IC<sub>50</sub> of  $59.78 \pm 10.58 \mu\text{M}$  (Figure 3C). Overall, these results demonstrate that even minor modifications to the variable region of the compound can have significant impacts on the 2-AI's ability to bind response regulators and provide support and that, like QseB, BfmR is also a cellular target of 2-AIs.

## 2-AIs Impact the Minimum Inhibitory Concentration of Antibiotics

Response regulators are often involved in antimicrobial resistance. For instance, QseB has been shown to play a

role in polymyxin B resistance (Mohapatra et al., 2007). The addition of AGL-600 and AGL-726 were able to lower the minimum inhibition concentration (MIC) of polymyxin B in *F. tularensis/novicida* (Milton et al., 2017). This finding provided further evidence that QseB is a cellular target of 2-AIs.

BfmR has been shown to mediate resistance to meropenem and colistin (Russo et al., 2016). 2-AIs that interact with BfmR *in vivo* may impact antibiotic resistance. To test the effects of the library of 2-AIs on antibiotic resistance, MIC lowering activity was evaluated for two strains of *A. baumannii*. Strain 1605 is a multidrug resistant *A. baumannii* isolated from military casualties (Tien et al., 2007) and strain 5075 is a highly virulent isolate often used as a model strain to evaluate antimicrobial treatments (Jacobs et al., 2014). Both strains were tested for increased sensitivity to meropenem, imipenem, and doripenem in the presence of our library of 2-AIs (Supplementary Table 1). Many of the compounds that interact with BfmR in the thermal



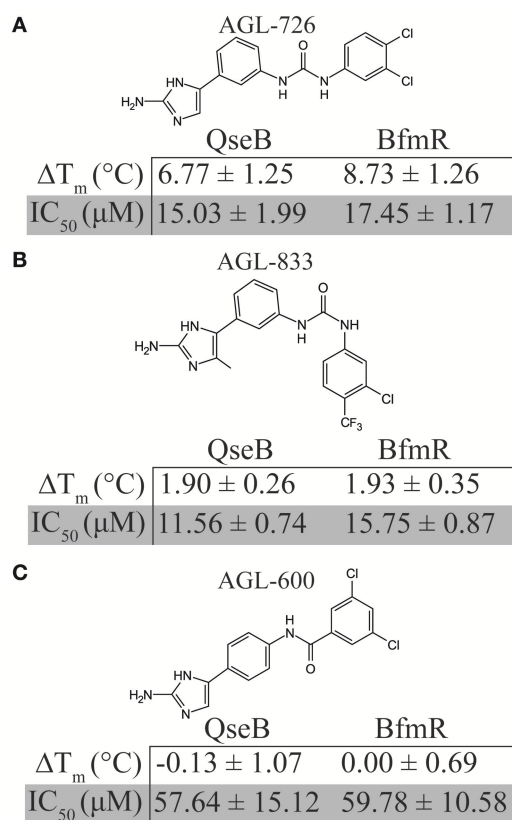


**FIGURE 3 |** Comparison of biofilm inhibition and BfmR binding properties for three select compounds across bacterial species. **(A)** AGL-726 binds BfmR and QseB with the highest change in  $T_m$ . This binding correlates with low  $IC_{50}$  values. **(B)** AGL-833 stimulates a minor increase in the  $T_m$ s of BfmR and QseB while still having potent biofilm inhibition properties. **(C)** AGL-600 binds very weakly, if at all, to BfmR and QseB, which probably contributes to a higher  $IC_{50}$  values for biofilm inhibition.

shift experiment have MIC lowering activity, specifically 726, 756, 770, 778, 786, 802, and 833. Five additional compounds which have biofilm inhibition  $IC_{50}$  values less than 100 μM (503, 600, 621, 754, and 773), also showed MIC lowering activity. These results further support that the response regulator BfmR is a cellular target of 2-AIs, and that the compounds can act as adjuvant therapies.

AGL-600, 726, and 833 all had potent MIC lowering activity (Table 1). All three compounds reduce the MIC in a dose-dependent manner. AGL-833 had to be used at lower concentrations due to having a lower MIC value than AGL-600 and 726 when tested in the absence of antibiotics, 12.5, 50, and 50 μM, respectively. Regardless, AGL-833 proved to be a potent MIC lowering adjuvant. Deletion of *bfmR* results in roughly a 2-fold lower MIC for meropenem than WT *A. baumannii* strain AB307-0294 (Russo et al., 2016). At concentrations four times lower than the MIC values of the 2-AIs alone, these compounds were able to reduce the MIC values of three carbapenem antibiotics at or beyond what was observed in a *bfmR* deletion mutant. While resistance likely varies greatly between strains, it

is highly probable that the MIC lowering activity seen in these compounds can be attributed to BfmR being a cellular target.

## Interactions between 2-AIs and Response Regulators

To further understand how 2-AIs are interacting with response regulators, we turned to structural biology techniques. The highly flexible nature of response regulators makes solving the full-length structure difficult. To date, we have solved the structures of the N-terminal receiver domains of QseB and BfmR using x-ray crystallography [PDB ID 5UIC and 5HM6 (Milton et al., 2017; Draughn and Milton et al. unpublished)], as well as the C-terminal DNA binding domain of BfmR [PDB ID 2NAZ (Draughn and Milton et al. unpublished)]. These structural domains can be combined using chemical crosslinking and molecular dynamics simulations to model full length response regulators (Olson et al., 2013, Draughn and Milton et al. unpublished). We have further employed molecular dynamics simulations and docking procedures to shed light on the interactions between 2-AIs and response regulators.

In lieu of a complete structure of QseB, we have used a homology model of PmrA from *Klebsiella pneumoniae* [PDB ID 4S04 and 4S05 (Lou et al., 2015)]. QseB and PmrA share 43% sequence identity and 61% sequence homology (Supplementary Figure 3). Alignment of the QseB N-terminal domain [PDB ID 5UIC (Milton et al., 2017)] with PmrA [PDB ID 4S05 (Lou et al., 2015)] crystal structures results in a Cα RMSD of 1.805 Å. Full length structures indicate that PmrA has a linker length of ~6 amino acids. Based on sequence alignment, we predicted that QseB has an ~8 amino acid linker. Combined, this information suggests that our PmrA derived model is a suitable stand-in for full length QseB. This model has allowed us to probe potential interactions between QseB and 2-AIs (Milton et al., 2017). From these studies, a binding interface between the N- and C-terminal domains was identified as the highest potential binding site. Similarly, an early model of BfmR identified the same 2-AI binding site (Thompson et al., 2012). This observation was supported by experimental finds which demonstrated that the N- and C-terminal domains of BfmR could bind a 2-AI independently. Both N- and C-terminal domain constructs of BfmR were independently pulled down by a 2-AI compound (Thompson et al., 2012). This suggests that a compound binding site lies at the interface between the two domains. All subsequent docking experiments for BfmR and QseB have identified some variation of the N- and C-terminal domain interface as the most favorable binding site for 2-AI compounds. Further structural studies will be necessary to confirm that the domain interface is the binding site and elucidate the specific residues that facilitate 2-AI compound binding.

As a follow up to prior studies employing docking with the current generation of 2-AI compounds (Milton et al., 2017), we performed “large-box” blind docking using Autodock VINA to the solution equilibrated “tucked” state of QseB. The low MMGBSA scored pose positions for compounds lie in cavities at the interface between the N- and C-terminal domains (Supplementary Figure 4). These poses have low RMSD

TABLE 1 | MIC lowering activity of AGL-600, 726, and 833.

		AGL-600					
		<i>A. baumannii</i> 1605			<i>A. baumannii</i> 5075		
Antibiotics		0 $\mu$ M	30 $\mu$ M	60 $\mu$ M	0 $\mu$ M	30 $\mu$ M	60 $\mu$ M
Imipenem	MIC ( $\mu$ g/mL)	32	–	4	32	2	–
	Fold reduction			8		16	
Meropenem	MIC ( $\mu$ g/mL)	32	–	4	32	2	–
	Fold reduction			8		16	
Doripenem	MIC ( $\mu$ g/mL)	32	–	8	32	2	–
	Fold reduction			4		16	

		AGL-726							
		<i>A. baumannii</i> 1605				<i>A. baumannii</i> 5075			
Antibiotics		0 $\mu$ M	10 $\mu$ M	15 $\mu$ M	30 $\mu$ M	0 $\mu$ M	10 $\mu$ M	15 $\mu$ M	30 $\mu$ M
Imipenem	MIC ( $\mu$ g/mL)	32	16	8	–	32	–	8	4
	Fold reduction		2	4				4	8
Meropenem	MIC ( $\mu$ g/mL)	32	8	6	–	32	–	4	2
	Fold reduction		4	5.3				8	16
Doripenem	MIC ( $\mu$ g/mL)	32	8	6.0	–	32	–	6	1
	Fold reduction		4	5.3				5.3	32

		AGL-833					
		<i>A. baumannii</i> 1605			<i>A. baumannii</i> 5075		
Antibiotics		0 $\mu$ M	2 $\mu$ M	4 $\mu$ M	0 $\mu$ M	2 $\mu$ M	4 $\mu$ M
Imipenem	MIC ( $\mu$ g/mL)	32	32	4	32	16	8
	Fold reduction		0	8		2	4
Meropenem	MIC ( $\mu$ g/mL)	32	32	4	32	32	4
	Fold reduction		0	8		0	8
Doripenem	MIC ( $\mu$ g/mL)	32	32	4	32	16	4
	Fold reduction		0	8		2	8

excursions over 30–60 ns while bound to the response regulator. This suggests that the compound binding sites identified are temporally stable and have reasonable residence times for ligands that bind with  $\mu$ M affinity.

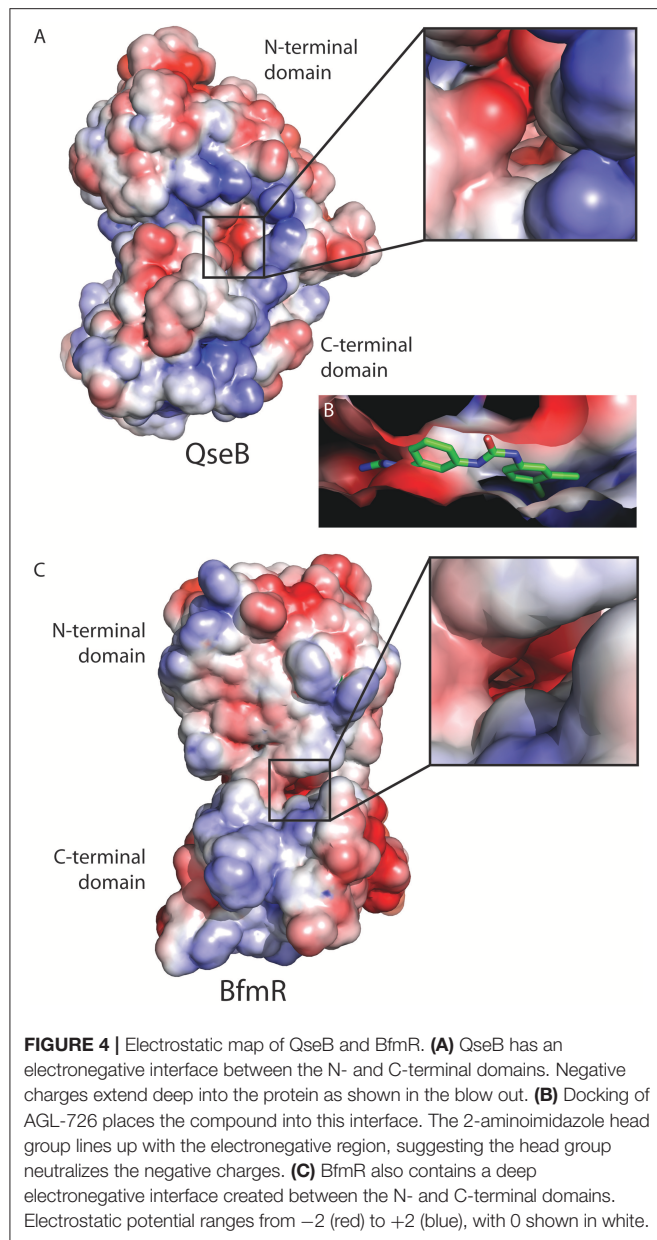
Examining the electrostatic properties of the interface between the N-terminal and C-terminal domains reveals an electronegative region in both QseB and BfmR. A concentrated electronegative region lines the inside of the interface central to the protein. This region is adjacent to where the flexible linker connects the two domains (Figures 4A,C). Similar patterns were observed in other full length response regulators ComE [PDB ID 4CBV (Boudes et al., 2014)] and KdpE [PDB ID 4KNY and 4KFC (Narayanan et al., 2014)], described below. Oddly, PmrA, for which the model of full length QseB is based, does not appear to have an electronegative interface [PDB ID 4S04 and 4S05 (Lou et al., 2015)]. This suggests that full length structural information will be very important for designing potent inhibitors. Docking of AGL-726 to QseB positions the compound within this interface (Figure 4B and Milton et al., 2017). The 2-aminoimidazole head

group docks within the electronegative region. This positioning was observed with many other 2-AIs (data not shown). BfmR and QseB share similar electrostatic topologies, providing evidence as to why the 2-aminoimidazole head group is required for compound efficacy. Depending on the response regulator, we propose that compounds can be tailored to interact with the exterior region of the interface while the conserved head group binds the electrostatic residues on the interior. This observation will help to guide the next generation of 2-AI derivatives.

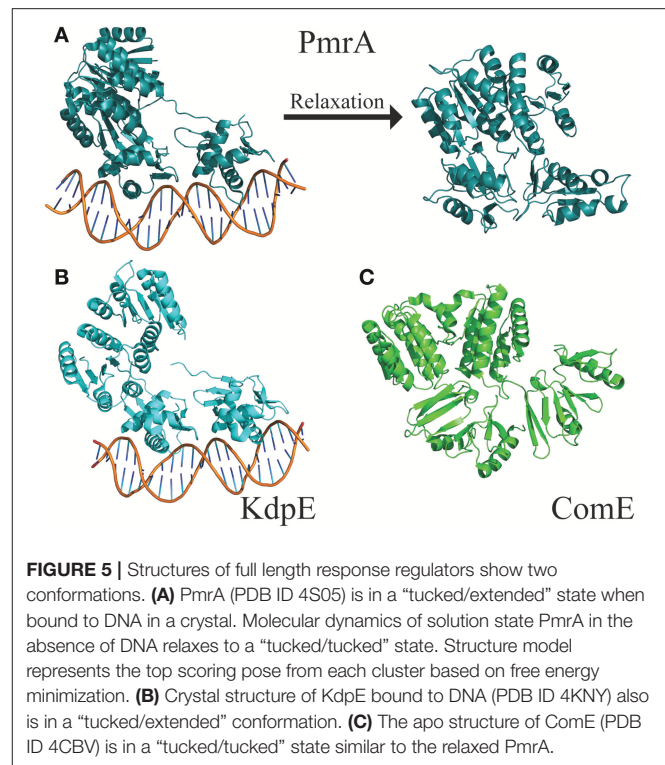
Response Regulator Dynamics

Flexibility likely plays a critical role in a response regulator’s ability to bind a variety of target DNA sequences. In fact, a DNA substrate is often used to lock down the mobile C-terminal domains in crystal structures. In order to understand how our compounds bind response regulators, it is important to understand the dynamics of the system.

The flexible linker connecting the N- and C-terminal domains allows response regulators to sample a wide range of states.



The “tucked” and “extended” states describe the relationship of the C-terminal DNA-binding domain to the N-terminal dimerization domain (Milton et al., 2017). These two extreme states have been observed in the crystal structures of PmrA from *K. pneumoniae* [PDB ID 4S04 and 4S05 (Lou et al., 2015)] and KdpE from *Escherichia coli* [PDB ID 4KFC and 4KNY (Narayanan et al., 2014)] (Figures 5A,B). Both structures are of DNA bound proteins that belong to the OmpR/PhoB family of response regulators. KdpE has a linker length of  $\sim 8$  amino acids and shares a 31% identity with 56% homology to QseB and 33% identity with 55% homology to PmrA (Supplementary Figure 3). Secondary structures of the N-terminal and C-terminal domains of QseB, PmrA, and KdpE are nearly identical structures with C $\alpha$  RMSDs of  $\sim 1.1$  Å for the N-terminus and  $\sim 1.5$  Å for



the C-terminus. Based on these crystal structures, thermal shift binding data, and molecular docking simulations, we previously proposed that compounds could bind either the “tucked” or “extended” state. In the model, compounds that favored the “tucked” conformation were tighter binders and more potent inhibitors. Molecular dynamics simulations allow for the model to be further explored.

The DNA was first removed from the full length crystal structure of PmrA [PDB ID 4S05 (Lou et al., 2015)] and immersed in a large box of TIP3P water. Molecular dynamics studies revealed that, following early equilibration, the “extended” chain of PmrA rapidly collapsed to a “tucked” conformation (Figure 5A) within the first 70 ns of the 250 ns simulation at 300 K. This suggests that there is likely a small or no energy barrier to folding to the “tucked” state. Examination of trajectory movies suggests the timescale for compaction may possibly be determined by the exclusion of intervening water molecules between the two C-terminal domains and low-energy gating transitions of a few residues in the linker chain. Following the C-terminal conformational transition, PmrA remains “tucked” with smaller scale dynamical fluctuations (Figure 6). Examining clustered conformations for the full duration of the simulation with this large amplitude transition, approximately 76% of the sampled populations take on a “tucked” conformation in the absence of DNA, with variations of the “extended” state present at short times. These percentages are not steady-state populations, *per se*, but merely reflect the conformational preferences for a simulation of this length. Supplementary Figure 5 shows that between 50 and 70 ns there is

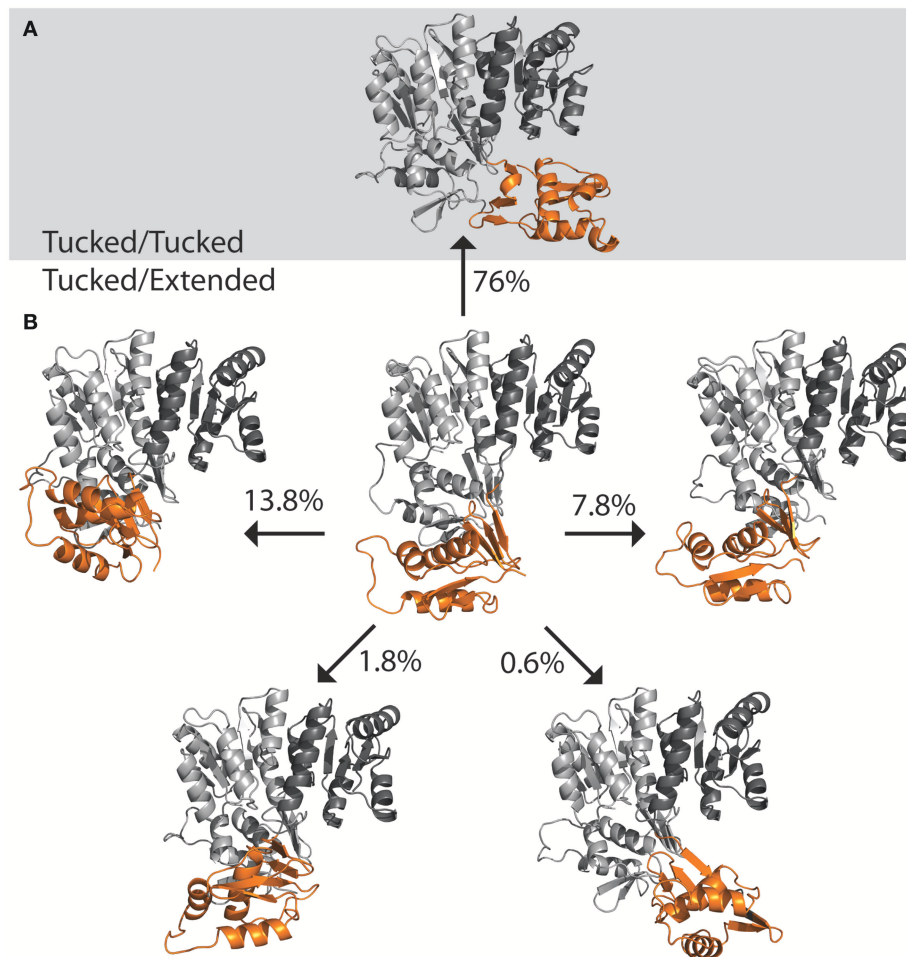


**FIGURE 6 |** Population distribution of PmrA. Having started with an “extended” state, the populations shifts to predominately “tucked” on a short time scale. **(A)** Molecular dynamics of PmrA (PDB ID 4S05) quickly relaxes to a “tucked/tucked” state and samples this state 76% of the time at a 250 ns time scale. **(B)** The PmrA crystal structure bound to DNA (center) begins in a “tucked/extended” state. Variations on the “tucked/extended” state are sampled for very short periods of time and account for small portions of the population at a given time. Structure models represent the top scoring pose from each cluster based on free energy minimization.

a significant increase in the RMSD of the sampled conformations as compared to the original starting structure. Investigation of the C $\alpha$  fluctuations at 70 ns reveals that the major contributor to change in RMSD is due to significant movement of the C-terminal residues of the “extended” state chain (Supplementary Figure 6). This is what one would expect for relaxing a system to a compact/energetically stable regime from a higher energetic extended state. Interestingly, the full length crystal structure of ComE [PDB ID 4CBV (Boudes et al., 2014)] has both dimer chains in the “tucked” conformation (**Figure 5C**). The lack of DNA may be attributed to this conformation. ComE is a member of the AlgR/AgrA/LytR family of transcription regulators. Its C-terminal DNA binding domain is distinct from the winged-helix-turn-helix found in OmpR/PhoB family. ComE does share some structural similarities to QseB, PmrA, and KdpE. A ~10 amino acid linker connects the two domains of ComE. The N-terminal domain has a 25% identity and 46% homology with C  $\alpha$  RMSD of 3.848 Å to QseB (Supplementary Figure 3). Since

no full length structures of OmpR/PhoB response regulators in a dimer conformation have been solved, ComE is the closest representation of a non-DNA bound response regulator dimer. Monomeric OmpR/PhoB family structures such as DrrB and MtrA have been solved in a “tucked” conformation, further suggesting that the “tucked” state is more favorable in solution, in the absence of DNA.

Based on these observations, we propose a potential mechanism for response regulator DNA binding. In solution, response regulators preferentially adopt a tucked conformation, occasionally sampling more extended poses. When a DNA substrate is identified, the N-terminal domain “kneels” over one of the C-terminal domains (**Figure 7**). This movement results in one dimer chain becoming tucked while the linker region of the other chain stretches out. Since 2-AIs likely bind to the interface between the N- and C-terminal domains, our working model proposes that they may impact the ability of the response regulator to “kneel” upon DNA binding (**Figure 7**).



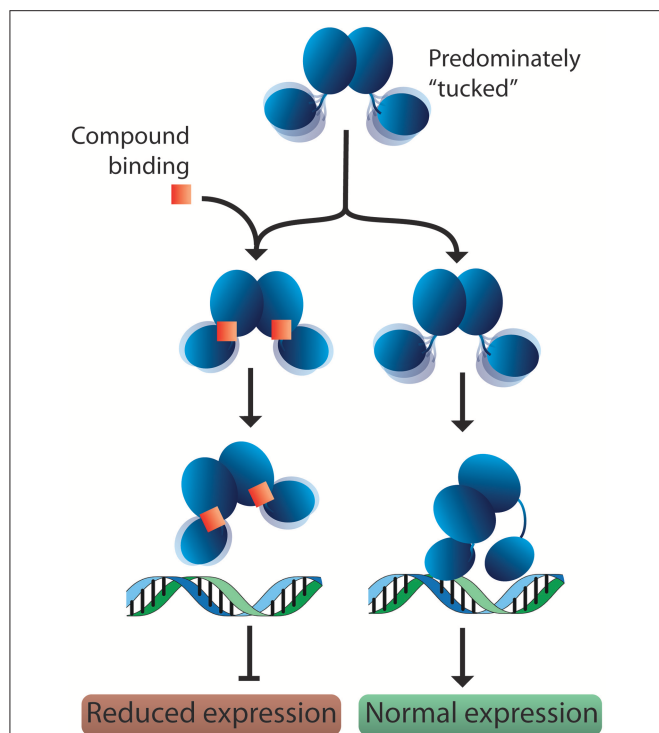


**FIGURE 7 |** Proposed model for response regulator DNA binding and 2-AI binding. In solution, response regulators are predominantly in the “tucked” conformation. In the absence of inhibitor, the response regulator is free to move the C-terminal domains. This assists in binding the target DNA and allows the N-terminal domain to “kneel” over one of the DNA-binding domains. Binding of a 2-AI compound likely increases the interactions between the N- and C-terminal domains, impacting the protein’s ability to position both DNA-binding domains on the promotor substrate and “kneel” over the N-terminal domain. Interfering with DNA binding or the protein conformation on the DNA would be expected to reduce the expression of downstream targets.

Both DNA binding domains are likely needed to sufficiently bind the target DNA sequence. Thus, a shift in equilibrium between “tucked” and “extended” states or trapping the response regulator in a “tucked” conformation may impact DNA binding and/or regulation of downstream targets. Further studies are needed to validate this hypothesis. With this in mind, 2-AIs designed to tightly bind the interface and facilitate interactions with both the N- and C-terminal domains should be excellent inhibitors.

## CONCLUSION

Using a combination of biochemical and cellular techniques, we confirmed that BfmR is a cellular target of 2-AI compounds. These results agree with our similar findings for QseB. Sampling of a library of compounds allowed for comparisons of behavior across multiple techniques, from which information about the most promising compounds can be deduced. Based on these experiments, AGL-726 and AGL-833 appear to have significant therapeutic potential, due to their ability to bind BfmR with relatively high affinities, inhibit biofilm formation, and increase

sensitivity to carbapenem derivatives. The confirmation of both QseB and BfmR as targets of 2-AI compounds and the identification of the same lead compounds suggests that studies to determine the inhibition mechanism in one system will translate to the other. Since *Francisella* encode only three response regulators, *Francisella* could be a model system for the determination of a 2-AI mechanism of action in *A. baumannii*. Understanding the interactions between response regulators and 2-AIs on a structural level is necessary to fully understand the mechanism of inhibition. This information will play a vital role in the development of even more potent compounds to combat antimicrobial resistance. Molecular dynamics simulations suggest that response regulators are prone to spend a majority of their time in the “tucked” state. As such, this state should be targeted for future drug design. We hypothesize that the binding of a 2-AI into the interface between the N-terminal and C-terminal domains will increase the interaction between these domains, stabilizing the “tucked” state. This binding could result in reduced sampling of the “extended” state. The work presented here lays the ground work for understanding how 2-AI compounds inhibit response regulators. Further studies are necessary to validate this working model. A better understanding of how 2-AIs interact with response regulators and the mechanisms involved in DNA binding will inform the development of more potent libraries of compounds with specific and broad range targets.

## AUTHOR CONTRIBUTIONS

MM: designed the research, performed biochemical experiments and wrote the manuscript; MM and CL: expressed and purified proteins; MM, BM, and BK: performed cellular experiments; DH: performed molecular dynamics studies; DJ: synthesized all compounds; DZ: provided all synthesized compounds; RT, RM, CM, and JC: supervised research.

## FUNDING

This project has been funded in part with Federal funds from the National Institute of Allergy and Infectious Diseases, National Institutes of Health, Department of Health and Human Services, under Contract No. HHSN272201500010C, grant RO1-GM055769, grant 1R41AI115915-01A1, and by the V Foundation for Cancer Research.

## ACKNOWLEDGMENTS

The authors would like to thank G. L. Draughn helpful discussions and A. J. Milton for critically reviewing the manuscript.

## SUPPLEMENTARY MATERIAL

The Supplementary Material for this article can be found online at: <https://www.frontiersin.org/articles/10.3389/fmolb.2018.00015/full#supplementary-material>

## REFERENCES

- Ballard, T. E., Richards, J. J., Wolfe, A. L., and Melander, C. (2008). Synthesis and antibiofilm activity of a second-generation reverse-amide oroidin library: a structure-activity relationship study. *Chem. Eur. J.* 14, 10745–10761. doi: 10.1002/chem.200801419
- Boudes, M., Sanchez, D., Graille, M., van Tilbeurgh, H., Durand, D., and Quevillon-Cheruel, S. (2014). Structural insights into the dimerization of the response regulator ComE from *Streptococcus pneumoniae*. *Nucleic Acids Res.* 42, 5302–5313. doi: 10.1093/nar/gku110
- Brackett, C. M., Melander, R. J., An, I. H., Krishnamurthy, A., Thompson, R. J., Cavanagh, J., et al. (2014). Small-molecule suppression of  $\beta$ -lactam resistance in multidrug-resistant gram-negative pathogens. *J. Med. Chem.* 57, 7450–7458. doi: 10.1021/jm501050e
- Case, D. A., Betz, R., Cerutti, D. S., Cheatham, T., Darden, T., Duke, R., et al. (2016). *Amber 2016*. San Francisco, CA: University of California. San Francisco.
- Dijkshoorn, L., Nemec, A., and Seifert, H. (2007). An increasing threat in hospitals: multidrug-resistant *Acinetobacter baumannii*. *Nat. Rev. Microbiol.* 5, 939–951. doi: 10.1038/nrmicro1789
- Donlan, R. M. (2002). Biofilms: microbial life on surfaces. *Emerg. Infect. Dis.* 8, 881–890. doi: 10.3201/eid0809.020063
- Donlan, R. M., and Costerton, J. W. (2002). Biofilms: survival mechanisms of clinically relevant microorganisms. *Clin. Microbiol. Rev.* 15, 167–193. doi: 10.1128/CMR.15.2.167-193.2002
- Durham-Colleran, M. W., Verhoeven, A. B., and van Hoek, M. L. (2010). *Francisella novicida* forms *in vitro* biofilms mediated by an orphan response regulator. *Microb. Ecol.* 59, 457–465. doi: 10.1007/s00248-009-9586-9
- Friesner, R. A., Murphy, R. B., Repasky, M. P., Frye, L. L., Greenwood, J. R., Halgren, T. A., et al. (2006). Extra precision glide: docking and scoring incorporating a model of hydrophobic enclosure for protein-ligand complexes. *J. Med. Chem.* 49, 6177–6196. doi: 10.1021/jm051256o
- Gao, R., and Stock, A. M. (2009). Biological insights from structures of two-component proteins. *Annu. Rev. Microbiol.* 63, 133–154. doi: 10.1146/annurev.micro.091208.073214
- González-Bello, C. (2017). Antibiotic adjuvants - a strategy to unlock bacterial resistance to antibiotics. *Bioorg. Med. Chem. Lett.* 27, 4221–4228. doi: 10.1016/j.bmcl.2017.08.027
- Greenidge, P. A., Kramer, C., Mozziconacci, J. C., and Wolf, R. M. (2013). MM/GBSA binding energy prediction on the PDBbind data set: successes, failures, and directions for further improvement. *J. Chem. Inf. Model.* 53, 201–209. doi: 10.1021/ci300425v
- Hou, T., Wang, J., Li, Y., and Wang, W. (2011). Assessing the performance of the molecular mechanics/Poisson Boltzmann surface area and molecular mechanics/generalized Born surface area methods. II. The accuracy of ranking poses generated from docking. *J. Comput. Chem.* 32, 866–877. doi: 10.1002/jcc.21666
- Imperi, F., Antunes, L. C., Blom, J., Villa, L., Iacono, M., Visca, P., et al. (2011). The genomics of *Acinetobacter baumannii*: insights into genome plasticity, antimicrobial resistance and pathogenicity. *IUBMB Life* 63, 1068–1074. doi: 10.1002/iub.531
- Jacobs, A. C., Thompson, M. G., Black, C. C., Kessler, J. L., Clark, L. P., McQueary, C. N., et al. (2014). AB5075, a highly virulent isolate of *Acinetobacter baumannii*, as a model strain for the evaluation of pathogenesis and antimicrobial treatments. *MBio* 5:e01076-14. doi: 10.1128/mBio.01076-14
- Kröger, C., Kary, S. C., Schauer, K., and Cameron, A. D. (2016). Genetic Regulation of virulence and antibiotic resistance in *Acinetobacter baumannii*. *Genes* 8:E12. doi: 10.3390/genes8010012
- Larsson, P., Oyston, P. C. F., Chain, P., Chu, M. C., Duffield, M., Fuxelius, H. H., et al. (2005). The complete genome sequence of *Francisella tularensis*, the causative agent of tularemia. *Nat. Genet.* 37, 153–159. doi: 10.1038/ng1499
- Liou, M. L., Soo, P. C., Ling, S. R., Kuo, H. Y., Tang, C. Y., and Chang, K. C. (2014). The sensor kinase BfmS mediates virulence in *Acinetobacter baumannii*. *J. Microbiol. Immunol. Infect. Wei Mian Yu Gan Ran Za Zhi* 47, 275–281. doi: 10.1016/j.jmii.2012.12.004
- Lo, M.-C., Aulabaugh, A., Jin, G., Cowling, R., Bard, J., Malamas, M., et al. (2004). Evaluation of fluorescence-based thermal shift assays for hit identification in drug discovery. *Anal. Biochem.* 332, 153–159. doi: 10.1016/j.ab.2004.04.031
- Lou, Y.-C., Weng, T.-H., Li, Y.-C., Kao, Y.-F., Lin, W.-F., Peng, H.-L., et al. (2015). Structure and dynamics of polymyxin-resistance-associated response regulator PmrA in complex with promoter DNA. *Nat. Commun.* 6:8838. doi: 10.1038/ncomms9838
- McConnell, M. J., Actis, L., and Pachón, J. (2013). *Acinetobacter baumannii*: human infections, factors contributing to pathogenesis and animal models. *FEMS Microbiol. Rev.* 37, 130–155. doi: 10.1111/j.1574-6976.2012.00344.x
- Melander, R. J., and Melander, C. (2017). The challenge of overcoming antibiotic resistance: an adjuvant approach? *ACS Infect. Dis.* 3, 559–563. doi: 10.1021/acsinfecdis.7b00071
- Milton, M. E., Allen, C. L., Feldmann, E. A., Bobay, B. G., Jung, D. K., Stephens, M. D., et al. (2017). Structure of the *Francisella* response regulator QseB receiver domain, and characterization of QseB inhibition by antibiofilm 2-aminoimidazole-based compounds. *Mol. Microbiol.* 106, 223–235. doi: 10.1111/mmi.13759
- Mohapatra, N. P., Soni, S., Bell, B. L., Warren, R., Ernst, R. K., Muszynski, A., et al. (2007). Identification of an orphan response regulator required for the virulence of *Francisella* spp. and transcription of pathogenicity island genes. *Infect. Immun.* 75, 3305–3314. doi: 10.1128/IAI.00351-07
- Narayanan, A., Kumar, S., Evrard, A. N., Paul, L. N., and Yernool, D. A. (2014). An asymmetric heterodomain interface stabilizes a response regulator-DNA complex. *Nat. Commun.* 5:3282. doi: 10.1038/ncomms4282
- Niesen, F. H., Berglund, H., and Vedadi, M. (2007). The use of differential scanning fluorimetry to detect ligand interactions that promote protein stability. *Nat. Protoc.* 2, 2212–2221. doi: 10.1038/nprot.2007.321
- O'Toole, G. A. (2011). Microtiter dish biofilm formation assay. *J. Vis. Exp.* 47:2437. doi: 10.3791/2437
- Olson, A. L., Liu, F., Tucker, A. T., Goshe, M. B., and Cavanagh, J. (2013). Chemical crosslinking and LC/MS analysis to determine protein domain orientation: application to AbrB. *Biochem. Biophys. Res. Commun.* 431, 253–257. doi: 10.1016/j.bbrc.2012.12.124
- Pantoliano, M. W., Petrella, E. C., Kwasnoski, J. D., Lobanov, V. S., Myslik, J., Graf, E., et al. (2001). High-density miniaturized thermal shift assays as a general strategy for drug discovery. *J. Biomol. Screen.* 6, 429–440. doi: 10.1177/108705710100600609
- Percival, S. L., Hill, K. E., Malic, S., Thomas, D. W., and Williams, D. W. (2011). Antimicrobial tolerance and the significance of persister cells in recalcitrant chronic wound biofilms. *Wound Repair Regen.* 19, 1–9. doi: 10.1111/j.1524-475X.2010.00651.x
- Perez, F., Hujer, A. M., Hujer, K. M., Decker, B. K., Rather, P. N., and Bonomo, R. A. (2007). Global challenge of multidrug-resistant *Acinetobacter baumannii*. *Antimicrob. Agents Chemother.* 51, 3471–3484. doi: 10.1128/AAC.01464-06
- Rasmussen, T. B., and Givskov, M. (2006). Quorum-sensing inhibitors as anti-pathogenic drugs. *Int. J. Med. Microbiol.* 296, 149–161. doi: 10.1016/j.ijmm.2006.02.005
- Rice, L. B. (2008). Federal funding for the study of antimicrobial resistance in nosocomial pathogens: no ESKAPE. *J. Infect. Dis.* 197, 1079–1081. doi: 10.1086/533452
- Richards, J. J., Ballard, T. E., and Melander, C. (2008a). Inhibition and dispersion of *Pseudomonas aeruginosa* biofilms with reverse amide 2-aminoimidazole oroidin analogues. *Org. Biomol. Chem.* 6:1356. doi: 10.1039/b719082d
- Richards, J. J., Huigens lii, R. W., Ballard, T. E., Basso, A., Cavanagh, J., and Melander, C. (2008b). Inhibition and dispersion of proteobacterial biofilms. *Chem. Commun* 14, 1698–700. doi: 10.1039/b719802g
- Rogers, S. A., and Melander, C. (2008). Construction and screening of a 2-aminoimidazole library identifies a small molecule capable of inhibiting and dispersing bacterial biofilms across order, class, and phylum. *Angew. Chem. Int. Ed Engl.* 47, 5229–5231. doi: 10.1002/anie.200800862
- Russo, T. A., Manohar, A., Beanan, J. M., Olson, R., MacDonald, U., Graham, J., et al. (2016). The response regulator BfmR is a potential drug target for *Acinetobacter baumannii*. *mSphere* 1:e00082-16. doi: 10.1128/mSphere.00082-16
- Sjöstedt, A. (2007). Tularemia: history, epidemiology, pathogen physiology, and clinical manifestations. *Ann. N.Y. Acad. Sci.* 1105, 1–29. doi: 10.1196/annals.1409.009
- Stock, A. M., Robinson, V. L., and Goudreau, P. N. (2000). Two-component signal transduction. *Annu. Rev. Biochem.* 69, 183–215. doi: 10.1146/annurev.biochem.69.1.183

- Stowe, S. D., Thompson, R. J., Peng, L., Su, Z., Blackledge, M. S., Draughn, G. L., et al. (2015). Membrane-permeabilizing activity of reverse-amide 2-aminoimidazole antibiofilm agents against *Acinetobacter baumannii*. *Curr. Drug Deliv.* 12, 223–230. doi: 10.2174/1567201811666140924125740
- Sutera, V., Levert, M., Burmeister, W. P., Schneider, D., and Maurin, M. (2014). Evolution toward high-level fluoroquinolone resistance in *Francisella* species. *J. Antimicrob. Chemother.* 69, 101–110. doi: 10.1093/jac/dkt321
- Thompson, R. J., Bobay, B. G., Stowe, S. D., Olson, A. L., Peng, L., Su, Z., et al. (2012). Identification of BfmR, a response regulator involved in biofilm development, as a Target for a 2-aminoimidazole-based anti-biofilm agent. *Biochem. Mosc.* 51, 9776–9778. doi: 10.1021/bi3015289
- Tien, H. C., Battad, A., Bryce, E. A., Fuller, J., Mulvey, M., Bernard, K., et al. (2007). Multi-drug resistant *Acinetobacter* infections in critically injured Canadian forces soldiers. *BMC Infect. Dis.* 7:95. doi: 10.1186/1471-2334-7-95
- Tomaras, A. P., Flagler, M. J., Dorsey, C. W., Gaddy, J. A., and Actis, L. A. (2008). Characterization of a two-component regulatory system from *Acinetobacter baumannii* that controls biofilm formation and cellular morphology. *Microbiol. Read. Engl.* 154, 3398–3409. doi: 10.1099/mic.0.2008/019471-0
- Trott, O., and Olson, A. J. (2010). AutoDock Vina: improving the speed and accuracy of docking with a new scoring function, efficient optimization and multithreading. *J. Comput. Chem.* 31, 455–461. doi: 10.1002/jcc.21334
- World Health Organization (2017). *Guidelines for the prevention and control of carbapenem-resistant Enterobacteriaceae, Acinetobacter baumannii and Pseudomonas aeruginosa in health care facilities*. World Health Organization Available online at: <http://www.who.int/iris/handle/10665/259462> (Accessed November 16, 2017).
- Wright, G. D. (2016). Antibiotic adjuvants: rescuing antibiotics from resistance. *Trends Microbiol.* 24, 862–871. doi: 10.1016/j.tim.2016.06.009
- Zhang, X., Wong, S. E., and Lightstone, F. C. (2014). Toward fully automated high performance computing drug discovery: a massively parallel virtual screening pipeline for docking and molecular mechanics/generalized born surface area rescoring to improve enrichment. *J. Chem. Inf. Model.* 54, 324–337. doi: 10.1021/ci4005145

**Conflict of Interest Statement:** Authors BK, DJ, and DZ were employed by the company Agile Sciences, Inc.

The other authors declare that the research was conducted in the absence of any commercial or financial relationships that could be construed as a potential conflict of interest.

Copyright © 2018 Milton, Minrovic, Harris, Kang, Jung, Lewis, Thompson, Melander, Zeng, Melander and Cavanagh. This is an open-access article distributed under the terms of the Creative Commons Attribution License (CC BY). The use, distribution or reproduction in other forums is permitted, provided the original author(s) and the copyright owner are credited and that the original publication in this journal is cited, in accordance with accepted academic practice. No use, distribution or reproduction is permitted which does not comply with these terms.



# Structure-Function Relationships of the Neisserial EptA Enzyme Responsible for Phosphoethanolamine Decoration of Lipid A: Rationale for Drug Targeting

Charlene M. Kahler<sup>1,2\*</sup>, K. L. Nawrocki<sup>3,4†</sup>, A. Anandan<sup>5</sup>, Alice Vrielink<sup>1,5</sup> and William M. Shafer<sup>3,4</sup>

## OPEN ACCESS

### Edited by:

Vassily Bavro,  
University of Essex, United Kingdom

### Reviewed by:

Alison Criss,  
University of Virginia, United States

Sunil D. Saroj,  
Symbiosis International University,  
India

Jessica M. A. Blair,  
University of Birmingham,  
United Kingdom

### \*Correspondence:

Charlene M. Kahler  
charlene.kahler@uwa.edu.au

### † Present address:

K. L. Nawrocki,  
Division of Pulmonary and Critical  
Care Medicine, Department of Internal  
Medicine, University of Michigan  
School of Medicine, Ann Arbor, MI,  
United States

### Specialty section:

This article was submitted to  
Antimicrobials, Resistance  
and Chemotherapy,  
a section of the journal  
Frontiers in Microbiology

**Received:** 04 June 2018

**Accepted:** 30 July 2018

**Published:** 21 August 2018

### Citation:

Kahler CM, Nawrocki KL,  
Anandan A, Vrielink A and  
Shafer WM (2018) Structure-Function  
Relationships of the Neisserial  
EptA Enzyme Responsible  
for Phosphoethanolamine Decoration  
of Lipid A: Rationale for Drug  
Targeting. *Front. Microbiol.* 9:1922.  
doi: 10.3389/fmicb.2018.01922

<sup>1</sup> The Marshall Center for Infectious Diseases Research and Training, School of Biomedical Sciences, University of Western Australia, Crawley, WA, Australia, <sup>2</sup> Perth Children's Hospital, Telethon Kids Institute, Subiaco, WA, Australia, <sup>3</sup> Department of Microbiology and Immunology, The Emory Antibiotic Resistance Center, Emory University School of Medicine, Atlanta, GA, United States, <sup>4</sup> Laboratories of Bacterial Pathogenesis, VA Medical Center, Decatur, GA, United States, <sup>5</sup> School of Molecular Sciences, University of Western Australia, Crawley, WA, Australia

Bacteria cause disease by two general mechanisms: the action of their toxins on host cells and induction of a pro-inflammatory response that can lead to a deleterious cytokine/chemokine response (e.g., the so-called cytokine storm) often seen in bacteremia/septicemia. These major mechanisms may overlap due to the action of surface structures that can have direct and indirect actions on phagocytic or non-phagocytic cells. In this respect, the lipid A (endotoxin) component of lipopolysaccharide (LPS) possessed by Gram-negative bacteria has been the subject of literally thousands of studies over the past century that clearly identified it as a key virulence factor in endotoxic shock. In addition to its capacity to modulate inflammatory responses, endotoxin can also modulate bacterial susceptibility to host antimicrobials, such as the host defense peptides termed cationic antimicrobial peptides. This review concentrates on the phosphoethanolamine (PEA) decoration of lipid A in the pathogenic species of the genus *Neisseria* [*N. gonorrhoeae* and *N. meningitidis*]. PEA decoration of lipid A is mediated by the enzyme EptA (formerly termed LptA) and promotes resistance to innate defense systems, induces the pro-inflammatory response and can influence the *in vivo* fitness of bacteria during infection. These important biological properties have driven efforts dealing with the biochemistry and structural biology of EptA that will facilitate the development of potential inhibitors that block PEA addition to lipid A.

**Keywords:** anti-virulence, phosphoethanolamine transferase, lipopolysaccharide, multidrug resistance, *N. meningitidis*, *N. gonorrhoeae*

## INTRODUCTION

The capacity of *Neisseria gonorrhoeae* (GC) and *N. meningitidis* (MC) to decorate their lipid A with phosphoethanolamine (PEA) has profound implications for their ability to survive host-derived antimicrobials and influence the host's pro-inflammatory response during infection. In the past decade a number of studies have been reported that advance our knowledge on the molecular mechanisms of this lipid A modification.



We propose that this strategy would render bacteria susceptible to innate host defenses and reduce the potentially damaging action of the pro-inflammatory response during infection. We posit that EptA inhibitors would serve as adjunctive therapeutics to counteract multidrug-resistant strains of *N. gonorrhoeae* (GC) that threaten the efficacy of currently used antibiotics. Accordingly, this review is concerned with bringing together results from molecular and structural studies that have focused attention on the enzyme EptA that is responsible for PEA decoration of lipid A in the context of biological studies that support this modification as a virulence factor.

## THE PATHOGENIC *Neisseria*, THEIR DISEASES AND TREATMENT/PREVENTION CONSIDERATIONS

*N. gonorrhoeae* causes the sexually transmitted infection termed gonorrhea with a world-wide yearly estimate of >78 million infections (Newman et al., 2015). Gonorrhea is an ancient disease with biblical references (Old Testament; Leviticus 15:1–3). It causes both symptomatic and (frequent) asymptomatic infections at genital and extra-genital sites in both men and women that can have serious consequences for the reproductive and general health of both sexes (summarized in Rice et al., 2017). Symptomatic disease is driven by the pro-inflammatory response and is highlighted by a substantial influx of neutrophils and marked increase in pro-inflammatory chemokines/cytokines. Most often, gonorrhea presents as uncomplicated urethritis in men and cervicitis in women. However, more invasive forms of disease can occur and include epididymitis, pelvic inflammatory disease (endometritis or salpingitis), or disseminated gonococcal infection (DGI) that can involve multiple organs and joints (infectious arthritis) (Rice, 2005). Women suffer the greatest medical complications from invasive GC infections, especially if there is fallopian tube involvement that can result in ectopic pregnancy, and long lasting damage to their reproductive health. Infected mothers can also transmit GC to their newborn during vaginal delivery resulting in ophthalmia neonatorum. Additional extra-genital infections (rectal and oral) in both sexes occur frequently. Finally, repeated GC infections can facilitate transmission or acquisition of the human immunodeficiency virus (HIV) (Malott et al., 2013).

In contrast to GC, MC is frequently carried as a commensal in the nasopharyngeal cavity by a high percentage of the population, but can enter the blood stream and quickly cause life-threatening disease. Invasive meningococcal disease (IMD) syndromes meningitis and/or fulminant septicemia seem to have appeared much later than gonorrhea in the evolution of *Homo sapiens*, with the earliest recorded reports from outbreaks in the early 1800s in Europe and the United States (reviewed in Stephens et al., 2007). Frequently, IMD occurs as localized endemic disease but can also be the cause of larger scale epidemics that include multiple countries and may span

continents over decades driven by serial introductions of new variants into susceptible populations by travelers (Yezli et al., 2016). Although sporadic outbreaks of IMD occur throughout Africa, prevalence is highest in the sub-Saharan belt consisting of parts of 26 countries which experiences 7000–180,000 IMD cases annually, typically in a seasonal pattern associated with the dry season (Borrow et al., 2017b). In this region, high temperatures and irritation of mucosal surfaces caused by dust are the most prominent risk factors associated with IMD. While it is not entirely clear why individuals develop IMD, prior events which perturb the mucosal innate immune system (viral infections, smoking, irritants such as dust and dry air) in addition to an increased risk of transmission via respiratory droplets (crowded living, salivary exchange through kissing) increase the probability of contracting IMD. The severity and morbidity of IMD is associated with perturbations in the complement and inflammatory cytokine cascade (Dale and Read, 2013) in addition to immunocompromised states such as asplenectomy (Dionne et al., 2017) and immunotherapy (Winthrop et al., 2018). The risk of repeated episodes of IMD and DGI increase in the absence of an intact functional complement system demonstrating the importance of this arm of the host defence against these infections.

Antibiotic resistance expressed by GC and MC has considerable implications for treatment options affecting severe complications and control of the disease in the community (reviewed in Unemo and Shafer, 2014); this topic, including the biochemistry, genetics and molecular biology of resistance, has been extensively reviewed (Unemo and Shafer, 2014). Briefly, from a historical perspective, beginning with the use of sulfonamides in 1938, which ended in 1942 due to resistance, the efficacy of every antibiotic that has been brought into clinical practice to treat gonorrhea has been removed (penicillin, tetracycline, and fluoroquinolones) or threatened for removal from the treatment regimen due to antimicrobial resistance. The prospect of untreatable gonorrhea due to resistance to approved antibiotics is cause for grave concern (Bolan et al., 2012). While empiric monotherapy was used previously to treat gonorrhea, the continued emergence of multidrug (MDR) resistant strains now requires dual antibiotic therapy consisting of azithromycin and ceftriaxone, but strains resistant to either antibiotic or both have emerged (Ohnishi et al., 2011; Fifer et al., 2016; reviewed in Unemo et al., 2016; Lahra et al., 2018; Public Health England, 2018; Wilely et al., 2018). It is also important to emphasize that the current treatment regimen is costly and not always available in less-resourced settings, which frequently have high incidences of gonorrhea. Clinical trials are in progress with new antibiotics and there is hope that new treatment options will soon be available, however, we should plan for GC to develop resistance to them in due course. In contrast to GC, MC does not appear to be particularly efficient in developing antibiotic resistance or, alternatively, at retaining resistance (a review of MC resistance to antibiotics can be found in Unemo and Shafer, 2014). Although frequently resistant to sulfonamides, MC have remained relatively susceptible to the antibiotics classically used for treatment and chemoprophylaxis but rare instances of penicillinase-producing strains have been reported. MC isolates

expressing decreased susceptibility to beta-lactams have emerged during the past two decades and have recently caused an ongoing outbreak since 2016 in Australia (Mowlaboccus et al., 2017). Decreased susceptibility and low-level resistance to ciprofloxacin and high-level resistance to rifampin, antibiotics used frequently for chemoprophylaxis to stop the spread of disease during outbreaks, have also been reported from many countries. Thus, while antibiotic resistance in MC is not at the threat level of GC, there is reason for concern that resistance will continue to evolve.

Efficacious vaccines, which are based upon the major capsular serogroups A, C, Y, and W that are responsible for the majority of IMD, have been successful in controlling epidemics (Borrow et al., 2017a). A four-component meningococcal serogroup B (4CMenB) vaccine, Bexsero®, has been recommended for pediatric immunization in several countries, including Australia, Canada, United Kingdom, and Italy (Kuhdari et al., 2016) and has shown effectiveness in children as a direct intervention against IMD. Due to the concern regarding emergence of MDR-GC strains and the lack of new antibiotics likely to reach the clinic in the immediate future, a renewed interest in developing a gonorrhea vaccine has developed after years of neglect since the failure of the pilin-based vaccine trials in the early 1980s (reviewed in Jerse and Deal, 2013). Encouragingly, in a population-based survey 4CMenB vaccination was associated with a reduced prevalence of gonorrhea in the vaccinated vs. unvaccinated cohorts in Canada and New Zealand (Petousis-Harris et al., 2017). This has raised the prospect that a vaccine directed toward GC is possible and recent data suggests that the NHBA (neisserial heparin binding antigen) component of 4CMenB raises a sufficiently cross-protective antibody response in mice to be a potential vaccine candidate (Pizza, 2018). In addition, other approaches such as the administration of IL-12 which reverses the immunosuppression by GC during urogenital tract infection is another means of raising a cross-protective antibody response to further infections (Liu et al., 2018). However, the development of a vaccine for GC infection remains elusive as there is no natural correlate of protection such as a protective antibody-response in humans, and further development in this area will need to continue.

## ANTI-VIRULENCE STRATEGIES BASED UPON MODELS OF IMD AND GONORRHEA INFECTION

While approaches to GC vaccination are underway, the prospect of increasing prevalence of MDR-GC is gaining momentum, with the appearance of isolates which are resistant to all classes of routinely used and approved antibiotics for treatment of gonorrhoea. Therefore, the development of novel antimicrobials is an area of intense interest. One approach that has gained momentum in the last decade, is the development of “anti-virulence” compounds which are designed to inhibit virulence thus enabling the natural immune responses of the host to clear the infection (Dickey et al., 2017). To be successful,

the virulence target to be inhibited must be essential for the development of disease by the infectious agent, should be tractable to structural studies (crystallography or NMR) and enable high-throughput screening strategies to be developed for identifying and optimizing candidate inhibitors.

The model of infection for GC has been excellently summarized by Quillin and Seifert (2018). Upon transmission, GC bind to the epithelial cells of the urogenital tract via type IV pili which retract enabling close contact and the formation of micro-colonies. The micro-colonies release inflammatory mediators: peptidoglycan, lipooligosaccharide (LOS), and outer membrane vesicles which result in the recruitment of neutrophils to the site of inflammation. Since the neutrophils are unable to clear the infection, the influx of neutrophils form a purulent exudate that then facilitates transmission to the urogenital tract of the next partner. *N. gonorrhoeae* can also colonize the nasopharynx and until recently this was considered transient and not a significant mode of transmission. However, antibiotic treatment failure is most commonly associated with nasopharyngeal carriage and often necessitates a nasopharyngeal swab test to ensure total cure after therapy (Unemo et al., 2016).

*Neisseria meningitidis* is most commonly carried asymptomatically in the nasopharynx of 10% of young adults. It is transmitted via the respiratory route in salivary droplets (Stephens et al., 2007). The MC model of colonization of the nasopharynx also involves type IV pili to initiate attachment and then close adhesion to the host epithelium when retracted. However, the meningococcal model of invasion also includes a wider variety of adhesins required for interaction with endothelial cells lining the blood vessels during IMD (Stephens et al., 2007).

Interestingly a single virulence factor, the ethanolamine transferase EptA (formerly termed lipid A phosphoethanolamine transferase LptA), has been shown to be required for multiple aspects of GC and MC pathogenesis including colonization, inflammation and survival in neutrophils, and we propose this enzyme has exciting potential as a target for development of anti-virulence compounds.

## FUNCTION OF EptA

EptA is an enzyme required for the decoration of lipid A of the LOS of the outer leaflet of the outer membrane of *Neisseria* spp. (Cox et al., 2003a). The LOS structure of the pathogenic *Neisseria* spp., is identical being composed of a conserved inner core consisting of heptose (Hep) and 3-deoxy-D-manno-2-octulosonic acid (KDO) attached to a lipid A moiety embedded in the outer membrane (Figure 1; Bartley and Kahler, 2014). Substitutions to this inner core are variable and contribute to the distinct immunoreactivity profiles of these structures. All structures have an  $\alpha$ -chain,  $\beta$ -chain, and  $\gamma$ -chain attached to the heptose residues, HepI and HepII, of the conserved inner core. The  $\alpha$ -chain attached to HepI is composed of either a lacto-N-neotetraose (LNT, Gal $\beta$ 1, 4GlcNAc $\beta$ 1, 3Gal $\beta$ 1, 4Glc where Gal is galactose, GlcNAc is N-acetyl-glucosamine and Glc is glucose) which mimics human glycosphingolipids such

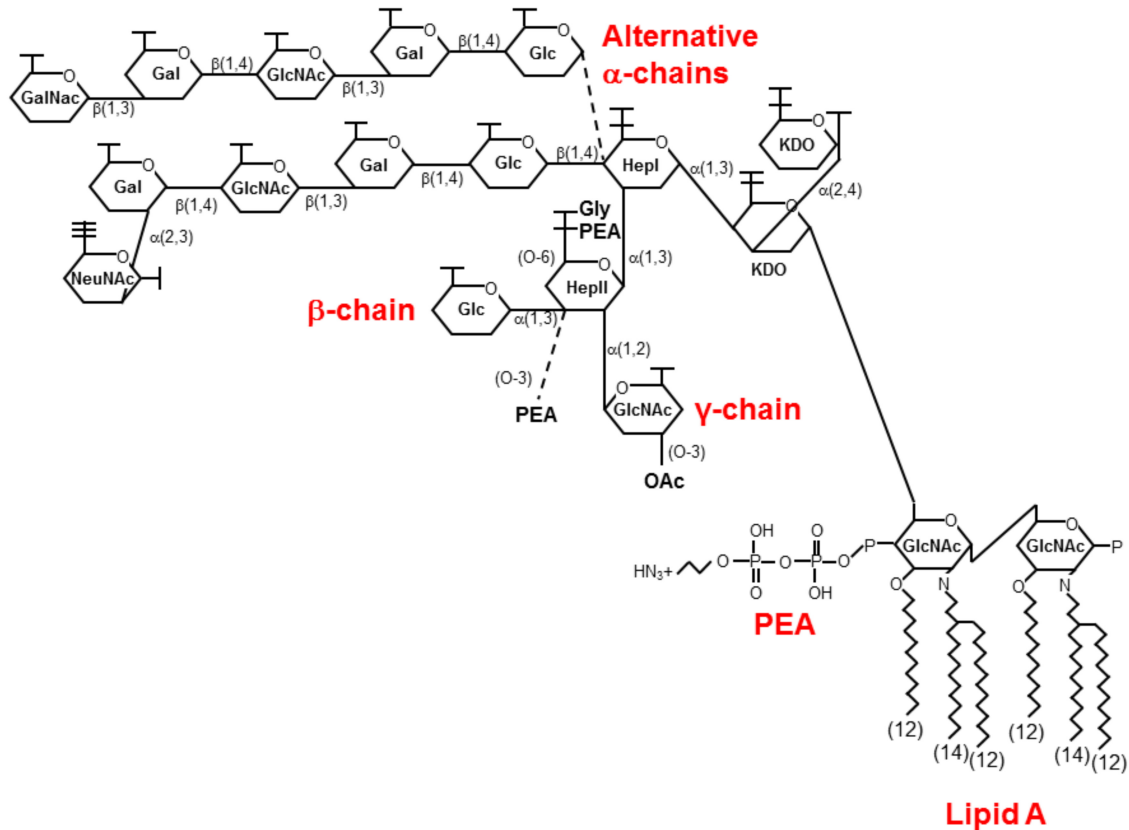


**FIGURE 1 |** The structure of LOS from pathogenic *Neisseria* spp. Shown is a predominant LOS isoform produced by the pathogenic *Neisseria*. The glycosidic  $\alpha$ ,  $\beta$ , and  $\gamma$  chains are attached to a conserved core of heptose (Hep) and keto-octulosonic residues (KDO) attached to lipid A. This figure shows two alternative  $\alpha$ -chains commonly expressed by *N. gonorrhoeae* terminating with GalNAc and *N. meningitidis* terminating in NeuNAc. Variable glycoforms are expressed upon the phase variable expression of various glycosyltransferases (reviewed in Bartley and Kahler, 2014). PEA is shown attached to the 4' position of lipid A in this representation, but variable phosphoforms have been identified with substitutions also occurring on the 1 position (see text and Lewis et al., 2009; John et al., 2012). Gal, galactose; Glc, glucose; GlcNAc, N-acetyl-glucosamine; NeuNAc, N-acetyl-neuraminic acid; P, phosphate; PEA, phosphoethanolamine; OAc, O-acetyl group.

as the human I erythrocyte antigen (Mandrell et al., 1988) or a di-galactose (Gal $\alpha$ 1, 4Gal) which mimics the human P<sup>k</sup> antigen (Mandrell and Apicella, 1993). The  $\beta$ -chain attached to HepII is also variable consisting of either O-3 linked PEA groups (Mackinnon et al., 2002), or a O-3 linked glucose (Banerjee et al., 1998) attached to HepII of the conserved inner core. Lastly the  $\gamma$ -chain attached to HepII is conserved with the addition of a  $\alpha$ -2 linked N-acetyl-glucosamine (GlcNAc) residue (Kahler et al., 1996) which is variably substituted with an O-acetyl group at position 3 or 6 (Kahler et al., 2006; Bartley and Kahler, 2014).

The lipid A structure is conserved within the *Neisseria* spp. (Johnson et al., 1975; John et al., 2012). All species produce a major hexaacyl lipid A with the hydroxyl groups at positions 3 and 3' carrying (R)-3-hydroxydodecanoic acid [12:0 (3-OH)] and the amino groups at positions 2 and 2' being substituted with (R)-3-(dodecanoyloxy)tetradecanoic acid [3-O (12:0)-14:0]. The  $\beta$ 1-6 linked di-glucosamine backbone of lipid A can be variably substituted at the 1 and 4' positions with phosphate, di-phosphate, O-phosphorylethanolamine, and O-pyro-phosphorylethanolamine (Zughaier et al., 2007). This

remarkable heterogeneity appears to be characteristic of GC, MC, *N. lactamica*, and some *N. polysacchareae* but not other commensal *Neisseria* spp. (John et al., 2012).

The lipid A phosphoforms in MC and GC are produced by EptA which is a cytoplasmic-membrane bound enzyme facing the periplasm encoded by a gene found in the pathogenic *Neisseria* but absent in most commensal species (Cox et al., 2003a; John et al., 2012). Once the LOS structure is processively synthesized in the cytoplasm (Bartley and Kahler, 2014) it is transported through the periplasm to the outer membrane by the ABC transporter complex consisting of lipopolysaccharide transport proteins (Lpt), LptBCFG. The lipopolysaccharide chaperone LptA transfers the LOS to the LptED complex in the outer membrane which inserts the LOS into the outer leaflet of the outer membrane (Bos et al., 2004). Only a proportion of lipid A is decorated with PEA headgroups and this can vary between strains by up to 60% of lipid A molecules (Liu M. et al., 2010; Liu X. et al., 2010; Piek et al., 2014; John et al., 2016). A number of transcriptional and post-translational mechanisms controlling EptA expression have been identified that collectively result in strain variation of lipid

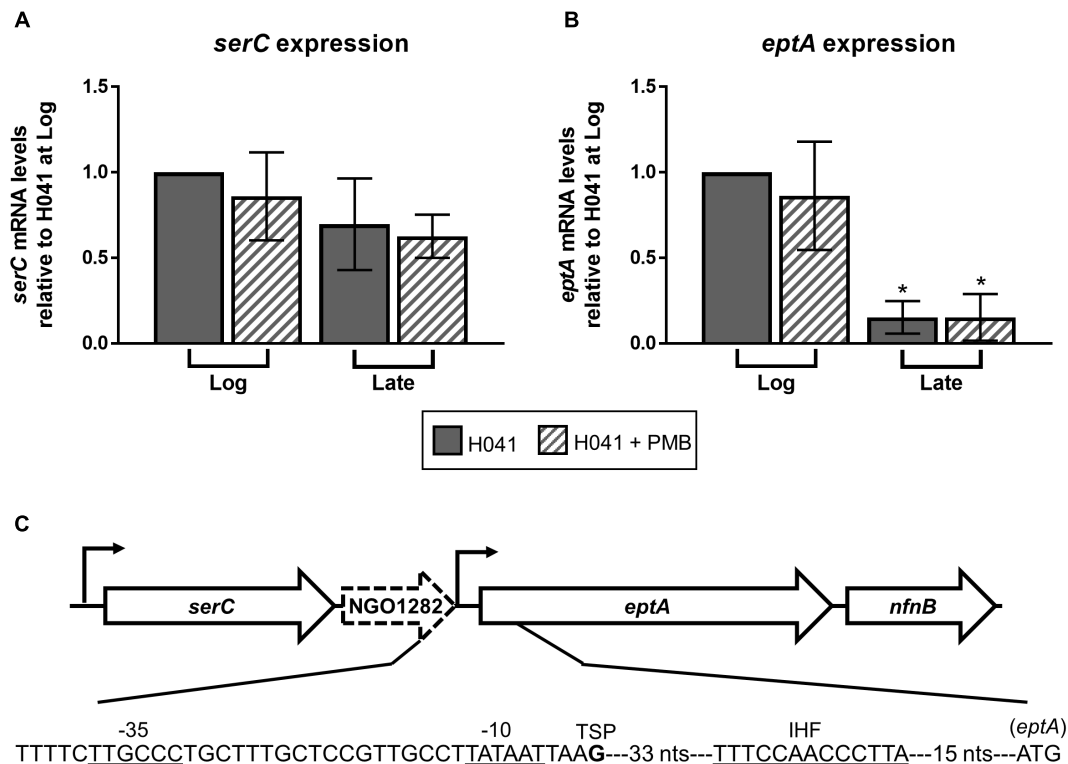


**FIGURE 2 |** Expression of *eptA* is growth phase-dependent. qRT-PCR analysis of (A) *serC* and (B) *eptA* expression in GC isolate H041 grown in GC broth with and without the addition of 1  $\mu$ g/ml polymyxin B (PMB). RNA samples were collected during logarithmic growth (Log, OD<sub>600</sub> of ~0.4) and at the end of logarithmic growth (Late, OD<sub>600</sub> of ~1.0) and subject to qRT-PCR using gene-specific primers. Primers *serC*\_qRT\_F (5'-TGTTGCCTGAAGCTGTGTTG-3') and *serC*\_qRT\_R (5'-TGTTCCGCATGATGCAGGAT-3') were used for *serC* expression. Primers *lptA*\_qRT\_F (5'-GGCATCGCGATGTTGCAATA-3') and *lptA*\_qRT\_R (5'-CACGACCGCCATATCCAATTG-3') were used for *eptA* expression. 16S rRNA expression was assessed with primers 16Smai\_qRT\_F (5'-CCATCGGTATTCCTCCACATCTCT-3') and 16Smai\_qRT\_R (5'-CGTAGGGTGCGAGCGTTAATC-3'). The means and standard deviations of three biological replicates are shown. The expression of *serC* and *eptA* were normalized to 16S rRNA expression at the Log timepoint without PMB treatment. Gene expression data were analyzed by ANOVA followed by Sidak's multiple comparisons test. \*Indicates  $P \leq 0.05$ . (C) Organization of *eptA* locus and position of promoters modified from Kandler et al. (2014). The *eptA* -10 and -35 promoter elements, transcriptional start point (TSP) is the bolded G nucleotide, putative integration host factor binding site (IHF) based on the consensus IHF-binding site in *E. coli* (11 matches of 13 bp) previously described in *N. gonorrhoeae* (Lee et al., 2006) as indicated by the underlined sequence, and the translational start codon are shown.

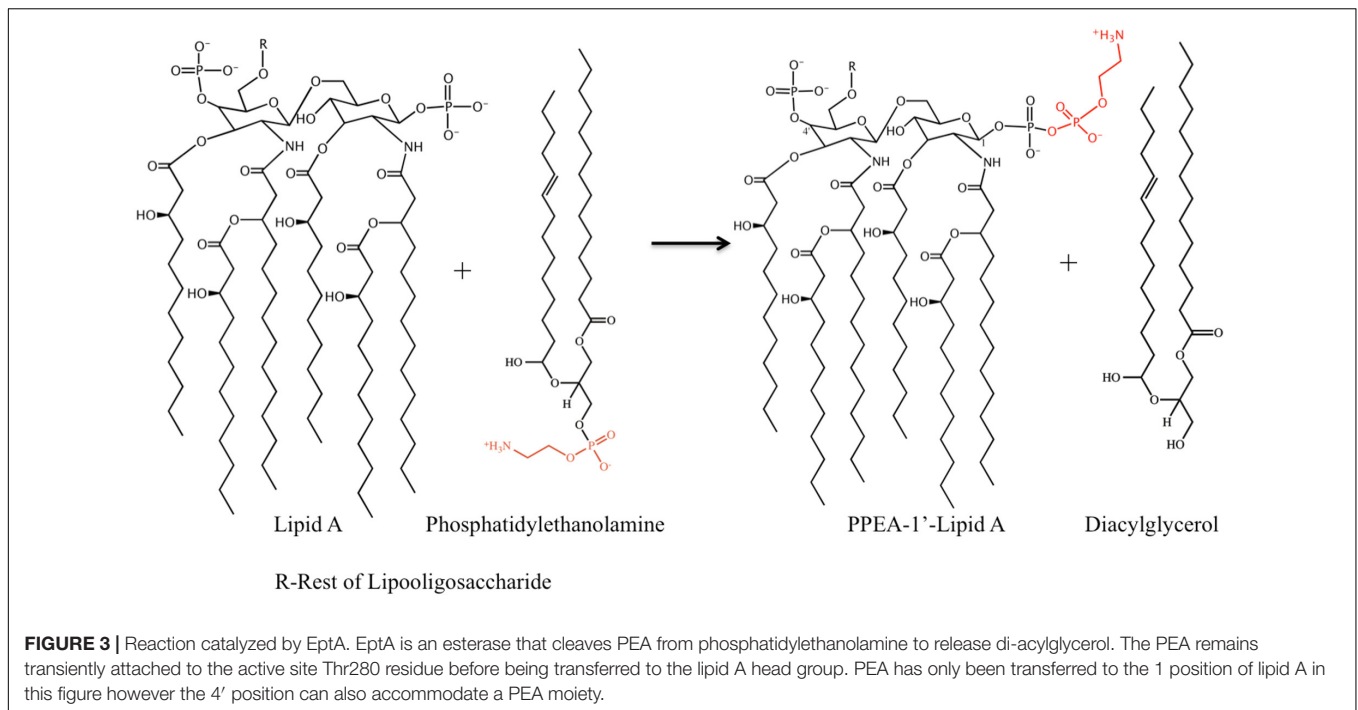
A phosphoforms. *eptA* is co-transcribed in an operon with *serC*, which encodes a putative phosphoserine aminotransferase, a hypothetical gene (*NGO1282*), and *nfnB*, which encodes a putative nitroreductase [Figure 2 below; (Kandler et al., 2014)]. Expression of *eptA*, but not *serC*, is growth phase-dependent with maximal expression observed at the mid-logarithmic phase in GC. It is not yet clear why transcription of *eptA* is maximal during exponential growth, but the presence of a putative integration host factor (IHF) binding site 37 bp downstream of -10 hexamer of the proximal *eptA* promoter might provide a mechanism (see Figure 2C for region of similarity with IHF-binding sites). Previous work by Hill et al. (1998) has shown that mRNA of IHF declines as GC enters stationary phase consistent with a potential means of influencing transcription in a growth phase dependent manner.

EptA expression is governed at the translational level by two means: phase variation of the open reading frame and protein stabilization by oxidoreductases. Translation of full-length EptA

is subject to high frequency mutation due to a phase variable poly-T track in the 5' end coding sequence (Kandler et al., 2014). In the "phase-on" position, the tract consists of 8 Ts. At a frequency of  $10^{-4}$  (4 logs greater than spontaneous mutation) a single T insertion occurs due to slipped-strand mispairing resulting in premature truncation of EptA (62 amino acid protein).

The second mechanism of post-translation control of EptA expression is a result of the requirement for disulfide bonds that improve stability of the protein in the periplasm. Five disulphide bonds are donated by oxidoreductases to EptA as it is transported via the Sec pathway into the periplasmic space. *N. gonorrhoeae* and MC contain a cohort of three oxidoreductases (DsbA1, DsbA2, and DsbA3) which are oxidized at the active site with a disulphide bond by membrane bound DsbB. The oxidoreductase rapidly and irreversibly donates the disulphide bond to thiol groups on substrate proteins resulting in the release of an oxidized substrate carrying a disulphide bond and a reduced oxidoreductase. DsbA1 and DsbA2 are paralogs, with





DsbA2 being encoded on a genetic island that is distributed in MC but absent in GC (Perrin et al., 2002). Both DsbA1 and DsbA2 are bound to the cytoplasmic membrane by a lipid-linked anchor (Tinsley et al., 2004) and have an overlapping repertoire of substrates involved in pilin biogenesis (Tinsley et al., 2004; Sinha et al., 2008). In contrast, DsbA3 is a soluble periplasmic enzyme, has a stronger oxidizing potential than that of the other DsbA enzymes and has no involvement with pilin biogenesis (Vivian et al., 2008, 2009). All three oxidoreductases have the capacity to introduce disulphide bonds into EptA, however, only the loss of DsbA3 resulted in protein instability and loss of function (Piek et al., 2014). Currently it is not clear whether this post-translational modification pathway is regulated as no change in expression of oxidoreductases has been detected in the many studies to-date on regulatory pathways in MC or GC (summarized in Piek and Kahler, 2012).

## STRUCTURE AND FUNCTIONAL MODEL OF EptA

EptA catalyzes the transfer of PEA from phosphatidylethanolamine (PtdE) to lipid A at 1 and/or 4' head group positions (Figure 3). EptA is an integral membrane protein consisting of an N-terminal transmembrane (TM) domain and a C-terminal soluble periplasmic-facing domain. The solved crystal structure of the soluble domain showed it adopts a hydrolase-type fold with a bound  $\text{Zn}^{2+}$  ion at the enzyme active site near to the catalytic nucleophile, Thr280 (Anandan et al., 2012; Wanty et al., 2013). The soluble domain, although retaining the esterase activity required for cleavage

of PtdE, was inactive as a lipid A transferase in bacterial cells suggesting that the TM domain is important for overall function. The solved 3D structure of full-length EptA revealed that the N-terminal TM domain was connected to the soluble domain by a bridging helix and an extended loop (Anandan et al., 2017; Figure 4).

The membrane domain contains five transmembrane helices (TMH1-5, Figure 4) oriented approximately parallel to one another and spanning the inner membrane in a previously uncharacterized fold. A patch of positively charged residues (Lys142, Lys144, Arg146, and Lys150) at the cytoplasmic end of TMH5 are likely to provide interactions with the phospholipid head groups at the inner membrane surface. The bridging helix (residues 194–208) has a highly unusual configuration in the structure and is linked to the soluble domain by an extended coiled region (residues 210–231). There is a large interface between the soluble and membrane domains which is conserved in all lipid A PEA transferases suggesting this region has a conserved function. Intrinsic tryptophan fluorescence experiments and molecular dynamics simulations has led to the proposal that the protein is highly dynamic in the membrane and support a model that the enzyme carries out catalysis through a “ping pong” kinetic mechanism. In this model, the first step requires EptA to bind PtdE using the small periplasmic helices (PH2 and PH2') located between TM3 and TMH4. PEA is cleaved from PtdE and transferred to the Thr280 residue to form an PEA-enzyme intermediate. The soluble domain then rotates away from the TM domain, resulting in an open conformation capable of accepting the larger lipid A into the binding site pocket and completing the transfer of the PEA from the enzyme intermediate to the 1 and 4' positions of lipid A.



of C4BP and fH to PorB and contributes to the ability of GC to resist complement-mediated killing by both the classical and alternative complement pathways.

Evasion of complement-mediated killing is commonly associated with escaping the ability of normal human serum to kill the organism once it enters the bloodstream. In this case, the role of complement resistance by MC during invasive disease is substantial in enabling bacteremia (Lewis and Ram, 2014). Female and male genital tract secretions have high levels of immunoglobulin IgG and complement factors (Birse et al., 2013; Horton and Vidarsson, 2013). In the model of cervicitis proposed by Edwards (2008), the lack of a detectable antibody response in uncomplicated gonococcal cervicitis means there is an absence of immunoglobulin to initiate the classical complement pathway. However, the binding of fH to the bacterial surface by PorB results in rapid inactivation of complement factor C3b to iC3b, which forms bridges with the host cell receptor CR3 (complement-receptor 3). CR-3 mediates endocytosis of the bacteria into the cervical epithelia potentially leading to the ability to colonize the mucosal surface without triggering an inflammatory response, a characteristic of the asymptomatic phase of gonorrhea seen in both sexes. Therefore, the interplay of complement-regulatory proteins on the gonococcal cell surface is closely associated with colonization events in men and women (Edwards and Apicella, 2004).

## ROLE OF EptA IN THE STIMULATION OF THE PRO-INFLAMMATORY RESPONSES OF MACROPHAGES AND NEUTROPHILS

While the endotoxins of MC and GC have an identical lipid A, most information on the structure and functional relationships that are necessary for eliciting the pro-inflammatory response has been conducted with meningococcal lipid A (Zughaier et al., 2005, 2007; Zimmer et al., 2007). Both endotoxins induce pro-inflammatory responses from cells via the Toll-like receptor (TLR) 4/myeloid differentiation factor 2 (MD-2) complex which sits in the host cell membrane and receives endotoxins from the soluble CD14 protein which binds endotoxins in serum (Park et al., 2009). Activation of TLR4/MD2 is dependent upon the conformational structural variations in lipid A, degree of lipid A phosphorylation, number and length of acyl chains, net charge of the molecule, and variations in hydrophobicity (Zimmer et al., 2007). The role of lipid A decorated with PEA headgroups in eliciting a stronger cytokine response was subsequently confirmed by John et al. (2012) and Liu M. et al. (2010) using purified lipid A with and without PEA decorations to elicit cytokine responses from cell monolayers. Packiam et al. (2014) further showed that purified LOS containing lipid A devoid of the PEA modification from a GC *eptA* mutant induced significantly lower levels of NF- $\kappa$ B in human embryonic kidney Toll-like receptor 4 (TLR4) cells and murine embryonic fibroblasts than wild-type LOS of the parent strain. Consistent with these tests, analysis of the chemokine/cytokine responses of female mice with lower genital tract infection showed that the parent GC strain possessing lipid A with PEA

decorations elicited a robust pro-inflammatory response that was significantly dampened in mice infected with the GC *eptA* null mutant; while markers of the anti-inflammatory response were not significantly different in mice infected with either strain.

The binding of lipid A to the TLR4/MD-2 complex on macrophages and neutrophils results in cellular activation, the release of cytokines, chemokines, reactive oxygen species (ROS), and nitric oxide which will kill phagocytosed bacteria. In the female mouse model of lower genital tract infection, Packiam et al. (2014) reported that the GC *eptA* mutant had a substantial fitness defect *in vivo* compared to the wild-type strain during a competitive, mixed infection. Hobbs et al. (2013) made similar observations in human male volunteers. They suggested that the observed fitness defect in the competitive infection model was due to the strong pro-inflammatory response elicited by the wild-type GC strain that was sufficient to activate macrophages and neutrophils which effectively killed the GC *eptA* mutants.

Macrophages and neutrophils kill bacteria by phagocytosis followed by the formation of a phagolysosome which utilizes oxidative mechanisms (ROS such as hydrogen peroxide, superoxide etc.) and non-oxidative mechanisms [serine proteases, cationic antimicrobial peptides (CAMPs), and iron sequestration] to kill the bacteria (Criss, 2014). Neutrophils will also secrete neutrophil extracellular traps (NETs) consisting of DNA coated with CAMPs such as LL-37 to trap the bacteria and kill them. Wild-type MC and GC evade killing by neutrophils by avoiding phagocytosis, engaging surface regulatory proteins that trigger an oxidative burst before the bacteria are phagocytosed, and using mechanisms that quench or detoxify ROS and resist CAMPs (Criss, 2014). The *eptA* mutants from MC and GC are exquisitely sensitive to killing by CAMPs and are rapidly killed by neutrophils as a result (Tzeng et al., 2005; Kandler et al., 2014; Handing and Criss, 2015; Tzeng and Stephens, 2015). Interestingly, decoration of lipid A with PEA has also been shown to interfere with the maturation of the phagolysosome by delaying fusion of azurophilic granules with maturing phagolysosomes (Johnson and Criss, 2013; Handing and Criss, 2015) and additionally dysregulates autophagy, a process which normally targets surface macromolecules including bacteria, to the phagolysosome (Zughaier et al., 2015).

## CONCLUSION

The decoration of lipid A with PEA in GC and MC is an essential pathogenesis factor that distinguishes these pathogens from most commensal *Neisseria* spp. This feature stimulates the pro-inflammatory responses during IMD and gonorrhea but also provides a protective role against clearance by innate immune cells such as neutrophils and macrophages that are attracted to the site of infection. In both instances, the engulfment of the bacteria leads to a frustrated innate immune response that results in chronic inflammation and in the case of GC infected neutrophils become vehicles for transmission between hosts.

We propose that inhibition of EptA will improve killing and clearance of these pathogens by neutrophils thus improving clearance of infection from mucosal surfaces and providing a mechanism that curtails transmission of GC in neutrophils. In addition, EptA enzymes are found in many gram-negative pathogens (e.g., *Escherichia coli*, *Salmonella enterica*, *Klebsiella pneumoniae*, etc.), rendering them resistant to colistin therapy (Gao et al., 2016). Detailed studies are underway to identify and optimize potential EptA-inhibitors that suppress expression (Daly et al., 2017) or inhibit the enzyme directly in these bacterial species. We suggest similar approaches to inhibition of EptA from *Neisseria* sp. will be prove to be a beneficial approach to the development of novel therapies. Therapeutics to boost the bactericidal activity of phagocytic cells are currently in development (Munguia and Nizet, 2017), which in combination with anti-EptA compounds, could be used as novel combination therapies to effectively reduce transmission of multi-drug resistant GC and MC isolates.

## AUTHOR CONTRIBUTIONS

CK and WS wrote the drafts of the manuscript with editorial changes and input by KN, AA, and AV. AA and KN prepared the figures and performed experiments described in the text.

## REFERENCES

- Anandan, A., Evans, G. L., Condic-Jurkic, K., O'mara, M. L., John, C. M., Phillips, N. J., et al. (2017). Structure of a lipid A phosphoethanolamine transferase suggests how conformational changes govern substrate binding. *Proc. Natl. Acad. Sci. U.S.A.* 114, 2218–2223. doi: 10.1073/pnas.1612927114
- Anandan, A., Piek, S., Kahler, C. M., and Vrielink, A. (2012). Cloning, expression, purification and crystallization of an endotoxin-biosynthesis enzyme from *Neisseria meningitidis*. *Acta Crystallogr. Sect. F Struct. Biol. Cryst. Commun.* 68, 1494–1497. doi: 10.1107/S1744309112042236
- Banerjee, A., Wang, R., Uljon, S. N., Rice, P. A., Gotschlich, E. C., and Stein, D. C. (1998). Identification of the gene (*lgtG*) encoding the lipooligosaccharide beta chain synthesizing glucosyl transferase from *Neisseria gonorrhoeae*. *Proc. Natl. Acad. Sci. U.S.A.* 95, 10872–10877. doi: 10.1073/pnas.95.18.10872
- Bartley, S. N., and Kahler, C. M. (2014). "The glycome of *Neisseria* spp.: how does this relate to pathogenesis?" in *Pathogenic Neisseria: Genomics, Molecular Biology and Disease Prevention*, eds J. K. Davies and C. M. Kahler (Norfolk: Caister Academic Press).
- Birse, K. M., Burgener, A., Westmacott, G. R., Mccorrister, S., Novak, R. M., and Ball, T. B. (2013). Unbiased proteomics analysis demonstrates significant variability in mucosal immune factor expression depending on the site and method of collection. *PLoS One* 8:e79505. doi: 10.1371/journal.pone.0079505
- Bolan, G. A., Sparling, P. F., and Wasserheit, J. N. (2012). The emerging threat of untreatable gonococcal infection. *N. Engl. J. Med.* 366, 485–487. doi: 10.1056/NEJMp1112456
- Borrow, R., Alarcon, P., Carlos, J., Caugant, D. A., Christensen, H., Debbag, R., et al. (2017a). The global meningococcal initiative: global epidemiology, the impact of vaccines on meningococcal disease and the importance of herd protection. *Exp. Rev. Vaccines* 16, 313–328. doi: 10.1080/14760584.2017.1258308
- Borrow, R., Caugant, D. A., Ceyhan, M., Christensen, H., Dinleyici, E. C., Findlow, J., et al. (2017b). Meningococcal disease in the Middle East and Africa: findings and updates from the global meningococcal initiative. *J. Infect.* 75, 1–11. doi: 10.1016/j.jinf.2017.04.007
- Bos, M. P., Tefsen, B., Geurtsen, J., and Tommassen, J. (2004). Identification of an outer membrane protein required for the transport of lipopolysaccharide

## FUNDING

This work was supported by VA Merit Award 510 1BX000112-07 (WS) from the Biomedical Laboratory Research and Development Service of the U.S. Department of Veterans Affairs and National Institutes of Health grant R37 AI21150 and U19 AI113170 (WS). WS is the recipient of a Senior Research Career Scientist Award from the Biomedical Laboratory Research and Development Service of the U.S. Department of Veterans Affairs. CK and AV were supported by the National Health and Medical Research Council Grants (APP1003697 and APP1078642).

## ACKNOWLEDGMENTS

AA acknowledges support through an Australian Postgraduate Award and the Fay Gale Fellowship from the University of Western Australia. The contents of this article are solely the responsibility of the authors and do not necessarily reflect the official views of the National Institutes of Health, the U.S. Department of Veterans Affairs, the United States Government or the National Health and Medical Research Council of Australia.

- to the bacterial cell surface. *Proc. Natl. Acad. Sci. U.S.A.* 101, 9417–9422. doi: 10.1073/pnas.0402340101
- Cox, A. D., Wright, J. C., Gidney, M. A., Lacelle, S., Plested, J. S., Martin, A., et al. (2003a). Identification of a novel inner-core oligosaccharide structure in *Neisseria meningitidis* lipopolysaccharide. *Eur. J. Biochem.* 270, 1759–1766.
- Cox, A. D., Wright, J. C., Li, J., Hood, D. W., Moxon, E. R., and Richards, J. C. (2003b). Phosphorylation of the lipid A region of meningococcal lipopolysaccharide: identification of a family of transferases that add phosphoethanolamine to lipopolysaccharide. *J. Bacteriol.* 185, 3270–3277.
- Criss, A. K. (2014). "Interactions of pathogenic *Neisseria* with neutrophils in the context of host immunity," in *Pathogenic Neisseria: Genomics, Molecular Biology and Disease Prevention*, eds J. K. Davies and C. M. Kahler (Norfolk: Caister Academic Press).
- Dale, A. P., and Read, R. C. (2013). Genetic susceptibility to meningococcal infection. *Exp. Rev. Anti Infect. Ther.* 11, 187–199. doi: 10.1586/eri.12.161
- Daly, S. M., Sturge, C. R., Felder-Scott, C. F., Geller, B. L., and Greenberg, D. E. (2017). MCR-1 inhibition with peptide-conjugated phosphorodiamidate morpholino oligomers restores sensitivity to polymyxin in *Escherichia coli*. *mBio* 8:e1315-17. doi: 10.1128/mBio.01315-17
- Dickey, S. W., Cheung, G. Y. C., and Otto, M. (2017). Different drugs for bad bugs: antivirulence strategies in the age of antibiotic resistance. *Nat. Rev. Drug Discov.* 16, 457–471. doi: 10.1038/nrd.2017.23
- Dionne, B., Dehority, W., Brett, M., and Howdieshell, T. R. (2017). The asplenic patient: post-insult immunocompetence, infection, and vaccination. *Surg. Infect (Larchmt)* 18, 536–544. doi: 10.1089/sur.2016.267
- Edwards, J. L. (2008). The role of complement in gonococcal infection of cervical epithelia. *Vaccine* 26(Suppl. 8), I56–I61. doi: 10.1016/j.vaccine.2008.11.055
- Edwards, J. L., and Apicella, M. A. (2004). The molecular mechanisms used by *Neisseria gonorrhoeae* to initiate infection differ between men and women. *Clin. Microbiol. Rev.* 17, 965–981. doi: 10.1128/CMR.17.4.965-981.2004
- Fifer, H., Natarajan, U., Jones, L., Alexander, S., Hughes, G., Golparian, D., et al. (2016). Failure of dual antimicrobial therapy in treatment of gonorrhea. *N. Engl. J. Med.* 374, 2504–2506. doi: 10.1056/NEJMc1512757



- Gao, R., Hu, Y., Li, Z., Sun, J., Wang, Q., Lin, J., et al. (2016). Dissemination and mechanism for the MCR-1 colistin resistance. *PLoS Pathog* 12:e1005957. doi: 10.1371/journal.ppat.1005957
- Handing, J. W., and Criss, A. K. (2015). The lipooligosaccharide-modifying enzyme LptA enhances gonococcal defence against human neutrophils. *Cell Microbiol.* 17, 910–921. doi: 10.1111/cmi.12411
- Hill, S. A., Belland, R. J., and Wilson, J. (1998). The *ihf* mRNA levels decline as *Neisseria gonorrhoeae* enters the stationary growth phase. *Gene* 215, 303–310. doi: 10.1016/S0378-1119(98)00285-6
- Hobbs, M. M., Anderson, J. E., Balthazar, J. T., Kandler, J. L., Carlson, R. W., Ganguly, J., et al. (2013). Lipid A's structure mediates *Neisseria gonorrhoeae* fitness during experimental infection of mice and men. *mBio* 4:e892-13. doi: 10.1128/mBio.00892-13
- Horton, R. E., and Vidarsson, G. (2013). Antibodies and their receptors: different potential roles in mucosal defense. *Front. Immunol.* 4:200. doi: 10.3389/fimmu.2013.00200
- Jerse, A. E., and Deal, C. D. (2013). Vaccine research for gonococcal infections: where are we? *Sex Transm. Infect.* 89(Suppl. 4), iv63–iv68. doi: 10.1136/sextrans-2013-051225
- John, C. M., Liu, M., Phillips, N. J., Yang, Z., Funk, C. R., Zimmerman, L. I., et al. (2012). Lack of lipid A pyrophosphorylation and functional *lptA* reduces inflammation by *Neisseria* commensals. *Infect. Immun.* 80, 4014–4026. doi: 10.1128/IAI.00506-12
- John, C. M., Phillips, N. J., Din, R., Liu, M., Rosenqvist, E., Hoiby, E. A., et al. (2016). Lipooligosaccharide structures of invasive and carrier isolates of *Neisseria meningitidis* are correlated with pathogenicity and carriage. *J. Biol. Chem.* 291, 3224–3238. doi: 10.1074/jbc.M115.666214
- Johnson, K. G., Perry, M. B., McDonald, I. J., and Russel, R. R. (1975). Cellular and free lipopolysaccharides of some species of *Neisseria*. *Can. J. Microbiol.* 21, 1969–1980. doi: 10.1139/m75-285
- Johnson, M. B., and Criss, A. K. (2013). *Neisseria gonorrhoeae* phagosomes delay fusion with primary granules to enhance bacterial survival inside human neutrophils. *Cell Microbiol.* 15, 1323–1340. doi: 10.1111/cmi.12117
- Kahler, C. M., Carlson, R. W., Rahman, M. M., Martin, L. E., and Stephens, D. S. (1996). Inner core biosynthesis of lipooligosaccharide (LOS) in *Neisseria meningitidis* serogroup B: identification and role in LOS assembly of the alpha1,2 *N*-acetylglucosamine transferase (RfaK). *J. Bacteriol.* 178, 1265–1273. doi: 10.1128/jb.178.5.1265-1273.1996
- Kahler, C. M., Lyons-Schindler, S., Choudhury, B., Glushka, J., Carlson, R. W., and Stephens, D. S. (2006). *O*-Acetylation of the terminal *N*-acetylglucosamine of the lipooligosaccharide inner core in *Neisseria meningitidis*. Influence on inner core structure and assembly. *J. Biol. Chem.* 281, 19939–19948. doi: 10.1074/jbc.M601308200
- Kandler, J. L., Joseph, S. J., Balthazar, J. T., Dhulipala, V., Read, T. D., Jerse, A. E., et al. (2014). Phase-variable expression of *lptA* modulates the resistance of *Neisseria gonorrhoeae* to cationic antimicrobial peptides. *Antimicrob. Agents Chemother.* 58, 4230–4233. doi: 10.1128/AAC.03108-14
- Kuhdari, P., Stefanati, A., Lupi, S., Valente, N., and Gabutti, G. (2016). Meningococcal B vaccination: real-world experience and future perspectives. *Pathog. Global Health* 110, 148–156. doi: 10.1080/20477724.2016.1195072
- Lahra, M. M., Martin, I., Demczuk, W., Jennison, A. V., Lee, K. I., Nakayama, S. I., et al. (2018). Cooperative recognition of internationally disseminated ceftriaxone-resistant *Neisseria gonorrhoeae* strain. *Emerg. Infect. Dis.* 24, 735–745.
- Lee, E.-H., Hill, S. A., Napier, R., and Shafer, W. M. (2006). Integration host factor is required for FarR repression of the *farAB*-encoded efflux pump of *Neisseria gonorrhoeae*. *Mol. Microbiol.* 60, 1381–1400. doi: 10.1111/j.1365-2958.2006.05185.x
- Lewis, L. A., Choudhury, B., Balthazar, J. T., Martin, L. E., Ram, S., Rice, P. A., et al. (2009). Phosphoethanolamine substitution of lipid A and resistance of *Neisseria gonorrhoeae* to cationic antimicrobial peptides and complement-mediated killing by normal human serum. *Infect. Immun.* 77, 1112–1120. doi: 10.1128/IAI.01280-08
- Lewis, L. A., and Ram, S. (2014). Meningococcal disease and the complement system. *Virulence* 5, 98–126. doi: 10.4161/viru.26515
- Lewis, L. A., Shafer, W. M., Dutta Ray, T., Ram, S., and Rice, P. A. (2013). Phosphoethanolamine residues on the lipid A moiety of *Neisseria gonorrhoeae* lipooligosaccharide modulate binding of complement inhibitors and resistance to complement killing. *Infect. Immun.* 81, 33–42. doi: 10.1128/IAI.00751-12
- Liu, M., John, C. M., and Jarvis, G. A. (2010). Phosphoryl moieties of lipid A from *Neisseria meningitidis* and *N. gonorrhoeae* lipooligosaccharides play an important role in activation of both MyD88- and TRIF-dependent TLR4-MD-2 signaling pathways. *J. Immunol.* 185, 6974–6984. doi: 10.4049/jimmunol.1000953
- Liu, X., Wetzler, L. M., Nascimento, L. O., and Massari, P. (2010). Human airway epithelial cell responses to *Neisseria lactamica* and purified porin via Toll-like receptor 2-dependent signaling. *Infect. Immun.* 78, 5314–5323. doi: 10.1128/IAI.00681-10
- Liu, Y., Perez, J., Hammer, L. A., Gallagher, H. C., De Jesus, M., Egilmez, N. K., et al. (2018). Intravaginal administration of interleukin 12 during genital gonococcal infection in mice induces immunity to heterologous strains of *Neisseria gonorrhoeae*. *mSphere* 3:e421-17.
- Mackinnon, F. G., Cox, A. D., Plested, J. S., Tang, C. M., Makepeace, K., Coull, P. A., et al. (2002). Identification of a gene (*lpt-3*) required for the addition of phosphoethanolamine to the lipopolysaccharide inner core of *Neisseria meningitidis* and its role in mediating susceptibility to bactericidal killing and opsonophagocytosis. *Mol. Microbiol.* 43, 931–943. doi: 10.1046/j.1365-2958.2002.02754.x
- Malott, R. J., Keller, B. O., Gaudet, R. G., Mccaw, S. E., Lai, C. C., Dobson-Belaire, W. N., et al. (2013). *Neisseria gonorrhoeae*-derived heptose elicits an innate immune response and drives HIV-1 expression. *Proc. Natl. Acad. Sci. U.S.A.* 110, 10234–10239. doi: 10.1073/pnas.1303738110
- Mandrell, R. E., and Apicella, M. A. (1993). Lipo-oligosaccharides (LOS) of mucosal pathogens: molecular mimicry and host-modification of LOS. *Immunobiology* 187, 382–402.
- Mandrell, R. E., Griffiss, J. M., and Macher, B. A. (1988). Lipooligosaccharides (LOS) of *Neisseria gonorrhoeae* and *Neisseria meningitidis* have components that are immunochemically similar to precursors of human blood group antigens. Carbohydrate sequence specificity of the mouse monoclonal antibodies that recognize crossreacting antigens on LOS and human erythrocytes. *J. Exp. Med.* 168, 107–126.
- Mowlaboccus, S., Jolley, K. A., Bray, J. E., Pang, S., Lee, Y. T., Bew, J. D., et al. (2017). Clonal expansion of new penicillin-resistant clade of *Neisseria meningitidis* serogroup W clonal complex 11, australia. *Emerg. Infect. Dis.* 23, 1364–1367. doi: 10.3201/eid2308.170259
- Munguia, J., and Nizet, V. (2017). Pharmacological targeting of the host-pathogen interaction: alternatives to classical antibiotics to combat drug-resistant superbugs. *Trends Pharmacol. Sci.* 38, 473–488. doi: 10.1016/j.tips.2017.02.003
- Newman, L., Rowley, J., Vander Hoorn, S., Wijesooriya, N. S., Unemo, M., Low, N., et al. (2015). Global estimates of the prevalence and incidence of four curable sexually transmitted infections in 2012 based on systematic review and global reporting. *PLoS One* 10:e0143304. doi: 10.1371/journal.pone.0143304
- Ohnishi, M., Golparian, D., Shimuta, K., Saika, T., Hoshina, S., Iwasaku, K., et al. (2011). Is *Neisseria gonorrhoeae* initiating a future era of untreatable gonorrhea?: detailed characterization of the first strain with high-level resistance to ceftriaxone. *Antimicrob. Agents Chemother.* 55, 3538–3545. doi: 10.1128/AAC.00325-11
- Packiam, M., Yedery, R. D., Begum, A. A., Carlson, R. W., Ganguly, J., Sempowski, G. D., et al. (2014). Phosphoethanolamine decoration of *Neisseria gonorrhoeae* lipid A plays a dual immunostimulatory and protective role during experimental genital tract infection. *Infect. Immun.* 82, 2170–2179. doi: 10.1128/IAI.01504-14
- Park, B. S., Song, D. H., Kim, H. M., Choi, B. S., Lee, H., and Lee, J. O. (2009). The structural basis of lipopolysaccharide recognition by the TLR4-MD-2 complex. *Nature* 458, 1191–1195. doi: 10.1038/nature07830
- Perrin, A., Bonacorsi, S., Carbone, E., Talibi, D., Dessen, P., Nassif, X., et al. (2002). Comparative genomics identifies the genetic islands that distinguish *Neisseria meningitidis*, the agent of cerebrospinal meningitis, from other *Neisseria* species. *Infect. Immun.* 70, 7063–7072.
- Petousis-Harris, H., Paynter, J., Morgan, J., Saxton, P., Mcardle, B., Goodyear-Smith, F., et al. (2017). Effectiveness of a group B outer membrane vesicle meningococcal vaccine against gonorrhoea in New Zealand: a retrospective case-control study. *Lancet* 390, 1603–1610. doi: 10.1016/S0140-6736(17)31449-6

- Public Health England (2018). *UK Case of Neisseria Gonorrhoeae with High-Level Resistance to Azithromycin and Resistance to Ceftriaxone Acquired Abroad. Health Protection Report Advanced Access Report*. London: Public Health England.
- Piek, S., and Kahler, C. M. (2012). A comparison of the endotoxin biosynthesis and protein oxidation pathways in the biogenesis of the outer membrane of *Escherichia coli* and *Neisseria meningitidis*. *Front. Cell Infect Microbiol.* 2:162. doi: 10.3389/fcimb.2012.00162
- Piek, S., Wang, Z., Ganguly, J., Lakey, A. M., Bartley, S. N., Mowlaboccus, S., et al. (2014). The role of oxidoreductases in determining the function of the neisserial lipid A phosphoethanolamine transferase required for resistance to polymyxin. *PLoS One* 9:e106513. doi: 10.1371/journal.pone.0106513
- Pizza, M., and Rappuoli, R. (2015). *Neisseria meningitidis*: pathogenesis and immunity. *Curr. Opin. Microbiol.* 23, 68–72. doi: 10.1016/j.mib.2014.11.006
- Pizza, M. S. (2018). *Vaccines For Neisseria Gonorrhoeae*. United States patent application 20180064801.
- Quillin, S. J., and Seifert, H. S. (2018). *Neisseria gonorrhoeae* host adaptation and pathogenesis. *Nat. Rev. Microbiol.* 16, 226–240. doi: 10.1038/nrmicro.2017.169
- Ram, S., Mackinnon, F. G., Gulati, S., Mcquillen, D. P., Vogel, U., Frosch, M., et al. (1999). The contrasting mechanisms of serum resistance of *Neisseria gonorrhoeae* and group B *Neisseria meningitidis*. *Mol. Immunol.* 36, 915–928.
- Ram, S., Shaughnessy, J., Deoliveira, R. B., Lewis, L. A., Gulati, S., and Rice, P. A. (2016). Utilizing complement evasion strategies to design complement-based antibacterial immunotherapeutics: lessons from the pathogenic neisseriae. *Immunobiology* 221, 1110–1123. doi: 10.1016/j.imbio.2016.05.016
- Rice, P. A. (2005). Gonococcal arthritis (disseminated gonococcal infection). *Infect. Dis. Clin. North Am.* 19, 853–861. doi: 10.1016/j.idc.2005.07.003
- Rice, P. A., Shafer, W. M., Ram, S., and Jerse, A. E. (2017). *Neisseria gonorrhoeae*: drug resistance, mouse models, and vaccine development. *Annu. Rev. Microbiol.* 71, 665–686. doi: 10.1146/annurev-micro-090816-093530
- Sinha, S., Ambur, O. H., Langford, P. R., Tonjum, T., and Kroll, J. S. (2008). Reduced DNA binding and uptake in the absence of DsbA1 and DsbA2 of *Neisseria meningitidis* due to inefficient folding of the outer-membrane secretin PilQ. *Microbiology* 154, 217–225. doi: 10.1099/mic.0.2007/010496-0
- Stephens, D. S., Greenwood, B., and Brandtzaeg, P. (2007). Epidemic meningitis, meningococcaemia, and *Neisseria meningitidis*. *Lancet* 369, 2196–2210. doi: 10.1016/S0140-6736(07)61016-2
- Takahashi, H., Carlson, R. W., Muszynski, A., Choudhury, B., Kim, K. S., Stephens, D. S., et al. (2008). Modification of lipooligosaccharide with phosphoethanolamine by LptA in *Neisseria meningitidis* enhances meningococcal adhesion to human endothelial and epithelial cells. *Infect. Immun.* 76, 5777–5789. doi: 10.1128/IAI.00676-08
- Tinsley, C. R., Voulhoux, R., Beretti, J. L., Tommassen, J., and Nassif, X. (2004). Three homologues, including two membrane-bound proteins, of the disulfide oxidoreductase DsbA in *Neisseria meningitidis*: effects on bacterial growth and biogenesis of functional type IV pili. *J. Biol. Chem.* 279, 27078–27087.
- Tommassen, J., and Arenas, J. (2017). Biological functions of the secretome of *Neisseria meningitidis*. *Front. Cell Infect Microbiol.* 7:256. doi: 10.3389/fcimb.2017.00256
- Tzeng, Y. L., Ambrose, K. D., Zughaier, S., Zhou, X., Miller, Y. K., Shafer, W. M., et al. (2005). Cationic antimicrobial peptide resistance in *Neisseria meningitidis*. *J. Bacteriol.* 187, 5387–5396.
- Tzeng, Y. L., and Stephens, D. S. (2015). Antimicrobial peptide resistance in *Neisseria meningitidis*. *Biochim. Biophys. Acta* 1848, 3026–3031. doi: 10.1016/j.bbame.2015.05.006
- Unemo, M., Del Rio, C., and Shafer, W. M. (2016). Antimicrobial resistance expressed by *Neisseria gonorrhoeae*: a major global public health problem in the 21st century. *Microbiol. Spectr.* 4. doi: 10.1128/microbiolspec.EI10-0009-2015 [Epub ahead of print].
- Unemo, M., and Shafer, W. M. (2014). Antimicrobial resistance in *Neisseria gonorrhoeae* in the 21st century: past, evolution, and future. *Clin. Microbiol. Rev.* 27, 587–613. doi: 10.1128/CMR.00010-14
- Vivian, J. P., Scoullar, J., Rimmer, K., Bushell, S. R., Beddoe, T., Wilce, M. C., et al. (2009). Structure and function of the oxidoreductase DsbA1 from *Neisseria meningitidis*. *J. Mol. Biol.* 394, 931–943. doi: 10.1016/j.jmb.2009.09.065
- Vivian, J. P., Scoullar, J., Robertson, A. L., Bottomley, S. P., Horne, J., Chin, Y., et al. (2008). Structural and biochemical characterization of the oxidoreductase NmDsbA3 from *Neisseria meningitidis*. *J. Biol. Chem.* 283, 32452–32461. doi: 10.1074/jbc.M803990200
- Wanty, C., Anandan, A., Piek, S., Walshe, J., Ganguly, J., Carlson, R. W., et al. (2013). The structure of the neisserial lipooligosaccharide phosphoethanolamine transferase A (LptA) required for resistance to polymyxin. *J. Mol. Biol.* 425, 3389–3402. doi: 10.1016/j.jmb.2013.06.029
- Whiley, D. M., Jennison, A., Pearson, J., and Lahra, M. M. (2018). Genetic characterisation of *Neisseria gonorrhoeae* resistant to both ceftriaxone and azithromycin. *Lancet Infect. Dis.* 18, 717–718. doi: 10.1016/S1473-3099(18)30340-2
- Winthrop, K. L., Mariette, X., Silva, J. T., Benamu, E., Calabrese, L. H., Dumusc, A., et al. (2018). ESCMID study group for infections in compromised hosts (ESGICH) consensus document on the safety of targeted and biological therapies: an infectious diseases perspective (Soluble immune effector molecules [II]: agents targeting interleukins, immunoglobulins and complement factors). *Clin. Microbiol. Infect.* 24, S21–S40. doi: 10.1016/j.cmi.2018.02.002
- Yezli, S., Assiri, A. M., Alhakeem, R. F., Turkistani, A. M., and Alotaibi, B. (2016). Meningococcal disease during the Hajj and Umrah mass gatherings. *Int. J. Infect. Dis.* 47, 60–64. doi: 10.1016/j.ijid.2016.04.007
- Zimmer, S. M., Zughaier, S. M., Tzeng, Y. L., and Stephens, D. S. (2007). Human MD-2 discrimination of meningococcal lipid A structures and activation of TLR4. *Glycobiology* 17, 847–856.
- Zughaier, S. M., Kandler, J. L., Balthazar, J. T., and Shafer, W. M. (2015). Phosphoethanolamine modification of *Neisseria gonorrhoeae* lipid A reduces autophagy flux in macrophages. *PLoS One* 10:e0144347. doi: 10.1371/journal.pone.0144347
- Zughaier, S. M., Lindner, B., Howe, J., Garidel, P., Koch, M. H., Brandenburg, K., et al. (2007). Physicochemical characterization and biological activity of lipooligosaccharides and lipid A from *Neisseria meningitidis*. *J. Endotoxin. Res.* 13, 343–357. doi: 10.1177/0968051907084435
- Zughaier, S. M., Zimmer, S. M., Datta, A., Carlson, R. W., and Stephens, D. S. (2005). Differential induction of the Toll-like receptor 4-MyD88-dependent and -independent signaling pathways by endotoxins. *Infect. Immun.* 73, 2940–2950.

**Conflict of Interest Statement:** The authors declare that the research was conducted in the absence of any commercial or financial relationships that could be construed as a potential conflict of interest.

Copyright © 2018 Kahler, Nawrocki, Anandan, Vrielink and Shafer. This is an open-access article distributed under the terms of the Creative Commons Attribution License (CC BY). The use, distribution or reproduction in other forums is permitted, provided the original author(s) and the copyright owner(s) are credited and that the original publication in this journal is cited, in accordance with accepted academic practice. No use, distribution or reproduction is permitted which does not comply with these terms.



# Bacterial Strategies to Preserve Cell Wall Integrity Against Environmental Threats

Akhilesh K. Yadav, Akbar Espaillet and Felipe Cava\*

Laboratory for Molecular Infection Medicine Sweden, Department of Molecular Biology, Umeå Centre for Microbial Research, Umeå University, Umeå, Sweden

## OPEN ACCESS

### Edited by:

Christopher Davies,  
Medical University of South Carolina,  
United States

### Reviewed by:

Joseph P. Dillard,  
University of Wisconsin–Madison,  
United States  
Ivo G. Boneca,  
Institut Pasteur, France

### \*Correspondence:

Felipe Cava  
felipe.cava@umu.se;  
felipe.cava@molbiol.umu.se

### Specialty section:

This article was submitted to  
Antimicrobials, Resistance  
and Chemotherapy,  
a section of the journal  
Frontiers in Microbiology

**Received:** 27 March 2018

**Accepted:** 13 August 2018

**Published:** 31 August 2018

### Citation:

Yadav AK, Espaillet A and Cava F  
(2018) Bacterial Strategies  
to Preserve Cell Wall Integrity Against  
Environmental Threats.  
Front. Microbiol. 9:2064.  
doi: 10.3389/fmicb.2018.02064

Bacterial cells are surrounded by an exoskeleton-like structure, the cell wall, composed primarily of the peptidoglycan (PG) sacculus. This structure is made up of glycan strands cross-linked by short peptides generating a covalent mesh that shapes bacteria and prevents their lysis due to their high internal osmotic pressure. Even though the PG is virtually universal in bacteria, there is a notable degree of diversity in its chemical structure. Modifications in both the sugars and peptides are known to be instrumental for bacteria to cope with diverse environmental challenges. In this review, we summarize and discuss the cell wall strategies to withstand biotic and abiotic environmental insults such as the effect of antibiotics targeting cell wall enzymes, predatory PG hydrolytic proteins, and PG signaling systems. Finally we will discuss the opportunities that species-specific PG variability might open to develop antimicrobial therapies.

**Keywords:** peptidoglycan, lysozyme, antibiotic resistance, innate immunity, plasticity

## INTRODUCTION

The presence of peptidoglycan (PG) as a key component of the bacterial cell wall is one of the defining characteristics of bacteria. PG is an exoskeleton-like macromolecule that envelopes the bacterial cell, preventing them from lysis through osmotic pressure and preserving their shape. PG is composed of  $\beta$ -1,4 linked glycan strands of *N*-acetyl muramic acid (NAM) and *N*-acetyl glucosamine (NAG), cross-linked by short peptide chains. The sugar moieties' composition is shared by both Gram-negative and Gram-positive bacteria while the nature of their peptides differ between them. In the majority of the analyzed Gram-negative bacteria the basic peptide structure is L-Ala-D-Glu-*meso*DAP-D-Ala-D-Ala while in Gram-positives, the most frequent third amino acid is Lys (Vollmer et al., 2008). Additionally, the cell wall is subjected to numerous changes associated with both the growth cycle and environmental challenges (e.g., antibiotic treatment) (Schneider and Sahl, 2010; Cava and de Pedro, 2014). These changes could occur both in the peptide and/or in the sugar moieties (Vollmer et al., 2008). For instance, PG peptide stems present D-amino acids, which have been suggested to serve as a protection from most of the secreted proteases. However, there are peptidases that can target specifically the muropeptide stems (Uehara and Bernhardt, 2011). Some of these PG-peptidases can target a bacterial cell by different means such as their injection via contact-dependent Type VI secretion system (T6SS). Recent studies have reported the existence of PG modifications, which work as protection mechanisms against these predatory enzymes (Espaillet et al., 2016). Similarly, the sugar moieties are also the target of diverse host secreted antimicrobials such as the lysozyme, a hydrolytic enzyme that cleaves the  $\beta$ -1, 4-glycosidic bond between the NAM and NAG. Some bacteria have devised strategies

to overcome host lysozyme-mediated lysis by chemical modification of the NAG and NAM sugars, thereby helping bacteria to evade the host immune system.

As cell wall is fundamental for survival, its chemical structure might follow the dynamics proposed by the Red Queen hypothesis effect (Liow et al., 2011), an evolutionary arms race where bacteria would alter the PG chemical structure in order to overcome specific threats to the cell wall. For example, structural variations in the basic moiety of the tracheal cytotoxin (i.e., NAG-anhydro-NAM-tetrapeptide) could lead to a weaker innate immune response (Luker et al., 1995; Knilans et al., 2017). Also, certain pathogens might manipulate the host metabolism as a strategy to evade the immune system and to increase their access to carbon sources (McConville, 2014; Passalacqua et al., 2016). In this review, we summarize PG modifications (**Figure 1** and **Table 1**) that confer protection to diverse antimicrobials, hydrolases and to the innate immune system.

## MODIFICATIONS IN PEPTIDOGLYCAN SUGAR MOIETIES

The sugars present in the glycan backbone of the PG possess the same central chemical skeleton. NAM is the lactic acid ether of NAG and the structural variations in both the sugars are limited to the  $-NH_2$  group at C-2 and the  $-OH$  group at C-6 of the sugars.

### N-Deacetylation of NAG

The N-deacetylation, removal of the acetyl group at position C-2, from NAG is catalyzed by the enzyme PgdA (Vollmer and Tomasz, 2000). NAG deacetylation is mostly reported in Gram-positive bacteria, e.g., *Bacillus cereus* (Psylinakis et al., 2005), *Enterococcus faecalis* (Benachour et al., 2012), *Clostridium difficile* (Peltier et al., 2011), *Streptococcus suis* and *Streptococcus iniae* (Fittipaldi et al., 2008; Milani et al., 2010). To our knowledge, *Helicobacter pylori* (Wang et al., 2009) and *Shigella flexneri* (Kaoukab-Raji et al., 2012) are the only Gram-negative bacteria having a putative NAG deacetylase homolog.

Mutants in *pgdA* in various bacterial strains are more sensitive to lysozyme and less virulent, thereby NAG deacetylation appears to protect cell wall integrity during infection and also plays a role in evading the host immune system (Vollmer and Tomasz, 2002; Boneca et al., 2007; Wang et al., 2009, 2010; Benachour et al., 2012). In fact, oxidative stress works as environmental trigger for PgdA induction in *H. pylori* (Wang et al., 2009) linking further its function to infection. In *Listeria monocytogenes*, the activity of PgdA is regulated by the cell division proteins GpsB and PBP1A. Deletion of *gpsB* in this bacterium causes an increase in deacetylated muropeptides that leads to a lysozyme resistance phenotype. This phenotype is, however, suppressed upon deletion of PBP1A, thereby underscoring that: (i) besides its PG synthetic activity, PBP1A also serves as an important regulatory partner (Claessen et al., 2008) and, (ii) the relevance of these protein-protein interactions to regulate PgdA cellular activity (Rismondo et al., 2016, 2018). In addition to protecting PG from lysozyme's action, NAG deacetylation plays also an important role in bacterial predation. *Bdellovibrio* is

a bacterium that preys on other Gram-negatives by invading their periplasmic space followed by the release of PG hydrolytic enzymes that digest the prey's cell wall. During this predator-prey interaction, *Bdellovibrio* deacetylates its own PG to prevent autolysis (Lambert et al., 2016). Similarly, deacetylation also enables coping with the presence of major autolysins in other bacteria, e.g., *Lactobacillus lactis* N-deacetylation decreases the susceptibility of PG to the major autolysin AcmA (Meyrand et al., 2007).

*Helicobacter pylori* PgdA deacetylase activity was suggested *in vitro* using an assay that measured the release of acetic acid from undigested PG (Wang et al., 2009). However, in another study, PgdA failed to deacetylate a variety of possible substrates (e.g., NAG, NAG<sub>3</sub>, etc.) (Shaik et al., 2011) suggesting that further studies will be necessary to identify the actual substrate of this enzyme.

N-deacetylation of NAG also helps the bacterium to evade the host immune system. *L. monocytogenes*' deacetylated PG presents a reduced recognition by the NOD1 receptor while PG from the *pgdA* mutant (fully acetylated PG) induces a massive NOD1-dependent IFN- $\beta$  response (Boneca et al., 2007). In a similar way, a fully N-deacetylated *H. pylori* PG (using the N-deacetylase from *B. cereus*) completely lost its ability to be sensed *in vitro* by both NOD1 and NOD2 receptors (Boneca et al., 2007), and *Bacillus anthracis* PG containing 88% deacetylated NAG induces very little or no NLRP3 inflammasome activation (Wolf et al., 2016). The reduced recognition of deacetylated PG by NOD1 results also from the inability of lysozyme to degrade it, which limits the availability of NOD1 agonist to the host and thus a weaker innate immune response. While in case of NOD2, the incapability of the receptor to sense the deacetylated PG also contributes to a weaker response (Boneca et al., 2007; Wang et al., 2009; Melnyk et al., 2015). Further details about the innate immune system are in the subsection "Chemical modifications as innate immune modulators."

### N-Deacetylation of NAM

PdaA and PdaC from *Bacillus subtilis* catalyze the removal of the acetyl group from the NAM. *pdaC* deletion mutant shows an increased sensitivity to lysozyme (Kobayashi et al., 2012), while the *pdaA* mutant fails to germinate, given that this activity is implicated in the  $\delta$ -lactam formation of *B. subtilis* spore cell wall (Fukushima et al., 2002). PdaA is active on denuded PG chains (i.e., PG pre-treated with CwlD, an N-acetylmuramoyl-L-alanine amidase, which cleaves the peptide stems) (Gilmour et al., 2004). Although, this activity is important for the spore cortex development in *B. subtilis*, homologs of this enzyme are also encoded in the genome of other non-spore forming microorganisms, e.g., *Rhizobium leguminosarum* (Fukushima et al., 2005). Therefore, the biological implications of PdaA like enzymes in non-sporulating bacteria still need to be determined. One hypothesis is that this activity could help bacteria to evade the innate immune system, as a study on various synthetic structural analogs of muramyl dipeptide (MDP) on NOD2 shows that the acetyl group in NAM is required for binding of MDP to the NOD2 receptor and the activation of the subsequent signaling cascade (Melnyk et al., 2015).



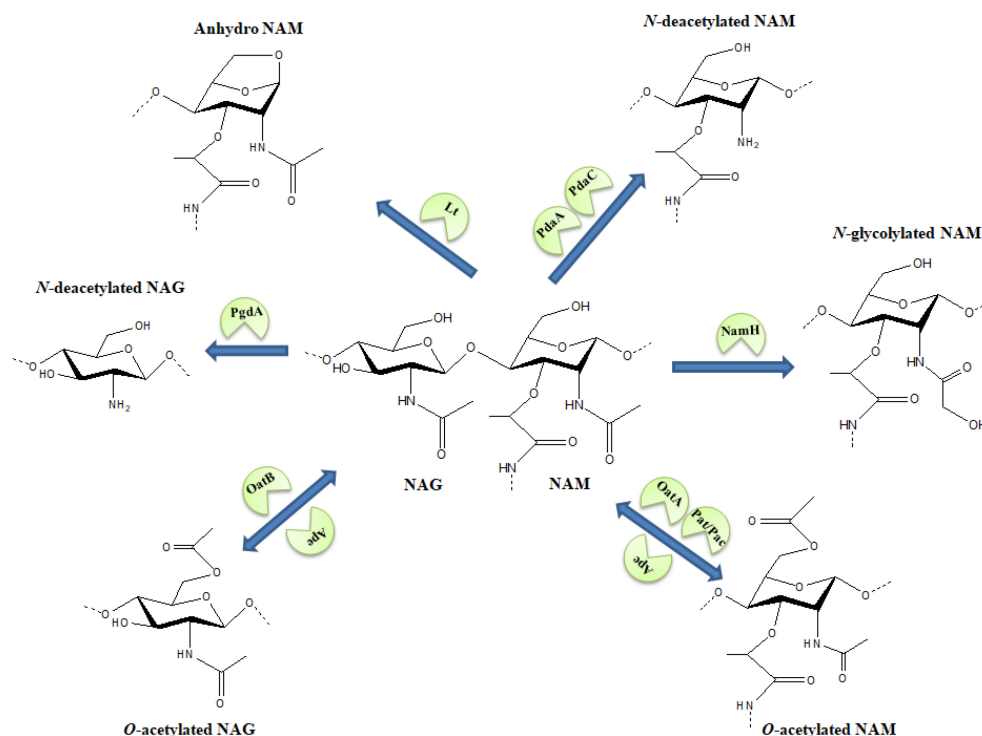


**FIGURE 1 |** Schematic representation of various modifications in the *N*-acetylmuramic acid (NAM) and *N*-acetylglucosamine (NAG) sugar structures. Arrows carry the responsible enzymes which catalyze the modification. O-acetylation of NAG or NAM is a reversible modification where OatA/OatB and Pat/Pac enzymes facilitate the O-acetylation of sugars while Ape works as a de-O-acetylase for the modification. Lr-lytic transglycosylase.

## N-Glycolylation of NAM

Four *Mycobacterium* species namely *Mycobacterium smegmatis*, *M. kansasii*, *M. tuberculosis*, and *M. phlei* present *N*-glycolylated NAM residues, a PG modification catalyzed by NamH (Azuma et al., 1970). In *M. smegmatis*, *namH* deletion causes increased susceptibility to  $\beta$ -lactam antibiotics and lysozyme (Raymond et al., 2005). Although, *N*-glycolylated NAM confers an enhanced NOD2 recognition, this PG modification seems to have a limited role in *M. tuberculosis* infection (Coulombe et al., 2009; Hansen et al., 2013).

The degree of *N*-glycolylation in the PG varies between species and in response to different antibiotics. *M. tuberculosis* treated with D-cycloserine contains only *N*-glycolyl muramic acid, while similarly treated *M. smegmatis* displays a mixture of *N*-glycolylated and *N*-acetylated PG. Similarly, vancomycin treatment of *M. smegmatis*, consisted of *N*-glycolyl NAM residues only, while in *M. tuberculosis*, this treatment produces a mixture of both the *N*-glycolyl and *N*-acetyl NAM residues (Mahapatra et al., 2005). Blocking PG synthesis at the precursor level (e.g., by vancomycin or D-cycloserine) increases *N*-glycolylation, which is in agreement with NamH being cytoplasmic and acting on the UDP precursor pool.

## O-Acetylation of NAM

*N*-acetyl muramic acid O-acetylation occurs at the OH group of the C6 of the sugar moiety. Acetylation of NAM seems to

be the most widespread PG modification across a great number of Gram-negative and Gram-positive bacteria. Conventionally, the NAM O-acetylation in Gram-positive bacteria is catalyzed by the O-acetyl transferase OatA (Bera et al., 2005; Rae et al., 2011; Bernard et al., 2012), whereas in Gram-negative bacteria is carried out by a family of enzymes, called Pat or Pac (Dillard and Hackett, 2005; Weadge et al., 2005; Moynihan and Clarke, 2010). Interestingly, *B. anthracis* uses both families of PG O-acetyltransferases, i.e., Oat and Pat/Pac. PatA1 and PatA2 is required for separation of *B. anthracis* cells, as well as for proper assembly and attachment of its S-layer (Laaberki et al., 2011). O-acetyl transferases Adr and OatA play an important role in cell division of *Streptococcus pneumoniae* and *Lactobacillus plantarum*, respectively (Bernard et al., 2012; Bonnet et al., 2017).

*N*-acetyl muramic acid O-acetylation confers lysozyme resistance (Bera et al., 2005; Shimada et al., 2010; Bernard et al., 2012) by preventing lysozyme binding to PG due to steric hindrance caused by the bulky acetyl group (Pushkaran et al., 2015). Deletion mutants of *pata* and *patB* in *Campylobacter jejuni* exhibited decreased lysozyme resistance and intracellular survival in macrophage cells (Iwata et al., 2016) while these activities have a minimal impact on *C. jejuni*'s growth and fitness *in vitro* (Ha et al., 2016). In Gram-negative bacteria, O-acetylation occurs as a result of the coordinated action of the enzymes PatA and PatB where PatA translocates the acetyl group from the cytoplasm to periplasm and PatB catalyzes the transfer of acetyl groups to NAM (Iwata et al., 2016). Deletion

**TABLE 1 |** List of bacterial species comprising various modifications in the sugar moieties of PG.

Modifications	Bacterial species	Reference
N-deacetylation of NAG	Gram-negative	
	<i>Helicobacter pylori</i>	Wang et al., 2009
	<i>Shigella flexneri</i>	Kaoukab-Raji et al., 2012
	Gram-positive	
	<i>Bacillus anthracis</i>	Psylinakis et al., 2005
	<i>Bacillus cereus</i>	Psylinakis et al., 2005
	<i>Bacillus subtilis</i>	Atrih et al., 1999
	<i>Clostridium difficile</i>	Peltier et al., 2011
	<i>Enterococcus faecalis</i>	Benachour et al., 2012
	<i>Lactobacillus fermentum</i>	Logardt and Neujahr, 1975
	<i>Lactobacillus lactis</i>	Meyrand et al., 2007
	<i>Listeria monocytogenes</i>	Boneca et al., 2007
	<i>Streptococcus iniae</i>	Milani et al., 2010
	<i>Streptococcus pneumoniae</i>	Vollmer and Tomasz, 2000
	<i>Streptococcus suis</i>	Fittipaldi et al., 2008
	<i>Bacillus subtilis</i>	Fukushima et al., 2005
N-deacetylation of NAM		
N-glycosylation of NAM	<i>Mycobacterium kansasii</i>	Azuma et al., 1970
	<i>Mycobacterium phlei</i>	Azuma et al., 1970
	<i>Mycobacterium smegmatis</i>	Azuma et al., 1970
	<i>Mycobacterium tuberculosis</i>	Azuma et al., 1970
O-acetylation of NAM	Gram-negative	
	<i>Agrobacterium tumefaciens</i>	Weadge et al., 2005
	<i>Bacteroides fragilis</i>	Weadge et al., 2005
	<i>Bacteroides thetaiotamicron</i>	Weadge et al., 2005
	<i>Bradyrhizobium japonicum</i>	Weadge et al., 2005
	<i>Campylobacter jejuni</i>	Ha et al., 2016
	<i>Chromobacterium violaceum</i>	Weadge et al., 2005
	<i>Helicobacter pylori</i>	Wang et al., 2012
	<i>Moraxella glucidolytica</i>	Martin et al., 1973
	<i>Morganella morganii</i>	Clarke, 1993
	<i>Neisseria gonorrhoeae</i>	Dillard and Hackett, 2005
	<i>Neisseria meningitidis</i>	Dillard and Hackett, 2005
	<i>Neisseria perflava</i>	Martin et al., 1973
	<i>Photobacterium luminescens</i>	Weadge et al., 2005
	<i>Providencia alcalifaciens</i>	Clarke, 1993
	<i>Providencia stuartii</i>	Clarke, 1993
	<i>Providencia rettgeri</i>	Clarke, 1993
	<i>Providencia heinbachae</i>	Clarke, 1993
	<i>Providencia rustigianii</i>	Clarke, 1993
	<i>Proteus mirabilis</i>	Clarke, 1993
	<i>Proteus myxofaciens</i>	Clarke, 1993
	<i>Proteus penneri</i>	Clarke, 1993
	<i>Proteus vulgaris</i>	Clarke, 1993
	<i>Pseudomonas alcaligenes</i>	Martin et al., 1973
	Gram-positive	
	<i>Bacillus anthracis</i>	Laaberki et al., 2011
	<i>Bacillus cereus</i>	Weadge et al., 2005
	<i>Bacillus subtilis</i>	Guariglia-Oropeza and Helmann, 2011

(Continued)

**TABLE 1 |** Continued

Modifications	Bacterial species	Reference
	<i>Enterococcus faecalis</i>	Pfeffer et al., 2006
	<i>Enterococcus durans</i>	Pfeffer et al., 2006
	<i>Enterococcus faecium</i>	Pfeffer et al., 2006
	<i>Enterococcus hirae</i>	Pfeffer et al., 2006
	<i>Lactobacillus casei</i>	Billot-Klein et al., 1997
	<i>Lactobacillus lactis</i>	Veiga et al., 2007
	<i>Lactobacillus plantarum</i>	Bernard et al., 2012
	<i>Lactobacillus fermentum</i>	Logardt and Neujahr, 1975
	<i>Lactobacillus acidophilus</i>	Coyette and Ghuysen, 1970
	<i>Listeria monocytogenes</i>	Rae et al., 2011
	<i>Macroccoccus caseolyticus</i>	Bera et al., 2006
	<i>Micrococcus luteus</i>	Brumfitt et al., 1958
	<i>Ruminococcus flavefaciens</i>	Weadge et al., 2005
	<i>Staphylococcus aureus</i>	Bera et al., 2006
	<i>Staphylococcus epidermidis</i>	Bera et al., 2006
	<i>Staphylococcus haemolyticus</i>	Bera et al., 2006
	<i>Staphylococcus hyicus</i>	Bera et al., 2006
	<i>Staphylococcus lugdunensis</i>	Bera et al., 2006
	<i>Staphylococcus saccharolyticus</i>	Bera et al., 2006
	<i>Staphylococcus saprophyticus</i>	Bera et al., 2006
O-acetylation of NAG	<i>Streptococcus pneumoniae</i>	Bonnet et al., 2017
	<i>Streptococcus faecalis</i>	Abrams, 1958
	<i>Lactobacillus plantarum</i>	Bernard et al., 2012
De-O-acetylation	<i>Campylobacter jejuni</i>	Ha et al., 2016
	<i>Neisseria meningitidis</i>	Veyrier et al., 2013
	<i>Neisseria gonorrhoeae</i>	Weadge and Clarke, 2006

mutant of *patA* in *H. pylori* is susceptible to lysozyme. Moreover, a simultaneous deletion of *patA* and the N-deacetylase *PgdA* makes *H. pylori* five times more sensitive to lysozyme and significantly impaired in intestinal colonization (Wang et al., 2012), highlighting the contribution of both enzymes in *H. pylori* virulence. Importantly, the absence of *PatB* and *Ape1* homologs in *H. pylori* suggests that further studies are needed to validate the role of *PatA* in the O-acetylation of this bacterium. In *Neisseria gonorrhoeae* and *Neisseria meningitidis*, *PacA*, and *PacB* are the enzymes required for NAM O-acetylation and associated lysozyme resistance (Dillard and Hackett, 2005). Lysozyme sensitivity of  $\Delta PacA$  in *N. gonorrhoeae* is dependent on the loss of two lytic transglycosylases *LtgA* and *LtgD*, which compromises the cell wall integrity and permits lysozyme to access the PG (Ragland et al., 2017). In vancomycin-resistant *E. faecalis*, vancomycin treatment increases cell wall O-acetylation, which leads to lysozyme resistance and enhanced virulence (Chang et al., 2017).

In some Gram-positive bacteria, e.g., *S. pneumoniae*, *L. monocytogenes*, and *B. anthracis* lysozyme resistance relies on both PG O-acetylation and N-deacetylation. Only a double mutant in both activities makes the PG susceptible to host lysozyme (Davis et al., 2008; Laaberki et al., 2011; Rae et al., 2011). The activity of *OatA* in *L. lactis* is regulated by the pyruvate oxidase *SpxB*, which is induced by the stress-responsive

two-component system, CesSR. Induction of OatA by this stress-signaling cascade renders lysozyme tolerance to *L. lactis* (Veiga et al., 2007).

Peptidoglycan O-acetylation also contributes to some physiological properties in bacteria other than providing the resistance to lysozyme. In *Staphylococcus aureus*, NAM O-acetylation helps to evade the immune system by repressing cytokine production required for differentiation of pro-inflammatory T helper cells (Sanchez et al., 2017). NAM O-acetylation also plays a role in septic arthritis. Gonococcal PG induces paw swelling in rats. Notably, O-acetylated PG fragments are more arthritogenic compared to non-O-acetylated PG (Fleming et al., 1986). These observations are further supported by a study in *S. aureus* strains which shows that the  $\Delta$ OatA mutant in *S. aureus* is less arthritogenic compared to its parental strain (Baranwal et al., 2017).

## O-Acetylation of NAG

Contrary to NAM O-acetylation, NAG O-acetylation is very infrequent in bacteria. To date, only *L. plantarum* has been reported to have O-acetylated NAG (Bernard et al., 2011). The O-acetylation reaction is catalyzed by the O-acetyltransferase OatB. Although O-acetylation of NAG plays no role in lysozyme resistance, it inhibits the activity of N-acetyl-glucosaminidase Acm2, a major autolysin of *L. plantarum* (Bernard et al., 2011).

## O-Deacetylation

As commented above, diverse bacterial species O-acetylate their PG to counteract lysozyme's cell wall hydrolytic activity. Additionally, O-acetylation also negatively regulates the activity of endogenous lytic transglycosylases, which require a free hydroxyl group at the C-6 position of NAM. Therefore, to coordinate both lytic and synthetic enzymes, bacteria encode the O-acetylsterase Ape for undoing the O-acetylation (Weadge et al., 2005). This activity is highly regulated as it only O-deacetylates mucopeptides with tripeptide stems. Mutants lacking *Ape1* in *C. jejuni* and *N. meningitidis* are defective in virulence and have increased chain length and altered cell size (Veyrier et al., 2013; Ha et al., 2016).

As lysozyme's PG hydrolytic activity is one of the first defense lines employed by the host immune system against bacterial pathogens, most of the above mentioned modifications in the PG glycan backbone that confer lysozyme resistance also improve virulence and/or persistence (Laaberki et al., 2011). For instance, viable but non-culturable (VBNC) *E. faecalis* cells have high levels of PG O-acetylation, which inhibits the action of lysozyme (Pfeffer et al., 2006). Interestingly, a study in staphylococci demonstrates that O-acetylation of NAM occurs only in the pathogenic strains and not in the non-pathogenic ones (Bera et al., 2006). In this context, it is important to study whether these PG modifying enzymes have emerged during evolution as a mechanism to cope with adverse conditions that a bacterium faces during infection. Further knowledge about the enzyme evolution might unleash the enormous functional diversity of cell wall related enzymes, and the evolutionary processes that gave rise to it.

## MODIFICATIONS IN PEPTIDE STEM

A structural change not only occurs in sugar moieties but also in the peptide stem (Vollmer et al., 2008). This peptide "editing" plays an important role in the fitness and adaptation of bacteria to diverse stress conditions such as those induced by toxic molecules, inter species competition, etc. Some of the chemical modifications and their biological implications are described further.

### Chemical Modifications Providing Antibiotic Resistance

The case of vancomycin resistance is one of the classical examples of a PG modification that provides antibiotic resistance. Vancomycin belongs to the family of the glycopeptide antibiotics. It affects the last step of PG synthesis by binding to the terminal D-Ala-D-Ala of the peptide chain and hence, it inhibits the cross-linking (i.e., transpeptidase) activity of PBPs, which ultimately leads to bacterial death (McGuinness et al., 2017). The resistance was first reported in *E. faecalis* but the same mechanism has been documented on different clinical isolates (Bugg et al., 1991).

Six types of vancomycin resistance have been reported in Enterococci, i.e., VanA, B, C, D, E and G (Courvalin, 2006). The VanA type confers the highest levels of vancomycin resistance (Arthur et al., 1996). This system is encoded by a specific conjugative operon, *VanA*, composed by three elements, (i) a two component system responsible for the detection of vancomycin and the induction of resistance genes; (ii) synthesis of D-Ala-D-Lac dipeptides, catalyzed by a set of genes which convert pyruvate to D-Lac. Then, a cytoplasmic ligase is able to attach D-Ala to the newly synthesized D-Lac; and (iii) a cytoplasmic peptidase that removes the terminal D-Ala-D-Ala of pre-existing peptide stems resulting in an increased pool of modified precursor (terminal D-Lac) over the canonical pool. Altogether, due to this minor change in the PG structure, vancomycin has less affinity to these peptide termini and consequently the bacterium survives in the presence of the antibiotic (McGuinness et al., 2017). The vancomycin resistant type VanC is similar to VanA but it changes the canonical pentapeptide termination from D-Ala-D-Ala to D-Ala-D-Ser, thanks to a transmembrane Ser-racemase. For more detailed information on the molecular basis of the other resistant types see Courvalin (2006).

The PG cross-linking is another structural property of the cell wall that bacteria can modulate to develop resistance to certain antibiotics. PG cross-linking is performed by the transpeptidase activity of high molecular weight PBPs, which uses the energy between the terminal D-Ala-D-Ala bond to cross-link the fourth D-Ala of one peptide stem with the third amino acid (*meso*-DAP or Lys) of an adjacent peptide (Vollmer et al., 2008). Contrary to this canonical DD-cross-link, some bacteria can also display a PG transpeptidase activity that cross-links the cell wall in a different manner. This atypical cross-link is done by a family of enzymes named LD-transpeptidases (Zhao et al., 2017), which connect two *meso* DAP residues from adjacent peptide stems. Indeed, *E. coli* presents 2–7% of its mucopeptides cross-linked by LD-transpeptidases (Glauner et al., 1988). Normally,

bacteria lacking this type of enzyme do not present any severe phenotype (Sanders and Pavelka, 2013). However, selection of certain mutations on sub-lethal concentrations of Ampicillin can provide high tolerance to different  $\beta$ -lactam antibiotics via a substitution of canonical DD- by non-canonical LD-cross-links. In *E. faecalis*, the mutation occurs in a cytoplasmic DD-carboxypeptidase which changes the mucopeptide precursor from penta- to tetra-peptide, favoring the substrate for the LD-transpeptidases (Mainardi et al., 2005). In the case of *E. coli*, it also requires an upregulation of one LD-transpeptidase YcbB, and the activation of the stringent response (Hugonnet et al., 2016). Even though these mutations have been selected under laboratory conditions they provide mechanistic insights about how bacteria can acquire high antibiotic tolerance to  $\beta$ -lactams.

## Chemical Modifications to Combat Bacterial Competition

Bacteria are usually encountered in polymicrobial communities where they establish different types of relations with their co-inhabitants that span from cooperative alliances to fierce competition (Peters et al., 2012). Recently, our group has documented an example of how certain PG modifications could shield the bacterial cell wall during competition (Espaillat et al., 2016). We discovered that the family Acetobacteraceae displays an atypical PG modification: an amidation on the L-center of *meso*DAP. Although this might seem a minor change, it confers a major selective advantage to specific type 6 secretion system (T6SS) driven cell wall effectors (i.e., DD-endopeptidases) that target the D-Ala-*meso*DAP cross-link. When a cross-linked mucopeptide presents this modification, the cleavage efficacy of these injected effectors is reduced, suggesting that this modification could be a resistance mechanism to the predatory bacteria. We also found that this bacterial family presented a novel LD-cross-link between the L-Ala on first position of one peptide moiety and the *meso*DAP of an adjacent peptide stem. This LD-cross-linkage also makes the cell wall more tolerant to predatory T6SS endopeptidases (Espaillat et al., 2016). In spite of these *in vitro* data, it remains unclear whether these PG modifications have emerged exclusively as a defensive strategy against surrounding competitors or if they play additional roles in other aspects of the lifestyle of the bacteria.

## Chemical Modifications as Innate Immune Modulators

The innate immune system is the first barrier that eukaryotes display against bacterial infections. In general, the innate immune system is able to recognize pathogen associated molecular patterns (PAMPs) that activate a response which ultimately depends on the molecular activator and the host. Usually, this response is characterized by the production of specific antibacterials (e.g., antimicrobial peptide, AMP) and also, in more complex hosts, the activation of inflammation (Wolf and Underhill, 2018).

One of these PAMPs is the bacterial PG, which is detected by pattern recognition receptors (PRR). Depending on the host, these PRRs could be present either on the surface or in the cytosol

of the intestinal epithelial cells (Chaput and Boneca, 2007). The PG can be either actively excreted by bacteria in case of *Bordetella pertussis* and *N. gonorrhoeae* (Wilson et al., 1991; Cloud and Dillard, 2002) or passively due to lysis. Here we give a concise overview of some important aspects on structural diversity in peptide stems and its recognition by the NOD receptors. For more details, there are a number of excellent reviews on PAMP recognition by, e.g., toll-like receptors (TLR), nucleotide-binding oligomerization domain-containing proteins (NOD) and PG recognition proteins (PGRP) (Chaput and Boneca, 2007; Sukhithasri et al., 2013; Wolf and Underhill, 2018).

In mammals, NODs are intracellular proteins which play an important role in PG detection. NOD1 recognizes GM-tri<sub>DAP</sub> (NAG-NAM-L-Ala-D-Glu-*meso*DAP) as a sensing motif to activate innate immune response. GM-tri<sub>DAP</sub> being conserved mainly in Gram-negative bacteria makes NOD1 quite specific of sensing these bacteria. NOD2 senses the MDP unit as well as GM-dipeptide, both found in Gram-positive and Gram-negative bacteria (Girardin et al., 2003a,b; Inohara et al., 2003). An *in vitro* study on NOD1 activation in human embryonic kidney cells shows the activation of nuclear factor-kappa B by the presence of *meso*-DAP and *meso*-lanthionine which along with non-sensing of GM-tetrapeptide by human NOD1 strengthens the necessity of an exposed *meso*-DAP in the NOD1 sensing motif (Tohno et al., 2008). Although it could be certainly informative to test the response of these NOD systems to all the possible known variations on the peptide stem, here we want to comment on two modifications on the third amino acid of the peptide stem. The amidation on the L-center of *meso*DAP in the PG of commensal bacteria of *Drosophila* induces a less potent response of the innate immune system, to not over stimulate the system and to have basal levels of AMP (Espaillat et al., 2016). Moreover, amidation on the D-center of *meso*DAP also produces a weaker NOD1 immune response on human cell lines (Girardin et al., 2003a; Vijayrajratnam et al., 2016). All above mentioned studies about the variations in the peptide stem are directly linked to low sensitivity to the innate immune system, which underlines the necessity of a detailed learning of all possible peptide stem modifications and their implication on the innate immune system.

## CONCLUSION

With just a few exceptions, PG is a universal component of the bacterial cell wall and thus, a main target of several host produced antimicrobials. Many bacterial pathogens have evolved mechanisms to combat different host defense strategies by modulating their PG structures. Modifications in the PG structure have direct implications on several processes ranging from lysozyme resistance, host immune response and antibiotic resistance. These modifications are important not only as adaptation to specific stresses but also since the cell wall is chemically edited, these modifications will likely have consequences in the activity of other PG-associated enzymes and what will be their physical interactions with these new



muropeptides. In this context, the lack of PG editing enzymes would not just make it difficult for bacteria to adapt to stress but also prime a domino effect of PG structural changes with negative consequences in cell wall integrity. This knowledge is valuable for the development of novel antibacterial combinatory therapies to sensitize pathogens that are otherwise non-susceptible to  $\beta$ -lactams. Also, the use of commensal bacteria with specific systems (e.g., T6SS effector against the modification) targeting this PG-editing could be instrumental to devise alternative enzyme-based therapies for the treatment of antibiotic resistant infectious diseases.

A comprehensive study on the PG-modulation strategies which empowers bacterial competition between communities is still in its infancy. Additional chemical analyses of more bacterial PGs is fundamental for gaining a comprehensive understanding of PG variability in nature, as well as under specific conditions (e.g., during infection). The role of bacterial PG persistence and pathogenicity has been a topic of extensive research in recent decades, but still there are many unanswered

questions. Continued efforts to understand the cell wall chemical diversity and adaptive enzymatic capacity will surely create new dimensions of antibiotic development strategies.

## AUTHOR CONTRIBUTIONS

All the authors contributed to the compilation of data and drafted the manuscript.

## FUNDING

AY and AE are thankful to The Swedish Research Council, Laboratory for Molecular Infection Medicine Sweden (MIMS) and UCMR for the financial support. Research in the Cava lab was supported by MIMS, the Knut and Alice Wallenberg Foundation (KAW), the Swedish Research Council and the Kempe Foundation.

## REFERENCES

- Abrams, A. (1958). O-acetyl groups in the cell wall of *Streptococcus faecalis*. *J. Biol. Chem.* 230, 949–959.
- Arthur, M., Depardieu, F., Reynolds, P., and Courvalin, P. (1996). Quantitative analysis of the metabolism of soluble cytoplasmic peptidoglycan precursors of glycopeptide-resistant enterococci. *Mol. Microbiol.* 21, 33–44. doi: 10.1046/j.1365-2958.1996.00617.x
- Atrih, A., Bacher, G., Allmaier, G., Williamson, M. P., and Foster, S. J. (1999). Analysis of peptidoglycan structure from vegetative cells of *Bacillus subtilis* 168 and role of PBP 5 in peptidoglycan maturation. *J. Bacteriol.* 181, 3956–3966.
- Azuma, I., Thomas, D. W., Adam, A., Ghuyssen, J. M., Bonaly, R., Petit, J. F., et al. (1970). Occurrence of N-glycolylmuramic acid in bacterial cell walls: a preliminary survey. *Biochim. Biophys. Acta* 208, 444–451. doi: 10.1016/0304-4165(70)90217-5
- Baranwal, G., Mohammad, M., Jarneborn, A., Reddy, B. R., Golla, A., Chakravarty, S., et al. (2017). Impact of cell wall peptidoglycan O-acetylation on the pathogenesis of *Staphylococcus aureus* in septic arthritis. *Int. J. Med. Microbiol.* 307, 388–397. doi: 10.1016/j.ijmm.2017.08.002
- Benachour, A., Ladjouzi, R., Le Jeune, A., Hébert, L., Thorpe, S., Courtin, P., et al. (2012). The lysozyme-induced peptidoglycan N-acetylglucosamine deacetylase PgdA (EF1843) is required for *Enterococcus faecalis* virulence. *J. Bacteriol.* 194, 6066–6073. doi: 10.1128/JB.00981-12
- Bera, A., Biswas, R., Herbert, S., and Götz, F. (2006). The presence of peptidoglycan O-acetyltransferase in various staphylococcal species correlates with lysozyme resistance and pathogenicity. *Infect. Immun.* 74, 4598–4604. doi: 10.1128/IAI.00301-06
- Bera, A., Herbert, S., Jakob, A., Vollmer, W., and Götz, F. (2005). Why are pathogenic staphylococci so lysozyme resistant? The peptidoglycan O-acetyltransferase OatA is the major determinant for lysozyme resistance of *Staphylococcus aureus*. *Mol. Microbiol.* 55, 778–787. doi: 10.1111/j.1365-2958.2004.04446.x
- Bernard, E., Rolain, T., Courtin, P., Guillot, A., Langella, P., Hols, P., et al. (2011). Characterization of O-acetylation of N-acetylglucosamine a novel structural variation of bacterial peptidoglycan. *J. Biol. Chem.* 286, 23950–23958. doi: 10.1074/jbc.M111.241414
- Bernard, E., Rolain, T., David, B., André, G., Dupres, V., Dufrêne, Y. F., et al. (2012). Dual role for the O-acetyltransferase OatA in peptidoglycan modification and control of cell septation in *Lactobacillus plantarum*. *PLoS One* 7:e47893. doi: 10.1371/journal.pone.0047893
- Billot-Klein, D., Legrand, R., Schoot, B., van Heijenoort, J., and Gutmann, L. (1997). Peptidoglycan structure of *Lactobacillus casei*, a species highly resistant to glycopeptide antibiotics. *J. Bacteriol.* 179, 6208–6212. doi: 10.1128/jb.179.19.6208-6212.1997
- Boneca, I. G., Dussurget, O., Cabanes, D., Nahori, M. A., Sousa, S., Lecuit, M., et al. (2007). A critical role for peptidoglycan N-deacetylation in *Listeria* evasion from the host innate immune system. *Proc. Natl. Acad. Sci. U.S.A.* 104, 997–1002. doi: 10.1073/pnas.0609672104
- Bonnet, J., Durmort, C., Jacq, M., Mortier-Barrière, I., Campo, N., Van Nieuwenhze, M. S., et al. (2017). Peptidoglycan O-acetylation is functionally related to cell wall biosynthesis and cell division in *Streptococcus pneumoniae*. *Mol. Microbiol.* 106, 832–846. doi: 10.1111/mmi.13849
- Brumfitt, W., Wardlaw, A. C., and Park, J. T. (1958). Development of lysozyme-resistance in *Micrococcus lysodeikticus* and its association with an increased O-acetyl content of the cell wall. *Nature* 181, 1783–1784. doi: 10.1038/1811783a0
- Bugg, T. D., Wright, G. D., Dutka-Malen, S., Arthur, M., Courvalin, P., and Walsh, C. T. (1991). Molecular basis for vancomycin resistance in *Enterococcus faecium* BM4147: biosynthesis of a depsipeptide peptidoglycan precursor by vancomycin resistance proteins VanH and VanA. *Biochemistry* 30, 10408–10415. doi: 10.1021/bi00107a007
- Cava, F., and de Pedro, M. A. (2014). Peptidoglycan plasticity in bacteria: emerging variability of the murein sacculus and their associated biological functions. *Curr. Opin. Microbiol.* 18, 46–53. doi: 10.1016/j.mib.2014.01.004
- Chang, J. D., Foster, E. E., Wallace, A. G., and Kim, S. J. (2017). Peptidoglycan O-acetylation increases in response to vancomycin treatment in vancomycin-resistant *Enterococcus faecalis*. *Sci. Rep.* 7:46500. doi: 10.1038/srep46500
- Chaput, C., and Boneca, I. G. (2007). Peptidoglycan detection by mammals and flies. *Microbes Infect.* 9, 637–647. doi: 10.1016/j.micinf.2007.01.022
- Claessen, D., Emmins, R., Hamoen, L. W., Daniel, R. A., Errington, J., and Edwards, D. H. (2008). Control of the cell elongation-division cycle by shuttling of PBP1 protein in *Bacillus subtilis*. *Mol. Microbiol.* 68, 1029–1046. doi: 10.1111/j.1365-2958.2008.06210.x
- Clarke, A. J. (1993). Extent of peptidoglycan O-acetylation in the tribe Proteaeae. *J. Bacteriol.* 175, 4550–4553. doi: 10.1128/jb.175.14.4550-4553.1993
- Cloud, K. A., and Dillard, J. P. (2002). A lytic transglycosylase of *Neisseria gonorrhoeae* is involved in peptidoglycan-derived cytotoxin production. *Infect. Immun.* 70, 2752–2757. doi: 10.1128/IAI.70.6.2752-2757.2002
- Coulombe, F., Divangahi, M., Veyrier, F., de Léséleuc, L., Gleason, J. L., Yang, Y., et al. (2009). Increased NOD2-mediated recognition of N-glycolylmuramyl dipeptide. *J. Exp. Med.* 206, 1709–1716. doi: 10.1084/jem.20081779
- Courvalin, P. (2006). Vancomycin resistance in gram-positive cocci. *Clin. Infect. Dis.* 42, S25–S34. doi: 10.1086/491711
- Coyette, J., and Ghuyssen, J. M. (1970). Structure of the walls of *Lactobacillus acidophilus* strain 63 AM. *Biochemistry* 9, 2935–2943. doi: 10.1021/bi00817a001

- Davis, K. M., Akinbi, H. T., Standish, A. J., and Weiser, J. N. (2008). Resistance to mucosal lysozyme compensates for the fitness deficit of peptidoglycan modifications by *Streptococcus pneumoniae*. *PLoS Pathog.* 4:e1000241. doi: 10.1371/journal.ppat.1000241
- Dillard, J. P., and Hackett, K. T. (2005). Mutations affecting peptidoglycan acetylation in *Neisseria gonorrhoeae* and *Neisseria meningitidis*. *Infect. Immun.* 73, 5697–5705. doi: 10.1128/IAI.73.9.5697-5705.2005
- Espallat, A., Forsmo, O., El Biari, K., Björk, R., Lemaitre, B., Trygg, J., et al. (2016). Chemometric analysis of bacterial peptidoglycan reveals atypical modifications that empower the cell wall against predatory enzymes and fly innate immunity. *J. Am. Chem. Soc.* 138, 9193–9204. doi: 10.1021/jacs.6b04430
- Fittipaldi, N., Sekizaki, T., Takamatsu, D., De La Cruz, Domínguez Punaro, M., Harel, J., et al. (2008). Significant contribution of the *pgdA* gene to the virulence of *Streptococcus suis*. *Mol. Microbiol.* 70, 1120–1135. doi: 10.1111/j.1365-2958.2008.06463.x
- Fleming, T. J., Wallsmith, D. E., and Rosenthal, R. S. (1986). Arthropathic properties of gonococcal peptidoglycan fragments: implications for the pathogenesis of disseminated gonococcal disease. *Infect. Immun.* 52, 600–608.
- Fukushima, T., Kitajima, T., and Sekiguchi, J. (2005). A polysaccharide deacetylase homologue, PdaA, in *Bacillus subtilis* acts as an *N*-acetylmuramic acid deacetylase *in vitro*. *J. Bacteriol.* 187, 1287–1292. doi: 10.1128/JB.187.4.1287-1292.2005
- Fukushima, T., Yamamoto, H., Atrih, A., Foster, S. J., and Sekiguchi, J. (2002). A polysaccharide deacetylase gene (*pdA*) is required for germination and for production of muramic  $\delta$ -lactam residues in the spore cortex of *Bacillus subtilis*. *J. Bacteriol.* 184, 6007–6015. doi: 10.1128/JB.184.21.6007-6015.2002
- Gilmore, M. E., Bandyopadhyay, D., Dean, A. M., Linnstaedt, S. D., and Popham, D. L. (2004). Production of muramic  $\delta$ -lactam in *Bacillus subtilis* spore peptidoglycan. *J. Bacteriol.* 186, 80–89. doi: 10.1128/JB.186.1.80-89.2004
- Girardin, S. E., Travassos, L. H., Hervé, M., Blanot, D., Boneca, I. G., Philpott, D. J., et al. (2003a). Peptidoglycan molecular requirements allowing detection by Nod1 and Nod2. *J. Biol. Chem.* 278, 41702–41708. doi: 10.1074/jbc.M307198200
- Girardin, S. E., Boneca, I. G., Carneiro, L. A., Antignac, A., Jéhanho, M., Viala, J., et al. (2003b). Nod1 detects a unique muropeptide from gram-negative bacterial peptidoglycan. *Science* 300, 1584–1587. doi: 10.1126/science.1084677
- Glauner, B., Hölte, J. V., and Schwarz, U. (1988). The composition of the murein of *Escherichia coli*. *J. Biol. Chem.* 263, 10088–10095.
- Guariglia-Oropeza, V., and Helmann, J. D. (2011). *Bacillus subtilis*  $\sigma^V$  confers lysozyme resistance by activation of two cell wall modification pathways, peptidoglycan *O*-acetylation and D-alanylation of teichoic acids. *J. Bacteriol.* 193, 6223–6232. doi: 10.1128/JB.06023-11
- Ha, R., Frirdich, E., Sychantha, D., Biboy, J., Taveirne, M. E., Johnson, J. G., et al. (2016). Accumulation of peptidoglycan *O*-acetylation leads to altered cell wall biochemistry and negatively impacts pathogenesis factors of *Campylobacter jejuni*. *J. Biol. Chem.* 291, 22686–22702. doi: 10.1074/jbc.M116.746404
- Hansen, J. M., Golchin, S. A., Veyrier, F. J., Domenech, P., Boneca, I. G., Azad, A. K., et al. (2013). *N*-glycosylated peptidoglycan contributes to the immunogenicity but not pathogenicity of *Mycobacterium tuberculosis*. *J. Infect. Dis.* 209, 1045–1054. doi: 10.1093/infdis/jit622
- Hugonnet, J. E., Mengin-Lecreux, D., Monton, A., den Blaauwen, T., Carbone, E., Veckerlé, C., et al. (2016). Factors essential for L,D-transpeptidase-mediated peptidoglycan cross-linking and  $\beta$ -lactam resistance in *Escherichia coli*. *eLife* 5:e19469. doi: 10.7554/eLife
- Inohara, N., Ogura, Y., Fontalba, A., Gutierrez, O., Pons, F., Crespo, J., et al. (2003). Host recognition of bacterial muramyl dipeptide mediated through nod2 implications for Crohn's disease. *J. Biol. Chem.* 278, 5509–5512. doi: 10.1074/jbc.C200673200
- Iwata, T., Watanabe, A., Kusumoto, M., and Akiba, M. (2016). Peptidoglycan acetylation of *Campylobacter jejuni* is essential for maintaining cell wall integrity and colonization in chicken intestines. *Appl. Environ. Microbiol.* 82, 6284–6290. doi: 10.1128/AEM.02068-16
- Kaoukab-Raji, A., Biskri, L., Bernardini, M. L., and Allaoui, A. (2012). Characterization of SfpdA, a *Shigella flexneri* peptidoglycan deacetylase required for bacterial persistence within polymorphonuclear neutrophils. *Microbes Infect.* 14, 619–627. doi: 10.1016/j.micinf.2012.01.009
- Knillans, K. J., Hackett, K. T., Anderson, J. E., Weng, C., Dillard, J. P., and Duncan, J. A. (2017). *Neisseria gonorrhoeae* lytic transglycosylases LtgA and LtgD reduce host innate immune signaling through TLR2 and NOD2. *ACS Infect. Dis.* 3, 624–633. doi: 10.1016/j.cel.2016.05.076
- Kobayashi, K., Sudarta, I. P., Kodama, T., Fukushima, T., Ara, K., Ozaki, K., et al. (2012). Identification and characterization of a novel polysaccharide deacetylase C (PdaC) from *Bacillus subtilis*. *J. Biol. Chem.* 287, 9765–9776. doi: 10.1074/jbc.M111.329490
- Laaberki, M. H., Pfeffer, J., Clarke, A. J., and Dworkin, J. (2011). *O*-Acetylation of peptidoglycan is required for proper cell separation and S-layer anchoring in *Bacillus anthracis*. *J. Biol. Chem.* 286, 5278–5288. doi: 10.1074/jbc.M110.183236
- Lambert, C., Lerner, T. R., Bui, N. K., Somers, H., Aizawa, S. I., Liddell, S., et al. (2016). Interrupting peptidoglycan deacetylation during *Bdellovibrio* predator-prey interaction prevents ultimate destruction of prey wall, liberating bacterial-ghosts. *Sci. Rep.* 6:26010. doi: 10.1038/srep26010
- Liow, L. H., Van Valen, L., and Stenseth, N. C. (2011). Red Queen: from populations to taxa and communities. *Trends Ecol. Evol.* 26, 349–358. doi: 10.1016/j.tree.2011.03.016
- Logardt, I. M., and Neujahr, H. Y. (1975). Lysis of modified walls from *Lactobacillus fermentum*. *J. Bacteriol.* 124, 73–77.
- Luker, K. E., Tyler, A. N., Marshall, G. R., and Goldman, W. E. (1995). Tracheal cytotoxin structural requirements for respiratory epithelial damage in pertussis. *Mol. Microbiol.* 16, 733–743. doi: 10.1111/j.1365-2958.1995.tb02434.x
- Mahapatra, S., Scherman, H., Brennan, P. J., and Crick, D. C. (2005). *N*-Glycosylation of the nucleotide precursors of peptidoglycan biosynthesis of *Mycobacterium* spp. is altered by drug treatment. *J. Bacteriol.* 187, 341–2347. doi: 10.1128/JB.187.7.2341-2347.2005
- Mainardi, J. L., Fourgeaud, M., Hugonnet, J. E., Dubost, L., Brouard, J. P., Ouazzani, J., et al. (2005). A novel peptidoglycan cross-linking enzyme for a  $\beta$ -lactam-resistant transpeptidation pathway. *J. Biol. Chem.* 280, 38146–38152. doi: 10.1074/jbc.M507384200
- Martin, J. P., Fleck, J., Mock, M., and Ghuysen, J. M. (1973). The wall peptidoglycans of *Neisseria perflava*, *Moraxella glucidolytica*, *Pseudomonas alcaligenes* and *Proteus vulgaris* strain P18. *FEBS J.* 38, 301–306. doi: 10.1111/j.1432-1033.1973.tb03062.x
- McConville, M. (2014). Open questions: microbes, metabolism and host-pathogen interactions. *BMC Biol.* 12:18. doi: 10.1186/1741-7007-12-18
- McGuinness, W. A., Malachowa, N., and DeLeo, F. R. (2017). Vancomycin resistance in *Staphylococcus aureus*. *Yale J. Boil. Med.* 90, 269–281.
- Melnik, J. E., Mohanan, V., Schaefer, A. K., Hou, C. W., and Grimes, C. L. (2015). Peptidoglycan modifications tune the stability and function of the innate immune receptor Nod2. *J. Am. Chem. Soc.* 137, 6987–6990. doi: 10.1021/jacs.5b01607
- Meyrand, M., Boughammoura, A., Courtin, P., Mezange, C., Guillot, A., and Chapot-Chartier, M. P. (2007). Peptidoglycan *N*-acetylglucosamine deacetylation decreases autolysis in *Lactococcus lactis*. *Microbiology* 153, 3275–3285. doi: 10.1099/mic.0.2007/005835-0
- Milani, C. J., Aziz, R. K., Locke, J. B., Dahesh, S., Nizet, V., and Buchanan, J. T. (2010). The novel polysaccharide deacetylase homologue Pdi contributes to virulence of the aquatic pathogen *Streptococcus iniae*. *Microbiology* 156, 543–554. doi: 10.1099/mic.0.028365-0
- Moynihan, P. J., and Clarke, A. J. (2010). *O*-acetylation of peptidoglycan in gram-negative bacteria: identification and characterization of peptidoglycan *O*-acetyltransferase in *Neisseria gonorrhoeae*. *J. Biol. Chem.* 285, 13264–13273. doi: 10.1074/jbc.M110.107086
- Passalacqua, K. D., Charbonneau, M. E., and O'Riordan, M. X. (2016). Bacterial metabolism shapes the host: pathogen interface. *Microbiol. Spectr.* 4:VMBF-0027-2015. doi: 10.1128/microbiolspec.VMBF-0027-2015
- Peltier, J., Courtin, P., El Meouche, L., Lemée, L., Chapot-Chartier, M. P., and Pons, J. L. (2011). *Clostridium difficile* has an original peptidoglycan structure with a high level of *N*-acetylglucosamine deacetylation and mainly 3-3 cross-links. *J. Biol. Chem.* 286, 29053–29062. doi: 10.1074/jbc.M111.259150
- Peters, B. M., Jabra-Rizk, M. A., O'May, G. A., Costerton, J. W., and Shirliff, M. E. (2012). Polymicrobial interactions: impact on pathogenesis and human disease. *Clin. Microbiol. Rev.* 25, 193–213.
- Pfeffer, J. M., Strating, H., Weadge, J. T., and Clarke, A. J. (2006). Peptidoglycan *O*-acetylation and autolysin profile of *Enterococcus faecalis* in the viable but nonculturable state. *J. Bacteriol.* 188, 902–908. doi: 10.1128/JB.188.3.902-908.2006

- Psylinakis, E., Boneca, I. G., Mavromatis, K., Deli, A., Hayhurst, E., Foster, S. J., et al. (2005). Peptidoglycan *N*-acetylglucosamine deacetylases from *Bacillus cereus*, highly conserved proteins in *Bacillus anthracis*. *J. Biol. Chem.* 280, 30856–30863. doi: 10.1074/jbc.M407426200
- Pushkaran, A. C., Nataraj, N., Nair, N., Götz, F., Biswas, R., and Mohan, C. G. (2015). Understanding the structure-function relationship of lysozyme resistance in *Staphylococcus aureus* by peptidoglycan *O*-acetylation using molecular docking, dynamics, and lysis assay. *J. Chem. Inf. Model.* 55, 760–770. doi: 10.1021/ci500734k
- Rae, C. S., Geissler, A., Adamson, P. C., and Portnoy, D. A. (2011). Mutations of the *Listeria monocytogenes* peptidoglycan *N*-deacetylase and *O*-acetylase result in enhanced lysozyme sensitivity, bacteriolysis, and hyperinduction of innate immune pathways. *Infect. Immun.* 79, 3596–3606. doi: 10.1128/IAI.00077-11
- Ragland, S. A., Schaub, R. E., Hackett, K. T., Dillard, J. P., and Criss, A. K. (2017). Two lytic transglycosylases in *Neisseria gonorrhoeae* impart resistance to killing by lysozyme and human neutrophils. *Cell. Microbiol.* 19:e12662. doi: 10.1111/cmi.12662
- Raymond, J. B., Mahapatra, S., Crick, D. C., and Pavelka, M. S. (2005). Identification of the *namH* gene, encoding the hydroxylase responsible for the *N*-glycosylation of the mycobacterial peptidoglycan. *J. Biol. Chem.* 280, 326–333. doi: 10.1074/jbc.M411006200
- Rismondo, J., Cleverley, R. M., Lane, H. V., Großhennig, S., Steglich, A., Möller, L., et al. (2016). Structure of the bacterial cell division determinant GpsB and its interaction with penicillin-binding proteins. *Mol. Microbiol.* 99, 978–998. doi: 10.1111/mmi.13279
- Rismondo, J., Wamp, S., Aldridge, C., Vollmer, W., and Halbedel, S. (2018). Stimulation of PgdA-dependent peptidoglycan *N*-deacetylation by GpsB-PBP A1 in *Listeria monocytogenes*. *Mol. Microbiol.* 107, 472–487. doi: 10.1111/mmi.13893
- Sanchez, M., Kolar, S. L., Müller, S., Reyes, C. N., Wolf, A. J., Ogawa, C., et al. (2017). *O*-Acetylation of peptidoglycan limits Helper T cell priming and permits *Staphylococcus aureus* reinfection. *Cell Host Microbe* 22, 543–551. doi: 10.1016/j.chom.2017.08.008
- Sanders, A. N., and Pavelka, M. S. (2013). Phenotypic analysis of *Escherichia coli* mutants lacking L,D-transpeptidases. *Microbiology* 159, 1842–1852. doi: 10.1099/mic.0.069211-0
- Schneider, T., and Sahl, H. G. (2010). An oldie but a goodie-cell wall biosynthesis as antibiotic target pathway. *Int. J. Med. Microbiol.* 300, 161–190. doi: 10.1016/j.ijmm.2009.10.005
- Shaik, M. M., Cendron, L., Percudani, R., and Zanotti, G. (2011). The structure of *Helicobacter pylori* HP0310 reveals an atypical peptidoglycan deacetylase. *PLoS One* 6:e19207. doi: 10.1371/journal.pone.0019207
- Shimada, T., Park, B. G., Wolf, A. J., Brikos, C., Goodridge, H. S., Becker, C. A., et al. (2010). *Staphylococcus aureus* evades lysozyme-based peptidoglycan digestion that links phagocytosis, inflammasome activation, and IL-1 $\beta$  secretion. *Cell Host Microbe* 7, 38–49. doi: 10.1016/j.chom.2009.12.008
- Sukhithasri, V., Nisha, N., Biswas, L., Kumar, V. A., and Biswas, R. (2013). Innate immune recognition of microbial cell wall components and microbial strategies to evade such recognitions. *Microbiol. Res.* 168, 396–406. doi: 10.1016/j.micres.2013.02.005
- Tohno, M., Shimazu, T., Aso, H., Uehara, A., Takada, H., Kawasaki, A., et al. (2008). Molecular cloning and functional characterization of porcine nucleotide-binding oligomerization domain-1 (n.d.) recognizing minimum agonists, meso-diaminopimelic acid and meso-lanthionine. *Mol. Immunol.* 45, 1807–1817. doi: 10.1016/j.molimm.2007.09.029
- Uehara, T., and Bernhardt, T. G. (2011). More than just lysins: peptidoglycan hydrolases tailor the cell wall. *Curr. Opin. Microbiol.* 14, 698–703. doi: 10.1016/j.mib.2011.10.003
- Veiga, P., Bulbarello-Sampieri, C., Furlan, S., Maisons, A., Chapot-Chartier, M. P., Erkelens, M., et al. (2007). SpxB regulates *O*-acetylation-dependent resistance of *Lactococcus lactis* peptidoglycan to hydrolysis. *J. Biol. Chem.* 282, 19342–19354. doi: 10.1074/jbc.M611308200
- Veyrier, F. J., Williams, A. H., Mesnage, S., Schmitt, C., Taha, M. K., and Boneca, I. G. (2013). De-*O*-acetylation of peptidoglycan regulates glycan chain extension and affects *in vivo* survival of *Neisseria meningitidis*. *Mol. Microbiol.* 87, 1100–1112. doi: 10.1111/mmi.12153
- Vijayarajratnam, S., Pushkaran, A. C., Balakrishnan, A., Vasudevan, A. K., Biswas, R., and Mohan, C. G. (2016). Bacterial peptidoglycan with amidated meso-diaminopimelic acid evades NOD1 recognition: an insight into NOD1 structure-recognition. *Biochem. J.* 473, 4573–4592. doi: 10.1042/BCJ20160817
- Vollmer, W., Blanot, D., and de Pedro, M. A. (2008). Peptidoglycan structure and architecture. *FEMS Microbiol. Rev.* 32, 149–167. doi: 10.1111/j.1574-6976.2007.00094.x
- Vollmer, W., and Tomasz, A. (2000). The *pgdA* gene encodes for a peptidoglycan *N*-acetylglucosamine deacetylase in *Streptococcus pneumoniae*. *J. Biol. Chem.* 275, 20496–20501. doi: 10.1074/jbc.M910189199
- Vollmer, W., and Tomasz, A. (2002). Peptidoglycan *N*-acetylglucosamine deacetylase, a putative virulence factor in *Streptococcus pneumoniae*. *Infect. Immun.* 70, 7176–7178. doi: 10.1128/IAI.70.12.7176-7178.2002
- Wang, G., Lo, L. F., Forsberg, L. S., and Maier, R. J. (2012). *Helicobacter pylori* peptidoglycan modifications confer lysozyme resistance and contribute to survival in the host. *mBio* 3, e409–e412. doi: 10.1128/mBio.00409-12
- Wang, G., Maier, S. E., Lo, L. F., Maier, G., Dosi, S., and Maier, R. J. (2010). Peptidoglycan deacetylation in *Helicobacter pylori* contributes to bacterial survival by mitigating host immune responses. *Infect. Immun.* 78, 4660–4666. doi: 10.1128/IAI.00307-10
- Wang, G., Olczak, A., Forsberg, L. S., and Maier, R. J. (2009). Oxidative stress-induced peptidoglycan deacetylase in *Helicobacter pylori*. *J. Biol. Chem.* 284, 6790–6800. doi: 10.1074/jbc.M808071200
- Weadge, J. T., and Clarke, A. J. (2006). Identification and characterization of *O*-acetylpeptidoglycan esterase: a novel enzyme discovered in *Neisseria gonorrhoeae*. *Biochemistry* 45, 839–851. doi: 10.1021/bi051679s
- Weadge, J. T., Pfeffer, J. M., and Clarke, A. J. (2005). Identification of a new family of enzymes with potential *O*-acetylpeptidoglycan esterase activity in both Gram-positive and Gram-negative bacteria. *BMC Microbiol.* 5:49. doi: 10.1186/1471-2180-5-49
- Wilson, R., Read, R., Thomas, M., Rutman, A., Harrison, K., Lund, V., et al. (1991). Effects of *Bordetella pertussis* infection on human respiratory epithelium *in vivo* and *in vitro*. *Infect. Immun.* 59, 337–345.
- Wolf, A. J., Reyes, C. N., Liang, W., Becker, C., Shimada, K., Wheeler, M. L., et al. (2016). Hexokinase is an innate immune receptor for the detection of bacterial peptidoglycan. *Cell* 166, 624–636. doi: 10.1016/j.cell.2016.05.076
- Wolf, A. J., and Underhill, D. M. (2018). Peptidoglycan recognition by the innate immune system. *Nat. Rev. Immunol.* 18, 243–254. doi: 10.1038/nri.2017.136
- Zhao, H., Patel, V., Helmann, J. D., and Dörr, T. (2017). Don't let sleeping dogmas lie: new views of peptidoglycan synthesis and its regulation. *Mol. Microbiol.* 106, 847–860. doi: 10.1111/mmi.13853

**Conflict of Interest Statement:** The authors declare that the research was conducted in the absence of any commercial or financial relationships that could be construed as a potential conflict of interest.

Copyright © 2018 Yadav, Espallat and Cava. This is an open-access article distributed under the terms of the Creative Commons Attribution License (CC BY). The use, distribution or reproduction in other forums is permitted, provided the original author(s) and the copyright owner(s) are credited and that the original publication in this journal is cited, in accordance with accepted academic practice. No use, distribution or reproduction is permitted which does not comply with these terms.



# The Mechanisms of Action of Ribosome-Targeting Peptide Antibiotics

Yury S. Polikanov<sup>1,2\*</sup>, Nikolay A. Aleksashin<sup>3</sup>, Bertrand Beckert<sup>4</sup> and Daniel N. Wilson<sup>4\*</sup>

<sup>1</sup> Department of Biological Sciences, University of Illinois at Chicago, Chicago, IL, United States, <sup>2</sup> Department of Medicinal Chemistry and Pharmacognosy, University of Illinois at Chicago, Chicago, IL, United States, <sup>3</sup> Center for Biomolecular Sciences, University of Illinois at Chicago, Chicago, IL, United States, <sup>4</sup> Institute for Biochemistry and Molecular Biology, University of Hamburg, Hamburg, Germany

## OPEN ACCESS

### Edited by:

Graeme L. Conn,  
Emory University School of Medicine,  
United States

### Reviewed by:

Jack A. Dunkle,  
University of Alabama, United States  
Adegboyega Oyelere,  
Georgia Institute of Technology,  
United States

### \*Correspondence:

Yury S. Polikanov  
yuryp@uic.edu  
Daniel N. Wilson  
wilson@chemie.uni-hamburg.de

### Specialty section:

This article was submitted to  
Structural Biology,  
a section of the journal  
Frontiers in Molecular Biosciences

**Received:** 25 February 2018

**Accepted:** 23 April 2018

**Published:** 14 May 2018

### Citation:

Polikanov YS, Aleksashin NA,  
Beckert B and Wilson DN (2018) The  
Mechanisms of Action of  
Ribosome-Targeting Peptide  
Antibiotics. *Front. Mol. Biosci.* 5:48.  
doi: 10.3389/fmolb.2018.00048

The ribosome is one of the major targets in the cell for clinically used antibiotics. However, the increase in multidrug resistant bacteria is rapidly reducing the effectiveness of our current arsenal of ribosome-targeting antibiotics, highlighting the need for the discovery of compounds with new scaffolds that bind to novel sites on the ribosome. One possible avenue for the development of new antimicrobial agents is by characterization and optimization of ribosome-targeting peptide antibiotics. Biochemical and structural data on ribosome-targeting peptide antibiotics illustrates the large diversity of scaffolds, binding interactions with the ribosome as well as mechanism of action to inhibit translation. The availability of high-resolution structures of ribosomes in complex with peptide antibiotics opens the way to structure-based design of these compounds as novel antimicrobial agents.

**Keywords:** proline-rich antimicrobial peptides, ribosome, translation, inhibitor, antibiotic

## THE RIBOSOME AND TRANSLATION AS AN ANTIBIOTIC TARGET

The ribosome is one of the most conserved and sophisticated macromolecular machines of the cell. It is composed of two unequal subunits, a small 30S and large 50S in bacteria, which join together to form a 70S ribosome. While each ribosomal subunit contains a large number of ribosomal proteins, it is the ribosomal RNA (rRNA) that plays the most critical functional role defining the ribosome as a ribozyme (Nissen et al., 2000). The small subunit decodes the genetic information delivered by messenger RNA (mRNA), whereas the large subunit hosts the catalytic peptidyl transferase center (PTC), where amino acids delivered by transfer RNAs (tRNAs) are linked into polypeptides (reviewed in Arenz and Wilson, 2016). The ribosome provides a platform for binding of the mRNA and transfer RNAs (tRNAs). The tRNAs have two functional ends, one carrying the amino acid and the other end containing the anticodon that recognizes the codon of the mRNA. The ribosome has three tRNA binding sites: the aminoacyl (A), peptidyl (P), and exit (E) sites. The A site binds the incoming aminoacyl-tRNA (aa-tRNA), the P site binds the



peptidyl-tRNA carrying the nascent polypeptide chain and the E site binds deacylated tRNA before it dissociates from the ribosome. For translation to proceed efficiently, many protein factors are needed, which sequentially guide the ribosome through the protein synthesis cycle (Figure 1). Translation is initiated on the 30S subunit with the help of initiation factors that recruit the initiator formyl-methionine tRNA (fMet-tRNA<sup>fMet</sup>) to the ribosomal P site where it recognizes the start codon of the mRNA. The 50S subunit associates with the 30S, forming

the 70S initiation complex that is primed for the elongation phase of protein synthesis. The second codon of the open reading frame located in the A site of the ribosome is decoded by the ternary complex, composed of aa-tRNA, elongation factor Tu (EF-Tu), and GTP. Decoding of the A-site codon by a cognate aa-tRNA triggers GTP hydrolysis on EF-Tu and release of the aa-tRNA into the A site. The CCA-3' terminus of aa-tRNA can then accommodate into the PTC of the 50S subunit, and the peptidyl transferase reaction occurs spontaneously extending the nascent

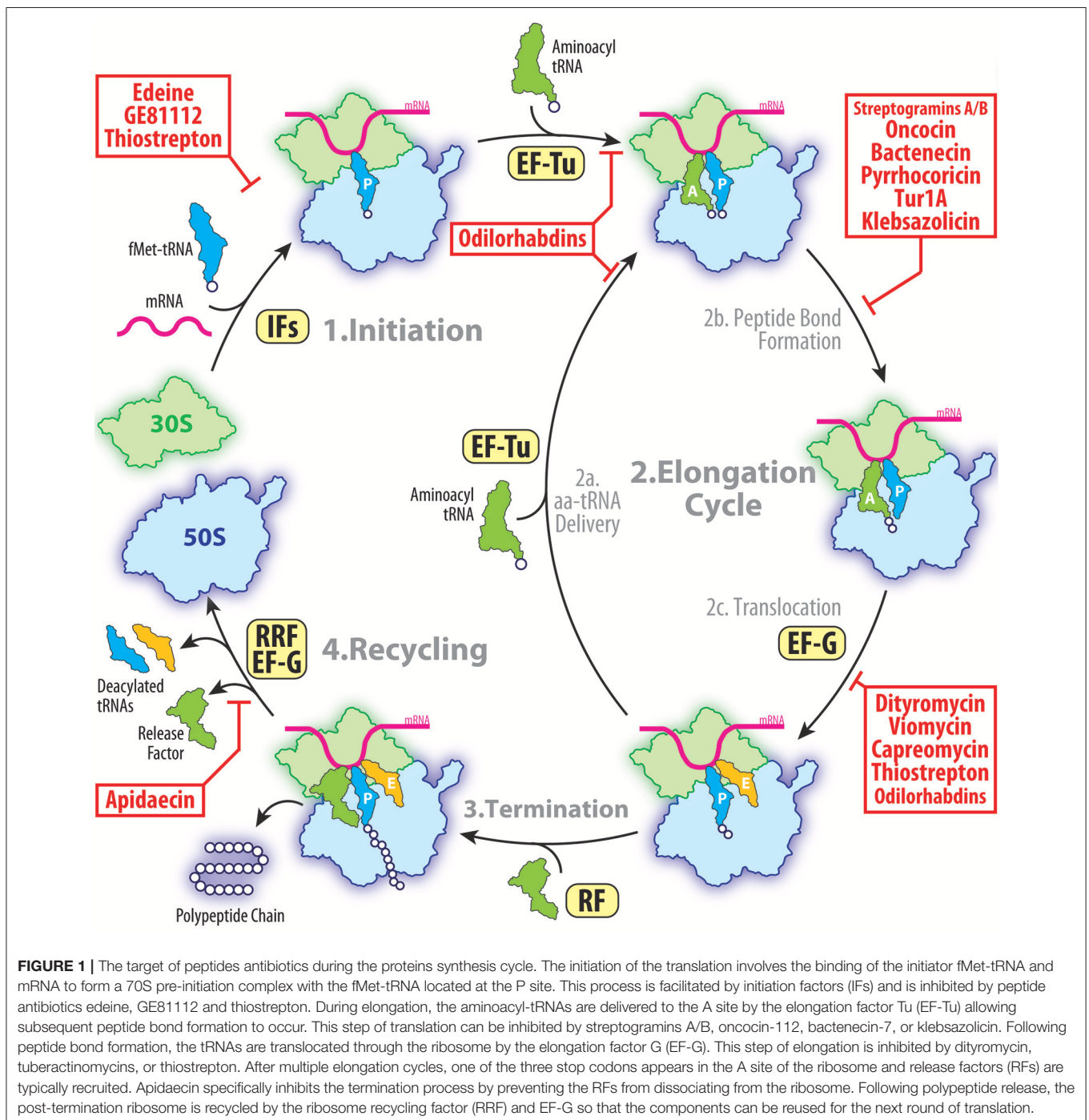


**FIGURE 1 |** The target of peptides antibiotics during the proteins synthesis cycle. The initiation of the translation involves the binding of the initiator fMet-tRNA and mRNA to form a 70S pre-initiation complex with the fMet-tRNA located at the P site. This process is facilitated by initiation factors (IFs) and is inhibited by peptide antibiotics edeine, GE81112 and thiostrepton. During elongation, the aminoacyl-tRNAs are delivered to the A site by the elongation factor Tu (EF-Tu) allowing subsequent peptide bond formation to occur. This step of translation can be inhibited by streptogramins A/B, oncocin-112, bactenecin-7, or klebsazolicin. Following peptide bond formation, the tRNAs are translocated through the ribosome by the elongation factor G (EF-G). This step of elongation is inhibited by dityromycin, tuberactinomycins, or thiostrepton. After multiple elongation cycles, one of the three stop codons appears in the A site of the ribosome and release factors (RFs) are typically recruited. Apidaecin specifically inhibits the termination process by preventing the RFs from dissociating from the ribosome. Following polypeptide release, the post-termination ribosome is recycled by the ribosome recycling factor (RRF) and EF-G so that the components can be reused for the next round of translation.

peptide chain by one amino acid residue. As the polypeptide is synthesized it passes through a tunnel on the large ribosomal subunit. The function of this exit tunnel appears to be not only to provide an unobstructed passage through the ribosome for newly synthesized polypeptide chains but in many cases to regulate translation itself. Specific elements within the tunnel monitor the amino acid sequence of the nascent polypeptide chain and can arrest translation in response to particular co-factors, such as drugs or metabolites (Ito and Chiba, 2013; Wilson et al., 2016). Following peptide bond formation, translocation of mRNA and tRNAs is catalyzed by the elongation factor EF-G. Translocation by EF-G shifts the deacylated tRNA from the P site to the E site and the peptidyl-tRNA from the A site to the P site. The elongation cycle of EF-Tu delivery of aa-tRNAs and subsequent translation by EF-G is repeated until a stop codon enters the A site. Release factors (RFs), such as RF1 and RF2, recognize the stop codon and promote hydrolysis of the peptidyl-tRNA in the P site, releasing the newly synthesized protein from the ribosome. The 70S ribosome is then recycled into individual subunits by the concerted action of EF-G and the ribosome recycling factor (RRF; **Figure 1**).

There is a diverse range of clinically important antibiotics that interfere with protein synthesis by binding at various functional centers of the ribosome and either freezing a particular conformation of the ribosome or hindering the binding of its ligands (Wilson, 2009, 2014). Although these antibiotics have been successfully employed during the past 70 years for the treatment of infectious diseases, the rapid spread of antibiotic resistance among pathogenic microorganisms has greatly limited the medical utility of our existing antibiotic arsenal. This poses a serious healthcare threat, highlighting the urgent need for new classes of compounds and/or improvement of existing antibiotics. The increase in multi-drug resistant pathogens has stimulated the development of new approaches to revive the natural products discovery pipeline and to enrich our treasure trove of structural scaffolds suitable for optimization by medicinal chemists. One such avenue is the discovery and optimization of peptide-based antibiotics. Peptide antibiotics provide an unmatched platform for rational drug design because most of them can be chemically synthesized. This allows the peptide antibiotics to be easily altered by simply changing the primary sequence of amino acids as well as incorporating non-natural amino acids and chemical moieties. The many natural product peptide antibiotics that have already been discovered usually fall into one of three classes: (i) ribosomally-synthesized peptides, such as proline-rich antimicrobial peptides (PrAMPs); (ii) ribosomally-synthesized and post-translationally modified peptides (RiPPs), such as klebsazolicin (KLB) and thiopeptides (thiostrepton, micrococcin); or (iii) peptides produced by non-ribosomal peptide synthetases (NRPSs), such as edeine and GE81112. With the exception of the streptogramins, none of the natural product peptide antibiotics that have been identified and characterized have so far been used clinically, however, the recent structures of these peptide antibiotics on the ribosome provides the opportunity to further develop these classes of potent antimicrobial agents. Here we provide an overview on the known ribosome-targeting peptide antibiotics that have been

biochemically and structurally characterized. The nine different classes are organized in the following sections based on whether they target the small or large subunit of the ribosome.

## PEPTIDE ANTIBIOTICS TARGETING THE SMALL RIBOSOMAL SUBUNIT

So far there are five main classes of peptide antibiotics that target the small ribosomal subunit (**Figures 2A–F**), two of which, target translation initiation, for example, edeine and GE81112 (**Figure 1**), whereas the other three, the dityromycin/GE82832, the tuberactinomycin (viomycin and capreomycin), and odorihabdin families, inhibit the translocation and/or decoding step (**Figures 1, 2A–F**). While edeine, GE81112, odorihabdins, and tuberactinomycins interact predominantly with the 16S rRNA to modulate tRNA binding (**Figures 2B,C,E,F**; Pioletti et al., 2001; Stanley et al., 2010; Fabbretti et al., 2016), dityromycin/GE82832 interact with ribosomal protein uS12 (**Figure 2D**) to inhibit translocation by trapping EF-G in a compact conformation on the ribosome (Bulkley et al., 2014; Lin et al., 2015).

### Edeine Inhibits Initiation Complex Formation

The edeine (EDE) class of antibiotics are pentapeptide amide antibiotics produced by the bacterium *Bacillus brevis* Vm4 (Gale et al., 1981). For example, the active isomer of edeine B has an N-terminal  $\beta$ -tyrosine residue linked to a C-terminal guanyspermidine moiety via glycine and three non-proteinogenic amino acids, 2,3-diaminopropanoic acid (DAPA), 2,6-diamino-7-hydroxyazelaic acid (DAHAA), and isoserine (**Figure 3A**; Westman et al., 2013). Edeines display activity against both Gram-positive and -negative bacteria, and also *Mycoplasma* sp. (Gale et al., 1981). X-ray structures reveal that EDE has a single binding site on the small 30S subunit, positioned on the solvent side of the platform, spanning between helices h24, h44, and h45 (Pioletti et al., 2001; **Figure 3B**). The guanyspermidine moiety of EDE overlaps with the position of the anticodon stem loop of a P-site tRNA (**Figure 3C**; Pioletti et al., 2001), consistent with the inhibition of binding of initiator tRNA to the P site of 30S subunits and 70S ribosomes (Dinos et al., 2004). Curiously, however, EDE does not inhibit binding of aa-tRNAs to the P site of 70S ribosomes in the absence of mRNA, leading to the suggestion that EDE may influence binding of the P-site tRNA indirectly *via* perturbing the path of the mRNA (Dinos et al., 2004). Binding of EDE induces base-pair formation between G693 and C795 (*E. coli* numbering is used throughout the text) at the tips of h23 and h24, respectively (**Figure 3D**; Pioletti et al., 2001), in agreement with the observation that EDE protects these nucleotides from chemical modification (Woodcock et al., 1991). The G693-C795 base-pair induced by EDE appears to obstruct the path of the mRNA and may therefore explain the indirect effect that EDE has on P-site tRNA binding. Whether direct or indirect, by blocking binding of the initiator tRNA to the 30S subunit, EDE inhibits formation of the 30S pre-initiation complex and thereby

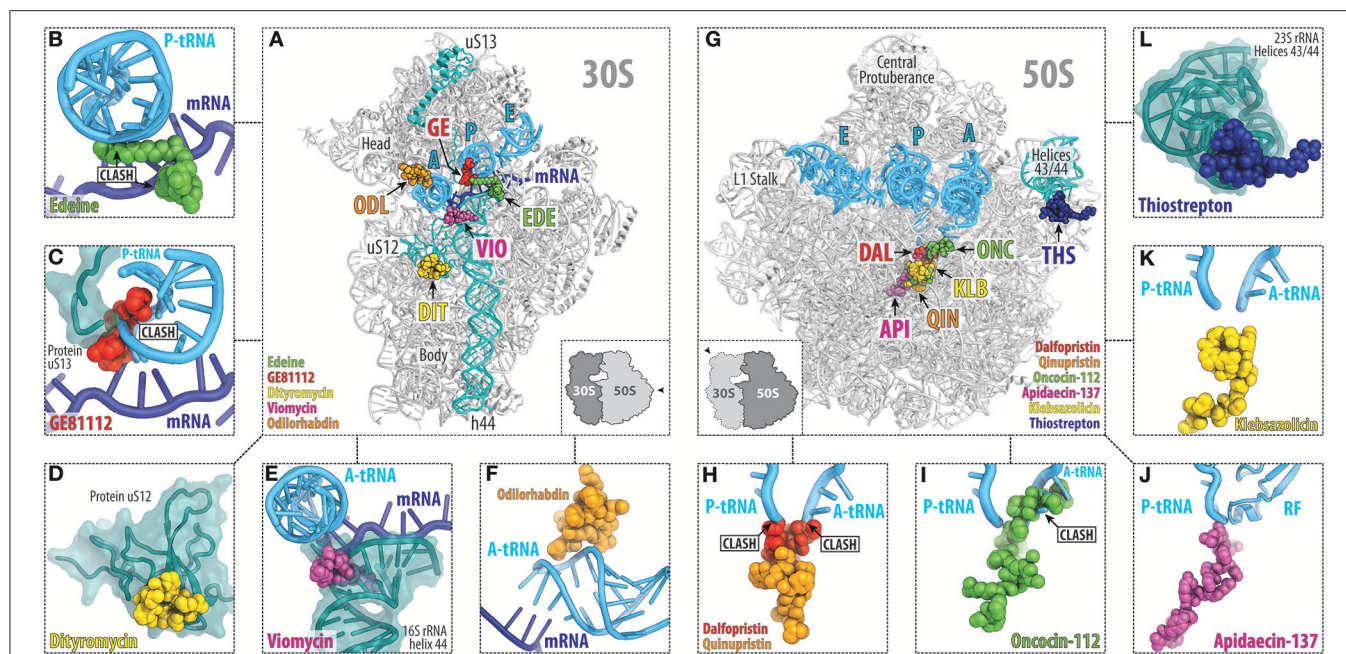


**FIGURE 2 |** Overview of the peptide antibiotics binding sites on the bacterial ribosome. Overview (A) and close-up views (B–F) of the binding sites of the peptide antibiotics (B) edeine B (EDE, green), (C) GE81112 (GE, red), (D) dityromycin (DIT, yellow), (E) viomycin (VIO, magenta), and (F) odilorhabdin (ODL, orange), which target the small (30S) ribosomal subunit. The mRNA (blue) and anticodon stem loop (ASL) of A-, P-, and E-site tRNAs (cyan) are shown, and 16S rRNA helix h44 as well as ribosomal proteins uS12 and uS13 are highlighted for reference. Overview (G) and close-up views (H–L) of the binding sites of the peptide antibiotics (H) streptogramin type A (dalfoprstin, DAL, red) and type B (quinupristin, QIN, orange), (I) oncocin-112 (ONC, green), (J) apidaecin-137 (API, magenta), (K) klebsazolicin (KLB, yellow), and (L) thiostrepton (THS, blue), which target the large (50S) ribosomal subunit. The relative position of A, P, and E-site tRNAs (cyan) are shown, and 23S rRNA helices H43/44 is highlighted for reference.

blocks association of the large subunit to form a competent 70S initiation complex.

EDE has also been shown to inhibit translation initiation on eukaryotic cytoplasmic ribosomes, such as in yeast (Gale et al., 1981). A recent crystal structure of the yeast 80S ribosome in complex with EDE reveals that although the binding site overlaps with that observed in bacteria, it adopts a markedly different conformation on the ribosome (Garreau de Loubresse et al., 2014). Rather than encroaching onto the P site as on the bacterial small ribosomal subunit, EDE is bound exclusively in the E site of the yeast small subunit (Garreau de Loubresse et al., 2014). Nevertheless, in yeast, EDE appears to also preclude stable binding of the initiator tRNA at the P site, which leads to continuous scanning of yeast 40S subunits (Kozak and Shatkin, 1978).

## GE81112 Targets Translation Initiation

The GE81112 family of non-ribosomally synthesized tetrapeptide antibiotics are produced by some *Streptomyces* species (Brandi et al., 2006a,b). The GE81112 biosynthetic gene cluster (*getA-N*) has been identified in *Streptomyces* sp. L-49973, leading to a linear model for GE81112 synthesis via a series of non-ribosomal peptide synthetases (NRPSs) and non-NRPS enzymes (Binz et al., 2010). GE81112 peptides are comprised of four L-amino acids: 3-hydroxyisovaleric acid (HPA), 2-amino-5-[(aminocarbonyl)oxy]-4-hydroxypentanoic acid (AAHPA)

followed by 5-amino-histidine and 5-chloro-2-imidazolyserine (CIS) residues (Figure 4A; Brandi et al., 2006a,b). Three distinct GE81112 congeners (A, B, and B1) have been identified, differing in molecular mass between 643 and 658 Da, with the most active and best studied being the B1 variant (658 Da; Figure 4A). GE81112 displays excellent activity against a variety of Gram-positive and Gram-negative bacteria (Brandi et al., 2006c; Maio et al., 2016). However, in rich media (e.g., LB broth), the inhibitory effects of GE81112 are suppressed because the uptake of GE81112 occurs via the oligopeptide permease Opp, which is blocked by the excess of various peptides present in the media competing with GE81112 for Opp binding (Brandi et al., 2006c; Maio et al., 2016). Indeed, the majority of spontaneous resistance mutations that arise in bacteria exposed to GE81112 lead to inactivation of the Opp transporter (Maio et al., 2016).

GE81112 was originally discovered in a high-throughput screen of Actinomycetes secondary metabolites that display inhibitory activity in an *E. coli* *in vitro* cell-free translation system, but not in a yeast system (Brandi et al., 2006a,b). To specifically select for novel translation initiation inhibitors, the screen was performed using two different mRNAs, a natural mRNA that is dependent on canonical translation initiation and a synthetic poly(U) mRNA that does not require canonical initiation events for translation to occur. The inhibition of translation *in vitro* by GE81112 from the screen was validated *in vivo* by showing that GE81112 inhibits the incorporation



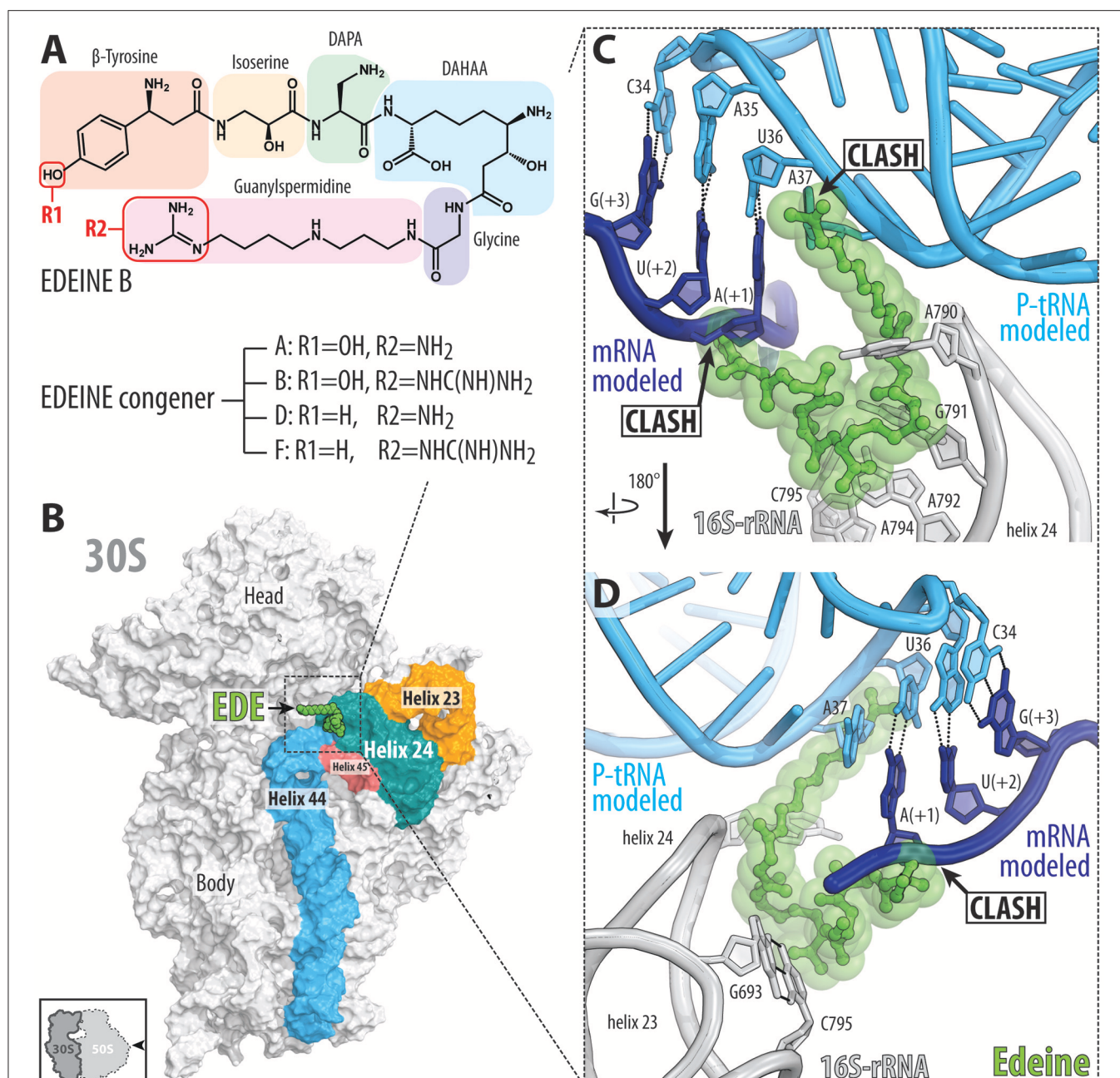


**FIGURE 3 |** Binding of the peptide antibiotic edeine is incompatible with the P-site tRNA and mRNA. **(A)** Chemical structure of the edeine B consisting of  $\beta$ -tyrosine, isoserine, DAPA (2,3-diaminopropanoic acid), DAHAA (2,6-diamino-7-hydroxyazelaic acid), and guanylspermidine moieties. **(B)** Overview of edeine B (EDE, green) binding site on the 30S subunit (PDB ID 1I95; Pioletti et al., 2001), with 16S rRNA helices h44 (blue), h45 (red), h23 (orange), and h24 (teal) shown for reference. The 30S subunit is viewed from the subunit interface as indicated by the inset at the bottom left. **(C,D)** Close-up view of EDE (green) binding site at the tip of helix h23 and h24 (gray) showing overlap of EDE with P-site tRNA (cyan) and first codon (+1) of the P-site mRNA (blue). Hydrogen bonding between the nucleotides G693-C795 of the 16S rRNA formed upon EDE binding is indicated with dashed lines in **(D)** (Pioletti et al., 2001).

of radiolabeled [<sup>14</sup>C]-phenylalanine, but not [<sup>3</sup>H]-thymidine or [<sup>3</sup>H]-uridine, thus, confirming GE81112 to be an inhibitor of protein synthesis, but not of DNA replication or RNA transcription (Brandi et al., 2006a,b). Subsequent experiments revealed that GE81112 does not inhibit *in vitro* translation when

using a human (HeLa) system, but is active in an archaeal (*Sulfolobus sulfataricus*) system (Brandi et al., 2006a,b) pointing to its selectivity against prokaryotic translation.

Initial biochemical assays suggested that GE81112 inhibited formation of the 30S pre-initiation complex (30S-PIC) by



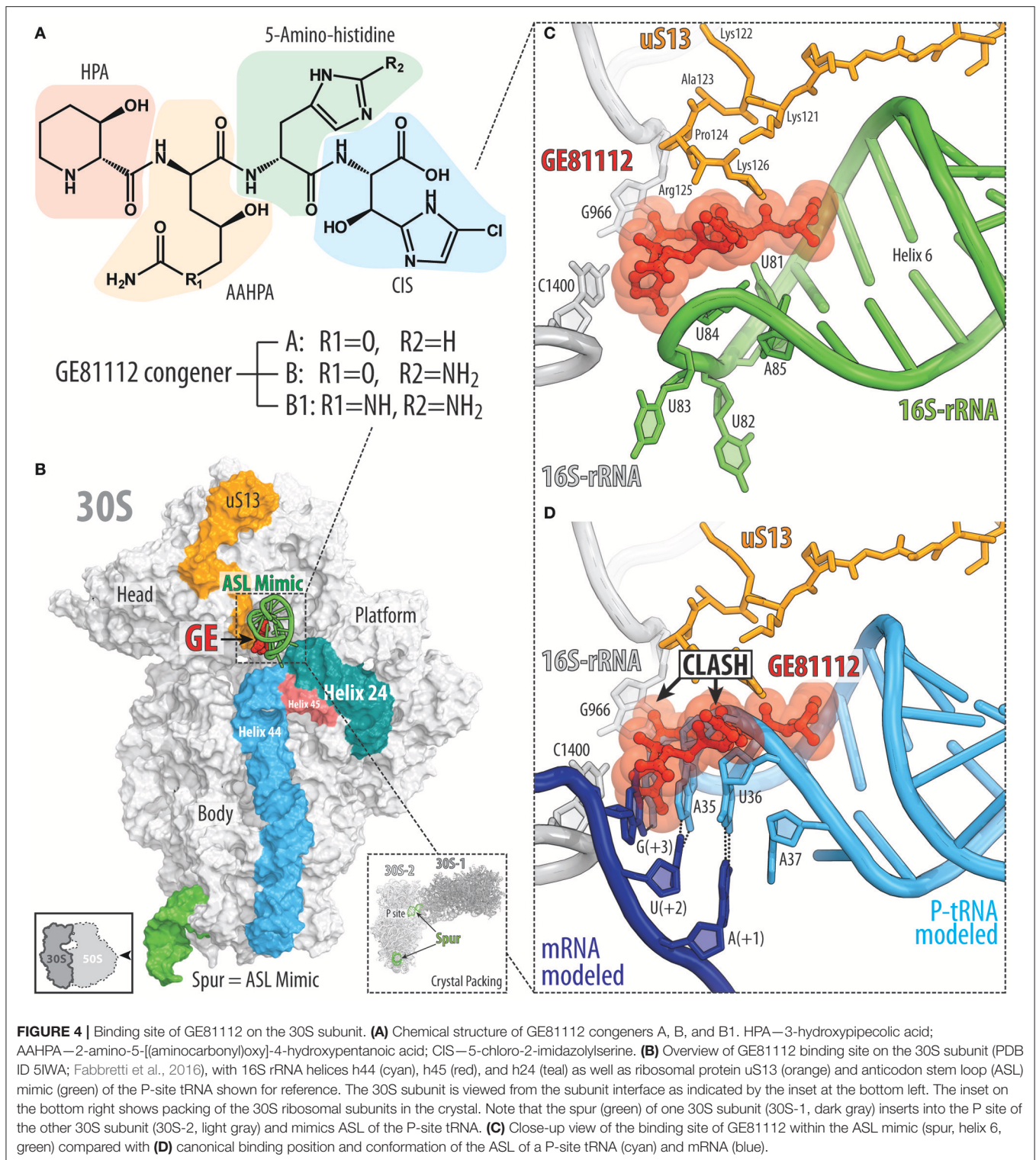


**FIGURE 4 |** Binding site of GE81112 on the 30S subunit. **(A)** Chemical structure of GE81112 congeners A, B, and B1. HPA—3-hydroxyproline; AAHPA—2-amino-5-[(aminocarbonyl)oxy]-4-hydroxypentanoic acid; CIS—5-chloro-2-imidazolyserine. **(B)** Overview of GE81112 binding site on the 30S subunit (PDB ID 5IWA; Fabbretti et al., 2016), with 16S rRNA helices h44 (cyan), h45 (red), and h24 (teal) as well as ribosomal protein uS13 (orange) and anticodon stem loop (ASL) mimic (green) of the P-site tRNA shown for reference. The 30S subunit is viewed from the subunit interface as indicated by the inset at the bottom left. The inset on the bottom right shows packing of the 30S ribosomal subunits in the crystal. Note that the spur (green) of one 30S subunit (30S-1, dark gray) inserts into the P site of the other 30S subunit (30S-2, light gray) and mimics ASL of the P-site tRNA. **(C)** Close-up view of the binding site of GE81112 within the ASL mimic (spur, helix 6, green) compared with **(D)** canonical binding position and conformation of the ASL of a P-site tRNA (cyan) and mRNA (blue).

preventing binding of the initiator fMet-tRNA to the 30S subunit (Brandt et al., 2006b). However, this model was subsequently revised, such that GE81112 does not interfere with the initial binding of the fMet-tRNA in the “unlocked” 30S-PIC, but prevents conversion of the “unlocked” into the “locked” 30S-PIC

(Fabbretti et al., 2016; Lopez-Alonso et al., 2017). Correct recognition of the start codon by the fMet-tRNA is thought to facilitate conversion from the “unlocked” to the “locked” 30S-PIC, which is accompanied by conformational changes in the ribosome and fMet-tRNA that promote joining of the

50S subunit to form the 70S initiation complex. Cryo-electron microscopy structures of the 30S-PIC formed in the presence of GE81112 revealed two distinct functional ribosomal states with the fMet-tRNA either directly engaged with the start codon, or shifted away and disengaged from the mRNA (Lopez-Alonso et al., 2017). Unfortunately, the resolution of the complexes did not allow visualization of GE81112 so it remains unclear whether both states represent unlocked 30S-PIC with GE81112 bound or whether the engaged state reflects the locked 30S-PIC in the absence of GE81112.

The structure of GE81112 on the *Thermus thermophilus* 30S subunit was determined using X-ray crystallography (Fabbretti et al., 2016). GE81112 was found to bind to helix 6 (h6) of the 16S rRNA, which forms the so-called spur of the 30S subunit (Figure 4B). Within the crystal, the individual 30S subunits are packed in such a way that the spur of one 30S subunit mimics the anticodon-stem-loop (ASL) of a tRNA and inserts into the P site of another 30S subunit, suggesting that GE81112 binds and interacts with the ASL of a P-site tRNA in the 30S-PIC (Figure 4C; Fabbretti et al., 2016). Binding of GE81112 to the 30S subunit induces distortions within the loop of h9, which mimics the anticodon of the P-site tRNA (Figures 4C,D), suggesting how GE81112 could prevent recognition of the start codon by the P-site tRNA. In addition to h9, GE81112 establishes extensive contact with the C-terminal extension of the ribosomal protein uS13 (Figures 4C,D). This interaction is, however, unlikely to be necessary for the action of GE81112 since it cannot occur in many other bacterial species, such as *E. coli*, because the C-terminal extension of the uS13 is significantly shorter.

Other than uS13, very few additional contacts of GE81112 are observed with the 30S subunit, suggesting that the P-site tRNA comprises the major determinant for GE81112 binding. The extensive interaction with P-site tRNA, rather than with the 16S rRNA, may explain the difficulty in obtaining spontaneous

resistance mutations to GE81112, even when the Opp transporter is overexpressed (Maio et al., 2016). However, 16S rRNA mutations A794G/U or G926A/C/U that mediate high level (up to 70-fold) kasugamycin resistance, also lead to a modest increase (10-fold) in GE81112 resistance, as monitored using *in vitro* mRNA translation assays (Maio et al., 2016). Similarly, the extensive interaction with P-site tRNA, rather than with 16S rRNA, may also explain the difficulty in using chemical modification techniques to map the GE81112 binding site on the 30S subunit (Brandi et al., 2006b). Nevertheless, chemical probing experiments revealed that binding of GE81112 induces conformational changes within the h44/h45/h24a interface of the 30S subunit (Brandi et al., 2006b; Fabbretti et al., 2016), which were proposed to favor the disengaged conformation of the initiator tRNA and prevent conversion to the “locked” 30S-PIC and thereby prevent 50S subunit joining (Fabbretti et al., 2016).

## GE82832/Dityromycin Targets the Translocation Step of Translation Elongation

While ribosomal protein uS13 contributes significantly to the binding of GE81112, ribosomal protein uS12 in the 30S subunit is the important determinant for binding of GE82832, a cyclic peptide antibiotic (Figure 5A) produced by *Streptosporangium cinnabarinum* (strain GE82832) that inhibits tRNA translocation by interacting with the 30S subunit (Brandi et al., 2006a). GE82832 is related to a poorly characterized antibiotic dityromycin that was discovered decades ago (Omura et al., 1977; Brandi et al., 2012). Characterization of both antibiotics has shown that they are structurally and functionally related, with both inhibiting EF-G-dependent tRNA translocation on the ribosome (Brandi et al., 2012). The crystal structure of the 70S ribosome in complex with dityromycin and GE82832 showed that these antibiotics are unique because

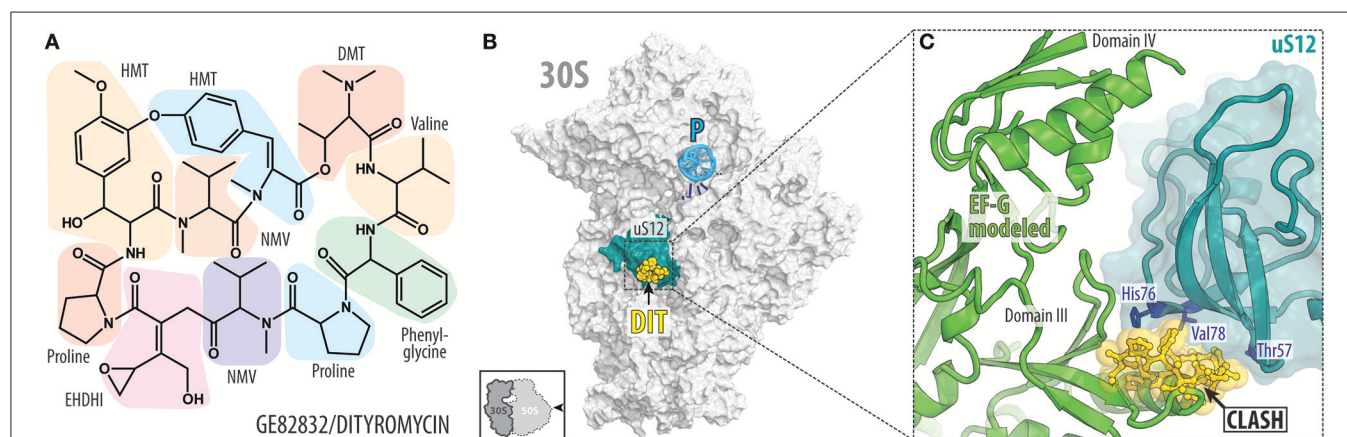


**FIGURE 5 |** GE82832/dityromycin bind to uS12 on the 30S subunit and inhibit translocation. **(A)** Chemical structure of the GE82832/dityromycin comprises proteinogenic (e.g., proline or valine) as well as non-proteinogenic amino acids, such as N,N-dimethyl-threonine (DMT), N-methyl-valine (NMV), epoxy-hydroxy-dehydro-isoleucine (EHDHI), or dihydroxyl-methyl tyrosine (HMT). **(B)** GE82832/dityromycin (DIT, yellow) interacts exclusively with the ribosomal protein uS12 (teal) on the 30S subunit (gray) (PDB ID 4NVY; Bulkley et al., 2014). The anticodon stem loop (ASL) of a P-site tRNA (cyan) and mRNA (blue) are shown for reference. The 30S subunit is viewed from the subunit interface, as indicated by the inset at the bottom left. **(C)** Overlap in the binding site of dityromycin (yellow) and domain III of EF-G (green). Residues within uS12 (teal) that are important for dityromycin binding are highlighted in blue.



they bind exclusively to ribosomal protein (uS12) rather than rRNA (**Figures 5B,C**; Bulkley et al., 2014). uS12 is positioned on the shoulder of the 30S subunit, where it reaches into the decoding center and acts as a control element in tRNA selection (Yates, 1979) and the translocation of tRNA-mRNA through the ribosome (Cukras et al., 2003).

The mechanism by which dityromycin and GE82832 interfere with tRNA and mRNA translocation has recently been elucidated using a crystal structure of EF-G bound to a dityromycin-70S ribosome complex (**Figure 5C**; Lin et al., 2015). The binding of dityromycin to protein uS12 traps EF-G in a compact conformation on the ribosome, inhibiting EF-G-mediated tRNA translocation. The binding site of GE82832/dityromycin also overlaps with that of ribosome recycling factor (RRF; Gao et al., 2007). Because RRF and EF-G work together in recycling, it is unclear whether the effects of GE82832/dityromycin on RRF could be disentangled from its effects on EF-G alone, but a superposition of RRF bound to both the *E. coli* Borovinskaya et al., 2007 and *T. thermophilus* (Weixlbaumer et al., 2007) ribosomes shows that RRF and GE82832/dityromycin share a contact point with uS12.

While the structure of GE82832/dityromycin in complex with the bacterial ribosome and EF-G explains its activity as a translocation inhibitor, it is also consistent with GE82832/dityromycin affecting the ability of EF-Tu to deliver aminoacyl-tRNA to the ribosomal A-site. The mutation of several residues of uS12 that are distant from the decoding center have been shown to increase miscoding errors. Two of these mutations, Thr57 and Val78 (*E. coli*; Agarwal et al., 2011), form part of the binding pocket for GE82832/dityromycin. Moreover, His76, the same residue that is critical for binding of GE82832/dityromycin to the ribosome (Brandi et al., 2012), is involved in EF-Tu signaling when codon recognition has taken place (Gregory et al., 2009). However, only at high concentrations (~10  $\mu$ M) does GE82832/dityromycin inhibit (~50%) the delivery of tRNA to the A-site in the absence of EF-Tu, whereas it has virtually no effect when EF-Tu is present (Brandi et al., 2006a). While this is likely due to the fact that aa-tRNA and EF-Tu simply outcompete the antibiotic from its binding site, it should be noted that overall protein synthesis and translocation are inhibited at the same rate by GE82832/dityromycin (Brandi et al., 2006a).

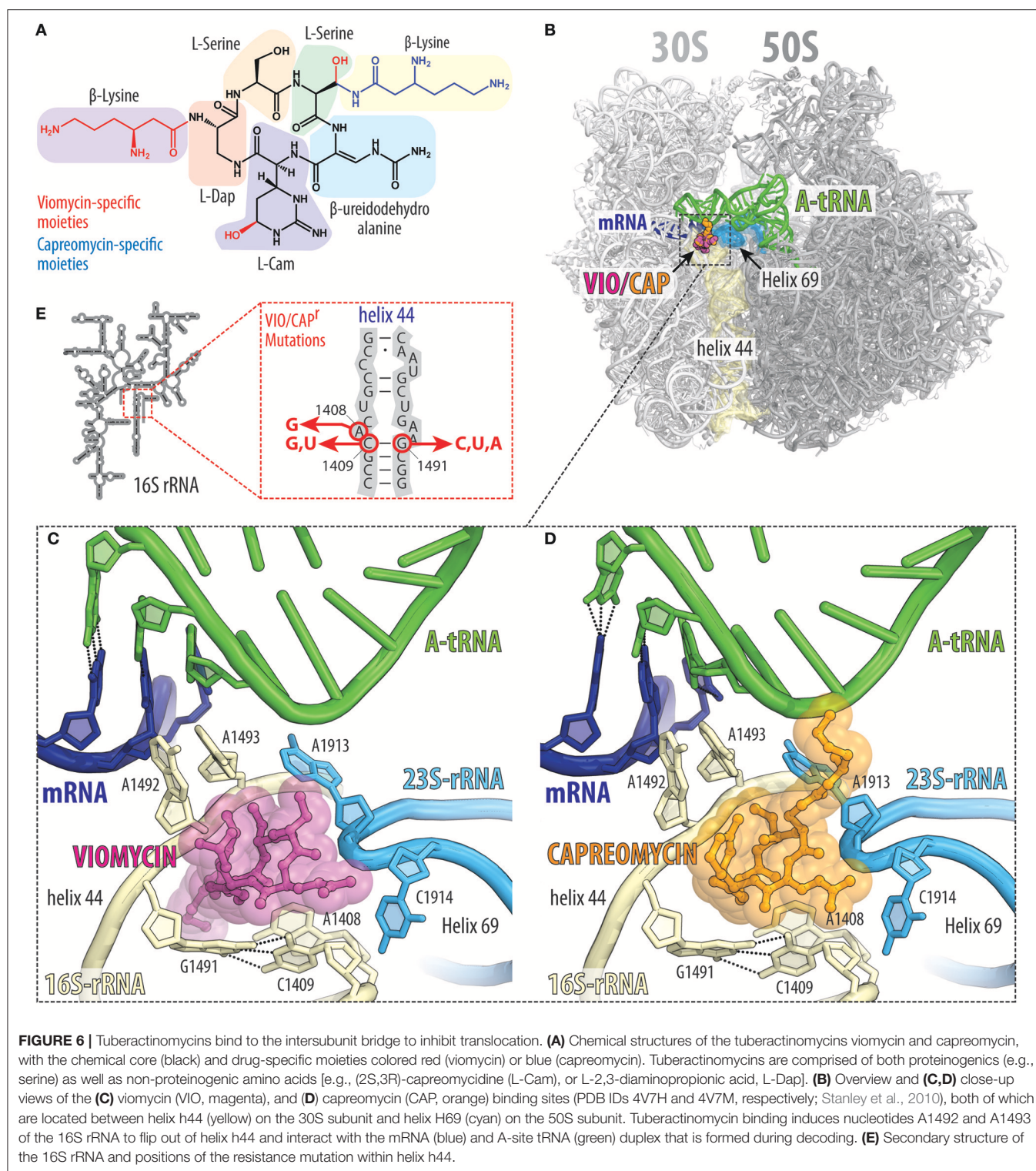
## The Tuberactinomycins Viomycin and Capreomycin Inhibit Translocation

Viomycin and capreomycin are cyclic pentapeptide antibiotics containing several non-canonical amino acids (**Figure 6A**), which are produced by non-ribosomal peptide synthetases (NRPSs) found in various *Streptomyces* species (Thomas et al., 2003). Viomycin and capreomycin are members of the tuberactinomycin family and display excellent activity against *Mycobacterium tuberculosis*, including multidrug resistant strains (Jain and Dixit, 2008). Tuberactinomycins have a single binding site on the ribosome that spans the ribosomal interface between h44 of the small 30S subunit and H69 of the large 50S subunit (**Figure 6B**; Stanley et al., 2010). Binding of the

tuberactinomycins within h44 requires nucleotides A1492 and A1493 to adopt a flipped-out conformation (**Figures 6C,D**; Stanley et al., 2010), as observed during decoding of aa-tRNA in the A-site (Ogle et al., 2003). This explains why the affinity of viomycin to the ribosome greatly increases upon binding of an A-site tRNA (Holm et al., 2016). Although the crystal structures of viomycin (and capreomycin) were on non-rotated ribosomes, biophysical studies indicate that viomycin stabilizes a rotated conformation of the ribosome with hybrid A/P- and P/E-tRNAs (Peske et al., 2004; Shoji et al., 2006; Ermolenko et al., 2007; Pan et al., 2007; Cornish et al., 2008; Ly et al., 2010; Wang et al., 2012). Thus, viomycin inhibits translation by trapping the ribosome in an intermediate state on the translocation pathway and can therefore be considered as a translocation inhibitor, as originally proposed in the 1970's (Liou and Tanaka, 1976; Modolell and Vazquez, 1977). Importantly, viomycin does not prevent binding of EF-G to the ribosome, nor GTP hydrolysis by EF-G (Modolell and Vazquez, 1977; Peske et al., 2004), however, by blocking translocation viomycin prevents release of EF-G from the ribosome and leads to multiple rounds of futile GTP hydrolysis by EF-G before translocation can occur (Holm et al., 2016). A pre-translocation complex with A/P and P/E hybrid site tRNAs and EF-G trapped by viomycin has been visualized by cryo-electron microscopy (Brilot et al., 2013).

The flipped-out conformations of A1492 and A1493 observed in the presence of viomycin (**Figure 6C**) or capreomycin (**Figure 6D**; Stanley et al., 2010) are analogous to those observed in the presence of the misreading inducing 2-deoxystreptamine aminoglycosides (Ogle et al., 2003). However, compared to aminoglycosides, the tuberactinomycin antibiotics induce little, if any, misreading on bacterial ribosomes (Marrero et al., 1980; Akbergenov et al., 2011). Nevertheless, translational misreading (Marrero et al., 1980; Wurmbach and Nierhaus, 1983) and stop codon suppression (Holm et al., 2016) has been reported when using tuberactinomycins in some *in vitro* translation systems. Stabilization of tRNAs in the A-site by viomycin has also been shown to promote back-translocation (Shoji et al., 2006). Viomycin also inhibits mRNA and tRNA release and splitting of ribosomal subunits (Hirokawa et al., 2002; Savelsbergh et al., 2009; Chen et al., 2017) that is normally mediated by RRF and EF-G during ribosome recycling. Additionally, viomycin has been reported to interfere with the canonical translation termination as well as the ArfA-RF2-dependent rescue system (Zeng and Jin, 2016).

Consistent with its binding site, resistance to viomycin results from ribosomes that have mutations or alterations in either the 16S or 23S rRNA (**Figure 6E**; Yamada et al., 1978; Maus et al., 2005; Johansen et al., 2006), as well as via inactivation of the TlyA methyltransferase that methylates nucleotides C1409 in h44 of the 30S subunit and C1920 in H69 of the 50S subunit (Johansen et al., 2006; Monshupanee et al., 2012). Capreomycin has been shown to disrupt the interaction between *M. tuberculosis* ribosomal proteins uL10 and bL12 (Lin et al., 2014), however, because resistance occurs via mutations in the 23S rRNA, it is likely that this is a secondary effect rather than the prime reason for translation inhibition.



## Odilorhabdins Cause Miscoding by Tethering tRNA to the Ribosome

Recently, a new class of modified peptide antibiotics, odilorhabdins (ODLs), has been discovered (Figure 7A; Pantel et al., 2018). Similarly to tuberactinomycins, ODLs are

produced by NRPSs, but from the Gram-negative bacteria *Xenorhabdus nematophila*, which live symbiotically with soil-dwelling nematodes. The first three naturally occurring ODLs were identified by screening the supernatants of 80 cultured *Xenorhabdus* strains for the presence of antimicrobial activity



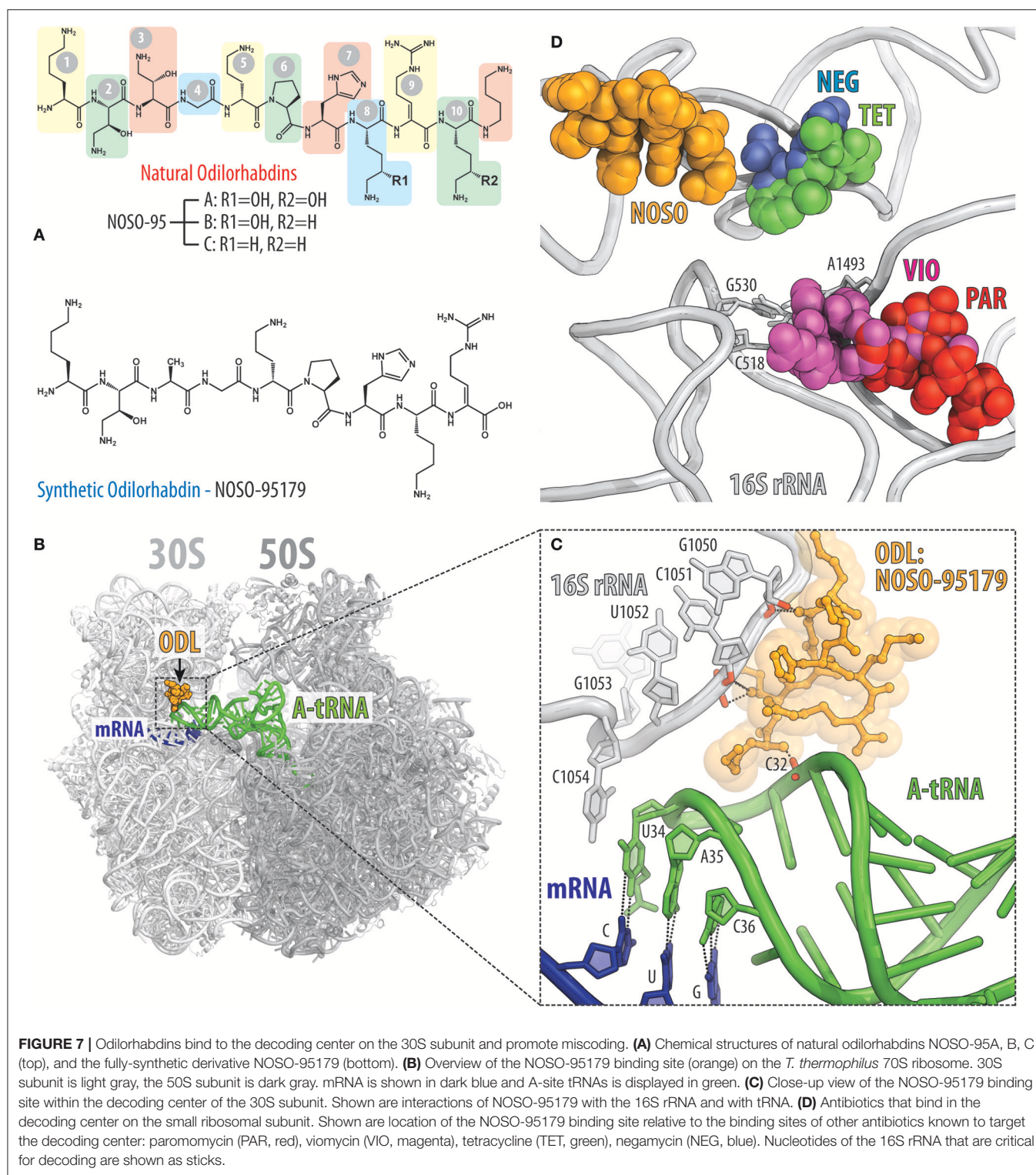


**FIGURE 7 |** Odilorhabdins bind to the decoding center on the 30S subunit and promote miscoding. **(A)** Chemical structures of natural odilorhabdins NOSO-95A, B, C (top), and the fully-synthetic derivative NOSO-95179 (bottom). **(B)** Overview of the NOSO-95179 binding site (orange) on the *T. thermophilus* 70S ribosome. 30S subunit is light gray, the 50S subunit is dark gray. mRNA is shown in dark blue and A-site tRNAs is displayed in green. **(C)** Close-up view of the NOSO-95179 binding site within the decoding center of the 30S subunit. Shown are interactions of NOSO-95179 with the 16S rRNA and with tRNA. **(D)** Antibiotics that bind in the decoding center on the small ribosomal subunit. Shown are location of the NOSO-95179 binding site relative to the binding sites of other antibiotics known to target the decoding center: paromomycin (PAR, red), viomycin (VIO, magenta), tetracycline (TET, green), negamycin (NEG, blue). Nucleotides of the 16S rRNA that are critical for decoding are shown as sticks.

(Pantel et al., 2018). These compounds with molecular weights of 1,296, 1,280, and 1,264 Da were isolated from the supernatant of *X. nematophila* strain K102 and were named NOSO-95A, NOSO-95B, and NOSO-95C, respectively (Figure 7A, top). These ODLs consist of 10 amino acids, including four types of

non-proteinogenic amino-acid residues:  $\alpha,\gamma$ -diamino- $\beta$ -hydroxy butyric acid [Dab( $\beta$ OH)] in positions 2 and 3;  $\delta$ -hydroxy lysine (Dhl) in positions 8 and 10;  $\alpha,\beta$ -dehydro arginine (Dha) in position 9; and  $\alpha,\delta$ -diamino butane (Dbt) in position 11 (Figure 7A, top). The peptidic nature and relative simplicity

of ODLs opened the way for improvement of their activity by modifying the chemical structure, resulting in the development of NOSO-95179 (**Figure 7A**, bottom), a derivative that exhibits better selectivity for bacterial vs. eukaryotic target compared to natural ODLs and thus, represents a preferable lead for further drug development. Overall, ODLs exhibit promising broad-spectrum bactericidal activity and are able to cure bacterial infections in animal models (Pantel et al., 2018).

ODLs bind to the decoding center of the bacterial ribosome at a site not exploited by any other known ribosome-targeting antibiotics (**Figures 7B,C**). In this binding site, ODLs simultaneously interact with the 16S rRNA as well as with the anticodon loop of the A-site tRNA. Interaction between the ODL and A-site tRNA increases the affinity of the aminoacyl-tRNA to the ribosome, resulting in a decreased accuracy of translation and impeding progression of the ribosome along the mRNA (**Figure 7C**; Pantel et al., 2018). Although, several classes of antibiotics also target the ribosomal decoding center, the binding site of ODLs is distinct from those of other inhibitors, such as tetracycline and negamycin as well as the tuberactinomycins and aminoglycosides (**Figure 7D**). Despite this, the overall mechanism of action of ODLs is conceptually similar to that of the aminoglycosides or negamycin, whose mode of translation inhibition depends on the drug concentration. At lower concentrations, these antibiotics induce amino acid misincorporation by reducing the fidelity of decoding, whereas at higher concentrations they interfere with translocation (Wang et al., 2012; Olivier et al., 2014; Polikanov et al., 2014; Pantel et al., 2018). Both activities likely reflect a tighter binding of the tRNA in the A site induced by the ODL. The direct interaction between ODL and tRNA anticodon not only promotes miscoding, but also likely hinders the transition of tRNA from the A site into the P site thus inhibiting translocation at the higher concentrations of the antibiotic.

## PEPTIDE ANTIBIOTICS TARGETING THE LARGE RIBOSOMAL SUBUNIT

Binding sites of the majority of peptide antibiotics that target the large 50S subunit cluster around the PTC where peptide bond formation occurs (**Figure 2G**), for example, streptogramin A (**Figure 2H**; Hansen et al., 2003; Noeske et al., 2014; Osterman et al., 2017), as well as within the nascent peptide exit tunnel, as seen for the streptogramins B (**Figure 2H**) and klebsazolicin (**Figures 2K**; Harms et al., 2004; Noeske et al., 2014; Meteleev et al., 2017). The binding sites of the PrAMPs (**Figures 2I,J**) span from the PTC into the nascent peptide exit tunnel (Graf et al., 2017) and thereby overlap the binding sites of both the streptogramin A and B compounds (**Figure 2H**). In contrast, the thiopeptide antibiotics, such as thiostrepton, have a distinct binding site from other clinically used antibiotics, which is located far from the PTC and exit tunnel. Instead, the binding site of the thiopeptides is located within the translation factor binding site on the large subunit and encompasses the components of the uL11 stalk base (**Figure 2L**; Harms et al., 2008).

## Streptogramin Antibiotics Act Synergistically on the Large Ribosomal Subunit

Streptogramin antibiotics are produced by several species of *Streptomyces* and comprise two structurally distinct subclasses: group A, which contain 23-membered macrocyclic polyketide/nonribosomal peptide hybrids and group B, which comprise 19-membered macrocyclic depsipeptides (**Figure 8A**; Li and Seiple, 2017). Streptogramins have been used as livestock feed additives for decades (Yates and Schaible, 1962) but were not approved by the FDA until the introduction of quinupristin-dalfopristin (Synercid) in 1999. The clinical use of this combination therapy is limited by its intravenous-only formulation and its narrow spectrum of activity, and is reserved for hospitalized patients with multidrug-resistant skin infections or with bacteremia caused by vancomycin-resistant *Enterococcus faecium* (Delgado et al., 2000). An orally bioavailable combination of semisynthetic streptogramins known as NXL-103 (flopristin-linopristin) underwent phase-II clinical trials in Pankuch et al. (2011), but has not progressed further in the clinic.

### Streptogramin A Antibiotics Target the Peptidyl Transferase Center

The binding site of group A streptogramins ( $S_A$ ) spans the A-site cleft and also encroaches into the P site of the bacterial ribosome (**Figures 2G, 8B**). Madumycin II (MADU), the simplest  $S_A$  antibiotic, inhibits the ribosome prior to the first cycle of peptide bond formation (Osterman et al., 2017). It allows binding of the tRNAs to the A and P sites, but prevents correct positioning of their CCA-ends into the PTC, thus making peptide bond formation impossible. Also, binding of MADU induces rearrangement of nucleotides U2506 and U2585 of the 23S rRNA resulting in the formation of the U2506-G2583 wobble base-pair that has been attributed to a catalytically inactive state of the PTC (Schmeing et al., 2005; Osterman et al., 2017). Virginiamycin M is another  $S_A$  antibiotic that binds in the PTC, causes rearrangements of nucleotides A2062 and U2585 (Hansen et al., 2003; Tu et al., 2005; Noeske et al., 2014) and inhibits binding of A- and P-site substrates (Pestka, 1969; Chinali et al., 1984). In this case, the oxazole ring of virginiamycin M reaches into the A-site cleft, where it establishes hydrophobic interactions.

### Streptogramin B Antibiotics Block Elongation of the Nascent Polypeptide Chain

The nascent polypeptide exit tunnel of the ribosome is targeted by group B streptogramins ( $S_B$ ), such as pristnamycin IA, quinupristin, and virginiamycin S (**Figure 8B**). Crystal structures of  $S_A$  (Hansen et al., 2003; Harms et al., 2004; Tu et al., 2005; Noeske et al., 2014; Osterman et al., 2017) and  $S_B$  (Harms et al., 2004; Tu et al., 2005; Noeske et al., 2014) antibiotics in complex with the ribosome show that both classes bind to adjacent, but not overlapping, sites on the ribosome, which explains their synergistic action (**Figure 8B**; Vannuffel and Cocito, 1996). As



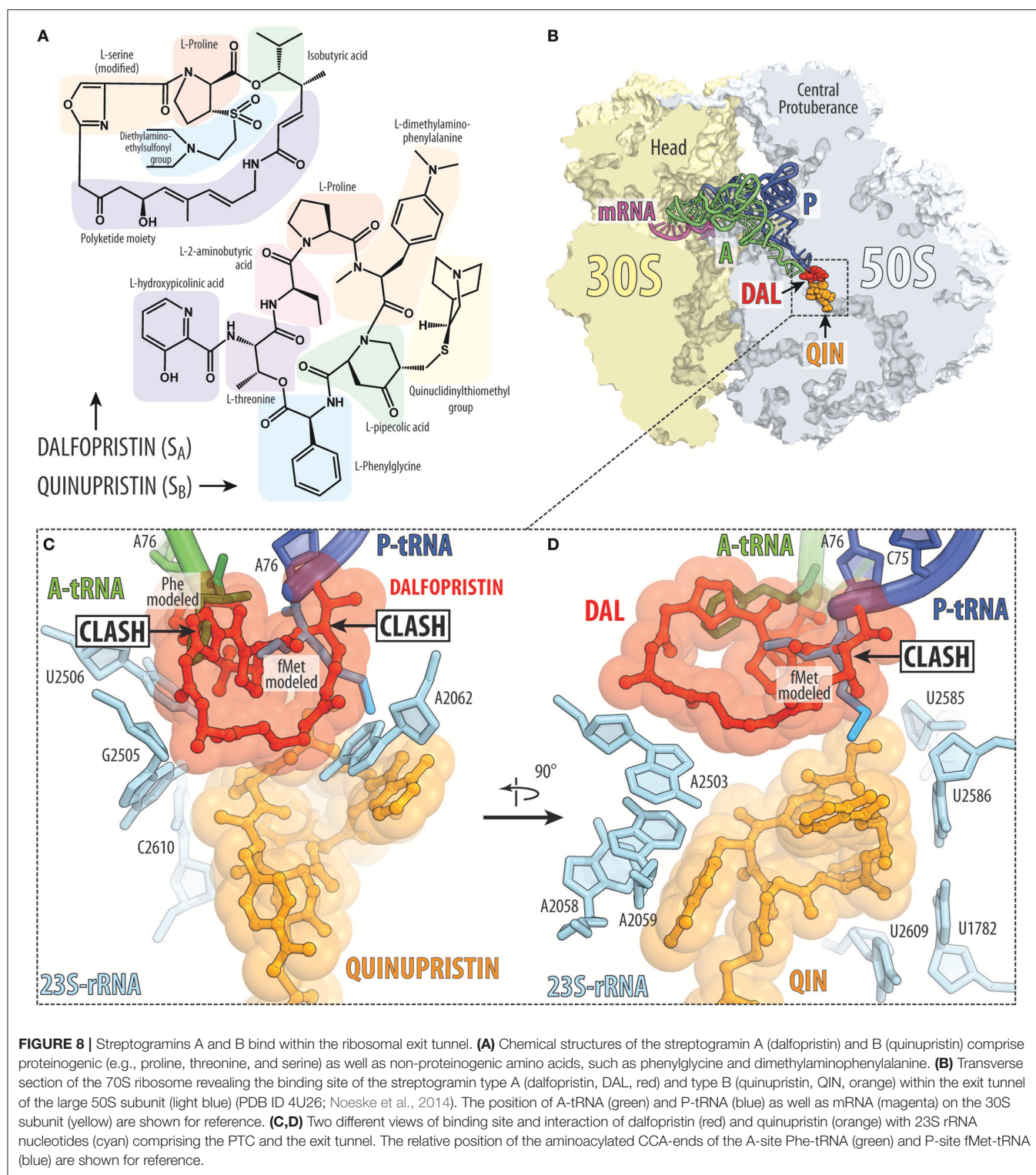


**FIGURE 8 |** Streptogramins A and B bind within the ribosomal exit tunnel. **(A)** Chemical structures of the streptogramin A (dalbopristin) and B (quinupristin) comprise proteinogenic (e.g., proline, threonine, and serine) as well as non-proteinogenic amino acids, such as phenylglycine and dimethylaminophenylalanine. **(B)** Transverse section of the 70S ribosome revealing the binding site of the streptogramin type A (dalbopristin, DAL, red) and type B (quinupristin, QIN, orange) within the exit tunnel of the large 50S subunit (light blue) (PDB ID 4U26; Noeske et al., 2014). The position of A-tRNA (green) and P-tRNA (blue) as well as mRNA (magenta) on the 30S subunit (yellow) are shown for reference. **(C,D)** Two different views of binding site and interaction of dalbopristin (red) and quinupristin (orange) with 23S rRNA nucleotides (cyan) comprising the PTC and the exit tunnel. The relative position of the aminoacylated CCA-ends of the A-site Phe-tRNA (green) and P-site fMet-tRNA (blue) are shown for reference.

discussed above, S<sub>A</sub> antibiotics bind at the PTC and prevent proper positioning of the A- and P-site tRNAs (**Figures 8C,D**), whereas S<sub>B</sub> antibiotics bind to a site that overlaps with that of macrolides and presumably interfere with the passage of the nascent peptide through the exit tunnel. Interestingly, nucleotide

A2062 of the 23S rRNA is sandwiched between the macrocyclic ring of S<sub>A</sub> compound (for example, dalbopristin) and the S<sub>B</sub> compound (for example quinupristin) (**Figure 8C**; Harms et al., 2004; Tu et al., 2005; Noeske et al., 2014), rationalizing why mutation A2062C in the 23S rRNA of *Streptococcus pneumoniae*

leads to  $S_A$  and  $S_B$  cross-resistance (Depardieu and Courvalin, 2001). Streptogramins have been approved for clinical use, such as Synercid, a mixture of the type A streptogramin dalbapristin and the type B streptogramin quinupristin (**Figure 8A**; Noeske et al., 2014), which are effective against methicillin-resistant *Staphylococcus aureus* (MRSA; Manzella, 2001).

A unique property of the streptogramin antibiotics is that groups A and B compounds act synergistically *in vivo* and *in vitro*, such that binding of the  $S_A$  compound promotes the binding of the corresponding  $S_B$  compound (Parfait et al., 1978). Due to this synergistic action, the concentration of each of the compounds in the mixture required to achieve the inhibitory action is significantly lower than the concentration of each of the compounds when they are used separately (Champney, 2001). The synergistic action also allows streptogramins to overcome some resistance mutations (Vannuffel et al., 1992; Canu and Leclercq, 2001). Moreover, by combining some  $S_A$  and  $S_B$  compounds it is possible to convert a bacteriostatic effect into a bactericidal lethality. The basis for the synergy between  $S_A$  and  $S_B$  is likely related to a rotation of nucleotide A2062 of the 23S rRNA that was observed upon binding of  $S_A$  compounds to the PTC (Hansen et al., 2003; Harms et al., 2004; Tu et al., 2005; Noeske et al., 2014; Osterman et al., 2017). In the new drug-induced conformation, A2062 can enhance binding of  $S_B$  compounds via additional stacking and/or hydrogen bond interactions. Indeed, mutations of A2062 can also lead to streptogramin resistance (Depardieu and Courvalin, 2001). In summary, the action of streptogramins is likely to block both A and P sites, and therefore function during initiation step (**Figure 1**) or by inducing peptidyl-tRNA drop-off at an early elongation step (**Figure 1**).

## Proline-Rich Antimicrobial Peptides Exhibit Distinct Mechanisms of Action

Unlike most antimicrobial peptides (AMPs), which kill bacteria by disrupting the bacterial membrane, the subclass of proline-rich antimicrobial peptides (PrAMPs) can pass through the bacterial membrane without damaging it and instead inhibit bacterial growth by targeting intracellular processes, such as protein synthesis (Casteels and Tempst, 1994; Mattiuzzo et al., 2007; Seefeldt et al., 2016; Graf et al., 2017). As suggested by their name, PrAMPs are AMPs rich in proline, but also contain many arginine residues. PrAMPs are products of the innate immune system and provide a first line of defense against invading bacteria. To date, PrAMPs have been found in many arthropods, such as insects and crustaceans, as well as in some mammals, such as cows, pigs, goats and sheep (Scocchi et al., 2011; Graf et al., 2017). PrAMPs are usually synthesized as inactive pre-pro-peptides that are matured *via* protease cleavage to yield the active PrAMP peptides. Non-lytic PrAMPs display excellent activity against Gram-negative bacteria, such as *E. coli*, but are generally less active against Gram-positive bacteria, such as *Bacillus subtilis*. This specificity is due to the fact that the uptake of PrAMPs occurs predominantly via the SbmA transporter (Mattiuzzo et al., 2007), but can also utilize the YjiL-MdtM transport system (Krizsan et al., 2015), which are present

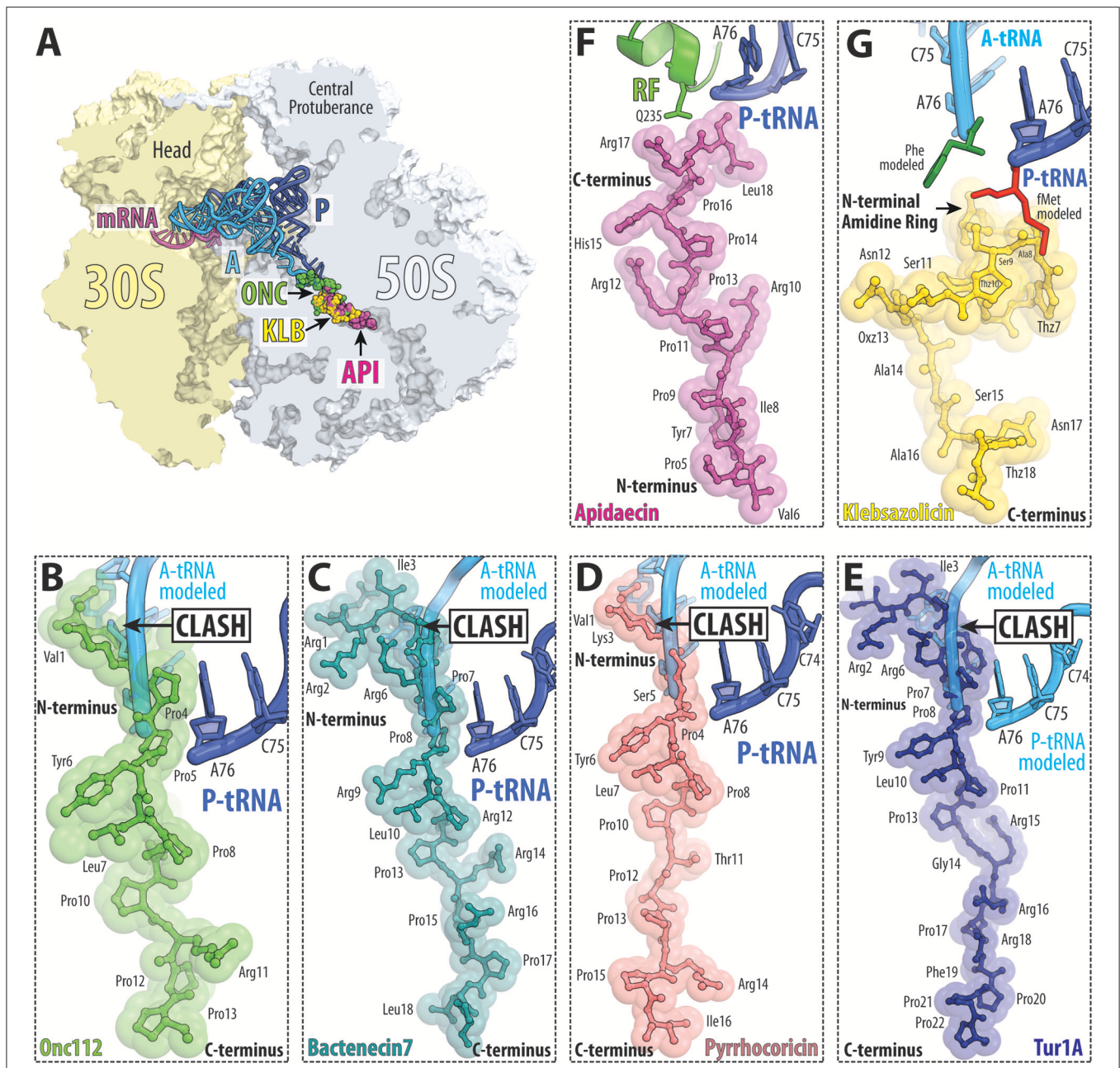
in most Gram-negative bacteria, but lacking in Gram-positive bacteria. Indeed, resistance to PrAMPs can arise due to deletion or mutation of the SbmA and MdtM transporters (Mattiuzzo et al., 2007; Krizsan et al., 2015; Seefeldt et al., 2015; Florin et al., 2017; Mardirossian et al., 2018). It should be noted that the mammalian PrAMPs, such as Bac7, are generally longer (~60 aa) than insect PrAMPs (~20 aa) and these additional C-terminal residues promote membrane permeabilization (Skerlavaj et al., 1990; Podda et al., 2006), suggesting a dual mode of uptake and action for these PrAMPs.

PrAMPs were shown to interact with the DnaK chaperone, thus initially suggesting that PrAMPs inhibit bacterial growth via interfering with DnaK mediated protein folding (Otvos et al., 2000). Subsequently, it was shown, however, that PrAMPs are equally effective at inhibiting bacterial strains where the gene encoding DnaK was inactivated (Krizsan et al., 2014). This suggested that another intracellular target for PrAMPs must exist. Indeed, PrAMPs were shown to bind to ribosomes and inhibit protein synthesis *in vivo* and *in vitro* (Krizsan et al., 2014; Mardirossian et al., 2014). Despite the diverse array of PrAMPs that have been so far identified, only a subset has been mechanistically investigated. Of the characterized PrAMPs, two distinct mechanisms of action have been identified, both of which involve inhibition of protein synthesis. The oncocin-like PrAMPs or type I PrAMPs allow translation initiation but prevent the transition into the elongation phase (Graf et al., 2017), whereas the apidaecin-like PrAMPs or type II PrAMPs allow translation initiation and elongation but block the translation termination phase (Florin et al., 2017).

### Type I (Oncocin-Like) PrAMPs

The type I PrAMPs encompass both insect and mammalian PrAMPs. One of the best-characterized members is Oncocin and Onc112, which are derivatives of a naturally occurring PrAMP from the milkweed bug *Oncopeltus fasciatus* (**Figures 9A,B**; Schneider and Dorn, 2001; Knappe et al., 2010, 2011). Other studied type I insect PrAMPs include pyrrhocoricin from the firebeetle *Pyrrhocoris apterus* and metalnikowin-1 from the green shield bug *Palomena prasina*. The best-characterized mammalian type I PrAMP is Bac7(1-16), a C-terminally truncated derivative of the naturally occurring bactericidin-7 (Bac7) PrAMP from the cow (*Bos taurus*). Recently, a type I PrAMP, Tur1A, was also identified from the bottlenose dolphin (*Tursiops truncatus*) (Mardirossian et al., 2018). Structural studies have revealed that type I PrAMPs bind within the ribosomal exit tunnel located on the large subunit (Roy et al., 2015; Seefeldt et al., 2015, 2016; Gagnon et al., 2016; Mardirossian et al., 2018). As expected from the high sequence identity, the insect PrAMPs Onc112, Pyr, Met, mammalian PrAMP Bac7(1-16) and dolphin PrAMP Tur1A bind with similar extended conformations within the exit tunnel (**Figures 9B–E**). The orientation of type I PrAMPs is inverted with respect to a nascent polypeptide chain, such that the N-terminus is located at the peptidyl transferase center (PTC) and the C-terminus extends into the ribosomal tunnel. Mutations of 23S rRNA nucleotides located within the ribosomal tunnel, such as A2503C, A2059C, and especially the A2503C/A2059C double mutation lead to increased resistance to Onc112, but





surprisingly not to Bac7 (Gagnon et al., 2016). Consistent with biochemical studies (Seefeldt et al., 2015, 2016; Gagnon et al., 2016), the structures reveal that the type I PrAMPs do not significantly overlap with the binding site of a P-site tRNA and thus allow translation initiation to occur uninhibited (Roy

et al., 2015; Seefeldt et al., 2015, 2016; Gagnon et al., 2016). By contrast, the N-terminal region of the type I PrAMPs sterically overlaps the binding site of the CCA-end of an A-site tRNA. This suggests that type I PrAMPs prevent the transition from initiation to elongation by blocking the binding and accommodation of

the aa-tRNA at the PTC on the large subunit (Graf et al., 2017).

## Type II (Apidaecin-Like) PrAMPs

The type II PrAMPs so far include only the insect PrAMPs belonging to the apidaecin subfamily. The best-characterized member is Api137, a derivative of the naturally occurring PrAMP apidaecin 1b from the honey bee *Apis mellifera*. Apidaecin-like PrAMPs are also found in other bees, wasps and hornets. Structural studies revealed that similar to type I PrAMPs, type II PrAMPs, such as Api137, also bind within the ribosomal exit tunnel (Figures 9A,F; Florin et al., 2017). However, the orientation of the type II PrAMPs is inverted with respect to type I PrAMPs, i.e., type II PrAMPs have the same orientation as a nascent polypeptide chain with the C-terminus located at the peptidyl transferase center (PTC) and the N-terminus extending down the ribosomal tunnel (Figure 9F). Biochemical studies show that Api137 does not inhibit translation initiation or elongation despite the overlap in binding site with the growing nascent polypeptide chain (Figure 9F). This paradox was resolved by the finding that Api137 has a very low affinity for empty ribosomes and require the presence of a termination release factor, RF1 or RF2, for stable binding (Florin et al., 2017). Presumably, the low affinity of Api137 in the absence of RF1/RF2 leads to its dissociation via prolongation of the nascent chain during translation elongation. During termination, Api137 does not interfere with binding of RF1/RF2 to the termination ribosome, nor with peptidyl-tRNA hydrolysis and release of the polypeptide by RF1/RF2. In fact, release of the polypeptide is a pre-requisite to allow Api137 to enter the ribosomal tunnel and engage its binding site. Following peptide release, however, binding of Api137 to the ribosome traps RF1/RF2 on the ribosome, even in the presence of RF3 (Florin et al., 2017). Thus, the action of Api137 needs to occur in the short time window following RF1/RF2-mediated peptide release, but before dissociation of RF1/RF2 from the ribosome.

Although the binding site of Api137 overlaps with type I PrAMPs, one major difference is that Api137 does not block entry of the A-site tRNA into the PTC. Instead, the C-terminus of the Api137 is positioned such that direct contact with RF1 and RF2 in the A site can occur. Specifically, Arg17 of Api137 can form direct hydrogen bond (H-bond) interactions with the sidechain of glutamine 235 (Q235) of the conserved GGQ motif. This is consistent with biochemical findings showing that mutations of Arg17 in Api137 decrease the ribosome affinity and reduce its inhibitory properties (Krizsan et al., 2014). In addition, the C-terminal carboxylate group of Api137 is within H-bond distance to the ribose hydroxyl of A76 of the deacylated P-site tRNA (Figure 9F), which could also contribute to trapping RF1/RF2 by preventing the ribosome from undergoing the RF3-stimulated transition into the rotated state required for RF1 or RF2 dissociation. Mutations in RF1 and RF2 as well as in ribosomal protein uL3 have been identified that confer resistance to Api137 (Florin et al., 2017). These mutations sites are located distant from the Api137 binding site and are therefore likely to confer resistance by altering RF1/RF2 binding such

that dissociation can occur even in the presence of Api137. Additionally, mutations within ribosomal tunnel can also confer resistance to Api137, including 23S rRNA mutations A2059C and A2503G, as identified for type I PrAMPs, such as Onc112, but also alterations within ribosomal proteins uL4 and uL22 rendered cells resistance to Api137 (Florin et al., 2017).

It should be noted that the number of ribosomes within a bacterial cell, such as *E. coli*, is much greater than the number of RF1 and RF2 molecules (by 200- and 25-fold, respectively; Bremer and Dennis, 1996; Schmidt et al., 2016) and therefore, Api137 can only trap RF1 and RF2 on a small subset of the available ribosomes. Nevertheless, this leads to a rapid depletion of the free pools of RF1 and RF2 in the cell, such that the vast majority of ribosomes become stalled during translation termination. Because of the absence of RF1 and RF2, an increased level of stop codon readthrough is observed on the termination stalled ribosomes. Surprisingly, the stop codon readthrough induced by Api137 is considerably higher than that induced by the classical misreading antibiotic streptomycin (Florin et al., 2017). Thus, in summary, type II PrAMPs such as Api137, have a dual mode of action to, on one hand, trap RF1 and RF2 on a minority of ribosomes within the cell and, on the other hand, to stall the majority of ribosomes at the termination phase due to the absence of available RFs, which in turn increases the rates of stop codon readthrough.

## Klebsazolicin Obstructs the Ribosomal Exit Tunnel

Klebsazolicin (KLB) is the first member of a new class of protein synthesis inhibitors, which comes from the opportunistic human pathogen *Klebsiella pneumoniae*, and was discovered recently using a genome mining approach (Metelev et al., 2017). This method allows one to harness a much greater chemical diversity and can result in the discovery of entirely new molecular scaffolds. Analysis of genomic data makes it possible to identify gene clusters encoding biosynthetic pathways for potential drug candidates, which may otherwise escape attention due to their inactivity under laboratory growth conditions (Doroghazi et al., 2014). Ribosomally-synthesized post-translationally modified peptides (RiPPs) are among the most abundant antimicrobial agents synthesized by various bacteria, including human microbiota (Donia et al., 2014; Donia and Fischbach, 2015).

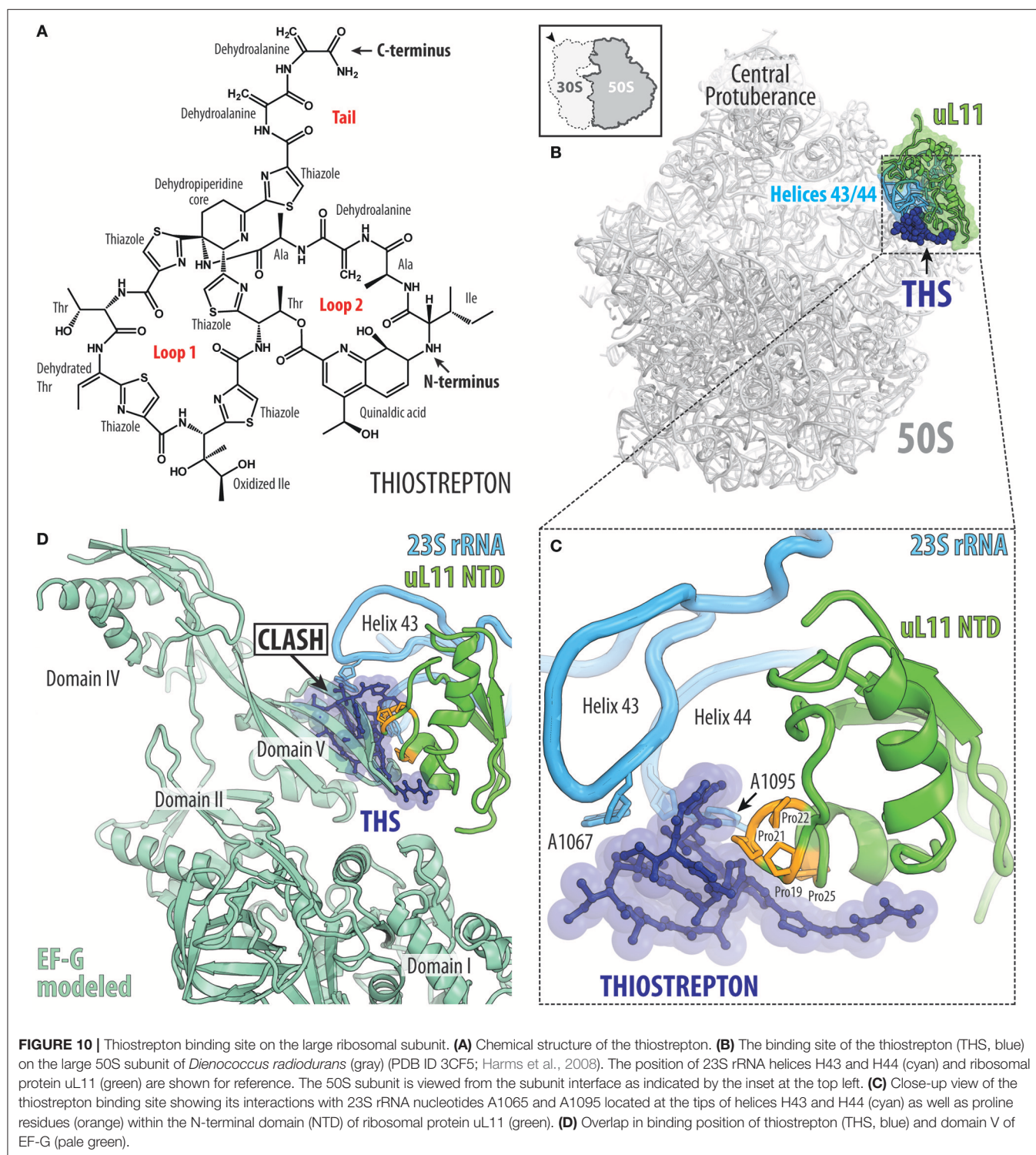
KLB is the first linear azole-containing RiPP for which the mode of binding to its target, the bacterial ribosome (Figures 9A,G), has been structurally characterized. KLB is synthesized on the ribosome as a precursor, which undergoes post-translational modifications by dedicated enzymes encoded in a compact gene cluster (Metelev et al., 2017). KLB appears to have a modular structure: its 14 N-terminal residues are essential for the inhibition of the ribosome, while its nine C-terminal residues are likely to be important for the uptake of the molecule and are not essential for ribosome binding (Metelev et al., 2017; Travin et al., 2018). It is likely that natural sensitivity/resistance to KLB is determined not by the differences in the ribosome target, but rather to differences in uptake. Moreover, KLB can be



expressed in a surrogate *E. coli* host (Metelev et al., 2017), which suggests avenues for future rational drug design: by changing the primary sequence of amino acids in the KLB precursor, it is possible to change properties of the final processed compound.

Structural analysis of the ribosome-KLB complex reveals that the compound binds in the nascent peptide exit tunnel to

a site that overlaps with the binding sites of macrolides,  $S_B$ , the PrAMPs, and significantly obstructs the tunnel (Figure 9G; Metelev et al., 2017). Similar to PrAMPs, KLB interacts with the ribosome mainly via stacking with rRNA bases. However, unlike PrAMPs, which bind the ribosome in an elongated conformation (Figures 9B–F), KLB adopts a compact, globular conformation



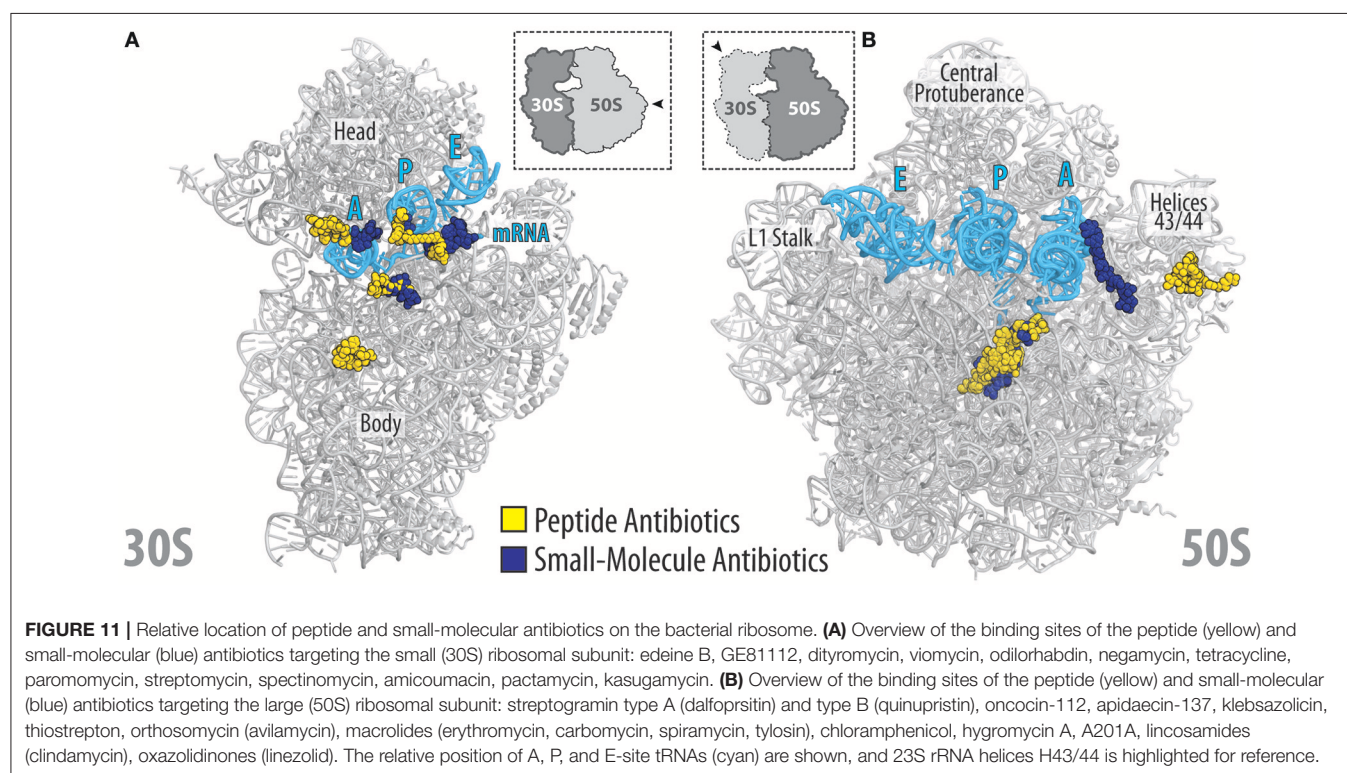
within the exit tunnel (**Figure 9G**). KLB inhibits protein synthesis by blocking the elongation after only three amino acids of the nascent peptide have been polymerized (Metelev et al., 2017). The KLB binding site does not overlap with the aminoacyl moieties of the A- and P-site tRNAs (**Figure 9G**) and the main occlusion point occurs around the macrolide binding site leaving some space between the PTC active site and the bound KLB molecule, so that the 2–3 amino acid long nascent peptide can fit. A unique and essential 6-membered amidine ring of KLB forms multiple interactions with the universally conserved nucleotides of the 23S rRNA at the heart of the PTC. For example, it forms two H-bonds with U2584, which resembles a non-canonical U-U base-pair.

## Thiopeptide Antibiotics That Interfere With Translation Factor Binding

There are an array of different thiopeptide antibiotics that inhibit translation either by interacting with translation factor EF-Tu, for example, GE2270A, or by directly binding to the ribosome, with the best characterized being thiostrepton, nosiheptide, and micrococcin (Bagley et al., 2005; Nicolaou et al., 2009). These antibiotics are synthesized as precursor polypeptides by the ribosome and then are post-translationally modified to yield the active compound (Wieland Brown et al., 2009). The chemical structure of thiostrepton can be separated into two loops (loop1 and 2) and a dehydroalanine tail, which are linked together by a tetrahydro-pyridin-3-ylamine moiety (**Figure 10A**). The 16 distinct chemical moieties that comprise thiostrepton include many thiazole rings as well as non-canonical and canonical amino acids, including for example, threonine, isoleucine, alanine and dehydroalanine (**Figure 10A**; Kelly et al., 2009).

The thiopeptide antibiotics are effective against Gram-positive bacteria, in particular, methicillin-resistant *Staphylococcus aureus* (MRSA), as well as against the malarial parasite *Plasmodium falciparum* (Aminake et al., 2011), but suffer from low water solubility and poor bioavailability, which has precluded their use in human medicine (Wilson, 2009).

The crystal structure of the *Deinococcus radiodurans* large subunit bound to thiostrepton (as well as nosiheptide and micrococcin; Harms et al., 2008) revealed that this class of antibiotics bind in a cleft formed between the N-terminal domain (NTD) of ribosomal protein uL11 and helices H43 and H44 of the 23S rRNA (**Figure 10B**). The solution NMR structure of thiostrepton compares well with the X-ray structure and reveals high flexibility of the dehydroalanine tail (Jonker et al., 2011). Within the cleft, thiostrepton interacts with nucleotides A1067 and A1095, located at the tips of H43 and H44, respectively, and the thiazole rings of thiostrepton stack upon the proline residues located in the NTD of uL11 (**Figure 10C**). This thiopeptide binding site is distinct when compared to other clinically used antibiotics and therefore cross-resistance with thiopeptides has not been reported. Nevertheless, mutations in A1067, A1095, or in the numerous proline residues of the uL11-NTD reduce thiopeptide binding and confer drug-resistance in bacteria and archaea (Wilson, 2009; Baumann et al., 2010). Furthermore, the producer of thiostrepton, *Streptomyces azureus*, inhibits drug binding to its own rRNA by 2'-O-methylation of position A1067 (Thompson et al., 1982). Eukaryotic 80S ribosomes are naturally resistant to thiostrepton, most probably due to sequence differences in uL11, which is in agreement with the observations that yeast 80S ribosomes bearing bacterial uL11 are sensitive to





the drug (Garcia-Marcos et al., 2007). The thiopeptide binding site on the large subunit sterically overlaps with the binding site of translation factors, such as the IF2, EF-Tu and EF-G (Figure 10D; Harms et al., 2008). Consistently, thiostrepton has been reported to inhibit IF2-dependent initiation complex formation (Brandi et al., 2004; Grigoriadou et al., 2007), EF-Tu delivery of the aa-tRNA to the A-site (Gonzalez et al., 2007) as well as accommodation of EF-G, which leads to inhibition of the translocation reaction (Rodnina et al., 1999; Seo et al., 2006; Pan et al., 2007; Mikolajka et al., 2011; Walter et al., 2012).

## CONCLUDING REMARKS

The available structures of peptide antibiotics on the ribosome illustrate the diverse manners in which these inhibitors interact with the ribosome and interfere with translation. High-resolution structures now open the way for structure-based design to develop peptide antibiotics with improved properties by identifying sites that can be modified to enable additional interaction with the ribosome. Similarly, the structures also identify residues that are not critical for ribosome binding and therefore can be utilized to optimize parameters such as uptake and retention, serum stability as well as reduced membrane permeabilization and toxicity. The proximity of the binding

sites of peptide antibiotics on the ribosome in relation to other classes of ribosome-targeting antibiotics (Figures 11A,B) also offers the opportunity to generate hybrid compounds that span over multiple binding sites. The increase in sequenced genomes coupled with improved data mining algorithms is leading to the identification of potential gene clusters encoding biosynthetic pathways for novel peptide antibiotics and PrAMPs. It will be interesting to see what novel ribosome-targeting peptide antibiotics these approaches will yield and to investigate their binding sites on the ribosome and mechanism of action to inhibit translation.

## AUTHOR CONTRIBUTIONS

YP and NA: prepared the figures; DW, BB, NA, and YP: wrote the manuscript.

## ACKNOWLEDGMENTS

We thank Dr. Maxim Svetlov for critical reading of the manuscript and valuable suggestions. This work was supported by Illinois State startup funds (to YP) and grants FOR1805, WI3285/8-1 (to DW) from the Deutsche Forschungsgemeinschaft (DFG).

## REFERENCES

- Agarwal, D., Gregory, S. T., and O'Connor, M. (2011). Error-prone and error-restrictive mutations affecting ribosomal protein S12. *J. Mol. Biol.* 410, 1–9. doi: 10.1016/j.jmb.2011.04.068
- Akbergenov, R., Shcherbakov, D., Matt, T., Dusch, S., Meyer, M., Wilson, D. N., et al. (2011). Molecular basis for the selectivity of antituberculosis compounds capreomycin and viomycin. *Antimicrob. Agents Chemother.* 55, 4712–4717. doi: 10.1128/AAC.00628-11
- Aminake, M. N., Schoof, S., Sologub, L., Leubner, M., Kirschner, M., Arndt, H. D., et al. (2011). Thiostrepton and derivatives exhibit antimalarial and gametocytocidal activity by dually targeting parasite proteasome and apicoplast. *Antimicrob. Agents Chemother.* 55, 1338–1348. doi: 10.1128/AAC.01096-10
- Arenz, S., and Wilson, D. N. (2016). Bacterial protein synthesis as a target for antibiotic inhibition. *Cold Spring Harbor Perspectives in Medicine*. 6:a025361. doi: 10.1101/cshperspect.a025361
- Bagley, M., Dale, J., Merritt, E., and Xiong, X. (2005). Thiopeptide antibiotics. *Chem. Rev.* 105, 685–714. doi: 10.1021/cr0300441
- Baumann, S., Schoof, S., Bolten, M., Haering, C., Takagi, M., Shin-ya, K., et al. (2010). Molecular determinants of microbial resistance to thiopeptide antibiotics. *J. Am. Chem. Soc.* 132, 6973–6981. doi: 10.1021/ja909317n
- Binz, T. M., Maffioli, S. I., Sosio, M., Donadio, S., and Muller, R. (2010). Insights into an unusual nonribosomal peptide synthetase biosynthesis: identification and characterization of the GE81112 biosynthetic gene cluster. *J. Biol. Chem.* 285, 32710–32719. doi: 10.1074/jbc.M110.146803
- Borovinskaya, M. A., Pai, R. D., Zhang, W., Schuwirth, B. S., Holton, J. M., Hirokawa, G., et al. (2007). Structural basis for aminoglycoside inhibition of bacterial ribosome recycling. *Nat. Struct. Mol. Biol.* 14, 727–732. doi: 10.1038/nsmb127
- Brandi, L., Fabbretti, A., Di Stefano, M., Lazzarini, A., Abbondi, M., and Gualerzi, C. O. (2006a). Characterization of GE82832, a Peptide inhibitor of translocation interacting with bacterial 30S ribosomal subunits. *RNA* 12, 1262–1270. doi: 10.1261/rna.61206
- Brandi, L., Fabbretti, A., La Teana, A., Abbondi, M., Losi, D., Donadio, S., et al. (2006b). Specific, efficient, and selective inhibition of prokaryotic translation initiation by a novel peptide antibiotic. *Proc. Natl. Acad. Sci. U.S.A.* 103, 39–44. doi: 10.1073/pnas.0507740102
- Brandi, L., Lazzarini, A., Cavaletti, L., Abbondi, M., Corti, E., Ciciliato, I., et al. (2006c). Novel tetrapeptide inhibitors of bacterial protein synthesis produced by a *Streptomyces* sp. *Biochemistry* 45, 3692–3702. doi: 10.1021/bi052540k
- Brandi, L., Maffioli, S., Donadio, S., Quaglia, F., Sette, M., Milon, P., et al. (2012). Structural and functional characterization of the bacterial translocation inhibitor GE82832. *FEBS Lett.* 586, 3373–3378. doi: 10.1016/j.febslet.2012.07.040
- Brandi, L., Marzi, S., Fabbretti, A., Fleischer, C., Hill, W., Lodmell, J., et al. (2004). The translation initiation functions of IF2: targets for thiostrepton inhibition. *J. Mol. Biol.* 335, 881–894. doi: 10.1016/j.jmb.2003.10.067
- Bremer, H., and Dennis, P. P. (1996). “Modulation of chemical composition and other parameters of the cell by growth rate,” in *Escherichia coli and Salmonella: Cellular and Molecular Biology*, eds F. C. Neidhardt, J. L. Ingraham, E. C. C. Lin, K. B. Low, B. Magasanik, W. S. Reznikow, M. Riley, M. Schaechter, and H. E. Umbarger (Washington, DC: ASM Press), 1553–1569.
- Brilot, A. F., Korostelev, A. A., Ermolenko, D. N., and Grigorieff, N. (2013). Structure of the ribosome with elongation factor G trapped in the pretranslocation state. *Proc. Natl. Acad. Sci. U.S.A.* 110, 20994–20999. doi: 10.1073/pnas.1311423110
- Bulkley, D., Brandi, L., Polikanov, Y. S., Fabbretti, A., O'Connor, M., Gualerzi, C. O., et al. (2014). The antibiotics dityromycin and GE82832 bind protein S12 and block EF-G-catalyzed translocation. *Cell Rep.* 6, 357–365. doi: 10.1016/j.celrep.2013.12.024
- Canu, A., and Leclercq, R. (2001). Overcoming bacterial resistance by dual target inhibition: the case of streptogramins. *Curr. Drug Targets Infect. Disord.* 1, 215–225. doi: 10.2174/1568005014606152
- Casteels, P., and Tempst, P. (1994). Apidaecin-type peptide antibiotics function through a non-poreforming mechanism involving stereospecificity. *Biochem. Biophys. Res. Commun.* 199, 339–345. doi: 10.1006/bbrc.1994.1234
- Champney, W. S. (2001). Bacterial ribosomal subunit synthesis: a novel antibiotic target. *Curr. Drug Targets Infect. Disord.* 1, 19–36. doi: 10.2174/1568005013343281

- Chen, Y., Kaji, A., Kaji, H., and Cooperman, B. S. (2017). The kinetic mechanism of bacterial ribosome recycling. *Nucleic Acids Res.* 45, 10168–10177. doi: 10.1093/nar/gkx694
- Chinali, G., Moureau, P., and Cocito, C. G. (1984). The action of virginiamycin M on the acceptor, donor, and catalytic sites of peptidyltransferase. *J. Biol. Chem.* 259, 9563–9568.
- Cornish, P. V., Ermolenko, D. N., Noller, H. F., and Ha, T. (2008). Spontaneous intersubunit rotation in single ribosomes. *Mol. Cell* 30, 578–588. doi: 10.1016/j.molcel.2008.05.004
- Cukras, A. R., Southworth, D. R., Brunelle, J. L., Culver, G. M., and Green, R. (2003). Ribosomal proteins S12 and S13 function as control elements for translocation of the mRNA:tRNA complex. *Mol. Cell* 12, 321–328. doi: 10.1016/S1097-2765(03)00275-2
- Delgado, G. Jr., Neuhauser, M. M., Bearden, D. T., and Danziger, L. H. (2000). Quinupristin-dalfopristin: an overview. *Pharmacotherapy* 20, 1469–1485. doi: 10.1592/phco.20.19.1469.34858
- Depardieu, F., and Courvalin, P. (2001). Mutation in 23S rRNA responsible for resistance to 16-membered macrolides and streptogramins in *Streptococcus pneumoniae*. *Antimicrob. Agents Chemother.* 45, 319–323. doi: 10.1128/AAC.45.1.319-323.2001
- Dinos, G., Wilson, D. N., Teraoka, Y., Szaflarski, W., Fucini, P., Kalpaxis, D., et al. (2004). Dissecting the ribosomal inhibition mechanisms of edeine and pactamycin: the universally conserved residues G693 and C795 regulate P-site tRNA binding. *Mol. Cell* 13, 113–124. doi: 10.1016/S1097-2765(04)00002-4
- Donia, M. S., Cimermancic, P., Schulze, C. J., Wieland Brown, L. C., Martin, J., Mitreva, M., et al. (2014). A systematic analysis of biosynthetic gene clusters in the human microbiome reveals a common family of antibiotics. *Cell* 158, 1402–1414. doi: 10.1016/j.cell.2014.08.032
- Donia, M. S., and Fischbach, M. A. (2015). HUMAN MICROBIOTA. Small molecules from the human microbiota. *Science* 349:1254766. doi: 10.1126/science.1254766
- Doroghazi, J. R., Albright, J. C., Goering, A. W., Ju, K. S., Haines, R. R., Tchaluikov, K. A., et al. (2014). A roadmap for natural product discovery based on large-scale genomics and metabolomics. *Nat. Chem. Biol.* 10, 963–968. doi: 10.1038/nchembio.1659
- Ermolenko, D. N., Majumdar, Z. K., Hickerson, R. P., Spiegel, P. C., Clegg, R. M., and Noller, H. F. (2007). Observation of intersubunit movement of the ribosome in solution using FRET. *J. Mol. Biol.* 370, 530–540. doi: 10.1016/j.jmb.2007.04.042
- Fabbretti, A., Schedlbauer, A., Brandi, L., Kaminishi, T., Giuliodori, A. M., Garofalo, R., et al. (2016). Inhibition of translation initiation complex formation by GE81112 unravels a 16S rRNA structural switch involved in P-site decoding. *Proc. Natl. Acad. Sci. U.S.A.* 113, E2286–E2295. doi: 10.1073/pnas.1521156113
- Florin, T., Maracci, C., Graf, M., Karki, P., Klepacki, D., Berninghausen, O., et al. (2017). An antimicrobial peptide that inhibits translation by trapping release factors on the ribosome. *Nat. Struct. Mol. Biol.* 24, 752–757. doi: 10.1038/nsmb.3439
- Gagnon, M. G., Roy, R. N., Lomakin, I. B., Florin, T., Mankin, A. S., and Steitz, T. A. (2016). Structures of proline-rich peptides bound to the ribosome reveal a common mechanism of protein synthesis inhibition. *Nucleic Acids Res.* 44, 2439–2450. doi: 10.1093/nar/gkw018
- Gale, E. F., Cundliffe, E., Reynolds, P. E., Richmond, M. H., and Waring, M. J., (eds.). (1981). “Antibiotic inhibitors of ribosome function,” in *The Molecular Basis of Antibiotic Action* (Bristol: John Wiley and sons), 278–379.
- Gao, N., Zavialov, A. V., Ehrenberg, M., and Frank, J. (2007). Specific interaction between EF-G and RRF and its implication for GTP-dependent ribosome splitting into subunits. *J. Mol. Biol.* 374, 1345–1358. doi: 10.1016/j.jmb.2007.10.021
- Garcia-Marcos, A., Morreale, A., Guarinos, E., Briones, E., Remacha, M., Ortiz, A. R., et al. (2007). *In vivo* assembling of bacterial ribosomal protein L11 into yeast ribosomes makes the particles sensitive to the prokaryotic specific antibiotic thiostrepton. *Nucleic Acids Res.* 35, 7109–7117. doi: 10.1093/nar/gkm773
- Garreau de Loubresse, N., Prokhorova, I., Holtkamp, W., Rodnina, M. V., Yusupova, G., and Yusupov, M. (2014). Structural basis for the inhibition of the eukaryotic ribosome. *Nature* 513, 517–522. doi: 10.1038/nature13737
- Gonzalez, R. L. Jr., Chu, S., and Puglisi, J. D. (2007). Thiostrepton inhibition of tRNA delivery to the ribosome. *RNA* 13, 2091–2097. doi: 10.1261/rna.499407
- Graf, M., Mardirossian, M., Nguyen, F., Seefeldt, A. C., Guichard, G., Scocchi, M., et al. (2017). Proline-rich antimicrobial peptides targeting protein synthesis. *Nat. Prod. Rep.* 34, 702–711. doi: 10.1039/C7NP00020K
- Gregory, S. T., Carr, J. F., and Dahlberg, A. E. (2009). A signal relay between ribosomal protein S12 and elongation factor EF-Tu during decoding of mRNA. *RNA* 15, 208–214. doi: 10.1261/rna.1355709
- Grigoriadou, C., Marzi, S., Kirillov, S., Gualerzi, C. O., and Cooperman, B. S. (2007). A quantitative kinetic scheme for 70S translation initiation complex formation. *J. Mol. Biol.* 373, 562–572. doi: 10.1016/j.jmb.2007.07.032
- Hansen, J. L., Moore, P. B., and Steitz, T. A. (2003). Structures of five antibiotics bound at the peptidyl transferase center of the large ribosomal subunit. *J. Mol. Biol.* 330, 1061–1075. doi: 10.1016/S0022-2836(03)00668-5
- Harms, J. M., Schlunzen, F., Fucini, P., Bartels, H., and Yonath, A. (2004). Alterations at the peptidyl transferase centre of the ribosome induced by the synergistic action of the streptogramins dalfopristin and quinupristin. *BMC Biol.* 2:4. doi: 10.1186/1741-7007-2-4
- Harms, J. M., Wilson, D. N., Schlunzen, F., Connell, S. R., Stachelhaus, T., Zaborowska, Z., et al. (2008). Translational regulation via L11: molecular switches on the ribosome turned on and off by thiostrepton and micrococin. *Mol. Cell* 30, 26–38. doi: 10.1016/j.molcel.2008.01.009
- Hirokawa, G., Kiel, M. C., Muto, A., Selmer, M., Raj, V. S., Liljas, A., et al. (2002). Post-termination complex disassembly by ribosome recycling factor, a functional tRNA mimic. *EMBO J.* 21, 2272–2281. doi: 10.1093/emboj/21.9.2272
- Holm, M., Borg, A., Ehrenberg, M., and Sanyal, S. (2016). Molecular mechanism of viomycin inhibition of peptide elongation in bacteria. *Proc. Natl. Acad. Sci. U.S.A.* 113, 978–983. doi: 10.1073/pnas.1517541113
- Ito, K., and Chiba, S. (2013). Arrest peptides: cis-acting modulators of translation. *Annu. Rev. Biochem.* 82, 171–202. doi: 10.1146/annurev-biochem-080211-105026
- Jain, A., and Dixit, P. (2008). Multidrug-resistant to extensively drug resistant tuberculosis: what is next? *J. Biosci.* 33, 605–616. doi: 10.1016/S0140-6736(10)60410-2
- Johansen, S. K., Maus, C. E., Plikaytis, B. B., and Douthwaite, S. (2006). Capreomycin binds across the ribosomal subunit interface using tlyA-encoded 2'-O-methylations in 16S and 23S rRNAs. *Mol. Cell* 23, 173–182. doi: 10.1016/j.molcel.2006.05.044
- Jonker, H. R., Baumann, S., Wolf, A., Schoof, S., Hiller, F., Schulte, K. W., et al. (2011). NMR structures of thiostrepton derivatives for characterization of the ribosomal binding site. *Angew. Chem. Int. Ed. Engl.* 50, 3308–3312. doi: 10.1002/anie.201003582
- Kelly, W. L., Pan, L., and Li, C. (2009). Thiostrepton biosynthesis: prototype for a new family of bacteriocins. *J. Am. Chem. Soc.* 131, 4327–4334. doi: 10.1021/ja807890a
- Knappe, D., Kabankov, N., and Hoffmann, R. (2011). Bactericidal oncocin derivatives with superior serum stabilities. *Int. J. Antimicrob. Agents* 37, 166–170. doi: 10.1016/j.ijantimicag.2010.10.028
- Knappe, D., Piantavigna, S., Hansen, A., Mechler, A., Binas, A., Nolte, O., et al. (2010). Oncocin (VDKPPYLPRPRPPRIYNH2): a novel antibacterial peptide optimized against gram-negative human pathogens. *J. Med. Chem.* 53, 5240–5247. doi: 10.1021/jm100378b
- Kozak, M., and Shatkin, A. J. (1978). Migration of 40S ribosomal subunits on messenger RNA in the presence of edeine. *J. Biol. Chem.* 253, 6568–6577.
- Krizsan, A., Knappe, D., and Hoffmann, R. (2015). Influence of the yjiL-mdtM gene cluster on the antibacterial activity of proline-rich antimicrobial peptides overcoming *Escherichia coli* resistance induced by the missing SbmA transporter system. *Antimicrob. Agents Chemother.* 59, 5992–5998. doi: 10.1128/AAC.01307-15
- Krizsan, A., Volke, D., Weinert, S., Strater, N., Knappe, D., and Hoffmann, R. (2014). Insect-derived proline-rich antimicrobial peptides kill bacteria by inhibiting bacterial protein translation at the 70S ribosome. *Angew. Chem. Int. Ed. Engl.* 53, 12236–12239. doi: 10.1002/anie.201407145
- Li, Q., and Seiple, I. B. (2017). Modular, scalable synthesis of group A streptogramin antibiotics. *J. Am. Chem. Soc.* 139, 13304–13307. doi: 10.1021/jacs.7b08577
- Lin, J., Gagnon, M. G., Bulkley, D., and Steitz, T. A. (2015). Conformational changes of elongation factor G on the ribosome during tRNA translocation. *Cell* 160, 219–227. doi: 10.1016/j.cell.2014.11.049

- Lin, Y., Li, Y., Zhu, N., Han, Y., Jiang, W., Wang, Y., et al. (2014). The antituberculosis antibiotic capreomycin inhibits protein synthesis by disrupting interaction between ribosomal proteins L12 and L10. *Antimicrob. Agents Chemother.* 58, 2038–2044. doi: 10.1128/AAC.02394-13
- Liou, Y., and Tanaka, N. (1976). Dual actions of viomycin on the ribosomal functions. *Biochem. Biophys. Res. Commun.* 71, 477–483. doi: 10.1016/0006-291X(76)90812-3
- Lopez-Alonso, J. P., Fabbretti, A., Kaminishi, T., Iturrioz, I., Brandi, L., Gil-Cardon, D., et al. (2017). Structure of a 30S pre-initiation complex stalled by GE81112 reveals structural parallels in bacterial and eukaryotic protein synthesis initiation pathways. *Nucleic Acids Res.* 45, 2179–2187. doi: 10.1093/nar/gkw1251
- Ly, C. T., Altuntop, M. E., and Wang, Y. (2010). Single-molecule study of viomycin's inhibition mechanism on ribosome translocation. *Biochemistry* 49, 9732–9738. doi: 10.1021/bi101029g
- Maio, A., Brandi, L., Donadio, S., and Gualerzi, C. O. (2016). The oligopeptide permease opp mediates illicit transport of the bacterial P-site decoding inhibitor GE81112. *Antibiotics* 5:E17. doi: 10.3390/antibiotics5020017
- Manzella, J. P. (2001). Quinupristin-dalfopristin: a new antibiotic for severe gram-positive infections. *Am. Fam. Phys.* 64, 1863–1866.
- Mardirossian, M., Grzela, R., Giglione, C., Meinel, T., Gennaro, R., Mergaert, P., et al. (2014). The host antimicrobial peptide Bac71-35 binds to bacterial ribosomal proteins and inhibits protein synthesis. *Chem. Biol.* 21, 1639–1647. doi: 10.1016/j.chembiol.2014.10.009
- Mardirossian, M., Pérébasquine, N., Benincasa, M., Gambato, S., Hofmann, S., Huter, P., et al. (2018). The dolphin proline-rich antimicrobial peptide Tur1A inhibits protein synthesis by targeting the bacterial ribosome. *Cell Chem. Biol.* doi: 10.1016/j.chembiol.2018.02.004. [Epub ahead of print].
- Marrero, P., Cabanas, M. J., and Modolell, J. (1980). Induction of translational errors (misreading) by tuberactinomycins and capreomycins. *Biochem. Biophys. Res. Commun.* 97, 1047–1052. doi: 10.1016/0006-291X(80)91481-3
- Mattiuzzo, M., Bandiera, A., Gennaro, R., Benincasa, M., Pacor, S., Antcheva, N., et al. (2007). Role of the *Escherichia coli* SbmA in the antimicrobial activity of proline-rich peptides. *Mol. Microbiol.* 66, 151–163. doi: 10.1111/j.1365-2958.2007.05903.x
- Maus, C. E., Plikaytis, B. B., and Shinnick, T. M. (2005). Molecular analysis of cross-resistance to capreomycin, kanamycin, amikacin, and viomycin in *Mycobacterium tuberculosis*. *Antimicrob. Agents Chemother.* 49, 3192–3197. doi: 10.1128/AAC.49.8.3192-3197.2005
- Metelev, M., Osterman, I. A., Ghilarov, D., Khabibullina, N. F., Komarova, E. S., Travin, D. Y., et al. (2017). Klebsazolicin inhibits 70S ribosome by obstructing the peptide exit tunnel. *Nat. Chem. Biol.* 13, 1129–1136. doi: 10.1038/nchembio.2462
- Mikolajka, A., Liu, H., Chen, Y., Starosta, A. L., Marquez, V., Ivanova, M., et al. (2011). Differential effects of thiopeptide and orthosomycin antibiotics on translational GTPases. *Chem. Biol.* 18, 589–600. doi: 10.1016/j.chembiol.2011.03.010
- Modolell, J., and Vazquez, D. (1977). The inhibition of ribosomal translocation by viomycin. *Eur. J. Biochem.* 81, 491–497. doi: 10.1111/j.1432-1033.1977.tb11974.x
- Monshupanee, T., Johansen, S. K., Dahlberg, A. E., and Douthwaite, S. (2012). Capreomycin susceptibility is increased by TlyA-directed 2'-O-methylation on both ribosomal subunits. *Mol. Microbiol.* 85, 1194–1203. doi: 10.1111/j.1365-2958.2012.08168.x
- Nicolaou, K. C., Chen, J. S., Edmonds, D. J., and Estrada, A. A. (2009). Recent advances in the chemistry and biology of naturally occurring antibiotics. *Angew. Chem. Int. Ed. Engl.* 48, 660–719. doi: 10.1002/anie.200801695
- Nissen, P., Hansen, J., Ban, N., Moore, P. B., and Steitz, T. A. (2000). The structural basis of ribosome activity in peptide bond synthesis. *Science* 289, 920–930. doi: 10.1126/science.289.5481.920
- Noeske, J., Huang, J., Olivier, N. B., Giacobbe, R. A., Zambrowski, M., and Cate, J. H. (2014). Synergy of streptogramin antibiotics occurs independently of their effects on translation. *Antimicrob. Agents Chemother.* 58, 5269–5279. doi: 10.1128/AAC.03389-14
- Ogle, J., Carter, A., and Ramakrishnan, V. (2003). Insights into the decoding mechanism from recent ribosome structures. *TIBS* 28, 259–266. doi: 10.1016/S0968-0004(03)00066-5
- Olivier, N. B., Altman, R. B., Noeske, J., Basarab, G. S., Code, E., Ferguson, A. D., et al. (2014). Negamycin induces translational stalling and miscoding by binding to the small subunit head domain of the *Escherichia coli* ribosome. *Proc. Natl. Acad. Sci. U.S.A.* 111, 16274–16279. doi: 10.1073/pnas.1414401111
- Omura, S., Iwai, Y., Hirano, A., Awaya, J., Suzuki, Y., and Matsumoto, K. (1977). New Antibiotic, Am-2504. *Agric. Biol. Chem.* 41, 1827–1828. doi: 10.1271/bbb1961.41.1827
- Osterman, I. A., Khabibullina, N. F., Komarova, E. S., Kasatsky, P., Kartsev, V. G., Bogdanov, A. A., et al. (2017). Madumycin II inhibits peptide bond formation by forcing the peptidyl transferase center into an inactive state. *Nucleic Acids Res.* 45, 7507–7514. doi: 10.1093/nar/gkx413
- Otvos, L. Jr., O, I., Rogers, M. E., Consolvo, P. J., Condie, B. A., Lovas, S., et al. (2000). Interaction between heat shock proteins and antimicrobial peptides. *Biochemistry* 39, 14150–14159. doi: 10.1021/bi0012843
- Pan, D., Kirillov, S. V., and Cooperman, B. S. (2007). Kinetically competent intermediates in the translocation step of protein synthesis. *Mol. Cell* 25, 519–529. doi: 10.1016/j.molcel.2007.01.014
- Pankuch, G. A., Lin, G., Clark, C., and Appelbaum, P. C. (2011). Time-kill activity of the streptogramin NXL 103 against Gram-positive and -negative bacteria. *Antimicrob. Agents Chemother.* 55, 1787–1791. doi: 10.1128/AAC.01159-10
- Pantel, L., Florin, T., Dobosz-Bartoszek, M., Racine, E., Sarciaux, M., Serri, M., et al. (2018). Odilorhabin, antibacterial agents that cause miscoding by binding at a new ribosomal site. *Mol. Cell* 70, 83–94. doi: 10.1016/j.molcel.2018.03.001
- Parfait, R., de Bethune, M. P., and Cocito, C. (1978). A spectrofluorimetric study of the interaction between virginiamycin S and bacterial ribosomes. *Mol. Gen. Genet.* 166, 45–51. doi: 10.1007/BF00379728
- Peske, F., Savelsbergh, A., Katunin, V. I., Rodnina, M. V., and Wintermeyer, W. (2004). Conformational changes of the small ribosomal subunit during elongation factor G-dependent tRNA-mRNA translocation. *J. Mol. Biol.* 343, 1183–1194. doi: 10.1016/j.jmb.2004.08.097
- Pestka, S. (1969). Studies on the formation of transfer ribonucleic acid-ribosome complexes. XI. Antibiotic effects on phenylalanyl-oligonucleotide binding to ribosomes. *Proc. Natl. Acad. Sci. U.S.A.* 64, 709–714. doi: 10.1073/pnas.64.2.709
- Pioletti, M., Schlunzen, F., Harms, J., Zarivach, R., Gluhmann, M., Avila, H., et al. (2001). Crystal structures of complexes of the small ribosomal subunit with tetracycline, edeine and IF3. *EMBO J.* 20, 1829–1839. doi: 10.1093/emboj/20.8.1829
- Podda, E., Benincasa, M., Pacor, S., Micali, F., Mattiuzzo, M., Gennaro, R., et al. (2006). Dual mode of action of Bac7, a proline-rich antibacterial peptide. *Biochim. Biophys. Acta* 1760, 1732–1740. doi: 10.1016/j.bbagen.2006.09.006
- Polikanov, Y. S., Szal, T., Jiang, F., Gupta, P., Matsuda, R., Shiozuka, M., et al. (2014). Negamycin interferes with decoding and translocation by simultaneous interaction with rRNA and tRNA. *Mol. Cell* 56, 541–550. doi: 10.1016/j.molcel.2014.09.021
- Rodnina, M. V., Savelsbergh, A., Matassova, N. B., Katunin, V. I., Semenov, Y. P., and Wintermeyer, W. (1999). Thiostrepton inhibits the turnover but not the GTPase of elongation factor G on the ribosome. *Proc. Natl. Acad. Sci. U.S.A.* 96, 9586–9590. doi: 10.1073/pnas.96.17.9586
- Roy, R. N., Lomakin, I. B., Gagnon, M. G., and Steitz, T. A. (2015). The mechanism of inhibition of protein synthesis by the proline-rich peptide oncocin. *Nat. Struct. Mol. Biol.* 22, 466–469. doi: 10.1038/nsmb.3031
- Savelsbergh, A., Rodnina, M. V., and Wintermeyer, W. (2009). Distinct functions of elongation factor G in ribosome recycling and translocation. *RNA* 15, 772–780. doi: 10.1261/rna.1592509
- Schmeing, T. M., Huang, K. S., Strobel, S. A., and Steitz, T. A. (2005). An induced-fit mechanism to promote peptide bond formation and exclude hydrolysis of peptidyl-tRNA. *Nature* 438, 520–524. doi: 10.1038/nature04152
- Schmidt, A., Kochanowski, K., Vedelaar, S., Ahrne, E., Volkmer, B., Callipo, L., et al. (2016). The quantitative and condition-dependent *Escherichia coli* proteome. *Nat. Biotechnol.* 34, 104–110. doi: 10.1038/nbt.3418
- Schneider, M., and Dorn, A. (2001). Differential infectivity of two *Pseudomonas* species and the immune response in the milkweed bug, *Oncopeltus fasciatus* (Insecta: Hemiptera). *J. Invertebr. Pathol.* 78, 135–140. doi: 10.1006/jipa.2001.5054
- Scocchi, M., Tossi, A., and Gennaro, R. (2011). Proline-rich antimicrobial peptides: converging to a non-lytic mechanism of action. *Cell. Mol. Life Sci.* 68, 2317–2330. doi: 10.1007/s00018-011-0721-7



- Seefeldt, A. C., Graf, M., Perebaskine, N., Nguyen, F., Arenz, S., Mardirossian, M., et al. (2016). Structure of the mammalian antimicrobial peptide Bac7(1-16) bound within the exit tunnel of a bacterial ribosome. *Nucleic Acids Res.* 44, 2429–2438. doi: 10.1093/nar/gkv1545
- Seefeldt, A. C., Nguyen, F., Antunes, S., Perebaskine, N., Graf, M., Arenz, S., et al. (2015). The proline-rich antimicrobial peptide Onc112 inhibits translation by blocking and destabilizing the initiation complex. *Nat. Struct. Mol. Biol.* 22, 470–475. doi: 10.1038/nsmb.3034
- Seo, H., Abedin, S., Kamp, D., Wilson, D. N., Nierhaus, K. H., and Cooperman, B. S. (2006). EF-G-dependent GTPase on the ribosome. Conformational change and fusidic acid inhibition. *Biochemistry* 45, 2504–2514. doi: 10.1021/bi0516677
- Shoji, S., Walker, S. E., and Fredrick, K. (2006). Reverse translocation of tRNA in the ribosome. *Mol. Cell* 24, 931–942. doi: 10.1016/j.molcel.2006.11.025
- Skerlavaj, B., Romeo, D., and Gennaro, R. (1990). Rapid membrane permeabilization and inhibition of vital functions of gram-negative bacteria by bactericins. *Infect. Immun.* 58, 3724–3730.
- Stanley, R. E., Blaha, G., Grodzicki, R. L., Strickler, M. D., and Steitz, T. A. (2010). The structures of the anti-tuberculosis antibiotics viomycin and capreomycin bound to the 70S ribosome. *Nat. Struct. Mol. Biol.* 17, 289–293. doi: 10.1038/nsmb.1755
- Thomas, M. G., Chan, Y. A., and Ozanick, S. G. (2003). Deciphering tuberactinomycin biosynthesis: isolation, sequencing, and annotation of the viomycin biosynthetic gene cluster. *Antimicrob. Agents Chemother.* 47, 2823–2830. doi: 10.1128/AAC.47.9.2823-2830.2003
- Thompson, C. J., Skinner, R. H., Thompson, J., Ward, J. M., Hopwood, D. A., and Cundliffe, E. (1982). Biochemical characterization of resistance determinants cloned from antibiotic-producing streptomycetes. *J. Bacteriol.* 151, 678–685.
- Travin, D. Y., Metele, M., Serebryakova, M., Komarova, E., Osterman, I. A., Ghilarov, D., et al. (2018). Biosynthesis of translation inhibitor Klebsazolicin proceeds through heterocyclisation and N-terminal amidine formation catalysed by a single YcaO enzyme. *J. Am. Chem. Soc.* 140, 5625–5633. doi: 10.1021/jacs.8b02277
- Tu, D., Blaha, G., Moore, P. B., and Steitz, T. A. (2005). Structures of MLSBK antibiotics bound to mutated large ribosomal subunits provide a structural explanation for resistance. *Cell* 121, 257–270. doi: 10.1016/j.cell.2005.02.005
- Vannuffel, P., and Cocito, C. (1996). Mechanism of action of streptogramins and macrolides. *Drugs* 51(Suppl. 1), 20–30. doi: 10.2165/00003495-199600511-00006
- Vannuffel, P., Di Giambattista, M., and Cocito, C. (1992). The role of rRNA bases in the interaction of peptidyltransferase inhibitors with bacterial ribosomes. *J. Biol. Chem.* 267, 16114–16120.
- Walter, J. D., Hunter, M., Cobb, M., Traeger, G., and Spiegel, P. C. (2012). Thiostrepton inhibits stable 70S ribosome binding and ribosome-dependent GTPase activation of elongation factor G and elongation factor 4. *Nucleic Acids Res.* 40, 360–370. doi: 10.1093/nar/gkr623
- Wang, L., Pulk, A., Wasserman, M. R., Feldman, M. B., Altman, R. B., Cate, J. H., et al. (2012). Allosteric control of the ribosome by small-molecule antibiotics. *Nat. Struct. Mol. Biol.* 19, 957–963. doi: 10.1038/nsmb.2360
- Weixlbaumer, A., Petry, S., Dunham, C. M., Selmer, M., Kelley, A. C., and Ramakrishnan, V. (2007). Crystal structure of the ribosome recycling factor bound to the ribosome. *Nat. Struct. Mol. Biol.* 14, 733–737. doi: 10.1038/nsmb1282
- Westman, E. L., Yan, M., Waglechner, N., Koteva, K., and Wright, G. D. (2013). Self resistance to the atypical cationic antimicrobial peptide edeine of *Brevibacillus brevis* Vm4 by the N-acetyltransferase EdeQ. *Chem. Biol.* 20, 983–990. doi: 10.1016/j.chembiol.2013.06.010
- Wieland Brown, L. C., Acker, M. G., Clardy, J., Walsh, C. T., and Fischbach, M. A. (2009). Thirteen posttranslational modifications convert a 14-residue peptide into the antibiotic thiocillin. *Proc. Natl. Acad. Sci. U.S.A.* 106, 2549–2553. doi: 10.1073/pnas.0900008106
- Wilson, D. N. (2009). The A-Z of bacterial translation inhibitors. *Crit. Rev. Biochem. Mol. Biol.* 44, 393–433. doi: 10.3109/10409230903307311
- Wilson, D. N. (2014). Ribosome-targeting antibiotics and bacterial resistance mechanisms. *Nat. Rev. Microbiol.* 12, 35–48. doi: 10.1038/nrmicro3155
- Wilson, D. N., Arenz, S., and Beckmann, R. (2016). Translation regulation via nascent polypeptide-mediated ribosome stalling. *Curr. Opin. Struct. Biol.* 37, 123–133. doi: 10.1016/j.sbi.2016.01.008
- Woodcock, J., Moazed, D., Cannon, M., Davies, J., and Noller, H. F. (1991). Interaction of antibiotics with A- and P-site-specific bases in 16S ribosomal RNA. *EMBO J.* 10, 3099–3103.
- Wurmbach, P., and Nierhaus, K. H. (1983). The inhibition pattern of antibiotics on the extent and accuracy of tRNA binding to the ribosome, and their effect on the subsequent steps in chain elongation. *Eur. J. Biochem.* 130, 9–12. doi: 10.1111/j.1432-1033.1983.tb07109.x
- Yamada, T., Mizuguchi, Y., Nierhaus, K. H., and Wittmann, H. G. (1978). Resistance to viomycin conferred by RNA of either ribosomal subunit. *Nature* 275, 460–461. doi: 10.1038/275460a0
- Yates, J. D., and Schaible, P. J. (1962). Virginiamycin as an antibiotic for poultry feeds. *Nature* 194, 183–184. doi: 10.1038/194183b0
- Yates, J. L. (1979). Role of ribosomal protein S12 in discrimination of aminoacyl-tRNA. *J. Biol. Chem.* 254, 11550–11554.
- Zeng, F., and Jin, H. (2016). Peptide release promoted by methylated RF2 and ArfA in nonstop translation is achieved by an induced-fit mechanism. *RNA* 22, 49–60. doi: 10.1261/rna.053082.115

**Conflict of Interest Statement:** The authors declare that the research was conducted in the absence of any commercial or financial relationships that could be construed as a potential conflict of interest.

Copyright © 2018 Polikanov, Aleksashin, Beckert and Wilson. This is an open-access article distributed under the terms of the Creative Commons Attribution License (CC BY). The use, distribution or reproduction in other forums is permitted, provided the original author(s) and the copyright owner are credited and that the original publication in this journal is cited, in accordance with accepted academic practice. No use, distribution or reproduction is permitted which does not comply with these terms.



# Tetracycline-Inactivating Enzymes

Jana L. Markley and Timothy A. Wencewicz\*

Department of Chemistry, Washington University in St. Louis, St. Louis, MO, United States

Tetracyclines have been foundational antibacterial agents for more than 70 years. Renewed interest in tetracycline antibiotics is being driven by advancements in tetracycline synthesis and strategic scaffold modifications designed to overcome established clinical resistance mechanisms including efflux and ribosome protection. Emerging new resistance mechanisms, including enzymatic antibiotic inactivation, threaten recent progress on bringing these next-generation tetracyclines to the clinic. Here we review the current state of knowledge on the structure, mechanism, and inhibition of tetracycline-inactivating enzymes.

**Keywords:** tetracycline destructases, enzymatic antibiotic inactivation, antibiotic adjuvants, tetracyclines, antibiotic resistance, flavin monooxygenase

## OPEN ACCESS

### Edited by:

Graeme L. Conn,  
Emory University School of Medicine,  
United States

### Reviewed by:

Pablo Sobrado,  
Virginia Tech, United States  
Yury S. Polikanov,  
The University of Illinois at Chicago,  
United States

### \*Correspondence:

Timothy A. Wencewicz  
wencewicz@wustl.edu

### Specialty section:

This article was submitted to  
Antimicrobials, Resistance  
and Chemotherapy,  
a section of the journal  
Frontiers in Microbiology

**Received:** 01 March 2018

**Accepted:** 04 May 2018

**Published:** 30 May 2018

### Citation:

Markley JL and Wencewicz TA  
(2018) Tetracycline-Inactivating  
Enzymes. *Front. Microbiol.* 9:1058.  
doi: 10.3389/fmicb.2018.01058

## INTRODUCTION

### Tetracycline Antibiotics

Tetracycline antibiotics were discovered in the 1940s and found widespread clinical use shortly thereafter (Duggar, 1948; Finlay et al., 1950; King et al., 1950; Roberts, 1996; Nelson and Levy, 2011). Naturally occurring tetracyclines are highly oxidized, type II polyketides composed of a linear fused tetracyclic scaffold with rings designated A, B, C, D (**Figure 1**; Stephens et al., 1952; Chopra and Roberts, 2001). Tetracyclines inhibit bacterial protein synthesis by binding to the 16S rRNA of the 30S bacterial ribosome subunit, preventing accommodation of incoming aminoacyl-tRNAs at the acceptor site (A-site) (Brodersen et al., 2000; Wilson, 2009). Tetracyclines make sequence-independent contacts with sugar phosphates in the primary binding site between h31 and h34. Both synthetic and semisynthetic tetracyclines have found clinical use as low cost, broad-spectrum, and orally available antimicrobial agents. The minimum active pharmacophore for bacterial ribosome inhibition is 6-deoxy-6-demethyltetracycline (McCormick et al., 1960; Chopra and Roberts, 2001). Chemical modification of positions 5–9 is well tolerated and can improve ribosome affinity, as is the case for the first and second generation scaffolds CTc and doxycycline. Modification of positions 1–4 and 10–12 strongly attenuates the antibacterial activity. The 1,3-diketone group at carbons 11 and 12 (pKa ~7) chelates Mg<sup>2+</sup> (Stephens et al., 1956; Jin et al., 2007). The tetracycline–Mg complex is the biologically active form that permeates the bacterial cell envelope (Schnappinger and Hillen, 1996) and binds to bacterial ribosomes (Jenner et al., 2013), transcription factors (Hinrichs et al., 1994), and aptamers (Xiao et al., 2008).

Chemical modification of the tetracycline scaffold has preserved this important class of antibiotics for >70 years against continuous waves of resistance determinants (Charest et al., 2005; Liu and Myers, 2016; Sun and Xiao, 2017). The unique 3D chemical shape of tetracycline arises

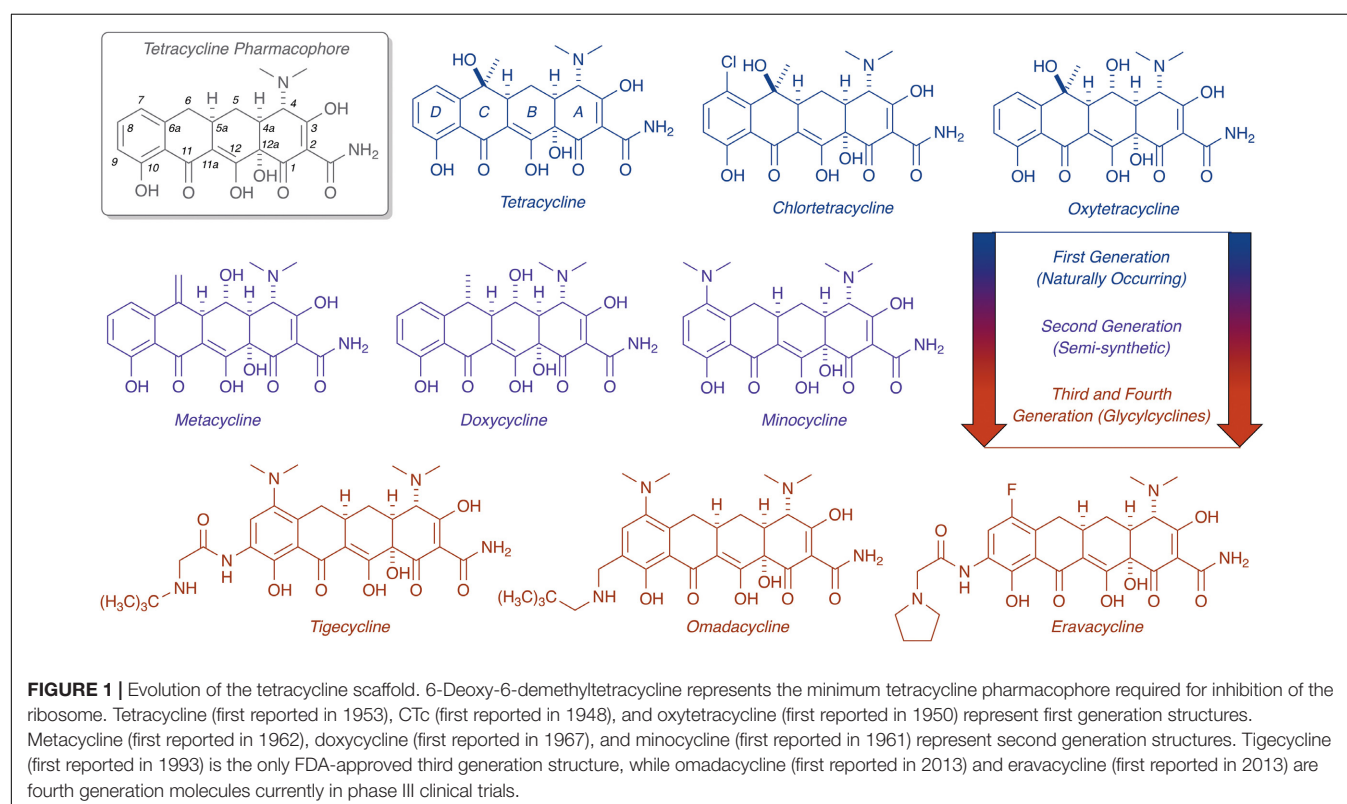
**Abbreviations:** ARG, antibiotic resistance gene; CTc, chlortetracycline; FAD, flavin adenine dinucleotide; FMO, flavin monooxygenase; NADPH, nicotinamide adenine dinucleotide phosphate reduced form; NADP<sup>+</sup>, nicotinamide adenine dinucleotide phosphate oxidized form.

from a bend in the structure at the A,B-ring juncture, and this seems to be a distinguishing feature from other tetracyclic polyketides that impart selectivity for ribosome binding (Brodersen et al., 2000; Stepanek et al., 2016). The D-ring of tetracyclines has proven to be robust toward semi-synthetic modifications, as highlighted by the bulky *N*-*t*-butyl-glycylamide side chain of the third generation antibiotic tigecycline, which plays a dual role in overcoming resistance and increasing affinity for the 30S ribosomal subunit (Jenner et al., 2013). Access to fully synthetic tetracyclines, including fourth generation compounds eravacycline (Ronn et al., 2013; Zhanel et al., 2016) and omadacycline (Tanaka et al., 2016) – both currently in phase III clinical trials – has rejuvenated clinical prospects for this drug class (Liu and Myers, 2016; Sun and Xiao, 2017). With the approval of next-generation tetracyclines on the horizon, new mechanisms of tetracycline resistance are certain to emerge as clinical use increases. Our ability to manage emerging resistance is critical to ensure future utility of tetracycline antibiotics and prevent a public health care crisis (Brown and Wright, 2016).

## Tetracycline Resistance

Resistance to tetracycline antibiotics was observed from the very start of clinical use (Schiott and Stenderup, 1954; Roberts, 1996). Despite widespread clinical resistance, tetracyclines continue to be important agents for treating a variety of human infections caused by Gram-negative and Gram-positive bacterial pathogens, along with atypical pathogens including mycoplasmas, nematodes, and parasitic protozoans (Chopra and Roberts, 2001). Tetracyclines are also widely used in

veterinary medicine and agricultural applications, including crop protection and intensive animal farming, which has contributed to the widespread dissemination of tetracycline resistance (Thaker et al., 2010; Surette and Wright, 2017). Molecular mechanisms of tetracycline resistance include efflux (Izaki and Arima, 1963; Levy and McMurtry, 1978; Kaneko et al., 1985), ribosome protection proteins (Burdett et al., 1982; Burdett, 1986, 1991, 1996), reduced permeability (Cohen et al., 1988), ribosome mutation (Ross et al., 1998), and enzymatic inactivation (Figure 2; Yang et al., 2004; Nguyen et al., 2014). Efflux pumps and ribosome protection proteins are the most common types of clinical resistance to tetracyclines and have been found in most human pathogens (Connell et al., 2003; Piddock, 2006; Thaker et al., 2010). Seven groups of efflux pumps have been identified that confer tetracycline resistance by decreasing the effective intracellular antibiotic concentration, with most members falling into the major facilitator superfamily (Guillaume et al., 2004; Piddock, 2006). Ribosome protection proteins are GTPases with homology to elongation factors that bind the ribosome analogously to elongation factors and chase bound tetracycline from the 30S ribosomal subunit (Connell et al., 2003; Jenner et al., 2013). Reduced drug permeability is achieved through morphological changes and the modification or reduced expression of porins and likely contributes to clinical tetracycline resistance (Cohen et al., 1988; Schnappinger and Hillen, 1996; Olesky et al., 2006; Justice et al., 2008). Ribosomal mutations are uncommon in clinical resistance to tetracyclines, probably due to the sequence-independent binding mode of tetracycline





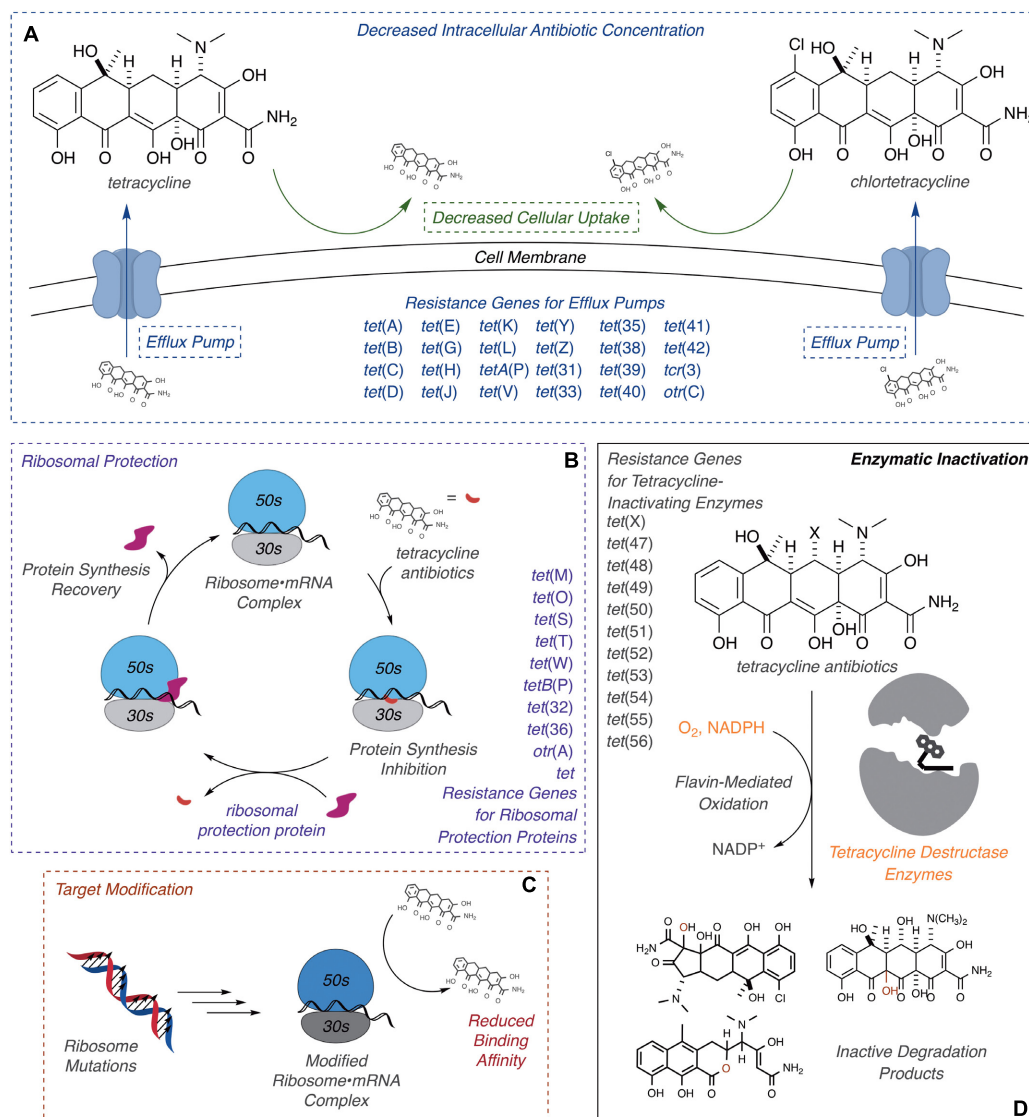


**FIGURE 2 |** Molecular mechanisms of tetracycline resistance. **(A)** Efflux, exclusion, **(B)** ribosome protection, **(C)** ribosome modification, and **(D)** enzymatic inactivation. Documented ARGs associated with each type of tetracycline resistance are provided.

to the 30S ribosomal subunit (Brodersen et al., 2000); still, some resistance-conferring mutations and deletions around the tetracycline-binding site have been reported (Ross et al., 1998; Gerritis et al., 2002; Trieber and Taylor, 2002). Some clinical isolates of *Helicobacter pylori* (Nonaka et al., 2005) and *Propionibacterium acnes* (Ross et al., 1998) carry point mutations in the 16S ribosome that confer tetracycline resistance, presumably through reduced tetracycline binding affinity. These ribosome mutations also confer tetracycline resistance in laboratory strains of *Escherichia coli* (Cocozaki et al., 2016). Similar resistance to tigecycline in *S. pneumonia*, arising from point mutations in ribosomal proteins and rRNA, has been introduced in the laboratory via successive passaging (Lupien et al., 2015). A more obscure resistance mechanism involves activation of  $Mg^{2+}$ -dependent purine nucleotide biosynthesis

via expression of the *tet34* gene product, a predicted xanthine-guanine phosphoribosyltransferase, which attenuates tetracycline antibacterial activity presumably by increasing the pool of GTP available to elongation factors to accelerate binding of aminoacyl-tRNAs to the 30S ribosomal subunit (Nonaka and Suzuki, 2002; Kim et al., 2003).

Third (tigecycline) and fourth generation (eravacycline and omadacycline) tetracyclines are known to overcome resistance via efflux and ribosome protection (Jenner et al., 2013; Zhanel et al., 2016; Tanaka et al., 2016). However, enzymatic inactivation has emerged as a new concern for these next-generation tetracyclines (Moore et al., 2005; Grossman et al., 2012, 2017). A family of FMOs, the tetracycline destructases (Forsberg et al., 2015), has been shown to selectively oxidize tetracyclines leading to covalent destruction of the antibiotic scaffold

(Yang et al., 2004). Unlike efflux, exclusion, ribosome protection, and ribosome modification, enzymatic inactivation permanently eliminates the tetracycline antibiotic challenge by decreasing intracellular and extracellular antibiotic concentrations (Davies, 1994; Wright, 2005). The clinical impact of enzymatic antibiotic inactivation can be devastating, as documented by the spread of broad-spectrum beta-lactamases across the globe (Bush and Jacoby, 2010; Brandt et al., 2017). The goal of this review is to highlight recent advances involving the structure, mechanism, and inhibition of tetracycline destructases to bring awareness and inspire solutions for this emerging type of tetracycline resistance.

## TETRACYCLINE DESTRUCTASES

### Antibiotic Destructases

The tetracycline destructases are part of a broadly defined family of enzymes, which we are calling the antibiotic destructases, that inactivate antibiotics via a wide variety of covalent modifications to the antibiotic scaffold (Davies, 1994; Wright, 2005). Antibiotic destructases are named to reflect the enzymatic activity associated with covalent modification of antibiotic scaffolds that permanently destroys antimicrobial activity and imparts resistance to producing microbes. Antibiotic destructases differ from xenobiotic modifying metabolic enzymes in regulation, catalytic efficiency, rate, and substrate specificity. Xenobiotic modifying enzymes perform housekeeping functions in the host, primarily clearance, and detoxification of xenobiotics (Krueger and Williams, 2005). The primary function of antibiotic destructases is gain of resistance. Thus, xenobiotic modifying enzymes tend to be broad in substrate scope at the cost of catalytic efficiency, while antibiotic destructases tend to be narrower in substrate scope with high specificity and catalytic efficiency toward a particular structural class of antibiotics (Wright, 2005).

Well-known examples of antibiotic destructases include beta-lactamases that hydrolyze the strained 4-membered lactam of beta-lactam antibiotics (Bush and Jacoby, 2010; Brandt et al., 2017), and aminoglycoside-inactivating enzymes including phosphotransferases, acetyltransferases, and adenylyltransferases that modify the free amine and hydroxyl groups of aminoglycoside antibiotics (Ramirez and Tolmasky, 2010). Known classes of antibiotic destructases (antibiotic substrates) include peptidases (bogorol, bacitracin) (Li et al., 2018), hydrolases (beta-lactams, macrolides) (Bush and Jacoby, 2010; Morar et al., 2012), thioltransferases (fosfomycin) (Rife et al., 2002; Thompson et al., 2013), epoxidases (fosfomycin) (Fillgrove et al., 2003), cyclopropanases (colibactin) (Tripathi et al., 2017), acyl transferases (aminoglycosides, chloramphenicol, glufosinate, tabtoxinine-beta-lactam, streptogramin) (Leslie, 1990; Botterman et al., 1991; Sugantino and Roderick, 2002; Ramirez and Tolmasky, 2010; Wenciewicz and Walsh, 2012; Favrot et al., 2016), methyl transferases (holomycin) (Li et al., 2012; Warrier et al., 2016), nucleotidyl transferases (aminoglycosides, lincosamide) (Morar et al., 2009; Ramirez and Tolmasky, 2010), ADP-ribosyltransferases (rifamycins) (Baysarowich et al., 2008), glycosyltransferases (aminoglycosides, rifamycins, macrolides) (Bolam et al., 2007; Ramirez and Tolmasky,

2010; Spanogiannopoulos et al., 2012), phosphotransferases (aminoglycosides, chloramphenicol, rifamycins, macrolides, viomycin) (Thiara and Cundliffe, 1995; Izard and Ellis, 2000; Ramirez and Tolmasky, 2010; Stogios et al., 2016; Fong et al., 2017), lyases (streptogramins) (Korczynska et al., 2007), and oxidoreductases (tetracyclines, rifamycins) (Park et al., 2017; Koteva et al., 2018). As antibiotic prospecting continues, the list of antibiotic destructases is certain to grow (Crofts et al., 2017; Li et al., 2018; Pawlowski et al., 2018).

Unlike other major classes of antibiotic resistance (efflux, exclusion, target modification), covalent inactivation by antibiotic destructases permanently neutralizes the antibiotic challenge and lowers intracellular and extracellular antibiotic concentrations. If antibiotic levels fall below the MIC, then resistance is achieved. Covalent modification of antibiotics can perturb target affinity, block cellular uptake, trigger efflux mechanisms, or lead to decomposition of the antibiotic (Wright, 2005). Genes encoding for antibiotic destructases are often present in operons that are co-transcribed with biosynthetic genes in the antibiotic producing microbe (Li et al., 2018). Co-transcription ensures self-protection during antibiotic biosynthesis (Bolam et al., 2007; Mack et al., 2014). Antibiotic destructases are often transferable through mobilized genetic elements such as plasmids (Davies and Davies, 2010). Once transformed into a host microbial cell, the expression of antibiotic destructases is often inducible and in some cases can be triggered specifically in response to antibiotic challenge (Llarrull et al., 2011). Antibiotic destructases can be excreted to the periplasm or even the extracellular space in order to destroy the antibiotic before it reaches the microbial cell. Resistance caused by antibiotic destructases can be overcome, in theory, by modifying the antibiotic scaffold to evade destructases (Syriopoulou et al., 1981), co-administration of a destructase inhibitor (Drawz and Bonomo, 2010), inhibition of destructase production or localization (Therien et al., 2012), or increasing intracellular concentrations to overcome destructase production (McPherson et al., 2012). Thus far, only modification of the antibiotic scaffold and co-administration of a destructase inhibitor have proven effective for overcoming resistance by antibiotic destructases in clinical infections (Fisher et al., 2005; Drawz and Bonomo, 2010).

Each class of antibiotic destructase represents a distinct chemical mode of antibiotic inactivation with the evolutionary potential to broaden or narrow substrate discrimination (Pawlowski et al., 2018). The evolutionary landscape leans heavily in favor of optimizing resistance enzymes due to the widespread selective pressure applied by broad-spectrum antibiotics. To prepare and respond to the emergence of antibiotic destructases, a thorough understanding of the genetic origins, dissemination, structure, and mechanism of the antibiotic destructase must be established. The rise of beta-lactamases in hospital- and community-acquired infections is the historical model for resistance via antibiotic destruction. Continuous innovation around the beta-lactam pharmacophore and co-administration of beta-lactamase inhibitors as adjuvants has maintained the clinical viability of this important antibiotic class (Bush, 2018). Most of the antibiotic-inactivating enzymes cited above do not represent

current clinical threats; however, each threatens to emerge pending widespread clinical use of the corresponding antibiotic class. The recent success of fourth generation tetracyclines in advanced clinical trials has raised concerns over selecting for tetracycline destructases that might compromise future clinical use of the entire tetracycline class of antibiotics.

## TetX – The Flagship Tetracycline-Inactivating Enzyme

Enzymatic inactivation of tetracyclines was first proposed as a resistance mechanism in 1984 (Guiney et al., 1984). A plasmid that conferred tetracycline resistance to *E. coli* with a strict requirement for aerobic growth was isolated from the human commensal *Bacteroides fragilis* (Matthews and Guiney, 1986; Park et al., 1987; Speer and Salyers, 1988). Plasmid mapping revealed the presence of a putative tetracycline efflux pump and a gene, *tetX*, encoding for a potentially novel tetracycline resistance enzyme that catalyzes tetracycline degradation (Park and Levy, 1988). Growth of *E. coli* carrying the *tetX* gene on an inducible plasmid yielded a distinctive brown colored growth phenotype, exclusively under aerobic conditions (Speer and Salyers, 1989). Spent media from tetracycline-treated cultures of *E. coli* expressing the *tetX* gene showed decreased tetracycline concentrations and loss of tetracycline activity against wild-type *E. coli*. Cell-free lysates of *E. coli* expressing *tetX* strictly required

exogenous NADPH for tetracycline inactivation, consistent with TetX being an NADPH-dependent oxidoreductase (Speer et al., 1991). Two additional variants of the *tetX* gene, *tetX1* and *tetX2*, were later identified in another *Bacteroides* transposon (Whittle et al., 2001).

In 2004, Wright and coworkers heterologously expressed TetX, TetX1, and TetX2 in *E. coli* and purified the recombinant proteins (Yang et al., 2004). TetX and TetX2 are 99% sequence identical, and both proteins co-purified with a bound flavin cofactor and proved to be active FMOs that degrade tetracyclines. TetX1 is a truncated variant that does not bind flavin and is thus not a true tetracycline resistance enzyme. TetX was shown to inactivate first, second, and third generation tetracyclines including tigecycline (Moore et al., 2005). Oxidation of oxytetracycline by TetX leads to formation of a variety of degradation products, including hydroxylation at C11a, the product of which was isolated and characterized by Wright and coworkers following an acid quench that provided the stabilized cyclic hemiketal (**Figure 3A**; alternate sites of oxidation and mechanistic considerations are discussed below in the section “Mechanisms of Tetracycline Oxidation”) (Yang et al., 2004). Presumably, modification at C11a will attenuate  $Mg^{2+}$  chelation and ribosome binding, which are both required for biological activity of oxytetracycline (Schnappinger and Hillen, 1996). Additionally, hydroxylation of C11a destabilizes

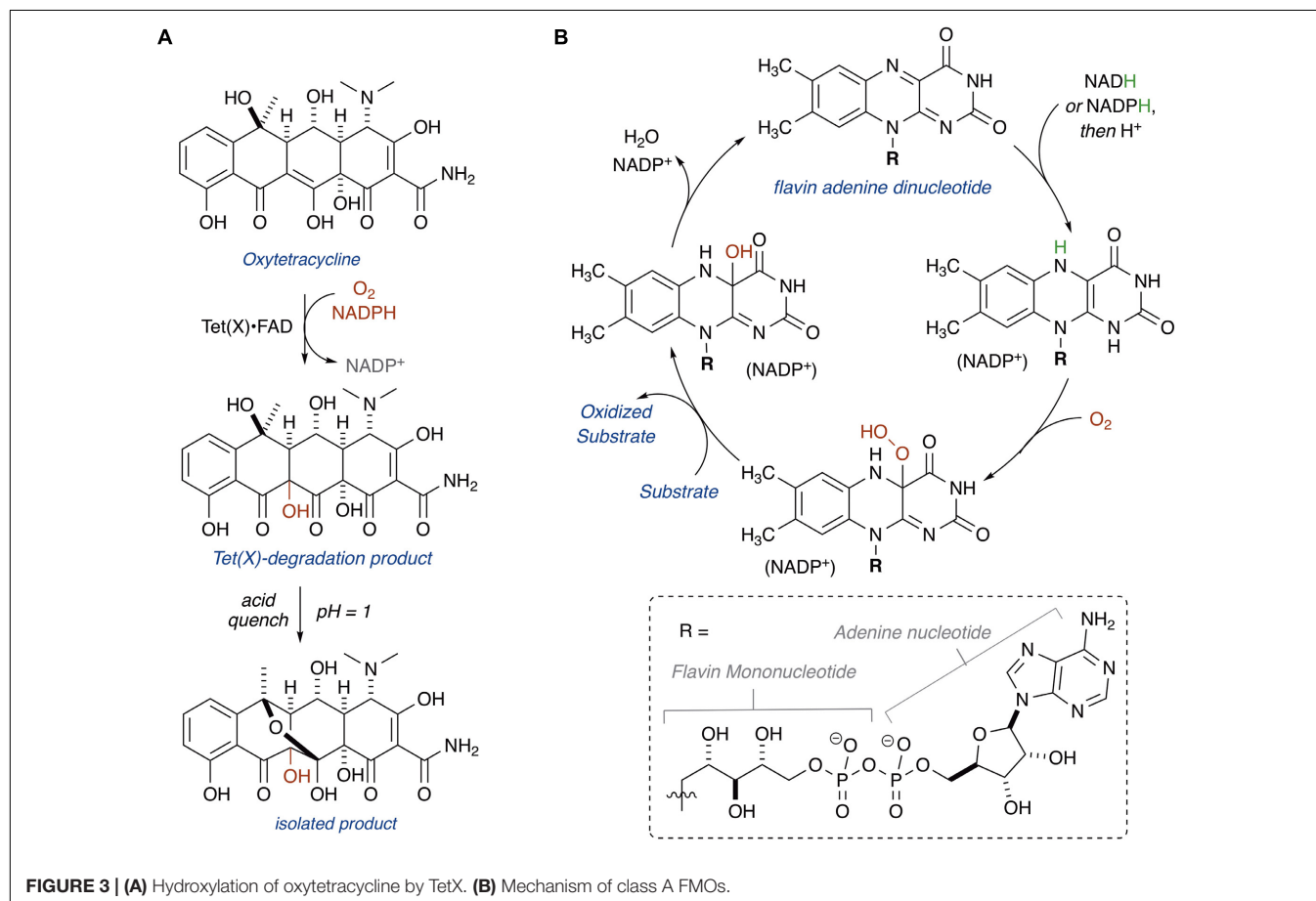


**FIGURE 3 | (A)** Hydroxylation of oxytetracycline by TetX. **(B)** Mechanism of class A FMOs.



the tetracycline scaffold leading to complex mixtures of non-enzymatic degradation products (Yang et al., 2004). X-ray crystal structures of TetX bound to 7-CTc, 7-iodotetracycline, minocycline, and tigecycline have been reported and confirmed TetX to be a class A FMO (structures are discussed below in the section “Structural Basis for Tetracycline Inactivation”) (Volkers et al., 2011, 2013). Similar to other class A FMOs, TetX is predicted to utilize NADPH to reduce the flavin cofactor in preparation for subsequent formation of a reactive C4a-peroxyflavin that transfers an electrophilic hydroxyl group to the nucleophilic C11a of the tetracycline enol (**Figure 3B**; van Berkel et al., 2006).

## Expanding the Tetracycline Destructase Family

Mobilization of *tetX* on transposons in *Bacteroides* suggests that dissemination of the tetracycline resistance gene into human pathogens is possible (Whittle et al., 2002). Indeed, in 2013, the *tetX* gene was found in a variety of MDR Gram-negative pathogens (*Enterobacter cloacae*, *Comamonas testosteroni*, *E. coli*, *Klebsiella pneumoniae*, *Delftia acidovorans*, and other members of Enterobacteriaceae and Pseudomonadaceae) isolated from a hospital in Sierra Leone (Leski et al., 2013). Several of the *tetX* harboring pathogens are on the CDC's list of ESKAPE pathogens (Santajit and Indrawattana, 2016), including *Pseudomonas aeruginosa* and *Acinetobacter baumannii* (Aminov, 2009, 2013; Deng et al., 2014). Although *tetX* has been found in human pathogens, there is yet to be a documented clinical case of tetracycline resistance caused by *tetX* or related genes encoding for tetracycline destructases. The *tetX* gene has also been observed in a variety of environmental bacteria, including *Myroides odoratimimus* (Ming et al., 2017), *Sphingobacterium* sp. (Ghosh et al., 2009, 2014), and *Flavobacterium psychrophilum* (Duchaud et al., 2018), and metagenomic samples including Chinese soil (Wang et al., 2017), human feces (Ohashi and Fujisawa, 2017), and hospital wastewater (Wang et al., 2018). The *tetX* gene is encountered in a wide range of ecosystems (human gut, soil, hospital wastewater) and is present on mobile genetic elements primed for horizontal gene transfer. This pattern of ARG dissemination is consistent with horizontal gene transfer of *tetX* between environmental bacteria and human pathogens, as has been observed for many other classes of ARGs (D'Costa et al., 2006; Forsberg et al., 2012; Crofts et al., 2017).

In 2015, a comprehensive functional metagenomic survey using tetracycline selection identified a new family of *tetX* homologs denoted as the tetracycline destructases (*tet49–tet55*) (Forsberg et al., 2015). The novel tetracycline destructase genes showed at most 24.4% amino acid sequence homology to TetX. Cloning, heterologous expression, and *in vitro* characterization of Tet49–Tet55 revealed that all nine enzymes were functional tetracycline-inactivating FMOs. Comparative gene analysis revealed a tenth tetracycline destructase gene, *tet56*, in the genome of the human pathogen *Legionella longbeachae*. Antibacterial susceptibility and *in vitro* tetracycline degradation assays proved that *tet56* is a true ARG that confers tetracycline resistance when expressed in *L. longbeachae*.

This expanded set of tetracycline destructases provided a unique opportunity to systematically explore substrate selectivity, characterize degradation products, screen for inhibitors, and compare structural features across the enzyme family. These studies led to several important crystal structures of Tet50, Tet51, Tet55, and Tet56 in a variety of functional states (see section “Structural Basis for Tetracycline Inactivation”) that provide mechanistic insight on the diverse oxidation patterns at play for tetracycline substrates (the section “Mechanisms of Tetracycline Oxidation”). These studies also led to the discovery of the first pan tetracycline destructase inhibitor that rescues tetracycline activity when co-administered to tetracycline destructase expressing bacteria (see section “Tetracycline Destructase Inhibitors, an Adjuvant Approach”) (Park et al., 2017).

## STRUCTURAL BASIS FOR TETRACYCLINE INACTIVATION

### Anatomy of a Tetracycline Destructase

TetX and all members of the tetracycline destructase family are structural homologs of class A FMOs. Class A FMOs are single component flavoprotein hydroxylases that utilize FAD cofactors and NAD(P)H electron donors to oxidize small molecule substrates—primarily through electrophilic hydroxylation of electron-rich olefins or aromatic rings by a transient, catalytic C4a-hydroperoxyflavin (*vide supra*, **Figure 3**) (van Berkel et al., 2006; Montersino and Berkel, 2013; Huijbers et al., 2014; Mascotti et al., 2016; Romero et al., 2018). In general, this particular type of FMO enzyme is characterized by a single Rossmann fold that binds FAD through non-covalent interactions with the adenosine monophosphate moiety, which is linked to the catalytic isoalloxazine fragment via a polyoxygenated alkyl chain. Flexibility in this alkyl linker is fundamentally important to the success of the catalytic cycle, which involves multiple, dynamic conformational changes in enzyme structure to establish distinct functional enzyme states differentiated by relative FAD activation and three-dimensional orientation (*vide infra*). TetX and members of the tetracycline destructase family are structurally similar and functionally homologous (Forsberg et al., 2015). As shown in **Figure 4**, the tetracycline-inactivating FMO enzymes are composed of two major domains – a lower FAD-binding domain (green) that exhibits the characteristic Rossmann fold and an upper tetracycline binding domain (pink) (Volkers et al., 2011; Park et al., 2017). The association of the two domains is stabilized by a C-terminal alpha-helix (purple), and specifically in the case of the tetracycline destructase family, a second C-terminal alpha-helix (cyan) is present near the tetracycline binding site, which plays an important role in substrate recognition and loading (Park et al., 2017).

While the exact sequence of events involving dynamic conformational changes to the enzyme during the catalytic cycle are currently unknown (see section “Tetracycline Destructase Inhibitors, an Adjuvant Approach” for a proposed model), two enzyme conformers have been observed via X-ray

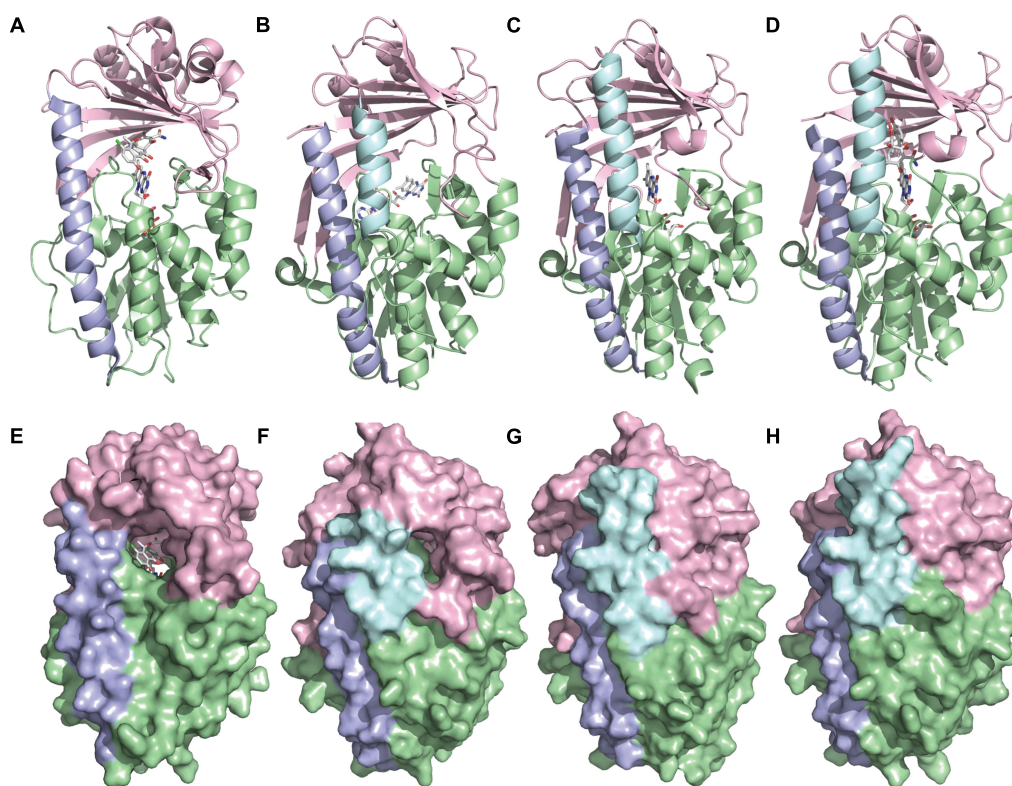


**FIGURE 4** | X-ray crystal structure of a tetracycline destructase with bound tetracycline substrate and flavin cofactor. The mobility of the flavin cofactor is highlighted by showing the FAD-IN and FAD-OUT conformations observed during structural studies. **(A)** X-ray crystal structure of CTC bound to TetX (FAD-IN conformation, PDB ID: 2y6r). **(B)** X-ray crystal structure of Tet50 with no bound substrate (FAD-OUT conformation, PDB ID: 5tue). **(C)** X-ray crystal structure of Tet50 with no bound substrate (FAD-IN conformation, PDB ID: 5tue). **(D)** X-ray crystal structure of CTC bound to Tet50 (FAD-IN conformation, PDB ID: 5tue). **(E)** Surface view of X-ray crystal structure of CTC bound to TetX (FAD-IN conformation, PDB ID: 2y6r). **(F)** Surface view of X-ray crystal structure of Tet50 with no bound substrate (FAD-OUT conformation, PDB ID: 5tue). **(G)** Surface view of X-ray crystal structure of Tet50 with no bound substrate (FAD-IN conformation, PDB ID: 5tue). **(H)** Surface view of X-ray crystal structure of CTC bound to Tet50 (FAD-IN conformation, PDB ID: 5tue). Images were generated using PyMOL v1.7.

crystallographic analysis which are distinct in both FAD-orientation and tertiary protein structure (**Figure 4**). The FAD-OUT conformer, in which the substrate loading channel is open and the FAD cofactor is pointed away from the tetracycline binding domain, allows for easy accommodation of the substrate and ready access of FAD to electron-donor NADPH to maintain a steady concentration of reduced FADH<sub>2</sub> primed for reactivation with molecular oxygen (shown for Tet50, **Figure 4B**, surface view **Figure 4F**). While the FAD-OUT conformation has not been experimentally observed for TetX, it has been observed in other class A-type FMO-enzymes (particularly StaC and RebC) (Ryan et al., 2008; Goldman et al., 2012) and is fundamentally important to maintain catalytic efficiency and relevant levels of antibiotic resistance.

Upon substrate and/or NADPH accommodation, several class A FMO enzymes undergo a series of discrete conformational changes that flip the activated FADH<sub>2</sub> toward the bound substrate and allow for both the protected formation of the reactive C4a-peroxyflavin from FADH<sub>2</sub> and molecular oxygen and subsequent substrate oxidation (Ghisla and Massey, 1989; Palfey and McDonald, 2010; Montersino and Berkel, 2013;

Huijbers et al., 2014). However, this FAD-IN conformer has been observed via X-ray crystallography for TetX and Tet50 in the *absence* of NADPH and substrate. A defined sequence of mechanistic events has been elucidated for prototypical class A FMO *p*-hydroxybenzoate hydroxylase (Eppink et al., 1998, 1999; Suemori, 2013). While the tetracycline-inactivating enzymes appear to be class A FMOs, the defined sequence of events, including NADPH-binding elements, and relevant extrapolation of these no-substrate, FAD-IN conformers to solution-phase enzyme dynamic processes remain currently unknown. Nevertheless, X-ray crystallographic analysis of the no substrate- and substrate-bound FAD-IN conformers of Tet50 and the substrate-bound FAD-IN conformer of TetX highlights several structural differences that may aid in the explanation of the unique, enzyme-specific antibiotic resistance phenotypes observed *in vitro* and in whole cell for each of these tetracycline-inactivating enzymes (Forsberg et al., 2015; Park et al., 2017).

In the absence of the second C-terminal “gatekeeper” helix observed in members of the tetracycline destructase families, the FAD-IN conformation for CTC bound to TetX utilizes several hydrophobic, mostly aromatic residues to shield the FAD-complex from C4a-peroxyflavin-reactive solvent molecules

(Figure 4A; Volkers et al., 2011). Indeed, the FAD cofactor is barely visible in the surface view of the CTc-bound, FAD-IN conformer of TetX (Figure 4E). However, a small, open pocket near the substrate-binding site allows for a portion of the substrate – in this case, CTc – to extend from the active site of the enzyme into solvent exposed space. In contrast, the substrate loading channel closes completely in the no substrate- and CTc-bound FAD-IN conformers of Tet50, where both the FAD and the substrate are shielded from solvent interaction by both the “gatekeeper helix” and a hydrophobic phenylalanine residue in the substrate-binding domain (Phe95, Figures 4C,D) (Park et al., 2017). This structural difference between FAD-IN conformers of TetX and Tet50 is highlighted in the surface views of each protein conformer shown in Figure 4 (TetX Figure 4E and Tet50 Figures 4G,H). In addition, the structure variability in FAD-IN conformation has important implications in substrate recognition and binding, as well as enzyme-substrate specificity and preference, that directly result in distinct tetracycline degradation profiles.

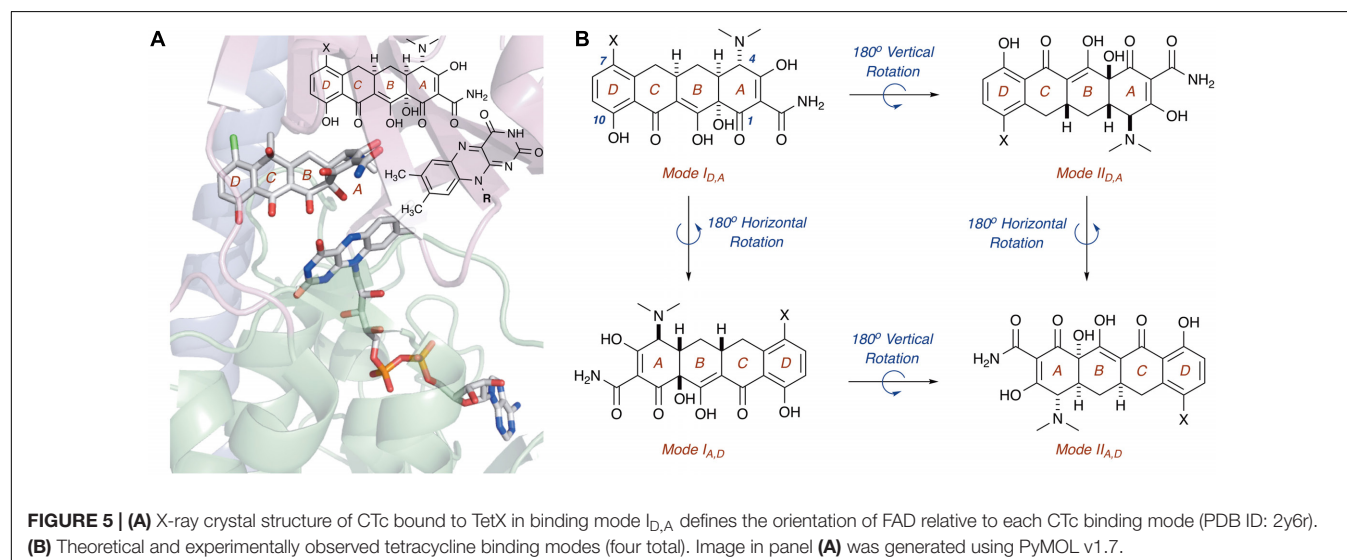
## Diverse Substrate-Binding Modes

As is the case with most class A FMO enzymes (van Berkel et al., 2006; Montersino and Berkel, 2013; Huijbers et al., 2014; Romero et al., 2018), the position of substrate oxidation is heavily dependent on the spatial orientation of the bound substrate in relation to the transient enzyme-associated C4a-peroxyflavin cofactor. Because active site flexibility can lead to product mixtures (as multiple binding modes can lead to multiple degradation products), it is important to correlate experimentally observed binding modes with potential sites of substrate oxidation that correspond to characterized oxidation products.

In this regard, the X-ray crystal structure of CTc bound to TetX can serve as a point of reference to help define spatial coordinates within the enzyme active site in which the tetracycline substrate can rotate/bind (Figure 5; Volkers et al., 2011). As is shown in Figure 5A, enzyme-bound CTc is located above the FAD

cofactor, which is extended toward the substrate-binding domain within the enzyme active site, as is consistent with the FAD-IN conformation. In addition, CTc is oriented in such a way that the A-ring (C1 proximal, C4 distal) is closest to the FAD cofactor, while the D-ring lies nearer the C-terminal alpha-helix (C10 proximal, C7 distal). Thus, this orientation can be defined as mode  $I_{D,A}$ , where the mode number (I or II) describes the proximal or distal position of the C1–C10 hemisphere of the molecule in relation to the FAD cofactor, and the subscript identifier describes the west-to-east (left-to-right) association of the D- and A-rings of the tetracycline substrate in relation to the FAD cofactor. Correspondingly, a  $180^\circ$  horizontal rotation of the tetracycline substrate bound in mode  $I_{D,A}$  (about a vertical axis) would result in substrate-binding mode  $I_{A,D}$  (C1,D-ring proximal), where the sole modification in binding mode is the relation of the A-ring (now west) and D-ring (now east) to the FAD cofactor (Figure 5B). The association of the C1–C10 hemisphere to the FAD isoalloxazine remains unchanged. In contrast, a  $180^\circ$  vertical rotation (about a horizontal axis) of the tetracycline substrate bound in mode  $I_{D,A}$  would result in the substrate-binding mode  $II_{D,A}$ , where the sole modification in binding mode is the relation of the C1–C10 hemisphere of the molecule in relation to the FAD cofactor (now distal). The association of the A- and D-rings to the FAD isoalloxazine remains unchanged. In this way, four potential binding modes for tetracycline substrates – modes  $I_{D,A}$ ,  $I_{A,D}$ ,  $II_{D,A}$ , and  $II_{A,D}$  – can be defined, and the oxidation of the tetracycline substrate will be binding-mode specific.

Of the four potential substrate-binding modes, only two have been experimentally observed via X-ray crystallography for the binding of substrates to tetracycline-inactivating enzymes (Figure 6; Volkers et al., 2011; Park et al., 2017). As described in the previous paragraph, CTc binds to TetX in mode  $I_{D,A}$ , and the primary substrate recognition elements are located in the substrate-binding domain, where hydrogen-bond donating residues (Q192, H234, and R213) interact with H-bond accepting ketone and amide functional groups on the A-ring of CTc





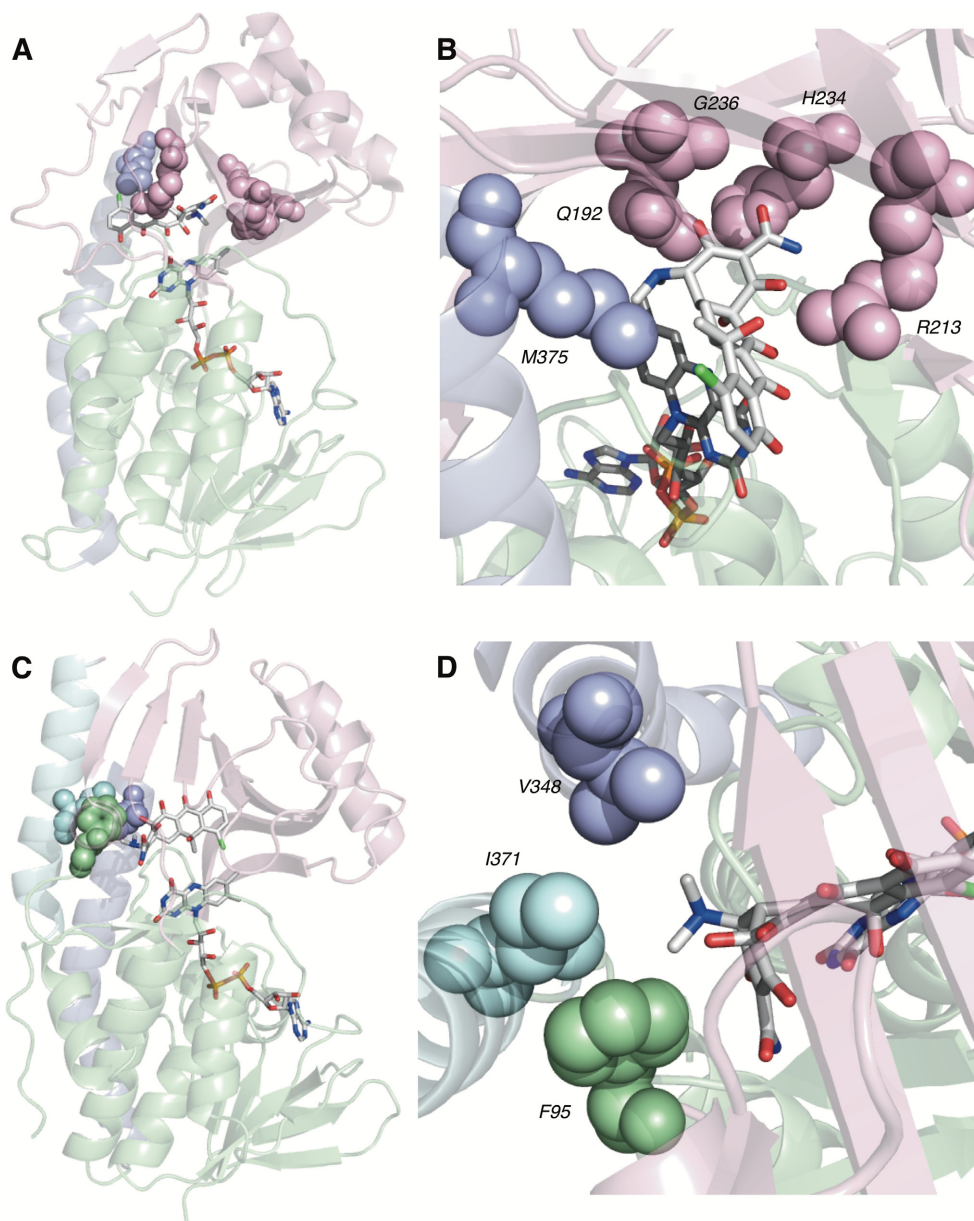


**FIGURE 6 |** Recognition elements of CTC A-ring for each experimentally observed substrate-binding mode. **(A)** X-ray structure of CTC bound to TetX in Mode I<sub>D,A</sub> (PDB ID: 2y6r). **(B)** Expanded X-ray structure of CTC bound to TetX in Mode I<sub>D,A</sub> with interacting structural residues highlighted and labeled (PDB ID: 2y6r). **(C)** X-ray structure of CTC bound to Tet50 in Mode II<sub>A,D</sub> (PDB ID: 5tui). **(D)** Expanded X-ray structure of CTC bound to Tet50 in Mode II<sub>A,D</sub> with interacting structural residues highlighted and labeled (PDB ID: 5tui). Images were generated using PyMOL v1.7.

(Figures 6A,B). While a number of hydrophobic residues in the substrate-binding domain also interact with the C- and D-rings of the enzyme-bound CTC (Volkers et al., 2011), the open cavity near the substrate loading channel of the FAD-IN conformer of TetX allows mostly weak interactions with the D-ring – which can also associate with readily available solvent molecules. In contrast, as shown in Figure 6C, CTC binds to Tet50 in mode II<sub>A,D</sub> (FAD-IN conformer shown), where several van der Waals interactions between the C-terminal stabilizing alpha-helix, the second C-terminal

“gatekeeper” helix, and a residue of the lower FAD-binding domain interact with the *N,N'*-(dimethyl)amino substituent of the now “west” tetracycline A-ring. The expanded view of the mode II<sub>A,D</sub> in Figure 6D highlights the important contribution of the second C-terminal “gatekeeper” helix – which is present in members of the tetracycline destructase family of enzymes but noticeably absent in TetX – to substrate recognition and accommodation. In turn, the substantial differences in experimentally observed substrate-binding modes for CTC-bound TetX and Tet50 account for the variability in

tetracycline degradation profiles observed for both enzymes, as the proximities of enzyme-reactive functional groups to the C4a-center of the FAD cofactor directly influence the nature of potential degradation cascades (Forsberg et al., 2015; Park et al., 2017).

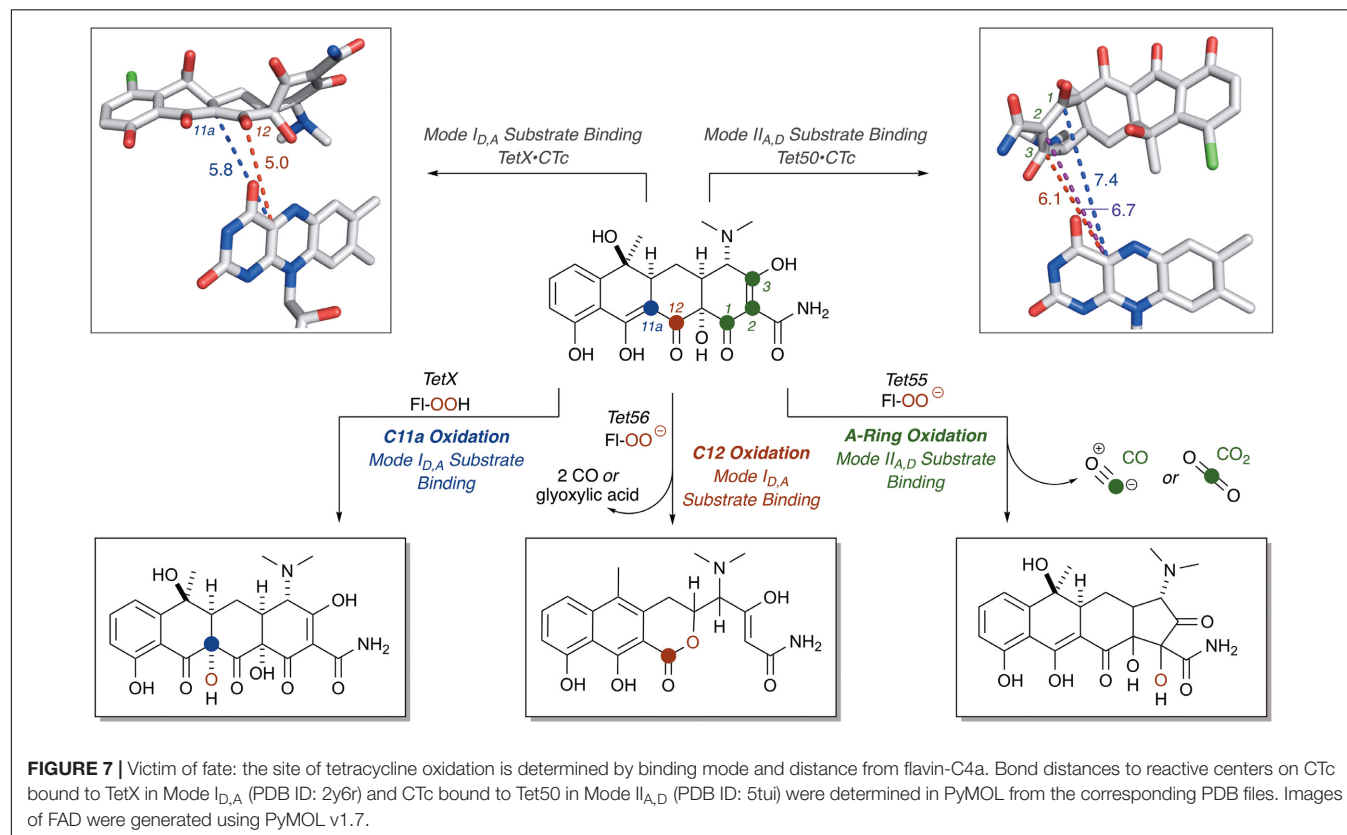
## MECHANISMS OF TETRACYCLINE OXIDATION

### Oxidative “Soft” Spots on the Tetracycline Scaffold

Due to the unstable nature of tetracyclines to light (Moore et al., 1983; Halling-Sorensen et al., 2002; Fuoco, 2015), heat (Nguyen et al., 2015), and acid or base (Yuen and Sokoloski, 1977), the enzymatic and non-enzymatic degradation profiles of tetracycline antibiotics are complex. The mixtures of products resulting from tetracycline oxidation are likely responsible for the distinct brown colored growth phenotype of *E. coli* expressing tetracycline destructases (Speer and Salyers, 1989; Yang et al., 2004; Forsberg et al., 2015). However, because the spatial orientation of the substrate in relation to the reactive C4a-peroxyflavin is fundamentally important to the mechanism of oxidation and tetracycline degradation, the experimentally observed binding modes of CTc bound to TetX and Tet50 can be used to identify potential, binding mode-specific, oxidative “soft” spots on the tetracycline scaffold. These oxidative “soft”

spots can then be used as starting points to propose potential non-enzymatic degradation cascades to explain experimentally observed degradation profiles (Yang et al., 2004; Forsberg et al., 2015; Park et al., 2017).

For CTc bound in mode I<sub>D,A</sub>, the proposed potential oxidative sites on CTc are the C11a-enol- and C12-carbonyl-carbon centers, at distances of 5.8 and 5.0 Å, respectively, from the C4a-position on the FAD cofactor (as determined from the X-ray crystal structure of CTc bound to TetX, **Figure 7**). This is consistent with the enzymatic hydroxylation of the C11a-center of oxytetracycline by TetX reported by Wright and coworkers in 2004, where acid-stabilizing hemiketal formation of the enzymatic degradation product allowed the authors to isolate and fully characterize the intermediate (see **Figure 3**, *vide supra*). For CTc bound in mode II<sub>A,D</sub>, where the A-ring is most accessible to C4a-peroxyflavin oxidation, the proposed potential oxidative sites on CTc are the C1-carbonyl, C2-enol, and C3-carbon centers at distances of 7.4, 6.7, and 6.1 Å, respectively (as determined from the X-ray crystal structure of CTc bound to Tet50, **Figure 7**). It appears that the tetracycline substrate is merely a victim of fate and the oxidative “soft spot” that aligns closest to the C4a-peroxyflavin will be oxidized. Properly defining the distance constraints between flavin-C4a and oxidation sites will enable some predictive capacity. A similar oxidative “soft spot” has been reported for the rifamycin monooxygenase (Rox) that hydroxylates the C2 position of the hydroxynaphthol leading to formation of a 1,2-naphthoquinone (Koteva et al., 2018; Liu et al., 2018).



In the rifamycin-Rox structure C2 is reported to be 4.7 Å from flavin-C4a.

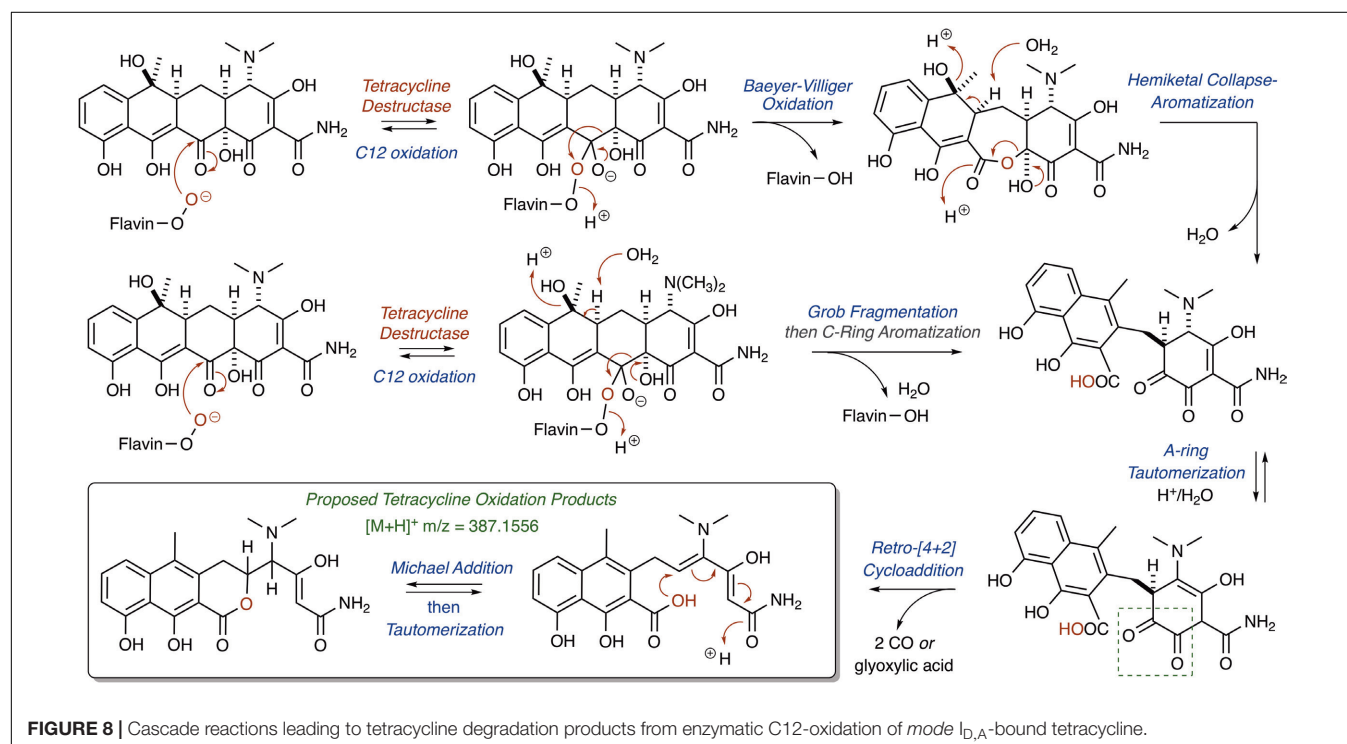
## Oxidation Initiates a Cascade of Chemistry

The highly conjugated nature of the tetracycline antibiotics enables chemical communication across the entire 4-ring structure, which – in turn – can result in a variety of non-enzyme catalyzed rearrangement cascades following the enzymatic oxidation of tetracycline substrates. Indeed, the complex nature of the enzymatic degradation profiles of tetracycline antibiotics and instability of oxidized degradation products implies that non-enzymatic cascade reactions must occur spontaneously in solution to result in a decrease of observed enzymatic degradation product. While the primary enzymatic degradation product of TetX monohydroxylation of oxytetracycline has been observed (Yang et al., 2004), several degradation cascades have been proposed to explain LCMS-observed degradation product formation resulting from the tetracycline destructase-mediated enzymatic oxidation of binding-mode-specific reactive “soft spots” on tetracycline scaffolds (Forsberg et al., 2015; Park et al., 2017).

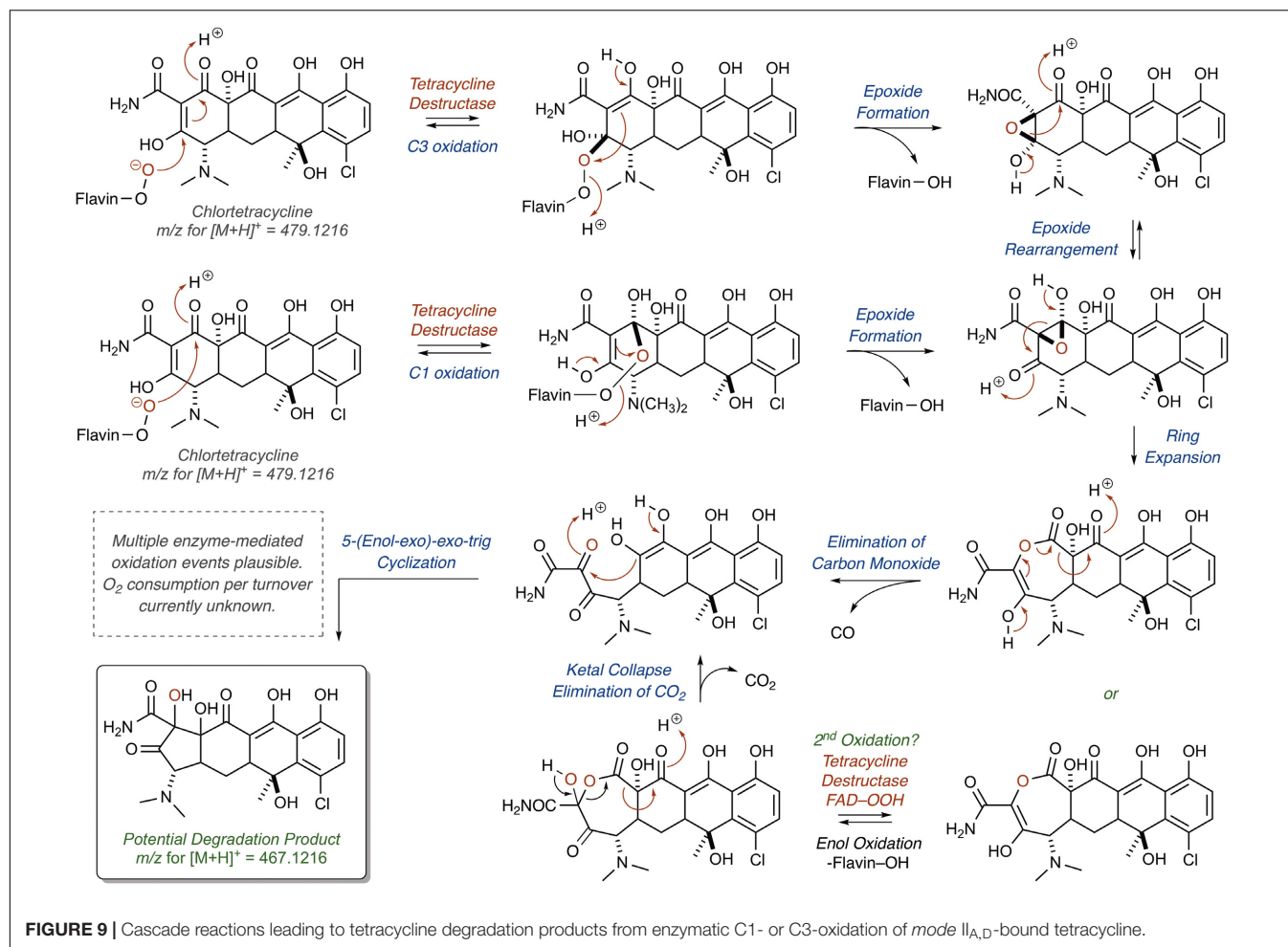
The nucleophilic or electrophilic nature of the intermediate C4a-peroxyflavin (pKa ~ 7–8; Favaudon, 1977; Kemal et al., 1977) within the enzyme active site can be ambiguous across class A FMO enzymes and is largely dependent upon protonation state (protonated C4a-peroxyflavin = electrophilic species; deprotonated C4a-peroxyflavin = nucleophilic species; Massey, 1994; Monterisino and Berkel, 2013; Huijbers et al., 2014). The majority act as electrophiles in the hydroxylation of

electron-rich aromatic rings (Wierenga et al., 1979), but Baeyer–Villiger chemistry has been observed when the substrate is an electrophilic carbonyl (Ryerson et al., 1982; Schwab et al., 1983; Walsh and Wencewicz, 2013). Thus, for the Tet56-mediated degradation of tetracycline resulting in the formation of major ion  $[M+H]^+$  387.1556, it is proposed that a nucleophilic C4a-flavinperoxide can add to the C12-ketone of tetracycline to form a transient, tetrahedral intermediate (Figure 8; Forsberg et al., 2015). This intermediate can undergo a Baeyer–Villiger-type ring expansion via a 1,2-alkyl-shift to eliminate the C4a-hydroxyflavin and provide an intermediate ester, which upon hemiketal collapse and rearomatization of the former C-ring can provide a naphthyl-substituted cyclohex-4-en-1,2-dione intermediate. Alternatively, the same tetrahedral intermediate can undergo a Grob fragmentation, followed by C-ring aromatization, to arrive at the same naphthyl-substituted cyclohex-4-en-1,2-dione intermediate. This cyclohex-4-en-1,2-dione can then tautomerize and undergo a retro[4+2]-cycloaddition to eliminate either two equivalents of carbon monoxide (CO) or one equivalent of transient oxoketene – that, upon hydrolysis, would provide an equivalent of glyoxylic acid – to afford the proposed degradation product as the naphthyl acid ( $[M+H]^+$   $m/z$  = 387.1556). Upon Michael addition and enol tautomerization, the naphthyl acid intermediate can provide the corresponding lactone ( $[M+H]^+$   $m/z$  = 387.1556).

Correspondingly, for the Tet55-mediated degradation of tetracycline resulting in the formation of major ion  $[M+H]^+$  467.1216, it is proposed that the nucleophilic addition of the C4a-flavinperoxide to either the C1- or C3-positions of the tetracycline substrate can result in the formation of two, rapidly interconverting epoxide species (Figure 9;







Park et al., 2017). These species can undergo a ring-expansion via collapse of the hemiketal-epoxide to provide an intermediate lactone, which upon elimination of one equivalent of CO and subsequent intramolecular 5-(enol-exo)-exo-trig cyclization of the resultant enol-containing alpha-ketoamide, could be converted to the proposed degradation product ( $[M+H]^+$  467.1216). Alternatively, the intermediate lactone could undergo a second enol oxidation, followed by ketal collapse and extrusion of carbon dioxide ( $\text{CO}_2$ ), to provide the same enol-containing alpha-ketoamide, which after intramolecular 5-(enol-exo)-exo-trig cyclization provides the corresponding degradation product.

Alternatively, hydroxylation of C2 with an electrophilic C4a-peroxyflavin would initiate a cascade resulting in the same degradation product (Figure 10;  $[M+H]^+$  467.1216). A similar hydroxylation of C2 in mithramycin biosynthesis initiates a ring opening cascade to provide the bioactive form of the DNA minor groove-binding molecule (Gibson et al., 2005). While the precise degradation products remain unknown for both the enzymatic oxidation and the following non-enzymatic degradation cascade, these mechanistic proposals may serve as useful models as more information becomes available en route to the elucidation of the enzymatic degradation of tetracycline antibiotics (Yang et al., 2004; Forsberg et al., 2015; Ghosh et al., 2015; Park et al.,

2017). It is noteworthy that a similar cascade event takes place for the Rox-mediated inactivation of rifamycin where oxidation of the C2 position of the hydroxynaphthalene leads to ring opening of the macrolactam and subsequent linearization of rifamycin (Koteva et al., 2018; Liu et al., 2018). A detailed understanding of enzymatic and non-enzymatic degradation cascades for tetracycline and other antibiotics is critical for designing future generations of molecules that overcome these resistance mechanisms and diagnostic tools to detect active antibiotic-inactivating enzymes in clinical samples. In fact, the degradation mechanisms of beta-lactam antibiotics by beta-lactamase enzymes were fundamentally important to the design of fluorogenic and chromogenic probes used in clinical diagnostic applications (O'Callaghan et al., 1972; Yu et al., 2012; Ghavami et al., 2015).

## TETRACYCLINE DESTRUCTASE INHIBITORS, AN ADJUVANT APPROACH

### Antibiotic Destructase Inhibitors

There are two clinically proven approaches to overcoming resistance by antibiotic destructases: (1) modification of the

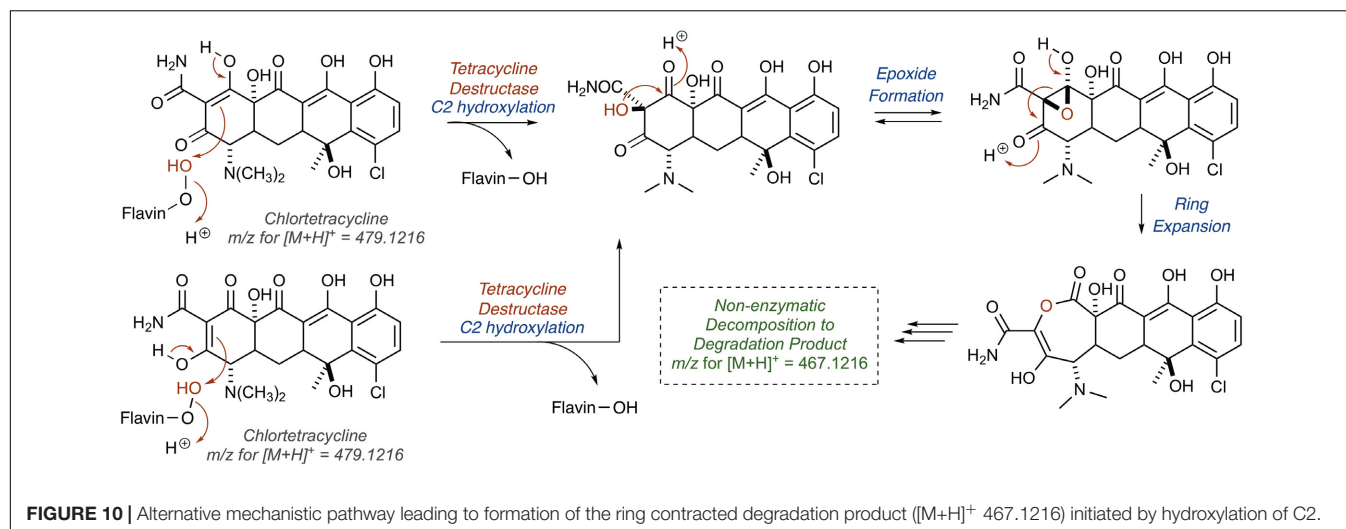


**FIGURE 10 |** Alternative mechanistic pathway leading to formation of the ring contracted degradation product ( $[M+H]^+$  467.1216) initiated by hydroxylation of C2.

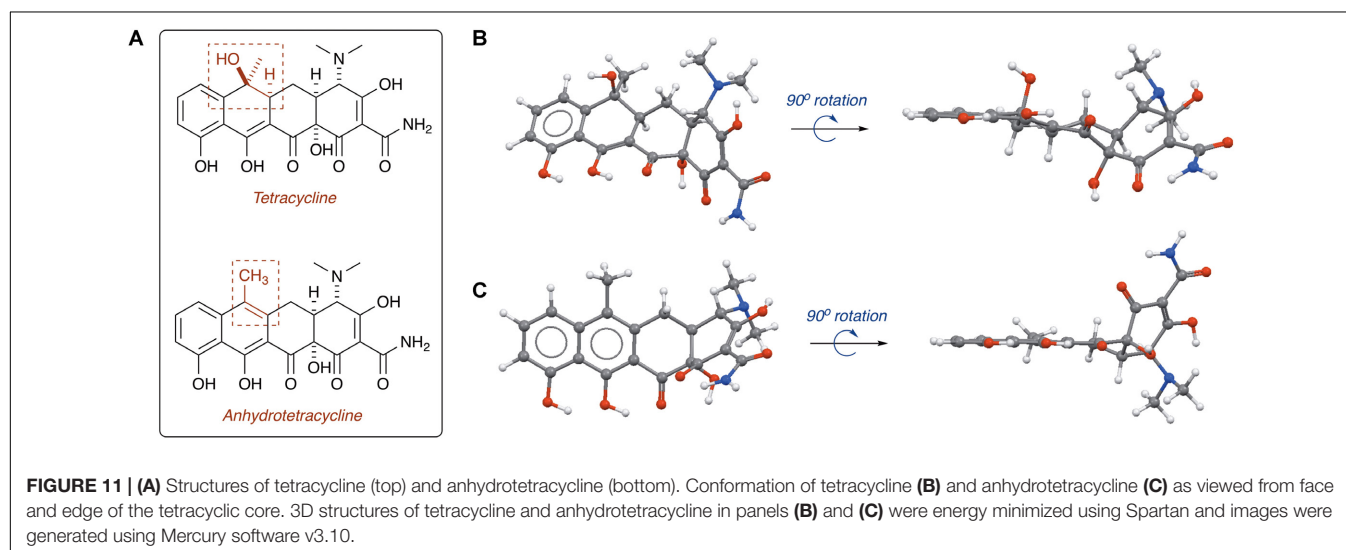


**FIGURE 11 | (A)** Structures of tetracycline (top) and anhydrotetracycline (bottom). Conformation of tetracycline **(B)** and anhydrotetracycline **(C)** as viewed from face and edge of the tetracyclic core. 3D structures of tetracycline and anhydrotetracycline in panels **(B)** and **(C)** were energy minimized using Spartan and images were generated using Mercury software v3.10.

antibiotic structure in a manner that prevents covalent modification (i.e., successive generations of beta-lactams) (Fisher et al., 2005); (2) co-administration of an adjuvant that inhibits production and/or catalytic activity of antibiotic destructases (i.e., beta-lactam/beta-lactamase inhibitor combinations) (Bush, 2018). Modern beta-lactam antibiotics are now fifth generation scaffold iterations, and it is rare to push new beta-lactams into the clinic without co-administration of a beta-lactamase inhibitor. The first beta-lactamase inhibitors, such as clavulanic acid isolated from *Streptomyces clavuligerus*, were found to be beta-lactams like the parent antibiotic (Reading and Cole, 1977). Nature seems to have invented this adjuvant approach long before medicinal chemists ever proposed the idea. In addition to clavulanic acid, *S. clavuligerus* also produces the cephalosporin antibiotic cepharmycin. The biosynthetic genes for both clavulanic acid and cepharmycin are colocalized in a “super cluster” operon, resulting in simultaneous production of the antibiotic and adjuvant to ensure efficacy against beta-lactamase-producing competitors (Ward and Hodgson, 1993). It

is conceivable that tetracycline producers can also biosynthesize tetracycline destructase inhibitors to protect the tetracycline antibiotic, though evidence of which has yet to be discovered.

## Anhydrotetracycline – The First Tetracycline Destructase Inhibitor

Tetracycline producers readily excrete analogs and shunt products during tetracycline biosynthesis (Pickens and Tang, 2010; Wang et al., 2013). One intermediate and shunt product in tetracycline biosynthesis, anhydrotetracycline, was found to be a poor substrate for the tetracycline destructases (Forsberg et al., 2015; Park et al., 2017). Only TetX was able to oxidize anhydrotetracycline, albeit very slowly, suggesting that tetracycline destructases can still bind anhydrotetracycline in the substrate-binding domain despite the subtle structural differences compared to the parent tetracycline (Figure 11). Dehydration of the tetracycline scaffold at C6 provides the more hydrophobic anhydrotetracycline with a flattened naphthalene C,D-ring system and some conformational changes

in the A,B-rings. Despite the subtle structural differences, tetracycline and anhydrotetracycline show remarkably different biological activity. Tetracyclines are potent ribosome inhibitors and have an overall bacteriostatic effect on cells (Wilson, 2009). Anhydrotetracyclines are weak ribosome inhibitors and have a bactericidal effect on cells, presumably through membrane depolarization (Rasmussen et al., 1991; Oliva et al., 1992). Anhydrotetracycline was able to rescue the activity of tetracyclines when co-administered in checkerboard antibacterial assays against *E. coli* expressing tetracycline destructases (Park et al., 2017). Furthermore, anhydrotetracycline was shown to be a potent inhibitor of tetracycline destructases *in vitro* at low micromolar levels. It remains unclear if anhydrotetracycline is acting as a true competitive inhibitor or a competitive (slow) substrate. These initial studies suggest that anhydrotetracycline is a viable tetracycline destructase lead inhibitor and sets the stage for developing tetracycline destructase inhibitors as adjuvants for use in combination therapy with tetracycline antibiotics. This also raises the question as to whether tetracycline-producing microbes excrete anhydrotetracycline with the tetracycline antibiotic to act synergistically as tetracycline destructase inhibitors and secondary antibiotics with an alternate mode of action (membrane depolarization). Mixtures of tetracycline and tetracycline degradation products, including anhydrotetracycline, have been shown to invert resistance selection and select against tetracycline efflux pumps (Palmer et al., 2010; Chait et al., 2011; Stone et al., 2016). Tetracycline destructases and associated degradation products might play a variety of roles beyond resistance in natural environments, including signaling and control of microbial populations (Yim et al., 2007).

## Structural and Mechanistic Basis for Inhibition

X-ray crystal structures of anhydrotetracycline bound to Tet50 revealed several important distinctions in the binding mode compared to the previously discussed structures of CTC bound to Tet50 and TetX (Figure 12; Park et al., 2017). First, a new binding orientation of the tetracyclic scaffold, Mode I<sub>A,D</sub>, was observed (see Figure 5 for reference). The flattened C,D-ring system enables anhydrotetracycline to bind deeper in the substrate-binding domain with the C6-methyl group filling a hydrophobic pocket lined by L198, T207, L205, M222, V181, P296, and Q44. This orientation pushes the flavin “out” and orients the gatekeeper helix so the active site is open to solvent. This binding mode is inaccessible to canonical tetracyclines with methylation and hydroxylation at C6 due to steric clashing. The anhydrotetracycline-stabilized Tet50 conformation is predicted to be catalytically incompetent; however, other binding modes with anhydrotetracycline might be possible based on the observed plasticity of the tetracycline destructases for CTC. Since TetX can slowly oxidize anhydrotetracycline, it seems possible that anhydrotetracyclines can bind in alternate modes similar to CTC that might enable the flavin cofactor to reach the catalytically competent “in” conformation. The gatekeeper helix might be the distinguishing structural

feature between TetX and other tetracycline destructases that determines conformational dynamics, substrate plasticity, catalytic efficiency, and susceptibility to inhibition. The structure of anhydrotetracycline bound to Tet50 should serve as a guide for structure-based drug design of improved tetracycline destructase inhibitors.

## Mechanistic Model for Catalysis and Inhibition

Based on the structural (the section “Structural Basis for Tetracycline Inactivation”), mechanistic (the section “Mechanisms of Tetracycline Oxidation”), and inhibition (the section “Tetracycline Destructase Inhibitors, an Adjuvant Approach”) studies of the tetracycline destructases, a generic model for the catalytic cycle of tetracycline inactivation and inhibition is proposed (Figure 13). The tetracycline destructase can exist in a resting state with the flavin in the oxidized form (I). As shown for other class A FMOs (Abdelwahab et al., 2016), substrate binding (II) can accelerate flavin reduction by NADPH (III) with the flavin dynamically moving between the FAD-IN and FAD-OUT states. The timing and location of C4a-peroxyflavin formation is unclear, but presumably, to oxidize the substrate, the C4a-peroxyflavin must move to the “in” conformation (IV). If the tetracycline destructase has a gatekeeper helix, then the enzyme active site will be closed when the flavin transitions from “out” to “in” and ultimately is positioned to oxidize the tetracycline substrate (V). Movement of the flavin to the “out” conformation will result in movement of the gatekeeper helix to open the active site and release the tetracycline product to complete the catalytic cycle (VI). The oxidized tetracycline products might be subject to further enzymatic oxidation or non-enzymatic cascade reactions leading to non-antibacterial tetracycline degradation products. Anhydrotetracycline is predicted to competitively bind in the substrate-binding domain, which can lead to formation of a stabilized tetracycline destructase inhibition complex with the flavin cofactor essentially “locked” in the unproductive “out” conformation (VII). Anhydrotetracycline is slowly oxidized by TetX; thus, it is conceivable that net destructase inhibition is achieved by anhydrotetracycline acting as a competitive (slow) substrate (VIII). FMOs are a diverse family of oxidoreductases that perform a staggering array of transformations (Walsh and Wencewicz, 2013). There are still many unanswered questions regarding the timing and mechanism of tetracycline inactivation and tetracycline destructase inhibition that will require further structural, mechanistic, and kinetic studies (Eswaramoorthy et al., 2006; van Berkel et al., 2006; Romero et al., 2018).

## FINAL THOUGHTS

### Tetracycline Destructases Represent an Emerging Threat to Next-Generation Tetracyclines

Antibiotic resistance is a moving target (Wright, 2007). Tetracyclines have kept pace through advancements in scaffold



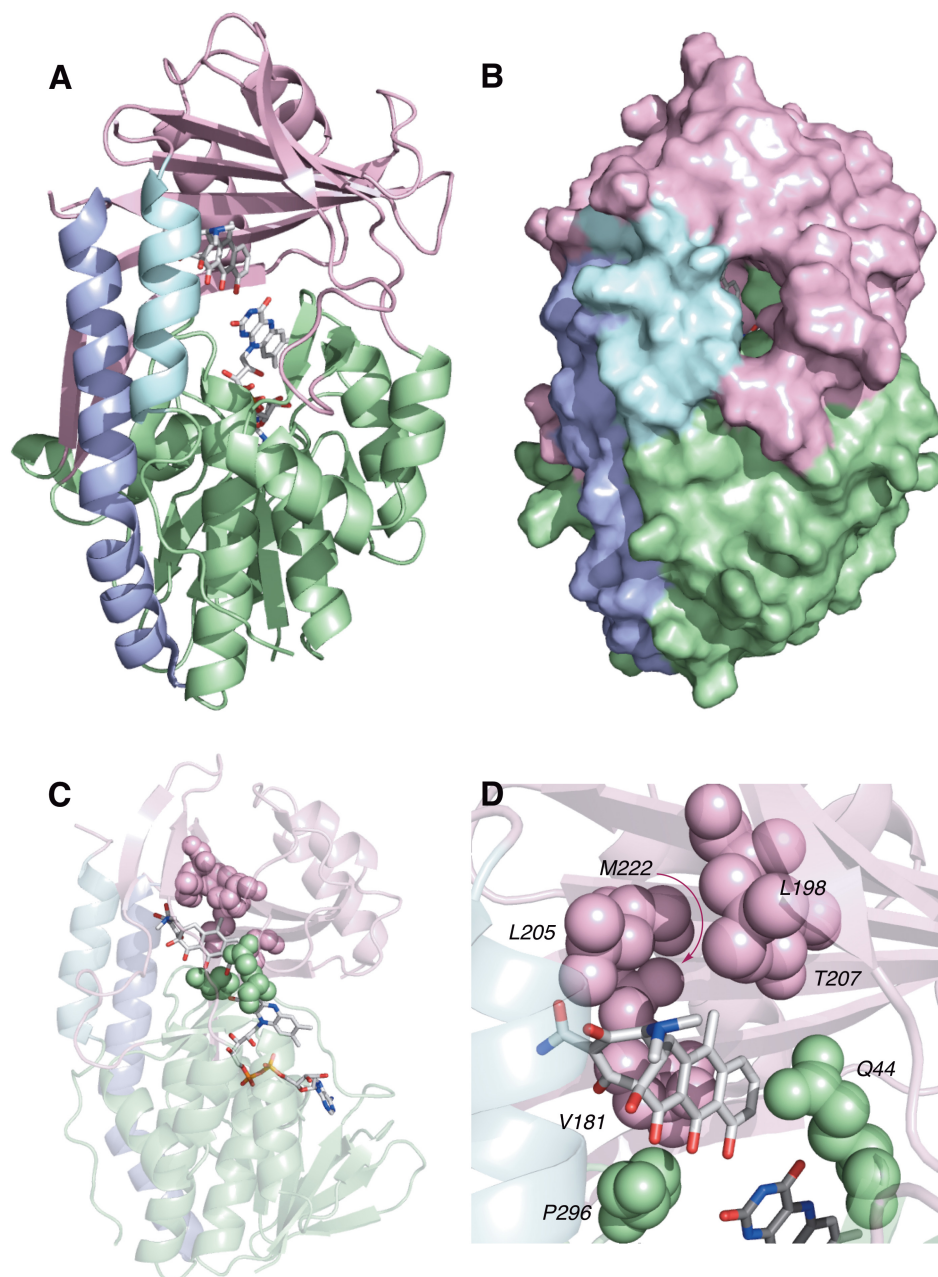
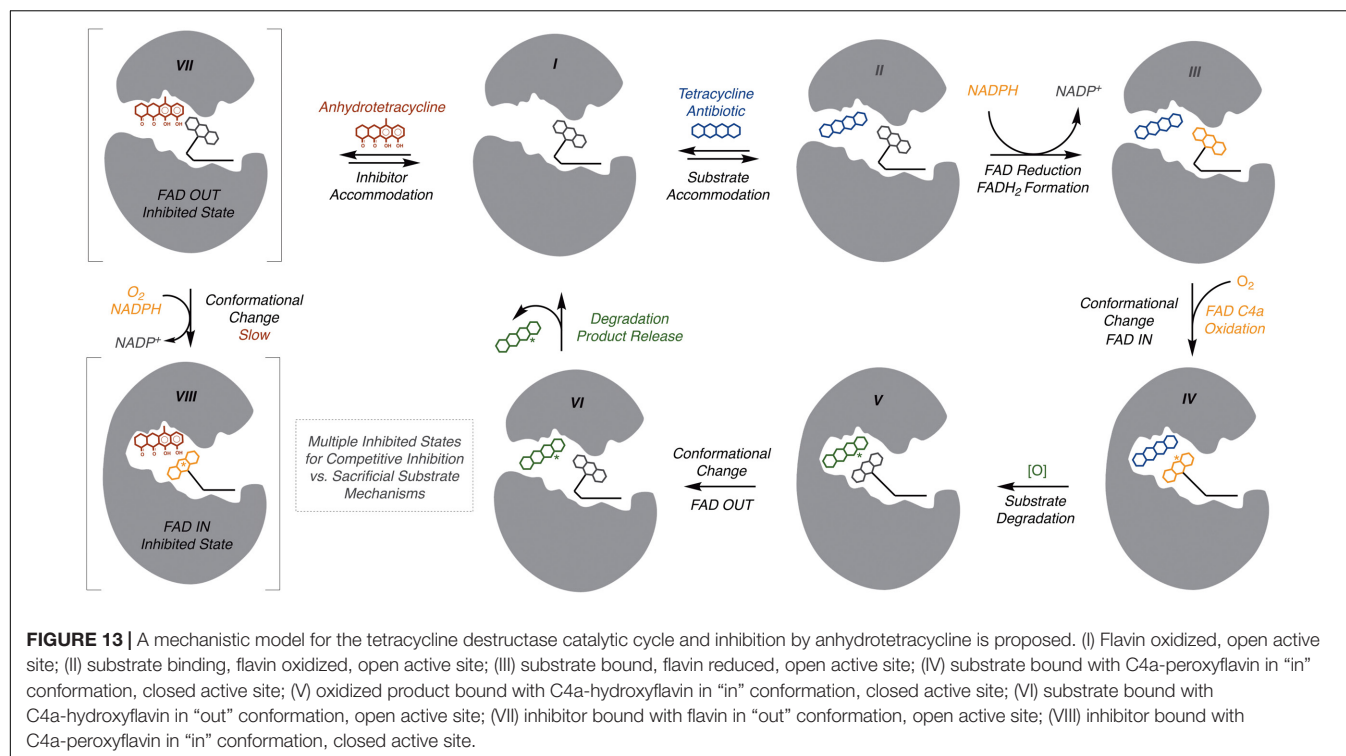


**FIGURE 12 | (A)** X-ray crystal structure of anhydrotetracycline bound to Tet50 in Mode I<sub>A,D</sub> (PDB accession number 5tuf). **(B)** Surface view of X-ray crystal structure of aTC bound to Tet50. **(C)** X-ray crystal structure of anhydrotetracycline bound to Tet50 in Mode I<sub>A,D</sub> with recognition residues highlighted. **(D)** Expanded X-ray crystal structure of anhydrotetracycline bound to Tet50 in Mode I<sub>A,D</sub> with recognition residues highlighted and labeled. Images were generated using PyMOL v1.7.

derivatization, semi-synthesis, biosynthesis, and total chemical synthesis (Chopra and Roberts, 2001; Liu and Myers, 2016; Sun and Xiao, 2017). Increased use of third (tigecycline) and fourth generation (eravacycline, omadacycline) tetracyclines that overcome resistance by efflux and ribosome protection threaten to select for new resistance mechanisms. The tetracycline destructases are FMOs that confer resistance to these next-generation tetracyclines via covalent inactivation (Moore et al., 2005; Grossman et al., 2012; Sutcliffe et al., 2013;

Volkers et al., 2013). Antibiotic oxidation is an emerging inactivation resistance strategy that has only been observed for one other antibiotic class, the rifamycins (Abdelwahab et al., 2016; Liu et al., 2016, 2018; Koteva et al., 2018). Resistance to rifamycin via enzymatic inactivation is not limited to FMOs; in fact, known rifamycin destructases include FMOs (Abdelwahab et al., 2016; Liu et al., 2016, 2018; Koteva et al., 2018), glycosyltransferases (Spanogiannopoulos et al., 2012), ADP-ribosyltransferases (Baysarowich et al.,



2008), and phosphotransferases (Stogios et al., 2016). Future prospecting for tetracycline ARGs will likely result in the discovery of non-FMO tetracycline destructases. Tetracyclines, and rifamycins, are sensitive to chemical photooxidation; so, it seems appropriate that the first tetracycline destructases, FMOs, exploit this reactivity (Moore et al., 1983). The relevance of FMO tetracycline destructases is presumably limited to aerobic infections due to the strict requirement of molecular oxygen for tetracycline inactivation (Guiney et al., 1984). Historically, tetracyclines have been found to be more effective against aerobic bacteria than anaerobic bacteria (Chow et al., 1975). Thus, acquisition and expression of tetracycline destructase FMO genes will be beneficial for aerobic and facultatively anaerobic pathogens that cause a variety of aerobic infections, including pulmonary, periodontal, skin, and post-surgical wound infections (Chopra and Roberts, 2001).

### Functional Prospecting Is Needed to Monitor the Dissemination of Tetracycline Destructase Genes in Human Pathogens

Tetracycline destructases have emerged on mobile genetic elements in human bacterial pathogens (Leski et al., 2013). It appears urgent to have a management plan for tetracycline destructases in place before a clinical crisis emerges. Functional metagenomics is an effective strategy to monitor the dissemination of tetracycline destructases in hospitals and should be continuously applied to patient samples and clinical isolates (Crofts et al., 2017). Tetracycline destructases, including

TetX, evolved in the presence of countless tetracycline variants in diverse environments and thus gained great substrate plasticity (Forsberg et al., 2015; Park et al., 2017). This explains the ability of TetX to oxidize never-before-seen synthetic tetracyclines, including the clinical antibiotics tigecycline and eravacycline, through flexibility in substrate-binding mode that allows for accommodation of tetracyclines with bulky D-ring substituents (Figure 14; Grossman et al., 2012; Sutcliffe et al., 2013). This same type of substrate plasticity has been well documented for the beta-lactamases and carries the risk of causing pan-resistance to an entire drug class (Bush and Jacoby, 2010). A recent study showed that random mutagenesis of the *tetX* gene readily provided TetX variants with significantly improved activity toward tigecycline inactivation (Linkevicius et al., 2016). This suggests that *tetX* is poised to emerge as a primary resistance mechanism under tigecycline selective pressure. Similar to tigecycline, fourth generation molecules like eravacycline and omadacycline possess bulky D-ring substituents that are accommodated and solvent exposed by the constitutively open TetX active site (Figure 14). Comprehensive study of the functional evolution and evolvability of the tetracycline destructases is merited to anticipate future enzyme variants that might emerge in human pathogens (Brandt et al., 2017; Crofts et al., 2017; Pawlowski et al., 2018). It will be interesting to look to tetracycline biosynthetic pathways for FMOs that introduce scaffold oxidations to see if these can undergo gain-of-function as destructases, which might point toward a pathway of evolution for the tetracycline destructases (Gibson et al., 2005; Pickens and Tang, 2010; Walsh and Wenciewicz, 2013; Wang et al., 2013).

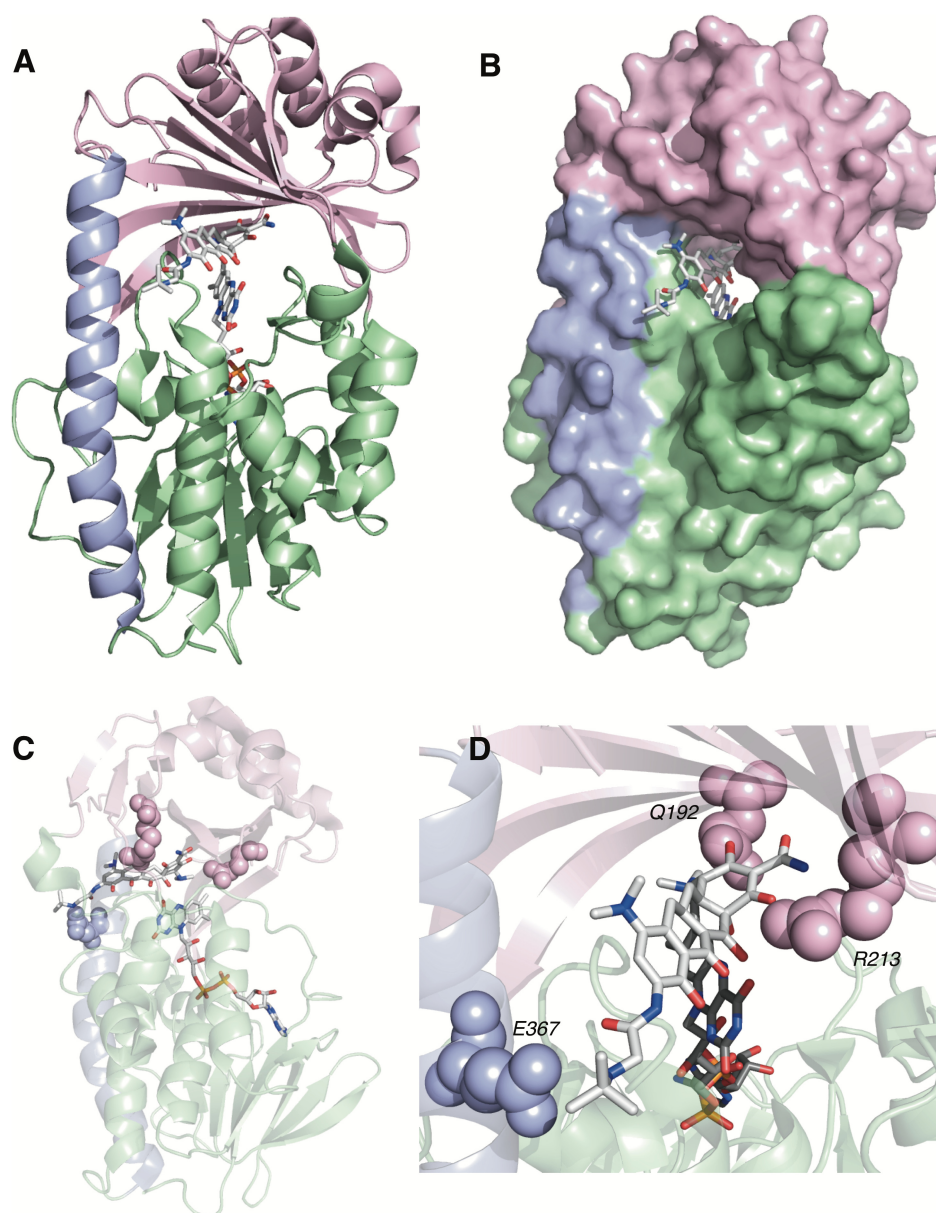


**FIGURE 14 |** (A) X-ray structure of tigecycline bound to TetX in Mode I<sub>D,A</sub> (PDB accession number 4a6n). (B) Surface view of X-ray structure of tigecycline bound to TetX in Mode I<sub>D,A</sub>. (C) X-ray structure of tigecycline bound to TetX in Mode I<sub>D,A</sub> with relevant substrate recognition interactions highlighted. (D) Expanded X-ray structure of tigecycline bound to TetX in Mode I<sub>D,A</sub> with relevant substrate recognition interactions highlighted for the A-ring (Q192, R213) and the D-ring *N*-*t*-butyl-glycylamide substituent (E367). Electron density for the C2-carboxamide bond was missing in the PDB file 4a6n. The C2-carboxamide bond was added using the create bond function in PyMOL. Images were generated using PyMOL v1.7.

## Inhibitors Are Needed as Tetracycline Adjuncts for Future Combination Therapy

Mechanistic and kinetic evaluation of tetracycline destructases have revealed an impressive capacity for substrate oxidation at diverse scaffold positions (Figure 7). Further studies will be needed to map oxidative soft spots to guide the synthesis of next-generation tetracyclines that block oxidation by tetracycline destructases and maintain high affinity for the bacterial ribosome.

The high degree of substrate plasticity of the tetracycline destructases suggests that inhibitors will likely be needed as adjuncts for combination therapies with tetracycline antibiotics. The history of beta-lactamases tells us that scaffold iteration is not enough, and it would be prudent to have inhibitors in hand before tetracycline destructases become a widespread clinical resistance mechanism. Anhydrotetracycline has emerged as the first tetracycline destructase inhibitor and shows potential to be a pan-destructase inhibitor. TetX can slowly oxidize



anhydrotetracycline; thus, models as both a competitive inhibitor and a competitive sacrificial substrate should be applied. Most beta-lactamase inhibitors are mechanism-based and act as both sacrificial substrates and covalent inhibitors, providing clinical evidence that this model of deconstructase inhibition is viable. The crystal structure of anhydrotetracycline bound to Tet50 in a novel binding mode that presumably locks the flavin cofactor in the “out” conformation is a good starting point for structure-based drug design (Figure 12; Park et al., 2017). Anhydrotetracyclines do have antibacterial activity as membrane disruptors and are capable of cell permeation even at sub-MIC levels relevant for tetracycline deconstructase inhibition when used in combination with tetracycline antibiotics (Rasmussen et al., 1991). In addition to anhydrotetracycline, a variety of inhibitor scaffolds would be beneficial, as history from beta-lactamases tells us that multiple inhibitor types will be needed to keep pace with the constantly evolving deconstructases (Drawz and Bonomo, 2010; Bush, 2018). For antibiotic resistance it is not a question of if, but when it will become a clinical problem, which begs the question: When will we take notice? Given the historical precedence for enzymatic antibiotic inactivation mechanisms to dominate resistance landscapes, it is conceivable that all next-generation tetracyclines will need to be co-administered with a tetracycline deconstructase inhibitor potentially in our lifetime. Therefore, a proactive approach to developing next-generation tetracyclines and tetracycline deconstructase inhibitors is the prudent solution to avoiding a clinical crisis . . . for now.

## REFERENCES

- Abdelwahab, H., Martin Del Campo, J. S., Dai, Y., Adly, C., El-Sohaimy, S., and Sobrado, P. (2016). Mechanism of rifampicin inactivation in *Nocardia farcinica*. *PLoS One* 11:e0162578. doi: 10.1371/journal.pone.0162578
- Aminov, R. I. (2009). The role of antibiotics and antibiotic resistance in nature. *Environ. Microbiol.* 11, 2970–2988. doi: 10.1111/j.1462-2920.2009.01972.x
- Aminov, R. I. (2013). Evolution in action: dissemination of *tet(X)* into pathogenic microbiota. *Front. Microbiol.* 4:192. doi: 10.3389/fmicb.2013.00192
- Baysarowich, J., Koteva, K., Hughes, D. W., Ejim, L., Griffiths, E., Zhang, K., et al. (2008). Rifamycin antibiotic resistance by ADP-ribosylation: structure and diversity of Arr. *Proc. Natl. Acad. Sci. U.S.A.* 105, 4886–4891. doi: 10.1073/pnas.0711939105
- Bolam, D. N., Roberts, S., Proctor, M. R., Turkenburg, J. P., Dodson, E. J., Martinez-Fleites, C., et al. (2007). The crystal structure of two macrolide glycosyltransferases provides a blueprint for host cell antibiotic immunity. *Proc. Natl. Acad. Sci. U.S.A.* 104, 5336–5341. doi: 10.1073/pnas.0607897104
- Botterman, J., Gosselé, V., Thoen, C., and Lauwereys, M. (1991). Characterization of phosphinothricin acetyltransferase and C-terminal enzymatically active fusion proteins. *Gene* 102, 33–37. doi: 10.1016/0378-1119(91)90534-1
- Brandt, C., Braun, S. D., Stein, C., Slickers, P., Ehrlich, R., Pletz, M. W., et al. (2017). *In silico* serine  $\beta$ -lactamases analysis reveals a huge potential resistome in environmental and pathogenic species. *Sci. Rep.* 7:43232. doi: 10.1038/srep43232
- Brodersen, D. E., Clemons, W. M. Jr., Carter, A. P., Morgan-Warren, R. J., Wimberly, B. T., and Ramakrishnan, V. (2000). The structural basis for the action of the antibiotics tetracycline, pactamycin, and hygromycin B on the 30S ribosomal subunit. *Cell* 103, 1143–1154. doi: 10.1016/S0092-8674(00)00216-6
- Brown, E. D., and Wright, G. D. (2016). Antibacterial drug discovery in the resistance era. *Nature* 529, 336–343. doi: 10.1038/nature17042
- Burdett, V. (1986). Streptococcal tetracycline resistance mediated at the level of protein synthesis. *J. Bacteriol.* 165, 564–569. doi: 10.1128/jb.165.2.564-569.1986
- Burdett, V. (1991). Purification and characterization of Tet(M), a protein that renders ribosomes resistant to tetracycline. *J. Biol. Chem.* 266, 2872–2877.
- Burdett, V. (1996). Tet(M)-promoted release of tetracycline from ribosomes is GTP dependent. *J. Bacteriol.* 178, 3246–3251. doi: 10.1128/jb.178.11.3246-3251.1996
- Burdett, V., Inamine, J., and Rajagopalan, S. (1982). Heterogeneity of tetracycline resistance determinants in *Streptococcus*. *J. Bacteriol.* 149, 995–1004.
- Bush, K. (2018). Game Changers: new  $\beta$ -lactamase inhibitor combinations targeting antibiotic resistance in gram-negative bacteria. *ACS Infect. Dis.* 4, 84–87. doi: 10.1021/acscinfecdis.7b00243
- Bush, K., and Jacoby, G. A. (2010). Updated functional classification of  $\beta$ -lactamases. *Antimicrob. Agents Chemother.* 54, 969–976. doi: 10.1128/AAC.01009-09
- Chait, R., Vetsigian, K., and Kishony, R. (2011). What counters antibiotic resistance in nature? *Nat. Chem. Biol.* 8, 2–5. doi: 10.1038/nchembio.745
- Charest, M. G., Lerner, C. D., Brubaker, J. D., Siegel, D. R., and Myers, A. G. (2005). A convergent enantioselective route to structurally diverse 6-deoxytetracycline antibiotics. *Science* 308, 395–398. doi: 10.1126/science.1109755
- Chopra, I., and Roberts, M. (2001). Tetracycline antibiotics: mode of action, applications, molecular biology, and epidemiology of bacterial resistance. *Microbiol. Mol. Biol. Rev.* 65, 232–260. doi: 10.1128/mmbr.65.2.232-260.2001
- Chow, A. W., Patten, V., and Guze, L. B. (1975). Comparative susceptibility of anaerobic bacteria to minocycline, doxycycline, and tetracycline. *Antimicrob. Agents Chemother.* 7, 46–49. doi: 10.1128/AAC.7.1.46
- Cocozaki, A. I., Altman, R. B., Huang, J., Buurman, E. T., Kazmirski, S. L., Doig, P., et al. (2016). Resistance mutations generate divergent antibiotic susceptibility profiles against translation inhibitors. *Proc. Natl. Acad. Sci. U.S.A.* 113, 8188–8193. doi: 10.1073/pnas.1605127113

## AUTHOR CONTRIBUTIONS

JM and TW wrote the manuscript and prepared the figures.

## FUNDING

TW and JM acknowledge the National Institute of Allergy and Infectious Diseases, National Institutes of Health, grant R01 123394 for supporting our work on tetracycline-inactivating enzymes.

## ACKNOWLEDGMENTS

A special acknowledgment is given to the tetracycline deconstructase research team at Washington University in St. Louis including Prof. Gautam Dantas (School of Medicine), Prof. Niraj Tolia (School of Medicine), Prof. Timothy Wencewicz (Department of Chemistry), Dr. Kevin Forsberg (Dantas Lab; currently at Fred Hutch Cancer Research Center), Dr. Jooyoung Park (Tolia Lab; currently at University of Washington), Dr. Jana Markley (Wencewicz Lab), Dr. Hirdesh Kumar (Tolia Lab), Dr. Jie Sun (Dantas Lab; currently at North Carolina State University), Andrew Gasparrini (Dantas Lab), Margaret Reck (Wencewicz Lab; currently at Carboline, St. Louis, MO, United States), Chanez Symister (Wencewicz Lab), Luting Fang (Wencewicz Lab), and Tayte Campbell (Dantas Lab).

- Cohen, S. P., McMurtry, L. M., and Levy, S. B. (1988). *marA* locus causes decreased expression of OmpF porin in multiple-antibiotic-resistant (Mar) mutants of *Escherichia coli*. *J. Bacteriol.* 170, 5416–5422. doi: 10.1128/jb.170.12.5416-5422
- Connell, S. R., Tracz, D. M., Nierhaus, K. H., and Taylor, D. E. (2003). Ribosomal protection proteins and their mechanism of tetracycline resistance. *Antimicrob. Agents Chemother.* 47, 3675–3681. doi: 10.1128/aac.47.12.3675-3681.2003
- Crofts, T. S., Gasparrini, A. J., and Dantas, G. (2017). Next-generation approaches to understand and combat the antibiotic resistome. *Nat. Rev. Microbiol.* 15, 422–434. doi: 10.1038/nrmicro.2017.28
- Davies, J. (1994). Inactivation of antibiotics and the dissemination of resistance genes. *Science* 264, 375–382. doi: 10.1126/science.8153624
- Davies, J., and Davies, D. (2010). Origins and evolution of antibiotic resistance. *Microbiol. Mol. Biol. Rev.* 74, 417–433. doi: 10.1128/mmb.00016-10
- D'Costa, V. M., McGrann, K. M., Hughes, D. W., and Wright, G. D. (2006). Sampling the antibiotic resistome. *Science* 311, 374–377. doi: 10.1126/science.1120800
- Deng, M., Zhu, M.-H., Li, J.-J., Bi, S., Sheng, Z.-K., Hu, F.-S., et al. (2014). Molecular epidemiology and mechanisms of tigecycline resistance in clinical isolates of *Acinetobacter baumannii* from a Chinese University Hospital. *Antimicrob. Agents Chemother.* 58, 297–303. doi: 10.1128/AAC.01727-13
- Drawz, S. M., and Bonomo, R. A. (2010). Three decades of  $\beta$ -lactamase inhibitors. *Clin. Microbiol. Rev.* 23, 160–201. doi: 10.1128/CMR.00037-09
- Duchaud, E., Rochat, T., Habib, C., Barbier, P., Loux, V., Guerin, C., et al. (2018). Genomic diversity and evolution of the fish pathogen *Flavobacterium psychrophilum*. *Front. Microbiol.* 9:138. doi: 10.3389/fmicb.2018.00138
- Duggar, B. M. (1948). Aureomycin: a product of the continuing search for new antibiotics. *Annu. N. Y. Acad. Sci.* 51, 17–32. doi: 10.1111/j.1749-6632.1948.tb27262.x
- Eppink, M. H. M., Overkamp, K. M., Schreuder, H. A., and van Berkel, W. J. H. (1999). Switch of the coenzyme specificity of *p*-hydroxybenzoate hydroxylase. *J. Mol. Biol.* 292, 87–96.
- Eppink, M. H. M., Schreuder, H. A., and van Berkel, W. J. H. (1998). Interdomain binding of NADPH in *p*-hydroxybenzoate hydroxylase as suggested by kinetic, crystallographic and modeling studies of histidine 162 and arginine 269 variants. *J. Biol. Chem.* 273, 21031–21039. doi: 10.1074/jbc.273.33.21031
- Eswaramoorthy, S., Bonanno, J. B., Burley, S. K., and Swaminathan, S. (2006). Mechanism of action of a flavin-containing monooxygenase. *Proc. Natl. Acad. Sci. U.S.A.* 103, 9832–9837. doi: 10.1073/pnas.0602398103
- Favaudon, V. (1977). Oxidation kinetics of 1,5-dihydroflavin by oxygen in non-aqueous solvent. *Eur. J. Biochem.* 78, 293–307. doi: 10.1111/j.1432-1033.1977.tb11740.x
- Favrot, L., Blanchard, J. S., and Vergnolle, O. (2016). Bacterial GCN5-related *N*-acetyltransferases: from resistance to regulation. *Biochemistry* 55, 989–1002. doi: 10.1021/acs.biochem.5b01269
- Fillgrove, K. L., Pakhomova, S., Newcomer, M. E., and Armstrong, R. N. (2003). Mechanistic diversity of fosfomycin resistance in pathogenic microorganisms. *J. Am. Chem. Soc.* 125, 15730–15731. doi: 10.1021/ja039307z
- Finlay, A. C., Hobby, G. L., Pan, S. Y., Regna, P. P., Routien, J. B., Seeley, G. M., et al. (1950). Terramycin, a new antibiotic. *Science* 111:85. doi: 10.1126/science.111.2874.85
- Fisher, J. F., Meroueh, S. O., and Mobashery, S. (2005). Bacterial resistance to  $\beta$ -lactam antibiotics: compelling opportunism, compelling opportunity. *Chem. Rev.* 105, 395–424. doi: 10.1021/cr030102i
- Fong, D. H., Burk, D. L., Blanchet, J., Yan, A. Y., and Berghuis, A. M. (2017). Structural basis for kinase-mediated macrolide antibiotic resistance. *Structure* 25, 750–761. doi: 10.1016/j.str.2017.03.007
- Forsberg, K. J., Patel, S., Wenciewicz, T. A., and Dantas, G. (2015). The tetracycline destructases: a novel family of tetracycline-inactivating enzymes. *Chem. Biol.* 22, 888–897. doi: 10.1016/j.chembiol.2015.05.017
- Forsberg, K. J., Reyes, A., Wang, B., Selleck, E. M., Sommer, M. O., and Dantas, G. (2012). The shared antibiotic resistome of soil bacteria and human pathogens. *Science* 337, 1107–1111. doi: 10.1126/science.1220761
- Fuoco, D. (2015). Cytotoxicity induced by tetracyclines via protein photooxidation. *Adv. Toxicol.* 2015:787129. doi: 10.1155/2015/787129
- Gerrits, M. M., de Zoete, M. R., Arents, N. L., Kuipers, E. J., and Kusters, J. G. (2002). 16S rRNA mutation-mediated tetracycline resistance in *Helicobacter pylori*. *Antimicrob. Agents Chemother.* 46, 2996–3000. doi: 10.1128/AAC.46.9.2996-3000.2002
- Ghavami, A., Labbe, G., Brem, J., Goodfellow, V. J., Marrone, L., Tanner, C. A., et al. (2015). Assay for drug discovery: synthesis and testing of nitrocefin analogues for use as  $\beta$ -lactamase substrates. *Anal. Biochem.* 486, 75–77. doi: 10.1016/j.ab.2015.06.032
- Ghisla, S., and Massey, V. (1989). Mechanisms of flavoprotein-catalyzed reactions. *Eur. J. Biochem.* 181, 1–17. doi: 10.1111/j.1432-1033.1989.tb14688.x
- Ghosh, S., LaPara, T. M., and Sadowsky, M. J. (2014). Draft genome sequence of *Sphingobacterium* sp. strain PM2-P1-29, a tetracycline-degrading TetX-expressing aerobic bacterium isolated from agricultural soil. *Genome Announc.* 2:e00963-14. doi: 10.1128/genomeA.00963-14
- Ghosh, S., LaPara, T. M., and Sadowsky, M. J. (2015). Transformation of tetracycline by TetX and its subsequent degradation in a heterologous host. *FEMS Microbiol. Ecol.* 91:fiv059. doi: 10.1093/femsec/fiv059
- Ghosh, S., Sadowsky, M. J., Roberts, M. C., Gralnick, J. A., and LaPara, T. M. (2009). *Sphingobacterium* sp. strain PM2-P1-29 harbours a functional *tet(X)* gene encoding for the degradation of tetracycline. *J. Appl. Microbiol.* 106, 1336–1342. doi: 10.1111/j.1365-2672.2008.04101.x
- Gibson, M., Nur-e-alam, M., Lipata, F., Oliveira, M. A., and Rohr, J. (2005). Characterization of kinetics and products of the Baeyer-Villiger oxygenase MtmOIV, the key enzyme of the biosynthetic pathway toward the natural product anticancer drug mithramycin from *Streptomyces argillaceus*. *J. Am. Chem. Soc.* 127, 17594–17595. doi: 10.1021/ja055750t
- Goldman, P. J., Ryan, K. S., Hamill, M. J., Howard-Jones, A. R., Walsh, C. T., Elliott, S. J., et al. (2012). An unusual role for a mobile flavin in StaC-like indolocarbazole biosynthetic enzymes. *Chem. Biol.* 19, 855–865. doi: 10.1016/j.chembiol.2012.05.016
- Grossman, T. H., Fyfe, C., O'Brien, W., Hackel, M., Minyard, M. B., Waites, K. B., et al. (2017). Fluorocycline TP-271 is potent against complicated community-acquired bacterial pneumonia pathogens. *mSphere* 2:e00004-17. doi: 10.1128/mSphere.00004-17
- Grossman, T. H., Starosta, A. L., Fyfe, C., O'Brien, W., Rothstein, D. M., Mikolajka, A., et al. (2012). Target- and resistance-based mechanistic studies with TP-434, a novel fluorocycline antibiotic. *Antimicrob. Agents Chemother.* 56, 2559–2564. doi: 10.1128/aac.06187-11
- Guillaume, G., Ledent, V., Moens, W., and Collard, J. M. (2004). Phylogeny of efflux-mediated tetracycline resistance genes and related proteins revisited. *Microb. Drug Resist.* 10, 11–26. doi: 10.1089/107662904323047754
- Guiney, D. G. Jr., Hasegawa, P., and Davis, C. E. (1984). Expression in *Escherichia coli* of cryptic tetracycline resistance genes from *Bacteroides* R plasmids. *Plasmid* 11, 248–252. doi: 10.1016/0147-619X(84)90031-3
- Halling-Sorensen, B., Sengelov, G., and Tjornelund, J. (2002). Toxicity of tetracyclines and tetracycline degradation products to environmentally relevant bacteria, including selected tetracycline-resistant bacteria. *Arch. Environ. Contam. Toxicol.* 42, 263–271. doi: 10.1007/s00244-001-0017-2
- Hinrichs, W., Kisker, C., Duvel, M., Muller, A., Tovar, K., Hillen, W., et al. (1994). Structure of the Tet repressor-tetracycline complex and regulation of antibiotic resistance. *Science* 264, 418–420. doi: 10.1126/science.8153629
- Huijbers, M. M. E., Montersino, S., Westphal, A. H., Tischler, D., and van Berkel, W. J. H. (2014). Flavin dependent monooxygenases. *Arch. Biochem. Biophys.* 544, 2–17. doi: 10.1016/j.abb.2013.12.005
- Izaki, K., and Arima, K. (1963). Disappearance of oxytetracycline accumulation in the cells of multiple drug-resistant *Escherichia coli*. *Nature* 200, 384–385. doi: 10.1038/200384a0
- Izard, T., and Ellis, J. (2000). The crystal structures of chloramphenicol phosphotransferase reveal a novel inactivation mechanism. *EMBO J.* 19, 2690–2700. doi: 10.1093/emboj/19.11.2690
- Jenner, L., Starosta, A. L., Terry, D. S., Mikolajka, A., Filonava, L., Yusupov, M., et al. (2013). Structural basis for potent inhibitory activity of the antibiotic tigecycline during protein synthesis. *Proc. Natl. Acad. Sci. U.S.A.* 110, 3812–3816. doi: 10.1073/pnas.1216691110
- Jin, L., Amaya-Mazo, X., Apel, M. E., Sankisa, S. S., Johnson, E., Zbyszynska, M. A., et al. (2007).  $\text{Ca}^{2+}$  and  $\text{Mg}^{2+}$  bind tetracycline with distinct stoichiometries and linked deprotonation. *Biophys. Chem.* 128, 185–196. doi: 10.1016/j.bpc.2007.04.005

- Justice, S. S., Hunstad, D. A., Cegelski, L., and Hultgren, S. J. (2008). Morphological plasticity as a bacterial survival strategy. *Nat. Rev. Microbiol.* 6, 162–168. doi: 10.1038/nrmicro1820
- Kaneko, M., Yamaguchi, A., and Sawai, T. (1985). Energetics of tetracycline efflux system encoded by Tn10 in *Escherichia coli*. *FEBS Lett.* 193, 194–198. doi: 10.1016/0014-5793(85)80149-6
- Kemal, C., Chan, T. W., and Bruce, T. C. (1977). Reaction of 3O2 with dihydroflavins. 1. N3,5-dimethyl-1,5-dihydrolumiflavin and 1,5-dihydroisalloxazines. *J. Am. Chem. Soc.* 99, 7272–7286. doi: 10.1021/ja00464a030
- Kim, S.-R., Nonaka, L., Oh, M. J., Lavilla-Pitogo, C. R., and Suzuki, S. (2003). Distribution of an oxytetracycline resistance determinant *tet(34)* among marine bacterial isolates of a *Vibrio* species. *Microbes Environ.* 18, 74–81. doi: 10.1264/jsm2.18.74
- King, E. Q., Lewis, C. N., Welch, H., Clark, E. A. Jr., Johnson, J. B., Lyons, J. B., et al. (1950). Clinical observations on the use of Terramycin hydrochloride. *J. Am. Med. Assoc.* 143, 1–4. doi: 10.1001/jama.1950.02910360003001
- Korczynska, M., Mukhtar, T. A., Wright, G. D., and Berghuis, A. M. (2007). Structural basis for streptogramin B resistance in *Staphylococcus aureus* by virginiamycin B lyase. *Proc. Natl. Acad. Sci. U.S.A.* 104, 10388–10393. doi: 10.1073/pnas.0701809104
- Koteva, K., Cox, G., Kelso, J. K., Surette, M. D., Zubyk, H. L., Ejim, L., et al. (2018). Rox, a rifamycin resistance Enzyme with an unprecedented mechanism of action. *Cell Chem. Biol.* 25, 403.e5–412.e5. doi: 10.1016/j.chembiol.2018.01.009
- Krueger, S. K., and Williams, D. E. (2005). Mammalian flavin-containing monooxygenases: structure/function, genetic polymorphisms and role in drug metabolism. *Pharmacol. Ther.* 106, 357–387. doi: 10.1016/j.pharmthera.2005.01.001
- Leski, T. A., Bangura, U., Jimmy, D. H., Ansumana, R., Lizewski, S. E., Stenger, D. A., et al. (2013). Multidrug-resistant *tet(X)*-containing hospital isolates in Sierra Leone. *Int. J. Antimicrob. Agents* 42, 83–86. doi: 10.1016/j.ijantimicag.2013.04.014
- Leslie, A. G. W. (1990). Refined crystal structure of type III chloramphenicol acetyltransferase at 1.75 Å resolution. *J. Mol. Biol.* 213, 167–186. doi: 10.1016/S0022-2836(05)80129-9
- Levy, S. B., and McMurry, L. (1978). Plasmid-determined tetracycline resistance involves new transport systems for tetracycline. *Nature* 276, 90–92. doi: 10.1038/276090a0
- Li, B., Forseth, R. R., Bowers, A. A., Schroeder, F. C., and Walsh, C. T. (2012). A backup plan for self-protection: S-methylation of holomycin biosynthetic intermediates in *Streptomyces clavuligerus*. *Chembiochem* 13, 2521–2526. doi: 10.1002/cbic.201200536
- Li, Y.-X., Zhong, Z., Hou, P., Zhang, W.-P., and Qian, P.-Y. (2018). Resistance to nonribosomal peptide antibiotics mediated by D-stereospecific peptidases. *Nat. Chem. Biol.* 14, 381–387. doi: 10.1038/s41589-018-0009-4
- Linkevicius, M., Sandegren, L., and Andersson, D. I. (2016). Potential of tetracycline resistance proteins to evolve tigecycline resistance. *Antimicrob. Agents Chemother.* 60, 789–796. doi: 10.1128/aac.02465-15
- Liu, F., and Myers, A. G. (2016). Development of a platform for the discovery and practical synthesis of new tetracycline antibiotics. *Curr. Opin. Chem. Biol.* 32, 48–57. doi: 10.1016/j.cbpa.2016.03.011
- Liu, L.-K., Abdelwahab, H., Martin Del Campo, J. S., Mehra-Chaudhary, R., Sobrado, P., and Tanner, J. J. (2016). The structure of the antibiotic deactivating, N-hydroxylating rifampicin monooxygenase. *J. Biol. Chem.* 291, 21553–21562. doi: 10.1074/jbc.M116.745315
- Liu, L.-K., Dai, Y., Abdelwahab, H., Sobrado, P., and Tanner, J. J. (2018). Structural evidence for rifampicin monooxygenase inactivating rifampicin by cleaving its ansa-bridge. *Biochemistry* 57, 2065–2068. doi: 10.1021/acs.biochem.8b00190
- Llarrull, L. I., Toth, M., Champion, M. M., and Mobashery, S. (2011). Activation of BlaR1 protein of methicillin-resistant *Staphylococcus aureus*, its proteolytic processing, and recovery from induction of resistance. *J. Biol. Chem.* 286, 38148–38158. doi: 10.1074/jbc.M111.288985
- Lupien, A., Gingras, H., Leprohon, P., and Ouellette, M. (2015). Induced tigecycline resistance in *Streptococcus pneumoniae* mutants reveals mutations in ribosomal proteins and rRNA. *J. Antimicrob. Chemother.* 70, 2973–2980. doi: 10.1093/jac/dkv211
- Mack, S., Xu, Y., and Nodwell, J. R. (2014). The expression of antibiotic resistance genes in antibiotic-producing bacteria. *Mol. Microbiol.* 93, 391–402. doi: 10.1111/mmi.12689
- Mascotti, M. L., Ayub, M. J., Furnham, N., Thornton, J. M., and Laskowski, R. A. (2016). Chopping and changing: the evolution of the flavin-dependent monooxygenases. *J. Mol. Biol.* 428, 3131–3146. doi: 10.1016/j.jmb.2016.07.003
- Massey, V. (1994). Activation of molecular oxygen by flavins and flavoproteins. *J. Biol. Chem.* 269, 22459–22462.
- Matthews, B. G., and Guiney, D. G. (1986). Characterization and mapping of regions encoding clindamycin resistance, tetracycline resistance, and a replication function on the *Bacteroides* R plasmid pCP1. *J. Bacteriol.* 167, 517–521. doi: 10.1128/jb.167.2.517-521.1986
- McCormick, J. R. D., Jensen, E. R., Miller, P. A., and Doerschuk, A. P. (1960). The 6-deoxytetracyclines. Further studies on the relationship between structure and antibacterial activity in the tetracycline series. *J. Am. Chem. Soc.* 82, 3381–3386. doi: 10.1021/ja01498a037
- McPherson, C. J., Aschenbrenner, L. M., Lacey, B. M., Fahnoe, K. C., Lemmon, M. M., Finegan, S. M., et al. (2012). Clinically relevant gram-negative resistance mechanisms have no effect on the efficacy of MC-1, a novel siderophore-conjugated monocarbam. *Antimicrob. Agents Chemother.* 56, 6334–6342. doi: 10.1128/aac.01345-12
- Ming, D.-S., Chen, Q.-Q., and Chen, X.-T. (2017). Analysis of resistance genes in pan-resistant *Myroides odoratimimus* clinical strain PR63039 using whole genome sequencing. *Microb. Pathog.* 112, 164–170. doi: 10.1016/j.micpath.2017.09.012
- Monterisino, S., and Berkel, W. J. H. V. (2013). “The flavin monooxygenases,” in *Handbook of Flavoproteins Vol II: Complex Flavoproteins, Dehydrogenases and Physical Methods*, eds R. Hille, S. Miller, and B. Palfey (Berlin: De Gruyter), 51–72.
- Moore, D. E., Fallon, M. P., and Burt, C. D. (1983). Photo-oxidation of tetracycline—a differential pulse polarographic study. *Int. J. Pharm.* 14, 133–142. doi: 10.1016/0378-5173(83)90088-1
- Moore, I. F., Hughes, D. W., and Wright, G. D. (2005). Tigecycline is modified by the flavin-dependent monooxygenase TetX. *Biochemistry* 44, 11829–11835. doi: 10.1021/bi0506066
- Morar, M., Bhullar, K., Hughes, D. W., Junop, M., and Wright, G. D. (2009). Structure and mechanism of the lincosamide antibiotic adenylyltransferase LinB. *Structure* 17, 1649–1659. doi: 10.1016/j.str.2009.10.013
- Morar, M., Pengelly, K., Koteva, K., and Wright, G. D. (2012). Mechanism and diversity of the erythromycin esterase family of enzymes. *Biochemistry* 51, 1740–1751. doi: 10.1021/bi201790u
- Nelson, M. L., and Levy, S. B. (2011). The history of the tetracyclines. *Annu. N. Y. Acad. Sci.* 1241, 17–32. doi: 10.1111/j.1749-6632.2011.06354.x
- Nguyen, F., Starosta, A. L., Arenz, S., Sohmen, D., Donhofer, A., and Wilson, D. N. (2014). Tetracycline antibiotics and resistance mechanisms. *Biol. Chem.* 395, 559–575. doi: 10.1515/hsz-2013-0292
- Nguyen, V., Nguyen, V., Li, C., and Zhou, G. (2015). The degradation of oxytetracycline during thermal treatments of chicken and pig meat and the toxic effects of degradation products of oxytetracycline on rats. *J. Food Sci. Technol.* 52, 2842–2850. doi: 10.1007/s13197-014-1306-x
- Nonaka, L., Connell, S. R., and Taylor, D. E. (2005). 16S rRNA mutations that confer tetracycline resistance in *Helicobacter pylori* decrease drug binding in *Escherichia coli* ribosomes. *J. Bacteriol.* 187, 3708–3712. doi: 10.1128/JB.187.11.3708-3712.2005
- Nonaka, L., and Suzuki, S. (2002). New Mg<sup>2+</sup>-dependent oxytetracycline resistance determinant *tet34* in *Vibrio* isolates from marine fish intestinal contents. *Antimicrob. Agents Chemother.* 46, 1550–1552. doi: 10.1128/AAC.46.5.1550-1552.2002
- O’Callaghan, C. H., Morris, A., Kirby, S. M., and Shingler, A. H. (1972). Novel method for detection of beta-lactamases by using a chromogenic cephalosporin substrate. *Antimicrob. Agents Chemother.* 1, 283–288. doi: 10.1128/AAC.1.4.283
- Ohashi, Y., and Fujisawa, T. (2017). Detection of antibiotic resistance genes in the feces of young adult Japanese. *Biosci. Microbiota Food Health* 36, 151–154. doi: 10.12938/bmfh.17-004
- Olesky, M., Zhao, S., Rosenberg, R. L., and Nicholas, R. A. (2006). Porin-mediated antibiotic resistance in *Neisseria gonorrhoeae*: Ion, solute, and antibiotic



- permeation through PIB proteins with *penB* mutations. *J. Bacteriol.* 188, 2300–2308.
- Oliva, B., Gordon, G., McNicholas, P., Ellestad, G., and Chopra, I. (1992). Evidence that tetracycline analogs whose primary target is not the bacterial ribosome cause lysis of *Escherichia coli*. *Antimicrob. Agents Chemother.* 36, 913–919. doi: 10.1128/AAC.36.5.913
- Palfe, B. A., and McDonald, C. A. (2010). Control of catalysis in flavin-dependent monooxygenases. *Arch. Biochem. Biophys.* 493, 26–36. doi: 10.1016/j.abb.2009.11.028
- Palmer, A. C., Angelino, E., and Kishony, R. (2010). Chemical decay of an antibiotic inverts selection for resistance. *Nat. Chem. Biol.* 6, 105–107. doi: 10.1038/nchembio.289
- Park, B. H., Hendricks, M., Malamy, M. H., Tally, F. P., and Levy, S. B. (1987). Cryptic tetracycline resistance determinant (class F) from *Bacteroides fragilis* mediates resistance in *Escherichia coli* by actively reducing tetracycline accumulation. *Antimicrob. Agents Chemother.* 31, 1739–1743. doi: 10.1128/aac.31.11.1739
- Park, B. H., and Levy, S. B. (1988). The cryptic tetracycline resistance determinant on Tn4400 mediates tetracycline degradation as well as tetracycline efflux. *Antimicrob. Agents Chemother.* 32, 1797–1800. doi: 10.1128/aac.32.12.1797
- Park, J., Gasparrini, A. J., Reck, M. R., Symister, C. T., Elliott, J. L., Vogel, J. P., et al. (2017). Plasticity, dynamics, and inhibition of emerging tetracycline resistance enzymes. *Nat. Chem. Biol.* 13, 730–736. doi: 10.1038/nchembio.2376
- Pawlowski, A. C., Stogios, P. J., Koteva, K., Skarina, T., Evdokimova, E., Savchenko, A., et al. (2018). The evolution of substrate discrimination in macrolide antibiotic resistance enzymes. *Nat. Commun.* 9:112. doi: 10.1038/s41467-017-02680-0
- Pickens, L. B., and Tang, Y. (2010). Oxytetracycline biosynthesis. *J. Biol. Chem.* 285, 27509–27515. doi: 10.1074/jbc.R110.130419
- Piddock, L. J. V. (2006). Clinically relevant chromosomally encoded multidrug resistance efflux pumps in bacteria. *Clin. Microbiol. Rev.* 19, 382–402. doi: 10.1128/CMR.19.2.382-402.2006
- Ramirez, M. S., and Tolmash, M. E. (2010). Aminoglycoside modifying enzymes. *Drug Resist. Updat.* 13, 151–171. doi: 10.1016/j.drug.2010.08.003
- Rasmussen, B., Noller, H. F., Daubresse, G., Oliva, B., Misulovin, Z., Rothstein, D. M., et al. (1991). Molecular basis of tetracycline action: identification of analogs whose primary target is not the bacterial ribosome. *Antimicrob. Agents Chemother.* 35, 2306–2311. doi: 10.1128/AAC.35.11.2306
- Reading, C., and Cole, M. (1977). Clavulanic acid: a beta-lactamase-inhibiting beta-lactam from *Streptomyces clavuligerus*. *Antimicrob. Agents Chemother.* 11, 852–857. doi: 10.1128/AAC.11.5.852
- Rife, C. L., Pharris, R. E., Newcomer, M. E., and Armstrong, R. N. (2002). Crystal structure of a genomically encoded fosfomycin resistance protein (FosA) at 1.19 Å resolution by MAD phasing off the L-III edge of  $\text{Ti}^{4+}$ . *J. Am. Chem. Soc.* 124, 11001–11003.
- Roberts, M. C. (1996). Tetracycline resistance determinants: mechanisms of action, regulation of expression, genetic mobility, and distribution. *FEMS Microbiol. Rev.* 19, 1–24. doi: 10.1111/j.1574-6976.1996.tb00251.x
- Romero, E., Gómez Castellanos, J. R., Gadda, G., Fraaije, M. W., and Mattevi, A. (2018). Same substrate, many reactions: oxygen activation in flavoenzymes. *Chem. Rev.* 118, 1742–1769. doi: 10.1021/acs.chemrev.7b00650
- Ronn, M., Zhijian, Z., Hogan, P. C., Zhang, W.-Y., Niu, J., Katz, C. E., et al. (2013). Process R&D of eravacycline: the first fully synthetic fluorocycline in clinical development. *Org. Process Res. Dev.* 17, 838–845. doi: 10.1021/op4000219
- Ross, J. I., Eady, E. A., Cove, J. H., and Cunliffe, W. J. (1998). 16S rRNA mutation associated with tetracycline resistance in a gram-positive bacterium. *Antimicrob. Agents Chemother.* 42, 1702–1705.
- Ryan, K. S., Chakraborty, S., Howard-Jones, A. R., Walsh, C. T., Ballou, D. P., and Drennan, C. L. (2008). The FAD cofactor of RebC shifts to an IN conformation upon flavin reduction. *Biochemistry* 47, 13506–13513. doi: 10.1021/bi801229w
- Ryerson, C. C., Ballou, D. P., and Walsh, C. (1982). Mechanistic studies on cyclohexanone oxygenase. *Biochemistry* 21, 2644–2655. doi: 10.1021/bi00540a011
- Santajit, S., and Indrawattana, N. (2016). Mechanisms of antimicrobial resistance in ESKAPE pathogens. *BioMed Res. Int.* 2016:2475067. doi: 10.1155/2016/2475067
- Schiott, C. R., and Stenderup, A. (1954). Terramycin-, aureomycin- and chloromycetin-dependent bacteria isolated from patients. *Acta Pathol. Microbiol. Scand.* 34, 410–416. doi: 10.1111/j.1699-0463.1954.tb00838.x
- Schnappinger, D., and Hillen, W. (1996). Tetracyclines: antibiotic action, uptake, and resistance mechanisms. *Arch. Microbiol.* 165, 359–369.
- Schwab, J. M., Li, W., and Thomas, L. P. (1983). Cyclohexanone oxygenase: stereochemistry, enantioselectivity, and regioselectivity of an enzyme-catalyzed Baeyer-Villiger reaction. *J. Am. Chem. Soc.* 105, 4800–4808. doi: 10.1021/ja00352a044
- Spanogiannopoulos, P., Thaker, M., Koteva, K., Waglehner, N., and Wright, G. D. (2012). Characterization of a rifampin-inactivating glycosyltransferase from a screen of environmental Actinomycetes. *Antimicrob. Agents Chemother.* 56, 5061–5069. doi: 10.1128/AAC.01166-12
- Speer, B. S., Bedzyk, L., and Salyers, A. A. (1991). Evidence that a novel tetracycline resistance gene found on two *Bacteroides* transposons encodes an NADP-requiring oxidoreductase. *J. Bacteriol.* 173, 176–183. doi: 10.1128/jb.173.1.176-183.1991
- Speer, B. S., and Salyers, A. A. (1988). Characterization of a novel tetracycline resistance that functions only in aerobically grown *Escherichia coli*. *J. Bacteriol.* 170, 1423–1429. doi: 10.1128/jb.170.4.1423-1429.1988
- Speer, B. S., and Salyers, A. A. (1989). Novel aerobic tetracycline resistance gene that chemically modifies tetracycline. *J. Bacteriol.* 171, 148–153. doi: 10.1128/jb.171.1.148-153.1989
- Stepanek, J. J., Lukezic, T., Teichert, I., Petkovic, H., and Bandow, J. E. (2016). Dual mechanism of action of the atypical tetracycline chelocardin. *Biochim. Biophys. Acta* 1864, 645–654. doi: 10.1016/j.bbapap.2016.03.004
- Stephens, C. R., Conover, L. H., Hochstein, F. A., Regna, P. P., Pilgrim, F. J., Bruning, K. J., et al. (1952). Terramycin. VIII. Structure of aureomycin and terramycin. *J. Am. Chem. Soc.* 74, 4976–4977. doi: 10.1021/ja011139a533
- Stephens, C. R., Murai, K., Brunings, K. J., and Woodward, R. B. (1956). Acidity constants of the tetracycline antibiotics. *J. Am. Chem. Soc.* 78, 4155–4158. doi: 10.1021/ja01597a081
- Stogios, P. J., Cox, G., Spanogiannopoulos, P., Pilon, M. C., Waglehner, N., Skarina, T., et al. (2016). Rifampin phosphotransferase is an unusual antibiotic resistance kinase. *Nat. Commun.* 7:11343. doi: 10.1038/ncomms11343
- Stone, L. K., Baym, M., Lieberman, T. D., Chait, R., Clardy, J., and Kishony, R. (2016). Compounds that select against the tetracycline-resistance efflux pump. *Nat. Chem. Biol.* 12, 902–904. doi: 10.1038/nchembio.2176
- Suemori, A. (2013). Conserved and non-conserved residues and their role in the structure and function of p-hydroxybenzoate hydroxylase. *Protein Eng. Des. Sel.* 26, 479–488. doi: 10.1093/protein/gzt026
- Sugantino, M., and Roderick, S. L. (2002). Crystal structure of Vat(D): an acetyltransferase that inactivates streptogramin group A antibiotics. *Biochemistry* 41, 2209–2216. doi: 10.1021/bi011991b
- Sun, C., and Xiao, X.-Y. (2017). “Fully synthetic tetracyclines: increasing chemical diversity to combat multidrug-resistant bacterial infections,” in *Topics in Medicinal Chemistry*, ed. J. F. Fisher (Berlin: Springer).
- Surette, M. D., and Wright, G. D. (2017). Lessons from the environmental antibiotic resistance. *Annu. Rev. Microbiol.* 71, 309–329. doi: 10.1146/annurev-micro-090816-093420
- Sutcliffe, J. A., O'Brien, W., Fyfe, C., and Grossman, T. H. (2013). Antibacterial activity of eravacycline (TP-434), a novel fluorocycline, against hospital and community pathogens. *Antimicrob. Agents Chemother.* 57, 5548–5558. doi: 10.1128/aac.01288-13
- Syriopoulou, V. P., Harding, A. L., Goldmann, D. A., and Smith, A. L. (1981). In vitro antibacterial activity of fluorinated analogs of chloramphenicol and thiamphenicol. *Antimicrob. Agents Chemother.* 19, 294–297. doi: 10.1128/AAC.19.2.294
- Tanaka, S. K., Steenbergen, J., and Villano, S. (2016). Discovery, pharmacology, and clinical profile of omadacycline, a novel aminomethylcycline antibiotic. *Bioorg. Med. Chem.* 24, 6409–6419. doi: 10.1016/j.bmc.2016.07.029
- Thaker, M., Spanogiannopoulos, P., and Wright, G. D. (2010). The tetracycline resistance. *Cell. Mol. Life Sci.* 67, 419–431. doi: 10.1007/s00018-009-0172-6
- Therien, A. G., Huber, J. L., Wilson, K. E., Beaulieu, P., Caron, A., Claveau, D., et al. (2012). Broadening the spectrum of  $\beta$ -lactam antibiotics through inhibition

- of signal peptidase type I. *Antimicrob. Agents Chemother.* 56, 4662–4670. doi: 10.1128/aac.00726-12
- Thiara, A. S., and Cundliffe, E. (1995). Analysis of two capreomycin-resistance determinants from *Streptomyces capreolus* and characterization of the action of their products. *Gene* 167, 121–126. doi: 10.1016/0378-1119(95)00702-4
- Thompson, M. K., Keithly, M. E., Harp, J., Cook, P. D., Jagessar, K. L., Sulikowski, G. A., et al. (2013). Structural and chemical aspects of resistance to the antibiotic fosfomycin conferred by FosB from *Bacillus cereus*. *Biochemistry* 52, 7350–7362. doi: 10.1021/bi4009648
- Trieber, C. A., and Taylor, D. E. (2002). Mutations in the 16S rRNA genes of *Helicobacter pylori* mediate resistance to tetracycline. *J. Bacteriol.* 184, 2131–2140. doi: 10.1128/JB.187.11.3708-3712.2005
- Tripathi, P., Shine, E. E., Healy, A. R., Kim, C. S., Herzon, S. B., Bruner, S. D., et al. (2017). ClbS is a cyclopropane hydrolase that confers colibactin resistance. *J. Am. Chem. Soc.* 139, 17719–17722. doi: 10.1021/jacs.7b09971
- van Berkel, W. J., Kamerbeek, N. M., and Fraaije, M. W. (2006). Flavoprotein monooxygenases, a diverse class of oxidative biocatalysts. *J. Biotechnol.* 124, 670–689. doi: 10.1016/j.jbiotec.2006.03.044
- Volkers, G., Damas, J. M., Palm, G. J., Panjikar, S., Soares, C. M., and Hinrichs, W. (2013). Putative dioxygen-binding sites and recognition of tigecycline and minocycline in the tetracycline-degrading monooxygenase TetX. *Acta Crystallogr. D* 69, 1758–1767. doi: 10.1107/s0907444913013802
- Volkers, G., Palm, G. J., Weiss, M. S., Wright, G. D., and Hinrichs, W. (2011). Structural basis for a new tetracycline resistance mechanism relying on the TetX monooxygenase. *FEBS Lett.* 585, 1061–1066. doi: 10.1016/j.febslet.2011.03.012
- Walsh, C. T., and Wencewicz, T. A. (2013). Flavoenzymes: versatile catalysts in biosynthetic pathways. *Nat. Prod. Rep.* 30, 175–200. doi: 10.1039/c2np20069d
- Wang, P., Bashiri, G., Gao, X., Sawaya, M. R., and Tang, Y. (2013). Uncovering the enzymes that catalyze the final steps in oxytetracycline biosynthesis. *J. Am. Chem. Soc.* 135, 7138–7141. doi: 10.1021/ja403516u
- Wang, Q., Wang, P., and Yang, Q. (2018). Occurrence and diversity of antibiotic resistance in untreated hospital wastewater. *Sci. Total Environ.* 621, 990–999. doi: 10.1016/j.scitotenv.2017.10.128
- Wang, S., Gao, X., Gao, Y., Li, Y., Cao, M., Xi, Z., et al. (2017). Tetracycline resistance genes identified from distinct soil environments in China by functional metagenomics. *Front. Microbiol.* 8:1406. doi: 10.3389/fmicb.2017.01406
- Ward, J. M., and Hodgson, J. E. (1993). The biosynthetic genes for clavulanic acid and cephamycin production occur as a ‘super-cluster’ in three *Streptomyces*. *FEMS Microbiol. Lett.* 110, 239–242. doi: 10.1111/j.1574-6968.1993.tb06326.x
- Warrier, T., Kapilashrami, K., Argyrou, A., Ioerger, T. R., Little, D., Murphy, K. C., et al. (2016). N-methylation of a bactericidal compound as a resistance mechanism in *Mycobacterium tuberculosis*. *Proc. Natl. Acad. Sci. U.S.A.* 113, E4523–E4530. doi: 10.1073/pnas.1606590113
- Wencewicz, T. A., and Walsh, C. T. (2012). *Pseudomonas syringae* self-protection from tabtoxinine-beta-lactam by ligase TblF and acetylase Ttr. *Biochemistry* 51, 7712–7725. doi: 10.1021/bi3011384
- Whittle, G., Hund, B. D., Shoemaker, N. B., and Salyers, A. A. (2001). Characterization of the 13-kilobase ermF region of the *Bacteroides* conjugative transposon CTnDOT. *Appl. Environ. Microbiol.* 67, 3488–3495. doi: 10.1128/AEM.67.8.3488-3495.2001
- Whittle, G., Shoemaker, N. B., and Salyers, A. A. (2002). The role of *Bacteroides* conjugative transposons in the dissemination of antibiotic resistance genes. *Cell. Mol. Life Sci.* 59, 2044–2054. doi: 10.1007/s000180200004
- Wierenga, R. K., de Jong, R. J., Kalkl, K. H., Hol, W. G. J., and Drenth, J. (1979). Crystal structure of p-hydroxybenzoate hydroxylase. *J. Mol. Biol.* 131, 55–73. doi: 10.1016/0022-2836(79)90301-2
- Wilson, D. N. (2009). The A-Z of bacterial translation inhibitors. *Crit. Rev. Biochem. Mol. Biol.* 44, 393–433. doi: 10.3109/10409230903307311
- Wright, G. D. (2005). Bacterial resistance to antibiotics: enzymatic degradation and modification. *Adv. Drug Deliv. Rev.* 57, 1451–1470. doi: 10.1016/j.addr.2005.04.002
- Wright, G. D. (2007). The antibiotic resistome: the nexus of chemical and genetic diversity. *Nat. Rev. Microbiol.* 5, 175–186. doi: 10.1038/nrmicro1614
- Xiao, H., Edwards, T. E., and Ferré-D’Amaré, A. R. (2008). Structural basis for specific, high-affinity tetracycline binding by an *in vitro* evolved aptamer and artificial riboswitch. *Chem. Biol.* 15, 1125–1137. doi: 10.1016/j.chembiol.2008.09.004
- Yang, W., Moore, I. F., Koteva, K. P., Bareich, D. C., Hughes, D. W., and Wright, G. D. (2004). TetX is a flavin-dependent monooxygenase conferring resistance to tetracycline antibiotics. *J. Biol. Chem.* 279, 52346–52352. doi: 10.1074/jbc.M409573200
- Yim, G., Huimi Wang, H., and Davies, J. (2007). Antibiotics as signalling molecules. *Philos. Trans. R. Soc. Lond. B Biol. Sci.* 362, 1195–1200. doi: 10.1098/rstb.2007.2044
- Yu, S., Vosbeek, A., Corbella, K., Severson, J., Schesser, J., and Sutton, L. D. (2012). A chromogenic cephalosporin for  $\beta$ -lactamase inhibitor screening assays. *Anal. Biochem.* 428, 96–98. doi: 10.1016/j.ab.2012.06.006
- Yuen, P. H., and Sokoloski, T. D. (1977). Kinetics of concomitant degradation of tetracycline to epitetracycline, anhydrotetracycline, and epianhydrotetracycline in acid phosphate solution. *J. Pharm. Sci.* 66, 1648–1650. doi: 10.1002/jps.2600661143
- Zhanel, G. G., Cheung, D., Adam, H., Zelenitsky, S., Golden, A., Schweizer, F., et al. (2016). Review of eravacycline, a novel fluorocycline antibacterial agent. *Drugs* 76, 567–588. doi: 10.1007/s40265-016-0545-8

**Conflict of Interest Statement:** The authors have filed a U.S. patent application (application 20170369864) on methods for treating bacterial infections caused by pathogens expressing tetracycline-inactivating enzymes.

Copyright © 2018 Markley and Wencewicz. This is an open-access article distributed under the terms of the Creative Commons Attribution License (CC BY). The use, distribution or reproduction in other forums is permitted, provided the original author(s) and the copyright owner are credited and that the original publication in this journal is cited, in accordance with accepted academic practice. No use, distribution or reproduction is permitted which does not comply with these terms.



# Look and Outlook on Enzyme-Mediated Macrolide Resistance

Tolou Golkar<sup>1†</sup>, Michał Zieliński<sup>1†</sup> and Albert M. Berghuis<sup>1,2\*</sup>

<sup>1</sup> Department of Biochemistry, McGill University, Montreal, QC, Canada, <sup>2</sup> Department of Microbiology & Immunology, McGill University, Montreal, QC, Canada

## OPEN ACCESS

### Edited by:

Graeme L. Conn,  
Emory University School of Medicine,  
United States

### Reviewed by:

Alexander Mankin,  
University of Illinois at Chicago,  
United States  
Martin Picard,  
UMR7099 Laboratoire de Biologie  
Physico-Chimique des Protéines  
Membranaires (LBPCPM), France  
Timothy Wencewicz,  
Washington University in St. Louis,  
United States

### \*Correspondence:

Albert M. Berghuis  
albert.berghuis@mcgill.ca

<sup>†</sup> These authors have contributed  
equally to this work

### Specialty section:

This article was submitted to  
Antimicrobials, Resistance  
and Chemotherapy,  
a section of the journal  
Frontiers in Microbiology

**Received:** 03 June 2018

**Accepted:** 31 July 2018

**Published:** 20 August 2018

### Citation:

Golkar T, Zieliński M and Berghuis AM  
(2018) Look and Outlook on  
Enzyme-Mediated Macrolide  
Resistance. *Front. Microbiol.* 9:1942.  
doi: 10.3389/fmicb.2018.01942

Since their discovery in the early 1950s, macrolide antibiotics have been used in both agriculture and medicine. Specifically, macrolides such as erythromycin and azithromycin have found use as substitutes for  $\beta$ -lactam antibiotics in patients with penicillin allergies. Given the extensive use of this class of antibiotics it is no surprise that resistance has spread among pathogenic bacteria. In these bacteria different mechanisms of resistance have been observed. Frequently observed are alterations in the target of macrolides, i.e., the ribosome, as well as upregulation of efflux pumps. However, drug modification is also increasingly observed. Two classes of enzymes have been implicated in macrolide detoxification: macrolide phosphotransferases and macrolide esterases. In this review, we present a comprehensive overview on what is known about macrolide resistance with an emphasis on the macrolide phosphotransferase and esterase enzymes. Furthermore, we explore how this information can assist in addressing resistance to macrolide antibiotics.

**Keywords:** antibiotic resistance mechanisms, macrolide resistance, macrolide phosphotransferase, erythromycin esterase, ketolides, macrolides, Ere, MPH

## INTRODUCTION

After  $\beta$ -lactams and aminoglycosides, macrolides were the third major class of microbial products to be discovered that possess antibiotic properties (Lewis, 2013). The archetypal macrolide, erythromycin, was first isolated in 1949 from the soil dwelling bacterium *Saccharopolyspora erythraea* in a Filipino environmental sample. Within, what is now considered a very short time, this macrolide antibiotic entered clinical practice in 1952. This kick-started the golden-era of macrolide discovery where a plethora of new macrolides were being frequently characterized. Furthermore, it fueled the development of next-generation macrolides using semi-synthetic approaches (Bryskier, 2000).

Initially, macrolides were primarily used for the treatment of upper respiratory tract, skin and soft tissue infections, as dictated by the pharmacological properties of these drugs. As next generation macrolides, improved upon the drug characteristics of these antibiotics, their usage was expanded. Specifically, macrolides now proved effective in the treatment of infections caused by Gram-positive bacteria (e.g., *Streptococcus pneumoniae*, *Streptococcus pyogenes*, *Staphylococcus aureus*), some Gram-negative (e.g., *Haemophilus influenzae*), as well as atypical pathogens (e.g., *Chlamydia trachomatis* – causative agents of chlamydia, *Treponema pallidum* – causative agents of syphilis, *Mycoplasma pneumoniae*). It has been noted that many of the infections that can be treated by next-generation cephalosporins also are treatable using macrolides (Zhanel et al., 2001).



Fortuitously, this provides a much-needed alternative treatment option for patients allergic to penicillins, and has thus increased the clinical application of these drugs (MacLaughlin et al., 2000). It should also be mentioned that the use of macrolides is not strictly restricted to antibiotics. Several macrolides are also in use or in clinical development for modulation of immune response including 12-membered EM-900, 23-membered tacrolimus and 31-membered rapamycin (Gomes et al., 2017).

## MACROLIDE ANTIBIOTICS

### Chemical Structure of Macrolides

Macrolide antibiotics are synthesized by polyketide-synthases present in various *Streptomyces* sp. The archetypal chemical structure for a macrolide antibiotic consists of a 12–18 membered lactone ring to which 1–3 different hexose moieties are directly or indirectly attached (see **Figure 1**). One of the hexose moieties is linked at the C5 position of the macrolactone ring and is either a desosamine or a mycaminoside sugar. If it is a mycaminoside, a second sugar, mycarose, is linked to this moiety, creating a disaccharide at the C5 position. A cladinose is frequently linked to the C3 position of the ring. Various additional substitutions on the macrolactone ring are observed creating extensive chemical diversity among macrolides (Omura, 2002).

Given the modular nature of macrolide antibiotics, which is a result of these molecules being synthesized by polyketide synthases, it is to be expected that a large number of different macrolides can be found in nature. A conservative estimate is that currently over 2000 different macrolides have been found by various groups (Omura, 2002). However, despite this abundance of molecules, only very few of these have thus far found clinical use. Clearly, not all macrolides possess the required pharmacological properties, to be sufficiently effective in the treatment of bacterial infections. Most notably, one of the persistent roadblocks for the clinical use of macrolide antibiotics has been their inherent susceptibility to acid degradation, which make them suboptimal for oral administration (Hassanzadeh et al., 2007). The desire to obtain improved pharmacokinetic properties has fueled the use of semi-synthetic approaches to create next-generation macrolides.

At present several semi-synthetic macrolides are in clinical use or in the later stages of clinical development (see **Figure 1**). Intriguingly, all of these are derivatives of the first macrolide to be clinically used, erythromycin. In the 1980s, Taisho Pharmaceuticals developed clarithromycin. This derivative of erythromycin is far more stable under acidic conditions, through a mere methylation of C6 hydroxyl group. (Morimoto et al., 1984). Around this time, azithromycin, was also developed by Pliva, as an effective antibiotic with increased acidic stability and improved pharmacokinetic properties (Girard et al., 1987). In the 1990s, under the pressure of rising resistance (see below), radical changes to the erythromycin scaffold were tested. Specifically, removal of erythromycin's cladinose sugar and oxidation of the remaining secondary alcohol to a keto group resulted in a scaffold that retained antibiotic activity, and that was additionally less

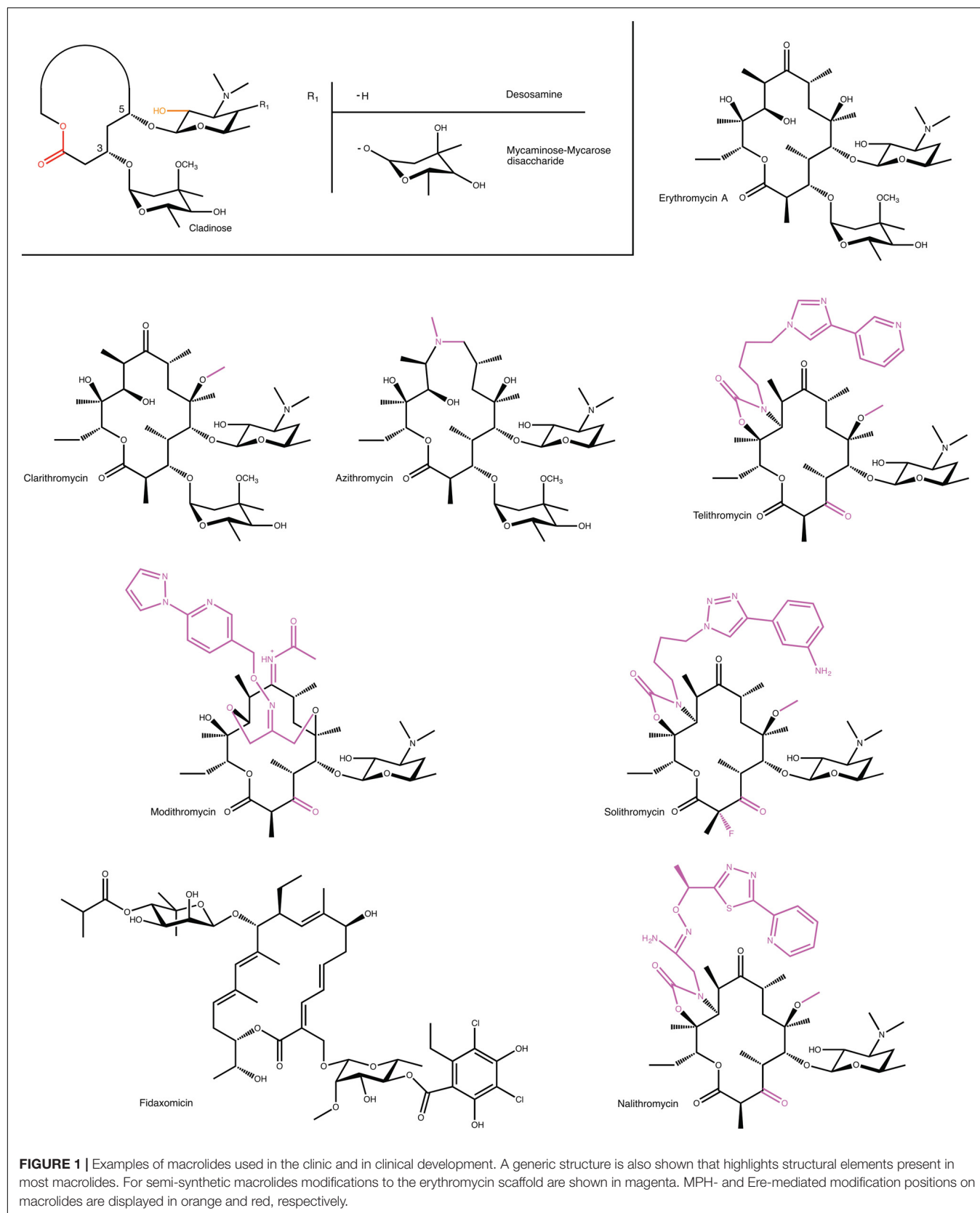
susceptible to some forms of macrolide resistance. This subclass of macrolides have since received their own name: ketolides (Bryskier, 2000).

Recently, two research areas have seen advances that will undoubtedly have a major impact on the development of new macrolides with improved antibiotic properties. The first is the increase in our understanding of how macrolides are synthesized by polyketide-synthases. This has opened the avenue to alter polyketide-synthases through protein engineering approaches, so as to create novel macrolides. Currently, this avenue is still in its infancy, but it shows great promise (Park et al., 2010). The second area is advances in the total synthesis of macrolides. Specifically, Seiple et al. (2016) reported the *de novo* synthesis of several bioactive macrolides from simple starting blocks, providing a feasible method for synthesis of thousands of chemically diverse macrolides. This group was not only able to change the number of atoms in the macrolactone ring, but also add extra moieties to the ring, and modify the sugars. This technology is currently being exploited by Macrolide Pharmaceuticals, a preclinical-stage company that is developing novel antibiotic compounds.

### Mechanism of Macrolide Antibacterial Activity

Through the study of the effects of erythromycin on bacteria it was found early on that macrolides had an impact on protein synthesis (Taubman et al., 1963). Subsequent studies revealed that this was due to binding of the macrolide to the ribosome (Taubman et al., 1966). Around that time, studies of chloramphenicol binding to the 50S ribosome, and interference of this binding by different classes of antibiotics, suggested that macrolides interact with the 50S subunit at a related site (Vazquez, 1966). This binding was also confirmed through studies of binding of erythromycin to ribosomes from antibiotic-sensitive and -resistant *Bacillus subtilis* 168 (Oleinick and Corcoran, 1969), through the fragment reaction studies (Celma et al., 1970) and through dimethyl sulfate and kethoxal probing (Moazed and Noller, 1987). Furthermore, this binding was shown genetically through two chloramphenicol-erythromycin resistance mutations on *Escherichia coli* 23 rRNA (Ettayebi et al., 1985). However, it took some time before the exact location and mechanism of ribosome binding and inhibition was determined through X-ray crystal structures of 50S and 30S ribosomal subunits and the intact 70S ribosome (Ban et al., 2000; Wimberly et al., 2000; Schlünzen et al., 2001, 2003; Tu et al., 2005).

Macrolides bind in the peptide exit tunnel of the large ribosomal subunit, immediately adjacent to the peptidyl transferase center. They block the lumen of the tunnel preventing an elongating polypeptide chain to pass through it, causing either a bacteriostatic effect or a bactericidal result, depending on the macrolide (Svetlov et al., 2017). It is noteworthy that this exact site in the bacterial ribosome is not only exploited by macrolides to exert an antibacterial effect, as also class B streptogramins and lincosamides bind in this location (Tu et al., 2005; Matzov et al., 2017). As discussed below, this has implications since certain mechanisms of resistance to these antibiotics also confer resistance to macrolides.



Despite the chemical diversity of macrolides, there is extensive similarity in how they bind to the ribosome (see **Figure 2**). First of all, the lactone rings, which possess a hydrophobic and a hydrophilic face, invariably bind to the ribosome with their hydrophobic face. The desosamine/mycaminose moiety at the C5 position makes specific hydrogen bond interactions with the nucleotide residues A2058 and A2059 (*E. coli* numbering). Furthermore, for those macrolides that possess a sugar at the C3 position, this cladinose group makes specific interactions with the base of nucleotide 2505, though this only contributes incrementally to the affinity of the macrolide for the 50S subunit (Hansen et al., 2002).

Intriguingly, for some 16-membered lactone ring macrolides, that also possess an acetaldehyde group at the C6 position, such as spiramycin, a covalent bond has been crystallographically observed between the macrolide's aldehyde group and the primary amine group at the N6 position of A2062, creating a carbinolamine linkage (Hansen et al., 2002). For this, the base of nucleotide 2062 of the 23S rRNA must reorient by almost 90 degrees so that it protrudes into the lumen of the tunnel. As the carbinolamine linkage is reversible, this observation does not imply irreversible binding of these macrolides to the ribosome.

For the ketolides sub-class, the absence of the specific interactions afforded by the cladinose group are compensated by interactions created by the cyclic carbamate moiety present in these antibiotics. The ketolides (because of the carbamate moiety and the quinolyl allyl group) have been reported to interact not only to the domain V of 23S rRNA but also with domain II (helix 35) and possibly domain IV (Hansen et al., 1999;

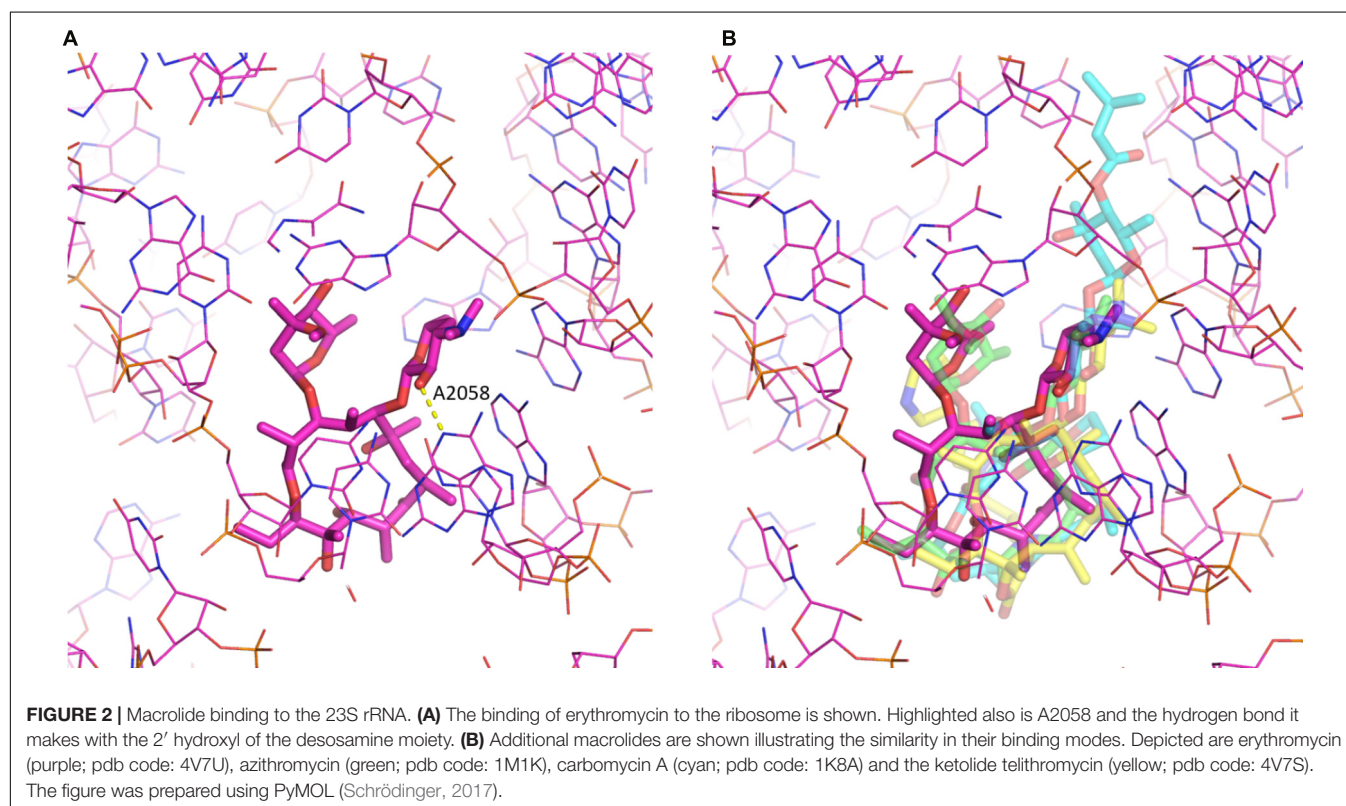
Xiong et al., 1999; Zhanel et al., 2001; Berisio et al., 2003; Schlünzen et al., 2003).

It is appropriate to mention here that while macrolides are known to interfere with protein synthesis through binding to the bacterial ribosome, this is not universally true. Noteworthy, the 18-membered ring macrolide, fidaxomicin, inhibits RNA polymerase (Artsimovitch et al., 2012).

## CLINICAL RESISTANCE TO MACROLIDE ANTIBIOTICS

Bacterial resistance to erythromycin was initially reported in *Staphylococci* in 1956, only a few years after its introduction into clinical practice (MacCabe and Gould, 1956). The first erythromycin-resistant strains of *Streptococci* were reported in the United Kingdom in 1959 and in North America in 1967 (Lowbury and Hurst, 1959; Dixon, 1968). Since that time, resistance has been detected in a large number of bacteria including *Staphylococcus* spp., *Streptococcus* spp., *Bacteroides* spp., *Enterococcus* spp., *Clostridium* spp., *Bacillus* spp., *Lactobacillus* spp., *M. pneumoniae*, *Campylobacter* spp., *Corynebacterium diphtheriae*, *Propionibacterium* and members of the Enterobacteriaceae (Leclercq and Courvalin, 1991; Weisblum, 1995; Zhanel et al., 2001).

The extend of macrolide resistance has becoming alarming depending on the bacterial pathogen and the location. For example, erythromycin-resistance *Campylobacter jejuni* rates have reached 22% in New Delhi, India (Ghosh et al., 2013). Also,





clarithromycin-resistant *Helicobacter pylori* has been on the rise in many countries over the past decade, with rates as high as ~30% in Japan and Italy, 40% in Turkey and 50% in China (Thung et al., 2016). In another study, the rate of macrolide resistance *S. pneumoniae* among outpatients of county hospitals in China was reported to be 89–96%. In the same study, the rate of macrolide resistance MRSA (methicillin-resistant *S. aureus*) was found up to 82% and for MSSA (methicillin-susceptible *S. aureus*) up to 63% (Xiao et al., 2015). Finally, the incidence of macrolide-resistant *M. pneumoniae* in Japan can go as high as 90% and in Zhejiang province of China to 100% (Pereyre et al., 2016).

As is discussed below, one of the mechanisms of resistance to macrolides is by target modification, i.e., alterations in the bacterial ribosome that compromise binding of the antibiotic. However, as previously mentioned, macrolides exploit the same pocket in the ribosome as several other antibiotics, specifically lincosamides and B streptogramins. This implies that the target modification observed in macrolide resistant bacteria may also confer resistance to lincosamides and B streptogramins. Indeed, this has been observed and the associated phenotype is now referred to as MLS<sub>B</sub> (Weisblum, 1995; Leclercq, 2002). Unfortunately, this also implies that certain forms of macrolides resistance are a far greater clinical and societal problem as they effectively negate usage of three different classes of antibiotics, substantially reducing the available armament of antibiotics for treating bacterial infections.

## MECHANISMS OF RESISTANCE TO MACROLIDE ANTIBIOTICS

As with other antibiotics, resistance to macrolide antibiotics is not confined to one single mechanism, but several mechanisms of resistance have been observed. Specifically, mechanisms to: (i) decrease the intracellular concentration of macrolides, (ii) alter the target (ribosome), (iii) protect the target (ribosome), and (iv) chemically modify the antibiotic are observed in clinical isolates.

### Decreased Intracellular Concentration

One way in which bacteria are able to evade the action of macrolides is to reduce the intracellular concentration through the use of efflux pumps. Several different families of pumps have been discovered including major facilitators superfamily (MFS), ATP-binding cassette (ABC) superfamily, multidrug and toxic compound extrusion (MATE) family, resistance-nodulation-division (RND) superfamily and small multidrug resistance (SMR) family (Gomes et al., 2017). These efflux pumps can be encoded on a chromosome or plasmids, and frequently provide resistance to multiple classes of antibiotics. Furthermore, they can often be upregulated in the presence of antibiotics (Ambrose et al., 2005).

Of particular relevance to macrolides are the Mef and Msr subfamilies of efflux pumps, which are encoded on plasmids and which are members of the MSF and ABC families, respectively. Since Mef proteins are members of the MSF family they do not use ATP as an energy source to pump the antibiotics to the exterior of the cell, instead they utilize secondary active transport,

where the energy of ATP is not used directly to transport macrolides across the membrane. This subfamily of proteins is one of the important determinants of the macrolide resistance, with Mef(A) and Mef(E) being the most commonly found. Msr subfamily of proteins are members of ABC family that use ATP as an energy source for active transport. Both Mef and Msr subfamily of proteins are capable of using 14- and 15-membered macrolides as substrates, including the ketolide telithromycin. We refer the reader to reviews for further information on macrolide pumps (Li and Nikaido, 2009; Gomes et al., 2017).

## Ribosome Modification

Three types of macrolide resistance conferring modifications to the ribosome have been observed in bacteria. Most prominently is methylation of the 23S rRNA by the members of the Erm family of methyltransferases. These enzymes catalyze the methylation of the N6 position of nucleotide A2058 in the 23S rRNA. This nucleotide makes specific interactions with the saccharide moiety located at the C5 position of the macrolactone ring, and methylation interferes with productive hydrogen bond formation. Mono-methylation of this nucleotide confers low-to-moderate resistance to macrolides, whereas di-methylation confers high resistance. It is important to note that di-methylation by Erm methyltransferases additionally confers high resistance to all MLS<sub>B</sub> antibiotics as well as the ketolide telithromycin, exacerbating antibiotic resistance (Poehlsgaard and Douthwaite, 2005; Roberts, 2008).

Besides methylation of the rRNA, mutations in the rRNA can also confer resistance. Mutation of A2058 will alter the ribosomal target site and prevent binding of macrolides, as well as lincosamides and group B streptogramins (Franceschi et al., 2004; Lambert, 2005; Tu et al., 2005). Furthermore, it has been shown that mutations of A2059 will confer macrolide and lincosamide resistance (Vester and Douthwaite, 2001; Leclercq, 2002). Numerous other mutations have been reported in both domains II and V that confer resistance to various macrolides, and this list is continuously expanding (Vester and Douthwaite, 2001; Hansen et al., 2002).

Mutations in some of the ribosomal proteins are also capable of conferring resistance. Specifically, alterations have been identified in the L4 and L22 ribosomal proteins. These alterations are single amino acid changes or could also consist of insertion/deletion of one or more amino acids to these proteins. These mutations have been documented in many clinical isolates, including *S. pneumoniae*, *H. influenzae*, and *E. coli* (Roberts, 2008). Mutations in L4 and L22 have been proposed to confer resistance through changing the shape of the peptide exit tunnel and distortion of the macrolide-binding site, which results in altered binding kinetics for macrolides (Gabashvili et al., 2001; Moore and Sauer, 2008; Lovmar et al., 2009; Wekselman et al., 2017).

## Ribosome Protection

Recently a new mechanism of resistance has been described for macrolides, mediated by members of the ABC-F subfamily of ATP-binding cassette proteins, such as MsrE (Sharkey et al., 2016; Su et al., 2018). Electron microscopy and biochemical studies for

MsrE show that this protein can bind to a stalled ribosome in which a peptidyl-tRNA is in the P-site. The ATP bound form of MsrE can then insert a needle-like domain that reaches the peptidyl transferase center and the adjacent peptide exit tunnel, i.e., the location where macrolides bind, where it pushes the antibiotic out of its binding site (Su et al., 2018). Note that since streptogramins and lincosamides also bind in this region of the ribosome, MsrE and/or homologs of this protein can confer resistance to other MLS<sub>B</sub> antibiotics. Although this is a novel mechanism of resistance to macrolides, it is reminiscent of what has previously been described for tetracyclines (Nguyen et al., 2014; Arenz et al., 2015).

## Drug Modification

A third mechanism of resistance to macrolides is the enzymatically catalyzed modification of these antibiotics. As a consequence of the alteration facilitated by specific enzymes, the modified macrolides are no longer capable to bind effectively to the 50S ribosome, and are thus unable to exert an antibiotic effect. Thus far two classes of enzymes have been identified in bacteria that confer resistance to macrolide antibiotics: macrolide phosphotransferases (MPHs) and Macrolide Esterases (Eres). Below these two classes of enzymes are discussed in greater detail.

It is worth noting that a third class of enzymes has been identified that modify macrolides, i.e., macrolide glycosyltransferases (Cundliffe, 1992; Quirós et al., 2000; Bolam et al., 2007). However, these enzymes are not involved in conferring antibiotic resistance as they are only present in

macrolide producing bacteria where they provide “host cell antibiotic immunity” (Fyfe et al., 2016). However, it is possible that in future this self-protection mechanism could be co-opted by other bacteria and transformed into a *bona-fide* antibiotic resistance mechanism.

## MACROLIDE PHOSPHOTRANSFERASES

In the search for novel mechanisms of resistance to macrolides, O'Hara, Kanda and Kono examined the ability of erythromycin-resistant clinical strains to detoxify macrolides, in the late 1980s. This search initially revealed that bacterial lysate from a clinical *E. coli* strains was able to phosphorylate oleandomycin, in 1988 (O'Hara et al., 1988). Subsequent work resulted in the purification and characterization of an enzyme that phosphorylated the hydroxyl group located at the 2' position of the C5 linked desosamine moiety of erythromycin and oleandomycin (see **Figure 3**). This enzyme was accordingly named macrolide 2'-phosphotransferase (O'Hara et al., 1989). Following this discovery several more enzymes have been found that show a similar activity. These MPHs all mediate the transfer of the  $\gamma$ -phosphate group from GTP onto the macrolide substrates and doing so confer resistance to a group of bacteria ranging from Gram-negative (*E. coli*, *Pseudomonas*, *Pasteurella*, *Klebsiella*, *Serratia*, *Shigella*) to Gram-positive (*Staphylococcus*) (Matsuoka et al., 1998, 2003; Nguyen et al., 2009; Ferjani et al., 2012; Mendes et al., 2017).

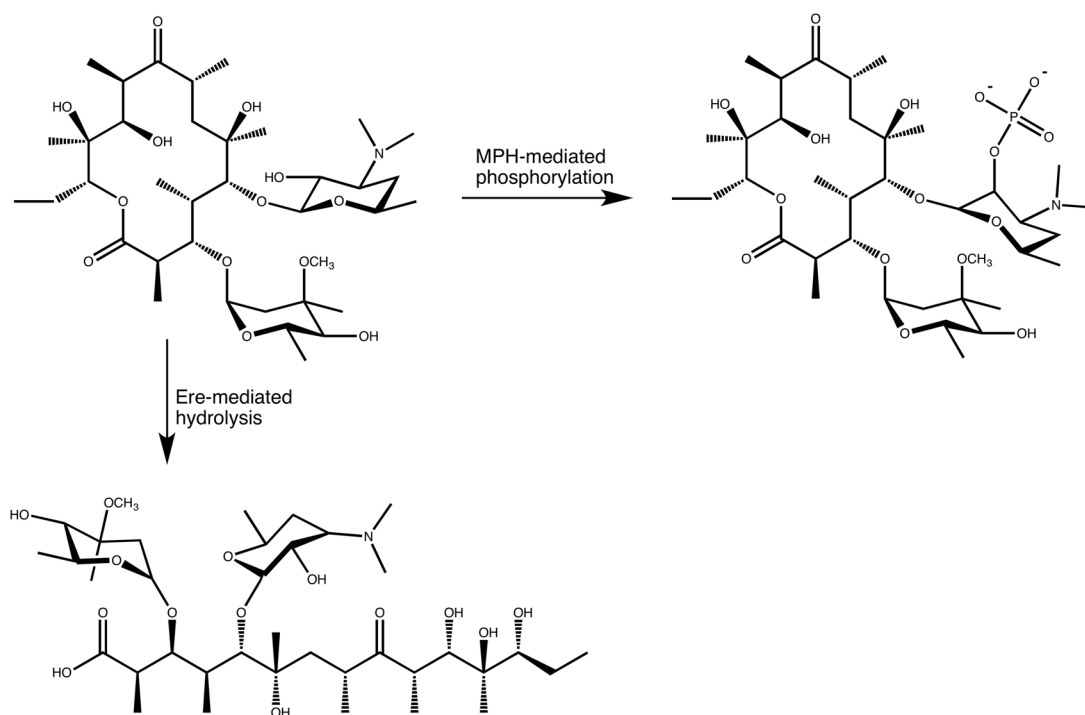


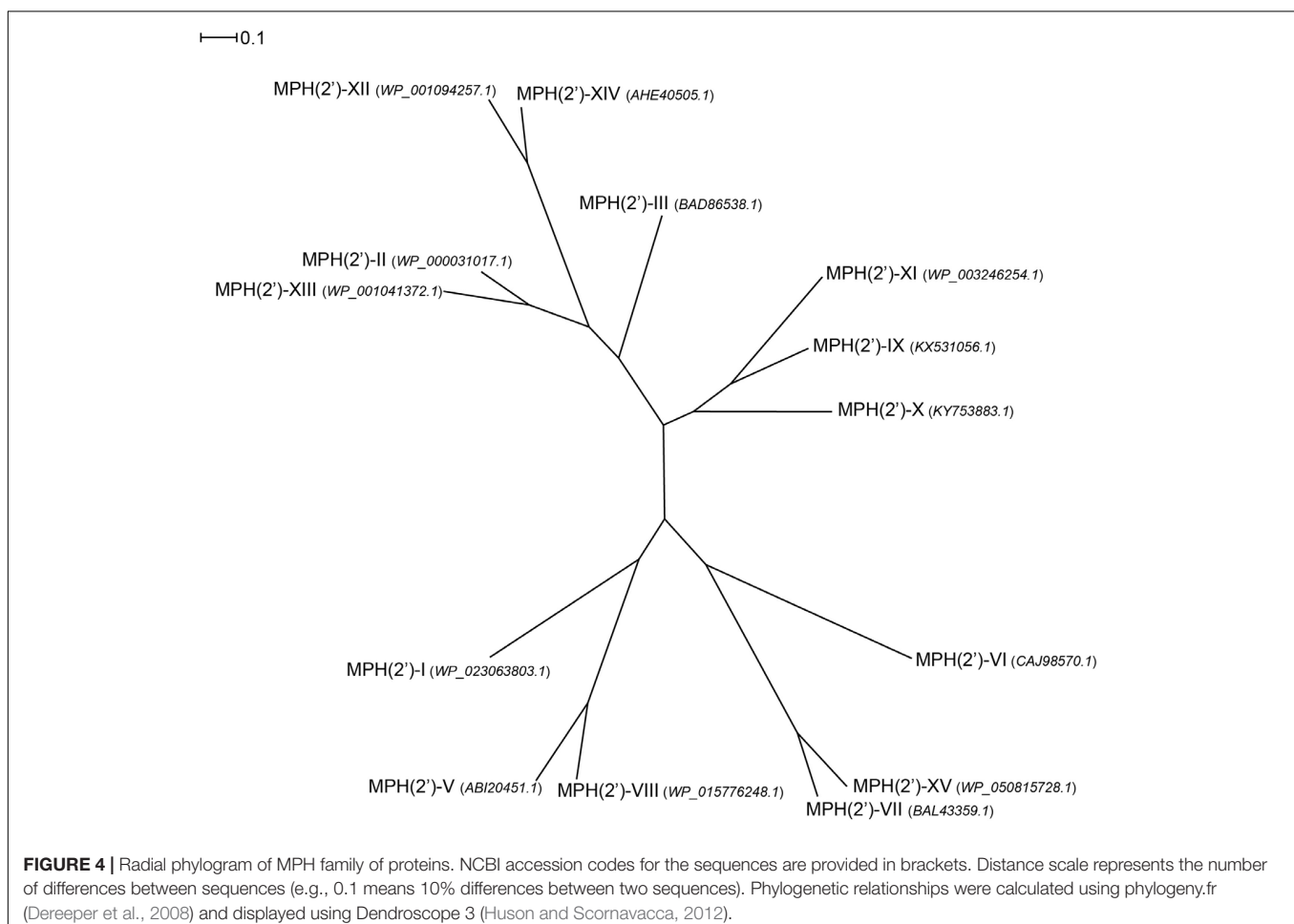
**FIGURE 3 |** Enzymatic modifications of erythromycin A catalyzed by MPH(2's) and Eres.

## Macrolide Phosphotransferase Family Members

At least 15 gene subtypes of MPHs have been reported, which are designated *mph*(A) to (O) (O'Hara et al., 1989; Kono et al., 1992; Kim et al., 1996; Matsuoka et al., 1998, 2003; Roberts et al., 1999; Schlüter et al., 2007; Pawlowski et al., 2016, 2018a). Here, we name their products MPH(2')-I to MPH(2')-XV, respectively, with the assumption that all these MPHs phosphorylate the hydroxyl on the C5 linked desosamine or mycaminoose moiety, which is present in all macrolides and ketolides that bind to the 23S rRNA where it forms a critical interaction with A2058 (see **Figure 2**). However, this is strictly only confirmed for MPH(2')-I, II, VIII, IX, and XI. Among these fifteen gene subtype of MPHs, *mph*(A), (B), and (C), which are encoded on mobile genetic elements, are found in clinical isolates of *E. coli*, *Salmonella* sp., *Klebsiella* sp., and *S. aureus*. Six more MPHs are encoded on mobile genetic elements, but are thus far only found in non-pathogenic bacteria, e.g., MPH(2')-XIV has been observed in *Exiguobacterium* and *Brachy bacterium*. However, this could readily change. The remaining six *mph* genes are chromosomally encoded in non-pathogenic bacteria, such as MPH(2')-VIII which is present in *Brachy bacterium faecium* and MPH(2')-XI which is present in *B. subtilis* 168.

Examination of the sequence diversity among 14 MPHs enzymes indicates that the various members can display extensive differences [only a partial sequence is available for the *mph*(D) gene]. For example, MPH(2')-I and II only share 36% identity. Though several sequences cluster together, e.g., MPH(2')-IX, X, and XI, with pairwise %identity of 46–54 (see **Figure 4**). Perhaps somewhat surprisingly, there is no real relationship between MPHs that cluster with whether they are chromosomally encoded or on mobile elements, or whether they are in pathogenic bacteria or in environmental isolates.

Macrolide phosphotransferases can confer resistance to a wide range of macrolide substrates, but this topic has not yet been thoroughly investigated, and much remains unknown about their substrate specificity profile. Comparing substrate specificity of the clinically relevant MPH(2')-I and II reveals that MPH(2')-I can only efficiently inactivate 14- and 15-membered lactone macrolides, whereas MPH(2')-II can additionally inactivate 16-membered lactone macrolides and the ketolide, telithromycin (Kono et al., 1992; Fong et al., 2017). A similar observation has been made for MPH(2')-XII and XIII, with MPH(2')-XII mirroring the substrate profile of MPH(2')-I and MPH(2')-XIII mirroring the substrate profile of MPH(2')-II (Wang et al., 2015). Also, MPH(2')-III has been shown to have the same





broad substrate specificity as MPH(2')-II (Chesneau et al., 2007). MPH(2')-IX from the environmental bacterium *Paenibacillus* sp. LC231 and MPH(2')-XI from *B. subtilis* 168 are unable to confer resistance to macrolides with a C3 cladinose in cell-based assays. Although, biochemical analysis of drug modification for both enzymes showed that they can use C3 cladinose containing macrolides as substrates but cannot inactivate 14-membered and 15-membered lactone macrolide as efficiently as macrolides without this moiety (Pawlowski et al., 2016, 2018a). Intriguingly, MPH(2')-X, which is a closer homolog to MPH(2')-IX than MPH(2')-XI, is able to effectively provide resistance to several cladinose containing macrolides (Pawlowski et al., 2018b). This observation underscores that sequence similarity among MPHs provides no indication to what the substrate profile for these enzymes might be.

## Structural Insights Into Macrolide Phosphotransferase Mediated Resistance

Fong et al. (2017) have recently reported the first three-dimensional structures for MPH enzymes. Specifically, MPH(2')-I and MPH(2')-II were determined, in their apo state, in complex with GTP analogs and in complex with several macrolides (see **Figure 5**). These structures confirm what sequence comparisons had suggested that MPHs are members of a large superfamily that also includes eukaryotic protein kinases (ePKs) and aminoglycoside phosphotransferases (APHs). The archetypal structure for the members of this superfamily is composed of an N-terminal lobe that contains a five-stranded  $\beta$ -sheet and C-terminal lobe that contains several  $\alpha$ -helices. In between these two lobes is the binding site for a tri-phosphate nucleotide that is used as the phosphoryl donor. The C-terminal lobe contains the substrate binding site, but the specific local architecture for this section can differ significantly between various members of the superfamily. For the two MPH enzymes, the architecture of their N-terminal lobe is similar to that seen for the N-terminal lobes of Ser/Thr and Tyr protein kinases, and APHs (Hon et al., 1997). The C-terminal lobe is largely identical to what is seen for a sub-family of APHs, the APH(2'') group, with which they share approximately 17% sequence identity (Shi and Berghuis, 2012). On the other hand, MPHs deviate from archetypal ePKs and APHs in the region between the N- and C-terminal lobes. In ePKs and APHs, the lobes are connected by a loop 5–12 residues in size, while in MPH (2')-I and MPH(2')-II the linker region is significantly larger, spanning approximately 25 residues (Fong et al., 2017).

As stated above, the sequence conservation in MPHs is not extensive (see **Figure 4**). However, as the structures of MPH(2')-I and MPH(2')-II reveal, this does not impact the fold of these enzymes, as their structures are highly similar (Fong et al., 2017). To further examine the sequence conservation, we mapped the extent of conservation onto the three-dimensional structure (see **Figure 5**). Not unsurprisingly, there are a very limited number of conserved residues among the 14 MPHs, and these include residues required for catalysis, e.g., coordination of the GTP associated  $Mg^{2+}$  ions. Intriguingly, the aspartate

responsible for abstraction of the proton of the macrolide 2' hydroxyl group, which is absolutely conserved in ePKs and APHs is apparently a glutamate in MPH(2')-VIII and MPH(2')-XV. Furthermore, there is conservation in the nucleotide binding pocket, rationalizing why all MPHs studied use GTP as the phosphoryl donor.

Examination of residue conservation in the macrolide binding area of MPHs reveals that this is not at all conserved. However, delving deeper into this, the chemical character of the macrolide binding pocket is similar in MPHs: generally hydrophobic with a region of negative charge around the conserved proton abstracting catalytic base (Fong et al., 2017). Structural studies of MPH(2')-I and MPH(2')-II showed that the relatively non-specific hydrophobic nature of the binding site and the fact that many of the interactions between the macrolides and the enzymes involve the lactone ring would facilitate the accommodation of a range of macrolide substrates.

The large contribution of non-specific hydrophobic interactions to the binding of macrolides to MPHs complicates the rationalization of these enzymes' substrate specificity, based on the three-dimensional structure. For example, while there is now ample structural data for MPH(2')-I and MPH(2')-II and their interactions with 14-, 15- and for MPH(2')-II 16-membered macrolactone rings, a structural reason for the inability for MPH(2')-I to phosphorylate 16-membered macrolides is not yet forthcoming (Fong et al., 2017). Recently, despite having structural data for MPHs, Wright and colleagues had to resort to using ancestral sequence reconstruction thus building an evolutionary path for MPH functional divergence and subsequent site-saturation combinatorial mutagenesis, to identify residues that dictate the preference of MPH(2')-IX for macrolides lacking the cladinose moiety (Pawlowski et al., 2018a). Intriguingly, the residues identified for impacting cladinose specificity were non-obvious as they were not in close proximity of the cladinose binding pocket. This further emphasizes the complexity in linking sequence to MPH substrate specificity.

## MACROLIDE ESTERASES

In the mid 1980s Courvalin and co-workers identified a plasmid in a clinical *E. coli* strain that conferred high level resistance to erythromycin, but not lincosamides or group B streptogramins, implying that the resistance mechanism was not caused by the at that time known Erm methyltransferases that methylate A2058 of the 23S rRNA (Andremont et al., 1986). Subsequent characterization of the enzyme encoded on the plasmid revealed that it exploits a feature present in all macrolides. In the biosynthesis of macrolides by polyketide synthases the macrolide aglycon is converted to a cyclic lactone, forming an ester bond. The enzyme identified by Courvalin and his team hydrolyzes this ester bond, thus linearizing the macrolide again, which is then no longer able to bind to its ribosomal binding site (Barthelemy et al., 1984) (see **Figure 3**). Actually, the exact product of the reaction catalyzed by the esterase has not been thoroughly identified. The current proposal is that the hydrolysed macrolide

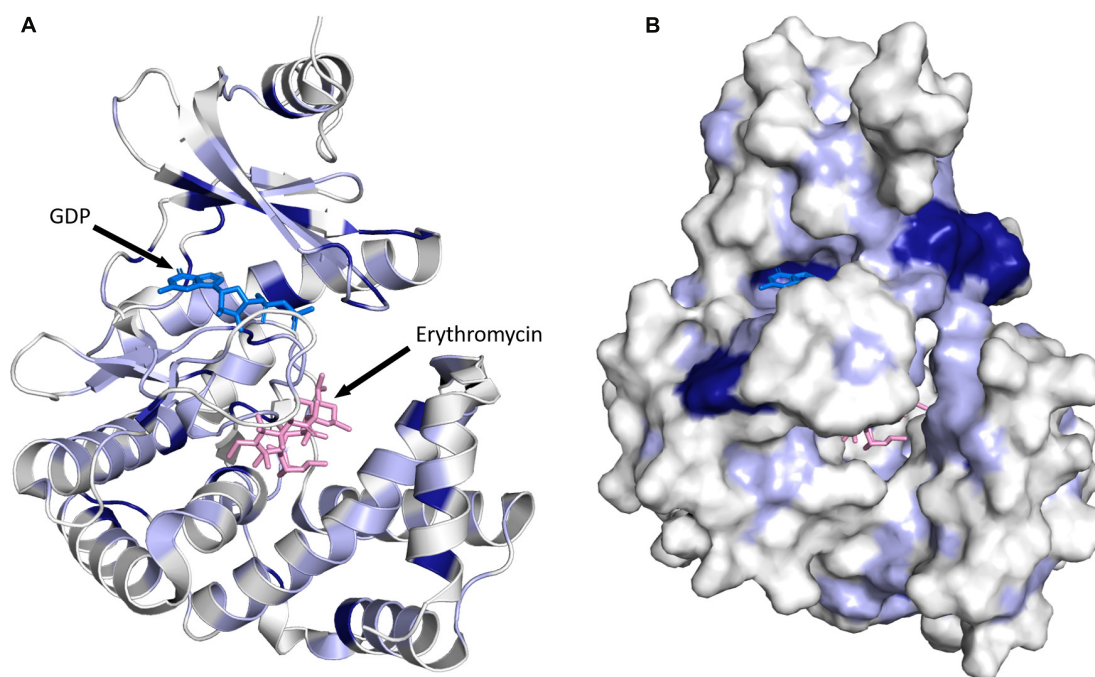


**FIGURE 5 |** Three-dimensional structure for MPHs. **(A)** MPH(2')-I in complex with GDP and erythromycin is shown. The color coding used illustrates sequence conservation within the 14 MPHs enzymes, with dark blue indicating completely conserved residues, light blue residues that are conserved among more than seven members, and white residues that are not conserved. **(B)** The enzyme is shown in surface representation. The figure was prepared using PyMOL (Schrödinger, 2017).

product is naturally very unstable and undergoes spontaneous rearrangement and dehydration. A detailed mechanism for this has been proposed (Barthelemy et al., 1984). Nonetheless, based on the presumed activity, the enzyme was therefore identified as an erythromycin esterase (Ere). Shortly after the discovery of the first erythromycin esterase, Courvalin and co-workers identified a second enzyme with a very similar activity, and additional members of this family have since been identified.

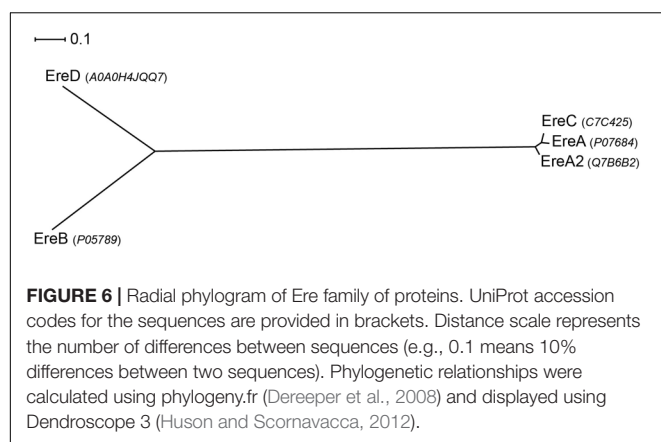
### Erythromycin Esterase Family Members

The first two members of the erythromycin esterase family, discovered by Courvalin and colleagues from clinical *E. coli* strains are known as EreA (Ounissi and Courvalin, 1985) and EreB (Arthur et al., 1986). Since then, three more erythromycin esterases have been discovered: EreA2 in multidrug-resistant *Vibrio cholerae* (Thungapathra et al., 2002), EreC in multidrug-resistant *Klebsiella pneumoniae* (Yong et al., 2009) and EreD in the duck pathogen *Riemerella anatipestifer* (Xing et al., 2015). Except for EreD, which is chromosomally encoded, all other Ere enzymes are encoded on mobile genetic elements, and thus are found in numerous different bacterial species, including environmental and clinical isolates. EreA enzyme is mostly found in environmental isolates, however, it has also been detected in *E. coli* and *S. aureus*. EreA2 is the vastly more clinically relevant cousin which has been detected in a multitude of important pathogens such as: *Pseudomonas* spp. (Kim et al., 2002; Kim and Cerniglia, 2005), *Salmonella indiana* (Zhao et al., 2017), *Klebsiella pneumoniae* (Abbassi et al., 2008), *E. coli* (Chang et al., 2000;

Ahmed and Shimamoto, 2011), non-typhoidal *Salmonella enterica* (Krauland et al., 2010), *Salmonella* spp. (Murphy et al., 2007), and *Vibrio cholera* (Thungapathra et al., 2002). EreB can be found in a range of pathogens including: *E. coli* (Arthur et al., 1986; Nakamura et al., 2000), MRSA (Schmitz et al., 2000b), MSSA (Schmitz et al., 2000a), *Staphylococcus saprophyticus* (Fernandez-Fuentes et al., 2014), *Klebsiella oxytoca* (Fuentes et al., 2014), and *Salmonella* spp. (Fuentes et al., 2014). The remaining two enzymes EreC and EreD, due to being a much newer addition to the family of Eres have stayed under the radar of macrolide-research community with only their discovery being published.

Sequence analyses of the five Ere family members reveals that there is extensive diversity in this small group. For example, EreB and EreC display the highest sequence divergence, with 44.8 and 23.0% sequence similarity and identity, respectively. In contrast, EreA, EreA2, and EreC enzymes share extensive sequence similarity with the %identity ranging between 90.0 and 92.6% (see Figure 6).

Presently, very limited information is available on the substrate specificities of Ere enzymes. One of the most in-depth studies on kinetics and substrate specificities of Eres focused solely on EreA and EreB and examined just five macrolides that also included one ketolide (Morar et al., 2012). The result showed that both enzymes are capable of cleaving 14-membered macrolides, and that EreB is able to also cleave 15-membered macrolides. However, neither enzyme is able to digest telithromycin, the sole ketolide tested. Surprisingly, despite the clinical relevance of EreA2 and EreC, no information is available



of substrate specificities of these two enzymes. For now it is assumed that due to high sequence similarity with EreA, they likely have a very similar substrate spectrum, being only able to degrade 14-membered macrolides (see **Figure 6**).

## Structural Insights Into Erythromycin Esterase Mediated Resistance

As of yet no three-dimensional structure has been determined of an erythromycin esterase, however, a search for homologous proteins with a known structure identified BcR135 and BcR136 as the closest homologs (PDB codes 3B55 and 2QGM, respectively). These two proteins are found in *Bacillus cereus* and are hypothesized to be involved in succinoglycan biosynthesis. The BcR135 and BcR136 sequences are 58.6% similar, and as is to be expected, they possess the exact same fold (Morar et al., 2012). The extent of sequence similarity of BcR135 and BcR136 vs. Eres is considerable, and ranges between 30.1 and 38.7% sequence similarity. Furthermore, similar to Eres they are both capable of cleaving the broad esterase substrate *p*-nitrophenyl butyrate (*p*-NPB). However, BcR136 has been proven not to possess macrolide esterase activity, and given the similarity between the two proteins, this also is likely true for BcR135. Intriguingly, the structure of BcR135 and BcR136 display a novel fold for esterase enzymes.

Given the extent of sequence similarity between BcR135 and BcR136 and the Eres enzymes, their structure can be used to generate a moderately accurate homology model of the resistance enzymes. We build a model of EreA based on BcR135, as it has been proposed that EreA is a metal-dependent esterase (Morar et al., 2012), and BcR135 has a  $\text{Ca}^{2+}$  present in its structure (note: EreB has not been reported to require a metal ion for catalysis) (PDB: 3B55). Subsequently, we used this EreA homology model to examine the sequence conservation among the five Ere enzymes (see **Figure 7**).

As shown in **Figure 7**, several completely conserved residues are located at the bottom of a groove, i.e., H40, E68, and H279. Note that these residues are also conserved in BcR135 and BcR136. It is tempting to speculate that this identifies the active site of the enzyme. This suggestion is further bolstered by the observation that the  $\text{Ca}^{2+}$  ion in BcR135 is coordinated to two

of these residues. In fact, Morar et al. (2012) have mutated these specific residues in EreB and shown that these mutations impact the catalytic activity of the enzyme. The authors speculate the role of H40 to be of a catalytic base that activates a water molecule which then becomes a nucleophile that will attack the ester bond of the macrolide. How this proposed mechanism could apply to the presumed metal dependent EreA enzyme is unclear. It is likely that EreA does not in fact require a metal ion for catalysis and that the calcium ion present in BcR135 is an artifact of the structure determination and does not reveal critical information on mechanism of catalysis.

The homology model of EreA also reveals that the walls of the groove, above the presumable active site, are somewhat less conserved. This could explain some of the reported differences in substrate specificity between EreA and EreB. However, given the very limited data available for the substrate spectrum of different Eres, combined with the complete absence of information on how a macrolide might actually bind to an Ere, further discussion on the structural basis of Ere substrate specificity is not feasible, and will need to wait until the three-dimensional structure of an Ere-macrolide complex has been determined.

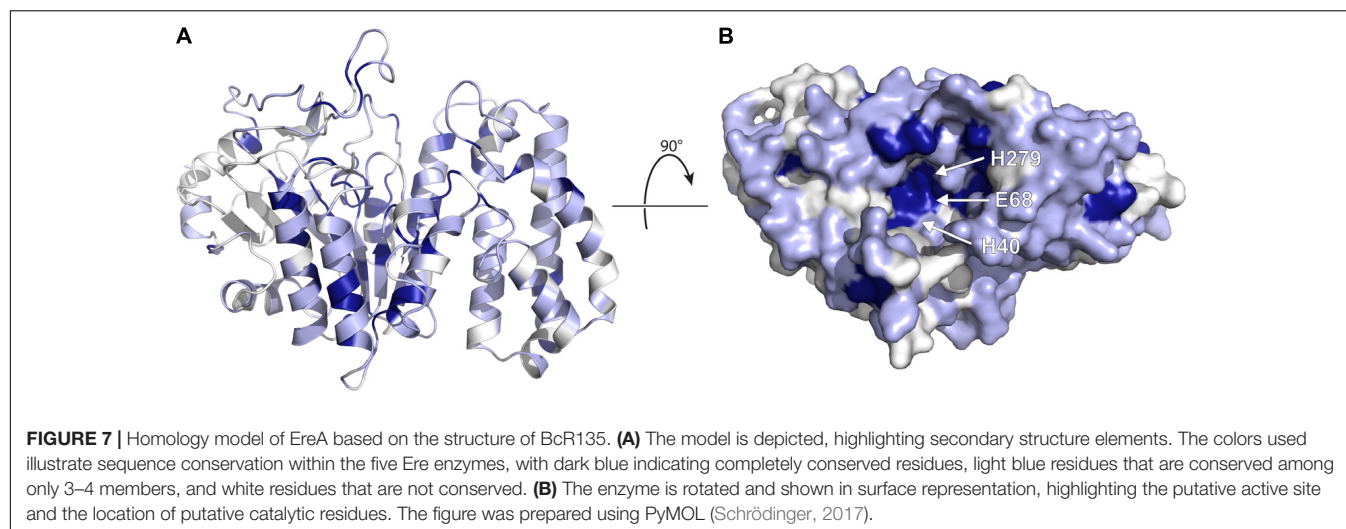
## COUNTERACTING MACROLIDE RESISTANCE

Three-dimensional structural information on how macrolides are rendered useless by various bacterial resistance mechanisms can be exploited for the development of therapies that are more resilient against such resistance. If additional detailed information is available for how macrolides bind to the ribosome, this can be also incorporated. Specifically, two distinct avenues are available for the rational development of improved therapies. First, information on features of the macrolide that are recognized by resistance mechanisms and contrasting this with how these drugs bind to ribosome can inform the design of next-generation macrolides, i.e., variants that are unable to bind to resistance proteins but that retain affinity for the ribosome. The second avenue for combating macrolide resistance is to develop inhibitors to the resistance proteins which can then be used as adjuvants to restore the activity of existing antibiotics. The validity of this strategy is illustrated by a familiar  $\beta$ -lactam antibiotic therapy where amoxicillin or ampicillin is co-administered with sulbactam or tazobactam, which inhibit some of the commonly encountered  $\beta$ -lactam resistance enzymes (Drawz and Bonomo, 2010). Below these two avenues are further explored.

## Avenues for Next-Generation Macrolide Antibiotic Development

When considering the design of a next-generation macrolide, it would be desirable if this design could address as many forms of clinically observed resistance as feasible. For macrolides, the challenge is to address: efflux pump action, di-methylation/mutation of the ribosome, and the action of MPHs and Eres. Unfortunately, efflux pumps are well-known for having a very broad range of action toward xenobiotics, leaving





ribosome alteration and antibiotic modification, as the resistance mechanisms that can potentially be addressed by improved design. Fortunately, three-dimensional structural information is available to assist in this design effort.

Ribosome alterations are largely centered on A2058 of the 23S rRNA, which makes a specific hydrogen-bond interaction with the C5-linked desosamine/mycaminose moiety of macrolides. This suggests that alterations in that group could be an avenue for exploration. However, the effectiveness of abolishing the hydrogen-bond between A2058 N6 and 2' hydroxyl of macrolides for precipitating resistance, suggests that merely removing this hydroxyl group on the macrolide will not be sufficient and compensatory interactions have to be engineered to maintain effective and specific binding affinity of the macrolide with the ribosome. Interestingly, the MPHs also target this same hydroxyl group for phosphorylation, and as such alterations in this part of the macrolide might simultaneously circumvent resistance by these enzymes. Alternatively, MPH mediated resistance could be addressed by interfering with the unique manner in which macrolides bind to these enzymes. Although macrolides bind in a similar way to the ribosome as to MPHs, the MPH-macrolide binding seems to be much more fitted. This becomes especially visible with 16-membered macrolides, where a section of C-9 to C-14 extends to the lumen of the exit tunnel whereas this particular section forms relatively close interaction with MPHs. As proposed by Fong et al. (2017) this feature is a potential avenue by which next generation macrolides could be altered to prevent interaction with MPH while at the same time retaining the ribosome binding.

As mentioned previously Ere enzymes take advantage of the ester linkage present in all macrolides and use a water molecule to hydrolyze the bond that cyclizes the macrolactone ring. One possible solution would be to create a macrolide which in place of an ester bond would have the far more stable amide bond. This in turn would no longer allow the Ere enzyme to perform its reaction. However, this will very likely represent a challenge from the point of view of synthesis. Even though the *de novo* synthesis of macrolides has been

described using chemical means, the protocol has been developed to utilize the ester linkage (Seiple et al., 2016). Furthermore, also polyketide synthases rely on the creation of cyclizing ester linkage (Park et al., 2010). An alternative approach would be to efficiently block the interaction between Ere and macrolide without impacting ribosome binding. For this to take place it would be helpful to obtain information on the structural details of an Ere-macrolide complex. However, even in the absence of this, we can note that when bound to the ribosome, the ester bond and neighboring atoms do not make specific interactions, and there is space to expand on the macrolide scaffold (Bulkley et al., 2010). It is unlikely that some of the viable expansions could also be accommodated when macrolides bind to Eres, given the need for catalysis, thus providing an avenue to engineer selectivity for the ribosome in the design.

It is appropriate to emphasize the breakthrough that both *de novo* synthesis and protein engineering of polyketide synthases represent. Prior to these two recent developments, efforts to modify the macrolide scaffold were extremely challenging. However, we are now approaching the situation that we are largely limited by our imagination. This places structural information for macrolides interactions with both the ribosome and with the proteins responsible for resistance, at the forefront to efficiently and effectively guide the exploration of macrolide chemical space for the development of next-generations antibiotics.

## Adjuvant Development of Macrolide Therapies

In the context of adjuvant development, it would be optimal to identify inhibitors of various clinically relevant mechanisms of macrolide resistance. Analogous to the design of next-generation macrolides, resistance mechanisms to be potentially addressed are: efflux pump action, alteration of the ribosome, and the action of MPHs and Eres. However, not all these mechanisms are amenable to inhibitor development. Specifically, mutations in the

ribosome cannot be addressed through inhibitors. Furthermore, not all enzymes are “drugable,” referring to presence of a distinct pocket that can be uniquely targeted by small molecules. In this respect, the homology model of EreA is discouraging as the pocket shown in **Figure 7** might be too shallow. This leaves efflux pumps, Erm methyltransferases and MPHs as potential targets for adjuvant development. For targeting pumps or ribosome alteration, we refer the reader to Van Bambeke and Lee (2006). Here we will discuss efforts to target MPHs for adjuvant development.

Human ePKs are primary targets for the treatment of cancer and have been extensively explored in drug discovery. To this end the pharmaceutical industry has significantly invested in the design and synthesis of large libraries of compounds that target these kinases. Structural resemblance of aminoglycoside and macrolide phosphotransferases to ePKs, specifically in the nucleotide binding region sparked the idea of repurposing ATP competitive kinase inhibitors against these antibiotic kinases. Soon after the structural homology between APHs and ePKs was uncovered, several known ATP competitive inhibitors of ePKs were assayed for their activity toward APHs. Isoquinoline sulfonamide derivatives, notably CKI-7 were among the first compounds discovered to inhibit some APHs such as APH(3′)-IIIa (Shi et al., 2013). Feasibility of using human protein kinase inhibitors against MPHs and APHs was also tested in a high throughput manner. The screening study clearly showed that although some of the inhibitors can be used against ATP-binding APHs, none were successful against MPHs which are GTP-binding kinases (Shakya et al., 2011).

The observation that an array of protein kinase inhibitors was unable to inhibit MPHs, as these enzymes are GTP-specific, is actually encouraging. A lingering concern in this effort has been the possibility of cross-reactivity of MPH inhibitors with human protein kinases. However, the MPHs’ GTP binding pocket appears to be sufficiently distinct from the ATP binding pocket in ePKs that selectivity is very likely feasible. However, the inability to find leads for MPHs in protein kinase inhibitor libraries implies that leveraging these libraries for adjuvant development is unlikely to be successful. An alternative to a “high-throughput” library screening approaches for inhibitor development is fragment-based drug discovery (Hajduk and Greer, 2007; Lamoree and Hubbard, 2017). This approach has several significant advantages over conventional high-throughput screening campaigns. Most notably, a large segment of chemical space can be surveyed using only a limited number of compounds, and it allows for the discovery of novel scaffolds. In fact, the consensus within the pharmaceutical industry is that fragment-based lead discovery outperforms high-throughput screening approaches as it is more reliable in identifying useful hits and ultimately provides higher quality leads (Hajduk and Greer, 2007). Fragment-based drug discovery does require the three-dimensional structure determination of fragment hits with their target, but this is not an insurmountable obstacle as high-resolution structures of 1.5 Å or better

have been obtained for both MPH(2′)-I and MPH(2′)-II (Fong et al., 2017). Given the structural data available for various MPHs, combined with fragment-based screening techniques, it is likely only a matter of time before inhibitors to this class of resistance enzymes will become available. Of course, it is realized that such an achievement would only be the first step in adjuvant development, but nonetheless a critical one in efforts to combat macrolide antibiotic resistance.

## CONCLUSION

Since their discovery almost 70 years ago, their introduction into clinical practice in 1952 and the first report of clinical resistance 4 years later, much has been learned about macrolides, their mode of action and the various mechanisms by which pathogenic bacteria are increasingly becoming resistant to these antibiotics. This wealth of information now sets the stage for the rational design of much needed therapies that can either overcome or counteract resistance to these antibiotics. The detailed structural insights obtained from the Nobel Prize winning research on how macrolides interact with the bacterial ribosome, combined with the growing information on macrolide resistance mechanisms, enables the rational development of next-generation macrolides. This is furthermore facilitated by recent advances in the synthesis of macrolide variants, either through protein engineering of polyketide synthases, or the *de novo* synthesis. Complementary, detailed structural studies of macrolide resistance mechanisms in conjunction with advanced approaches to inhibitor development, such as fragment-based screening can accelerate the development of macrolide adjuvants. Much research remains to be accomplished, but there is reason for optimism that macrolides may remain a valuable resource to combat bacterial infections.

## AUTHOR CONTRIBUTIONS

All authors listed have made a substantial, direct and intellectual contribution to the work, and approved it for publication.

## FUNDING

The research on macrolide resistance conducted by the authors has been supported by a Grant from the Canadian Institutes of Health Research awarded to AMB. This study has been funded by CIHR Operating Grant MOP-13107.

## ACKNOWLEDGMENTS

We would like to thank members of the Berghuis lab for helpful discussions.

## REFERENCES

- Abbassi, M. S., Torres, C., Achour, W., Vinué, L., Sáenz, Y., Costa, D., et al. (2008). Genetic characterisation of CTX-M-15-producing *Klebsiella pneumoniae* and *Escherichia coli* strains isolated from stem cell transplant patients in Tunisia. *Int. J. Antimicrob. Agents* 32, 308–314. doi: 10.1016/j.ijantimicag.2008.04.009
- Ahmed, A. M., and Shimamoto, T. (2011). Molecular characterization of antimicrobial resistance in Gram-negative bacteria isolated from bovine mastitis in Egypt. *Microbiol. Immunol.* 55, 318–327. doi: 10.1111/j.1348-0421.2011.00323.x
- Ambrose, K. D., Nisbet, R., and Stephens, D. S. (2005). Macrolide efflux in *Streptococcus pneumoniae* is mediated by a dual efflux pump (mel and mef) and is erythromycin inducible. *Antimicrob. Agents Chemother.* 49, 4203–4209. doi: 10.1128/AAC.49.10.4203-4209.2005
- Andremont, A., Gerbaud, G., and Courvalin, P. (1986). Plasmid-mediated high-level resistance to erythromycin in *Escherichia coli*. *Antimicrob. Agents Chemother.* 29, 515–518. doi: 10.1128/AAC.29.3.515
- Arenz, S., Nguyen, F., Beckmann, R., and Wilson, D. N. (2015). Cryo-EM structure of the tetracycline resistance protein TetM in complex with a translating ribosome at 3.9-Å resolution. *Proc. Natl. Acad. Sci. U.S.A.* 112, 5401–5406. doi: 10.1073/pnas.1501775112
- Arthur, M., Autissier, D., and Courvalin, P. (1986). Analysis of the nucleotide sequence of the ereB gene encoding the erythromycin esterase type II. *Nucleic Acids Res.* 14, 4987–4999. doi: 10.1093/nar/14.12.4987
- Artsmovitch, I., Seddon, J., and Sears, P. (2012). Fidaxomicin is an inhibitor of the initiation of bacterial RNA synthesis. *Clin. Infect. Dis.* 55, S127–S131. doi: 10.1093/cid/cis358
- Ban, N., Nissen, P., Hansen, J., Moore, P. B., and Steitz, T. A. (2000). The complete atomic structure of the large ribosomal subunit at 2.4 Å resolution. *Science* 289, 905–920. doi: 10.1126/science.289.5481.905
- Barthelemy, P., Autissier, D., Gerbaud, G., and Courvalin, P. (1984). Enzymic hydrolysis of erythromycin by a strain of *Escherichia coli*. *J. Antibiot.* 37, 1692–1696. doi: 10.7164/antibiotics.37.1692
- Berisio, R., Harms, J., Schlunzen, F., Zarivach, R., Hansen, H. A., Fucini, P., et al. (2003). Structural insight into the antibiotic action of telithromycin against resistant mutants. *J. Bacteriol.* 185, 4276–4279. doi: 10.1128/JB.185.14.4276-4279.2003
- Bolam, D. N., Roberts, S., Proctor, M. R., Turkenburg, J. P., Dodson, E. J., Martinez-Fleites, C., et al. (2007). The crystal structure of two macrolide glycosyltransferases provides a blueprint for host cell antibiotic immunity. *Proc. Natl. Acad. Sci. U.S.A.* 104, 5336–5341. doi: 10.1073/pnas.0607897104
- Bryskier, A. (2000). Ketolid—telithromycin, an example of a new class of antibacterial agents. *Clin. Microbiol. Infect.* 6, 661–669. doi: 10.1046/j.1469-0691.2000.00185.x
- Bulkley, D., Innis, C. A., Blaha, G., and Steitz, T. A. (2010). Revisiting the structures of several antibiotics bound to the bacterial ribosome. *Proc. Natl. Acad. Sci. U.S.A.* 107, 17158–17163. doi: 10.1073/pnas.1008685107
- Celma, M., Monro, R., and Vazquez, D. (1970). Substrate and antibiotic binding sites at the peptidyl transferase centre of *E. coli* ribosomes. *FEBS Lett.* 6, 273–277. doi: 10.1016/0014-5793(70)80076-X
- Chang, C.-Y., Chang, L.-L., Chang, Y.-H., Lee, T.-M., and Chang, S.-F. (2000). Characterisation of drug resistance gene cassettes associated with class 1 integrons in clinical isolates of *Escherichia coli* from Taiwan, ROC. *J. Med. Microbiol.* 49, 1097–1102. doi: 10.1099/0022-1317-49-12-1097
- Chesneau, O., Tsvetkova, K., and Courvalin, P. (2007). Resistance phenotypes conferred by macrolide phosphotransferases. *FEMS Microbiol. Lett.* 269, 317–322. doi: 10.1111/j.1574-6968.2007.00643.x
- Cundliffe, E. (1992). Glycosylation of macrolide antibiotics in extracts of *Streptomyces lividans*. *Antimicrob. Agents Chemother.* 36, 348–352. doi: 10.1128/AAC.36.2.348
- Dereeper, A., Guignon, V., Blanc, G., Audic, S., Buffet, S., Chevenet, F., et al. (2008). Phylogeny.fr: robust phylogenetic analysis for the non-specialist. *Nucleic Acids Res.* 36, W465–W469. doi: 10.1093/nar/gkn180
- Dixon, J. (1968). Group A *Streptococcus* resistant to erythromycin and lincomycin. *Can. Med. Assoc. J.* 99, 1093–1094.
- Drawz, S. M., and Bonomo, R. A. (2010). Three decades of  $\beta$ -lactamase inhibitors. *Clin. Microbiol. Rev.* 23, 160–201. doi: 10.1128/CMR.00037-09
- Ettayebi, M., Prasad, S. M., and Morgan, E. A. (1985). Chloramphenicol-erythromycin resistance mutations in a 23S rRNA gene of *Escherichia coli*. *J. Bacteriol.* 162, 551–557.
- Ferjani, A., Baccouche, A., Marzouk, M., Tarchouna, M., and Boukadida, J. (2012). *Escherichia coli* as reservoir for macrolide resistance genes. *Clin. Microbiol. Infect.* 18:335. doi: 10.3201/eid1510.090696
- Fernandez-Fuentes, M. A., Abriouel, H., Morente, E. O., Pulido, R. P., and Galvez, A. (2014). Genetic determinants of antimicrobial resistance in Gram positive bacteria from organic foods. *Int. J. Food Microbiol.* 172, 49–56. doi: 10.1016/j.ijfoodmicro.2013.11.032
- Fong, D. H., Burk, D. L., Blanchet, J., Yan, A. Y., and Berghuis, A. M. (2017). Structural basis for kinase-mediated macrolide antibiotic resistance. *Structure* 25, 750.e5–761.e5. doi: 10.1016/j.str.2017.03.007
- Franceschi, F., Kanyo, Z., Sherer, E., and Sutcliffe, J. (2004). Macrolide resistance from the ribosome perspective. *Curr. Drug Targets Infect. Disord.* 4, 177–191. doi: 10.2174/1568005043340740
- Fuentes, M. A. F., Morente, E. O., Abriouel, H., Pulido, R. P., and Galvez, A. (2014). Antimicrobial resistance determinants in antibiotic and biocide-resistant gram-negative bacteria from organic foods. *Food Control* 37, 9–14. doi: 10.1016/j.foodcont.2013.08.041
- Fyfe, C., Grossman, T. H., Kerstein, K., and Sutcliffe, J. (2016). Resistance to macrolide antibiotics in public health pathogens. *Cold Spring Harb. Perspect. Med.* 6:a025395. doi: 10.1101/cshperspect.a025395
- Gabashvili, I. S., Gregory, S. T., Valle, M., Grassucci, R., Worbs, M., Wahl, M. C., et al. (2001). The polypeptide tunnel system in the ribosome and its gating in erythromycin resistance mutants of L4 and L22. *Mol. Cell* 8, 181–188. doi: 10.1016/S1097-2765(01)00293-3
- Ghosh, R., Uppal, B., Aggarwal, P., Chakravarti, A., and Jha, A. K. (2013). Increasing antimicrobial resistance of *Campylobacter jejuni* isolated from paediatric diarrhea cases in a tertiary care hospital of New Delhi, India. *J. Clin. Diagn. Res.* 7, 247–249. doi: 10.7860/JCDR/2013/5267.2738
- Girard, A. E., Girard, D., English, A. R., Gootz, T. D., Cimochoowski, C. R., Faiella, J. A., et al. (1987). Pharmacokinetic and in vivo studies with azithromycin (CP-62,993), a new macrolide with an extended half-life and excellent tissue distribution. *Antimicrob. Agents Chemother.* 31, 1948–1954. doi: 10.1128/AAC.31.12.1948
- Gomes, C., Martínez-Puchol, S., Palma, N., Horna, G., Ruiz-Roldán, L., Pons, M. J., et al. (2017). Macrolide resistance mechanisms in *Enterobacteriaceae*: focus on azithromycin. *Crit. Rev. Microbiol.* 43, 1–30. doi: 10.3109/1040841X.2015.1136261
- Hajduk, P. J., and Greer, J. (2007). A decade of fragment-based drug design: strategic advances and lessons learned. *Nat. Rev. Drug Discov.* 6, 211–219. doi: 10.1038/nrd2220
- Hansen, J. L., Ippolito, J. A., Ban, N., Nissen, P., Moore, P. B., and Steitz, T. A. (2002). The structures of four macrolide antibiotics bound to the large ribosomal subunit. *Mol. Cell* 10, 117–128. doi: 10.1016/S1097-2765(02)00570-1
- Hansen, L. H., Mauvais, P., and Douthwaite, S. (1999). The macrolide–ketolide antibiotic binding site is formed by structures in domains II and V of 23S ribosomal RNA. *Mol. Microbiol.* 31, 623–631. doi: 10.1046/j.1365-2958.1999.01202.x
- Hassanzadeh, A., Barber, J., Morris, G. A., and Gorry, P. A. (2007). Mechanism for the degradation of erythromycin A and erythromycin A 2'-ethyl succinate in acidic aqueous solution. *J. Phys. Chem. A* 111, 10098–10104. doi: 10.1021/jp073030y
- Hon, W.-C., McKay, G. A., Thompson, P. R., Sweet, R. M., Yang, D. S., Wright, G. D., et al. (1997). Structure of an enzyme required for aminoglycoside antibiotic resistance reveals homology to eukaryotic protein kinases. *Cell* 89, 887–895. doi: 10.1016/S0092-8674(00)80274-3
- Huson, D. H., and Scornavacca, C. (2012). Dendroscope 3: an interactive tool for rooted phylogenetic trees and networks. *Syst. Biol.* 61, 1061–1067. doi: 10.1093/sysbio/sys062
- Kim, S., Baek, M., Choi, S., Kim, B., and Choi, E. (1996). Nucleotide sequence, expression and transcriptional analysis of the *Escherichia coli* mphK gene encoding macrolide-phosphotransferase K. *Mol. Cells* 6, 153–160.
- Kim, Y. H., and Cerniglia, C. E. (2005). Influence of erythromycin A on the microbial populations in aquaculture sediment microcosms. *Aquat. Toxicol.* 73, 230–241. doi: 10.1016/j.aquatox.2005.03.013



- Kim, Y. H., Cha, C. J., and Cerniglia, C. E. (2002). Purification and characterization of an erythromycin esterase from an erythromycin-resistant *Pseudomonas* sp. *FEMS Microbiol. Lett.* 210, 239–244. doi: 10.1111/j.1574-6968.2002.tb11187.x
- Kono, M., O'hara, K., and Ebisu, T. (1992). Purification and characterization of macrolide 2'-phosphotransferase type II from a strain of *Escherichia coli* highly resistant to macrolide antibiotics. *FEMS Microbiol. Lett.* 97, 89–94. doi: 10.1016/0378-1097(92)90369-Y
- Krauland, M., Harrison, L., Paterson, D., and Marsh, J. (2010). Novel integron gene cassette arrays identified in a global collection of multi-drug resistant non-typhoidal *Salmonella enterica*. *Curr. Microbiol.* 60, 217–223. doi: 10.1007/s00284-009-9527-3
- Lambert, P. A. (2005). Bacterial resistance to antibiotics: modified target sites. *Adv. Drug Deliv. Rev.* 57, 1471–1485. doi: 10.1016/j.addr.2005.04.003
- Lamoree, B., and Hubbard, R. E. (2017). Current perspectives in fragment-based lead discovery (FBLD). *Essays Biochem.* 61, 453–464. doi: 10.1042/EBC20170028
- Leclercq, R. (2002). Mechanisms of resistance to macrolides and lincosamides: nature of the resistance elements and their clinical implications. *Clin. Infect. Dis.* 34, 482–492. doi: 10.1086/324626
- Leclercq, R., and Courvalin, P. (1991). Bacterial resistance to macrolide, lincosamide, and streptogramin antibiotics by target modification. *Antimicrob. Agents Chemother.* 35, 1267–1272. doi: 10.1128/AAC.35.7.1267
- Lewis, K. (2013). Platforms for antibiotic discovery. *Nat. Rev. Drug Discov.* 12, 371–387. doi: 10.1038/nrd3975
- Li, X. Z., and Nikaido, H. (2009). Efflux-mediated drug resistance in bacteria: an update. *Drugs* 69, 1555–1623. doi: 10.2165/11317030-000000000-00000
- Lovmar, M., Nilsson, K., Lukk, E., Vimberg, V., Tenson, T., and Ehrenberg, M. (2009). Erythromycin resistance by L4/L22 mutations and resistance masking by drug efflux pump deficiency. *EMBO J.* 28, 736–744. doi: 10.1038/emboj.2009.17
- Lowbury, E., and Hurst, L. (1959). The sensitivity of Staphylococci and other wound bacteria to erythromycin, oleandomycin, and spiramycin. *J. Clin. Pathol.* 12, 163–169. doi: 10.1136/jcp.12.2.163
- MacCabe, A. F., and Gould, J. C. (1956). The epidemiology of an erythromycin resistant Staphylococcus. *Scot. Med. J.* 1, 223–226. doi: 10.1177/003693305600100701
- MacLaughlin, E. J., Saseen, J. J., and Malone, D. C. (2000). Costs of  $\beta$ -lactam allergies: selection and costs of antibiotics for patients with a reported  $\beta$ -lactam allergy. *Arch. Fam. Med.* 9, 722–726. doi: 10.1001/archfam.9.8.722
- Matsuoka, M., Endou, K., Kobayashi, H., Inoue, M., and Nakajima, Y. (1998). A plasmid that encodes three genes for resistance to macrolide antibiotics in *Staphylococcus aureus*. *FEMS Microbiol. Lett.* 167, 221–227. doi: 10.1111/j.1574-6968.1998.tb13232.x
- Matsuoka, M., Inoue, M., Endo, Y., and Nakajima, Y. (2003). Characteristic expression of three genes, *msr* (A), *mph* (C) and *erm* (Y), that confer resistance to macrolide antibiotics on *Staphylococcus aureus*. *FEMS Microbiol. Lett.* 220, 287–293. doi: 10.1016/S0378-1097(03)00134-4
- Matzov, D., Eyal, Z., Benhamou, R. I., Shalev-Benami, M., Halfon, Y., Krupkin, M., et al. (2017). Structural insights of lincosamides targeting the ribosome of *Staphylococcus aureus*. *Nucleic Acids Res.* 45, 10284–10292. doi: 10.1093/nar/gkx658
- Mendes, R. E., Castanheira, M., Farrell, D. J., Flamm, R. K., Sader, H. S., and Jones, R. N. (2017). Prevalence of macrolide–lincosamide resistance and multidrug resistance phenotypes in Streptococcal isolates causing infections in European hospitals: evaluation of the in vitro activity of oritavancin and comparator agents. *J. Glob. Antimicrob. Resist.* 8, 28–32. doi: 10.1016/j.jgar.2016.08.013
- Moazed, D., and Noller, H. F. (1987). Chloramphenicol, erythromycin, carbomycin and vernamycin B protect overlapping sites in the peptidyl transferase region of 23S ribosomal RNA. *Biochimie* 69, 879–884. doi: 10.1016/0300-9084(87)90215-X
- Moore, S. D., and Sauer, R. T. (2008). Revisiting the mechanism of macrolide-antibiotic resistance mediated by ribosomal protein L22. *Proc. Natl. Acad. Sci. U.S.A.* 105, 18261–18266. doi: 10.1073/pnas.0810357105
- Morar, M., Pengelly, K., Koteva, K., and Wright, G. D. (2012). Mechanism and diversity of the erythromycin esterase family of enzymes. *Biochemistry* 51, 1740–1751. doi: 10.1021/bi201790u
- Morimoto, S., Takahashi, Y., Watanabe, Y., and Omura, S. (1984). Chemical modification of erythromycins. I. Synthesis and antibacterial activity of 6-O-methylethylerythromycins A. *J. Antibiot.* 37, 187–189. doi: 10.7164/antibiotics.37.187
- Murphy, B. P., O'mahony, R., Buckley, J. F., Shine, P., Fidelma Boyd, E., Gilroy, D., et al. (2007). Investigation of a global collection of nontyphoidal *Salmonella* of various serotypes cultured between 1953 and 2004 for the presence of class 1 integrons. *FEMS Microbiol. Lett.* 266, 170–176. doi: 10.1111/j.1574-6968.2006.00537.x
- Nakamura, A., Nakazawa, K., Miyakozawa, T., Mizukoshi, S., Tsurubuchi, K., Nakagawa, M., et al. (2000). Macrolide esterase-producing *Escherichia coli* clinically isolated in Japan. *J. Antibiot.* 53, 516–524. doi: 10.7164/antibiotics.53.516
- Nguyen, F., Starosta, A. L., Arenz, S., Sohmen, D., Dönhöfer, A., and Wilson, D. N. (2014). Tetracycline antibiotics and resistance mechanisms. *Biol. Chem.* 395, 559–575. doi: 10.1515/hsz-2013-0292
- Nguyen, M. C. P., Woerther, P.-L., Bouvet, M., Andremont, A., Leclercq, R., and Canu, A. (2009). *Escherichia coli* as reservoir for macrolide resistance genes. *Emerg. Infect. Dis.* 15, 1648–1650. doi: 10.3201/eid1510.090696
- O'Hara, K., Kanda, T., and Kono, M. (1988). Structure of a phosphorylated derivative of oleandomycin, obtained by reaction of oleandomycin with an extract of an erythromycin-resistant strain of *Escherichia coli*. *J. Antibiot.* 41, 823–827. doi: 10.7164/antibiotics.41.823
- O'Hara, K., Kanda, T., Ohmiya, K., Ebisu, T., and Kono, M. (1989). Purification and characterization of macrolide 2'-phosphotransferase from a strain of *Escherichia coli* that is highly resistant to erythromycin. *Antimicrob. Agents Chemother.* 33, 1354–1357. doi: 10.1128/AAC.33.8.1354
- Oleinick, N. L., and Corcoran, J. W. (1969). Two types of binding of erythromycin to ribosomes from antibiotic-sensitive and-resistant *Bacillus subtilis* 168. *J. Biol. Chem.* 244, 727–735.
- Omura, S. (2002). *Macrolide Antibiotics: Chemistry, Biology, and Practice*. New York, NY: Elsevier.
- Ounissi, H., and Courvalin, P. (1985). Nucleotide sequence of the gene *ereA* encoding the erythromycin esterase in *Escherichia coli*. *Gene* 35, 271–278. doi: 10.1016/0378-1119(85)90005-8
- Park, S. R., Han, A. R., Ban, Y.-H., Yoo, Y. J., Kim, E. J., and Yoon, Y. J. (2010). Genetic engineering of macrolide biosynthesis: past advances, current state, and future prospects. *Appl. Microbiol. Biotechnol.* 85, 1227–1239. doi: 10.1007/s00253-009-2326-8
- Pawlowski, A. C., Stogios, P. J., Koteva, K., Skarina, T., Evdokimova, E., Savchenko, A., et al. (2018a). The evolution of substrate discrimination in macrolide antibiotic resistance enzymes. *Nat. Commun.* 9:112. doi: 10.1038/s41467-017-02680-0
- Pawlowski, A. C., Wang, W., Koteva, K., Barton, H. A., McArthur, A. G., and Wright, G. D. (2016). A diverse intrinsic antibiotic resistome from a cave bacterium. *Nat. Commun.* 7:13803. doi: 10.1038/ncomms13803
- Pawlowski, A. C., Westman, E. L., Koteva, K., Waglechner, N., and Wright, G. D. (2018b). The complex resistomes of Paenibacillaceae reflect diverse antibiotic chemical ecologies. *ISME J.* 12, 885–897. doi: 10.1038/s41396-017-0017-5
- Pereyre, S., Goret, J., and Bébér, C. (2016). *Mycoplasma pneumoniae*: current knowledge on macrolide resistance and treatment. *Front. Microbiol.* 7:974. doi: 10.3389/fmicb.2016.00974
- Poehlsgaard, J., and Douthwaite, S. (2005). The bacterial ribosome as a target for antibiotics. *Nat. Rev. Microbiol.* 3, 870–881. doi: 10.1038/nrmicro1265
- Quirós, L. M., Carbajo, R. J., Braña, A. F., and Salas, J. A. (2000). Glycosylation of Macrolide Antibiotics purification and kinetic studies of a macrolide glycosyltransferase from *Streptomyces antibioticus*. *J. Biol. Chem.* 275, 11713–11720. doi: 10.1074/jbc.275.16.11713
- Roberts, M. C. (2008). Update on macrolide–lincosamide–streptogramin, ketolide, and oxazolidinone resistance genes. *FEMS Microbiol. Lett.* 282, 147–159. doi: 10.1111/j.1574-6968.2008.01145.x
- Roberts, M. C., Sutcliffe, J., Courvalin, P., Jensen, L. B., Rood, J., and Seppala, H. (1999). Nomenclature for macrolide and macrolide-lincosamide-streptogramin B resistance determinants. *Antimicrob. Agents Chemother.* 43, 2823–2830.
- Schlünzen, F., Harms, J. M., Franceschi, F., Hansen, H. A., Bartels, H., Zarivach, R., et al. (2003). Structural basis for the antibiotic activity of ketolides and azalides. *Structure* 11, 329–338. doi: 10.1016/S0969-2126(03)00022-4

- Schlünzen, F., Zarivach, R., Harms, J., Bashan, A., Tocilj, A., Albrecht, R., et al. (2001). Structural basis for the interaction of antibiotics with the peptidyl transferase centre in eubacteria. *Nature* 413, 814–821. doi: 10.1038/35101544
- Schlüter, A., Szczepanowski, R., Kurz, N., Schneiker, S., Krahn, I., and Pühler, A. (2007). Erythromycin resistance-conferring plasmid pRSB105, isolated from a sewage treatment plant, harbors a new macrolide resistance determinant, an integron-containing Tn402-like element, and a large region of unknown function. *Appl. Environ. Microbiol.* 73, 1952–1960. doi: 10.1128/AEM.02159-06
- Schmitz, F. J., Petridou, J., Fluit, A. C., Hadding, U., Peters, G., Von Eiff, C., et al. (2000a). Distribution of macrolide-resistance genes in *Staphylococcus aureus* blood-culture isolates from fifteen German university hospitals. *Eur. J. Clin. Microbiol. Infect. Dis.* 19, 385–387.
- Schmitz, F.-J., Sadurski, R., Kray, A., Boos, M., Geisel, R., Köhrer, K., et al. (2000b). Prevalence of macrolide-resistance genes in *Staphylococcus aureus* and *Enterococcus faecium* isolates from 24 European university hospitals. *J. Antimicrob. Chemother.* 45, 891–894.
- Schrödinger, LLC (2017). *The PyMOL Molecular Graphics System, Version 1.8.2015*. New York, NY: Schrödinger, LLC.
- Seiple, I. B., Zhang, Z., Jakubec, P., Langlois-Mercier, A., Wright, P. M., Hog, D. T., et al. (2016). A platform for the discovery of new macrolide antibiotics. *Nature* 533, 338–345. doi: 10.1038/nature17967
- Shakya, T., Stogios, P. J., Wagelchner, N., Evdokimova, E., Ejim, L., Blanchard, J. E., et al. (2011). A small molecule discrimination map of the antibiotic resistance kinome. *Chem. Biol.* 18, 1591–1601. doi: 10.1016/j.chembiol.2011.10.018
- Sharkey, L. K., Edwards, T. A., and O'Neill, A. J. (2016). ABC-F proteins mediate antibiotic resistance through ribosomal protection. *mBio* 7:e01975-15. doi: 10.1128/mBio.01975-15
- Shi, K., and Berghuis, A. M. (2012). Structural basis for dual nucleotide selectivity of aminoglycoside 2''-phosphotransferase IVa provides insight on determinants of nucleotide specificity of aminoglycoside kinases. *J. Biol. Chem.* 287, 13094–13102. doi: 10.1074/jbc.M112.349670
- Shi, K., Caldwell, S. J., Fong, D. H., and Berghuis, A. M. (2013). Prospects for circumventing aminoglycoside kinase mediated antibiotic resistance. *Front. Cell. Infect. Microbiol.* 3:22. doi: 10.3389/fcimb.2013.00022
- Su, W., Kumar, V., Ding, Y., Ero, R., Serra, A., Lee, B. S. T., et al. (2018). Ribosome protection by antibiotic resistance ATP-binding cassette protein. *Proc. Natl. Acad. Sci. U.S.A.* 115, 5157–5162. doi: 10.1073/pnas.1803313115
- Svetlov, M. S., Vázquez-Laslop, N., and Mankin, A. S. (2017). Kinetics of drug-ribosome interactions defines the cidal activity of macrolide antibiotics. *Proc. Natl. Acad. Sci. U.S.A.* 114, 13673–13678. doi: 10.1073/pnas.1717168115
- Taubman, S., So, A., Young, F., Davie, E., and Corcoran, J. (1963). Effect of erythromycin on protein biosynthesis in *Bacillus subtilis*. *Antimicrob. Agents Chemother.* 161, 395–401.
- Taubman, S. B., Jones, N. R., Young, F. E., and Corcoran, J. W. (1966). Sensitivity and resistance to erythromycin in *Bacillus subtilis* 168: the ribosomal binding of erythromycin and chloramphenicol. *Biochim. Biophys. Acta* 123, 438–440. doi: 10.1016/0005-2787(66)90301-7
- Thung, I., Aramin, H., Vavinskaya, V., Gupta, S., Park, J., Crowe, S., et al. (2016). The global emergence of *Helicobacter pylori* antibiotic resistance. *Aliment. Pharmacol. Ther.* 43, 514–533. doi: 10.1111/apt.13497
- Thungapathra, M., Amita, Sinha, K. K., Chaudhuri, S. R., Garg, P., Ramamurthy, T., et al. (2002). Occurrence of Antibiotic Resistance Gene Cassettes aac(6')-Ib, dfrA5, dfrA12, and ereA2 in Class I Integrons in Non-O1, Non-O139 *Vibrio cholerae* Strains in India. *Antimicrob. Agents Chemother.* 46, 2948–2955. doi: 10.1128/AAC.46.9.2948-2955.2002
- Tu, D., Blaha, G., Moore, P. B., and Steitz, T. A. (2005). Structures of MLS B K antibiotics bound to mutated large ribosomal subunits provide a structural explanation for resistance. *Cell* 121, 257–270. doi: 10.1016/j.cell.2005.02.005
- Van Bambeke, F., and Lee, V. J. (2006). Inhibitors of bacterial efflux pumps as adjuvants in antibiotic treatments and diagnostic tools for detection of resistance by efflux. *Recent Pat. Antiinfect. Drug Discov.* 1, 157–175. doi: 10.2174/157489106777452692
- Vazquez, D. (1966). Binding of chloramphenicol to ribosomes the effect of a number of antibiotics. *Biochim. Biophys. Acta* 114, 277–288. doi: 10.1016/0005-2787(66)90309-1
- Vester, B., and Douthwaite, S. (2001). Macrolide resistance conferred by base substitutions in 23S rRNA. *Antimicrob. Agents Chemother.* 45, 1–12. doi: 10.1128/AAC.45.1.1-12.2001
- Wang, C., Sui, Z., Leclercq, S. O., Zhang, G., Zhao, M., Chen, W., et al. (2015). Functional characterization and phylogenetic analysis of acquired and intrinsic macrolide phosphotransferases in the *Bacillus cereus* group. *Environ. Microbiol.* 17, 1560–1573. doi: 10.1111/1462-2920.12578
- Weisblum, B. (1995). Erythromycin resistance by ribosome modification. *Antimicrob. Agents Chemother.* 39, 577–585. doi: 10.1128/AAC.39.3.577
- Wekselman, I., Zimmerman, E., Davidovich, C., Belousoff, M., Matzov, D., Krupkin, M., et al. (2017). The ribosomal protein uL22 modulates the shape of the protein exit tunnel. *Structure* 25, 1233.e3–1241.e3. doi: 10.1016/j.str.2017.06.004
- Wimberly, B. T., Brodersen, D. E., Clemons, W. M. Jr., Morgan-Warren, R. J., Carter, A. P., Vonnrhein, C., et al. (2000). Structure of the 30S ribosomal subunit. *Nature* 407, 327–339. doi: 10.1038/35030006
- Xiao, Y., Wei, Z., Shen, P., Ji, J., Sun, Z., Yu, H., et al. (2015). Bacterial-resistance among outpatients of county hospitals in China: significant geographic distinctions and minor differences between central cities. *Microbes Infect.* 17, 417–425. doi: 10.1016/j.micinf.2015.02.001
- Xing, L., Yu, H., Qi, J., Jiang, P., Sun, B., Cui, J., et al. (2015). ErmF and ereD are responsible for erythromycin resistance in *Riemerella anatipestifer*. *PLoS One* 10:e0131078. doi: 10.1371/journal.pone.0131078
- Xiong, L., Shah, S., Mauvais, P., and Mankin, A. S. (1999). A ketolide resistance mutation in domain II of 23S rRNA reveals the proximity of hairpin 35 to the peptidyl transferase centre. *Mol. Microbiol.* 31, 633–639. doi: 10.1046/j.1365-2958.1999.01203.x
- Yong, D., Toleman, M. A., Giske, C. G., Cho, H. S., Sundman, K., Lee, K., et al. (2009). Characterization of a new metallo- $\beta$ -lactamase gene, bla(NDM-1), and a novel erythromycin esterase gene carried on a unique genetic structure in *Klebsiella pneumoniae* sequence type 14 from India. *Antimicrob. Agents Chemother.* 53, 5046–5054. doi: 10.1128/AAC.00774-09
- Zhan, G. G., Dueck, M., Hoban, D. J., Vercaigne, L. M., Embil, J. M., Gin, A. S., et al. (2001). Review of macrolides and ketolides. *Drugs* 61, 443–498. doi: 10.2165/00003495-200161040-00003
- Zhao, X., Ye, C., Chang, W., and Sun, S. (2017). Serotype distribution, antimicrobial resistance, and class 1 integrons profiles of *Salmonella* from animals in slaughterhouses in Shandong Province, China. *Front. Microbiol.* 8:1049. doi: 10.3389/fmicb.2017.01049

**Conflict of Interest Statement:** The authors declare that the research was conducted in the absence of any commercial or financial relationships that could be construed as a potential conflict of interest.

Copyright © 2018 Golkar, Zieliński and Berghuis. This is an open-access article distributed under the terms of the Creative Commons Attribution License (CC BY). The use, distribution or reproduction in other forums is permitted, provided the original author(s) and the copyright owner(s) are credited and that the original publication in this journal is cited, in accordance with accepted academic practice. No use, distribution or reproduction is permitted which does not comply with these terms.



## OPEN ACCESS

## Edited by:

Christopher Davies,  
Medical University of South Carolina,  
United States

## Reviewed by:

Yusuke Minato,  
University of Minnesota Twin Cities,  
United States  
Jeremy Derrick,  
University of Manchester,  
United Kingdom

## \*Correspondence:

Richard E. Lee  
richard.lee@stjude.org  
Stephen W. White  
stephen.white@stjude.org

## †Present Address:

Yinan Wu,  
LakePharma, Inc., Belmont, CA,  
United States  
Stefan Gajewski,  
Nurix, Inc., San Francisco, CA,  
United States

‡These authors have contributed  
equally to this work.

## Specialty section:

This article was submitted to  
Antimicrobials, Resistance and  
Chemotherapy,  
a section of the journal  
Frontiers in Microbiology

Received: 08 March 2018

Accepted: 06 June 2018

Published: 17 July 2018

## Citation:

Griffith EC, Wallace MJ, Wu Y,  
Kumar G, Gajewski S, Jackson P,  
Phelps GA, Zheng Z, Rock CO,  
Lee RE and White SW (2018) The  
Structural and Functional Basis for  
Recurring Sulfa Drug Resistance  
Mutations in *Staphylococcus aureus*  
Dihydropteroate Synthase.  
Front. Microbiol. 9:1369.  
doi: 10.3389/fmicb.2018.01369

# The Structural and Functional Basis for Recurring Sulfa Drug Resistance Mutations in *Staphylococcus aureus* Dihydropteroate Synthase

Elizabeth C. Griffith<sup>1‡</sup>, Miranda J. Wallace<sup>1,2‡</sup>, Yinan Wu<sup>3†</sup>, Gyanendra Kumar<sup>3</sup>,  
Stefan Gajewski<sup>3†</sup>, Pamela Jackson<sup>4</sup>, Gregory A. Phelps<sup>1,5</sup>, Zhong Zheng<sup>1</sup>,  
Charles O. Rock<sup>4</sup>, Richard E. Lee<sup>1\*</sup> and Stephen W. White<sup>2,3\*</sup>

<sup>1</sup> Department of Chemical Biology & Therapeutics, St. Jude Children's Research Hospital, Memphis, TN, United States,

<sup>2</sup> Department of Microbiology, Immunology, and Biochemistry, University of Tennessee Health Science Center, Memphis, TN, United States, <sup>3</sup> Structural Biology, St. Jude Children's Research Hospital, Memphis, TN, United States, <sup>4</sup> Infectious Diseases, St. Jude Children's Research Hospital, Memphis, TN, United States, <sup>5</sup> Pharmaceutical Sciences, University of Tennessee Health Science Center, Memphis, TN, United States

*Staphylococcal* species are a leading cause of bacterial drug-resistant infections and associated mortality. One strategy to combat bacterial drug resistance is to revisit compromised targets, and to circumvent resistance mechanisms using structure-assisted drug discovery. The folate pathway is an ideal candidate for this approach. Antifolates target an essential metabolic pathway, and the necessary detailed structural information is now available for most enzymes in this pathway. Dihydropteroate synthase (DHPS) is the target of the sulfonamide class of drugs, and its well characterized mechanism facilitates detailed analyses of how drug resistance has evolved. Here, we surveyed clinical genetic sequencing data in *S. aureus* to distinguish natural amino acid variations in DHPS from those that are associated with sulfonamide resistance. Five mutations were identified, F17L, S18L, T51M, E208K, and KE257\_dup. Their contribution to resistance and their cost to the catalytic properties of DHPS were evaluated using a combination of biochemical, biophysical and microbiological susceptibility studies. These studies show that F17L, S18L, and T51M directly lead to sulfonamide resistance while unexpectedly increasing susceptibility to trimethoprim, which targets the downstream enzyme dihydrofolate reductase. The secondary mutations E208K and KE257\_dup restore trimethoprim susceptibility closer to wild-type levels while further increasing sulfonamide resistance. Structural studies reveal that these mutations appear to selectively disfavor the binding of the sulfonamides by sterically blocking an outer ring moiety that is not present in the substrate. This emphasizes that new inhibitors must be designed that strictly stay within the substrate volume in the context of the transition state.

**Keywords:** infectious disease, antibiotics, drug discovery, fitness cost, kinetics, drug susceptibility, bacterial genetics



## INTRODUCTION

Sulfonamides are the oldest class of synthetic antibiotics. They have been in clinical use for over 75 years, with proven efficacy against many microbial infections (Domagk, 1935; Bermingham and Derrick, 2002). Sulfonamides target the enzyme dihydropteroate synthase (DHPS) that catalyzes a key step in microbial folate biosynthesis, the production of 7,8-dihydropteroate from *para*-aminobenzoic acid (*p*ABA) and dihydropterin pyrophosphate (DHPP). Sulfonamides exert their antimicrobial action in two ways, by directly competing with the substrate *p*ABA and through the formation of pterin-sulfa dead-end metabolic products (Roland et al., 1979). Prokaryotes and lower eukaryotes rely on this pathway for the *de novo* synthesis of folate that is a critically important cell metabolite, and disruption of folate biosynthesis therefore severely curtails their growth. In contrast, higher eukaryotes obtain folate directly from their diet and have dispensed with the pathway. The universal presence of DHPS in lower organisms and its absence in higher organisms explains why sulfonamides have been successful as broad-spectrum antimicrobials (Bermingham and Derrick, 2002).

Today, sulfonamides are mainly used in a fix dose combination with trimethoprim (TMP), a dihydrofolate reductase (DHFR) inhibitor. Co-trimoxazole, a combination of sulfamethoxazole (SMX), and TMP, is the most commonly prescribed. This cheap and orally bioavailable combination is used as a second-line therapy to treat a wide variety of bacterial infections including urinary tract infections (UTIs), bronchitis, traveler's diarrhea, and methicillin-resistant *Staphylococcus aureus* (MRSA) infections. Application of co-trimoxazole prophylaxis to prevent *Pneumocystis jirovecii* infections in immunosuppressed patients, such as those undergoing intensive cancer chemotherapy or with advanced HIV infections, has also emerged as a particularly important clinical application (Bermingham and Derrick, 2002).

The emergence of multidrug and pan resistant bacterial pathogens is an alarming and increasing phenomenon that requires immediate action (Boucher et al., 2009). To tackle this problem, we are revisiting previously identified antimicrobial targets and applying new strategies to develop inhibitors that are less prone to resistance mechanisms. Key to this approach is gaining an improved understanding of the targets' biochemical mechanisms, active site structures and resistance mechanisms. In many ways, DHPS is the perfect candidate for such an approach. Structurally and mechanistically, DHPS has been well characterized. The crystal structures of DHPS have been determined from 15 microbial species within the last 20 years, and more recent structural and computational studies from our group have revealed the ordered  $S_N1$  catalytic mechanism and the detailed configuration of the near transition state (Yun et al., 2012). These new insights have already enabled us to generate pyridazine derivatives with improved DHPS inhibition, identify allosteric inhibitors that hinder product release, and develop inhibitory pterin-sulfa conjugates (Zhao et al., 2012, 2016; Hammoudeh et al., 2014).

In this study, we focus on the structural and mechanistic basis of sulfonamide resistance in *S. aureus* DHPS (*Sa*DHPS), and analyze how recurring resistance mutations can selectively disfavor the binding of sulfonamides while retaining the necessary fitness of the enzyme. Crystal structures of DHPS containing pterin•PPi•Mg•*p*ABA and pterin•PPi•Mg•sulfonamide have revealed that *p*ABA and sulfonamides occupy the same locale in the near transition state (Yun et al., 2012). Our focus will be on this locale and how the resistance mutations modulate its structure and dynamics to selectively disfavor the binding of the drug. Our studies proceeded in three stages; (1) bioinformatics analysis to identify the key resistance mutations across organisms, (2) biochemical, resistance and fitness analyses of these mutations in DHPS from *S. aureus*, and (3) structural and computational analyses to understand the mechanistic basis of these mutations. Our goal is to use these results to support ongoing drug discovery efforts toward this enzyme and to develop lead compounds that are not cross-resistant to sulfonamides.

## RESULTS

### Primary and Secondary Mutations Confer Sulfonamide Resistance

The increasing prevalence of MRSA during the past two decades and the associated sequencing of clinical isolates has generated a large dataset of *Sa*DHPS sequence variations in the DHPS-encoding *folP* gene, including those that are found in sulfonamide resistant strains. We rigorously analyzed the available data up to and including 2014 to identify variations that are clearly associated with sulfonamide resistance. We identified two classes of resistance-associated mutations; primary mutations that are directly associated with sulfonamide resistance and secondary mutations that are only found in the presence of the primary mutations. An important goal of this analysis was to differentiate these mutations from the natural variations in *Sa*DHPS that are present in sulfonamide susceptible strains but do not directly contribute to resistance. The results of this survey are summarized in **Table 1**. F17L, S18L, and T51M emerge as primary mutations; F17L occurs at the highest frequency, and S18L and T51M were each observed in less than 1% of sequences surveyed as single variants. E208K and KE257\_dup (a duplication/insertion of Lys-Glu at position 257) were categorized as secondary mutations. E208K is found with both F17L and T51M, and KE257\_dup is only found with F17L. The primary mutation S18L is not found with either of the two secondary mutations. In an earlier study, Hampele and coauthors identified 15 mutations among nine sulfonamide-resistant MRSA clinical isolates that are not present in the sulfonamide susceptible *S. aureus* Rosenbach 25923 strain (Hampele et al., 1997). Although this study also identified F17L, T51M, E208K and KE257\_dup, our analysis showed that the 11 remaining mutations are found in sulfonamide susceptible *S. aureus* strain NCTC 8325 and are apparently natural polymorphisms in *Sa*DHPS that

**TABLE 1** | Survey of DHPS variants and known resistance to sulfonamides.

Sequence Background	25923	8325*	8325	25923	8325	8325	25923	8325	25923	8325
Resistance Mutations	None	None	F17L KE257_dup	T51M E208K	T51M E208K	F17L E208K	F17L	F17L	T51M	S18L
% Sequences (n = 136)	28	49	3	8	1.5	3.7	3	2	0.7	0.7
Hampele Strain			Group 1	Group 2	Group 3	Group 4				
Hampele MIC (μg/mL)			256->1024	256->1024	>1024	>1024				
Sulfonamide resistant	No	No	Yes	Yes	Yes	Yes	ND	ND	ND	ND

Hampele strain group and MIC values have previously been published (Hampele et al., 1997). \*Indicates that among the wild type folP genes surveyed and categorized as having an 8325 background, 31% lacked the natural variations T59S and L64M seen in the *S. aureus* strain Rosenbach 25923 (Supplementary Table 1).

do not contribute to sulfonamide resistance (Supplementary Table 1).

A survey of other organisms was conducted to determine which of these mutations is conserved across species (Table 2). Mutations equivalent to F17L were found in *Neisseria meningitidis* and *Escherichia coli*, and mutations equivalent to T51M were found in *Plasmodium* species, *Pneumocystis carinii*, *Mycobacterium leprae*, and *Streptococcus pneumoniae* (Dallas et al., 1992; Fermer et al., 1995; Lane et al., 1997; Maskell et al., 1997; Wang et al., 1997b; Elena et al., 1998; Kazanjian et al., 1998; Mei et al., 1998; Kai et al., 1999; Williams et al., 2000; Pornthanakasem et al., 2016). A mutation homologous to E208K was also found in *Plasmodium* species but not in conjunction with any of the primary mutations (Pornthanakasem et al., 2016). We did not identify mutations equivalent to S18L or KE257\_dup in other species. Alignment of DHPS sequences from *S. aureus* strains NCTC 8325 and Rosenbach 25923, and nine other microbial pathogens reveals that the primary mutations occur at highly conserved regions of the sequence while the secondary mutations occur in less conserved regions (Figure 1).

## Thermal Stabilities of Sulfonamide Resistant SaDHPS Mutants

To explore how the resistance mutations identified in this study affect the stability of SaDHPS, the “wild type” enzyme from sulfonamide-susceptible strain Rosenbach 25923 and eight defined mutant enzymes were generated, expressed in *E. coli* and purified. Five of the mutant enzymes contained the single mutations F17L, S18L, T51M, E208K, and KE257\_dup, and three contained the clinically observed double mutations F17L/E208K, T51M/E208K, and F17L/KE257\_dup. The DHPS from sulfonamide susceptible *S. aureus* strain NCTC 8325 that harbors the 11 background variations not associated with sulfonamide resistance was also expressed and purified as a further control.

Thermal shift assays were employed to measure the denaturation temperatures ( $T_M$ ) of the purified proteins and to assess whether the mutations affect their stabilities

**TABLE 2** | DHPS mutations associated with sulfonamide resistance in *S. aureus*, and their homologs in *E. coli* (Dallas et al., 1992), *N. meningitidis* (Ferner et al., 1995), *B. anthracis* (Yun et al., 2012), *S. pneumoniae* (Maskell et al., 1997), *P. falciparum* (Wang et al., 1997a), *P. vivax* (Pornthanakasem et al., 2016), *M. leprae* (Kai et al., 1999), and *P. carinii* (Mei et al., 1998).

Classification	Mutation	Location	Similar Mutations in Other Microbial Species
Primary	F17L	Loop 1	<i>E. coli</i> , <i>N. meningitidis</i> , <i>B. anthracis</i>
	S18L	Loop 1	None
	T51M	Loop 2	<i>S. pneumoniae</i> *, <i>P. falciparum</i> *, <i>P. vivax</i> *, <i>M. leprae</i> *, <i>P. carinii</i>
Secondary	E208K	α-helix Loop 7	<i>P. falciparum</i> <sup>†</sup> , <i>P. vivax</i> <sup>†</sup>
	KE257_Dup	α-helix 8	None

\*<sup>†</sup>, Indicate that mutations align with T51M and E208K, respectively, but are not strictly conserved (Figure 1).

(Table 3). These experiments were performed using Sypro-Orange that fluoresces when exposed to the hydrophobic interior of unfolded proteins upon denaturation. The SaDHPS primary mutations did not significantly alter the  $T_M$ , falling within 1°C of wild type 25923. In contrast, the secondary mutations E208K and KE257\_dup both result in a 3–4°C drop in  $T_M$ , revealing that these secondary mutations destabilize the protein structure. Addition of the F17L or T51M mutations to E208K maintains the 3–4°C drop in  $T_M$  whereas addition of the F17L mutation to KE257\_dup restores the stability of the protein. These results are consistent with the SaDHPS crystal structure (Hampele et al., 1997). F17, S18, and T51 are in the two flexible loops 1 and 2 that are disordered in the absence of substrates and unlikely to contribute to the stability of the protein fold. In contrast, E208 is part of a salt bridge array involving R176, R204, and K207 that appears to stabilize this region of the protein. The structural basis for the reduction in stability produced by the KE257\_dup mutation is not so obvious and it may simply result from its location at the dimer interface. However, the compensation

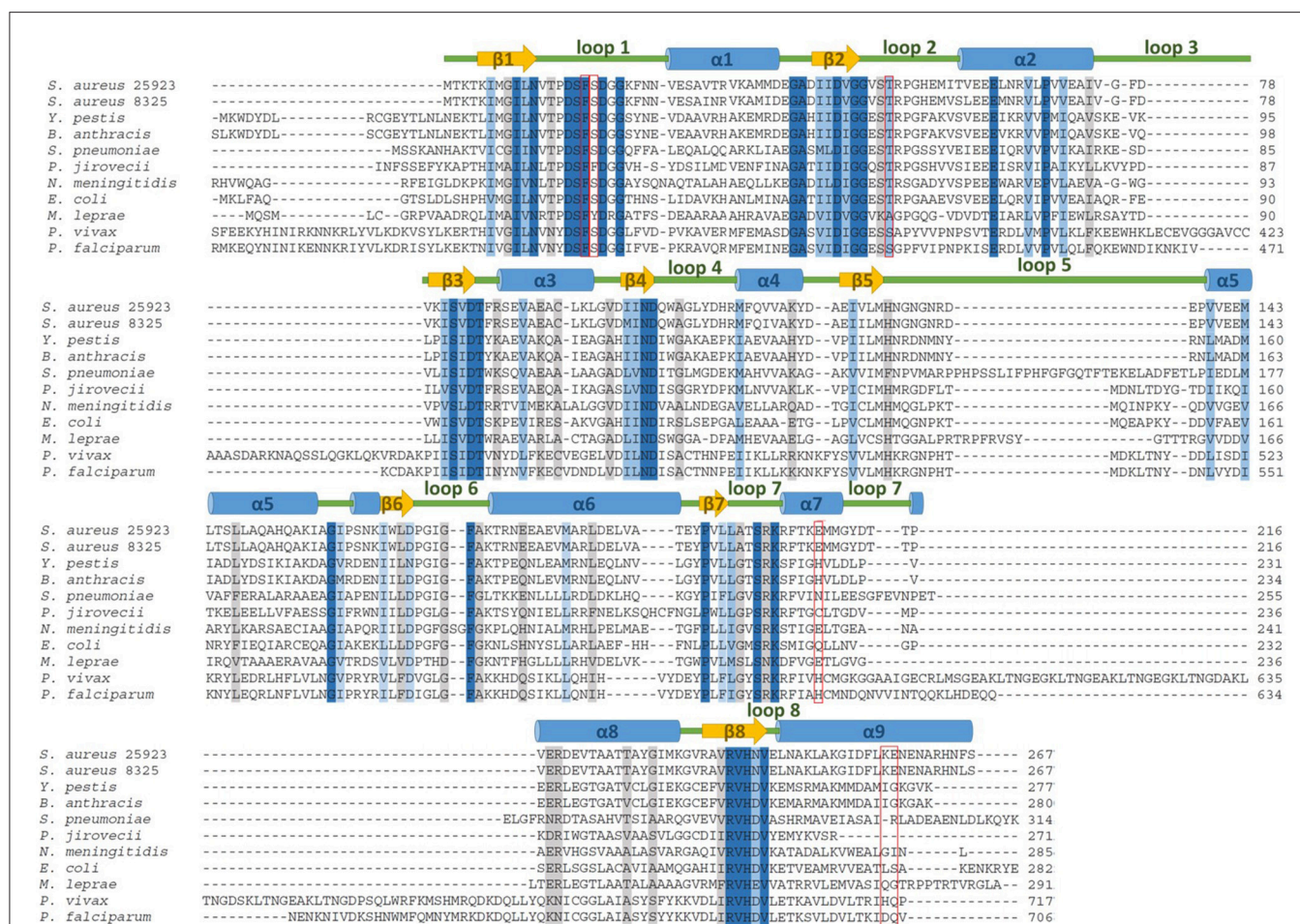


**FIGURE 1 |** DHPS amino acid sequence alignment for *S. aureus* wild type representatives used in this study and nine other clinically relevant microbial pathogens. The five mutations that directly contribute to sulfonamide resistance are boxed in red. Amino acids that are 100% conserved, highly conserved and weakly conserved are highlighted in dark blue, light blue, and gray, respectively.

in stability provided by F17L suggests that it may involve the dynamic allosteric communication between the interface and the active site that we previously described (Hammoud et al., 2014). The DHPS from NCTC 8325 is  $\sim 4^\circ\text{C}$  more stable than wild type DHPS from Rosenbach 25923, indicating that the 11 background mutations generate an inherently more stable enzyme.

## Catalytic Properties of Sulfonamide Resistant SaDHPS Mutants

We then analyzed the kinetic properties of the purified proteins (Table 4). The  $K_M$  values for DHPP, *p*A<sub>BA</sub> and SMX were measured using a colorimetric assay that monitors the release of pyrophosphate. The  $K_i$  values of SMX were derived from a radiometric assay that monitors the incorporation of  $^{14}\text{C}$ -labeled *p*A<sub>BA</sub> into the 7,8-dihydropteroate product. The  $K_{cat}$  values for *p*A<sub>BA</sub> and SMX were also derived from the colorimetric assay. The primary mutations F17L, S18L and T51M impart a slight increase in the  $K_M$  for DHPP, but significantly larger increases for *p*A<sub>BA</sub>. In contrast, the effects are reversed for the secondary

mutations where the increases in the DHPP  $K_M$  values are more pronounced than those for *p*A<sub>BA</sub>. When the primary and secondary mutations are combined, they consistently lower the *p*A<sub>BA</sub>  $K_M$  values toward that of the wild type protein and increase the DHPP  $K_M$  values to those seen in the secondary mutations alone. As anticipated, the  $K_M$  and  $K_i$  values for SMX showed that the drug efficiently binds and inhibits the wild type enzyme. F17L, both alone and in combination with the two secondary mutations, decreases the binding and inhibition of SMX, but this was not the case with T51M where the effects were less obvious. S18L also significantly increased the  $K_M$  for SMX but it was not possible to measure the  $K_i$  value for technical reasons. The same was true for the secondary mutations alone.

The kinetic data confirmed that SMX is a *bona fide* substrate of DHPS, although the turnover rates with the natural substrate *p*A<sub>BA</sub>, as reflected in the  $K_{cat}$  values, were consistently lower for all the variants. The individual mutations, both primary and secondary, decreased the turnover rates for both ligands, which confirms that the catalytic efficiency is compromised by each mutation. Somewhat surprisingly, apart from F17L/KE257\_dup,



there was an additive decrease in turnover rates for both *pABA* and *SMX* when the primary and secondary mutations are combined. Thus, the “rescue” of the *pABA*  $K_M$  by the secondary mutations does not translate into a similar rescue of  $K_{cat}$ .

### Resistant Mutations and Antibacterial MIC Values

To determine the individual effects of the identified resistance mutations in *S. aureus*, we measured the MIC values of isogenic strains that only contained the mutant DHPS enzymes (Supplementary Table 1). It was first necessary to perform allelic replacements of the wild type *folP* gene with the mutant genes to generate the required strains in a USA300 AH1263 background, and this was successful for seven of the eight mutants that were biochemically analyzed. We failed to generate an isogenic strain containing the T51M/E208K double mutation after several attempts, and we therefore used the COL *S. aureus* strain that naturally harbors these mutations for

select experiments. We and others have found that metabolic intermediates and nutrients in standard testing media can mask the action of antibiotics, including sulfonamides, and that minimal inhibitory concentration (MIC) determinations are more easily and accurately performed in minimal media (Zlitni et al., 2013; Zhao et al., 2016). We therefore measured the MICs of the nine *S. aureus* strains in minimal SSM9PR media lacking *pABA* and several products of folate biosynthesis (Reed et al., 2015). We used chloramphenicol (CAM) as the control antibiotic that does not act through the folate pathway, and it has an MIC of 3.1–4.2  $\mu\text{g/mL}$  for all strains tested. The results are summarized in Table 5. The most notable increase in resistance by a primary mutation occurred in the T51M mutant with dapsone, which is a structurally distinct member of the sulfonamide class. It is therefore significant that a homologous loop 2 mutation is also observed in *M. leprae* and two malarial strains (Table 2), for which dapsone is a common treatment option (Matsuoka, 2010).

Individually, the primary mutations increased the MIC for most of the 10 sulfonamides tested in this study, but not markedly. F17L had the greatest impact, but only 4- to 5-fold for three of the sulfonamides. S18L and T51M had minimal effect, and the same was true for the two secondary mutations, apart from T51M with dapsone. In contrast, the combination of primary and secondary mutations dramatically increased the MIC values for all 10 sulfonamides. The largest effect was observed with T51M/E208K (Table 5), but this may be related to strain variability because this double mutation was evaluated in the COL *S. aureus* strain rather than as an allelic replacement in USA300 AH1263.

TMP targets DHFR within the folate pathway downstream of DHPS, and changes in the TMP MIC may indicate fitness costs associated with DHPS mutations. The primary resistance mutations significantly decreased TMP MIC, but the secondary mutations alone had negligible effect. When combined, the secondary mutations decreased the effect of the F17L mutant. Addition of *pABA* to the testing media universally restored the TMP MICs closer to wild type for all the mutants. This could indicate that defects in catalysis caused by primary

**TABLE 3 |** Changes in thermal stabilization of DHPS imparted by the observed sulfonamide resistant variations.

DHPS Variant		$T_M$ ( $^{\circ}\text{C}$ )	$\Delta T_M$ ( $^{\circ}\text{C}$ )
Rosenbach 25923		38.63 $\pm$ 0.09	
NCTC 8325		42.48 $\pm$ 0.01	
Primary mutation	F17L	39.14 $\pm$ 0.0	0.51
	S18L	39.52 $\pm$ 0.003	0.89
	T51M	38.7 $\pm$ 0.09	0.07
Secondary mutation	E208K	34.89 $\pm$ 0.04	−3.74
	KE257_dup	34.26 $\pm$ 0.1	−4.37
Double mutation	F17L E208K	34.77 $\pm$ 0.05	−3.86
	F17L KE257_dup	40.34 $\pm$ 0.14	1.71
	T51M E208K	35.67 $\pm$ 0.05	−2.96

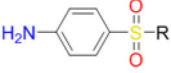
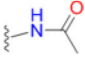
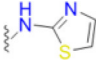
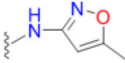
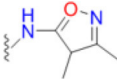
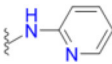
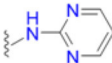
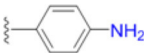
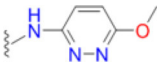
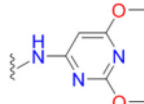
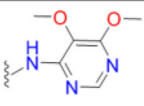
Changes in melting temperature ( $\Delta T_M$ ) are relative to the Rosenbach 25923 wild type DHPS enzyme.

**TABLE 4 |** Kinetic characterization of *S. aureus* DHPS variants.

saDHPS Variant		Native Substrate		SMX Antibiotic		Substrate Turnover	
		$K_M$ DHPP ( $\mu\text{M}$ )	$K_M$ pABA ( $\mu\text{M}$ )	$K_M$ SMX ( $\mu\text{M}$ )	$K_i$ SMX ( $\mu\text{M}$ )	$K_{cat}$ pABA ( $\text{s}^{-1}$ )	$K_{cat}$ SMX ( $\text{s}^{-1}$ )
Primary mutation	Wild Type	10.0 ( $\pm$ 1.4)	3.1 ( $\pm$ 0.9)	5.9 ( $\pm$ 0.2)	1.3 ( $\pm$ 0.5)	4.5 ( $\pm$ 0.4)	2.2 ( $\pm$ 0.1)
	F17L	18.3 ( $\pm$ 4.7)	40.2 ( $\pm$ 6.1)	202 ( $\pm$ 54)	94.1 ( $\pm$ 23.7)	1.7 ( $\pm$ 0.3)	1.0 ( $\pm$ 0.1)
	S18L	10.2 ( $\pm$ 1.8)	26.2 ( $\pm$ 0.2)	140 ( $\pm$ 40)	ND	3.4 ( $\pm$ 0.2)	1.6 ( $\pm$ 0.1)
	T51M	12.1 ( $\pm$ 2.6)	29.8 ( $\pm$ 13.2)	3.9 ( $\pm$ 1.6)	10.0 ( $\pm$ 0.68)	1.9 ( $\pm$ 0.2)	0.8 ( $\pm$ 0.1)
Secondary mutation	E208K	34.5 ( $\pm$ 2.2)	15.7 ( $\pm$ 4.5)	ND	ND	3.1 ( $\pm$ 0.0)	1.5 ( $\pm$ 0.1)
	KE257_Dup	21.1 ( $\pm$ 1.6)	5.3 ( $\pm$ 3.0)	ND	ND	1.8 ( $\pm$ 0.0)	0.9 ( $\pm$ 0.2)
Double mutants	F17L E208K	21.3 ( $\pm$ 6.8)	13.1 ( $\pm$ 2.6)	167.5 ( $\pm$ 43.6)	362.1 ( $\pm$ 33.3)	0.5 ( $\pm$ 0.0)	0.3 ( $\pm$ 0.1)
	T51M E208K	38.1 ( $\pm$ 1.5)	9.2 ( $\pm$ 3.5)	5.7 ( $\pm$ 3.0)	29.0 ( $\pm$ 2.7)	0.5 ( $\pm$ 0.1)	0.3 ( $\pm$ 0.0)
	F17L KE257_Dup	22.3 ( $\pm$ 5.6)	14.3 ( $\pm$ 3.3)	26.0 ( $\pm$ 6.0)	158.9 ( $\pm$ 31.7)	3.6 ( $\pm$ 0.3)	2.1 ( $\pm$ 0.2)

DHPP, pABA and SMX  $K_M$  and  $K_{cat}$  values were measured using a colorimetric assay that monitors pyrophosphate release. A radiometric assay that monitors  $^{14}\text{C}$ -labeled pABA incorporation into 7,8-dihydropteroate was used to determine the SMX  $K_i$  values.

TABLE 5 |  $\mu\text{g/ml}$  MIC<sub>80</sub> values for DHPS variants.

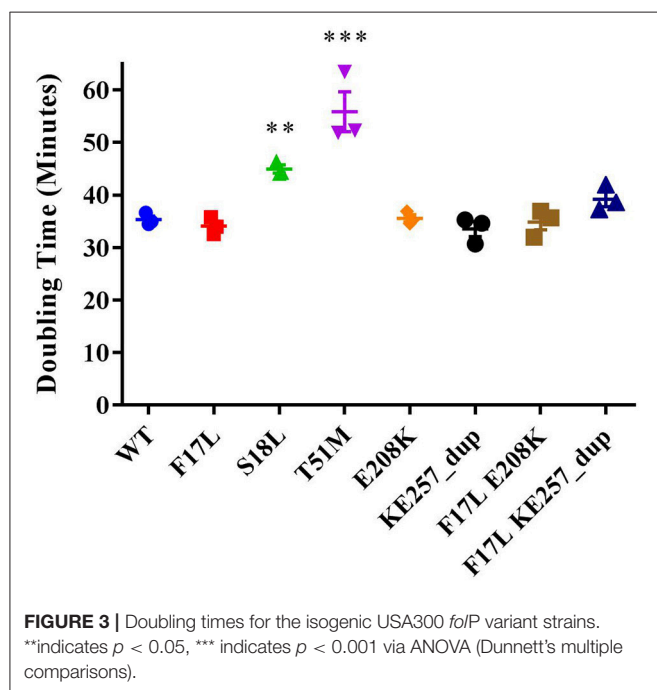
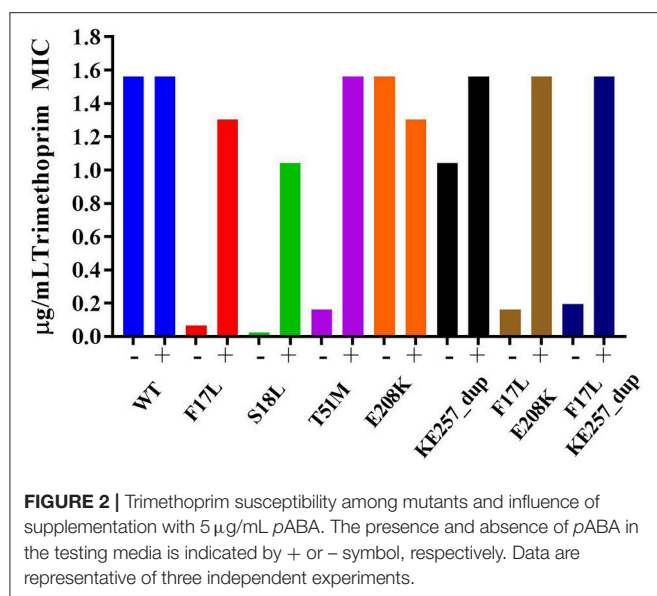
<div></div>	Primary mutation				Secondary mutation		Double mutation			
	R	WT	F17L	S18L	T51M	E208K	KE257_dup	F17L E208K	F17L KE257_dup	T51M E208K*
Sulfacetamide		25	41.7	20.8	12.5	50	41.7	200	133.3	200 – >200
Sulfathiazole		2.6	12.5	4.2	3.1	8.3	8.3	41.7	41.7	83.3
Sulfamethoxazole		4.2	16.7	10.4	6.3	8.3	8.3	50	41.7	66.7
Sulfisoxazole		2.1	6.3	5.2	2.1	6.3	6.3	25	25	58
Sulfapyridine		33.3	100	50	66.7	50	50	200	200 – >200	>200
Sulfadiazine		10.4	25	25	8.3	20.8	20.8	83.3	83.3	200
Dapsone		16.7	20.8	6.3	50	33.3	29.2	50	66.7	200 – >200
Sulfamethoxypyridazine		7.3	25.0	25.0	7.3	12.5	16.7	83.3	83.3	133.3
Sulfadimethoxine		2.6	12.5	4.2	3.6	8.3	8.3	33.3	25	66.7
Sulfadoxine		25	33.3	41.7	12.5	50	41.7	200	83.3	200 – >200
Chloramphenicol		4.2	4.2	3.1	3.1	3.1	3.1	3.1	3.1	3.1
Trimethoprim		1.6	0.065	0.024	0.16	1.6	1.0	0.16	0.20	2.1
Sulfamethoxazole <sup>§</sup>		0.39	0.78	0.33	0.39	0.52	0.65	1.6	1.6	3.1
Trimethoprim		0.021	0.041	0.017	0.021	0.027	0.034	0.082	0.082	0.16

MIC<sub>80</sub> values reported are an average of three experiments. Apart from T51M/E208K, all mutants were cloned via allelic replacement into an isogenic USA300 AH1263 panel. \*T51M/E208K values were derived from the COL *S. aureus* strain (Supplementary Table 1). <sup>§</sup>The SMX/TMP combination MICs at the bottom of the Table represent co-trimoxazole at a ratio of 19:1.

mutations in DHPS cause the downstream enzyme DHFR to become more crucial for overall pathway function, resulting in heightened susceptibility to DHFR inhibition as indicated by the lowered TMP MICs (Figure 2). The supplementation of *p*A<sub>BA</sub> may boost DHPS catalytic output, thus returning the TMP MICs to wild type levels. Appreciable increases in the co-trimoxazole SMX/TMP combination MICs were only observed with the double mutants, likely because the heightened TMP susceptibility of primary mutants drives the combination MIC closer to wild type levels despite having resistance to SMX (Table 5).

### Fitness Studies of the folP Mutants

The kinetic data showed that the primary resistance mutations raise the *K<sub>M</sub>* of *p*A<sub>BA</sub> and the secondary mutations lower the *p*A<sub>BA</sub> *K<sub>M</sub>* back toward the value observed in the wild type enzyme. Furthermore, the TMP MIC testing revealed fitness consequences imposed by primary mutations at later stages of the folate biosynthesis pathway that could be restored by secondary mutation. Thus, the secondary mutations appear to restore the fitness of DHPS that is impaired by the primary mutations. To test whether these apparent changes in fitness of the isolated enzyme affect bacterial cell growth, the doubling



times for the eight isogenic strains were measured (Figure 3). The strain harboring T51M had the slowest growth rate, but F17L did not have an altered growth rate. This was surprising because F17L had the highest consequence to *pABA* binding (Table 4). However, the neighboring mutation S18L also had a significantly increased doubling time relative to the wild type enzymes. The remaining four mutations had no significant effect on doubling time.

To test whether the changes in fitness might become apparent *in vivo*, the isogenic *S. aureus* strains were subjected to a wax moth larvae infection study (Figure 4). In this model

system, the larvae were infected with *S. aureus* strains from our isogenic panel of DHPS variants (Supplementary Table 1) and larval mortality rates were monitored. It was assumed that any significant decrease in the virulence of a particular strain would reflect the fitness cost associated with its introduced DHPS variant. Overall mortality rates at the end of the 72-h survival study indicated that the T51M mutant displayed the least virulence, consistent with the cell growth studies, but there were no significant changes in mortality-based virulence among any of the mutants according to Mantel Cox (Log-Rank) analysis. However, the wax moth larval model did respond as predicted in the presence of SMX. When administered 100 mg/kg SMX daily, the larvae could be rescued from the susceptible wild type strain, but every mutant strain was resistant to the antibiotic.

## Structural and Biophysical Analyses of the *pABA*/SMX Binding Pocket

Having revealed the importance of Phe17, Ser18, and Thr51 in sulfa drug resistance, we re-examined their structural roles in the context of the near-transition state structure. We first modeled and energy minimized the structures of the *Sa*DHPS near transition states in the presence of *pABA* and SMX using our previously determined crystal structures of *Yp*DHPS (Yun et al., 2012). This proved to be very straightforward because the residues are highly conserved in the DHPS active site locale. Like all DHPS structures, loops 1 and 2 are disordered in the absence of substrates but become ordered in the near-transition state to create the *pABA*-binding pocket and to structurally and chemically optimize the substrates for catalysis (Yun et al., 2012). This *Sa*DHPS active site locale is shown in Figure 5A, which highlights the roles of Phe17, Ser18, and Thr51. Phe17, together with Pro53, Phe172, and Lys203 create the *pABA*-binding pocket, with the side chain rings of Phe17, Pro53, and Phe172 forming edge-to-face interactions with the phenyl ring of *pABA*. The adjacent Ser18 does not interact with *pABA* but appears to stabilize loop1 in this region. Meanwhile, the hydroxyl group of Thr51 forms hydrogen bonds with the amino group of *pABA* and an oxygen of the pyrophosphate group that has been released from DHPP prior to the  $S_N1$  reaction that forms the product (Yun et al., 2012). Thr51 appears to help align the amino group for bond formation to the C11 carbon atom of the pterin substrate.

To gain more insights into the formation of the transition state ordered loop structure and the binding of *pABA* and sulfonamides, we used isothermal titration calorimetry (ITC). ITC revealed that, while *pABA* and pyrophosphate are both absolutely required to generate the *pABA*-binding pocket, the pterin moiety of DHPP is not necessary (Figure 6). This is consistent with the ordered loop structure that makes multiple conserved interactions with the enclosed *pABA* and pyrophosphate while the pterin moiety is independently accommodated in an adjacent preformed pocket (Figure 5A). The binding thermodynamics of SMX are almost identical to those of *pABA* (Figure 6), which is consistent with our published structures that show that both occupy the binding pocket created by loops 1 and 2 in almost identical fashion



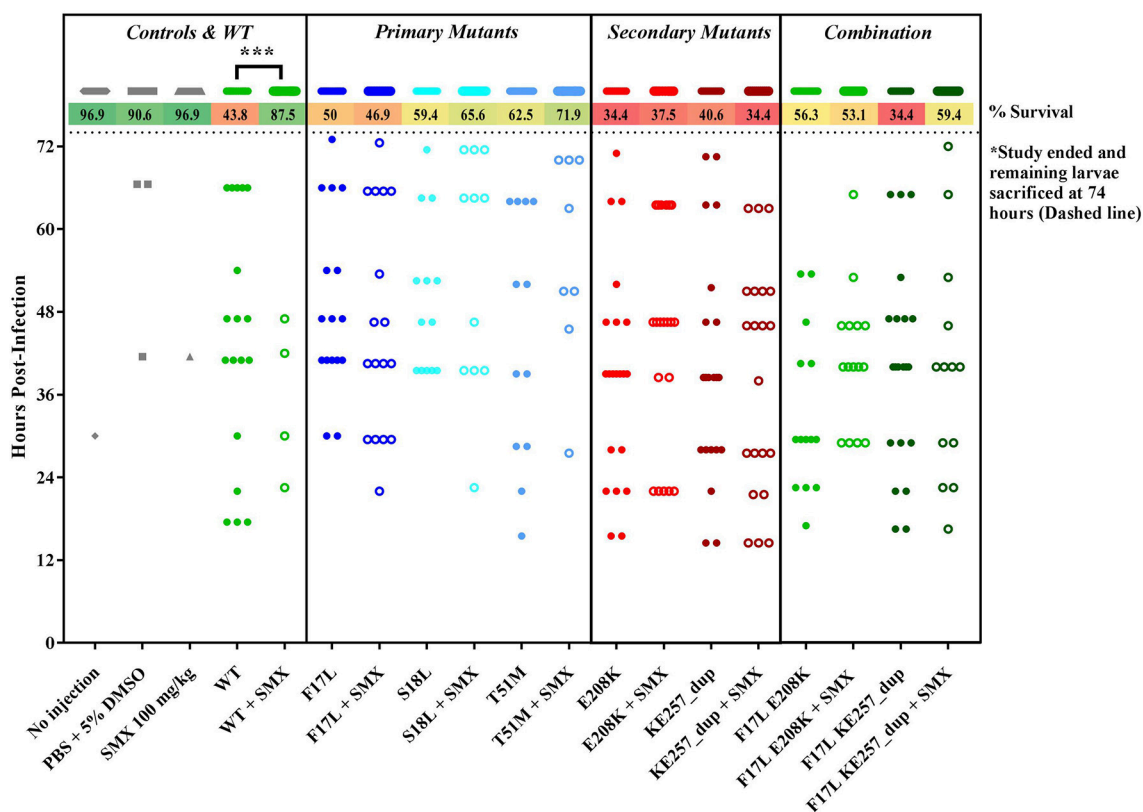


**FIGURE 4 |** Wax moth larvae rescue study with isogenic USA300 *folP* variants. All groups contain 32 larvae and each data point indicates an observed death. Percentage survival at the end of the study is listed at the top. \*\*\* indicates  $P < 0.001$  via Mantel Cox (Log-Rank) survival analysis.

(Yun et al., 2012). In the presence of pyrophosphate, *pABA* and SMX have negative free energy ( $-6.9$  and  $-6.8$  kcal/mol respectively) reflecting a spontaneous binding interaction. The negative enthalpy measured in these studies is indicative of binding interactions driven by hydrogen bonding or  $\pi$ -stacking, again consistent with our structures. Finally, the significant entropic penalty associated with the binding of *pABA* and SMX is consistent with the observed ordering of loops 1 and 2.

## Structural Analyses of SaDHPS F17L/E208K

We crystallized SaDHPS F17L/E208K and determined its structure in the absence of ligands (apo) and with our previously published (Zhao et al., 2016) inhibitory pterin-sulfisoxazole conjugate compound 1530 (Figures 5B,C, respectively). In the published SaDHPS wild type structures, Phe17 within loop1 is either distant from the active site locale or missing (Hampele et al., 1997). However, in our two F17L/E208K structures, F17L and loop1 adopt a conformation that is similar but not identical to the known conformation of loop1 in the near transition state (compare the position of Phe17 in Figure 5A with the positions of Leu17 in Figures 5B,C). We have previously shown that compound 1530 binds to the wild type DHPS active site locale in a similar fashion to the pterin substrate and SMX in the

near transition state (Yun et al., 2012; Zhao et al., 2016). In the F17L/E208K mutant structure complexed with compound 1530, Leu17 is directly adjacent to, and may therefore sterically impact, the oxazole ring of sulfisoxazole (Figure 5C).

The structural consequences of the E208K mutation are apparent from our two structures. In the wild type SaDHPS structures, Glu208 forms a salt bridge with Arg176 and the adjacent Glu179 forms a salt bridge with Arg204 (Figure 5D). Arg176 and Arg204 also interact via a  $\pi$ -stacking interaction to stabilize this 4-residue cluster. When the E208K mutation is introduced, Arg176 relocates to form a salt bridge with Glu179 and Arg204 is displaced (Figures 5B,C). The structures suggest three ways in which the E208K mutation can contribute to resistance. First, the relocated Arg204 is adjacent to the oxazole ring in the 1530 complex (Figure 5C) and may sterically interfere with the transition state binding of sulfa drugs that have similar moieties (Table 5). The relocated Arg204 does not impact the phenyl ring of 1530 and should therefore have minimal impact on the binding of *pABA* that occupies the same location. Second, the relocated Arg204 may form a stabilizing salt bridge with the carboxyl group of *pABA* and thereby compensate for the negative impact on *pABA* binding of the F17L and T51M mutations. The equivalent of this interaction with the negatively charged sulfone of sulfisoxazole is visible in Figure 5C. Finally, disruption of the Arg176/Glu179/Arg204/Glu208 salt bridge substructure

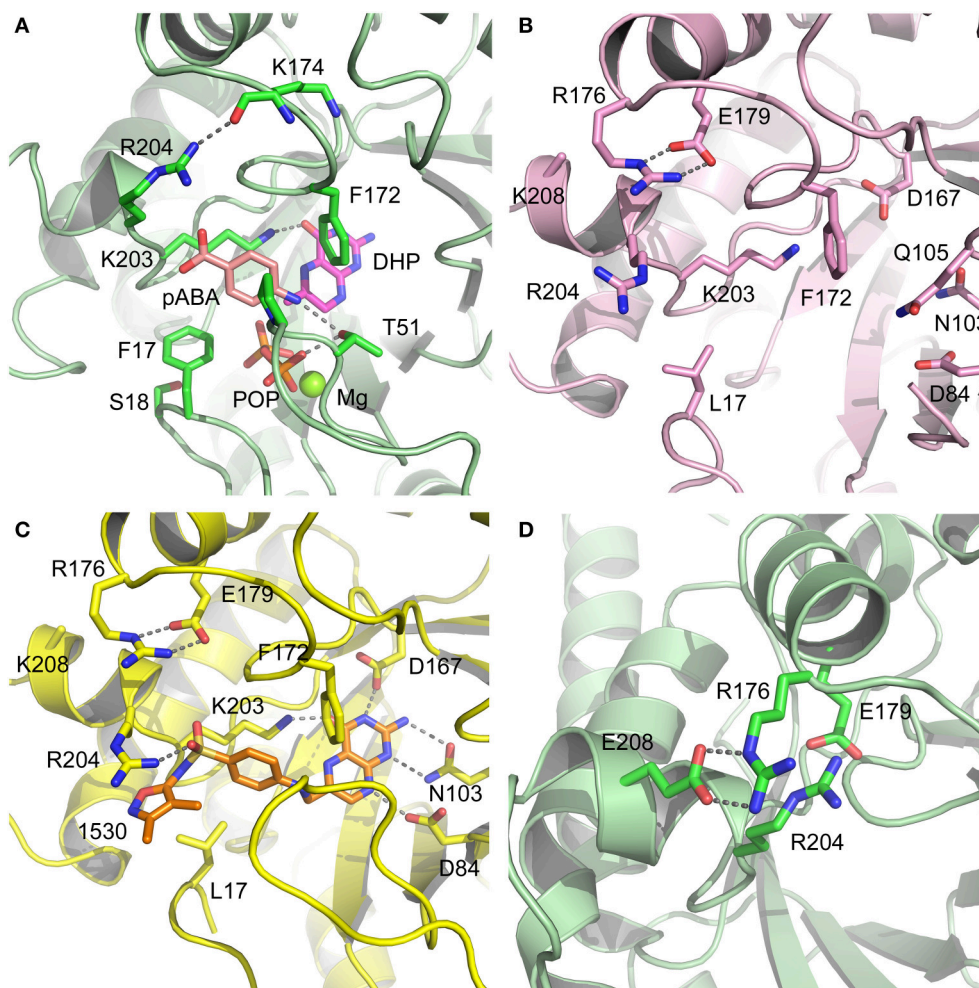


**FIGURE 5 | DHPS active site locale.** (A) The modeled *S. aureus* DHPS transition state based on the published *Y. pestis* structure (3TYZ) highlighting the *pABA* environment. The protein backbone is shown in pale green cartoon, the residues are in stick representation with green carbon, *pABA* and DHP are in stick representation with salmon and magenta carbons, respectively, and pyrophosphate is orange. The essential  $Mg^{2+}$  ion is shown as a fluorescent green ball. (B) The mutated salt bridge arrangement in the crystal structure of SaDHPS-F17L-E208K. The protein backbone is shown in purple cartoon, and the residues are in stick representation with purple carbons. (C) The mutated salt bridge arrangement in the crystal structure of the SaDHPS-F17L-E208K-1530 compound complex. The protein backbone is shown in yellow cartoon, the residues are in stick representation with yellow carbons, and compound 1530 is in stick representation with orange carbons. (D) The wild type SaDHPS salt bridge arrangement adjacent to the active site locale from the previously published crystal structure (1AD1). The coloring is the same as (A). In all figures, the dashed gray lines indicate salt-bridges and hydrogen bonds.

may introduce some local flexibility to facilitate the distortions of the *pABA*-binding site caused by the F17L, S18L, and T51M mutations. This is consistent with the thermal shift assay data for E208K (Table 3).

### Modeling Studies of F17L, S18L, and T51M in the Transition State

We failed to obtain crystal structures of F17L, S18L, and T51M and we therefore turned to modeling and energy minimization to gain further insights into their roles in resistance. We introduced the three mutations independently into the two modeled SaDHPS transition state structures containing *pABA* or SMX, and performed energy minimization. The side chain of Leu17 is predicted to adopt the same rotamer in the *pABA*

and SMX complexes that minimally impacts the transition state structure. However, while this rotamer maintains a favorable and close interaction with *pABA*, it sterically impacts the methylisoxazole ring of SMX. In the case of T51M, the mutation appears to have an indirect affect by impacting the location of Pro53 in loop2. As described above, Pro53 loosely forms part of the *pABA* binding pocket, but it forms a tight van der Waals interaction with the methylisoxazole ring of SMX. The modeling suggests that any movement of Pro53 toward the methylisoxazole ring caused by T51M would selectively disfavor the binding of SMX compared to *pABA*. Modeling with S18L did not yield a clear answer, but we suggest that it also acts indirectly to impact the position of the adjacent Phe17. The conclusions from these modeling studies are summarized in Figure 7.

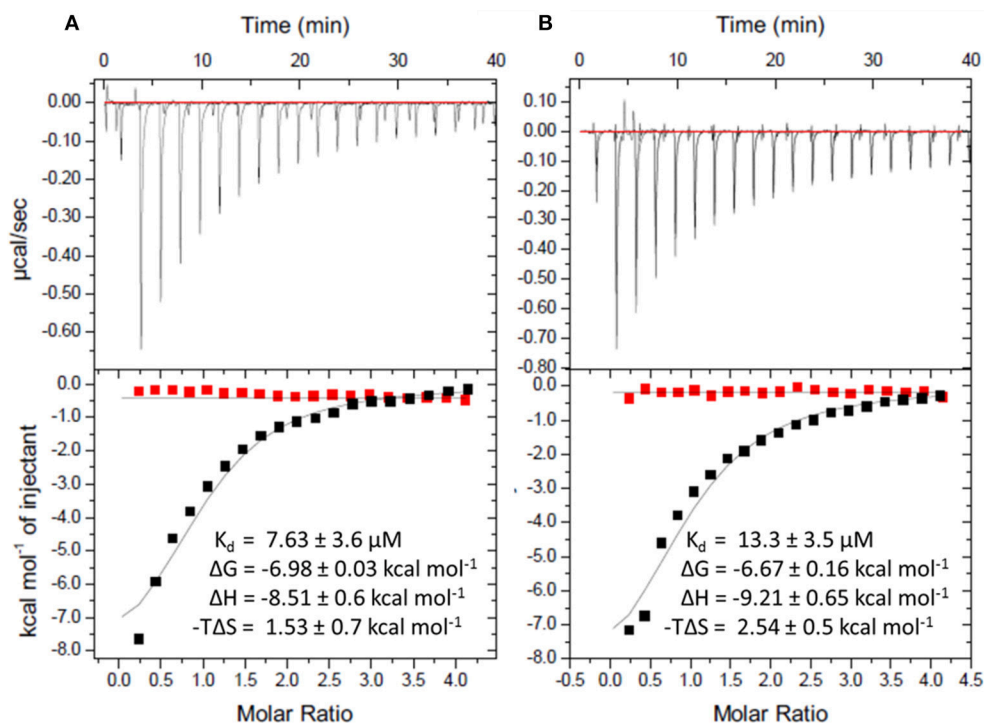


**FIGURE 6 |** Isothermal titration calorimetric analysis of *pABA* or SMX binding to DHPS in the presence and absence of sodium pyrophosphate. Trace of the calorimetric titration of  $19 \times 2 \mu\text{l}$  aliquots of  $500 \mu\text{M}$  *pABA* (A) or SMX (B) into  $25 \mu\text{M}$  DHPS (top) and integrated binding isotherms (bottom). Red squares represent the heat of binding in the absence of sodium pyrophosphate. Black squares represent heat of binding in the presence of  $10 \text{ mM}$  sodium pyrophosphate. The solid black lines represent the best fit to a one site model. The derived thermodynamic parameters are shown as insets in the lower panel.

## DISCUSSION

The output of novel antibiotic classes has been greatly reduced in recent years, and there is a crucial need for new orally bioavailable antimicrobials effective against pathogenic *Staphylococci* such as MRSA and vancomycin-resistant *S. aureus* (VRSA). The folate biosynthesis pathway remains a viable target for inhibitor development due to the essentiality of this pathway in microbes. Indeed, sulfonamides that target the DHPS enzyme in the folate pathway remain a useful treatment option for common infection types such as UTIs, skin and soft tissue infections, and osteomyelitis (Liu et al., 2011). Opportunities for new therapies that target the folate pathway are afforded by continuing advances in our understanding of the catalytic mechanisms of DHPS and other component enzymes such as 6-hydroxymethyl-7,8-dihydropterin pyrophosphokinase (Shi et al., 2012; Dennis et al., 2016), and powerful new technologies to probe and exploit these mechanisms. In this study, we have analyzed the sequences of DHPS from sulfonamide resistant clinical isolates of *S. aureus* to identify the biochemical and structural basis of resistance. This information will be invaluable for developing new therapeutics that target DHPS and minimize the potential for resistance.

We have demonstrated using bioinformatics, biochemistry and microbiological analyses that five mutations in the enzyme DHPS directly contribute to sulfonamide resistance. We designated three of these mutations, Phe17, Ser18, and Thr51, as

“primary” because one of these mutations is consistently present in resistant strains, and two mutations, E208K and KE257\_dup, as “secondary” because they only appear in the presence of the primary mutations. Our crystallographic and modeling analyses reveal how these mutations achieve this resistance at the structural level. The three amino acids altered by primary mutations are highly conserved and have fundamental roles in creating the transition state structure in which two otherwise flexible loops become ordered by the pyrophosphate of DHPP and create a pocket that is bound and stabilized by *pABA* (Yun et al., 2012). ITC data reported here confirm this mechanism. Sulfonamides are exquisite mimics of *pABA* that can also engage this pocket, and we demonstrate by measuring the  $K_M$  values that the primary mutations have a greater negative impact on sulfonamide binding compared to *pABA*. Previous studies have also reported this phenomenon (Fermer and Swedberg, 1997; Vedantam and Nichols, 1998; Gibreel and Sköold, 1999; Haasum et al., 2001; Levy et al., 2008). The secondary mutations partially restore *pABA* binding to the wild type levels but do not restore the catalytic efficiency that is significantly reduced by the primary mutations. This is consistent with a recent study on clinical mutations in *Plasmodium* species that showed similar additive increases in sulfonamide  $K_i$  and whole-cell resistance (Pornthanakasem et al., 2016).

Thus, the mechanism of resistance is based on increasing the  $K_M$  of the sulfonamides compared to *pABA*, and the organism



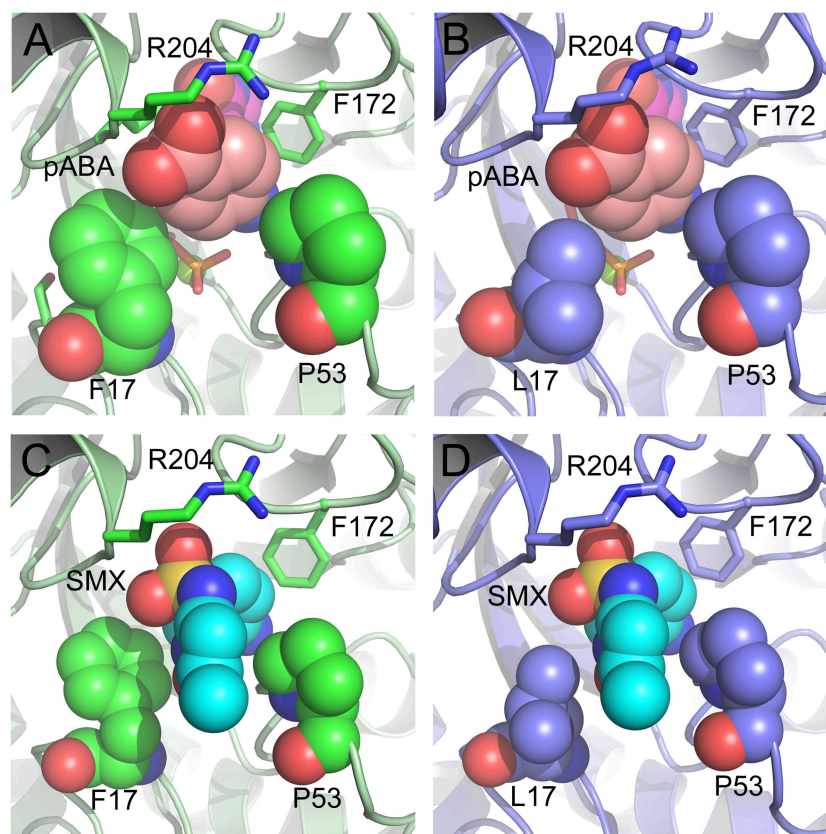


**FIGURE 7** | Close up view of the wild type and F17L mutant of SaDHPS in complex with *p*ABA and sulfamethoxazole (SMX). **(A)** Wild type with *p*ABA. **(B)** F17L with *p*ABA. **(C)** Wild type with SMX. **(D)** F17L with SMX. Color scheme – wild type SaDHPS, green carbons and ribbon; F17L SaDHPS, violet carbons and ribbon; *p*ABA, salmon carbons; SMX, cyan carbons. The complexes were modeled using the YpDHPS transition state complexes (PDB ID: 3TYZ and 3TZF).

can apparently survive with a less efficient DHPS enzyme under drug selective pressure. Our structural studies reveal that the discrimination between the binding of sulfonamides compared to *p*ABA is via the electron deficient outer ring, exemplified by methylisoxazole in SMX, that is required to generate the negative charge on the sulfone that mimics the carboxyl group of *p*ABA. As shown in **Figures 5, 7**, all three primary mutations appear to impact this ring and therefore the binding of the entire drug. The same is also true for the E208K secondary mutation that leads to a reorganization of a salt bridge structure adjacent to the active site locale that also appears to disfavor the binding of sulfonamides via this outer ring moiety. The way in which KE257\_dup functions at the dimer interface is less apparent. We suggest that it operates allosterically based on our previous studies that identified inhibitory compounds that bind at the dimer interface, rigidify the dimer and significantly slow down the release of product (Hammoudeh et al., 2014). Overall, the data are most consistent for the F17L/E208K double mutant. The kinetics, sulfonamide susceptibility, crystal structures and modeling all present a consistent picture of how these two mutations work in concert to efficiently produce high levels of resistance. This double mutation results in a high level of

resistance and is frequently observed in sulfonamide resistant strains of *S. aureus*.

Avoiding resistance is a key component of any successful drug discovery regime, as has been shown with other notoriously mutable targets such as the essential NS3/4A protease component of the hepatitis C virus (HCV). Structural studies with this protease indicated that the most marked increases in resistance are seen among inhibitors that extend beyond the “substrate envelope,” or consensus volume assumed by native substrate binding (Romano et al., 2010). Our studies reveal the same basic mechanism of resistance in DHPS but also show the importance of secondary mutations that can partially offset the negative impact of primary resistance mutations on enzyme function. Developing inhibitors that only occupy the volume assumed by native substrates will continue to be a key strategy in our drug discovery efforts on DHPS and other key enzymes in the folate pathway (Yun et al., 2014). An important conclusion from our studies is that continued development of the sulfonamide scaffold focused on the ring extending beyond the native substrate binding pocket is fundamentally flawed. Historically, structure activity relationship efforts to improve the efficacy of sulfonamides have focused on the outer ring which also produces more favorable potency and ADME properties.

Although sulfanilamide and sulfacetamide lack this ring moiety, they are significantly less potent, and all potent sulfonamides are therefore inherently vulnerable to this mechanism of resistance (Greenwood, 2010).

Our studies demonstrate that the biochemical data derived from the resistance mutations do not necessarily translate into cellular MIC or fitness measurements. The flow of precursors from other metabolic pathways and uptake of exogenous metabolites contributes to resistance and fitness within the folate pathway. Our results also reflect that there is direct interplay between the enzymes within the folate pathway. Thus, we observed a modulation of TMP growth inhibition by both primary DHPS mutations and exogenously provided *p*ABA. This “*p*ABA rescue” effect has been observed with novel inhibitors generated by our group (Zhao et al., 2016), and with MAC173979, a *p*ABA biosynthesis inhibitor discovered by Zlitni et al. (2013). We also demonstrate that resistance to DHPS inhibitors increases sensitivity to TMP. This indirect consequence toward the susceptibility of the downstream enzyme DHFR is consistent with the mutual potentiation effects recently described between SMX and TMP (Minato et al., 2018). In these studies, TMP is shown to potentiate SMX by limiting production of the 7,8-dihydropteroate precursor DHPP, and SMX is shown to potentiate TMP by ultimately limiting 7,8-dihydrofolate production. The latter potentiation effect is similar to the results observed with the primary mutations in our study which hinder biochemical function.

Secondary mutations are not observed by themselves in our genetic survey of clinical isolates, perhaps due to its limited size. E208K when combined with F17L, clearly contributes to resistance and partially restores the binding of *p*ABA, and one might expect these benefits to be present without F17L. Our data show that this is not the case and that E208K fails to provide an advantage under the selective pressure of sulfonamide treatment.

Class modification is a highly successful strategy to develop improved antimicrobial agents that continue to engage clinically validated targets, but are engineered to avoid limiting resistance mechanisms (Silver, 2011). Many groups, including ours, are applying this strategy toward the folate biosynthesis pathway, within which DHPS remains a promising target (Bermingham and Derrick, 2002; Lombardo et al., 2016). Numerous pathogenic species acquire sulfonamide resistance through equivalent mutations to those we have characterized in this study. The findings from our work describes the structural and biochemical basis of sulfonamide resistance in *S. aureus*, which can now be used for the future development of next generation DHPS inhibitors suitable for the treatment of many multidrug-resistant pathogens.

## MATERIALS AND METHODS

### Genetic Survey of *folP* Variations Contributing to Sulfonamide Resistance

Comparative analyses of the DHPS amino acid sequences were performed against a set of 56 *S. aureus* reference strains and 80 non-redundant *S. aureus* DHPS sequences from GenBank

using BLAST (Benson et al., 2005; Pruitt et al., 2005; Boratyn et al., 2012). Sequence variances in DHPS were recorded and compared. Based on these analyses, sequences were separated into the two wild type backgrounds, and 8 subgroups containing at least one of the 5 variations that contribute to sulfonamide resistance or a combination of them. Sulfonamide susceptibility data for each isolate, where available, were associated with the sequencing data. Amino acid sequence alignments were performed using Clustal Omega (Goujon et al., 2010; Sievers et al., 2011).

### SaDHPS Expression and Purification

The *folP* gene of *S. aureus* Rosenbach 25923 DHPS (EMBL accession number Z84573) and those of the F17L, S18L, T51M, E208K, KE257\_dup, T51M/E208K, F17L/E208K, and F17L/KE257\_dup mutants were synthesized into the pET16b vector by GenScript to produce the protein with a N-terminal 10xHis tag. These plasmids were used to transform competent *E. coli* BL21[DE3] cells. Resultant cell lines were used to inoculate 1L LB broth containing 50 µg/mL Ampicillin (added as a selective agent). These cultures were incubated at 37°C with shaking at 225 RPM until they reached an OD<sub>600</sub> of 0.5. These cultures were then induced with 1 mM IPTG and incubated overnight at 18°C with shaking at 225 rpm. Cell pellets were collected with centrifugation at 3700 RCF and resuspended in a lysis buffer consisting of 50 mM Tris pH 8, 500 mM NaCl, 5 mM imidazole, lysozyme, and protease inhibitor cocktail (Roche 11-836-170-001). Cells were lysed by sonication and cell debris was cleared with centrifugation at 14,000 rpm. Crude lysate was further clarified by filtration through a 0.22 µm filter. DHPS was purified from crude lysate in two steps. Crude lysate was applied to a GE HisTrap HP 5 ml column at a rate of 0.2 ml/min. The column was then washed with 200 ml Buffer A consisting of 50 mM Tris, 500 mM NaCl, and 5 mM imidazole, pH 8. DHPS was eluted from the GE HisTrap HP 5 ml column using a gradient of 5–500 mM imidazole. Elution fractions were collected and those with an elevated UV spectrum at 280 were pooled. Pooled fractions were then applied to a HiPrep 16/60 Sephacryl S-200 HR column at a rate of 0.5 ml/min. The column was then washed with 2 column volumes elution buffer consisting of 50 mM HEPES, 150 mM NaCl, and 1 mM DTT at pH 7.6. Elution fractions were collected and examined via SDS-PAGE. Those fractions yielding a single band at approximately 32 kDa were pooled as a final product of purification. Samples were flash frozen using liquid nitrogen and stored for a maximum of 6 months at –80°C.

### DHPS Kinetic Characterization

All kinetic characterization experiments were carried out in 50 mM HEPES with 10 mM MgCl<sub>2</sub> at pH 7.6. Two kinetic analyses were employed. The first measures the pyrophosphate that is released by the DHPS reaction. The pyrophosphate is converted to orthophosphate using yeast inorganic pyrophosphatase, and the PiColor Lock Gold assay (Innova Biosciences) was used to detect orthophosphate. The *K<sub>M</sub>* values for the two substrates *p*ABA and DHPP were individually

measured by maintaining one of the substrates at a concentration that was at least 20-fold in excess of the established  $K_d$ .

The second kinetic analysis employed a radiometric assay that measures  $^{14}\text{C}$ -labeled *p*A<sub>BA</sub> incorporation into the 7,8-dihydropteroate product. The reaction was carried out for 30 min at 37°C in a total volume of 100 and 10  $\mu\text{l}$  aliquots were removed at intervals of 5 min. Ice-cold 50% acetic acid was added to stop the reaction. Reaction products were loaded onto PEI TLC cellulose plates (Analtech 205016) followed by development in 100 mM  $\text{NaPO}_4$ , pH 7. Phos-Screen exposure was followed by Typhoon imaging. Inhibition constants were determined by maintaining substrate levels at their  $K_d$ . SMX was added at concentration ranges between 0 and 10 mM. The  $K_i$  values were determined using the one-site Fit  $K_i$  equation.

### Thermal Stability Studies

The stability of wild-type and variant DHPS was assessed using a thermal stability assay. Sypro-Orange was added to a 10  $\mu\text{M}$  sample of DHPS in the same buffer conditions used for kinetic studies, resulting in a final concentration of 5X. The fluorescence of the solution was then measured over a range of temperatures (23–99°C). Resultant data were fit to the Boltzmann equation resulting in the melting temperature of the protein ( $T_M$ ).

### Isothermal Titration Studies

Binding of *p*A<sub>BA</sub> or SMX to DHPS in the presence or absence of 10 mM sodium pyrophosphate was performed on an iTC200 (MicroCal) at 25°C. Wild type DHPS was dialyzed into 2 L ITC buffer (50 mM HEPES pH 7.6, 5 mM  $\text{MgCl}_2$ ) overnight at 4°C. Standard ITC experiments were performed in 50 mM HEPES, 5 mM  $\text{MgCl}_2$ , and 2.5% DMSO. The iTC200 Microcalorimeter was set to deliver  $19 \times 2 \mu\text{l}$  injections of 500  $\mu\text{M}$  ligand at 150 s intervals into 200  $\mu\text{l}$  of 25  $\mu\text{M}$  protein solution. All experiments were completed in triplicate. Data were analyzed using MicroCal Origin 7.0 software using a one-site binding model with  $n$  values fixed at 1.

### Allelic Replacement to Generate Isogenic USA300 AH1263 *folP* Mutants

The gene encoding *S. aureus folP* from wild-type strain NCTC 8325 was cloned into the PCR2.1TOPO vector. Site-directed mutagenesis was employed to generate eight variants of this gene with confirmed sulfonamide-resistance mutations present singly or in their observed clinical combination which included F17L, S18L, T51M, E208K, KE257\_dup, F17L/E208K, F17L/KE257\_dup, and T51M/E208K. These genes were sub-cloned into the shuttle vector pJB38, which has a temperature-sensitive *S. aureus* origin of replication. After transformation of *S. aureus* USA300 AH1263 with the pJB38 plasmids, growth at 43°C in the presence of chloramphenicol (CAM) allowed for plasmid integration, after which the bacteria were sub-cultured and allowed to grow at 30°C. Growth on anhydrous tetracycline allowed for the killing of cells that still contained the pJB38 plasmid. Absence of the plasmid was further confirmed by testing for sensitivity to CAM followed by sequencing of the *folP* gene, which was PCR amplified from the genomic DNA of each

mutant. All of the isogenic mutants were successfully generated with the exception of T51M/E208K.

### Minimum Inhibitory Concentration Assay (MIC)

MIC testing was carried out in SSM9PR media (Reed et al., 2015). When necessary, *p*A<sub>BA</sub> was added to achieve a final concentration of 5  $\mu\text{g/ml}$ . Antifolates were serially diluted in 100  $\mu\text{l}$ /well 2-fold across 96 well plates. Colonies of each *S. aureus* wild type or mutant strain to be tested were resuspended in media to a mid-log  $\text{OD}_{600}$  between 0.3 and 0.6, after which they were further diluted to an  $\text{OD}_{600}$  of 0.001, which allowed for 100  $\mu\text{l}$  of bacterial suspension containing  $10^5$  CFU to be added to each well. After 16 h of incubation at 37°C, the concentration at which 80% growth inhibition had occurred was determined visually.

### Growth Curve Analysis

Each strain studied was streaked onto LB agar and grown overnight. The overnight cultures were further diluted 1:100 in LB and the  $\text{OD}_{600}$  was read every 30 min. Doubling times were calculated using the linear range of the growth curve of each mutant using the following equation (Reeve et al., 2016):

$$\text{Doubling time} = \frac{\Delta \text{Time} \times \log 2}{\log(\text{Final conc.}) - \log(\text{initial conc.})}$$

The growth curve experiment was performed with three biological replicates for each mutant. The calculated doubling times were compared using One-Way ANOVA Dunnett's Multiple Comparisons Test.

### Wax Moth Larvae Infection Study

*Galleria mellonella* larvae were purchased from Fisher Scientific (14-726-369) in their final instar stage. Larvae were stored at 13°C prior to experimentation and used within seven days of receipt. The larvae used in each experiment were obtained in a single batch and normalized for size. Each sample group contained 32 subjects. Each experiment had at least two control groups including a group that was maintained with no manipulation and a group that was injected with the vehicle solution 10  $\mu\text{l}$  PBS/5% DMSO. For the rescue experiments, larvae were injected with SMX at 100 mg/kg daily in PBS/5% DMSO solution. To prepare the inoculum, *S. aureus* strains with chromosomal DHPS mutations of interest were streaked onto LB agar and incubated at 37°C overnight. A single colony was then used to inoculate 5 ml LB broth which was brought to mid-log at 37°C with shaking at 225 RPM. Cells were collected via centrifugation and suspended in PBS. Cell density was normalized to yield a 10  $\mu\text{l}$  injection volume containing  $5.9 \times 10^5$  CFU, which has an  $\text{LD}_{50}$  at approximately 72 h for the wild type strain. During the course of the experiment, larvae were contained in petri dishes at 37°C. Over a period of 72 h, sample groups were checked for mortality, which was defined by lack of motility and alteration in color. Mortality data were analyzed using GraphPad Prism, with the Log-rank (Mantel-Cox) test used to determine statistically significant changes in mortality for each



mutant compared to the wild type strain. The same statistical test was used to determine significant alterations in mortality due to SMX treatment for each strain tested.

## Crystallography

SaDHPS-F17L/E208K was brought to a concentration of 20 mg/ml in crystallization buffer (50 mM HEPES pH 7.6, 150 mM NaCl, and 1 mM DTT). Initial crystallization conditions were determined using the JCSG I-IV screens wherein 200 nl of SaDHPS were added to 200 nl of well solution in a sitting drop plate and incubated at 8°, 18°, and 23°C. Initial crystals were optimized to produce the final conditions of 0.2 M sodium nitrate, 20% PEG 3350, 75 mM NaCl, 25 mM HEPES, pH 7.6 at 18°C. Crystals were soaked overnight in compound 1530 at a 3:1 molar ratio to generate the complex structure. Twenty-five percent glycerol was added to the crystallization buffer as a cryoprotectant, and crystals were flash frozen in liquid nitrogen prior to data collection at 100°K. X-ray data were collected at Southeast Regional Collaborative Access Team (SER-CAT) 22-ID beamline at the Advanced Photon Source, Argonne National Laboratory. Diffraction images were indexed and integrated with XDS (Kabsch, 2010), and scaled and merged with aimless (CCP4) in space group P43. The structure was solved with PHASER (McCoy et al., 2007) using the published SaDHPS coordinates (PDB 1AD4) as the search model. Reciprocal space refinement was carried out in PHENIX (Afonine et al., 2012) using twin law h,-k,-l, NCS restraints, and TLS definitions in the final cycles. Ligand restraints were created with eLBOW (Moriarty et al., 2009) and real space refinement was performed using COOT (Emsley and Cowtan, 2004). Both structures have been deposited in Protein Data Bank with accession codes 6CLU and 6CLV. Data collection and refinement statistics are reported in Supplementary Table 2.

## Modeling and Computational Studies

The SaDHPS transition state complexes with *p*ABA and sulfamethoxazole were modeled based on the crystal structures of *Yersinia pestis* DHPS in the near transition state complex with *p*ABA (3TYZ) and sulfamethoxazole (3TZF) using the program COOT (Emsley and Cowtan, 2004) and energy minimized using the program MOE (Molecular Operating Environment [MOE],

2018). The Amber ff12 force field was used for the protein and OPLS-AA for the small molecules. The system was energy minimized to 0.1 kcal/mol/Å<sup>2</sup>.

## AUTHOR CONTRIBUTIONS

RL, SW, and CR oversaw and directed the research. They also contributed to the writing of the manuscript. EG performed the kinetic experiments, isothermal calorimetry, genetic survey of folP genes in *S. aureus*, and crystallized as well as collected the X-ray data. She also contributed to writing the manuscript. MW participated in generating the isogenic USA300 mutant panel, performed the minimal inhibitory concentration testing, and fitness studies. She also contributed to writing the manuscript. YW and GK processed the X-ray crystallography data and refined the structures. SG performed the modeling studies and contributed to writing the manuscript. PJ participated in generating the isogenic USA300 mutant panel. ZZ performed the initial bioinformatics analysis. GP participated in the wax moth larvae fitness study and helped to analyze the data.

## ACKNOWLEDGMENTS

We would like to acknowledge the Lead Discovery Informatics team at St. Jude Children's Research Hospital for their assistance in computational analysis of sulfonamide resistance mutations in DHPS. Use of the Advanced Photon Source was supported by the U. S. Department of Energy, Office of Science, Office of Basic Energy Sciences, under Contract No. W-31-109-Eng-38. Funding was provided by NIH grants AI070721 and GMO34496, and the American Lebanese Syrian Associated Charities (ALSAC).

## SUPPLEMENTARY MATERIAL

The Supplementary Material for this article can be found online at: <https://www.frontiersin.org/articles/10.3389/fmicb.2018.01369/full#supplementary-material>

## REFERENCES

- Afonine, P. V., Grosse-Kunstleve, R. W., Echols, N., Headd, J. J., Moriarty, N. W., Mustyakimov, M., et al. (2012). Towards automated crystallographic structure refinement with phenix.refine. *Acta Crystallogr. D Biol. Crystallogr.* 68, 352–367. doi: 10.1107/S0907444912001308
- Benson, D. A., Karsch-Mizrachi, I., Lipman, D. J., Ostell, J., and Wheeler, D. L. (2005). GenBank. *Nucleic Acids Res.* 33, D34–D38. doi: 10.1093/nar/gki063
- Bermingham, A., and Derrick, J. P. (2002). The folic acid biosynthesis pathway in bacteria: evaluation of potential for antibacterial drug discovery. *Bioessays* 24, 637–648. doi: 10.1002/bies.10114
- Boratyn, G. M., Schäffer, A. A., Agarwala, R., Altschul, S. F., Lipman, D. J., and Madden, T. L. (2012). Domain enhanced lookup time accelerated BLAST. *Biol. Direct* 7:12. doi: 10.1186/1745-6150-7-12
- Boucher, H. W., Talbot, G. H., Bradley, J. S., Edwards, J. E., Gilbert, D., Rice, L. B., et al. (2009). Bad bugs, no drugs: no ESKAPE! An update from the Infectious Diseases Society of America. *Clin. Infect. Dis.* 48, 1–12. doi: 10.1086/595011
- Dallas, W. S., Gowen, J. E., Ray, P. H., Cox, M. J., and Dev, I. K. (1992). Cloning, sequencing, and enhanced expression of the dihydropteroate synthase gene of *Escherichia coli* MC4100. *J. Bacteriol.* 174, 5961–5970. doi: 10.1128/jb.174.18.5961-5970.1992
- Dennis, M. L., Pitcher, N. P., Lee, M. D., Debono, A. J., Wang, Z. C., Harjani, J. R., et al. (2016). Structural basis for the selective binding of inhibitors to 6-Hydroxymethyl-7,8-dihydropterin Pyrophosphokinase from *Staphylococcus aureus* and *Escherichia coli*. *J. Med. Chem.* 59, 5248–5263. doi: 10.1021/acs.jmedchem.6b00002
- Domagk, G. (1935). Chemotherapie der bakteriellen Infektionen. *Angewandte Chemie* 48, 657–667. doi: 10.1002/ange.19350484202

- Elena, S. F., Ekunwe, L., Hajela, N., Oden, S. A., and Lenski, R. E. (1998). Distribution of fitness effects caused by random insertion mutations in *Escherichia coli*. *Genetica* 102–103, 349–358. doi: 10.1023/A:1017031008316
- Emsley, P., and Cowtan, K. (2004). Coot: model-building tools for molecular graphics. *Acta Crystallogr. D Biol. Crystallogr.* 60(Pt 12 Pt 1), 2126–2132. doi: 10.1107/S0907444904019158
- Fermer, C., Kristiansen, B. E., Sköld, O., and Swedberg, G. (1995). Sulfonamide resistance in *Neisseria meningitidis* as defined by site-directed mutagenesis could have its origin in other species. *J. Bacteriol.* 177, 4669–4675. doi: 10.1128/jb.177.16.4669-4675.1995
- Fermer, C., and Swedberg, G. (1997). Adaptation to sulfonamide resistance in *Neisseria meningitidis* may have required compensatory changes to retain enzyme function: kinetic analysis of dihydropteroate synthases from *N. meningitidis* expressed in a knockout mutant of *Escherichia coli*. *J. Bacteriol.* 179, 831–837. doi: 10.1128/jb.179.3.831-837.1997
- Gibrel, A., and Sköld, O. (1999). Sulfonamide resistance in clinical isolates of *Campylobacter jejuni*: mutational changes in the chromosomal dihydropteroate synthase. *Antimicrob. Agents Chemother.* 43, 2156–2160.
- Goujon, M., McWilliam, H., Li, W., Valentin, F., Squizzato, S., Paern, J., et al. (2010). A new bioinformatics analysis tools framework at EMBL-EBI. *Nucleic Acids Res.* 38, W695–W699. doi: 10.1093/nar/gkq313
- Greenwood, D. (2010). “Sulfonamides,” in *Antibiotic and Chemotherapy*. Nottingham, UK: Elsevier B.V.
- Haasum, Y., Strom, K., Wehlie, R., Luna, V., Roberts, M. C., Maskell, J. P., et al. (2001). Amino acid repetitions in the dihydropteroate synthase of *Streptococcus pneumoniae* lead to sulfonamide resistance with limited effects on substrate K(m). *Antimicrob. Agents Chemother.* 45, 805–809. doi: 10.1128/AAC.45.3.805-809.2001
- Hammoudeh, D. I., Date, M., Yun, M. K., Zhang, W., Boyd, V. A., Viacava Follis, A., et al. (2014). Identification and characterization of an allosteric inhibitory site on dihydropteroate synthase. *ACS Chem. Biol.* 9, 1294–1302. doi: 10.1021/cb500038g
- Hampele, I. C., D’arcy, A., Dale, G. E., Kostrewa, D., Nielsen, J., Oefner, C., et al. (1997). Structure and function of the dihydropteroate synthase from *Staphylococcus aureus*. *J. Mol. Biol.* 268, 21–30. doi: 10.1006/jmbi.1997.0944
- Kabsch, W. (2010). XDS. *Acta Cryst. D* 66, 125–132. doi: 10.1107/S0907444909047337
- Kai, M., Matsuoka, M., Nakata, N., Maeda, S., Gidoh, M., Maeda, Y., et al. (1999). Diaminodiphenylsulfone resistance of *Mycobacterium leprae* due to mutations in the dihydropteroate synthase gene. *FEMS Microbiol. Lett.* 177, 231–235. doi: 10.1111/j.1574-6968.1999.tb13737.x
- Kazanjian, P., Locke, A. B., Hossler, P. A., Lane, B. R., Bartlett, M. S., Smith, J. W., et al. (1998). Pneumocystis carinii mutations associated with sulfa and sulfone prophylaxis failures in AIDS patients. *AIDS* 12, 873–878. doi: 10.1097/00002030-199808000-00009
- Lane, B. R., Ast, J. C., Hossler, P. A., Mindell, D. P., Bartlett, M. S., Smith, J. W., et al. (1997). Dihydropteroate synthase polymorphisms in *Pneumocystis carinii*. *J. Infect. Dis.* 175, 482–485. doi: 10.1093/infdis/175.2.482
- Levy, C., Minnis, D., and Derrick, J. P. (2008). Dihydropteroate synthase from *Streptococcus pneumoniae*: structure, ligand recognition and mechanism of sulfonamide resistance. *Biochem. J.* 412, 379–388. doi: 10.1042/BJ20071598
- Liu, C., Bayer, A., Cosgrove, S. E., Daum, R. S., Fridkin, S. K., Gorwitz, R. J., et al. (2011). Clinical practice guidelines by the infectious diseases society of america for the treatment of methicillin-resistant *Staphylococcus aureus* infections in adults and children: executive summary. *Clin. Infect. Dis.* 52, 285–292. doi: 10.1093/cid/cir034
- Lombardo, M. N., G-Davanandan, M., Wright, D. L., and Anderson, A. C. (2016). Crystal structures of trimethoprim-resistant DfrA1 rationalizes potent inhibition by propargyl-linked antifolates. *ACS Infect. Dis.* 2, 149–156. doi: 10.1021/acsinfecdis.5b00129
- Maskell, J. P., Sefton, A. M., and Hall, L. M. (1997). Mechanism of sulfonamide resistance in clinical isolates of *Streptococcus pneumoniae*. *Antimicrob. Agents Chemother.* 41, 2121–2126.
- Matsuoka, M. (2010). Drug resistance in leprosy. *Jpn. J. Infect. Dis.* 63, 1–7.
- McCoy, A. J., Grosse-Kunstleve, R. W., Adams, P. D., Winn, M. D., Storoni, L. C., and Read, R. J. (2007). Phaser crystallographic software. *J. Appl. Cryst.* 40, 658–674. doi: 10.1107/S0021889807021206
- Mei, Q., Gurunathan, S., Masur, H., and Kovacs, J. A. (1998). Failure of cotrimoxazole in *Pneumocystis carinii* infection and mutations in dihydropteroate synthase gene. *Lancet* 351, 1631–1632. doi: 10.1016/S0140-6736(05)77687-X
- Minato, Y., Dawadi, S., Kordus, S. L., Sivanandam, A., Aldrich, C. C., and Baughn, A. D. (2018). Mutual potentiation drives synergy between trimethoprim and sulfamethoxazole. *Nat. Commun.* 9:1003. doi: 10.1038/s41467-018-03447-x
- Molecular Operating Environment [MOE] (2018). *Molecular Operating Environment [MOE] 2016.08*. Montreal, QC: Computational Chemistry Group ULC.
- Moriarty, N. W., Grosse-Kunstleve, R. W., and Adams, P. D. (2009). Electronic Ligand Builder and Optimization Workbench (eLBOW): a tool for ligand coordinate and restraint generation. *Acta Crystallogr. D Biol. Crystallogr.* 65, 1074–1080. doi: 10.1107/S0907444909029436
- Pornthanakase, W., Riangrunroj, P., Chitnumsub, P., Ittarat, W., Kongkasuriyachai, D., Uthaiipibull, C., et al. (2016). Role of plasmodium vivax dihydropteroate synthase polymorphisms in sulfa drug resistance. *Antimicrob. Agents Chemother.* 60, 4453–4463. doi: 10.1128/AAC.01835-15
- Pruitt, K. D., Tatusova, T., and Maglott, D. R. (2005). NCBI Reference Sequence (RefSeq): a curated non-redundant sequence database of genomes, transcripts and proteins. *Nucleic Acids Res.* 33, D501–504. doi: 10.1093/nar/gki025
- Reed, P., Attilano, M. L., Alves, R., Hoiczky, E., Sher, X., Reichmann, N. T., et al. (2015). *Staphylococcus aureus* survives with a minimal peptidoglycan synthesis machine but sacrifices virulence and antibiotic resistance. *PLoS Pathog.* 11:e1004891. doi: 10.1371/journal.ppat.1004891
- Reeve, S. M., Scocchera, E. W., N. G.D., Keshipeddy, S., Krucinska, J., Hajian, B., et al. (2016). MRSA isolates from united states hospitals carry dfrg and dfrk resistance genes and succumb to propargyl-linked antifolates. *Cell Chem. Biol.* 23, 1458–1467. doi: 10.1016/j.chembiol.2016.11.007
- Roland, S., Ferone, R., Harvey, R. J., Styles, V. L., and Morrison, R. W. (1979). The characteristics and significance of sulfonamides as substrates for *Escherichia coli* dihydropteroate synthase. *J. Biol. Chem.* 254, 10337–10345.
- Romano, K. P., Ali, A., Royer, W. E., and Schiffer, C. A. (2010). Drug resistance against HCV NS3/4A inhibitors is defined by the balance of substrate recognition versus inhibitor binding. *Proc. Natl. Acad. Sci. U.S.A.* 49, 20986–20991. doi: 10.1073/pnas.1006370107
- Shi, G., Shaw, G., Liang, Y. H., Subburaman, P., Li, Y., Wu, Y., et al. (2012). Bisubstrate analogue inhibitors of 6-hydroxymethyl-7,8-dihydropterin pyrophosphokinase: new design with improved properties. *Bioorg. Med. Chem.* 20, 47–57. doi: 10.1016/j.bmc.2011.11.032
- Sievers, F., Wilm, A., Dineen, D., Gibson, T. J., Karplus, K., Li, W., et al. (2011). Fast, scalable generation of high-quality protein multiple sequence alignments using Clustal Omega. *Mol. Syst. Biol.* 7:539. doi: 10.1038/msb.2011.75
- Silver, L. L. (2011). Challenges of antibacterial discovery. *Clin. Microbiol. Rev.* 24, 71–109. doi: 10.1128/CMR.00030-10
- Vedantam, G., and Nichols, B. P. (1998). Characterization of a mutationally altered dihydropteroate synthase contributing to sulfathiazole resistance in *Escherichia coli*. *Microb. Drug Resist.* 4, 91–97. doi: 10.1089/mdr.1998.4.91
- Wang, P., Lee, C. S., Bayoumi, R., Djimde, A., Doumbo, O., Swedberg, G., et al. (1997a). Resistance to antifolates in *Plasmodium falciparum* monitored by sequence analysis of dihydropteroate synthetase and dihydrofolate reductase alleles in a large number of field samples of diverse origins. *Mol. Biochem. Parasitol.* 89, 161–177. doi: 10.1016/S0166-6851(97)00114-X
- Wang, P., Sims, P. F., and Hyde, J. E. (1997b). A modified *in vitro* sulfadoxine susceptibility assay for *Plasmodium falciparum* suitable for investigating Fansidar resistance. *Parasitology* 115 (Pt 3), 223–230. doi: 10.1017/S0031182097001431
- Williams, D. L., Spring, L., Harris, E., Roche, P., and Gillis, T. P. (2000). Dihydropteroate synthase of *Mycobacterium leprae* and dapson resistance. *Antimicrob. Agents Chemother.* 44, 1530–1537. doi: 10.1128/AAC.44.6.1530-1537.2000
- Yun, M. K., Hoagland, D., Kumar, G., Waddell, M. B., Rock, C. O., Lee, R. E., et al. (2014). The identification, analysis and structure-based development of novel inhibitors of 6-hydroxymethyl-7,8-dihydropterin pyrophosphokinase. *Bioorg. Med. Chem.* 22, 2157–2165. doi: 10.1016/j.bmc.2014.02.022
- Yun, M. K., Wu, Y., Li, Z., Zhao, Y., Waddell, M. B., Ferreira, A. M., et al. (2012). Catalysis and sulfa drug resistance in dihydropteroate synthase. *Science* 335, 1110–1114. doi: 10.1126/science.1214641

- Zhao, Y., Hammoudeh, D., Yun, M. K., Qi, J., White, S. W., and Lee, R. E. (2012). Structure-based design of novel pyrimido[4,5-c]pyridazine derivatives as dihydropteroate synthase inhibitors with increased affinity. *ChemMedChem* 7, 861–870. doi: 10.1002/cmdc.201200049
- Zhao, Y., Shadrack, W. R., Wallace, M. J., Wu, Y., Griffith, E. C., Qi, J., et al. (2016). Pterin-sulfa conjugates as dihydropteroate synthase inhibitors and antibacterial agents. *Bioorg. Med. Chem. Lett.* 26, 3950–3954. doi: 10.1016/j.bmcl.2016.07.006
- Zlitni, S., Ferruccio, L. F., and Brown, E. D. (2013). Metabolic suppression identifies new antibacterial inhibitors under nutrient limitation. *Nat. Chem. Biol.* 9, 796–804. doi: 10.1038/nchembio.1361

**Conflict of Interest Statement:** The authors declare that the research was conducted in the absence of any commercial or financial relationships that could be construed as a potential conflict of interest.

Copyright © 2018 Griffith, Wallace, Wu, Kumar, Gajewski, Jackson, Phelps, Zheng, Rock, Lee and White. This is an open-access article distributed under the terms of the Creative Commons Attribution License (CC BY). The use, distribution or reproduction in other forums is permitted, provided the original author(s) and the copyright owner(s) are credited and that the original publication in this journal is cited, in accordance with accepted academic practice. No use, distribution or reproduction is permitted which does not comply with these terms.





# Structural and Mechanistic Basis for Extended-Spectrum Drug-Resistance Mutations in Altering the Specificity of TEM, CTX-M, and KPC $\beta$ -lactamases

Timothy Palzkill<sup>1,2\*</sup>

<sup>1</sup> Department of Pharmacology and Chemical Biology, Baylor College of Medicine, Houston, TX, United States, <sup>2</sup> Department of Biochemistry and Molecular Biology, Baylor College of Medicine, Houston, TX, United States

## OPEN ACCESS

### Edited by:

Christopher Davies,  
Medical University of South Carolina,  
United States

### Reviewed by:

Focco Van Den Akker,  
Case Western Reserve University,  
United States  
Sergei Vakulenko,  
University of Notre Dame,  
United States

### \*Correspondence:

Timothy Palzkill  
timothyp@bcm.edu

### Specialty section:

This article was submitted to  
Structural Biology,  
a section of the journal  
Frontiers in Molecular Biosciences

**Received:** 27 December 2017

**Accepted:** 08 February 2018

**Published:** 23 February 2018

### Citation:

Palzkill T (2018) Structural and Mechanistic Basis for Extended-Spectrum Drug-Resistance Mutations in Altering the Specificity of TEM, CTX-M, and KPC  $\beta$ -lactamases. *Front. Mol. Biosci.* 5:16. doi: 10.3389/fmolb.2018.00016

The most common mechanism of resistance to  $\beta$ -lactam antibiotics in Gram-negative bacteria is the production of  $\beta$ -lactamases that hydrolyze the drugs. Class A  $\beta$ -lactamases are serine active-site hydrolases that include the common TEM, CTX-M, and KPC enzymes. The TEM enzymes readily hydrolyze penicillins and older cephalosporins. Oxyimino-cephalosporins, such as cefotaxime and ceftazidime, however, are poor substrates for TEM-1 and were introduced, in part, to circumvent  $\beta$ -lactamase-mediated resistance. Nevertheless, the use of these antibiotics has led to evolution of numerous variants of TEM with mutations that significantly increase the hydrolysis of the newer cephalosporins. The CTX-M enzymes emerged in the late 1980s and hydrolyze penicillins and older cephalosporins and derive their name from the ability to also hydrolyze cefotaxime. The CTX-M enzymes, however, do not efficiently hydrolyze ceftazidime. Variants of CTX-M enzymes, however, have evolved that exhibit increased hydrolysis of ceftazidime. Finally, the KPC enzyme emerged in the 1990s and is characterized by its broad specificity that includes penicillins, most cephalosporins, and carbapenems. The KPC enzyme, however, does not efficiently hydrolyze ceftazidime. As with the TEM and CTX-M enzymes, variants have recently evolved that extend the spectrum of KPC  $\beta$ -lactamase to include ceftazidime. This review discusses the structural and mechanistic basis for the expanded substrate specificity of each of these enzymes that result from natural mutations that confer oxyimino-cephalosporin resistance. For the TEM enzyme, extended-spectrum mutations act by establishing new interactions with the cephalosporin. These mutations increase the conformational heterogeneity of the active site to create sub-states that better accommodate the larger drugs. The mutations expanding the spectrum of CTX-M enzymes also affect the flexibility and conformation of the active site to accommodate ceftazidime. Although structural data are limited, extended-spectrum mutations in KPC may act by mediating new, direct interactions with substrate and/or altering conformations of the active site. In many cases,

mutations that expand the substrate profile of these enzymes simultaneously decrease the thermodynamic stability. This leads to the emergence of additional global suppressor mutations that help correct the stability defects leading to increased protein expression and increased antibiotic resistance.

**Keywords:**  $\beta$ -lactamase,  $\beta$ -lactam antibiotics, protein evolution, antibiotic resistance, enzyme structure, enzyme mechanism

## INTRODUCTION

$\beta$ -lactam antibiotics are the most often-used antimicrobials representing ~65% of antibiotic usage worldwide (Livermore, 2006). The  $\beta$ -lactams act by inhibiting bacterial cell wall biosynthesis. Specifically, they are covalent inhibitors of transpeptidase enzymes, commonly referred to as penicillin-binding proteins (PBPs). These enzymes catalyze a cross-linking reaction of pentapeptides present in the peptidoglycan layer of the cell wall (Lovering et al., 2012).

The most common mechanism of resistance to  $\beta$ -lactam antibiotics is the bacterial production of  $\beta$ -lactamases (Fisher et al., 2005). These enzymes catalyze the hydrolysis of the amide bond present in the  $\beta$ -lactam ring resulting in a product that is an ineffective inhibitor of the PBPs.  $\beta$ -lactamases can be distributed into four classes (A, B, C, and D) based on primary amino acid sequence homology (Ambler, 1980; Fisher et al., 2005). Classes A, C, and D are serine hydrolases that function similarly to classical serine proteases such as chymotrypsin. They catalyze attack of the catalytic serine on the carbonyl carbon of the amide bond to form a covalent acyl-enzyme intermediate that is subsequently hydrolyzed by a water molecule that has been activated by a general base. Class B  $\beta$ -lactamases are zinc metallo-enzymes that contain one or two zinc ions that coordinate a hydroxide ion for direct attack on the carbonyl carbon of the amide and do not proceed through a covalent acyl-enzyme (Palzkill, 2013).

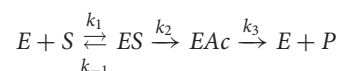
Class A  $\beta$ -lactamases are often encoded on plasmids that can move by conjugation and, as a result, these enzymes are widespread sources of resistance (Bush and Fisher, 2011). Class A  $\beta$ -lactamases are a particular problem for resistance in Gram-negative bacteria including the ESKAPE pathogens (*Enterococcus faecium*, *Staphylococcus aureus*, *Klebsiella pneumoniae*, *Acinetobacter baumannii*, *Pseudomonas aeruginosa*, and *Enterobacter* species; Pendleton et al., 2013). Individual class A  $\beta$ -lactamases display a range of substrate specificities although, as a group, they are commonly known for the efficient hydrolysis of penicillins and early generation cephalosporins. The extensive use of these antibiotics and subsequent spread of class A  $\beta$ -lactamases has led to widespread resistance (Bush and Fisher, 2011). This was countered in the 1980s with the introduction of oxyimino-cephalosporins, which are still good PBP inhibitors but poor substrates for  $\beta$ -lactamases. Mechanism-based inhibitors that target the  $\beta$ -lactamases were also developed to combat resistance (Drawz and Bonomo, 2010). The introduction and subsequent use of both these agents, however, placed selective pressure on bacteria resulting in the evolution of variants of class A enzymes that have gained the ability to hydrolyze oxyimino-cephalosporins or that avoid the action of  $\beta$ -lactamase

inhibitors (Petrosino et al., 1998; Gniadkowski, 2008; Salverda et al., 2010).

This review will focus on three groups of class A  $\beta$ -lactamases that have evolved in response to the use of oxyimino-cephalosporins such as cefotaxime and ceftazidime and that are widespread sources of resistance in Gram-negative bacteria (Bonomo, 2017). These groups of enzymes include the TEM, CTX-M, and KPC  $\beta$ -lactamases. Although the evolution of resistance to mechanism-based inhibitors is clearly an important source of resistance, the focus of this review is on the evolution of enzymes with higher activity for catalysis of oxyimino-cephalosporins (Figure 1).

## KINETICS OF $\beta$ -LACTAM HYDROLYSIS BY CLASS A $\beta$ -LACTAMASES

In order to understand the means by which the TEM, CTX-M, and KPC enzymes and variants inactivate oxyimino-cephalosporins, it is useful to review the kinetics and mechanism by which class A  $\beta$ -lactamases catalyze hydrolysis of  $\beta$ -lactams. Class A  $\beta$ -lactamases are serine hydrolases with a mechanism similar to serine proteases. After formation of the enzyme-substrate complex (ES), the active-site serine attacks and forms a covalent, acyl-enzyme intermediate (EAc). Subsequent catalysis of the hydrolysis of the acyl-enzyme generates the inactive, hydrolyzed  $\beta$ -lactamase product (P) (Hedstrom, 2002; Galleni and Frere, 2007).



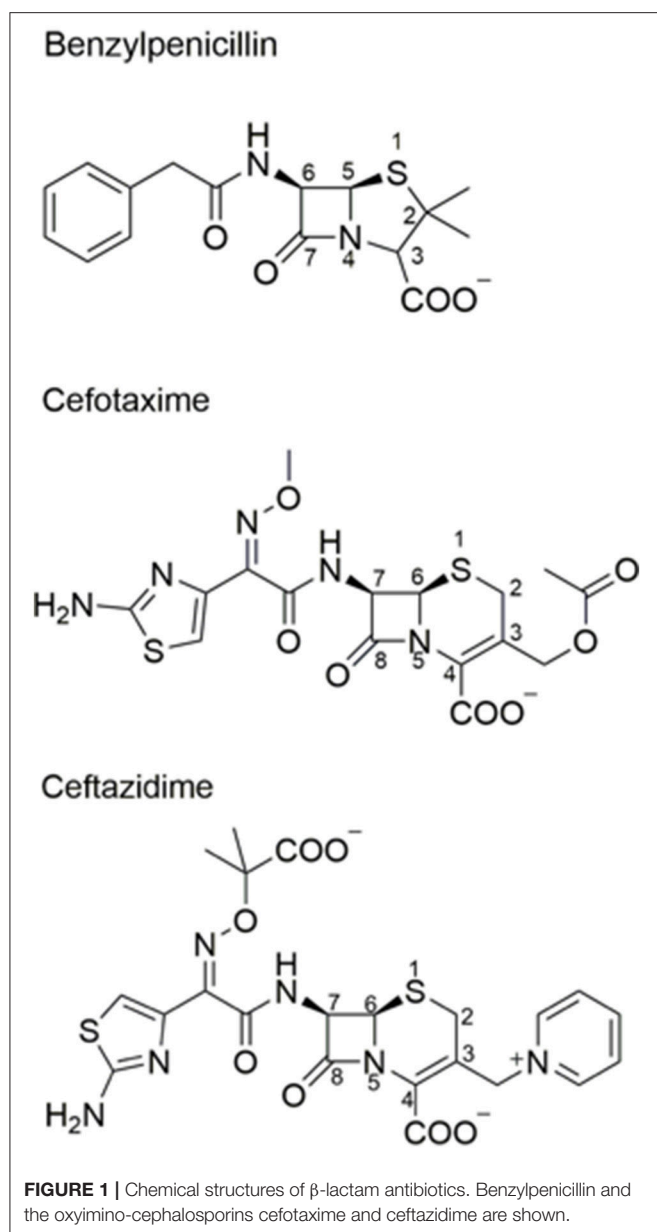
Based on this mechanism, the Michaelis-Menten kinetic parameters are described by the following equations.

$$k_{cat} = k_2 k_3 / (k_2 + k_3) \quad (1)$$

$$K_M = k_3 (k_{-1} + k_2) / k_1 (k_2 + k_3) \quad (2)$$

$$k_{cat} / K_M = k_1 k_2 / (k_{-1} + k_2) \quad (3)$$

For  $\beta$ -lactamases, the kinetic parameters  $k_{cat}$ ,  $K_M$ , and  $k_{cat}/K_M$  are composite constants that depend on the rates of multiple steps in the reaction.  $k_{cat}$  reflects the magnitude and relationship between the acylation ( $k_2$ ) and deacylation ( $k_3$ ) rate constants (Equation 1).  $K_M$  is often regarded as an indication of affinity between the substrate and enzyme, i.e., that  $K_M$  approximates  $K_s$ , which is  $k_{-1}/k_1$ . However, in the  $\beta$ -lactamase mechanism,  $K_M$  is also dependent on  $k_2$  and  $k_3$  (Equation 2; Raquet et al., 1994). Assuming  $k_{-1} > k_2$ ,  $K_M$  approximates substrate affinity ( $K_s$ ) when the acylation rate ( $k_2$ ) is much slower than the deacylation rate



( $k_3$ ), which is often not the case with  $\beta$ -lactam substrates. When deacylation is rate limiting ( $k_2 > k_3$ ), the value of  $K_M$  is lower than  $K_S$  and overestimates the affinity of the enzyme for substrate. Amino acid substitutions in  $\beta$ -lactamases that result in changes in  $K_M$  can be due to changes in  $K_S$ ,  $k_2$  or  $k_3$ , or a combination thereof. Finally,  $k_{cat}/K_M$  reflects the rates of steps occurring up to the formation of the acyl-enzyme. The deacylation rate ( $k_3$ ) does not contribute to the value of  $k_{cat}/K_M$  as seen in equation 3.

## CLASS A $\beta$ -LACTAMASE MECHANISM

Class A  $\beta$ -lactamases utilize a set of conserved amino acid residues in the active site to promote substrate binding,

acyl-enzyme formation, and subsequent deacylation to release product. The class A enzymes contain a  $\beta$  and an  $\alpha/\beta$  domain, with the active site situated between these closely connected domains (Herzberg and Moulton, 1987; Strynadka et al., 1992). Residues Ser70, Ser130, Asn132, Glu166, Asn170, Lys234, Ser/Thr235, Gly236, and Ala/Ser/Thr237 (Ambler numbering scheme; Ambler et al., 1991) are important contributors to substrate binding and catalysis (**Figure 2**). The hydroxyl oxygen of Ser70 serves as the nucleophile for attack on the carbonyl carbon of the amide bond (Strynadka et al., 1992; Fisher and Mobashery, 2009). The main chain NH groups of Ser70 and Ala237 act as the oxyanion hole and make hydrogen bonding interactions to stabilize the negative charge that develops on the carbonyl oxygen tetrahedral intermediate during acylation and deacylation (Strynadka et al., 1992). Although the details are controversial, Lys73, Glu166 and a catalytic water are thought to participate in abstracting the proton to activate Ser70 (Herzberg and Moulton, 1987; Strynadka et al., 1992; Damblon et al., 1996; Minasov et al., 2002; Meroueh et al., 2005). Ser130 has been proposed to serve as a proton shuttle between Lys73 and the leaving group nitrogen (Strynadka et al., 1992). Asn132 forms a hydrogen bond with the acyl-amide group in the C6/7 side chain of penicillins and cephalosporins for binding and positioning of substrate. Lys234 and Ser/Thr235 make interactions with the C3/C4 substrate carboxylate found on all penicillins, cephalosporins and carbapenems and therefore are important for substrate binding. This interaction may also contribute to stabilization of the acylation and deacylation transition states to facilitate catalysis (Strynadka et al., 1992; Delmas et al., 2010; Fonseca et al., 2012). Glu166 serves as the general base for activating the catalytic water for the deacylation step and amino acid substitutions at this position lead to accumulation of the acyl-enzyme intermediate (Adachi et al., 1991; Delaire et al., 1991; Escobar et al., 1991; Strynadka et al., 1992). Asn170 forms a hydrogen bond to Glu166 and an active site water to help position the residue for activating the water. Both Glu166 and Asn170 are found on an omega loop structure that forms the base of the active site in class A  $\beta$ -lactamases (**Figure 2**). As discussed below, the omega loop plays an important role in the evolution of increased oxyimino-cephalosporin hydrolysis in class A enzymes. The residues described above are important for catalysis of all  $\beta$ -lactam substrates and mutations at these positions reduce activity. Thus, they form the core residues required for catalysis. Mutations leading to increased catalysis of oxyimino-cephalosporins occur at residues other than these core positions.

## TEM EXTENDED-SPECTRUM $\beta$ -LACTAMASES (ESBLs)

TEM-1  $\beta$ -lactamase was reported in 1963 in *E. coli* and *Salmonella* (Datta and Kontomichalou, 1965). It subsequently spread among Enterobacteriaceae and other Gram-negative pathogens to become a widespread source of  $\beta$ -lactam resistance. TEM-1 efficiently catalyzes the hydrolysis of penicillins and early generation cephalosporins and provides high-level bacterial



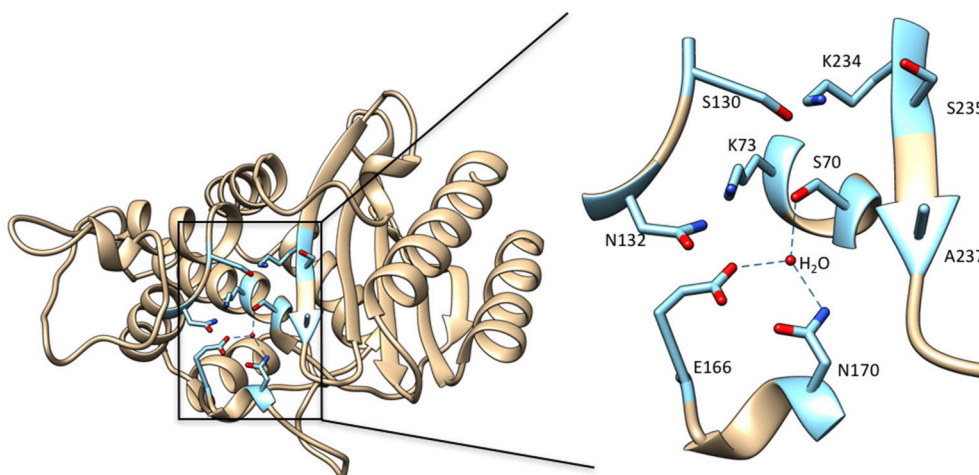


**FIGURE 2 | Left:** Ribbon diagram of TEM-1  $\beta$ -lactamase (PDB ID: 1BTL). Key active site residues that are implicated in substrate binding and catalysis and highlighted in cyan. **Right:** Enlarged view of the boxed region of the active site with the active site residues labeled. The deacylation water molecule is shown as a red sphere with hydrogen bonds from this water to Ser70, Glu166, and Asn170 shown as dotted lines. Hydrogen bonds between residues are not shown.

resistance to these drugs. In part due to the widespread presence of TEM-1, the oxyimino-cephalosporins were introduced in the 1980s (Bush, 2002). The oxyimino-cephalosporins, such as cefotaxime and ceftazidime, include an oxyimino side chain at the C7 position (**Figure 1**). The large and inflexible oxyimino side chain is difficult to accommodate into the active site of TEM-1, resulting in slow rates of hydrolysis (**Table 1**). Ceftazidime differs from cefotaxime by having an even larger side chain that includes a carboxylate group (**Figure 1**). The increased bulk of ceftazidime is associated with a further reduction in rates of catalysis by TEM-1 compared to cefotaxime (**Table 2**).

The kinetic parameters for oxyimino-cephalosporin hydrolysis by TEM-1 reveal low  $k_{\text{cat}}$  and  $k_{\text{cat}}/K_M$  values and high  $K_M$  values compared with good substrates such as ampicillin or benzylpenicillin. There have been a large number of studies on cefotaxime hydrolysis by TEM-1 and a list of kinetic parameters is compiled in **Table 1**. The list is likely not comprehensive and there is some variation in assay conditions such as 25°C vs. 30°C but the majority of the listed results were obtained using similar buffer conditions. There is some variation in published values, particularly with regard to  $K_M$ .  $K_M$  is generally high and in several studies it was too high to measure accurately (**Table 1**). The  $k_{\text{cat}}/K_M$  values, however, are relatively consistent and average  $\sim 1.7 \times 10^3 \text{ M}^{-1}\text{s}^{-1}$  (**Table 1**). Published kinetic parameters for ceftazidime hydrolysis also exhibit variation in  $K_M$  but with  $K_M$  generally high (**Table 2**). However,  $k_{\text{cat}}/K_M$  values are quite consistent and average  $\sim 40 \text{ M}^{-1}\text{s}^{-1}$ . Therefore, both cefotaxime and ceftazidime are poor substrates for TEM-1  $\beta$ -lactamase. Ceftazidime, however, is a particularly poor substrate with an  $\sim 45$ -fold lower  $k_{\text{cat}}/K_M$  value than that observed for cefotaxime hydrolysis. Published  $k_{\text{cat}}/K_M$  values for benzylpenicillin hydrolysis are in the range of  $10^7$ – $10^8 \text{ M}^{-1}\text{s}^{-1}$  and therefore cefotaxime and ceftazidime hydrolysis is  $10^4$ – $10^6$ -fold less efficient (Christensen et al., 1990). Since  $k_{\text{cat}}/K_M$  reflects the events occurring up to formation

of the acyl-enzyme, the low  $k_{\text{cat}}/K_M$  values for cefotaxime and ceftazidime hydrolysis reflect low affinity for substrate binding and/or a slow acylation reaction. Indeed, estimates of  $K_s$  for the binding of cefotaxime and ceftazidime to TEM-1 reveal poor affinity with values of 3.8 and 9.9 mM, respectively (Vakulenko et al., 1999). The rate-limiting step for cefotaxime hydrolysis by TEM-1 has been shown to be the acylation step ( $k_2$ ) (Saves et al., 1995). Taken together, these results are consistent with the large, inflexible oxyimino side chain of cefotaxime being poorly accommodated in the active site of TEM-1.

Since the introduction of oxyimino-cephalosporins into clinical practice, variants of TEM-1 with amino acid substitutions that result in increased hydrolysis have been emerging (Petrosino et al., 1998; Salverda et al., 2010; Pimenta et al., 2014). Each unique variant is given a new number and these variants are termed TEM extended spectrum  $\beta$ -lactamases (ESBLs). The number of TEM variants is now greater than 200 (Salverda et al., 2010; Pimenta et al., 2014). The most common substitutions in TEM enzymes displaying enhanced oxyimino-cephalosporin hydrolysis include E104K, R164S/H, M182T, A237T, G238S, and E240K (**Figure 3**). The effects of these substitutions have been studied extensively using kinetic, biophysical, and structural tools to determine the mechanism by which resistance to oxyimino-cephalosporins is evolving.

## G238S AND R164S SUBSTITUTIONS

The R164S and G238S substitutions are associated with the largest increases in cefotaxime and ceftazidime hydrolysis when introduced into the TEM-1 enzyme. These substitutions are likely the driver substitutions for clinically relevant resistance and are the most often observed in TEM ESBLs. The G238S substitution is predominantly associated with enhanced hydrolysis of cefotaxime and increased resistance. Residue 238 is situated on

**TABLE 1** | Kinetic parameters for cefotaxime hydrolysis by TEM-1  $\beta$ -lactamase and mutants.

Enzyme	$k_{\text{cat}}$ ( $\text{s}^{-1}$ )	$K_M$ ( $\mu\text{M}$ )	$k_{\text{cat}}/K_M$ ( $\text{M}^{-1} \text{s}^{-1}$ )	Buffer	References
TEM-1 wt	0.25	450	$5.6 \times 10^2$	0.1 M phosphate, pH7.0, 25°C	Sowek et al., 1991
TEM-1 wt	9.0	6,000	$1.5 \times 10^3$	50 mM phosphate, pH7.0, 30°C	Raquet et al., 1994
TEM-1 wt	2	1,100	$1.8 \times 10^3$	pH7.0, 37°C	Petit et al., 1995
TEM-1 wt	2.5	1,684	$1.5 \times 10^3$	10 mM sodium bicarbonate, pH7.0, 37°C	Saves et al., 1995
TEM-1 wt	0.18	230	$7.8 \times 10^2$	50 mM phosphate, 100 mM NaCl, pH7.0, 25°C	Vakulenko et al., 1999
TEM-1 wt	nd <sup>a</sup>	nd	$3.9 \times 10^3$	50 mM phosphate, pH7.0, 30°C	Venkatachalam et al., 1994
TEM-1 wt	nd	nd	$2.8 \times 10^3$	50 mM phosphate, pH7.0, 30°C	Cantu and Palzkill, 1998
TEM-1 wt	0.64	308	$2.1 \times 10^3$	50 mM phosphate, pH7.0, 25°C	Wang et al., 2002
TEM-1 wt	nd	nd	$2.1 \times 10^3$	50 mM phosphate, pH7.0, 30°C	Brown et al., 2010
TEM-1 wt	nd	nd	$1.0 \times 10^3$	100 mM phosphate, pH7.0, 25°C	Dellus-Gur et al., 2015
TEM-1 wt	nd	nd	$2.0 \times 10^3$	50 mM phosphate, pH7.0, 10% glycerol, 25°C	Hart et al., 2016
TEM-1 wt	0.17	750	$1.5 \times 10^2$	100 mM phosphate, pH7.0, 25°C	Knies et al., 2017
Avg(SD)	2.1 (3.2)	1,500 (2,050)	$1.7 \times 10^3$ ( $1.0 \times 10^3$ )		
TEM R164S	2.4	230	$1.0 \times 10^4$	0.1 M phosphate, pH7.0, 25°C	Sowek et al., 1991
TEM R164S	0.2	174	$1.1 \times 10^3$	50 mM phosphate, 100 mM NaCl, pH7.0, 25°C	Vakulenko et al., 1999
TEM R164S	1.8	201	$8.8 \times 10^3$	50 mM phosphate, pH7.0, 25°C	Wang et al., 2002
TEM R164S	2.5	536	$4.7 \times 10^3$	100 mM phosphate, pH7.0, 25°C	Dellus-Gur et al., 2015
TEM R164S <sup>b</sup>	1.5	100	$1.5 \times 10^4$	50 mM phosphate, pH7.0, 30°C	Raquet et al., 1994
Avg(SD)	1.7 (1)	250 (170)	$7.9 \times 10^3$ ( $5.3 \times 10^3$ )		
TEM G238S	66	290	$2.3 \times 10^5$	50 mM phosphate, pH7.0, 30°C	Raquet et al., 1994
TEM G238S <sup>b</sup>	20	188	$1.1 \times 10^5$	10 mM sodium bicarbonate, pH7.0, 37°C	Saves et al., 1995
TEM G238S	7.5	577	$1.3 \times 10^4$	50 mM phosphate, pH7.0, 30°C	Viadiu et al., 1995
TEM G238S	16	124	$1.4 \times 10^5$	50 mM phosphate, pH7.0, 30°C	Cantu and Palzkill, 1998
TEM G238S	42	234	$1.8 \times 10^5$	50 mM phosphate, pH7.0, 25°C	Wang et al., 2002
TEM G238S	50	403	$1.3 \times 10^5$	100 mM phosphate, pH7.0, 25°C	Dellus-Gur et al., 2015
TEM G238S	50	190	$2.6 \times 10^5$	50 mM phosphate, pH7.0, 10% glycerol, 25°C	Hart et al., 2016
TEM G238S	14	700	$2.2 \times 10^4$	100 mM phosphate, pH7.0, 25°C	Knies et al., 2017
Avg(SD)	33 (21)	340 (200)	$1.4 \times 10^5$ ( $8.9 \times 10^4$ )		
TEM E104K	2.5	470	$5.3 \times 10^3$	0.1 M phosphate, pH7.0, 25°C	Sowek et al., 1991
TEM E104K	25	1,000	$2.5 \times 10^4$	pH7.0, 37°C	Petit et al., 1995
TEM E104K	9.3	980	$9.4 \times 10^3$	50 mM phosphate, pH7.0, 25°C	Wang et al., 2002
TEM E104K	nd	nd	$1.2 \times 10^4$	50 mM phosphate, pH7.0, 10% glycerol, 25°C	Hart et al., 2016
TEM E104K	3.9	5,000	$6.0 \times 10^2$	100 mM phosphate, pH7.0, 25°C	Knies et al., 2017
Avg(SD)	10 (10)	1,870 (2,110)	$1.0 \times 10^4$ ( $9.2 \times 10^3$ )		
TEM E240K	0.66	140	$4.7 \times 10^3$	0.1 M phosphate, pH7.0, 25°C	Sowek et al., 1991
TEM E240K	nd	nd	$8.5 \times 10^3$	50 mM phosphate, pH7.0, 30°C	Venkatachalam et al., 1994
Avg(SD)	–	–	$6.6 \times 10^3$ ( $2.7 \times 10^3$ )		

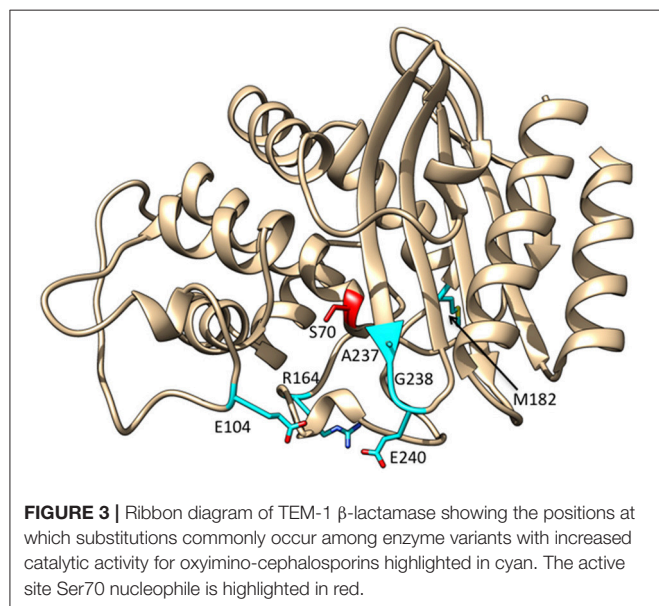
<sup>a</sup>nd, not determined.<sup>b</sup>Enzyme also contains Q39K substitution.

the  $\beta 3$  strand that forms a side of the active site (**Figure 3**). A number of studies have shown that the G238S substitution, when introduced into the TEM-1 enzyme, results in an  $\sim 80$ -fold increase in  $k_{\text{cat}}/K_M$  for cefotaxime hydrolysis compared to wild-type TEM-1 and has a value of  $\sim 1.4 \times 10^5 \text{ M}^{-1}\text{s}^{-1}$  (**Table 1**). It is somewhat difficult to estimate the changes in  $k_{\text{cat}}$  and  $K_M$  relative to TEM-1 as they are often not determined for wild type because of high  $K_M$  values. However, it is clear that  $K_M$  for cefotaxime hydrolysis is reduced for G238S compared to TEM-1 as the value is consistently measurable and is in the range of 300  $\mu\text{M}$  while  $k_{\text{cat}}$  is in the range of 30  $\text{s}^{-1}$  (**Table 1**). Saves et al.

utilized electrospray mass spectroscopy to determine acylation ( $k_2$ ) and deacylation ( $k_3$ ) rates for TEM-1 and the G238S mutant and found acylation is rate-limiting for cefotaxime hydrolysis for TEM-1, as noted above (Saves et al., 1995). Acylation remains rate-limiting for the G238S enzyme but  $k_2$  is increased nearly 10-fold (Saves et al., 1995). A significant portion of the increase in  $k_{\text{cat}}/K_M$  observed for the G238S enzyme is thus due to an increase in the acylation rate. Although values for  $K_s$  for G238S with cefotaxime have not been determined, the fact that acylation is rate-limiting indicates  $K_M$  is an approximation of  $K_s$ . Since the  $K_M$  for cefotaxime is reduced for the G238S enzyme compared to

**TABLE 2 |** Kinetic parameters for ceftazidime hydrolysis by TEM-1  $\beta$ -lactamase and mutants.

Enzyme	$k_{\text{cat}}$ ( $\text{s}^{-1}$ )	$K_M$ ( $\mu\text{M}$ )	$k_{\text{cat}}/K_M$ ( $\text{M}^{-1}\text{s}^{-1}$ )	Buffer	References
TEM-1 wt	0.0016	80	20	0.1 M phosphate, pH7.0, 25°C	Sowek et al., 1991
TEM-1 wt	0.3	4,300	70	50 mM phosphate, pH7.0, 30°C	Raquet et al., 1994
TEM-1 wt	nd <sup>a</sup>	nd	21	50 mM phosphate, pH7.0, 30°C	Venkatachalam et al., 1994
TEM-1 wt	0.02	300	66	pH7.0, 37°C	Petit et al., 1995
TEM-1 wt	nd	nd	55	50 mM phosphate, pH7.0, 30°C	Cantu et al., 1996
TEM-1 wt	0.008	200	40	50 mM phosphate, 100 mM NaCl, pH7.0, 25°C	Vakulenko et al., 1999
TEM-1 wt	0.018	557	32	50 mM phosphate, pH7.0, 25°C	Wang et al., 2002
Avg(SD)	0.07 (0.13)	1,090 (1,800)	43 (21)		
TEM R164S	3.4	260	$1.3 \times 10^4$	0.1 M phosphate, pH7.0, 25°C	Sowek et al., 1991
TEM R164S <sup>b</sup>	9	1,000	$9.0 \times 10^3$	50 mM phosphate, pH7.0, 30°C	Raquet et al., 1994
TEM R164S	1.4	270	$5.2 \times 10^3$	50 mM phosphate, 100 mM NaCl, pH7.0, 25°C	Vakulenko et al., 1999
TEM R164S	8.5	1,600	$5.3 \times 10^3$	50 mM phosphate, pH7.0, 25°C	Wang et al., 2002
Avg(SD)	5.6 (3.8)	780 (650)	$8.1 \times 10^3$ ( $3.7 \times 10^3$ )		
TEM G238S	0.9	532	$1.6 \times 10^3$	50 mM phosphate, pH7.0, 30°C	Venkatachalam et al., 1994
TEM G238S	26	5,200	$5.0 \times 10^3$	50 mM phosphate, pH7.0, 30°C	Raquet et al., 1994
TEM G238S	0.55	897	$6.1 \times 10^2$	50 mM phosphate, pH7.0, 25°C	Wang et al., 2002
TEM G238S	1.0	343	$3.0 \times 10^3$	50 mM phosphate, pH7.0, 30°C	Cantu and Palzkill, 1998
Avg(SD)	7 (13)	1,740 (2,320)	$2.6 \times 10^3$ ( $1.9 \times 10^3$ )		
TEM E104K	0.07	150	$4.5 \times 10^2$	0.1 M phosphate, pH7.0, 25°C	Sowek et al., 1991
TEM E104K	0.3	80	$3.7 \times 10^3$	pH7.0, 37°C	Petit et al., 1995
TEM E104K	0.41	760	$5.4 \times 10^2$	50 mM phosphate, pH7.0, 25°C	Wang et al., 2002
Avg(SD)	0.26 (0.17)	330 (370)	$1.6 \times 10^3$ ( $1.9 \times 10^3$ )		
TEM E240K	0.28	460	$6.1 \times 10^2$	0.1 M phosphate, pH7.0, 25°C	Sowek et al., 1991
TEM E240K	nd	nd	$1.7 \times 10^3$	50 mM phosphate, pH7.0, 30°C	Venkatachalam et al., 1994
Avg(SD)	–	–	$1.2 \times 10^3$ ( $7.7 \times 10^2$ )		

<sup>a</sup>nd, not determined.<sup>b</sup>Enzyme also contains Q39K substitution.

TEM-1 (Table 1), this suggests that the increased affinity of the G238S enzyme for cefotaxime also contributes to the increase in  $k_{\text{cat}}/K_M$ .

The G238S substitution in TEM-1 also results in increased ceftazidime hydrolysis, albeit to a lesser extent than that observed for cefotaxime, with a  $k_{\text{cat}}/K_M$  value of  $\sim 2.5 \times 10^3 \text{ M}^{-1}\text{s}^{-1}$  (Table 2). This is a 60-fold increase over that observed for TEM-1. As with cefotaxime,  $k_{\text{cat}}$  and  $K_M$  comparisons to wild-type TEM-1 are difficult. However, the  $K_M$  for ceftazidime hydrolysis is reduced to a measurable range for G238S with a value of  $\sim 1,700 \mu\text{M}$  while  $k_{\text{cat}}$  is roughly  $7 \text{ s}^{-1}$ , although there is high variance in published values (Table 2). A comparison of  $k_{\text{cat}}/K_M$  values for G238S reveals a 60-fold higher catalytic efficiency for cefotaxime vs. ceftazidime hydrolysis.

While the G238S substitution increases the rate of cefotaxime and ceftazidime hydrolysis, it significantly decreases the rate of hydrolysis of penicillins. For example,  $k_{\text{cat}}/K_M$  for ampicillin hydrolysis is reduced 10-fold compared to wild-type TEM-1 while  $k_{\text{cat}}$  is decreased  $\sim 50$ -fold (Dellus-Gur et al., 2015). Very similar effects were observed for hydrolysis of benzylpenicillin by the G238S enzyme (Cantu and Palzkill, 1998). Because  $k_{\text{cat}}$  is decreased, the effect of G238S is not simply on binding affinity for penicillins but includes reduced rates of acylation ( $k_2$ ), deacylation ( $k_3$ ), or both. Christensen et al. determined that, for TEM-1, the rates of acylation and deacylation are fast ( $>1,000 \text{ s}^{-1}$ ) and neither is rate-limiting for benzylpenicillin hydrolysis (Christensen et al., 1990). Using mass spectroscopy, Saves et al. determined that, for the G238S enzyme,  $k_3$  is greatly

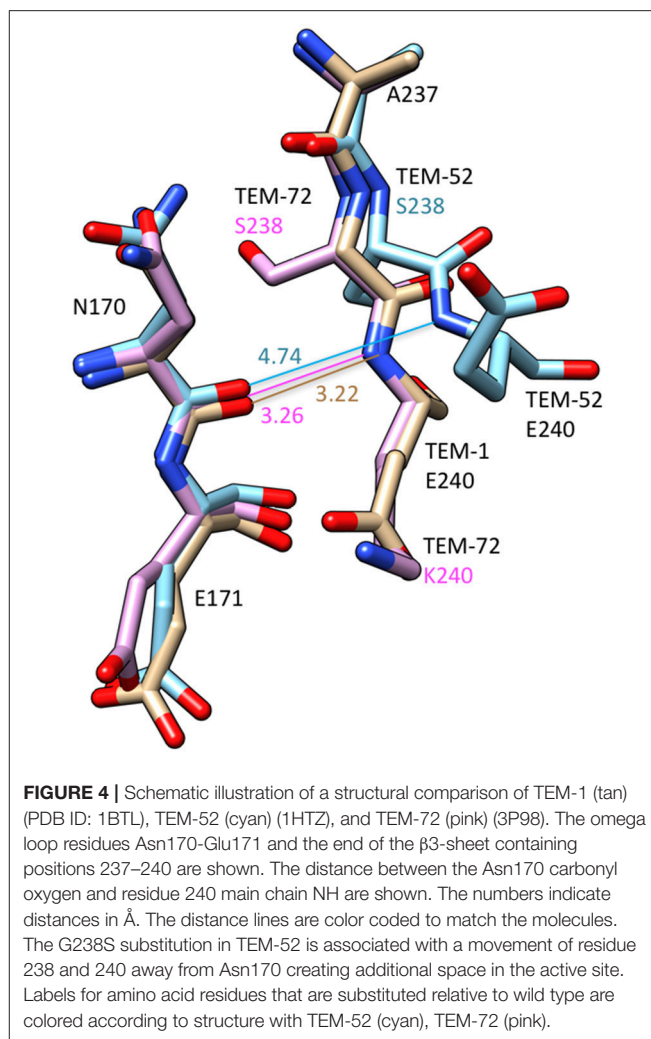


reduced and is rate-limiting for hydrolysis of benzylpenicillin (Saves et al., 1995). Based on these results, it was suggested the G238S substitution may affect the positioning of the omega loop and alter the action of the Glu166 general base, which is present on the loop, resulting in a decreased deacylation rate (Saves et al., 1995).

Two models have been proposed to explain the mechanism of the G238S substitution. One model involves a hydrogen bond between the side chain hydroxyl of the Ser238 residue and the oxime group of the oxyimino-cephalosporins that would improve affinity of the enzyme for the antibiotics and thereby increase catalytic efficiency (Huletsky et al., 1993). The second model suggests that steric conflicts of the Ser238 side chain with residue Asn170 would lead to movement of the  $\beta$ 3 strand or movement of the omega loop thereby causing expansion of the active site to accommodate the larger oxyimino-cephalosporin side chain (Saves et al., 1995; Cantu and Palzkill, 1998). An analysis of kinetic parameters of a series of substitutions at position 238 supported the steric conflict model in that  $k_{\text{cat}}/K_M$  for oxyimino-cephalosporin hydrolysis correlated more closely with side-chain volume than hydrogen bonding potential (Cantu and Palzkill, 1998). In addition, docking and molecular dynamics studies of the G238S mutant with cefotaxime have suggested Ser238 does not hydrogen bond to cefotaxime in the complex (Singh and Dominy, 2012).

The structures of TEM variants from clinical isolates containing multiple substitutions including G238S have been determined. The structure of the TEM-52 enzyme containing the E104K/M182T/G238S substitutions shows the position of the loop region of residues 238–243 is moved by 2.8 Å to widen the active site to accommodate the bulkier side chains of oxyimino-cephalosporins (**Figure 4**). It was also noted that lysine from the E104K substitution is oriented toward the active site (Orencia et al., 2001). In addition, the structure of the TEM-72 enzyme containing the Q39K, M182T, G238S, and E240K substitutions has been determined (Docquier et al., 2011). Curiously, the TEM-72 enzyme does not show the movement of the 238–243 loop and the active site is not expanded (**Figure 4**). This could be due to the presence of the E240K substitution adjacent to G238S somehow restraining the conformation. Note, however, that TEM-1 containing the G238S/E240K double mutant has higher catalytic efficiency for cefotaxime hydrolysis than G238S alone, indicating cefotaxime is accommodated into the active site in the simultaneous presence of G238S and E240K (Venkatachalam et al., 1994). Finally, the structure of a TEM G238A mutant has been determined and, similar to TEM-52, shows an expansion of the active site, however, the expansion is due to movement of the omega loop because of steric conflict with the substituted alanine (Wang et al., 2002).

The X-ray crystal structure of the G238S mutant has also been determined in a TEM-1 enzyme that also contains stabilizing substitutions that enhance protein expression and crystallization (Dellus-Gur et al., 2015). These substitutions did not influence the catalytic properties of the enzyme compared to G238S without the stabilizing substitutions. The G238S structures were determined under cryogenic conditions and at room temperature (Dellus-Gur et al., 2015). The G238S enzyme exists in two



well-defined conformations of the active site loop at the end of the  $\beta$ 3-strand containing residue 238. One of these is a more open conformation that could accommodate cefotaxime (Dellus-Gur et al., 2015). Taken together, the structural results on G238S suggest, TEM-72 notwithstanding, the substitution is associated with increased space to accommodate substrate and are broadly consistent with the steric conflict model.

The R164S substitution results in increased hydrolysis of both cefotaxime and ceftazidime, although it is most often associated with TEM ESBLs providing increased resistance to ceftazidime. Several studies reveal the R164S substitution results in a roughly 5-fold increase in  $k_{\text{cat}}/K_M$  for cefotaxime hydrolysis compared to TEM-1 with a value of  $\sim 8.0 \times 10^3 \text{ M}^{-1}\text{s}^{-1}$  (**Table 1**). Although cefotaxime  $K_M$  values are often too high to measure for TEM-1,  $K_M$  is measurable for R164S with values in the range of 250  $\mu\text{M}$  and  $k_{\text{cat}}$  in the range of  $2 \text{ s}^{-1}$  (**Table 1**). In contrast to the relatively modest increase in cefotaxime hydrolysis mediated by R164S, this substitution is associated with an  $\sim 200$ -fold increase in  $k_{\text{cat}}/K_M$  for ceftazidime hydrolysis compared to TEM-1 with a value of  $\sim 8.0 \times 10^3 \text{ M}^{-1}\text{s}^{-1}$  compared to  $40 \text{ M}^{-1}\text{s}^{-1}$  for TEM-1 (**Table 2**). The increased catalytic efficiency is associated

with a consistently measurable  $K_M$  for R164S with a value of  $\sim 800 \mu\text{M}$  and a  $k_{\text{cat}}$  of  $\sim 6 \text{ s}^{-1}$ . The large increase in  $k_{\text{cat}}/K_M$  for ceftazidime hydrolysis by R164S relative to TEM-1 may explain why the substitution is often associated with ESBLs with high ceftazidime resistance. Because  $k_{\text{cat}}/K_M$  is a reflection of rates occurring up to the formation of the acyl-enzyme, the increase in  $k_{\text{cat}}/K_M$  relative to TEM-1 for both cefotaxime and ceftazidime hydrolysis by R164S suggests the substitution is associated with a decrease in  $K_s$  (increased affinity) and/or an increase in  $k_2$ .

As with G238S, the R164S substitution is associated with decreased penicillin hydrolysis. For example, the  $k_{\text{cat}}$  for ampicillin hydrolysis is decreased 25-fold and  $k_{\text{cat}}/K_M$  is decreased 13-fold for the R164S enzyme relative to wild-type TEM-1 (Dellus-Gur et al., 2015). Similarly, for benzylpenicillin hydrolysis,  $k_{\text{cat}}$  is decreased 70-fold and  $k_{\text{cat}}/K_M$  is decreased 14-fold (Vakulenko et al., 1999). There are no reported values for  $K_s$ ,  $k_2$  or  $k_3$  for penicillin hydrolysis but the 25- and 70-fold reductions in  $k_{\text{cat}}$  suggests  $k_2$  and/or  $k_3$  values are significantly lower for penicillin hydrolysis by R164S relative to TEM-1.

Several groups have investigated the structural basis of the change in substrate specificity provided by R164S. Mobashery and colleagues noted that the R164S substitution would create a cavity in the middle of the omega loop and the top of the loop containing Pro167 and Asn170 would collapse to fill the void. This rearrangement creates additional space in the active site (Vakulenko et al., 1999). The structure of TEM-64 (E104K/R164S/M182T), which contains the R164S substitution, has been determined (Wang et al., 2002). It was found the omega loop has an altered conformation where the short helix in the region of residue 170 unwinds and Asn170 moves by  $4.5 \text{ \AA}$  to create a cavity in the active site that could better accommodate the C7 $\beta$  side chain of oxyimino-cephalosporins (Wang et al., 2002; Figure 5). The structure of the R164S mutant has also been determined in a TEM-1 enzyme that, like G238S described above, also contains stabilizing substitutions that enhance protein expression and crystallization without affecting kinetic parameters (Dellus-Gur et al., 2015). Similar to G238S described above, structures were determined at cryogenic conditions and room temperature. The structure of R164S showed the omega loop is conformationally heterogeneous (Dellus-Gur et al., 2015). An ensemble of different conformations of the omega loop are present, some of which better accommodate cefotaxime. Binding of oxyimino-cephalosporins is proposed to shift the ensemble toward catalytically active conformations. The structure of a covalently bound boronic-acid analog showed less conformational heterogeneity, supporting this view (Dellus-Gur et al., 2015).

## E104K AND E240K SUBSTITUTIONS

The E104K and E240K substitutions are also associated with increases in the hydrolysis of cefotaxime and ceftazidime. Although these substitutions have been found individually in ESBLs, they are often found in association with the G238S or R164S substitutions. The E104K substitution has been studied by several groups and exhibits an  $\sim 6$ -fold increase in  $k_{\text{cat}}/K_M$

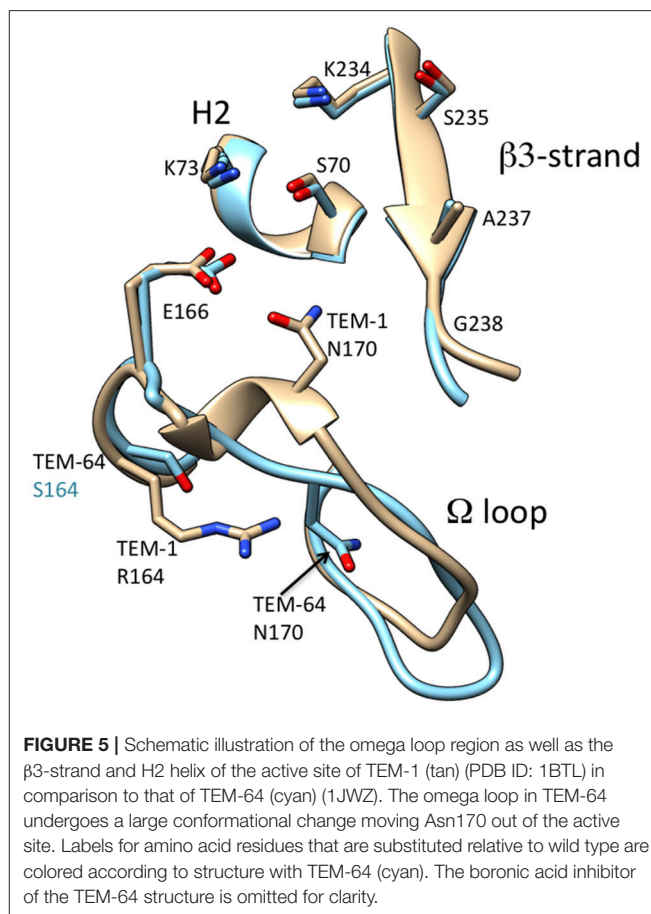


**FIGURE 5** | Schematic illustration of the omega loop region as well as the  $\beta 3$ -strand and H2 helix of the active site of TEM-1 (tan) (PDB ID: 1BTL) in comparison to that of TEM-64 (cyan) (1JWZ). The omega loop in TEM-64 undergoes a large conformational change moving Asn170 out of the active site. Labels for amino acid residues that are substituted relative to wild type are colored according to structure with TEM-64 (cyan). The boronic acid inhibitor of the TEM-64 structure is omitted for clarity.

for cefotaxime hydrolysis compared to TEM-1 with a value of  $1.0 \times 10^4 \text{ M}^{-1}\text{s}^{-1}$  (Table 1).  $K_M$  is consistently measurable for TEM-1 containing the E104K substitution with an average of  $1,800 \mu\text{M}$ , although with high variance in values.  $k_{\text{cat}}$  is likely also increased relative to TEM-1 and has a value of  $\sim 10 \text{ s}^{-1}$  (Table 1). For ceftazidime hydrolysis, the E104K substitution is associated with an  $\sim 40$ -fold increase in  $k_{\text{cat}}/K_M$  compared to TEM-1 (Table 2). The  $K_M$  value for E104K with ceftazidime is in a measurable range with a value of  $\sim 300 \mu\text{M}$  while  $k_{\text{cat}}$  is  $\sim 0.3 \text{ s}^{-1}$  (Table 2). There are no published results on  $K_s$ ,  $k_2$  or  $k_3$  for E104K for these substrates but the increased  $k_{\text{cat}}/K_M$  values suggest minimally that  $K_s$  is reduced and/or  $k_2$  is increased by the substitution. It has been suggested that electrostatic interactions of E104K could increase binding of oxyimino-cephalosporins. Docking and molecular dynamics, however, suggest the lysine at position 104 does not directly interact with bound cefotaxime, although ceftazidime was not examined (Sowek et al., 1991; Singh and Dominy, 2012).

In contrast to the R164S and G238S substitutions, the E104K substitution has little effect on the hydrolysis of penicillins. The kinetic parameters for benzylpenicillin hydrolysis are very similar to TEM-1 with high  $k_{\text{cat}}$ , low  $K_M$  and very high  $k_{\text{cat}}/K_M$  values (Sowek et al., 1991; Hart et al., 2016). Similarly, kinetic parameters are largely unchanged for hydrolysis of 6-furylacrylpenicillanic acid (FAP) (Wang

et al., 2002). These results suggest the E104K substitution does not significantly modify active site structures that are necessary for penicillin hydrolysis. Substitutions in TEM-1 that increase oxyimino-cephalosporin hydrolysis therefore need not reduce hydrolysis rates of excellent substrates such as penicillins.

The E240K substitution has been evaluated in multiple publications and exhibits an  $\sim 4$ -fold increase in  $k_{\text{cat}}/K_M$  for cefotaxime hydrolysis compared to TEM-1 with a value of  $\sim 6.6 \times 10^3 \text{ M}^{-1}\text{s}^{-1}$  (Table 1). The  $K_M$  for cefotaxime hydrolysis is decreased to a measurable value of  $\sim 140 \mu\text{M}$  while  $k_{\text{cat}}$  is low and has a value of  $\sim 0.5 \text{ s}^{-1}$ . With regard to ceftazidime hydrolysis, the E240K substitution results in a roughly 30-fold increase in  $k_{\text{cat}}/K_M$  compared to TEM-1 (Table 2). Similar to the E104K substitution, the E240K substitution results in only modest changes in kinetic parameters for hydrolysis of penicillins such as benzylpenicillin (Sowek et al., 1991). Thus, like E104K, the E240K enzyme is an excellent penicillinase. Finally, a comparison of the effects of E104K vs. E240K on  $k_{\text{cat}}/K_M$  for cefotaxime and ceftazidime reveals that both substitutions result in a  $\sim 5$ -fold increase for cefotaxime but a 30–40-fold increase for ceftazidime relative to TEM-1, indicating these substitutions have the largest impact on ceftazidime hydrolysis.

## A237T SUBSTITUTION

The A237T substitution occurs more rarely than R164S or G238S among TEM ESBLs and when it occurs, it is associated with other substitutions, particularly R164S (www.lahey.org/studies/webt.asp). The A237T substitution was first identified in a selection for mutants of TEM-1 with increased cephalosporin C resistance (Hall and Knowles, 1976). There have been relatively few detailed biochemical studies of the effect of the A237T substitution. Healy et al. showed with purified enzyme that the A237T substitution results in a 2-fold decrease in  $k_{\text{cat}}$  but a modest (1.3-fold) increase in  $k_{\text{cat}}/K_M$  for hydrolysis of the cephalosporins cephalothin and cephalosporin C (Healy et al., 1989). In addition, they showed the substitution reduces hydrolysis of benzylpenicillin and ampicillin with a 7-fold decrease in  $k_{\text{cat}}$  and a  $\sim 10$ -fold decrease in  $k_{\text{cat}}/K_M$ . The A237T substitution also decreases the thermal stability of the enzyme by  $5^\circ\text{C}$ . Further, Cantu et al. made similar observations with regard to the negative effect of A237T on benzylpenicillin and ampicillin hydrolysis and also showed the substitution causes a modest 1.3-fold increase in  $k_{\text{cat}}/K_M$  for cefotaxime (Cantu et al., 1997). A further suggestion that the A237T substitution increases cefotaxime hydrolysis comes from a study showing that TEM-24 (Q39K/E104K/R164S/A237T/E240K) exhibits a  $\sim 10$ -fold higher  $V_{\text{max}}/K_M$  value for cefotaxime hydrolysis relative to TEM-46 (Q39K/E104K/R164S/E240K) (Chanal-Claris et al., 1997). There is no structural information available on a TEM A237T mutant; however, by analogy to structures of the class A enzymes Toho-1, CTX-M-9, and CTX-M-14 in complex with cefotaxime, it is possible that the hydroxyl group of Thr237 makes a hydrogen bond to the C4 carboxylate group to enhance

cefotaxime hydrolysis (Shimamura et al., 2002; Delmas et al., 2010; Adamski et al., 2015).

## M182T SUBSTITUTION

The M182T substitution is found in many TEM ESBL enzymes as well as inhibitor resistant enzymes. M182T is found in combination with other amino acid substitutions in ESBLs (www.lahey.org/studies/webt.asp). In contrast to the substitutions described above, residue 182 is not in the vicinity of the active site (Figure 3). The M182T substitution, when introduced by itself into the TEM-1 enzyme, does not alter substrate specificity (Sideraki et al., 2001; Wang et al., 2002). Instead, M182T acts by increasing thermodynamic stability and suppressing aggregation (Sideraki et al., 2001; Wang et al., 2002). A role for the M182T substitution in ESBL evolution was found in a genetic study to identify intragenic second-site suppressor mutations of folding and stability mutants in TEM-1  $\beta$ -lactamase (Huang and Palzkill, 1997). For this purpose, a destabilizing mutation in the hydrophobic core (L76N) was introduced into TEM-1. This resulted in rapid proteolysis of the enzyme in *E. coli* and a large reduction in ampicillin resistance. Suppressor mutations (i.e., mutations that restored ampicillin resistance to *E. coli* containing the TEM-1 L76N gene) were selected after random introduction of point mutations in the TEM gene (Huang and Palzkill, 1997). Using this approach, mutants that reverted the L76N substitution to leucine and isoleucine were discovered; however, the most common suppressor was M182T, which is located 17Å from residue 76 (Huang and Palzkill, 1997). The M182T substitution was shown to restore protein expression levels of TEM-1 L76N in *E. coli* and, importantly, restored expression of other destabilizing mutations in TEM-1. Based on these results, it was suggested that in natural ESBLs, M182T acts as a suppressor of folding and stability defects associated with substitutions that increase catalysis of extended-spectrum cephalosporins or cause inhibitor resistance (Huang and Palzkill, 1997). It was named a “global suppressor” based on similar properties to intragenic second-site stabilizing mutations that had previously been observed in staphylococcus nuclease that were named global suppressors (Shortle and Lin, 1985).

It was later shown that the TEM-1 L76N substitution results in misfolding leading to aggregation and proteolysis of the enzyme in the periplasmic space of *E. coli* (Sideraki et al., 2001). The addition of the M182T substitution restored the accumulation of active, folded enzyme in the periplasm and suppressed the formation of aggregates. It was also shown that, in guanidinium hydrochloride denaturation experiments, M182T did not act on the final stability of the L76N enzyme (Sideraki et al., 2001). Subsequently, it has been shown using circular dichroism (CD) measurements at increasing temperatures that M182T does increase the thermodynamic stability of the wild-type TEM-1 enzyme (Wang et al., 2002). In addition, it was shown using the CD assay that TEM mutations that increase oxyimino-cephalosporin hydrolysis such as R164S and G238S, also decrease the thermodynamic stability of the enzyme, i.e., there is a stability-function trade-off (Wang et al., 2002). Previous



studies had also shown that R164S and G238S have reduced stability relative to wild-type TEM-1 (Raquet et al., 1995). Adding the M182T substitution to the G238S enzyme results in increased thermodynamic stability suggesting that M182T compensates for TEM ESBL substitutions that trade off protein stability for improved oxyimino-cephalosporin hydrolysis (Wang et al., 2002).

Consistent with the results of Wang et al. (2002), Knies et al. recently showed that M182T increases the thermostability of wild type TEM-1, that the G238S substitution results in lower thermostability of TEM-1, and that the M182T substitution restores stability to the M182T/G238S mutant (Knies et al., 2017). These authors note, however, that the increased thermostability does not correlate with increased cefotaxime MICs. They go on to suggest that the effects of the mutations on other factors may be important, such as folding/misfolding or kinetic stability (Knies et al., 2017). Studies on *in vivo* (in periplasm) folding kinetics and propensity for misfolded products of TEM ESBL mutants such as G238S and the influence of mutations including M182T on such folding will be of interest to further address the *in vivo* effect of ESBL substitutions and the role of global suppressor substitutions.

There have been multiple proposals for the structural basis by which M182T increases enzyme thermostability. Farzaneh et al. proposed that the threonine at position 182 results in a new hydrogen bond between residue 182 and the main chain carbonyl group of residue 64 (Farzaneh et al., 1996). This would provide an additional link between the  $\alpha$  and  $\alpha\beta$  domains of  $\beta$ -lactamase and possibly increase stability. Alternatively, it has been shown that Thr182 acts as an N-cap residue for the residue 183-195  $\alpha$ -helix by forming an additional hydrogen bond to Ala185 that would be expected to increase stability (Minasov et al., 2002).

Finally, it is also noteworthy that several groups have now shown that there are, in fact, many substitutions in TEM-1 that increase the stability of the enzyme including V31R, I47V, F60Y, P62S, G78A, V80I, S82H, G92D, R120G, E147G, H153R, M182T, A184V, T188I, L201P, I208M, A224V, E240H, R241H, I247V, T265M, R275Q, R275L, and N276D (Bershtein et al., 2008; Kather et al., 2008; Marciano et al., 2008; Brown et al., 2010; Deng et al., 2012). A number of these substitutions have been observed in TEM ESBL or inhibitor-resistant enzymes from clinical isolates including G92D, R120G, H153R, M182T, A184V, A224V, T265M, R275Q, and N276D (Brown et al., 2010). Therefore, suppression of folding and stability defects is likely achieved by several mutational pathways in natural variants.

## MULTIPLE SUBSTITUTIONS AND EPISTASIS IN TEM ESBLs

TEM ESBLs from resistant clinical isolates contain 1–5 substitutions and multiply substituted enzymes are the rule with single substitutions being relatively rare ([www.lahey.org/studies/webt.asp](http://www.lahey.org/studies/webt.asp)). Many ESBLs contain a core substitution of either R164S or G238S with additional substitutions such as E104K, M182T, A237T or E240K. Enzymes containing R164S are more often associated with high ceftazidime resistance while

those with G238S are associated with high cefotaxime resistance. This is related to the fact, as discussed above, that the R164S substitution gives a large increase in  $k_{\text{cat}}/K_M$  for ceftazidime relative to wild type TEM-1 and G238S gives a large increase in cefotaxime  $k_{\text{cat}}/K_M$  relative to wild type. This categorization is an oversimplification, however, in that R164S does moderately increase cefotaxime hydrolysis and G238S moderately increases ceftazidime hydrolysis relative to wild-type TEM-1.

The addition of substitutions to R164S and G238S mutations results in increased oxyimino-cephalosporin hydrolysis. For example, the addition of E104K to R164S results in a 30-fold increase in  $k_{\text{cat}}/K_M$  for ceftazidime and a 2.4-fold increase for cefotaxime hydrolysis relative to the R164S enzyme (Sowek et al., 1991). Addition of the E240K substitution to R164S results in a 7-fold increase in  $k_{\text{cat}}/K_M$  for ceftazidime but only a modest 1.2-fold increase for cefotaxime hydrolysis (Sowek et al., 1991). Further, the addition of E104K to the G238S enzyme results in a 15-fold increase in  $k_{\text{cat}}/K_M$  for ceftazidime and a 10-fold increase for cefotaxime hydrolysis relative to the G238S enzyme (Wang et al., 2002). The addition of E240K to the G238S enzyme results in a 37-fold increase in  $k_{\text{cat}}/K_M$  for ceftazidime and a 2.6-fold increase for cefotaxime hydrolysis relative to G238S (Venkatachalam et al., 1994). Taken together, these findings show that the E104K and E240K substitutions increase  $k_{\text{cat}}/K_M$  of either R164S or G238S for both ceftazidime and cefotaxime. However, the effect is more pronounced for ceftazidime. It has been noted by Sowek et al., the effect of E104K and E240K on ceftazidime hydrolysis may be due to favorable electrostatic interactions of lysine in either position with the carboxylate group found in the C7 $\beta$  side chain of ceftazidime (Sowek et al., 1991).

R164S or G238S mutations in combination with E104K or E240K generally result in additive effects on catalysis where the combination of two substitutions that each increase hydrolysis leads to even higher levels of hydrolysis in the double mutant. Additive combinations reveal that the two substitutions have independent effects on catalysis (Wells, 1990). However, not all substitutions associated with TEM ESBLs are additive. For example, the combination of E104K and E240K, each of which increases  $k_{\text{cat}}/K_M$  for cefotaxime hydrolysis when introduced individually into the TEM-1 enzyme, results in an E104K/E240K double mutant that hydrolyzes cefotaxime with a  $k_{\text{cat}}/K_M$  at the same level as the E104K substitution alone (Hart et al., 2016). Similarly, the addition of E104K to a R164S/E240K enzyme results in an E104K/R164S/E240K mutant that exhibits the same  $k_{\text{cat}}/K_M$  value for cefotaxime hydrolysis as the R164S/E240K enzyme (Sowek et al., 1991). Therefore, in these examples, the presence of E240K negates the effect of E104K (and vice versa). The lack of additivity means that the two mutations interact, directly or indirectly, and that the interaction has a negative effect on hydrolysis.

Non-additive effects of mutations are termed epistasis (de Visser and Krug, 2014; Dellus-Gur et al., 2015). Epistasis is an important element of evolution because it determines what mutational pathways are accessible to natural selection (de Visser and Krug, 2014; Dellus-Gur et al., 2015). Indeed, these effects

have been highlighted for a TEM mutant consisting of a promoter mutation (g4205a) as well as the amino acid substitutions A42G/E104K/M182T/G238S. This variant provides high-level cefotaxime resistance to *E. coli* (Stemmer, 1994; Orenca et al., 2001). Weinreich et al. showed that out of the  $5! = 120$  mutational pathways leading from wild type to the final mutant, 102 were selectively inaccessible paths in that some of the individual mutations do not increase cefotaxime resistance on all allelic backgrounds. Because some increase in cefotaxime resistance is required for selection of intermediate mutations, mutational pathways that include a step with no selection advantage will be dead-ends. Thus, negative epistasis excludes some of the possible pathways by which complex mutations may arise (Weinreich et al., 2006).

A well-studied example of epistasis in the TEM system from a structural and functional standpoint is the combination of R164S with G238S. The combination of R164S and G238S, each of which increase resistance toward cefotaxime and ceftazidime, results in a double mutant R164S/G238S with reduced resistance toward each of these (Giakkoupi et al., 2000). The  $k_{\text{cat}}/K_M$  for cefotaxime hydrolysis by the R164S/G238S double mutant is the same as R164S and 20-fold lower than that for G238S, indicating negative epistasis between the substitutions (Dellus-Gur et al., 2015). In each case, the  $k_{\text{cat}}/K_M$  for the double mutant is significantly smaller than the  $k_{\text{cat}}/K_M$  expected if the two mutations were simply additive.

In order to understand the molecular basis of the observed epistasis, the structure of the R164S/G238S double mutant was determined by Dellus-Gur et al. in the context of other stabilizing substitutions that do not impact kinetic parameters as described above for G238S and R164S (Dellus-Gur et al., 2015). As noted above, the G238S substitution induced two dominant conformations of the G238-loop while the R164S substitution induced an ensemble of conformations of the omega loop. The R164S/G238S double mutant exhibited a wider ensemble of conformations than the single mutants (Dellus-Gur et al., 2015). In addition, a non-native interaction between residues 171 and 240 is present which results in a dominant, large change in the position of the catalytically important residue Asn170. It was suggested that the entropic cost of the substrate selecting from the many conformations, in addition to the unfavorable position of Asn170 results in the low  $k_{\text{cat}}$  for cefotaxime hydrolysis by the double mutant, thereby accounting for the negative epistatic effect of introducing the second mutation (Dellus-Gur et al., 2015). Based on the results, the authors suggest there is a delicate balance between the adaptive benefit of increased structural freedom to allow oxyimino-cephalosporin access to the active site and the cost of diluting the catalytically optimal conformation among many non-productive conformations that decreases catalytic efficiency (Dellus-Gur et al., 2015). This study also provides evidence for the importance of conformational ensembles or sub-states in enzyme action and evolution. The coexistence of multiple sub-states has been referred to as “floppiness” and is recognized as an important component of enzyme catalytic efficiency and evolution (Tokuriki and Tawfik, 2009a; Bar-Even et al., 2015).

## COMPUTATIONAL STUDIES OF CONFORMATIONAL HETEROGENEITY OF TEM ESBLs

Computational studies also support a role for conformational flexibility in the evolution of altered specificity in the TEM-1 enzyme. It has been shown through docking and molecular dynamics that the G238S and E104K substitutions induce changes in the conformation of the omega loop as well as regions consisting of residues 86–118, 213–229, and 267–271 upon binding cefotaxime (Singh and Dominy, 2012). In addition, a study has demonstrated flexibility in TEM-1 and greater flexibility in ancestral  $\beta$ -lactamases that exhibit broader substrate specificity, thereby linking flexibility with broad specificity (Zou et al., 2015). Further, hidden allosteric sites have been discovered in the TEM enzyme (Horn and Shoichet, 2004; Bowman et al., 2015). These sites are binding pockets that are not present in the crystal structure but become available as the protein structure fluctuates in solution. Such a site was discovered via structure determination of a small molecule inhibitor that was found bound in a pocket 16 Å from the active site that is not apparent in the apoenzyme (Horn and Shoichet, 2004). The conformational changes associated with small molecule binding in the cryptic pocket were communicated to the active site resulting in movement of a key active site residue thereby inhibiting the enzyme (Horn and Shoichet, 2004). Hidden allosteric sites that are sampled among TEM-1 conformations have also been discovered computationally and thiol labeling experiments support their presence in TEM-1 (Bowman and Geissler, 2012; Bowman et al., 2015). Taken together, these studies support a role for conformational heterogeneity in  $\beta$ -lactamases and its potential impact on catalysis via communication with the active site.

Recently, molecular dynamics simulations and Markov State Models (MSMs) were used to examine the mechanism of action of the TEM-1 wild type, E104K, and G238S substitutions on cefotaxime hydrolysis (Hart et al., 2016). The authors showed that docking of cefotaxime into static TEM ESBL structures shows a poor correlation with  $k_{\text{cat}}/K_M$  of the variants, suggesting the static structures do not contain sufficient information to understand the function of the enzymes. The correlation was improved using “Boltzman docking” where MSMs based on molecular dynamics simulations were weighted to the contribution of each state by its equilibrium probability (Hart et al., 2016). The results suggested that consideration of enzyme conformational sub-states rather than a single structure provides more relevant information on TEM ESBL activity against cefotaxime. Next, the authors used MSMs constructed based on molecular dynamics of wild type TEM-1 and the E104K/G238S enzyme that hydrolyzes cefotaxime >1,000-fold faster than wild type and identified states that are more populated by E104K/G238S than by wild type. Interestingly, it was found that the “cefotaximase states” resembled the wild-type structure while the omega loop in the wild type undergoes substantial rearrangements (Hart et al., 2016). This suggests that E104K/G238S hydrolyzes cefotaxime more efficiently than wild type because the omega loop is actually more constrained

in a conformation that will accommodate cefotaxime in the double mutant while the wild-type TEM-1 samples many non-productive conformations. Support for this model was obtained by chemical footprinting and the construction of mutations predicted to preferentially occupy active conformational states (Hart et al., 2016). These findings suggest that, contrary to the view that the active site needs to become more open to accommodate cefotaxime, for productive catalysis it needs to be more constrained to limit non-productive sub-states (Hart et al., 2016). Examination of the most populated states of E104K/G238S cefotaximase indicated the serine at position 238 and lysine at position 104 act to pin down the omega loop to limit non-productive conformations (Hart et al., 2016). These results again highlight the importance of conformational sub-states and provide a different view from the idea that the expansion of the TEM-1 active site by ESBL mutations to accommodate oxyimino-cephalosporins is the causative basis of enhanced catalytic efficiency.

## CTX-M $\beta$ -LACTAMASE VARIANTS AND CEFTAZIDIME HYDROLYSIS

CTX-M  $\beta$ -lactamases are class A enzymes that are characterized by the ability to efficiently hydrolyze cefotaxime (Bonnet, 2004). These enzymes have spread globally to become the most widespread ESBLs in Gram-negative bacteria (Cantón et al., 2012). The CTX-M ESBLs are divided into five clusters based on amino acid sequence homology including CTX-M-1, CTX-M-2, CTX-M-8, CTX-M-9, and CTX-M-25 with the names based on the prominent member of each subgroup (D'Andrea et al., 2013). The subgroups differ from one another by >10% amino acid sequence divergence and each subgroup contains a number of variants that differ from one another by <5% sequence divergence (D'Andrea et al., 2013). The CTX-M enzymes are ~35% identical to TEM-1  $\beta$ -lactamase.

The Toho-1 (CTX-M-44), CTX-M-9, and CTX-M-14 enzymes have been the most intensively studied in terms of structure and mechanism (Shimamura et al., 2002; Chen et al., 2005; Delmas et al., 2010). Toho-1 is in the CTX-M-2 subfamily while CTX-M-9 and -14 are in the CTX-M-9 subfamily and differ only in a V231A substitution in CTX-M-9 relative to CTX-M-14 (Chen et al., 2005; D'Andrea et al., 2013). In addition, CTX-M-9 and CTX-M-14 exhibit similar kinetic parameters for  $\beta$ -lactam substrate hydrolysis (Chen et al., 2005). Therefore, structure and function conclusions from studies of one of these enzymes are likely to apply to the others.

The focus here will be on CTX-M-14 and the role of amino acid substitutions found in variants that increase ceftazidime hydrolysis. In contrast to TEM-1, the CTX-M enzymes are excellent catalysts for the hydrolysis of cefotaxime (Bonnet, 2004). With regard to CTX-M-14,  $k_{\text{cat}}$  is in the range of 200–400  $\text{s}^{-1}$  and  $K_M \sim 100 \mu\text{M}$  while  $k_{\text{cat}}/K_M$  is  $\sim 3.0 \times 10^6 \text{ M}^{-1}\text{s}^{-1}$  (Chen et al., 2005; Adamski et al., 2015; Patel et al., 2015). Thus, the  $k_{\text{cat}}/K_M$  value for cefotaxime hydrolysis by CTX-M-14 is about 1,500-fold higher than that for TEM-1. Structural studies of CTX-M-14 and CTX-M-9 apoenzymes reveal that,

contrary to the expectation that a wider active site would better accommodate cefotaxime, the active site is narrower than that observed for TEM-1 (Chen et al., 2005; Delmas et al., 2010). X-ray structures of CTX-M-14 and CTX-M-9 in the presence of cefotaxime show that the active site expands significantly with cefotaxime bound in the active site (Delmas et al., 2010; Adamski et al., 2015). These structures were solved using an S70G substitution of the nucleophile for acylation in order to trap the unhydrolyzed substrate (Delmas et al., 2010). The expansion is accompanied by the breaking of a hydrogen bond between the main chain carbonyl oxygen of Asn170 and the main chain NH of Asp240 that connects to omega loop the  $\beta$ -3 strand (Delmas et al., 2010) (Figure 6). Note that this is a similar region of the active site as that of TEM-1 where the G238S substitution increases the hydrolysis of oxyimino-cephalosporins and the proposed effect of increasing the size of the active site is similar.

Although CTX-M enzymes rapidly hydrolyze cefotaxime, the related oxyimino-cephalosporin ceftazidime is poorly hydrolyzed (Bonnet, 2004). Determinations of kinetic parameters for CTX-M-14 for ceftazidime reveal high  $K_M$  values of  $>600 \mu\text{M}$ ,  $k_{\text{cat}}$  values  $<5 \text{ s}^{-1}$  and a  $k_{\text{cat}}/K_M$  of  $1\text{--}5 \times 10^3 \text{ M}^{-1}\text{s}^{-1}$  (Chen et al., 2005; Patel et al., 2015). This  $k_{\text{cat}}/K_M$  value is ~1,000-fold less than  $k_{\text{cat}}/K_M$  for cefotaxime hydrolysis by CTX-M-14. Note, however, that this  $k_{\text{cat}}/K_M$  value for ceftazidime is still ~100-fold higher than that observed for TEM-1 indicating CTX-M is a significantly better catalyst for this substrate than TEM-1. The difference in  $k_{\text{cat}}/K_M$  for ceftotaxime vs. ceftazidime by CTX-M enzymes is due to the extra bulk of the C7 $\beta$  side chain of ceftazidime that contains a carboxypropyl group replacing the methyl group found in cefotaxime. This leads to steric clashes in binding ceftazidime in the CTX-M active site (Delmas et al., 2008).

## CTX-M D240G SUBSTITUTION

As noted, the CTX-M enzymes hydrolyze ceftazidime poorly compared to cefotaxime. In the last 15 years, however, variants have emerged that are able to hydrolyze ceftazidime (Bonnet, 2004; Cantón et al., 2012; D'Andrea et al., 2013). In particular, the D240G and P167S substitutions occur individually in multiple CTX-M subgroups where they enhance ceftazidime hydrolysis (Bonnet et al., 2001, 2003; Cartelle et al., 2004; Kimura et al., 2004; Ishii et al., 2007). For example, the D240G substitution has been identified in the CTX-M-1, -2, -9, and -25 subfamilies while the P167S substitution has been identified in variants belonging to the CTX-M-1 and -9 subfamilies (D'Andrea et al., 2013). CTX-M variants containing D240G or P167S from clinical isolates are associated with increased MIC values for ceftazidime and the introduction of the substitutions into CTX-M-14 results in increased ceftazidime MICs for *E. coli* containing the mutants vs. the wild-type CTX-M-14 (Patel et al., 2015).

The D240G substitution, when introduced into CTX-M-14 or CTX-M-9, results in a 10-fold increase in  $k_{\text{cat}}/K_M$  for ceftazidime hydrolysis (Bonnet et al., 2003; Chen et al., 2005; Patel et al., 2015). Residue 240 is at the end of the  $\beta$ 3-strand that flanks the active site and also contains Thr235 and Ser237



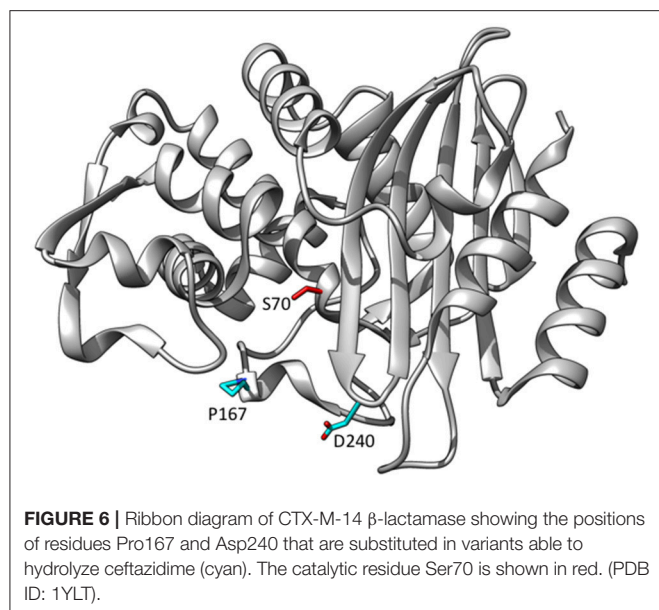


**FIGURE 6** | Ribbon diagram of CTX-M-14 β-lactamase showing the positions of residues Pro167 and Asp240 that are substituted in variants able to hydrolyze ceftazidime (cyan). The catalytic residue Ser70 is shown in red. (PDB ID: 1YLT).

that make direct interactions with the C4 carboxylate group of cephalosporins (Delmas et al., 2010; Adamski et al., 2015; **Figure 6**). The X-ray crystal structure of CTX-M-14 containing the D240G substitution (CTX-M-27) has been determined, and anisotropic B-factor analysis demonstrated increased flexibility of the β3- strand that forms the side of the active site (Chen et al., 2005). This increase in flexibility is thought to expand its substrate profile by allowing access to the bulkier ceftazidime molecule (Chen et al., 2005).

The effect of the D240G substitution was further investigated by determining the structure of CTX-M-9 with the D240G substitution in complex with a glycyboronic acid containing the C7β oximino side chain of ceftazidime which forms a covalent adduct with Ser70 and places the ceftazidime side chain in a similar position as cefotaxime in the Toho-1 E166A-cefotaxime structure (Shimamura et al., 2002; Delmas et al., 2008). A comparison of the positioning of the ceftazidime side chain in the D240G mutant to its position in the wild type CTX-M-9 revealed that the aminothiazole ring was positioned deeper into the active site, more resembling the position of the aminothiazole ring in cefotaxime structures (Delmas et al., 2008). This positioning, in turn, led to more optimal contacts of the NH of the amide group of the ceftazidime side chain with the Ser237 main chain oxygen. Molecular dynamics simulations of ceftazidime acyl-enzyme structures of CTX-M-9 and the D240G mutant based on the ceftazidime-like boronic acid structures also suggested more optimal contacts of Thr235 with the C4 carboxylate of ceftazidime. A new hydrogen bond is observed between the amino group of the aminothiazole ring and the Pro167 backbone oxygen, along with an improved Ser237 main chain O interaction with the amide group (Delmas et al., 2008). Thus, the D240G substitution, via deeper positioning of the aminothiazole ring, appears to improve interactions with ceftazidime with multiple active site groups (Delmas et al., 2008).

## CTX-M P167S SUBSTITUTION

The CTX-M P167S substitution, when introduced into CTX-M-14, results in a 10-fold increase in  $k_{cat}/K_M$  for ceftazidime hydrolysis, similar to that observed for D240G (Patel et al., 2015). Pro167 resides on the omega loop and the peptide bond between Glu166 and Pro167 is in the *cis* configuration (**Figure 6**). The *cis* peptide bond contributes strongly to the conformation of the omega loop and particularly the positioning of Asn170 (Patel et al., 2017). Pro167 is largely conserved among class A β-lactamases, including TEM-1, and is a *cis*-proline in these enzymes (Philippon et al., 2016).

Molecular dynamics simulations based on the structure of the Toho-1 (CTX-M-44) enzyme have been performed to assess the effect of the P167S substitution (Kimura et al., 2004). The results suggested that in the P167S enzyme, the aminothiazole ring is displaced to prevent steric clash with Ser167 causing the C4 carboxylate of ceftazidime to hydrogen bond to Ser130 and Ser237 and enhancing hydrolysis (Kimura et al., 2004).

The CTX-M-14 β-lactamase has also been used as a model system to examine the structural changes caused by the P167S substitution that are associated with increased ceftazidime hydrolysis. A number of X-ray structures of CTX-M-14 P167S were solved that enabled an evaluation of the changes in structure between the apoenzyme, the initial enzyme complex with ceftazidime, and the formation of the ceftazidime-acyl enzyme (Patel et al., 2017). The S70G mutation was introduced to P167S to prevent acyl-enzyme formation and capture the structure of the enzyme-substrate complex and the E166A mutation was introduced to P167S to prevent deacylation of the acyl-enzyme to observe the acyl-enzyme structure. It was observed that the P167S apoenzyme closely resembled CTX-M-14 and the peptide bond preceding Ser167 was *cis*, despite a non-prolyl *cis* peptide bond being very energetically unfavorable (Jorgensen and Gao, 1988; Patel et al., 2017). The S70G/P167S structure in complex with ceftazidime revealed that the substrate bound with the C8 carbonyl oxygen in the oxyanion hole, as expected for a productive complex. The C4 carboxylate was bound by Thr235 but the C7β side chain was more solvent exposed due to steric constraints with the omega loop (**Figure 7**). The omega loop retained the conformation observed for the wild-type CTX-M-14 and P167S enzymes, and the peptide bond preceding Ser167 was also *cis* (Patel et al., 2017; **Figure 8**). The addition of E166A to the P167S enzyme to create E166A/P167S also showed the omega loop in a closed conformation in the apoenzyme structure, similar to the wild type and P167S apoenzymes (**Figure 8**). However, the peptide bond preceding Ser167 was *trans*. The addition of ceftazidime to E166A/P167S to form an acyl-enzyme resulted in a *trans* peptide bond preceding Ser167 and a large conformational change of the omega loop with Asn170 moving 4.2 Å out of the active site to create a pocket to accommodate the ceftazidime side chain (Patel et al., 2017; **Figures 7, 8**). This resulted in the aminothiazole ring sinking deeply into the active site in a buried position (**Figure 7**). These results suggested that both the Ser167 substitution and the presence of acylated ceftazidime are required for the conformational change. Finally, in order to show that the conformational change was due to

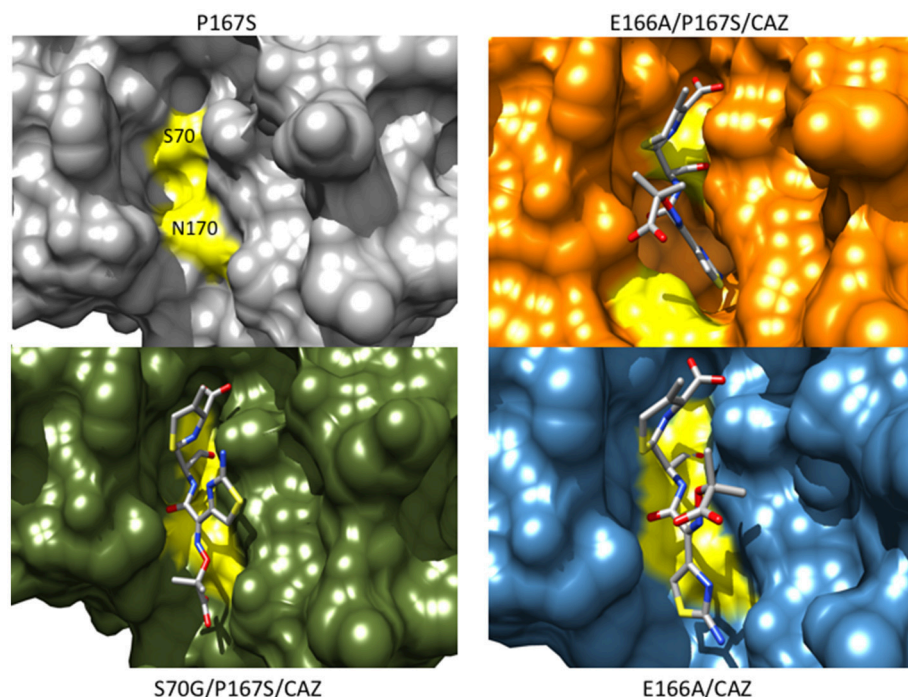


**FIGURE 7 |** Protein surface representations of the CTX-M-14 P167S (gray) (PDB ID:5TWD), S70G/P167S with ceftazidime (green) (5TWE), E166A/P167S with acylated ceftazidime (orange) (5TW6) and E166A with acylated ceftazidime (blue) (5U53) are shown. The positions of Ser70 and Asn170 on the CTX-M structure are shown in yellow illustrating the movement of the omega loop in the E166A/P167S/CAZ acyl-enzyme separates Ser70 and Asn170 to create space in the active site to accommodate ceftazidime.

the P167S substitution and not the E166A substitution that was used to trap the acyl-enzyme, the structure of E166A in complex with ceftazidime was determined. This showed the acyl-ceftazidime in the active site with Pro167 in the *cis* configuration and the omega loop in the closed conformation indicating the P167S substitution is required for the conformational change (Figures 7, 8). Therefore, the P167S substitution and the presence of acylated ceftazidime were both necessary to drive the structure toward a *trans* peptide bond at residue 167 and to induce conformational change of the omega loop (Patel et al., 2017).

It is interesting to note that the structure of the CTX-M-9 D140G enzyme in complex with the ceftazidime-like boronic acid inhibitor and the CTX-M-14 E166A/P167S enzyme with acylated ceftazidime show the aminothiazole ring sinking to a deeper position in the active site relative to CTX-M-9 or CTX-M-14, respectively (Delmas et al., 2008; Patel et al., 2017). This suggests the P167S and D240G substitutions utilize different paths to a broadly similar end result—altered positioning of the aminothiazole ring and better contacts of substrate with the enzyme. In addition, the TEM-64 (E104K/R164S/M182T) ESBL enzyme with increased activity toward ceftazidime also displays a similar conformational change of the omega loop when complexed to a boronic acid inhibitor (Wang et al., 2002). Finally, a TEM-1 triple mutant (W165Y/E166Y/P167G) selected from a random mutagenesis experiment for increased hydrolysis of ceftazidime displays a large conformational change of the omega loop creating space to accommodate ceftazidime (Stojanowski

et al., 2015). These studies suggest that enlargement of the active site via movement of the omega loop, which results in a shift of the Asn170 residue, is an important mechanism by which mutations can lead to hydrolysis of the bulky ceftazidime molecule in class A  $\beta$ -lactamases.

## STABILIZING SUBSTITUTIONS IN CTX-M NATURAL VARIANTS

It has been demonstrated that the P167S and D240G substitutions both destabilize the CTX-M enzyme (Chen et al., 2005; Patel et al., 2015). As indicated above, the CTX-M family consists of a large number of variants containing amino acid substitutions (D'Andrea et al., 2013). Many of the substitutions are located outside of the active site and their effect on CTX-M structure and function is largely unknown. The A77V substitution is found in multiple subfamilies including the CTX-M-1, CTX-M-9, and CTX-M-25 groups (Patel et al., 2015). In addition, A77V has been found associated with either the P167S or D240G substitutions in each of these subfamilies. Using the CTX-M-14 model system, addition of the A77V substitution to either a P167S or D240G enzyme results in enhanced steady-state protein expression levels in *E. coli* relative to the P167S or D240G single mutants (Patel et al., 2015). In addition, the A77V/P167S and A77V/D240G enzymes exhibit increased thermal stability *in vitro* compared to the P167S and D240G enzymes (Patel et al.,

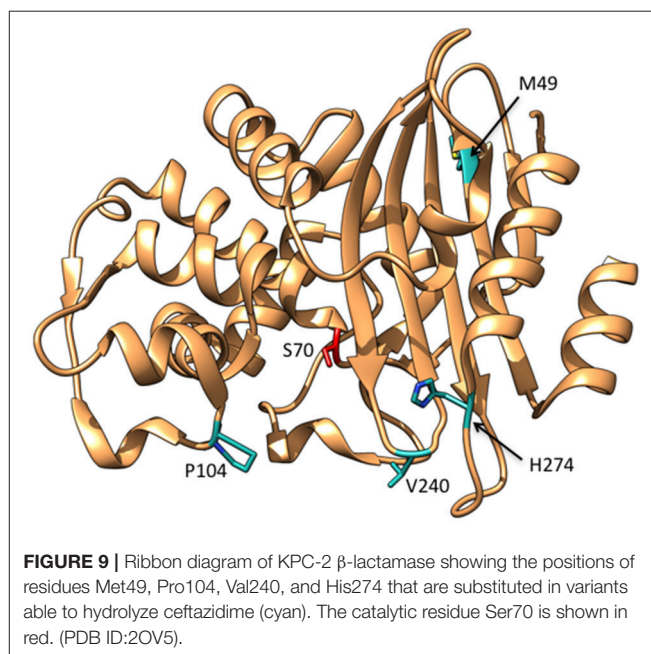
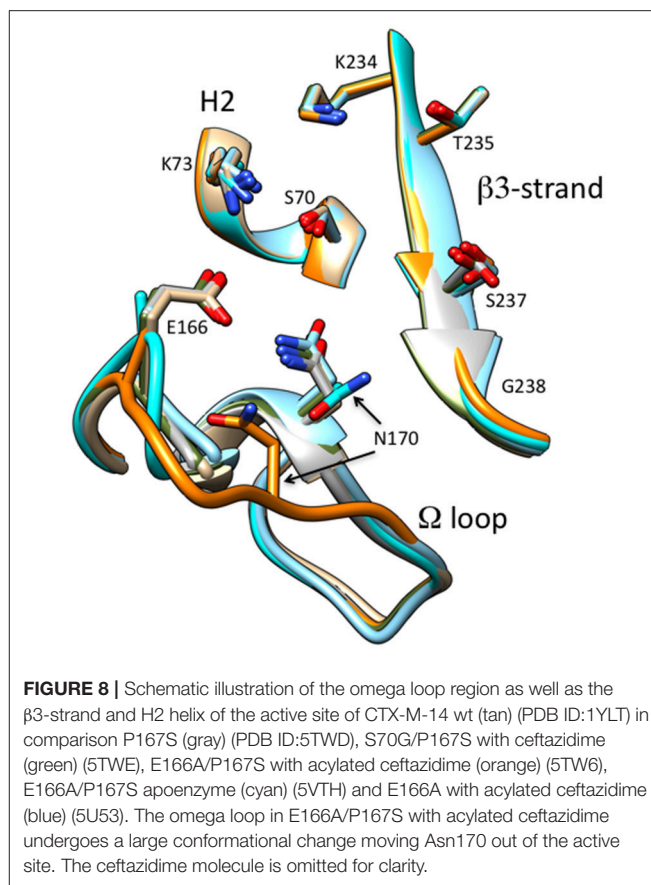
2015). Based on these results, A77V has been suggested to be a global suppressor for CTX-M, analogous to M182T for TEM-1. Given the large number of substitutions among CTX-M variants, it is likely that other global suppressors are present in the family of clinical variants.

## KPC $\beta$ -LACTAMASE VARIANTS AND CEFTAZIDIME HYDROLYSIS

KPC-2  $\beta$ -lactamase is a class A enzyme that hydrolyzes a broad range of  $\beta$ -lactam antibiotics including penicillins, cephalosporins and carbapenems. This enzyme also efficiently hydrolyzes cefotaxime but only poorly hydrolyzes ceftazidime. The value for  $k_{\text{cat}}/K_M$  for cefotaxime hydrolysis is  $\sim 3.0 \times 10^5 \text{ M}^{-1}\text{s}^{-1}$  (Yigit et al., 2003; Levitt et al., 2012) while  $k_{\text{cat}}/K_M$  for ceftazidime is  $\sim 1.0 \times 10^3 \text{ M}^{-1}\text{s}^{-1}$  (Mehta et al., 2015). By comparison,  $k_{\text{cat}}/K_M$  for ceftazidime for KPC-2 is 25-fold higher than that for TEM-1 and similar to the  $k_{\text{cat}}/K_M$  value for CTX-M-14. KPC-2 is an important clinical problem due to its broad substrate profile and wide distribution in enteric bacteria (Nordmann et al., 2009). The problem is compounded by the evolution of KPC variants that with increased ceftazidime hydrolysis rates and resistance (Mehta et al., 2015; Naas et al., 2016). Over 20 variants of KPC have been identified that contain a range of amino acid substitutions (Naas et al., 2016).

A detailed study of the KPC-3 to KPC-11 variants showed that these enzymes exhibit increased  $k_{\text{cat}}/K_M$  values for ceftazidime hydrolysis compared to KPC-2 (Mehta et al., 2015). Amino acid substitutions found among these enzymes include M49I, P104R, P104L, V240G, V240A, and H274Y (Figure 9). The P104R single substitution was found to increase  $k_{\text{cat}}/K_M$  for ceftazidime by 10-fold compared to KPC-2 while P104L exhibited a more modest 2.5-fold increase (Mehta et al., 2015). The V240G substitution increased  $k_{\text{cat}}/K_M$  for ceftazidime by 5-fold and H274Y resulted in a 10-fold increase. Double mutants containing combinations of the single substitutions exhibited further increases in  $k_{\text{cat}}/K_M$ . For example, the V240G/H274Y, P104R/V240G, and P104R/H274Y enzymes displayed 40-, 50-, and 75-fold increases in  $k_{\text{cat}}/K_M$ , respectively, for ceftazidime relative to KPC-2 (Mehta et al., 2015). In contrast, the M49I/H274Y enzyme exhibited similar catalytic efficiency as the H274Y enzyme, suggesting that M49I does not contribute to ceftazidime hydrolysis; however, the M49I substitution alone was not studied. Further, it was shown that the P104R, V240G, and H274Y substitutions act additively rather than cooperatively, i.e., there is no epistasis, when combined into the double mutants. This indicates that the substitutions act independently and do not influence each other's function when present in the double mutants. This would also suggest that the order in which the mutations occur to form the double mutant is not important (Mehta et al., 2015).

There is currently no structural information on the variants so there is limited understanding of their effect on KPC or the mechanism by which they alter specificity. However, molecular modeling of the substitutions onto the KPC-2 structure and computational docking of ceftazidime suggested that the P104R



and H274Y substitutions could create new hydrogen bonding interactions with the C7 $\beta$ -oxymino side chain of ceftazidime (Mehta et al., 2015). Note that the P104R substitution is in



the same region of the proteins as the E104K substitution that commonly occurs in TEM ESBL variants. In addition, the V240G substitution is analogous to the CTX-M D240G substitution and could act by a similar mechanism of increasing flexibility of the  $\beta$ 3 strand and allowing the aminothiazole ring of ceftazidime to sink deeper into the active site upon binding (Chen et al., 2005; Delmas et al., 2008). Finally, the H274Y substitution appears to be unique to the KPC variants.

As noted above, several substitutions in TEM and CTX-M that increase oxyimino-cephalosporin hydrolysis also decrease stability (Wang et al., 2002; Chen et al., 2005; Patel et al., 2015; Knies et al., 2017). A similar pattern was observed with the substitutions found in the KPC-3 to KPC-11 variants. There was a strong inverse correlation between  $k_{\text{cat}}/K_M$  for ceftazidime hydrolysis and the  $T_m$  of the enzymes (Mehta et al., 2015). However, the  $T_m$  for the wild type KPC-2 (66°C) is significantly higher than that for TEM or CTX-M and even the most unstable KPC variant is more stable than wild-type TEM-1 (Mehta et al., 2015). Therefore, the high stability of KPC-2 may serve as a buffer to allow the accumulation of substitutions without causing unfolding of the enzyme. This type of stability buffer has been noted previously as a mechanism to enhance protein evolvability (Bloom and Arnold, 2009; Tokuriki and Tawfik, 2009b).

## CONCLUSIONS

The use of oxyimino-cephalosporins in the clinical setting has led to the evolution of variants of TEM-1, CTX-M, and KPC enzymes that can hydrolyze these drugs. The TEM-1 enzyme does not efficiently hydrolyze either cefotaxime or ceftazidime but there are now many variants that exhibit increased hydrolysis of these drugs. Initial isolates of CTX-M and KPC enzymes hydrolyze cefotaxime but not ceftazidime; however, variants now exist that hydrolyze ceftazidime. For TEM-1, recent studies have pointed to the importance of conformational heterogeneity of variants with ESBL substitutions. Rather than adopting a single, stable conformation, some variants exist in multiple

sub-states of conformations that contain active conformers that can accommodate oxyimino-cephalosporins. One study also indicates that sampling of non-productive sub-states underlies the failure of mutant combinations such as R164S/G238S and, in another study, wild-type TEM-1 itself, to hydrolyze oxyimino-cephalosporins. Studies with TEM-1 have also indicated that several ESBL substitutions increase catalytic activity but are associated with a cost in stability. Global suppressor mutations then occur to compensate for the stability loss. It will be of interest to examine the folding, aggregation and stability effects of ESBL mutations and the compensatory effects of suppressors *in vivo* in the periplasm. The substitutions associated with ceftazidime hydrolysis in CTX-M are different than those observed in TEM, but act through conformational changes in similar regions of the active site as TEM-1. KPC variants are in analogous positions as some TEM and CTX-M substitutions and may act similarly. Conformational heterogeneity and the existence of sub-states have not been examined for CTX-M or KPC variants but may also be an important contributor to the function of these ESBL enzymes.

## AUTHOR CONTRIBUTIONS

The author confirms being the sole contributor of this work and approved it for publication.

## FUNDING

$\beta$ -lactamase research in the author's laboratory is funded by National Institutes of Health grants AI32956 and AI106863.

## ACKNOWLEDGMENTS

The author wishes to thank Drs. Jin Wang and Jianwei Chen for assistance with preparation of **Figure 1**. In addition, the author thanks Drs. Hiram Gilbert and B.V.V. Prasad for discussions and comments on the manuscript.

## REFERENCES

- Adachi, H., Ohta, T., and Matsuzawa, H. (1991). Site-directed mutants, at position 166, of RTEM-1 beta-lactamase that form a stable acyl-enzyme intermediate with penicillin. *J. Biol. Chem.* 266, 3186–3191.
- Adamski, C. J., Cardenas, A. M., Brown, N. G., Horton, L. B., Sankaran, B., Prasad, B. V., et al. (2015). Molecular basis for the catalytic specificity of the CTX-M extended spectrum  $\beta$ -lactamases. *Biochemistry* 54, 447–457. doi: 10.1021/bi501195g
- Ambler, R. P., Coulson, F. W., Frere, J. M., Ghuyssen, J. M., Joris, B., Forsman, M., et al. (1991). A standard numbering scheme for the class A  $\beta$ -lactamases. *Biochem. J.* 276, 269–272. doi: 10.1042/bj2760269
- Ambler, R. P. (1980). The structure of beta-lactamases. *Phil. Trans. R. Soc. Lond. B Biol. Sci.* 289, 321–331. doi: 10.1098/rstb.1980.0049
- Bar-Even, A., Milo, R., Noor, E., and Tawfik, D. S. (2015). The moderately efficient enzyme: futile encounters and enzyme floppiness. *Biochemistry* 54, 4969–4977. doi: 10.1021/acs.biochem.5b00621
- Bershtein, S., Goldin, K., and Tawfik, D. S. (2008). Intense neutral drifts yield robust and evolvable consensus proteins. *J. Mol. Biol.* 379, 1029–1044. doi: 10.1016/j.jmb.2008.04.024
- Bloom, J. D., and Arnold, F. H. (2009). In the light of directed evolution: pathways of adaptive protein evolution. *Proc. Natl. Acad. Sci. U.S.A.* 106(Suppl. 1), 9995–10000. doi: 10.1073/pnas.0901522106
- Bonnet, R., Dutour, C., Sampaio, J. L. M., Chanal, C., Sirot, D., Labia, R., et al. (2001). Novel cefotaximase (CTX-M-16) with increased catalytic efficiency due to substitution Asp-240-Gly. *Antimicrob. Agents Chemother.* 45, 2269–2275. doi: 10.1128/AAC.45.8.2269-2275.2001
- Bonnet, R., Recule, C., Baraduc, R., Chanal, C., Sirot, D., De Champs, C., et al. (2003). Effect of D240G substitution in a novel ESBL CTX-M-27. *J. Antimicrob. Chemother.* 52, 29–35. doi: 10.1093/jac/dkg256
- Bonnet, R. (2004). Growing group of extended-spectrum  $\beta$ -lactamases: the CTX-M enzymes. *Antimicrob. Agents Chemother.* 48, 1–14. doi: 10.1128/AAC.48.1.1-14.2004
- Bonomo, R. A. (2017).  $\beta$ -lactamases: a focus on current challenges. *Cold Spring Harb. Perspect. Med.* 7:a025239. doi: 10.1101/cshperspect.a025239
- Bowman, G. R., and Geissler, P. L. (2012). Equilibrium fluctuations of a single folded protein reveal a multitude of potential cryptic allosteric sites. *Proc. Natl. Acad. Sci. U.S.A.* 109, 11681–11686. doi: 10.1073/pnas.1209309109
- Bowman, G. R., Bolin, E. R., Hart, K. M., Maguire, B. C., and Marqusee, S. (2015). Discovery of multiple hidden allosteric sites by combining Markov

- state models and experiments. *Proc. Natl. Acad. Sci. U.S.A.* 112, 2734–2739. doi: 10.1073/pnas.1417811112
- Brown, N. G., Pennington, J. M., Huang, W., Ayvaz, T., and Palzkill, T. (2010). Multiple global suppressors of protein stability defects facilitate the evolution of extended-spectrum TEM  $\beta$ -lactamases. *J. Mol. Biol.* 404, 832–846. doi: 10.1016/j.jmb.2010.10.008
- Bush, K., and Fisher, J. F. (2011). Epidemiological expansion, structural studies, and clinical challenges of new  $\beta$ -lactamases from Gram-negative bacteria. *Ann. Rev. Microbiol.* 65, 455–478. doi: 10.1146/annurev-micro-090110-102911
- Bush, K. (2002). The impact of  $\beta$ -lactamases on the development of novel antimicrobial agents. *Curr. Opin. Invest. Drugs* 3, 1284–1290.
- Cantón, R., González-Alba, J. M., and Galán, J. C. (2012). CTX-M enzymes: origin and diffusion. *Front. Microbiol.* 3:110. doi: 10.3389/fmicb.2012.00110
- Cantu, C. III., and Palzkill, T. (1998). The role of residue 238 of TEM-1  $\beta$ -lactamase in the hydrolysis of extended-spectrum antibiotics. *J. Biol. Chem.* 273, 26603–26609. doi: 10.1074/jbc.273.41.26603
- Cantu, C. III., Huang, W., and Palzkill, T. (1996). Selection and characterization of amino acid substitutions at residues 237–240 of TEM-1  $\beta$ -lactamase with altered substrate specificity for aztreonam and ceftazidime. *J. Biol. Chem.* 271, 22538–22545. doi: 10.1074/jbc.271.37.22538
- Cantu, C. III., Huang, W., and Palzkill, T. (1997). Cephalosporin substrate specificity determinants of TEM-1  $\beta$ -lactamase. *J. Biol. Chem.* 272, 29144–29150. doi: 10.1074/jbc.272.46.29144
- Cartelle, M., del Mar Tomas, M., Molina, F., Moure, R., Villanueva, R., and Bou, G. (2004). High-level resistance to ceftazidime conferred by a novel enzyme, CTX-M-32, derived from CTX-M-1 through a single Asp240-Gly substitution. *Antimicrob. Agents Chemother.* 48, 2308–2313. doi: 10.1128/AAC.48.6.2308-2313.2004
- Chanal-Claris, C., Siro, J., Bret, L., Chatron, P., Labia, R., and Siro, J. (1997). Novel extended-spectrum TEM-type  $\beta$ -lactamase from an *Escherichia coli* isolate resistant to ceftazidime and susceptible to cephalothin. *Antimicrob. Agents Chemother.* 41, 715–716.
- Chen, Y., Delmas, J., Siro, J., Shoichet, B., and Bonnet, R. (2005). Atomic resolution structures of CTX-M  $\beta$ -lactamases: extended spectrum activities from increased mobility and decreased stability. *J. Mol. Biol.* 348, 349–362. doi: 10.1016/j.jmb.2005.02.010
- Christensen, H., Martin, M., and Waley, G. (1990).  $\beta$ -Lactamases as fully efficient enzymes. *Biochem. J.* 266, 853–861.
- Damblon, C., Raquet, X., Lian, L. Y., Lamotte-Brasseur, J., Fonze, E., Charlier, P., et al. (1996). The catalytic mechanism of  $\beta$ -lactamases: NMR titration of an active-site lysine residue of the TEM-1 enzyme. *Proc. Natl. Acad. Sci. U.S.A.* 93, 1747–1752. doi: 10.1073/pnas.93.5.1747
- D'Andrea, M. M., Arena, F., Pallecchi, L., and Rossolini, G. M. (2013). CTX-M-type  $\beta$ -lactamases: a successful story of antibiotic resistance. *Int. J. Med. Microbiol.* 303, 305–317. doi: 10.1016/j.ijmm.2013.02.008
- Datta, N., and Kontomichalou, P. (1965). Penicillinase synthesis controlled by infectious R factors in *Enterobacteriaceae*. *Nature* 208, 239–241. doi: 10.1038/208239a0
- de Visser, J. A., and Krug, J. (2014). Empirical fitness landscapes and the predictability of evolution. *Nat. Rev. Genet.* 15, 480–490. doi: 10.1038/nrg3744
- Delaire, M., Lenfant, F., Labia, R., and Masson, J. M. (1991). Site-directed mutagenesis on TEM-1  $\beta$ -lactamase: role of Glu166 in catalysis and substrate binding. *Protein Eng.* 4, 805–810. doi: 10.1093/protein/4.7.805
- Dellus-Gur, E., Elias, M., Caselli, E., Prati, F., Salverda, M. L. M., De Visser, J. A. G. M., et al. (2015). Negative epistasis and evolvability in TEM-1  $\beta$ -lactamase - the thin line between an enzyme's conformational freedom and disorder. *J. Mol. Biol.* 427, 2396–2409. doi: 10.1016/j.jmb.2015.05.011
- Delmas, J., Chen, Y., Prati, F., Robin, F., Shoichet, B. K., and Bonnet, R. (2008). Structure and dynamics of CTX-M enzymes reveal insights into substrate accommodation by extended-spectrum  $\beta$ -lactamases. *J. Mol. Biol.* 375, 192–201. doi: 10.1016/j.jmb.2007.10.026
- Delmas, J., Leyssene, D., Dubois, D., Birck, C., Vazeille, E., Robin, F., et al. (2010). Structural insights into substrate recognition and product expulsion in CTX-M enzymes. *J. Mol. Biol.* 400, 108–120. doi: 10.1016/j.jmb.2010.04.062
- Deng, Z., Huang, W., Bakkalbasi, E., Brown, N. G., Adamski, C. J., Rice, K., et al. (2012). Deep sequencing of systematic combinatorial libraries reveals  $\beta$ -lactamase sequence constraints at high resolution. *J. Mol. Biol.* 424, 150–167. doi: 10.1016/j.jmb.2012.09.014
- Docquier, J. D., Benvenuti, M., Calderone, V., Rossolini, G. M., and Gangani, S. (2011). Structure of the extended-spectrum  $\beta$ -lactamase TEM-72 inhibited by citrate. *Acta Crystallogr. Sect. F Struct. Biol. Cryst. Commun.* 67, 303–306. doi: 10.1107/S1744309110054680
- Drawz, S. M., and Bonomo, R. A. (2010). Three decades of  $\beta$ -lactamase inhibitors. *Clin. Microbiol. Rev.* 23, 160–201. doi: 10.1128/CMR.00037-09
- Escobar, W. A., Tan, A. K., and Fink, A. L. (1991). Site-directed mutagenesis of  $\beta$ -lactamase leading to accumulation of an acyl-enzyme intermediate. *Biochemistry* 30, 10783–10787. doi: 10.1021/bi00108a025
- Farzaneh, S., Chaibi, E. B., Peduzzi, J., Barthelemy, M., Labia, R., Blazquez, J., et al. (1996). Implication of Ile-69 and Thr-182 residues in kinetic characteristics of IRT-3 (TEM-32)  $\beta$ -lactamase. *Antimicrob. Agents Chemother.* 40, 2434–2436.
- Fisher, J. F., and Mobashery, S. (2009). Three decades of the class A  $\beta$ -lactamase acyl-enzyme. *Curr. Prot. Pept. Sci.* 10, 401–407. doi: 10.2174/138920309789351967
- Fisher, J. F., Meroueh, S. O., and Mobashery, S. (2005). Bacterial resistance to  $\beta$ -lactam antibiotics: compelling opportunism, compelling opportunity. *Chem. Rev.* 105, 395–424. doi: 10.1021/cr030102i
- Fonseca, F., Chudyk, E. I., Van Der Kamp, M. W., Correia, A., Mulholland, A. J., and Spencer, J. (2012). The basis for carbapenem hydrolysis by class A  $\beta$ -lactamases: a combined investigation using crystallography and simulations. *J. Amer. Chem. Soc.* 134, 18275–18285. doi: 10.1021/ja304460j
- Galleni, M., and Frere, J. M. (2007). “Kinetics of  $\beta$ -lactamases and penicillin-binding proteins,” in *Enzyme-Mediated Resistance to Antibiotics: Mechanisms, Dissemination, and Prospects for Inhibition*, eds R. A. Bonomo and M. E. Tolmasky (Washington, DC: ASM Press), 67–79.
- Giakkoupi, P., Tzelepi, E., Tassios, P. T., Legakis, N. J., and Tzouveleakis, L. S. (2000). Detrimental effect of the combination of R164S with G238S in TEM-1  $\beta$ -lactamase on the extended-spectrum activity conferred by each single mutation. *J. Antimicrob. Chemother.* 45, 101–104. doi: 10.1093/jac/45.1.101
- Gniadkowski, M. (2008). Evolution of extended-spectrum  $\beta$ -lactamases by mutation. *Clin. Microb. Infect.* 14, 11–32. doi: 10.1111/j.1469-0691.2007.01854.x
- Hall, A., and Knowles, J. R. (1976). Directed selective pressure on a  $\beta$ -lactamase to analyse molecular changes involved in the development of enzyme function. *Nature* 264, 803–804. doi: 10.1038/264803a0
- Hart, K. M., Ho, C. M., Dutta, S., Gross, M. L., and Bowman, G. R. (2016). Modelling proteins' hidden conformations to predict antibiotic resistance. *Nat. Commun.* 7:12965. doi: 10.1038/ncomms12965
- Healy, W. J., Labgold, M. R., and Richards, J. H. (1989). Substrate preferences in class A  $\beta$ -lactamases: preference for penams vs. cepheems. The role of residue 237. *Proteins Struct. Func. Genet.* 6, 275–283. doi: 10.1002/prot.340060310
- Hedstrom, L. (2002). Serine protease mechanism and specificity. *Chem. Rev.* 102, 4501–4523. doi: 10.1021/cr000033x
- Herzberg, O., and Moul, J. (1987). Bacterial resistance to  $\beta$ -lactam antibiotics: crystal structure of  $\beta$ -lactamase from *Staphylococcus aureus* PC1 at 2.5 Å resolution. *Science* 236, 694–701. doi: 10.1126/science.3107125
- Horn, J. R., and Shoichet, B. K. (2004). Allosteric inhibition through core disruption. *J. Mol. Biol.* 336, 1283–1291. doi: 10.1016/j.jmb.2003.12.068
- Huang, W., and Palzkill, T. (1997). A natural polymorphism in  $\beta$ -lactamase is a global suppressor. *Proc. Natl. Acad. Sci. U.S.A.* 94, 8801–8806. doi: 10.1073/pnas.94.16.8801
- Huletsky, A., Knox, J. R., and Levesque, R. C. (1993). Role of Ser-238 and Lys-240 in the hydrolysis of third-generation cephalosporins by SHV-type  $\beta$ -lactamases probed by site-directed mutagenesis and three-dimensional modeling. *J. Biol. Chem.* 268, 3690–3697.
- Ishii, Y., Galleni, M., Ma, L., Frere, J. M., and Yamaguchi, K. (2007). Biochemical characterisation of the CTX-M-14  $\beta$ -lactamase. *Int. J. Antimicrob. Agents* 29, 159–164. doi: 10.1016/j.ijantimicag.2006.09.005
- Jorgensen, W. L., and Gao, J. (1988). Cis-trans energy difference for the peptide bond in the gas phase and in aqueous solution. *J. Amer. Chem. Soc.* 110, 4212–4216. doi: 10.1021/ja00221a020

- Kather, I., Jakob, R. P., Dobbek, H., and Schmid, F. X. (2008). Increased folding stability of TEM-1 beta-lactamase by *in vitro* selection. *J. Mol. Biol.* 383, 238–251. doi: 10.1016/j.jmb.2008.07.082
- Kimura, S., Ishiguro, M., Ishii, Y., Alba, J., and Yamaguchi, K. (2004). Role of a mutation at position 167 of CTX-M-19 in ceftazidime hydrolysis. *Antimicrob. Agents Chemother.* 48, 1454–1460. doi: 10.1128/AAC.48.5.1454-1460.2004
- Knies, J. L., Cai, F., and Weinreich, D. M. (2017). Enzyme efficiency but not thermostability drives cefotaxime resistance evolution in TEM-1  $\beta$ -lactamase. *Mol. Biol. Evol.* 34, 1040–1054. doi: 10.1093/molbev/msx053
- Levitt, P. S., Papp-Wallace, K. M., Taracila, M. A., Hujer, A. M., Winkler, M. L., Smith, K. M., et al. (2012). Exploring the role of a conserved class A residue in the W-loop of KPC-2  $\beta$ -lactamase. *J. Biol. Chem.* 287, 31783–31793. doi: 10.1074/jbc.M112.348540
- Livermore, D. M. (2006). The  $\beta$ -lactamase threat in enterobacteriaceae, pseudomonas and acinetobacter. *Trends Microbiol.* 14, 413–420. doi: 10.1016/j.tim.2006.07.008
- Lovering, A. L., Safadi, S. S., and Strynadka, N. C. (2012). Structural perspective of peptidoglycan biosynthesis and assembly. *Ann. Rev. Biochem.* 2012, 451–478. doi: 10.1146/annurev-biochem-061809-112742
- Marciano, D. C., Pennington, J. M., Wang, X., Wang, J., Chen, Y., Thomas, V. L., et al. (2008). Genetic and structural characterization of an L201P global suppressor substitution in TEM-1 beta-lactamase. *J. Mol. Biol.* 384, 151–164. doi: 10.1016/j.jmb.2008.09.009
- Mehta, S. C., Rice, K., and Palzkill, T. (2015). Natural variants of the KPC-2 carbapenemase have evolved increased catalytic efficiency for ceftazidime hydrolysis at the cost of enzyme stability. *PLoS Pathog.* 11:e1004949. doi: 10.1371/journal.ppat.1004949
- Meroueh, S. O., Fisher, J. F., Schlegel, H. B., and Mobashery, S. (2005). Ab initio QM/MM study of class A  $\beta$ -lactamase acylation: dual participation of Glu166 and Lys73 in concerted base promotion of Ser70. *J. Amer. Chem. Soc.* 127, 15397–15407. doi: 10.1021/ja051592u
- Minasov, G., Wang, X., and Shoichet, B. K. (2002). An ultrahigh resolution structure of TEM-1 beta-lactamase suggests a role for Glu166 as the general base in acylation. *J. Am. Chem. Soc.* 124, 5333–5340. doi: 10.1021/ja0259640
- Naas, T., Dortet, L., and Iorga, B. I. (2016). Structural and functional aspects of class A carbapenemases. *Curr. Drug Targets* 17, 1006–1028. doi: 10.2174/1389450117666160310144501
- Nordmann, P., Cuzon, G., and Naas, T. (2009). The real threat of *Klebsiella pneumoniae* carbapenemase-producing bacteria. *Lancet Infect. Dis.* 9, 228–236. doi: 10.1016/S1473-3099(09)70054-4
- Orencia, M. C., Yoon, J. S., Ness, J. E., Stemmer, W. P. C., and Stevens, R. C. (2001). Predicting the emergence of antibiotic resistance by directed evolution and structural analysis. *Nat. Struct. Biol.* 8, 238–242. doi: 10.1038/84981
- Palzkill, T. (2013). Metallo- $\beta$ -lactamase structure and function. *Ann. N.Y. Acad. Sci.* 1277, 91–104. doi: 10.1111/j.1749-6632.2012.06796.x
- Patel, M. P., Fryszcyn, B. G., and Palzkill, T. (2015). Characterization of the global stabilizing substitution A77V and its role in the evolution of CTX-M  $\beta$ -lactamases. *Antimicrob. Agents Chemother.* 59, 6741–6748. doi: 10.1128/AAC.00618-15
- Patel, M. P., Hu, L., Stojanowski, V., Sankaran, B., Prasad, B. V., and Palzkill, T. (2017). The drug-resistant variant P167S expands the substrate profile of CTX-M  $\beta$ -lactamases for oxymino-cephalosporin antibiotics by enlarging the active site upon acylation. *Biochemistry* 56, 3443–3453. doi: 10.1021/acs.biochem.7b00176
- Pendleton, J. N., Gorman, S. P., and Gilmore, B. F. (2013). Clinical relevance of the ESXAPe pathogens. *Expert Rev. Anti. Infect. Ther.* 11, 297–308. doi: 10.1586/eri.13.12
- Petit, A., Maveyraud, L., Lenfant, F., Samama, J. P., Labia, R., and Masson, J. M. (1995). Multiple substitutions at position 104 of  $\beta$ -lactamase TEM-1: assessing the role of this residue in substrate specificity. *Biochem. J.* 305, 33–40. doi: 10.1042/bj3050033
- Petrosino, J., Cantu Iii, C., and Palzkill, T. (1998).  $\beta$ -lactamases: protein evolution in real time. *Trends Microbiol.* 6, 323–327. doi: 10.1016/S0966-842X(98)01317-1
- Philippon, A., Slama, P., Deny, P., and Labia, R. (2016). A structure-based classification of class A  $\beta$ -lactamases, a broadly diverse family of enzymes. *Clin. Microb. Rev.* 29, 29–57. doi: 10.1128/CMR.00019-15
- Pimenta, A. C., Fernandes, R., and Moreira, I. S. (2014). Evolution of drug resistance: insight on TEM-1  $\beta$ -lactamases structure and activity and  $\beta$ -lactam antibiotics. *Mini Rev. Med. Chem.* 14, 111–122. doi: 10.2174/1389557514666140123145809
- Raquet, X., Lamotte-Brasseur, J., Fonze, E., Goussard, S., Courvalin, P., and Frere, J. M. (1994). TEM beta-lactamase mutants hydrolysing third-generation cephalosporins-A kinetic and molecular modelling analysis. *J. Mol. Biol.* 244, 625–639. doi: 10.1006/jmbi.1994.1756
- Raquet, X., Vanhove, M., Lamotte-Brasseur, J., Goussard, S., Courvalin, P., and Frere, J. M. (1995). Stability of TEM beta-lactamase mutants hydrolyzing third generation cephalosporins. *Proteins* 23, 63–72. doi: 10.1002/prot.340230108
- Salverda, M. L. M., De Visser, J. A. G. M., and Barlow, M. (2010). Natural evolution of TEM-1  $\beta$ -lactamase: experimental reconstruction and clinical relevance. *FEMS Microbiol. Rev.* 2010, 1–22. doi: 10.1111/j.1574-6976.2010.00222.x
- Saves, I., Burlet-Schiltz, O., Maveyraud, L., Samama, J. P., Prome, J. C., and Masson, J. M. (1995). Mass spectral kinetic study of acylation and deacylation during hydrolysis of penicillins and cefotaxime by  $\beta$ -lactamase TEM-1 and the G238S mutant. *Biochemistry* 34, 11660–11667. doi: 10.1021/bi00037a003
- Shimamura, T., Ibuka, A., Fushinobu, S., Wakagi, T., Ishiguro, M., Ishii, Y., et al. (2002). Acyl-intermediate structures of the extended-spectrum class A  $\beta$ -lactamase, Toho-1, in complex with cefotaxime, cephalothin, and benzylpenicillin. *J. Biol. Chem.* 277, 46601–46608. doi: 10.1074/jbc.M207884200
- Shortle, D., and Lin, B. (1985). Genetic analysis of *Staphylococcal nuclease*: identification of three intragenic “global suppressors” of nuclease minus mutations. *Genetics* 110, 539–555.
- Sideraki, V., Huang, W., Palzkill, T., and Gilbert, H. F. (2001). A secondary drug resistance mutation of TEM-1 beta-lactamase that suppresses misfolding and aggregation. *Proc. Natl. Acad. Sci. U.S.A.* 98, 283–288. doi: 10.1073/pnas.011454198
- Singh, M. K., and Dominy, B. N. (2012). The evolution of cefotaximase activity in the TEM-1  $\beta$ -lactamase. *J. Mol. Biol.* 415, 205–220. doi: 10.1016/j.jmb.2011.10.041
- Sowek, J. A., Singer, S. B., Ohringer, S., Malley, M. F., Dougherty, T. J., Gougoutas, J. Z., et al. (1991). Substitution of lysine at position 104 or 240 of TEM-1pTZ18R  $\beta$ -lactamase enhances the effect of serine-164 substitution on hydrolysis or affinity for cephalosporins and the monobactam aztreonam. *Biochemistry* 30, 3179–3188. doi: 10.1021/bi00227a004
- Stemmer, W. (1994). Rapid evolution of a protein *in vitro* by DNA shuffling. *Nature* 370, 389–391. doi: 10.1038/370389a0
- Stojanowski, V., Chow, D. C., Hu, L., Sankaran, B., Gilbert, H. F., Prasad, B. V., et al. (2015). A triple mutant in the  $\Omega$ -loop of TEM-1  $\beta$ -lactamase changes the substrate profile via a large conformational change and an altered general base for catalysis. *J. Biol. Chem.* 290, 10382–10394. doi: 10.1074/jbc.M114.633438
- Strynadka, N. C. J., Adachi, H., Jensen, S. E., Johns, K., Sielecki, A., Betzel, C., et al. (1992). Molecular structure of the acyl-enzyme intermediate in  $\beta$ -lactam hydrolysis at 1.7 Å resolution. *Nature* 359, 700–705. doi: 10.1038/359700a0
- Tokuriki, N., and Tawfik, D. S. (2009a). Protein dynamism and evolvability. *Science* 324, 203–207. doi: 10.1126/science.1169375
- Tokuriki, N., and Tawfik, D. S. (2009b). Stability effects of mutations and protein evolvability. *Curr. Opin. Struct. Biol.* 19, 596–604. doi: 10.1016/j.sbi.2009.08.003
- Vakulenko, S. B., Taibi-Tronche, P., Toth, M., Massova, L., Lerner, S. A., and Mobashery, S. (1999). Effects on substrate profile by mutational substitutions at positions 164 and 179 of the class A TEMpUC19  $\beta$ -lactamase from *Escherichia coli*. *J. Biol. Chem.* 274, 23052–23060. doi: 10.1074/jbc.274.33.23052
- Venkatachalam, K. V., Huang, W., Larocco, M., and Palzkill, T. (1994). Characterization of TEM-1  $\beta$ -lactamase mutants from positions 238 to 241 with increased catalytic efficiency for ceftazidime. *J. Biol. Chem.* 269, 23444–23450.
- Viadiu, H., Osuna, J., Fink, A. L., and Soberon, X. (1995). A new TEM  $\beta$ -lactamase double mutant with broadened specificity reveals substrate-dependent functional interactions. *J. Biol. Chem.* 270, 781–787. doi: 10.1074/jbc.270.2.781
- Wang, X., Minasov, G., and Shoichet, B. K. (2002). Evolution of an antibiotic resistance enzyme constrained by stability and activity trade-offs. *J. Mol. Biol.* 320, 85–95. doi: 10.1016/S0022-2836(02)00400-X
- Weinreich, D. M., Delaney, N. F., Depristo, M. A., and Hartl, D. L. (2006). Darwinian evolution can follow only very few mutational paths to fitter proteins. *Science* 312, 111–114. doi: 10.1126/science.1123539



- Wells, J. A. (1990). Additivity of mutational effects in proteins. *Biochemistry* 29, 8509–8517. doi: 10.1021/bi00489a001
- Yigit, H., Queenan, A. M., Rasheed, J. K., Biddle, J. W., Domenech-Sanchez, A., Alberti, S., et al. (2003). Carbapenem-resistant strain of *Klebsiella oxytoca* harboring carbapenem-hydrolyzing  $\beta$ -lactamase KPC-2. *Antimicrob. Agents Chemother.* 47, 3881–3889. doi: 10.1128/AAC.47.12.3881-3889.2003
- Zou, T., Risso, V. A., Gavira, J. A., Sanchez-Ruiz, J. M., and Ozkan, S. B. (2015). Evolution of conformational dynamics determines the conversion of a promiscuous generalist into a specialist enzyme. *Mol. Biol. Evol.* 32, 132–143. doi: 10.1093/molbev/msu281

**Conflict of Interest Statement:** The author declares that the research was conducted in the absence of any commercial or financial relationships that could be construed as a potential conflict of interest.

Copyright © 2018 Palzkill. This is an open-access article distributed under the terms of the Creative Commons Attribution License (CC BY). The use, distribution or reproduction in other forums is permitted, provided the original author(s) and the copyright owner are credited and that the original publication in this journal is cited, in accordance with accepted academic practice. No use, distribution or reproduction is permitted which does not comply with these terms.



# Exploring Additional Dimensions of Complexity in Inhibitor Design for Serine $\beta$ -Lactamases: Mechanistic and Intra- and Inter-molecular Chemistry Approaches

Focco van den Akker<sup>1\*</sup> and Robert A. Bonomo<sup>1,2,3,4</sup>

## OPEN ACCESS

### Edited by:

Christopher Davies,  
Medical University of South Carolina,  
United States

### Reviewed by:

Yu Chen,  
University of South Florida,  
United States  
Sergei Vakulenko,  
University of Notre Dame,  
United States

### \*Correspondence:

Focco van den Akker  
focco.vandenakker@case.edu

### Specialty section:

This article was submitted to  
Antimicrobials, Resistance and  
Chemotherapy,  
a section of the journal  
Frontiers in Microbiology

**Received:** 25 January 2018

**Accepted:** 19 March 2018

**Published:** 05 April 2018

### Citation:

van den Akker F and Bonomo RA  
(2018) Exploring Additional  
Dimensions of Complexity in Inhibitor  
Design for Serine  $\beta$ -Lactamases:  
Mechanistic and Intra- and  
Inter-molecular Chemistry  
Approaches. *Front. Microbiol.* 9:622.  
doi: 10.3389/fmicb.2018.00622

<sup>1</sup> Department of Biochemistry, Case Western Reserve University School of Medicine, Cleveland, OH, United States,

<sup>2</sup> Medicine, Pharmacology, Molecular Biology and Microbiology, Proteomics and Bioinformatics, Case Western Reserve

University School of Medicine, Cleveland, OH, United States, <sup>3</sup> Medical Service and Geriatric Research, Education, and

Clinical Centers (GRECC), Louis Stokes Cleveland Department of Veterans Affairs Medical Center, Cleveland, OH,

United States, <sup>4</sup> Case Western Reserve University-VA Medical Center for Antimicrobial Resistance and Epidemiology (Case  
VA CARES), Cleveland, OH, United States

As a bacterial resistance strategy, serine  $\beta$ -lactamases have evolved from cell wall synthesizing enzymes known as penicillin-binding proteins (PBP), by not only covalently binding  $\beta$ -lactam antibiotics but, also acquiring mechanisms of deacylating these antibiotics. This critical deacylation step leads to release of hydrolyzed and inactivated  $\beta$ -lactams, thereby providing resistance for the bacteria against these antibiotics targeting the cell wall. To combat  $\beta$ -lactamase-mediated antibiotic resistance, numerous  $\beta$ -lactamase inhibitors were developed that utilize various strategies to inactivate the  $\beta$ -lactamase. Most of these compounds are “mechanism-based” inhibitors that in some manner mimic the  $\beta$ -lactam substrate, having a carbonyl moiety and a negatively charged carboxyl or sulfate group. These compounds form a covalent adduct with the catalytic serine via an initial acylation step. To increase the life-time of the inhibitory covalent adduct intermediates, a remarkable array of different strategies was employed to improve inhibition potency. Such approaches include post-acylation intra- and intermolecular chemical rearrangements as well as affecting the deacylation water. These approaches transform the inhibitor design process from a 3-dimensional problem (i.e., XYZ coordinates) to one with additional dimensions of complexity as the reaction coordinate and time spent at each chemical state need to be taken into consideration. This review highlights the mechanistic intricacies of the design efforts of the  $\beta$ -lactamase inhibitors which so far have resulted in the development of “two generations” and 5 clinically available inhibitors.

**Keywords:** beta-lactamase, structural biology, enzyme inhibitors, transition state, antibacterial agents

Resistance against  $\beta$ -lactam antibiotics is in large part mediated by  $\beta$ -lactamases. The expression of  $\beta$ -lactamases protects the intended targets of these antibiotics, the penicillin binding proteins (PBPs), transpeptidase and carboxypeptidase enzymes critical in the synthesis of peptidoglycan and the bacterial cell wall (Nikolaidis et al., 2014).  $\beta$ -lactamases provide this protection as they have evolved from PBPs to recognize  $\beta$ -lactams, yet have also acquired a deacylation machinery to inactivate/hydrolyze  $\beta$ -lactam antibiotics (Fisher and Mobashery, 2009). There are four classes of  $\beta$ -lactamases, A–D, with Classes A, C, and D being serine  $\beta$ -lactamases that have PBPs as a shared common ancestor; Class B is reserved for the structurally unrelated metallo  $\beta$ -lactamases (Bush, 2013).

The serine  $\beta$ -lactamases contain key motifs or features to recognize and facilitate the  $\beta$ -lactam for hydrolysis: (1) a polar pocket optimized to attract the carboxyl moieties of  $\beta$ -lactams; (2) an oxyanion hole to attract and stabilize the carbonyl oxygen of the  $\beta$ -lactam ring; (3) a catalytic serine hydroxyl moiety that attacks the carbonyl carbon atom which leads to breakage of the carbonyl carbon nitrogen bond in the  $\beta$ -lactam; (4) conserved residues involved in a deacylation step not present in PBPs (Class A  $\beta$ -lactamases utilize for example a deacylation water that is primed by E166/N170 in the omega loop, a structural motif not present in PBPs). These features are complemented by an intricate hydrogen bonding network involving conserved Lys and Ser/Tyr hydroxyl moieties, in addition to a likely substrate-assisted hydrogen donation step that aids in the catalytic mechanism of some of these enzymes (e.g., Class C  $\beta$ -lactamases; Bulychev et al., 1997; Patera et al., 2000). These above steps have been investigated for different  $\beta$ -lactamases (Strynadka et al., 1992; Bulychev et al., 1997; Chen et al., 2006; Docquier and Mangani, 2016) as well as analyzed with QM/MM calculations [(Meroueh et al., 2005; Li et al., 2011; Sgrignani et al., 2014, 2016; Tripathi and Nair, 2016; Lizana and Delgado, 2017)]. To combat the  $\beta$ -lactamase-mediated resistance against  $\beta$ -lactam antibiotics, many different  $\beta$ -lactamase inhibitors (BLIs) were developed often using novel strategies to overcome the deacylation machinery of  $\beta$ -lactamases (Papp-Wallace and Bonomo, 2016). This review summarizes the remarkable breadth of inhibitor development strategies often involving additional chemical bond rearrangements post-acylation. These chemical and mechanistic strategies might also be useful for targeting other enzymes. Overall, the successful efforts in this arena have led to five  $\beta$ -lactamase inhibitors being approved for clinical use and others that are still in preclinical development.

## CLAVULANIC ACID, SULBACTAM, AND TAZOBACTAM; THE “FIRST GENERATION”

The first BLIs that were approved by the FDA were clavulanic acid, sulbactam, and tazobactam (Figure 1) (Page, 2000; Drawz and Bonomo, 2010). Each of these BLIs was paired with a  $\beta$ -lactam (amoxicillin/clavulanic acid, ticarcillin/clavulanic acid, ampicillin/sulbactam, cefoperazone/sulbactam, and piperacillin/tazobactam). These three inhibitors shared several

features with  $\beta$ -lactamase substrates, such as penicillin, including a  $\beta$ -lactam ring fused to a 5-membered ring containing a carboxylate moiety. Sulbactam and tazobactam are penicillanic acid sulfones and differ in the C2 substituent which is a methyl group for sulbactam and a triazolyl containing moiety for tazobactam (Figure 1). In contrast, clavulanic acid is a clavam with sulfone replaced by an oxygen. The latter inhibitor differs from the other two inhibitors at the C2 position. The serine  $\beta$ -lactamases recognize the inhibitors by positioning the carboxyl moiety and carbonyl moieties in conserved regions in the active site as was observed in the pre-acylation Michaelis-Menten complex of sulbactam bound to the S70C mutant of SHV-1  $\beta$ -lactamase (Figure 2A; Rodkey et al., 2012). The carboxyl moiety is in a pocket with hydrogen bond donors T235, S130, and within electrostatic interaction distances of R244 and K234 (Figure 2A). The carbonyl oxygen is positioned in the oxyanion hole formed by backbone nitrogens of residues 70 and 237 thereby priming the carbonyl carbon for nucleophilic attack by the hydroxyl moiety of the catalytic S70 as well as to stabilize the transition state. Finally, the hydrophobic part of the ring systems of sulbactam form hydrophobic interactions with the aromatic face of the side chain of Y105. Overall, this binding mode is similar to how these enzymes recognize  $\beta$ -lactam substrates (Beadle et al., 2002).

All three “first generation” inhibitors are mechanism-based compounds and inhibit serine  $\beta$ -lactamases by limiting deacylation *via* additional post-acylation reaction pathways that can promote semi-stable intermediates including *trans*-enamine (Figure 2B) and *cis*-enamine (Figure 2C) inhibitory species (Figure 1A; Padayatti et al., 2004, 2005; Totir et al., 2006). The enamine species both yield a double bond in the vicinity of, and thereby a conjugated system with, the carbonyl bond (Figure 1A). This conjugation is thought to decrease the carbonyl carbon's susceptibility to nucleophilic attack by the deacylation water thus preventing deacylation.

A second inhibitory mechanism for these inhibitors likely entails fashioning an eventual irreversible inhibitory species that appears after several turn-over events; this inhibitory species is postulated to involve fragmentation of the inhibitor yielding covalent modifications on either S130 and/or the catalytic S70 residue (Figures 1A, 2C; Kuzin et al., 2001; Sun et al., 2004).

## DEFINING THE IMPORTANCE OF A LONG-LIVED INTERMEDIATE: SA2-13

Efforts to improve the longevity of the *trans*-enamine intermediate have yielded the inhibitor SA2-13 which increases the lifetime of this intermediate by 10-fold over tazobactam as observed in the measured  $k_{obs,react}$  (Padayatti et al., 2006). This improvement was accomplished by changing the C2 substituent to a carboxyl linker such that the latter moiety occupies the carboxyl binding pocket thereby forming a U-shaped covalent adduct that stabilizes the *trans*-enamine intermediate (Padayatti et al., 2006; Sampson et al., 2011; Ke et al., 2012c; Rodkey et al., 2014; Figure 2D). SA2-13 thus positions its two carboxyl moieties in the carboxyl binding pocket during two separate



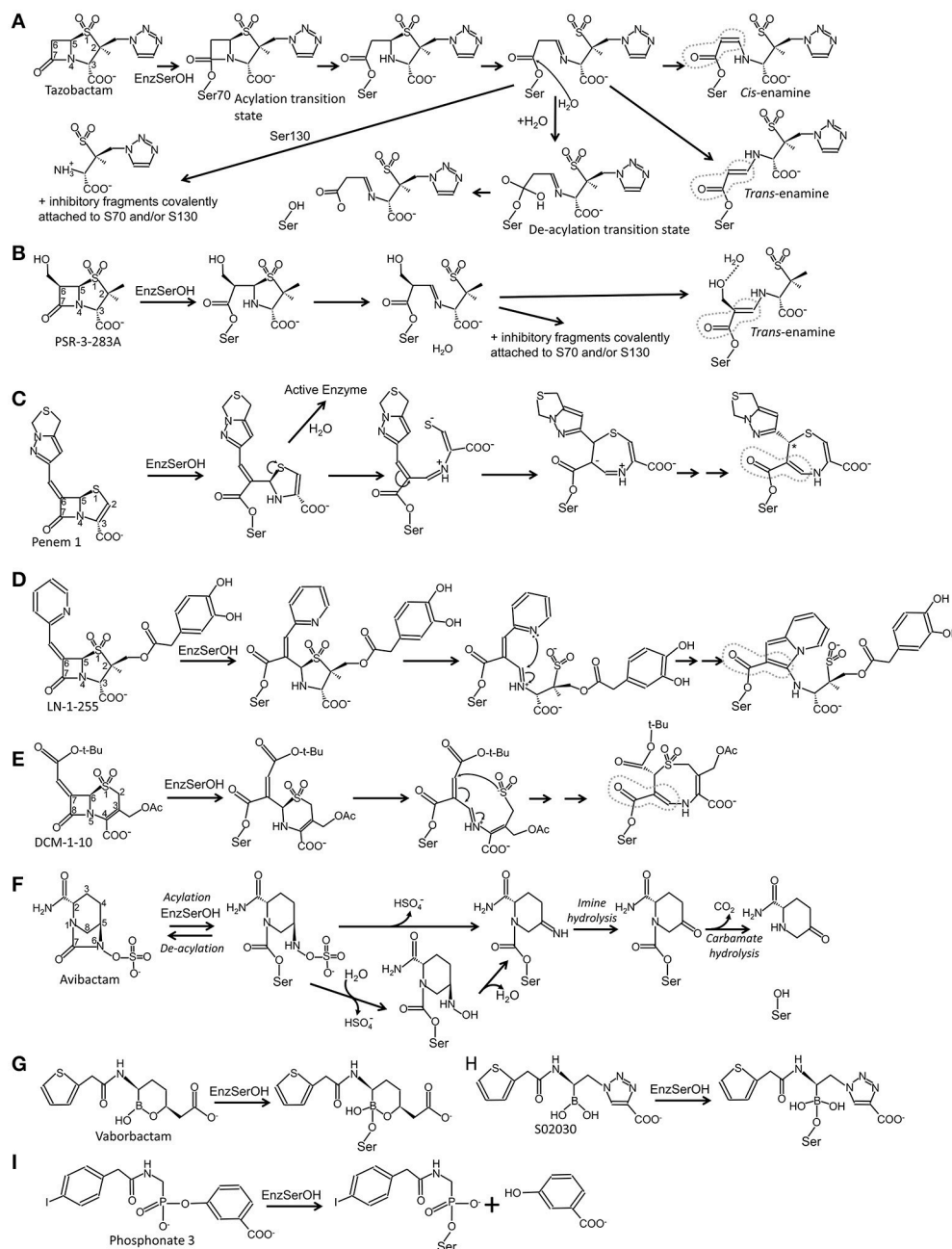


**FIGURE 1 |** Schematic diagrams of different approaches of mechanism-based inhibition of serine  $\beta$ -lactamases. **(A)** Inhibition by tazobactam; **(B)** inhibition by PSR-3-283A; **(C)** inhibition by penem 1; **(D)** inhibition by LN-1-255; **(E)** inhibition by DCM-1-10; **(F)** inhibition by avibactam; **(G)** inhibition by vaborbactam; **(H)** inhibition by S02030; **(I)** inhibition by phosphonate 3. Instances where there is conjugation with the double bond of the carbonyl moiety are highlighted by a dashed gray line.

steps in its reaction with the  $\beta$ -lactamase. The position of the original carboxyl moiety in the SA2-13 complex leads to a minor steric and electrostatic repulsion with residues in the omega-loop such that binding of SA2-13 to Extended-Spectrum- $\beta$ -Lactamase (ESBL) mutants of SHV-1 causes complete disorder of the omega loop; this disorder further enhancing SA2-13's inhibitory efficacy toward ESBLs as this loop harbors residues needed for deacylation (Sampson et al., 2011).

## SLOWING THE DEACYLATION RATE: 6 $\beta$ -HYDROXYMETHYL CONTAINING INHIBITORS

The addition of a 6 $\beta$ -hydroxy-methyl moiety to a penicillanic acid sulfone improved certain inhibitory characteristics specifically slowing down the deacylation rate (Bitha et al., 1999a,b; Papp-Wallace et al., 2012; Che et al., 2015). The basis of

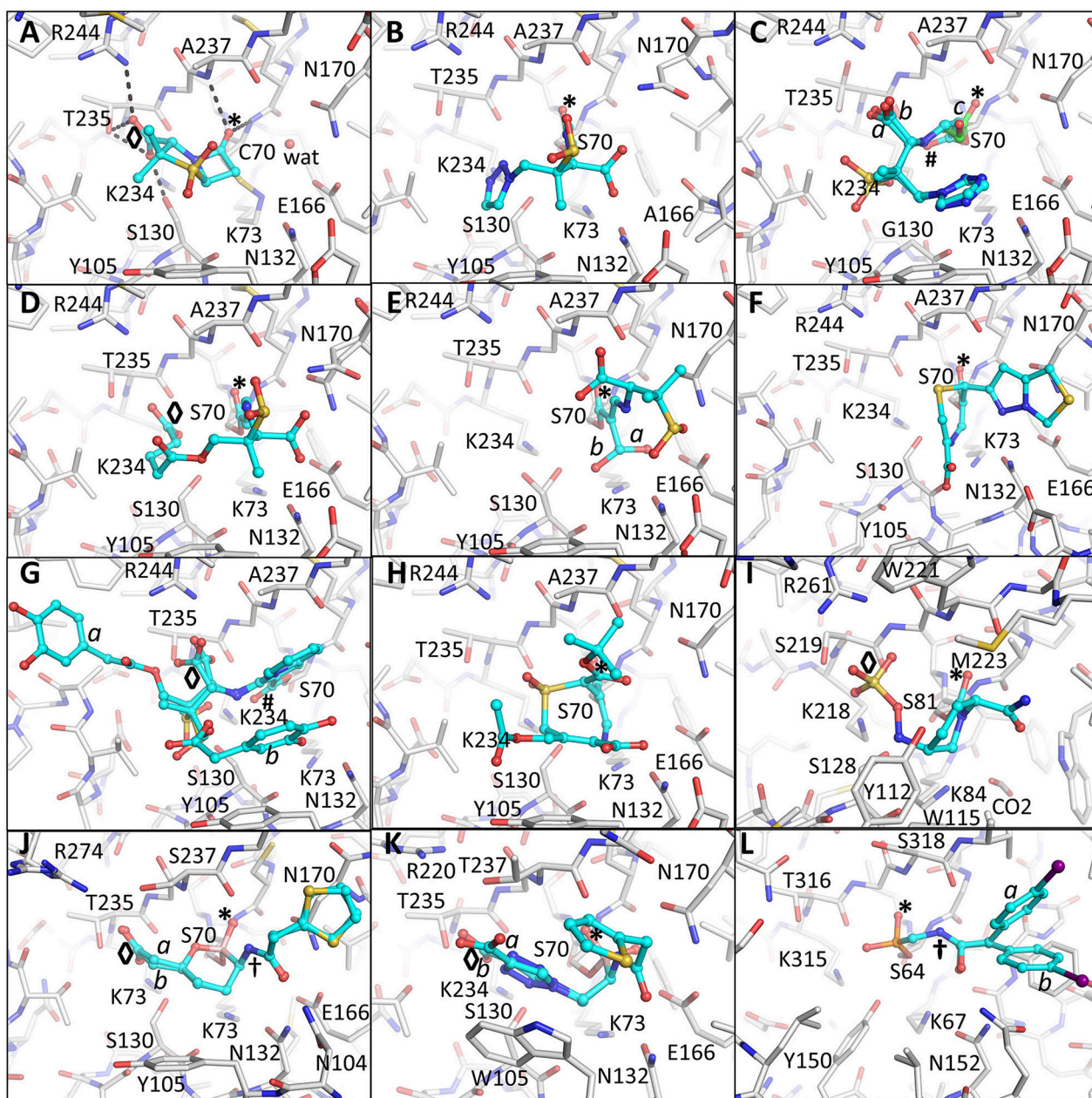


**FIGURE 2 |** Crystallographically determined binding modes of  $\beta$ -lactamase inhibitors. **(A)** Sulbactam bound in a pre-acylation/Michaelis-Menten binding mode in the S70C mutant of SHV-1  $\beta$ -lactamase. The S70C mutations changes the reactivity of the catalytic S70 nucleophile; the C70 residue forms a covalent sulfonamide bond with the conserved K73 allowing capture of the pre-acylation complex. Hydrogen bonds between the carboxyl and carbonyl oxygens are depicted as dashed black lines. The occupied carboxyl pocket and oxanion hole are labeled “o” and “\*”, respectively. These labels are used through subsequent panels of this figure where applicable. The deacylation water is shown as a solid red sphere labeled “wat”; **(B)** tazobactam, in the *trans*-enamine conformation, bound to the deacylation deficient E166A mutant of SHV-1; **(C)** tazobactam, in the *cis*-enamine conformation, bound to the inhibitor-resistant S130G mutant of SHV-1. Tazobactam adopts three conformations two of which are *cis*-enamine (0.33 occupancy with cyan carbon atoms each labeled “a” and “b”) and a fragmented species with green carbon atoms labeled “c” (also 0.33 occupancy). These labels for alternate conformations are used when needed in subsequent panels of this Figure. The *cis*-enamine and fragmented species have their carbonyl oxygens positioned outside (labeled “#”) and inside the oxanion hole (labeled “\*”), respectively; **(D)** SA2-13 complexed to SHV-1; **(E)** PSR-2-283A complexed to SHV-1. The hydroxymethyl moiety was observed to be in two conformations (labeled “a” and “b”). The major conformation hydrogen bonds with the deacylation water (not shown) and the second conformation does not. Residue S130 is also in two conformations; **(F)** penem 1 bound to SHV-1; **(G)** LN-1-255 complexed to SHV-1. Two conformations of the tail of LN-1-255 are observed (“a” and “b”); **(H)** DCM-1-10 bound to SHV-1; **(I)** Avibactam bound to Class D OXA-24  $\beta$ -lactamase; **(J)** Vaborbactam complexed to CTX-M-15. Two conformations for vaborbactam were observed. The amide moiety of vaborbactam (labeled “†”) makes hydrogen bonds across the active site groove; **(K)** S02030 bound to KPC-2. Two conformations were observed for the carboxyl-triazole moiety (labeled “a” and “b”); **(L)** Phosphonate 3 complexed to P99  $\beta$ -lactamase. The iodobenzene ring was present in two conformations. Like in vaborbactam, the amide moiety of phosphonate 3 makes hydrogen bonds across the active site.

this effect is attributed to the presence of the hydroxyl-methyl moiety interacting with the deacylation water when in the *trans*-enamine or imine intermediate state of the inhibitor (**Figures 1B, 2E**). This interaction can thereby either (1) sterically prevent the deacylation water from being able to nucleophilically attack the carbonyl carbon; and/or (2) negatively alter the nucleophilic properties of the deacylation water (Che et al., 2015). These inhibitors were also observed to undergo fragmentation yielding inhibitory adducts to Class A and C  $\beta$ -lactamases (Papp-Wallace et al., 2012). A 6- $\alpha$ -hydroxymethyl penicillanate variant yielded a similar inhibitory binding mode when bound to TEM-1 with the hydroxymethyl moiety also interacting with the deacylation water (Maveyraud et al., 1996).

## PENEM; A STRATEGIC DESIGN THAT ENHANCES THE ACYL INTERMEDIATE

To take advantage of and to increase the longevity of the semi-stable acyl-enzyme imine intermediate, reactive groups were added at the C6 position such as the alkylidene group in penems (**Figure 1C**; Nukaga et al., 2003; Venkatesan et al., 2004a,b, 2008; Mansour et al., 2007; Ke et al., 2012b). The design was to, when in the imine intermediate, allow the nucleophilic sulfur to react with the carbon in the alkylidene group *via* a 7-*endo-trig* rearrangement. This reaction would form a new 7-membered ring that *via* additional rearrangements can lead to an enamine species that conjugates with the carbonyl carbon bond (**Figure 1C**). This in turn limits deacylation by decreasing the susceptibility of the carbonyl carbon to nucleophilic attack of the deacylation water. This 7-membered ring enamine intermediate was crystallographically observed for penem 1 with the carbonyl oxygen situated in the oxyanion hole with deacylation likely being diminished due to this conjugation (**Figures 1C, 2F**; Ke et al., 2012b).

The alkylidene moiety at the C6 position can have different aromatic 1-, 2-, or 3-ring systems as substituents of which penem 1 contains a 2-ring heterocycle substitution (Bulychev et al., 1995; Ke et al., 2012b). When combined with piperacillin, penem 1 lowered MIC values from 64–2,048 to 4–8  $\mu\text{g/ml}$  for *Escherichia coli* expressing SHV-1, SHV-2, and the inhibitor-resistant R244S variant (Ke et al., 2012b).

## 6-ALKYLIDENE-2' $\beta$ -SUBSTITUTED PENAM SULFONES: LN-1-255 AND NOVEL CHEMISTRY

Like the penems above, alkylidene group containing reactive groups were added at the C6 position of penam sulfones (Chen et al., 1987; Buynak et al., 1999; Phillips et al., 2005; Kalp et al., 2007; Che et al., 2012). In particular, the pyridylethylidene moiety in LN-1-255 is potent since, when in the imine intermediate, the nitrogen of the pyridyl group reacts with the carbon atom of the imine bond to form a bicyclic ring (**Figure 1D**; Buynak et al., 1999; Pattanaik et al., 2009). The carbonyl carbon is now conjugated with the newly formed bicyclic ring; to maintain its conjugation and thus planarity with

this bulky ring, the carbonyl oxygen “flips out” of the oxyanion hole (labeled “#” in **Figure 2G**). This oxygen movement and the resulting conjugation renders the carbonyl bond very resistant to deacylation making the inhibitor even more efficient with a lower turn-over number compared to tazobactam (Pattanaik et al., 2009).

Remarkably, LN-1-255 and other 6-alkylidene-2' $\beta$ -substituted penam sulfones are also potent Class D  $\beta$ -lactamase inhibitors and have a similar mechanism of enzyme inhibition (Bou et al., 2010). An additional improvement for LN-1-255 included adding a dihydroxy-phenyl catechol moiety at the C2 position of the penam sulfone. This moiety is a siderophore and could allow improved uptake of LN-1-255 *via* bacterial iron-acquisition siderophore channels (Pattanaik et al., 2009). Presently, LN-1-255 is undergoing preclinical studies to establish its efficacy in treating infections.

## 7-ALKYLIDENECEPHALOSPORIN SULFONES

Like in LN-1-255 and penem 1, the alkylidene moiety can also be incorporated on the equivalent position in cephalosporin sulfones, at the 7 position (Buynak et al., 2000). Such a 7-alkylideneccephalosporin sulfone is DCM-1-10 (**Figure 1E**). DCM-1-10 undergoes a similar acyl-forming inhibitory mechanism, yet deviates from penem 1 in that it is the sulfone that reacts with the carbon of the alkylidene moiety thus forming an 8 atom cyclic intermediate (**Figures 1E, 2H**). The carbonyl oxygen remains in the oxyanion hole yet the intermediate is likely protected from deacylation by the stabilizing effect on the carbonyl bond by being conjugated with a neighboring double bond (**Figure 1E**; Rodkey et al., 2013). DCM-1-10 has only modest potency as its  $\text{IC}_{50}$  is 4- and 27-fold higher for clavulanic acid and tazobactam, respectively. Nevertheless, the turnover numbers for DCM-1-10 are similar to tazobactam and the  $k_{\text{obs,react}}$  is significantly slower compared to tazobactam and clavulanic acid indicating that DCM-1-10 can form a relatively stable inhibitory complex (Rodkey et al., 2013).

## DIAZABICYCLOOCTANE INHIBITORS; THE “SECOND GENERATION”

Avibactam (NXL104) is a diazabicyclooctane (DBO) (Coleman, 2011) and is the 4th  $\beta$ -lactamase inhibitor that was FDA approved as part of the formulation ceftazidime/avibactam (in 2015). Unlike the above described inhibitors, avibactam inhibition of serine  $\beta$ -lactamases is mostly reversible (**Figure 1F**; Ehmann et al., 2012, 2013). Avibactam is chemically distinct from the other inhibitors in that its rings are arranged differently with the strained 4-atom  $\beta$ -lactam ring being absent. Nevertheless, avibactam contains a carbonyl bond adjacent to a ring nitrogen. The carboxyl moiety, present in all previously discussed inhibitors, is replaced by a negatively charged sulfate moiety. For proper recognition in the active site, the same distance between the carbonyl oxygen and the negatively charged oxygens of the sulfate group is maintained relative to its equivalent



atoms in the above  $\beta$ -lactam containing inhibitors: the negatively charged oxygens (in either the carboxyl or sulfate moiety) and the carbonyl oxygen are separated by 4 atoms in both classes of inhibitors (**Figure 1**).

Avibactam forms an acyl-enzyme complex with the serine  $\beta$ -lactamase upon breakage of the C-N bond and concomitant opening of the 5-membered ring (**Figure 1F**). Interestingly, avibactam can be removed from the enzyme via deacylation and ring closure resulting in an intact avibactam molecule being liberated. A number of crystal structures have been determined of avibactam complexes with representatives from all three serine  $\beta$ -lactamase classes (Xu et al., 2012; Lahiri et al., 2013, 2014, 2015; King et al., 2015; Krishnan et al., 2015; Calvopiña et al., 2017; Jin et al., 2017; Lohans et al., 2017).

Despite the mostly reversible mode of inhibition (a property not evident with the other BLIs listed above), some  $\beta$ -lactamases are capable of slowly desulfating avibactam once bound to the enzyme resulting in inactivation of avibactam upon carbamate hydrolysis (Ehmann et al., 2012, 2013; **Figure 1F**). Avibactam forms similar acyl-enzyme complexes in Class A, C, and D  $\beta$ -lactamases (Xu et al., 2012; Lahiri et al., 2013, 2015; King et al., 2015; Krishnan et al., 2015) in which the sulfate moiety is occupying the carboxyl binding pocket and the carbonyl oxygen is situated in the oxyanion hole (**Figure 2I**). One possible explanation that the acyl-enzyme is likely resistant to attack by the deacylation water could be due to having a nitrogen atom bonded to the carbonyl carbon atom (**Figure 1F**) thereby likely altering this bond as well as its local environment. The chirality of this tertiary amine, when bound to  $\beta$ -lactamase, can vary from S, R, or planar (Krishnan et al., 2015). Additional DBO  $\beta$ -lactamase inhibitors are currently being developed with improved efficacies with some having dual action potential by also inhibiting PBPs (Ambrose et al., 2017; Durand-Réville et al., 2017; Moya et al., 2017a,b; Shapiro et al., 2017; Zhanel et al., 2018). The DBOs in preclinical development are listed in **Table 1**; additional DBO analogs in earlier stages of development can be found here (King et al., 2016; Wang et al., 2016; Durand-Réville et al., 2017).

## BORONIC ACID AND PHOSPHONATE TRANSITION STATE ANALOGS

Elucidation of the reaction scheme of mechanism-based inhibition BLIs (**Figure 1A**) suggested that transition states can be mimicked to obtain potent inhibitors. The reaction scheme indicates that a transition state exists for both the acylation and the deacylation component of the reaction; exploiting these transition states for developing new BLIs will be discussed next.

The cyclic boronic acid inhibitor vaborbactam (RPX7009; Hecker et al., 2015; Lomovskaya et al., 2017) was recently FDA approved (meropenem/vaborbactam) and its complex with CTX-M-15 and P99  $\beta$ -lactamases was crystallographically determined (Hecker et al., 2015; **Figures 1G, 2J**). Vaborbactam mimics  $\beta$ -lactamase inhibitors/substrates (**Figure 2J**) by having (1) a boron atom, like the carbonyl carbon, that can be the recipient of nucleophilic attack by the catalytic serine; (2) a carboxyl moiety that occupies the carboxyl binding pocket; (3)

a hydroxyl moiety mimicking the carbonyl oxygen; (4) a ring system that makes hydrophobic interactions with the Y/W side chain often found in  $\beta$ -lactamase active sites; and (5) an amide moiety, found in the penicillin substrate, that can interact with the different atoms across the active site cleft (with a backbone oxygen of T237 on one side of the cleft and the amide moieties of both Asn132 and Asn102 on the other end). When bound to the active site, vaborbactam adopts an acylation transition state binding mode with its exocyclic boron oxygen in the oxyanion hole (**Figure 2J**). Like DBOs that can reversibly acylate and deacylate, vaborbactam can be a reversible  $\beta$ -lactamase inhibitor (Hecker et al., 2015; Lomovskaya et al., 2017). Cyclic boronate inhibitors can have broad spectrum efficacy as some are capable of inhibiting all 4 classes of  $\beta$ -lactamases including metallo  $\beta$ -lactamases (Cahill et al., 2017). Furthermore, these inhibitors have potential beyond inhibiting  $\beta$ -lactamases as a cyclic boronate inhibitor was shown to inhibit PBP5 (Brem et al., 2016).

A different boronic acid inhibitor is S02030 which when complexed to KPC-2 binds in a deacylation transition state mode (**Figures 1H, 2K**; Nguyen et al., 2016). This is in sharp contrast to vaborbactam. S02030 possesses two boron hydroxyl groups: one of them occupies the oxyanion hole whereas the second hydroxyl occupies the pocket normally harboring the deacylation water, but this water is now displaced (**Figure 2K**); these hydroxyl interactions were also observed in a KPC-2 complex with a small boronic acid fragment molecule (Ke et al., 2012a). S02030 is very potent at inhibiting  $\beta$ -lactamases observed in *Klebsiella pneumoniae* and *E. coli* species. Developing boronic acid  $\beta$ -lactamase inhibitors is a promising approach as has been shown for a number of different  $\beta$ -lactamases (Tondi et al., 2010, 2014; Powers et al., 2014; Bouza et al., 2017; Werner et al., 2017; Caselli et al., 2018).

In addition to boronic acid analogs, phosphonates also behave as transition state BLIs. Phosphonates are unique mechanism-based BLIs; the nucleophilic attack of the catalytic serine leads to bond breakage and release of part of the molecule adjacent to the phosphonate (**Figure 1I**). The structure of phosphonate 3 bound to P99  $\beta$ -lactamase reveals the phosphorous atom covalently bonded to the catalytic serine (**Figure 2L**; Lobkovsky et al., 1994). Furthermore, one of the phosphonate oxygen atoms is in the oxyanion hole and the amide moiety makes hydrogen bond interactions across the active site cleft like vaborbactam (**Figures 2J, 2L**). Like with boronic acids, phosphonates have also been used to probe binding modes of transition states of  $\beta$ -lactams such as the phosphonate transition state analog of a cephalosporin bound to a Class C  $\beta$ -lactamase (Nukaga et al., 2004).

## ADDITIONAL INHIBITOR DESIGN APPROACHES

In addition to these mechanism-based  $\beta$ -lactamase inhibitors, some groups have targeted developing non-covalent  $\beta$ -lactamase inhibitors (Eidam et al., 2012; Nichols et al., 2014). This approach is often initiated by starting from small fragments

**TABLE 1** | Promising DBO inhibitors in pre-clinical development or FDA approved.

DBO name	Characteristics	References
Avibactam (NXL104)	Currently only FDA approved DBO $\beta$ -lactamase inhibitor. Partnered with ceftazidime	Reviewed in Coleman, 2011
WCK 4234	Active against <i>Pseudomonas</i> and <i>Acinetobacter</i> Class A, C, and D $\beta$ -lactamases. Partnered with imipenem or meropenem	Mushtaq et al., 2017
WCK 5107 (Zidebactam)	Active against <i>A. baumannii</i> , <i>Enterobacteriaceae</i> , and <i>Pseudomonas aeruginosa</i> . Dual target inhibitor ( <i>P.a.</i> PBP2). Partnered with cefepime or sulbactam	Livermore et al., 2017; Moya et al., 2017a,b; Sader et al., 2017a,b
WCK 5153	Active against <i>A. baumannii</i> and <i>P. aeruginosa</i> . Dual target inhibitor ( <i>P.a.</i> PBP2). Partnered with cefepime or sulbactam	Moya et al., 2017a,b
ETX2514	Active against Gram-negative bacteria including <i>A. baumannii</i> and <i>P. aeruginosa</i> . Dual target inhibitor ( <i>A. b.</i> PBP2). Partnered with sulbactam	Durand-Réville et al., 2017; McLeod et al., 2017; Shapiro et al., 2017
Relebactam (MK-7655)	Active against <i>Enterobacteriaceae</i> , <i>Klebsiella pneumoniae</i> , and <i>Pseudomonas</i> . Partnered with imipenem	Livermore et al., 2013; Blizzard et al., 2014; Lapuebla et al., 2015; Haidar et al., 2017; Lob et al., 2017
Nacubactam (OP0595)	Active against <i>Enterobacteriaceae</i> , <i>P. aeruginosa</i> , and <i>K. pneumoniae</i> . Dual target activity (inhibits PBP2) and has “enhancer”-activity. Partnered with cefepime, piperacillin, or meropenem	Livermore et al., 2015; Morinaka et al., 2015, 2017

and exploiting hydrogen bond, electrostatic, and van der Waals interactions similar those observed in the mechanism-based inhibitor complexes. Despite not having a covalent bond with the catalytic serine, this approach can yield nano-molar affinity  $\beta$ -lactamase inhibitors (Eidam et al., 2012; Nichols et al., 2014). An important challenge here is the need to demonstrate “broad class” inhibition as was seen with DBOs. Alternatively, “narrow spectrum” inhibitors should not be discounted for therapeutic purposes as they will likely cause less damage to the patients beneficial microbiome (Boucher et al., 2017). Another approach is to utilize naturally observed protein inhibitors of  $\beta$ -lactamases from *Streptomyces*, termed  $\beta$ -lactamase inhibitor proteins (BLIPs), which can be altered to modulate  $\beta$ -lactamase specificity (Brown et al., 2013; Chow et al., 2016; Adamski and Palzkill, 2017a,b); peptides derived from BLIPs have been shown to have antimicrobial activity (Alaybeyoglu et al., 2015).

## CONCLUSION

BLI development has made tremendous progress during the last decades and exploited numerous different chemical and/or mechanistic strategies. This includes unusual (post-acylation) reactions that can involve both intra- and/or inter-molecular rearrangements. Different areas of the reaction coordinate space have been exploited to arrive at novel and promising compounds. Despite all the progress resulting in now 5 inhibitors clinically available, resistance against these  $\beta$ -lactamase inhibitors has occurred including against avibactam (Wright et al., 2017);

resistance against vaborbactam has not been observed yet, as the inhibitor has only recently been FDA approved (Zhanel et al., 2018). Therefore, continued efforts in this field are needed to develop BLIs with novel properties such as the dual action DBO inhibitors that are in preclinical development. Also, developing BLIs that target both metallo- $\beta$ -lactamases (Class B) and serine based enzymes (Classes A, C, and D) remains a goal of the future.

## AUTHOR CONTRIBUTIONS

FvdA has written the initial draft manuscript and prepared the figures. FvdA and RB have contributed to editing the manuscript.

## ACKNOWLEDGMENTS

Research reported in this publication was supported in part by the National Institute of Allergy and Infectious Diseases of the National Institutes of Health under Award Numbers R01AI100560, R01AI063517, R21AI114508, and R01AI072219 to RB. This study was supported in part by funds and/or facilities provided by the Cleveland Department of Veterans Affairs, Award Number 1I01BX001974 to RB from the Biomedical Laboratory Research & Development Service of the VA Office of Research and Development and the Geriatric Research Education and Clinical Center VISN 10 to RB. The content is solely the responsibility of the authors and does not necessarily represent the official views of the National Institutes of Health or the Department of Veterans Affairs.

## REFERENCES

- Adamski, C. J., and Palzkill, T. (2017a). Systematic substitutions at BLIP position 50 result in changes in binding specificity for class A  $\beta$ -lactamases. *BMC Biochem.* 18:2. doi: 10.1186/s12858-017-0077-1
- Adamski, C. J., and Palzkill, T. (2017b). BLIP-II employs differential hotspot residues to bind structurally similar staphylococcus aureus PBP2a and class A  $\beta$ -lactamases. *Biochemistry* 56, 1075–1084. doi: 10.1021/acs.biochem.6b00978
- Alaybeyoglu, B., Akbulut, B. S., and Ozkirimli, E. (2015). A novel chimeric peptide with antimicrobial activity. *J. Pept. Sci.* 21, 294–301. doi: 10.1002/psc.2739

- Ambrose, P. G., VanScoy, B. D., Trang, M., McCauley-Miller, J., Conde, H., Bhavnani, S. M., et al. (2017). Pharmacokinetics-pharmacodynamics of CB-618 in combination with cefepime, ceftazidime, ceftolozane, or meropenem: the pharmacological basis for a stand-alone beta-lactamase inhibitor. *Antimicrob. Agents Chemother.* 61:e00630-17. doi: 10.1128/AAC.00630-17
- Beadle, B. M., Trehan, I., Focia, P. J., and Shoichet, B. K. (2002). Structural milestones in the reaction pathway of an amide hydrolase: substrate, acyl, and product complexes of cephalothin with AmpC  $\beta$ -lactamase. *Structure* 10, 413–424. doi: 10.1016/S0969-2126(02)00725-6
- Bitha, P., Li, Z., Francisco, G. D., Rasmussen, B. A., and Lin, Y. I. (1999a). 6-(1-Hydroxyalkyl)penam sulfone derivatives as inhibitors of class A and class C beta-lactamases I. *Bioorg. Med. Chem. Lett.* 9, 991–996.
- Bitha, P., Li, Z., Francisco, G. D., Yang, Y., Petersen, P. J., Lenoy, E., et al. (1999b). 6-(1-Hydroxyalkyl)penam sulfone derivatives as inhibitors of class A and class C beta-lactamases II. *Bioorg. Med. Chem. Lett.* 9, 997–1002.
- Blizzard, T. A., Chen, H., Kim, S., Wu, J., Bodner, R., Gude, C., et al. (2014). Discovery of MK-7655, a beta-lactamase inhibitor for combination with Primaxin(R). *Bioorg. Med. Chem. Lett.* 24, 780–785. doi: 10.1016/j.bmcl.2013.12.101
- Bou, G., Santillana, E., Sheri, A., Beceiro, A., Sampson, J. M., Kalp, M., et al. (2010). Design, synthesis, and crystal structures of 6-alkylidene-2'-substituted penicillanic acid sulfones as potent inhibitors of *Acinetobacter baumannii* OXA-24 carbapenemase. *J. Am. Chem. Soc.* 132, 13320–13331. doi: 10.1021/ja104092z
- Boucher, H. W., Ambrose, P. G., Chambers, H. F., Ebright, R. H., Jezek, A., Murray, B. E., et al. (2017). White paper: developing antimicrobial drugs for resistant pathogens, narrow-spectrum indications, and unmet needs. *J. Infect. Dis.* 216, 228–236. doi: 10.1093/infdis/jix211
- Bouza, A. A., Swanson, H. C., Smolen, K. A., VanDine, A. L., Taracila, M. A., Romagnoli, C., et al. (2017). Structure-based analysis of boronic acids as inhibitors of acinetobacter-derived cephalosporinase-7, a unique class c beta-lactamase. *ACS Infect. Dis.* 4, 325–336. doi: 10.1021/acscinfecdis.7b00152
- Brem, J., Cain, R., Cahill, S., McDonough, M. A., Clifton, I. J., Jimenez-Castellanos, J. C., et al. (2016). Structural basis of metallo-beta-lactamase, serine-beta-lactamase and penicillin-binding protein inhibition by cyclic boronates. *Nat. Commun.* 7:12406. doi: 10.1038/ncomms12406
- Brown, N. G., Chow, D. C., and Palzkill, T. (2013). BLIP-II is a highly potent inhibitor of *Klebsiella pneumoniae* carbapenemase (KPC-2). *Antimicrob. Agents Chemother.* 57, 3398–3401. doi: 10.1128/AAC.00215-13
- Bulychev, A., Massova, I., Lerner, S. A., and Mobashery, S. (1995). Penem BRL 42715: an effective inactivator of beta-lactamases. *J. Am. Chem. Soc.* 117, 4797–4800. doi: 10.1021/ja00122a009
- Bulychev, A., Massova, I., Miyashita, K., and Mobashery, S. (1997). Nuances of mechanisms and their implications for evolution of the versatile beta-lactamase activity: from biosynthetic enzymes to drug resistance factors. *J. Am. Chem. Soc.* 119, 7619–7625.
- Bush, K. (2013). The ABCD's of beta-lactamase nomenclature. *J. Infect. Chemother.* 19, 549–559. doi: 10.1007/s10156-013-0640-7
- Buynak, J. D., Doppalapudi, V. R., and Adam, G. (2000). The synthesis and evaluation of 3-substituted-7-(alkylidene)cephalosporin sulfones as beta-lactamase inhibitors. *Bioorg. Med. Chem. Lett.* 10, 853–857. doi: 10.1016/S0960-894X(00)00098-6
- Buynak, J. D., Rao, A. S., Doppalapudi, V. R., Adam, G., Petersen, P. J., and Nidamarthy, S. D. (1999). The synthesis and evaluation of 6-alkylidene-2'-beta-substituted penam sulfones as beta-lactamase inhibitors. *Bioorg. Med. Chem. Lett.* 9, 1997–2002. doi: 10.1016/S0960-894X(99)00325-X
- Cahill, S. T., Cain, R., Wang, D. Y., Lohans, C. T., Wareham, D. W., Oswin, H. P., et al. (2017). Cyclic boronates inhibit all classes of beta-lactamases. *Antimicrob. Agents Chemother.* 61:e02260-16. doi: 10.1128/AAC.02260-16
- Calvo-piña, K., Hinchliffe, P., Brem, J., Heesom, K. J., Johnson, S., Cain, R., et al. (2017). Structural/mechanistic insights into the efficacy of nonclassical beta-lactamase inhibitors against extensively drug resistant *Stenotrophomonas maltophilia* clinical isolates. *Mol. Microbiol.* 106, 492–504. doi: 10.1111/mmi.13831
- Caselli, E., Romagnoli, C., Powers, R. A., Taracila, M. A., Bouza, A. A., Swanson, H. C., et al. (2018). Inhibition of acinetobacter-derived cephalosporinase: exploring the carboxylate recognition site using novel beta-lactamase inhibitors. *ACS Infect. Dis.* 4, 337–348. doi: 10.1021/acscinfecdis.7b00153
- Che, T., Bonomo, R. A., Shanmugam, S., Bethel, C. R., Pusztai-Carey, M., Buynak, J. D., et al. (2012). Carboxylation and decarboxylation of active site lys 84 controls the activity of OXA-24 beta-lactamase of *Acinetobacter baumannii*: raman crystallographic and solution evidence. *J. Am. Chem. Soc.* 134, 11206–11215. doi: 10.1021/ja303168n
- Che, T., Rodkey, E. A., Bethel, C. R., Shanmugam, S., Ding, Z., Pusztai-Carey, M., et al. (2015). Detecting a quasi-stable imine species on the reaction pathway of SHV-1 beta-lactamase and 6beta-(Hydroxymethyl)penicillanic acid sulfone. *Biochemistry* 54, 734–743. doi: 10.1021/bi501197t
- Chen, Y. L., Chang, C. W., Hedberg, K., Guarino, K., Welch, W. M., Kiessling, L., et al. (1987). Structure-activity relationships of 6-(heterocycl)-methylene penam sulfones; a new class of beta-lactamase inhibitors. *J. Antibiot.* 40, 803–822.
- Chen, Y., Minasov, G., Roth, T. A., Prati, F., and Shoichet, B. K. (2006). The deacylation mechanism of AmpC beta-lactamase at ultrahigh resolution. *J. Am. Chem. Soc.* 128, 2970–2976. doi: 10.1021/ja056806m
- Chow, D. C., Rice, K., Huang, W., Atmar, R. L., and Palzkill, T. (2016). Engineering specificity from broad to narrow: design of a beta-lactamase inhibitory protein (BLIP) variant that exclusively binds and detects KPC beta-lactamase. *ACS Infect. Dis.* 2, 969–979. doi: 10.1021/acscinfecdis.6b00160
- Coleman, K. (2011). Diazabicyclooctanes (DBOs): a potent new class of non-beta-lactam beta-lactamase inhibitors. *Curr. Opin. Microbiol.* 14, 550–555. doi: 10.1016/j.mib.2011.07.026
- Docquier, J. D., and Mangani, S. (2016). Structure-function relationships of class D carbapenemases. *Curr. Drug Targets* 17, 1061–1071. doi: 10.2174/1389450116666150825115824
- Drawz, S. M., and Bonomo, R. A. (2010). Three decades of  $\beta$ -lactamase inhibitors. *Clin. Microbiol. Rev.* 23, 160–201. doi: 10.1128/CMR.00037-09
- Durand-Réville, T. F., Guler, S., Comita-Prevoir, J., Chen, B., Bifulco, N., Huynh, H., et al. (2017). ETX2514 is a broad-spectrum beta-lactamase inhibitor for the treatment of drug-resistant Gram-negative bacteria including *Acinetobacter baumannii*. *Nat. Microbiol.* 2:17104. doi: 10.1038/nmicrobiol.2017.104
- Ehmann, D. E., Jahic, H., Ross, P. L., Gu, R. F., Hu, J., Durand-Réville, T. F., et al. (2013). Kinetics of avibactam inhibition against Class, A, C, and D beta-lactamases. *J. Biol. Chem.* 288, 27960–27971. doi: 10.1074/jbc.M113.485979
- Ehmann, D. E., Jahic, H., Ross, P. L., Gu, R. F., Hu, J., Kern, G., et al. (2012). Avibactam is a covalent, reversible, non-beta-lactam beta-lactamase inhibitor. *Proc. Natl. Acad. Sci. U.S.A.* 109, 11663–11668. doi: 10.1073/pnas.1205073109
- Eidam, O., Romagnoli, C., Dalmasso, G., Barelier, S., Caselli, E., Bonnet, R., et al. (2012). Fragment-guided design of subnanomolar beta-lactamase inhibitors active *in vivo*. *Proc. Natl. Acad. Sci. U.S.A.* 109, 17448–17453. doi: 10.1073/pnas.1208337109
- Fisher, J. F., and Mobashery, S. (2009). Three decades of the class A beta-lactamase acyl-enzyme. *Curr. Protein Pept. Sci.* 10, 401–407. doi: 10.2174/138920309789351967
- Haidar, G., Clancy, C. J., Chen, L., Samanta, P., Shields, R. K., Kreiswirth, B. N., et al. (2017). Identifying spectra of activity and therapeutic niches for ceftazidime-avibactam and imipenem-relebactam against carbapenem-resistant *Enterobacteriaceae*. *Antimicrob. Agents Chemother.* 61, e00642–e00647. doi: 10.1128/AAC.00642-17
- Hecker, S. J., Reddy, K. R., Totrov, M., Hirst, G. C., Lomovskaya, O., Griffith, D. C., et al. (2015). Discovery of a cyclic boronic acid beta-lactamase inhibitor (RPX7009) with utility vs class A serine carbapenemases. *J. Med. Chem.* 58, 3682–3692. doi: 10.1021/acs.jmedchem.5b00127
- Jin, W., Wachino, J. I., Yamaguchi, Y., Kimura, K., Kumar, A., Yamada, M., et al. (2017). Structural insights into the TLA-3 extended-spectrum beta-lactamase and its inhibition by avibactam and OP0595. *Antimicrob. Agents Chemother.* 61:e00501-17. doi: 10.1128/AAC.00501-17
- Kalp, M., Sheri, A., Buynak, J. D., Bethel, C. R., Bonomo, R. A., and Carey, P. R. (2007). Efficient inhibition of class A and class D  $\beta$ -lactamases by Michaelis complexes. *J. Biol. Chem.* 282, 21588–21591. doi: 10.1074/jbc.C700080200
- Ke, W., Bethel, C. R., Papp-Wallace, K. M., Pagadala, S. R., Nottingham, M., Fernandez, D., et al. (2012a). Crystal structures of KPC-2  $\beta$ -lactamase in complex with 3-nitrophenyl boronic acid and the penam sulfone PSR-3-226. *Antimicrob. Agents Chemother.* 56, 2713–2718. doi: 10.1128/AAC.06099-11
- Ke, W., Pattanaik, P., Bethel, C. R., Sheri, A., Buynak, J. D., Bonomo, R. A., et al. (2012b). Structures of SHV-1  $\beta$ -lactamase with penem and penam sulfone



- inhibitors that form cyclic intermediates stabilized by carbonyl conjugation. *PLoS ONE* 7:e49035. doi: 10.1371/journal.pone.0049035
- Ke, W., Rodkey, E. A., Sampson, J. M., Skalweit, M. J., Sheri, A., Pagadala, S. R., et al. (2012c). The importance of the *trans*-enamine intermediate as a  $\beta$ -lactamase inhibition strategy probed in inhibitor-resistant SHV  $\beta$ -lactamase variants. *Chem. Med. Chem.* 7, 1002–1008. doi: 10.1002/cmdc.201200006
- King, A. M., King, D. T., French, S., Brouillette, E., Asli, A., Alexander, J. A., et al. (2016). Structural and kinetic characterization of diazabicyclooctanes as dual inhibitors of both serine- $\beta$ -lactamases and penicillin-binding proteins. *ACS Chem. Biol.* 11, 864–868. doi: 10.1021/acscmbio.5b00944
- King, D. T., King, A. M., Lal, S. M., Wright, G. D., and Strynadka, N. C. (2015). Molecular mechanism of avibactam mediated beta-lactamase inhibition. *ACS Infect. Dis.* 1, 175–184. doi: 10.1021/acsfeddis.5b00007
- Krishnan, N. P., Nguyen, N. Q., Papp-Wallace, K. M., Bonomo, R. A., and van den Akker, F. (2015). Inhibition of klebsiella beta-lactamases (SHV-1 and KPC-2) by avibactam: a structural study. *PLoS ONE* 10:e0136813. doi: 10.1371/journal.pone.0136813
- Kuzin, A. P., Nukaga, M., Nukaga, Y., Hujer, A., Bonomo, R. A., and Knox, J. R. (2001). Inhibition of the SHV-1  $\beta$ -lactamase by sulfones: crystallographic observation of two reaction intermediates with tazobactam. *Biochemistry* 40, 1861–1866. doi: 10.1021/bi0022745
- Lahiri, S. D., Johnstone, M. R., Ross, P. L., McLaughlin, R. E., Olivier, N. B., and Alm, R. A. (2014). Avibactam and class C beta-lactamases: mechanism of inhibition, conservation of the binding pocket, and implications for resistance. *Antimicrob. Agents Chemother.* 58, 5704–5713. doi: 10.1128/AAC.03057-14
- Lahiri, S. D., Mangani, S., Durand-Reville, T., Benvenuti, M., De Luca, F., Sanyal, G., et al. (2013). Structural insight into potent broad-spectrum inhibition with reversible recyclization mechanism: avibactam in complex with CTX-M-15 and *Pseudomonas aeruginosa* AmpC beta-lactamases. *Antimicrob. Agents Chemother.* 57, 2496–2505. doi: 10.1128/AAC.02247-12
- Lahiri, S. D., Mangani, S., Jahic, H., Benvenuti, M., Durand-Reville, T. F., De Luca, F., et al. (2015). Molecular basis of selective inhibition and slow reversibility of avibactam against class D carbapenemases: a structure-guided study of OXA-24 and OXA-48. *ACS Chem. Biol.* 10, 591–600. doi: 10.1021/cb500703p
- Lapuebla, A., Abdallah, M., Olafisoye, O., Cortes, C., Urban, C., Landman, D., et al. (2015). Activity of imipenem with relebactam against gram-negative pathogens from New York city. *Antimicrob. Agents Chemother.* 59, 5029–5031. doi: 10.1128/AAC.00830-15
- Li, R., Liao, J. M., Gu, C. R., Wang, Y. T., and Chen, C. L. (2011). Theoretical investigation on reaction of sulbactam with wild-type SHV-1 beta-lactamase: acylation, tautomerization, and deacylation. *J. Phys. Chem. B* 115, 10298–10310. doi: 10.1021/jp111572v
- Livermore, D. M., Mushtaq, S., Warner, M., Vickers, A., and Woodford, N. (2017). *In vitro* activity of cefepime/zidebactam (WCK 5222) against Gram-negative bacteria. *J. Antimicrob. Chemother.* 72, 1373–1385. doi: 10.1093/jac/dkw593
- Livermore, D. M., Mushtaq, S., Warner, M., and Woodford, N. (2015). Activity of OP0595/beta-lactam combinations against Gram-negative bacteria with extended-spectrum, AmpC and carbapenem-hydrolysing beta-lactamases. *J. Antimicrob. Chemother.* 70, 3032–3041. doi: 10.1093/jac/dkv239
- Livermore, D. M., Warner, M., and Mushtaq, S. (2013). Activity of MK-7655 combined with imipenem against *Enterobacteriaceae* and *Pseudomonas aeruginosa*. *J. Antimicrob. Chemother.* 68, 2286–2290. doi: 10.1093/jac/dkt178
- Lizana, I., and Delgado, E. J. (2017). A QM/MM study on the enzymatic inactivation of cefotaxime. *J. Mol. Model.* 23:209. doi: 10.1007/s00894-017-3379-8
- Lob, S. H., Hackel, M. A., Kazmierczak, K. M., Young, K., Motyl, M. R., Karlowsky, J. A., et al. (2017). *In vitro* activity of imipenem-relebactam against gram-negative ESKAPE pathogens isolated by clinical laboratories in the United States in 2015 (Results from the SMART Global Surveillance Program). *Antimicrob. Agents Chemother.* 61:e02209-16. doi: 10.1128/AAC.02209-16
- Lobkovsky, E., Billings, E. M., Moews, P. C., Rahil, J., Pratt, R. F., and Knox, J. R. (1994). Crystallographic structure of a phosphonate derivative of the *Enterobacter cloacae* P99 cephalosporinase: mechanistic interpretation of a beta-lactamase transition-state analog. *Biochemistry* 33, 6762–6772. doi: 10.1021/bi00188a004
- Lohans, C. T., Wang, D. Y., Jorgensen, C., Cahill, S. T., Clifton, I. J., McDonough, M. A., et al. (2017). (13)C-Carbamylation as a mechanistic probe for the inhibition of class D beta-lactamases by avibactam and halide ions. *Organ. Biomol. Chem.* 15 6024–6032. doi: 10.1039/C7OB01514C
- Lomovskaya, O., Sun, D., Rubio-Aparicio, D., Nelson, K., Tsivkovski, R., Griffith, D. C., et al. (2017). Vaborbactam: spectrum of beta-lactamase inhibition and impact of resistance mechanisms on activity in *Enterobacteriaceae*. *Antimicrob. Agents Chemother.* 61, e01443–e01417. doi: 10.1128/AAC.01443-17
- Mansour, T. S., Agarwal, A., Venkatesan, A., Abe, T., Mihira, A., Takasaki, T., et al. (2007). On the absolute configuration in 1,4-dihydrothiazepine covalent complexes derived from inhibition of class A and C beta-lactamases with 6-methylidene penems. *Chem. Med. Chem.* 2, 1713–1716. doi: 10.1002/cmdc.200700144
- Maveyraud, L., Massova, I., Bircik, I., Miyashita, K., Samama, J. P., and Mobashery, S. (1996). Crystal structure of 6 $\alpha$ -(hydroxymethyl)penicillanate complexed to the TEM-1 beta-lactamase from *Escherichia coli*: evidence on the mechanism of action of a novel inhibitor designed by a computer-aided process. *J. Am. Chem. Soc.* 118, 7435–7440.
- McLeod, S. M., Shapiro, A. B., Moussa, S. H., Johnstone, M., McLaughlin, R. E., de Jonge, B. L. M., et al. (2017). Frequency and mechanism of spontaneous resistance to sulbactam combined with the novel beta-lactamase inhibitor ETX2514 in clinical isolates of *Acinetobacter baumannii*. *Antimicrob. Agents Chemother.* 62, e01576–e01517. doi: 10.1128/AAC.01576-17
- Meroueh, S. O., Fisher, J. F., Schlegel, H. B., and Mobashery, S. (2005). Ab initio QM/MM study of class A beta-lactamase acylation: dual participation of Glu166 and Lys73 in a concerted base promotion of Ser70. *J. Am. Chem. Soc.* 127, 15397–15407. doi: 10.1021/ja051592u
- Morinaka, A., Tsutsumi, Y., Yamada, K., Takayama, Y., Sakakibara, S., Takata, T., et al. (2017). *In vitro* and *in vivo* activities of the diazabicyclooctane OP0595 against AmpC-derepressed *Pseudomonas aeruginosa*. *J. Antibiot.* 70, 246–250. doi: 10.1038/ja.2016.150
- Morinaka, A., Tsutsumi, Y., Yamada, M., Suzuki, K., Watanabe, T., Abe, T., et al. (2015). OP0595, a new diazabicyclooctane: mode of action as a serine beta-lactamase inhibitor, antibiotic and beta-lactam ‘enhancer’. *J. Antimicrob. Chemother.* 70, 2779–2786. doi: 10.1093/jac/dkv166
- Moya, B., Barcelo, I. M., Bhagwat, S., Patel, M., Bou, G., Papp-Wallace, K. M., et al. (2017a). Potent beta-lactam enhancer activity of zidebactam and WCK 5153 against *Acinetobacter baumannii*, including carbapenemase-producing clinical isolates. *Antimicrob. Agents Chemother.* 61:01238-17. doi: 10.1128/AAC.01238-17
- Moya, B., Barcelo, I. M., Bhagwat, S., Patel, M., Bou, G., Papp-Wallace, K. M., et al. (2017b). WCK 5107 (Zidebactam) and WCK 5153 are novel inhibitors of BBP2 showing potent “beta-lactam enhancer” activity against *Pseudomonas aeruginosa*, including multidrug-resistant metallo-beta-lactamase-producing high-risk clones. *Antimicrob. Agents Chemother.* 61:e02529-16. doi: 10.1128/AAC.02529-16
- Mushtaq, S., Vickers, A., Woodford, N., and Livermore, D. M. (2017). WCK 4234, a novel diazabicyclooctane potentiating carbapenems against *Enterobacteriaceae*, *Pseudomonas* and *Acinetobacter* with class A, C and D beta-lactamases. *J. Antimicrob. Chemother.* 72, 1688–1695. doi: 10.1093/jac/dkw035
- Nguyen, N. Q., Krishnan, N. P., Rojas, L. J., Prati, F., Caselli, E., Romagnoli, C., et al. (2016). Crystal structures of KPC-2 and SHV-1 beta-lactamases in complex with the boronic acid transition state analog S02030. *Antimicrob. Agents Chemother.* 60, 1760–1766. doi: 10.1128/AAC.02643-15
- Nichols, D. A., Renslo, A. R., and Chen, Y. (2014). Fragment-based inhibitor discovery against beta-lactamase. *Future Med. Chem.* 6, 413–427. doi: 10.4155/fmc.14.10
- Nikolaidis, I., Favini-Stabile, S., and Dessen, A. (2014). Resistance to antibiotics targeted to the bacterial cell wall. *Protein Sci.* 23, 243–259. doi: 10.1002/pro.2414
- Nukaga, M., Abe, T., Venkatesan, A. M., Mansour, T. S., Bonomo, R. A., and Knox, J. R. (2003). Inhibition of class A and class C  $\beta$ -lactamases by penems: crystallographic structures of a novel 1,4-thiazepine intermediate. *Biochemistry* 42, 13152–13159. doi: 10.1021/bi034986b
- Nukaga, M., Kumar, S., Nukaga, K., Pratt, R. F., and Knox, J. R. (2004). Hydrolysis of third-generation cephalosporins by class C beta-lactamases. Structures of a transition state analog of cefotaxime in wild-type and extended spectrum enzymes. *J. Biol. Chem.* 279, 9344–9352. doi: 10.1074/jbc.M312356200
- Padayatti, P. S., Helfand, M. S., Totir, M. A., Carey, M. P., Carey, P. R., Bonomo, R. A., et al. (2005). High resolution crystal structures of the *trans*-enamine intermediates formed by sulbactam and clavulanic acid and E166A

- SHV-1  $\beta$ -lactamase. *J. Biol. Chem.* 280, 34900–34907. doi: 10.1074/jbc.M50533200
- Padayatti, P. S., Helfand, M. S., Totir, M. A., Carey, M. P., Hujer, H. M., Carey, P. R., et al. (2004). Tazobactam forms a stoichiometric *trans*-enamine intermediate in the E166A variant of SHV-1  $\beta$ -lactamase: 1.63 Å crystal structure. *Biochemistry* 43, 843–848. doi: 10.1021/bi035985m
- Padayatti, P. S., Sheri, A., Totir, M. A., Helfand, M. S., Carey, M. P., Anderson, V. E., et al. (2006). Rational design of a  $\beta$ -lactamase inhibitor achieved via stabilization of the *trans*-enamine intermediate: 1.28 Å crystal structure of wt SHV-1 complex with a penam sulfone. *J. Am. Chem. Soc.* 128, 13235–13242. doi: 10.1021/ja063715w
- Page, M. G. P. (2000).  $\beta$ -Lactamase inhibitors. *Drug Resist. Updat.* 3, 109–125. doi: 10.1054/drup.2000.0137
- Papp-Wallace, K. M., Bethel, C. R., Gootz, T. D., Shang, W., Stroth, J., Lau, W., et al. (2012). Inactivation of a class A and a class C  $\beta$ -lactamase by 6 $\beta$ -(hydroxymethyl)penicillanic acid sulfone. *Biochem. Pharmacol.* 83, 462–471. doi: 10.1016/j.bcp.2011.11.015
- Papp-Wallace, K. M., and Bonomo, R. A. (2016). New beta-lactamase inhibitors in the clinic. *Infect. Dis. Clin. North Am.* 30, 441–464. doi: 10.1016/j.idc.2016.02.007
- Patera, A., Blaszczak, L. C., and Shoichet, B. (2000). Crystal structures of substrate and inhibitor complexes with AmpC beta-lactamase: possible implications for substrate-assisted catalysis. *J. Am. Chem. Soc.* 122, 10504–10512. doi: 10.1021/ja001676x
- Pattanaik, P., Bethel, C. R., Hujer, A. M., Hujer, K. M., Distler, A. M., Taracila, M., et al. (2009). Strategic design of an effective  $\beta$ -lactamase inhibitor: LN-1-255, a 6-alkylidene-2'-substituted penicillin sulfone. *J. Biol. Chem.* 284, 945–953. doi: 10.1074/jbc.M806833200
- Phillips, O. A., Reddy, A. V., Setti, E. L., Spevak, P., Czajkowski, D. P., Atwal, H., et al. (2005). Synthesis and biological evaluation of penam sulfones as inhibitors of beta-lactamases. *Bioorg. Med. Chem.* 13, 2847–2858. doi: 10.1016/j.bmc.2005.02.020
- Powers, R. A., Swanson, H. C., Taracila, M. A., Florek, N. W., Romagnoli, C., Caselli, E., et al. (2014). Biochemical and structural analysis of inhibitors targeting the ADC-7 cephalosporinase of *Acinetobacter baumannii*. *Biochemistry* 53, 7670–7679. doi: 10.1021/bi500887n
- Rodkey, E. A., Drawz, S. M., Sampson, J. M., Bethel, C. R., Bonomo, R. A. and van den Akker, F. (2012). Crystal structure of a pre-acylation complex of the  $\beta$ -lactamase inhibitor sulbactam bound to a sulfenamide bond-containing thiol-beta-lactamase. *J. Am. Chem. Soc.* 134, 16798–16804. doi: 10.1021/ja3073676
- Rodkey, E. A., McLeod, D. C., Bethel, C. R., Smith, K. M., Xu, Y., Chai, W., et al. (2013). beta-Lactamase inhibition by 7-alkylidenecephalosporin sulfones: allylic transposition and formation of an unprecedented stabilized acyl-enzyme. *J. Am. Chem. Soc.* 135, 18358–18369. doi: 10.1021/ja403598g
- Rodkey, E. A., Winkler, M. L., Bethel, C. R., Pagadala, S. R., Buynak, J. D., Bonomo, R. A., et al. (2014). Penam sulfones and beta-lactamase inhibition: SA2-13 and the importance of the C2 side chain length and composition. *PLoS ONE* 9:e85892. doi: 10.1371/journal.pone.0085892
- Sader, H. S., Castanheira, M., Huband, M., Jones, R. N., and Flamm, R. K. (2017a). WCK 5222 (Cefepime-Zidebactam) antimicrobial activity against clinical isolates of gram-negative bacteria collected worldwide in 2015. *Antimicrob. Agents Chemother.* 61:e00072-17. doi: 10.1128/AAC.00072-17
- Sader, H. S., Rhomberg, P. R., Flamm, R. K., Jones, R. N., and Castanheira, M. (2017b). WCK 5222 (cefepime/zidebactam) antimicrobial activity tested against Gram-negative organisms producing clinically relevant beta-lactamases. *J. Antimicrob. Chemother.* 72, 1696–1703. doi: 10.1093/jac/dkx050
- Sampson, J. M., Ke, W., Bethel, C. R., Pagadala, S. R., Nottingham, M. D., Bonomo, R. A., et al. (2011). Ligand-dependent disorder of the  $\Omega$ -loop observed in extended-spectrum SHV-type  $\beta$ -lactamase. *Antimicrob. Agents Chemother.* 55, 2303–2309. doi: 10.1128/AAC.01360-10
- Sgrignani, J., Grazioso, G., and De Amici, M. (2016). Insight into the mechanism of hydrolysis of meropenem by OXA-23 serine-beta-lactamase gained by quantum mechanics/molecular mechanics calculations. *Biochemistry* 55, 5191–5200. doi: 10.1021/acs.biochem.6b00461
- Sgrignani, J., Grazioso, G., De Amici, M., and Colombo, G. (2014). Inactivation of TEM-1 by avibactam (NXL-104): insights from quantum mechanics/molecular mechanics metadynamics simulations. *Biochemistry* 53, 5174–5185. doi: 10.1021/bi500589x
- Shapiro, A. B., Gao, N., Jahic, H., Carter, N. M., Chen, A., and Miller, A. A. (2017). Reversibility of covalent, broad-spectrum serine beta-lactamase inhibition by the diazabicyclooctenone ETX2514. *ACS Infect. Dis.* 3, 833–844. doi: 10.1021/acsinfecdis.7b00113
- Strynadka, N. C., Adachi, H., Jensen, S. E., Johns, K., Sielecki, A., Betzel, C., et al. (1992). Molecular structure of the acyl-enzyme intermediate in  $\beta$ -lactam hydrolysis at 1.7 Å resolution. *Nature* 359, 700–705.
- Sun, T., Bethel, C. R., Bonomo, R. A., and Knox, J. R. (2004). Inhibitor-resistant class A  $\beta$ -lactamases: consequences of the Ser130-to-Gly mutation seen in Apo and tazobactam structures of the SHV-1 variant. *Biochemistry* 43, 14111–14117. doi: 10.1021/bi0487903
- Tondi, D., Calo, S., Shoichet, B. K., and Costi, M. P. (2010). Structural study of phenyl boronic acid derivatives as AmpC beta-lactamase inhibitors. *Bioorg. Med. Chem. Lett.* 20, 3416–3419. doi: 10.1016/j.bmcl.2010.04.007
- Tondi, D., Venturelli, A., Bonnet, R., Pozzi, C., Shoichet, B. K., and Costi, M. P. (2014). Targeting class A and C serine beta-lactamases with a broad-spectrum boronic acid derivative. *J. Med. Chem.* 57, 5449–5458. doi: 10.1021/jm5006572
- Totir, M. A., Padayatti, P. S., Helfand, M. S., Carey, M. P., Bonomo, R. A., Carey, P. R., et al. (2006). Effect of the inhibitor-resistant M69V substitution on the structures and populations of *trans*-enamine beta-lactamase intermediates. *Biochemistry* 45, 11895–11904. doi: 10.1021/bi060990m
- Tripathi, R., and Nair, N. N. (2016). Deacylation mechanism and kinetics of acyl-enzyme complex of class C beta-lactamase and cephalothin. *J. Phys. Chem. B* 120, 2681–2690. doi: 10.1021/acs.jpcc.5b11623
- Venkatesan, A. M., Agarwal, A., Abe, T., Ushirogouchi, H., Ado, M., Tsuyoshi, T., et al. (2008). 5,5,6-Fused tricycles bearing imidazole and pyrazole 6-methylidene penems as broad-spectrum inhibitors of beta-lactamases. *Bioorg. Med. Chem.* 16, 1890–1902. doi: 10.1016/j.bmc.2007.11.006
- Venkatesan, A. M., Agarwal, A., Abe, T., Ushirogouchi, H., Yamamura, I., Kumagai, T., et al. (2004a). Novel imidazole substituted 6-methylidene-penems as broad-spectrum beta-lactamase inhibitors. *Bioorg. Med. Chem.* 12, 5807–5817. doi: 10.1016/j.bmc.2004.08.039
- Venkatesan, A. M., Gu, Y., Dos, S. O., Abe, T., Agarwal, A., Yang, Y., et al. (2004b). Structure-activity relationship of 6-methylidene penems bearing tricyclic heterocycles as broad-spectrum beta-lactamase inhibitors: crystallographic structures show unexpected binding of 1,4-thiazepine intermediates. *J. Med. Chem.* 47, 6556–6568. doi: 10.1021/jm049680x
- Wang, D. Y., Abboud, M. I., Markoulides, M. S., Brem, J., and Schofield, C. J. (2016). The road to avibactam: the first clinically useful non-beta-lactam working somewhat like a beta-lactam. *Future Med. Chem.* 8, 1063–1084. doi: 10.4155/fmc-2016-0078
- Werner, J. P., Mitchell, J. M., Taracila, M. A., Bonomo, R. A., and Powers, R. A. (2017). Exploring the potential of boronic acids as inhibitors of OXA-24/40 beta-lactamase. *Protein Sci.* 26, 515–526. doi: 10.1002/pro.3100
- Wright, H., Bonomo, R. A., and Paterson, D. L. (2017). New agents for the treatment of infections with Gram-negative bacteria: restoring the miracle or false dawn? *Clin. Microbiol. Infect.* 23, 704–712. doi: 10.1016/j.cmi.2017.09.001
- Xu, H., Hazra, S., and Blanchard, J. S. (2012). NXL104 irreversibly inhibits the beta-lactamase from *Mycobacterium tuberculosis*. *Biochemistry* 51, 4551–4557. doi: 10.1021/bi300508r
- Zhanell, G. G., Lawrence, C. K., Adam, H., Schweizer, F., Zelenitsky, S., Zhanell, M., et al. (2018). Imipenem-relebactam and meropenem-vaborbactam: two novel carbapenem-beta-lactamase inhibitor combinations. *Drugs* 78, 65–98. doi: 10.1007/s40265-017-0851-9

**Conflict of Interest Statement:** The authors declare that the research was conducted in the absence of any commercial or financial relationships that could be construed as a potential conflict of interest.

Copyright © 2018 van den Akker and Bonomo. This is an open-access article distributed under the terms of the Creative Commons Attribution License (CC BY). The use, distribution or reproduction in other forums is permitted, provided the original author(s) and the copyright owner are credited and that the original publication in this journal is cited, in accordance with accepted academic practice. No use, distribution or reproduction is permitted which does not comply with these terms.

# Advantages of publishing in Frontiers



## OPEN ACCESS

Articles are free to read  
for greatest visibility  
and readership



## FAST PUBLICATION

Around 90 days  
from submission  
to decision



## HIGH QUALITY PEER-REVIEW

Rigorous, collaborative,  
and constructive  
peer-review



## TRANSPARENT PEER-REVIEW

Editors and reviewers  
acknowledged by name  
on published articles

## Frontiers

Avenue du Tribunal-Fédéral 34  
1005 Lausanne | Switzerland

**Visit us:** [www.frontiersin.org](http://www.frontiersin.org)

**Contact us:** [info@frontiersin.org](mailto:info@frontiersin.org) | +41 21 510 17 00



## REPRODUCIBILITY OF RESEARCH

Support open data  
and methods to enhance  
research reproducibility



## DIGITAL PUBLISHING

Articles designed  
for optimal readership  
across devices



## FOLLOW US

[@frontiersin](https://twitter.com/frontiersin)



## IMPACT METRICS

Advanced article metrics  
track visibility across  
digital media



## EXTENSIVE PROMOTION

Marketing  
and promotion  
of impactful research



## LOOP RESEARCH NETWORK

Our network  
increases your  
article's readership